Richard Ha
Christopher E. Comstock
Elizabeth A. Morris
Editors

Breast MRI Teaching Atlas

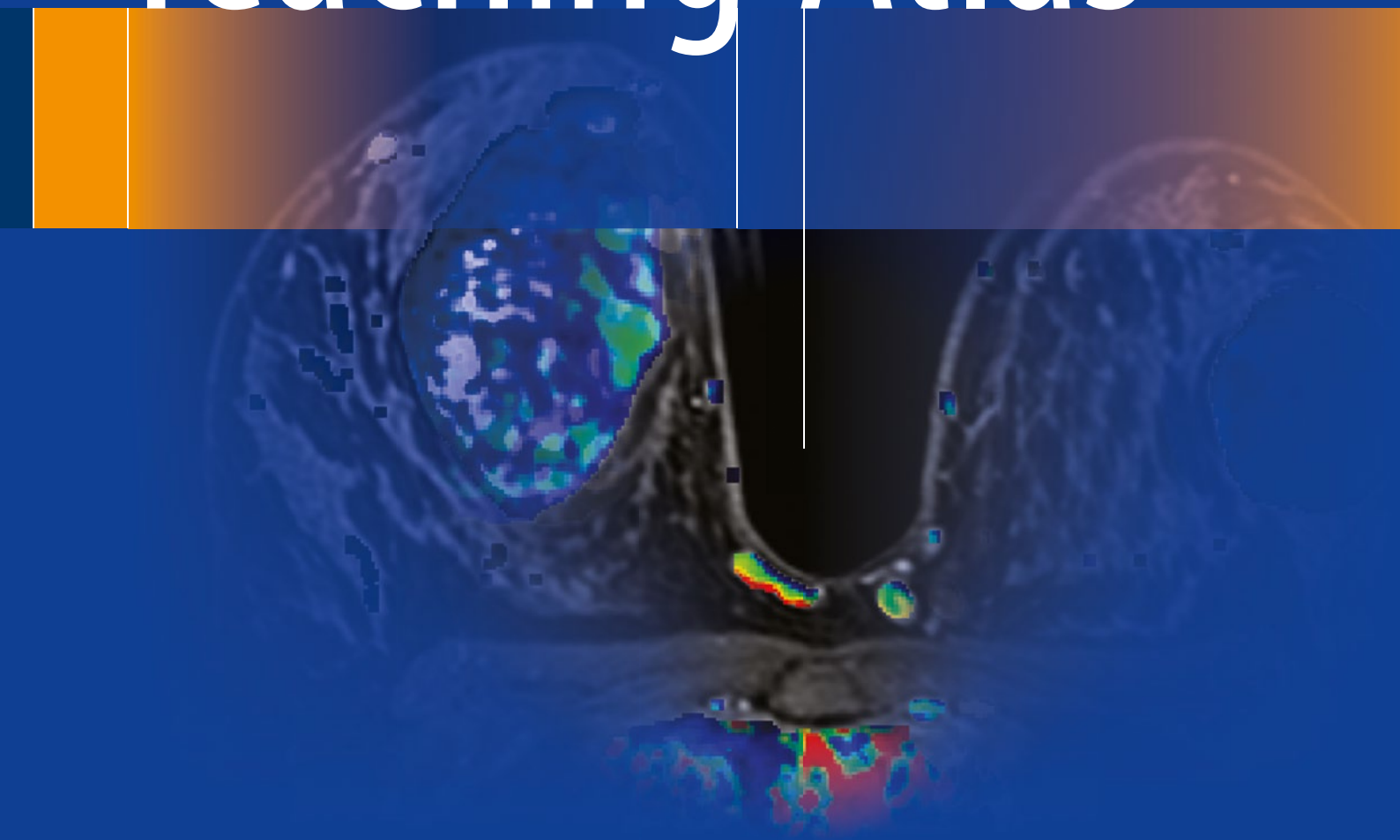

Springer

Breast MRI Teaching Atlas

Richard Ha • Christopher E. Comstock
Elizabeth A. Morris
Editors

Breast MRI Teaching Atlas

Springer

Editors
Richard Ha, MD
Director of Education and Research
Division of Breast Imaging
Assistant Professor of Radiology
Columbia University Medical Center
New York, NY
USA

Christopher E. Comstock, MD
Breast Imaging Service
Memorial Sloan-Kettering Cancer Center
New York, NY
USA

Associate Professor of Radiology
Weill Cornell Medical College
New York, NY
USA

Elizabeth A. Morris, MD
Chief, Breast Imaging Service
Memorial Sloan-Kettering Cancer Center
New York, NY
USA

Professor of Radiology
Weill Cornell Medical College
New York, NY
USA

ISBN 978-1-4939-6407-9 ISBN 978-1-4939-6409-3 (eBook)
DOI 10.1007/978-1-4939-6409-3

Library of Congress Control Number: 2017936197

Printed on acid-free paper

This Springer imprint is published by Springer Nature
The registered company is Springer Science+Business Media LLC
The registered company address is: 233 Spring Street, New York, NY 10013, U.S.A.

To my loving parents (Kyungsub and Kehui Ha), my beautiful wife Karen, and my little princesses Madeleine and Esme, who have given my life joy and make me appreciate every day.

Richard Ha, MD

To my daughters Abby and Bronwyn.

Elizabeth A. Morris, MD

Preface

The purpose of the *Breast MRI Teaching Atlas* is to serve as a basic introduction to breast MRI. This book is case based, emphasizing pertinent breast MRI findings and common indications for breast MRI. The chapters are broadly separated based on benign and malignant breast pathology as well as commonly encountered breast MRI findings. Brief teaching points accompany each case, highlighting the importance of the findings rather than long and exhaustive discussion. The target audience for this book is medical students, residents, and breast imaging fellows, with the intention of being readable over a short period of time to provide an introduction to breast MRI. This book may also serve as a review for practicing general radiologists and clinicians involved in the care of breast cancer patients including surgeons, oncologists, and obstetricians/gynecologists.

New York, NY, USA — Richard Ha, MD
New York, NY, USA — Christopher E. Comstock, MD
New York, NY, USA — Elizabeth A. Morris, MD

Contents

Contributors

Rend Al-Khalili, MD Staff Radiologist, Washington Radiology Associates, Fairfax, Virginia, VA, USA

Christopher E. Comstock, MD Breast Imaging Service, Memorial Sloan-Kettering Cancer Center, New York, NY, USA

Associate Professor of Radiology, Weill Cornell Medical College, New York, NY, USA

Lauren Friedlander, MD Director of Breast and Body Imaging Fellowship, Division of Breast Imaging, Assistant Professor of Radiology, Columbia University Medical Center, New York, NY, USA

Richard Ha, MD Director of Education and Research, Division of Breast Imaging, Assistant Professor of Radiology, Columbia University Medical Center, New York, NY, USA

Victoria Mango, MD Director of Breast and Body Imaging Fellowship, Breast Imaging Service, Memorial Sloan-Kettering Cancer Center, Assistant Professor of Radiology, Weill Cornell Medical College, New York, NY, USA

Elizabeth A. Morris, MD Chief, Breast Imaging Service, Memorial Sloan-Kettering Cancer Center, New York, NY, USA

Professor of Radiology, Weill Cornell Medical College, New York, NY, USA

Dustin Nguyen, DO Staff Radiologist, Radiology Associates of North Texas, Fort Worth, Texas, TX, USA

Habib Rahbar, MD Breast Imaging Section, Associate Professor of Radiology, University of Washington School of Medicine, Seattle, Washington, WA, USA

Karen Weinshelbaum, MD Department of Radiology, Newark Beth Israel Medical Center, Newark, NJ, USA

Ralph Wynn, MD Section Head, Division of Breast Imaging, Associate Professor of Radiology, Columbia University Medical Center, New York, NY, USA

Breast MRI Basics

1

Victoria Mango, Habib Rahbar, Ralph Wynn,
Lauren Friedlander, and Richard Ha

V. Mango, MD
Director of Breast and Body Imaging Fellowship,
Breast Imaging Service, Memorial Sloan-Kettering Cancer Center,
Assistant Professor of Radiology, Weill Cornell Medical College,
New York, NY, USA
e-mail: vlm2125@columbia.edu

H. Rahbar, MD
Breast Imaging Section, Associate Professor of Radiology,
University of Washington School of Medicine,
Seattle, Washington, USA
e-mail: hrahbar@uw.edu

R. Wynn, MD
Section Head, Division of Breast Imaging, Associate Professor
of Radiology, Columbia University Medical Center,
New York, NY, USA
e-mail: rtw2120@columbia.edu

L. Friedlander, MD
Director of Breast and Body Imaging Fellowship,
Division of Breast Imaging, Assistant Professor of Radiology,
Columbia University Medical Center, New York, NY, USA
e-mail: lf2386@columbia.edu

R. Ha, MD (✉)
Director of Education and Research,
Division of Breast Imaging, Assistant Professor of Radiology,
Columbia University Medical Center, New York, NY, USA
e-mail: rh2616@cumc.columbia.edu

R. Ha et al. (eds.), Breast MRI Teaching Atlas, DOI 10.1007/978-1-4939-6409-3_1

1.1 History

Four patients with T1-weighted sequence findings (Figs. 1.1, 1.2, 1.3, 1.4, 1.5, 1.6, 1.7, and 1.8).

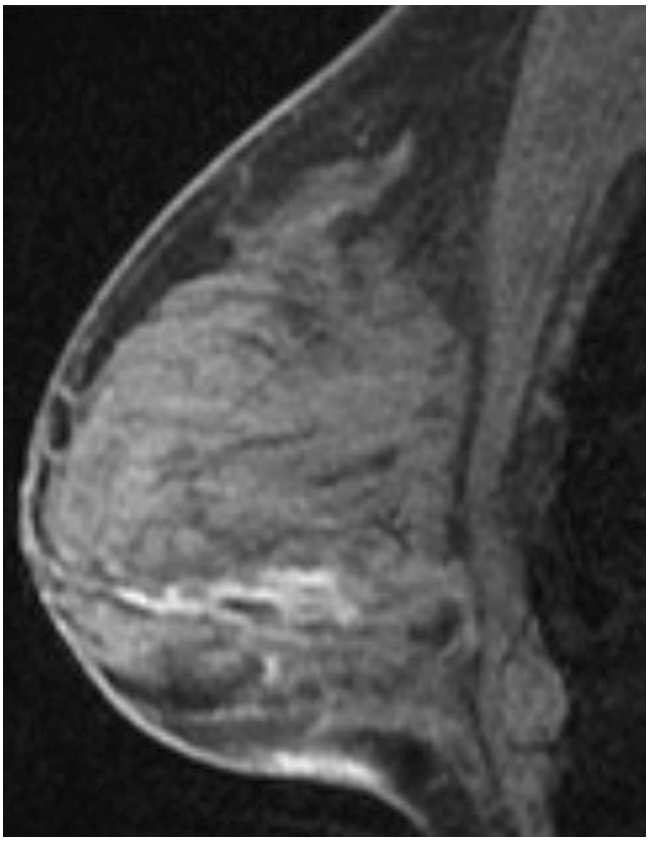

Fig. 1.1 Sagittal T1 fat-saturated pre-contrast image of the right breast

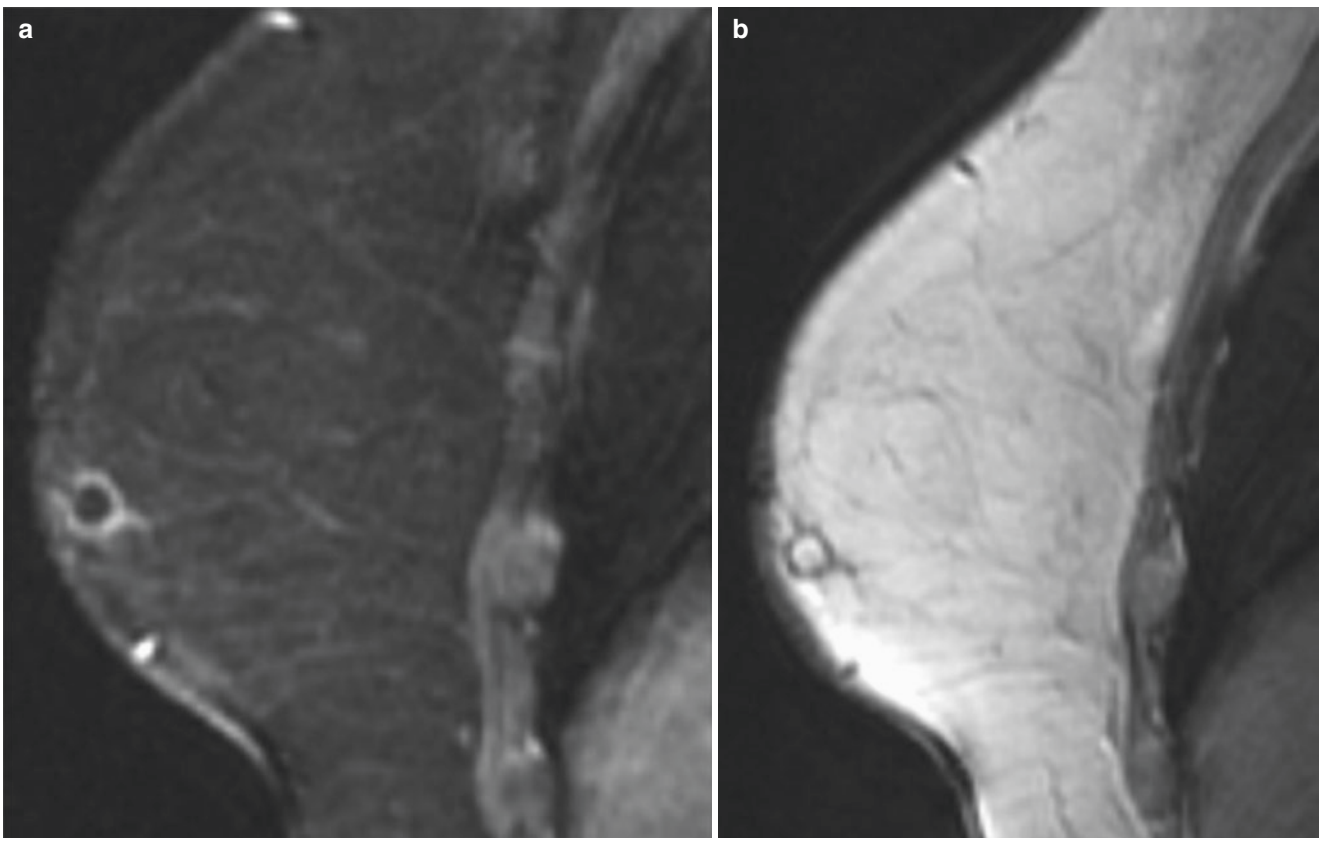

Fig. 1.2 Sagittal T1 fat-saturated post-contrast image of the right breast (**a**) and corresponding T1 non–fat-saturated image (**b**)

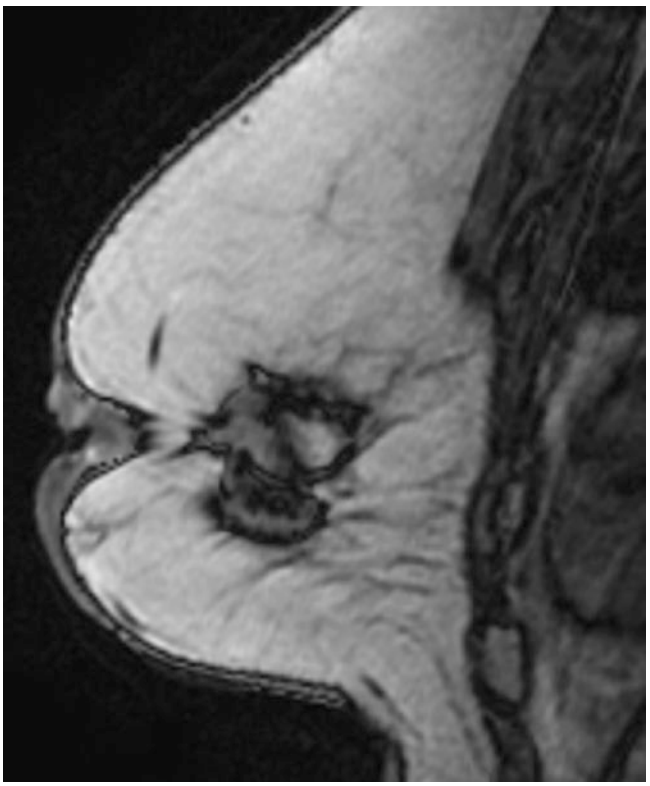

Fig. 1.3 Sagittal T1 non–fat-saturated image of the left breast

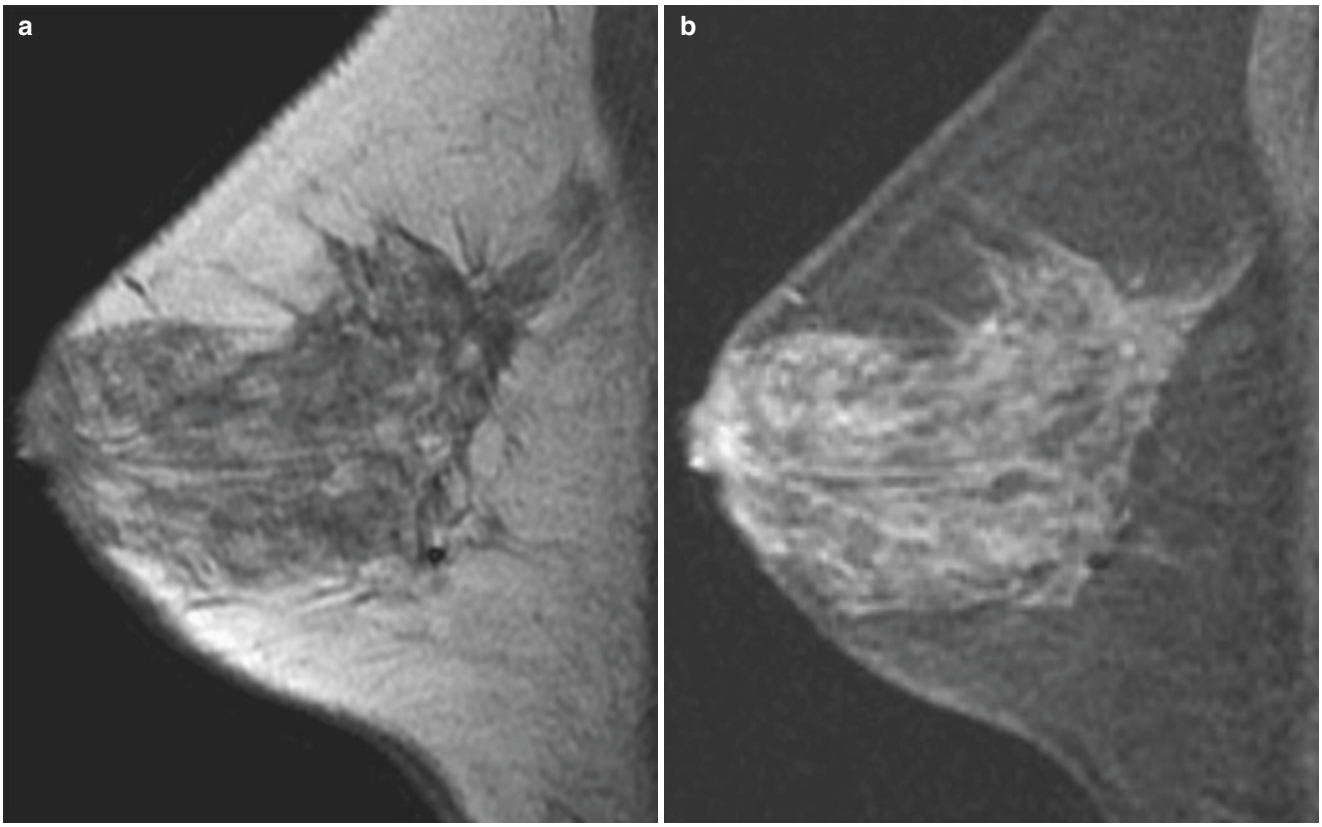

Fig. 1.4 Sagittal T1 non–fat-saturated image of the right breast (**a**) and corresponding T1 fat-saturated sequences (**b**)

1.1 T1-Weighted Sequence

Teaching Points Breast MRI should be performed on systems with at least 1.5 Tesla magnet strength with a dedicated breast coil. Usually, a pre-contrast T1-weighted gradient-echo sequence without fat saturation is the first sequence performed after the scout images. A T1-weighted non–fat-saturated sequence is obtained bilaterally, including axillae and chest wall, to distinguish fat from water-based tissues. The pre-contrast T1-weighted sequence is typically used to assess the amount of fibroglandular tissue and can be particularly helpful in documenting the presence of high-signal hemorrhagic or proteinaceous fluid-filled, dilated ducts (Fig. 1.1). Radiologists should be aware of these T1-hyperintense ducts, which can cause potential misregistration artifact related to patient motion, leading to an apparent suspicious linear nonmass enhancement on post-contrast subtracted images. It is important to assess the pre-contrast T1 sequence before evaluating the post-contrast images. T1 non–fat-saturated images can be helpful in evaluating for fat necrosis by identifying central fat (Fig. 1.2). Biopsy clip artifact and architectural distortion can be better seen on the non–fat-saturated T1 sequence (Figs. 1.3 and 1.4).

Image Findings

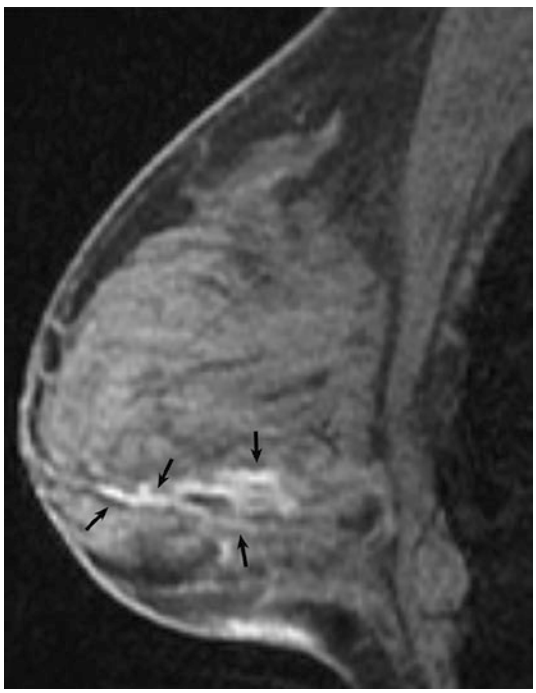

Fig. 1.5 Hemorrhagic or proteinaceous debris in ducts. Sagittal T1 fat-saturated pre-contrast image of the right breast demonstrates several linear hyperintensities (*arrows*) in a ductal distribution in the lower breast, compatible with hemorrhagic or proteinaceous debris

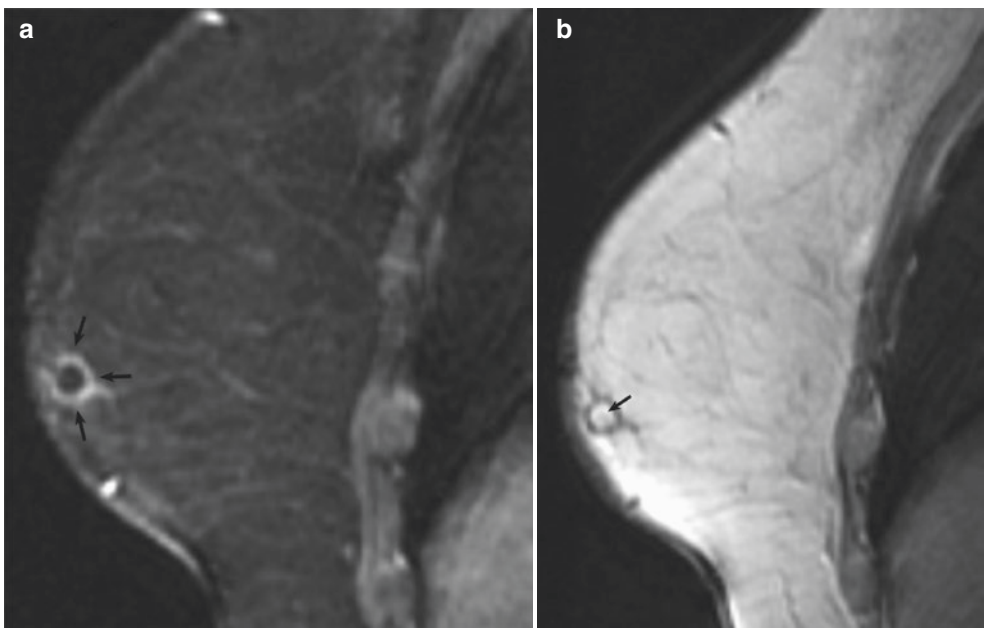

Fig. 1.6 Fat necrosis. (**a**) Sagittal T1 fat-saturated post-contrast image of the right breast demonstrates indeterminate rim enhancement (*arrows*). (**b**) The T1 non–fat-saturated image shows central fat (*arrow*), compatible with benign fat necrosis

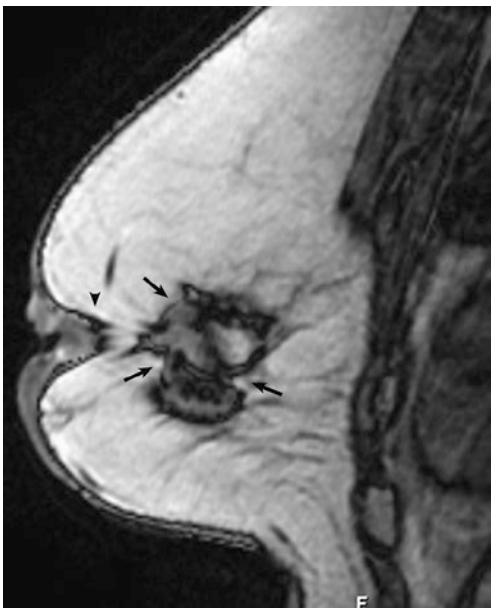

Fig. 1.7 Architectural distortion. In a patient with prior lumpectomy, the sagittal T1 non–fat-saturated image of the left breast illustrates architectural distortion in the central breast (*arrows*) and associated nipple retraction (*arrowhead*)

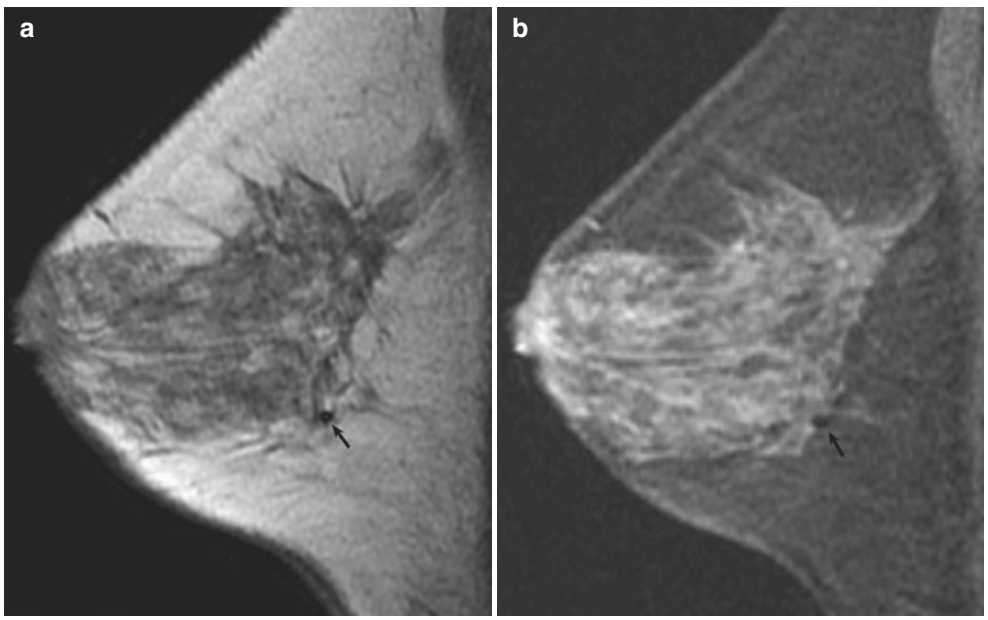

Fig. 1.8 Susceptibility artifact from biopsy clip. The susceptibility artifact from a biopsy clip (*arrow*) is more prominent on the T1 non–fat-saturated image of the right breast (**a**) than on the T1 fat-saturated sequences (**b**)

1.2 History

Four patients illustrating the range of the amount of fibroglandular tissue on breast MRI (Figs. 1.9, 1.10, 1.11, and 1.12).

1.2 Fibroglandular Tissue

Teaching Points At mammography, breast density is represented by the amount of fibroglandular tissue (FGT) in contrast to fat measured in two-dimensional views that may not reflect an accurate assessment. Breast MRI provides strong soft-tissue contrast between FGT and fat, and a more accurate three-dimensional coverage of the entire breast. Evaluation of the amount of FGT is usually done on the T1-weighted sequences with and without fat suppression. According to the American College of Radiology (ACR) guidelines, the amount of FGT should be described in the Breast MRI report using the BI-RADS® four assessment categories of breast composition, which are defined by the visually estimated content of FGT within the breasts.

The amount of fibroglandular tissue (breast density) has been established as an independent risk factor associated with the development of breast cancer, which is three to five times higher in women with mammographically dense breasts than in women with predominantly fatty breasts.

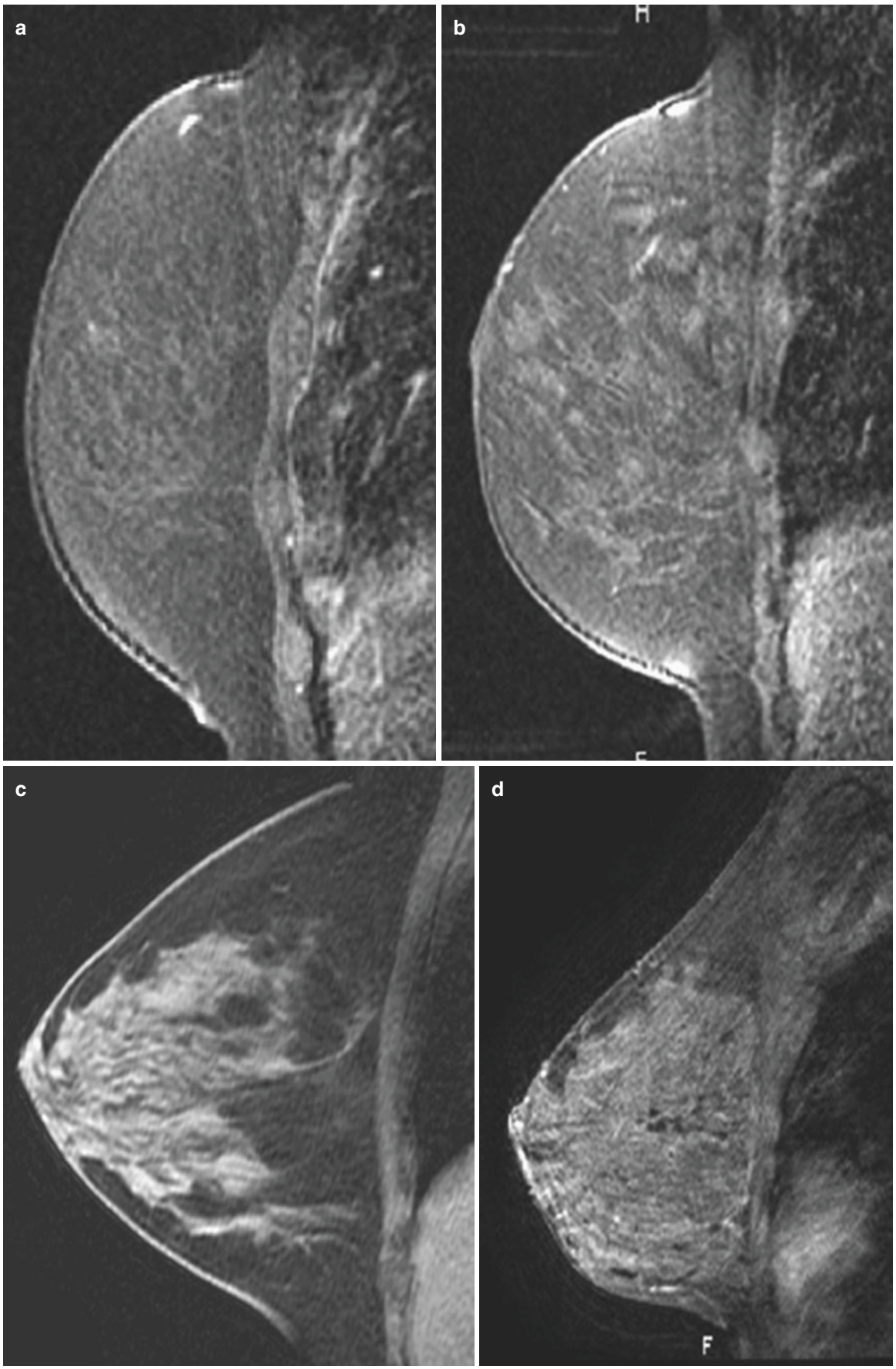

Fig. 1.9, 1.10, 1.11, and 1.12 Selected sagittal T1 post-contrast image (**a**) right breast demonstrates an almost entirely fatty breast (**b**) right breast shows scattered fibroglandular tissue. Selected sagittal T1 pre-contrast image (**c**) right breast demonstrates heterogeneous fibroglandular tissue. Selected sagittal T1 post-contrast image (**d**) left breast demonstrates extreme fibroglandular tissue

1.3 History

Four patients illustrating the range of background parenchymal enhancement seen on breast MRI (Figs. 1.13, 1.14, 1.15, and 1.16).

1.3 Background Parenchymal Enhancement

Teaching Points The 5th edition of the ACR BI-RADS® (Breast Imaging Reporting and Data System) Atlas recommends that the amount of background parenchymal enhancement (BPE) be categorized in the MRI report as "minimal," "mild," "moderate," or "marked" to describe the volume and intensity of the BPE. Research into the association of BPE and breast cancer risk indicates a likely increase in the risk for breast cancer, which may be as high (3–4×) as the more-established risk associated with mammographic dense breasts.

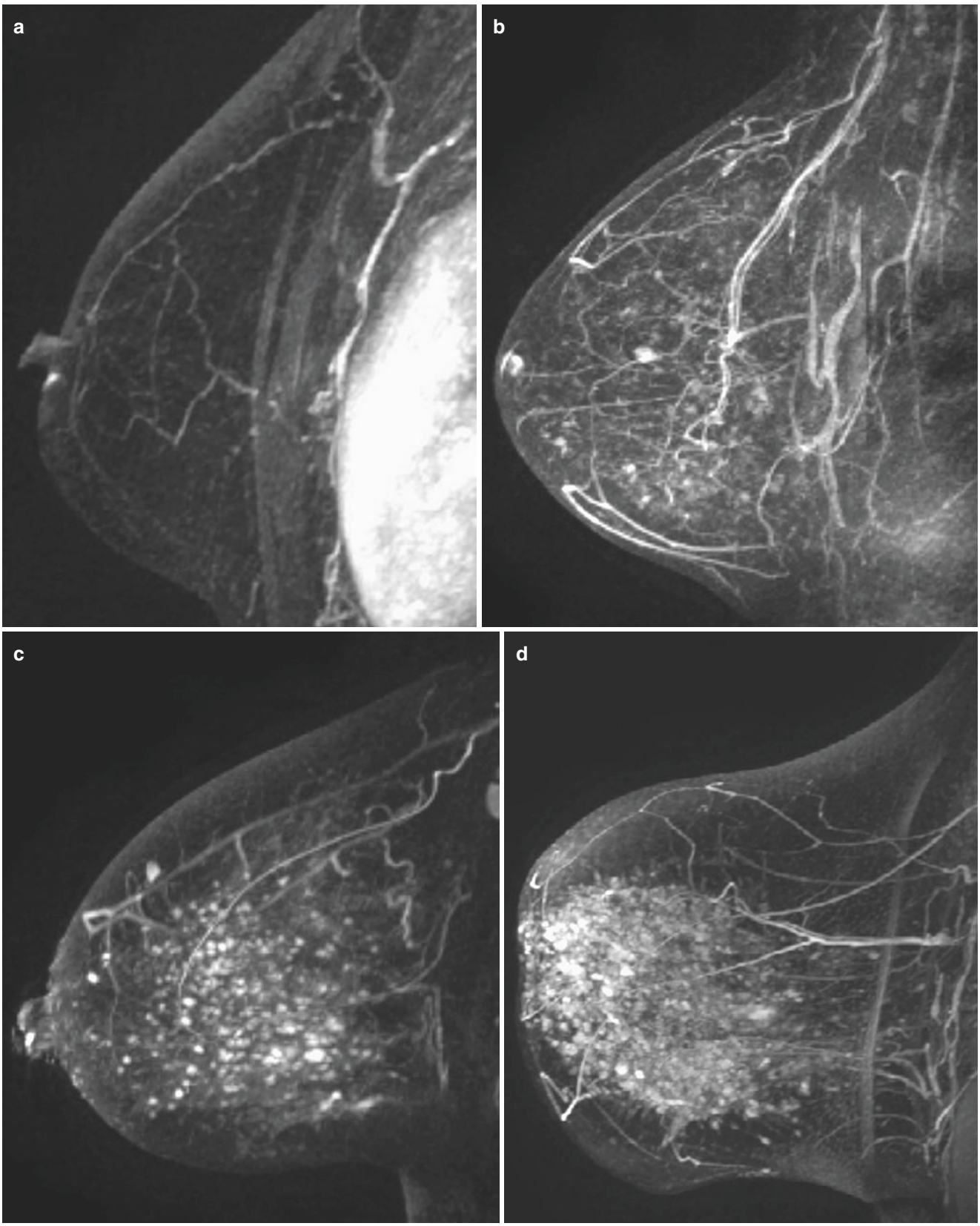

Fig. 1.13, 1.14, 1.15, and 1.16 Sagittal T1 post-contrast 3D maximum intensity projection (MIP) image (**a**) left breast demonstrates minimal background parenchymal enhancement (**b**) right breast demonstrates mild background parenchymal enhancement (**c**) right breast demonstrates moderate background parenchymal enhancement (**d**) right breast demonstrates marked background parenchymal enhancement

1.4 History

67-year-old woman with newly diagnosed right breast cancer (Figs. 1.17, 1.18, 1.19, and 1.20).

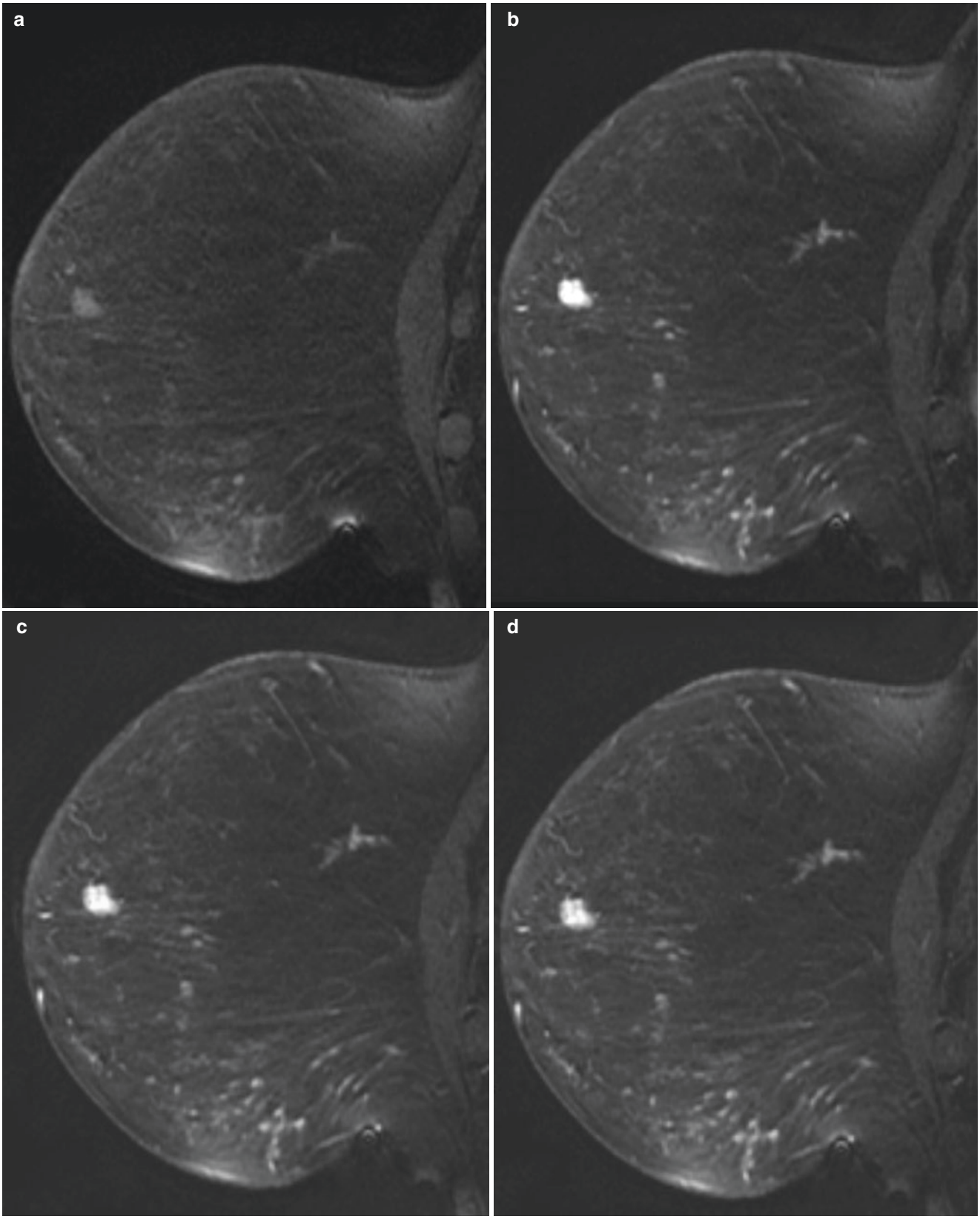

Fig. 1.17 T1-weighted fat-saturated pre-contrast image (**a**) and three consecutive post-contrast images (**b**–**d**) demonstrate 1.5-cm, mildly irregular enhancing mass in the anterior upper right breast

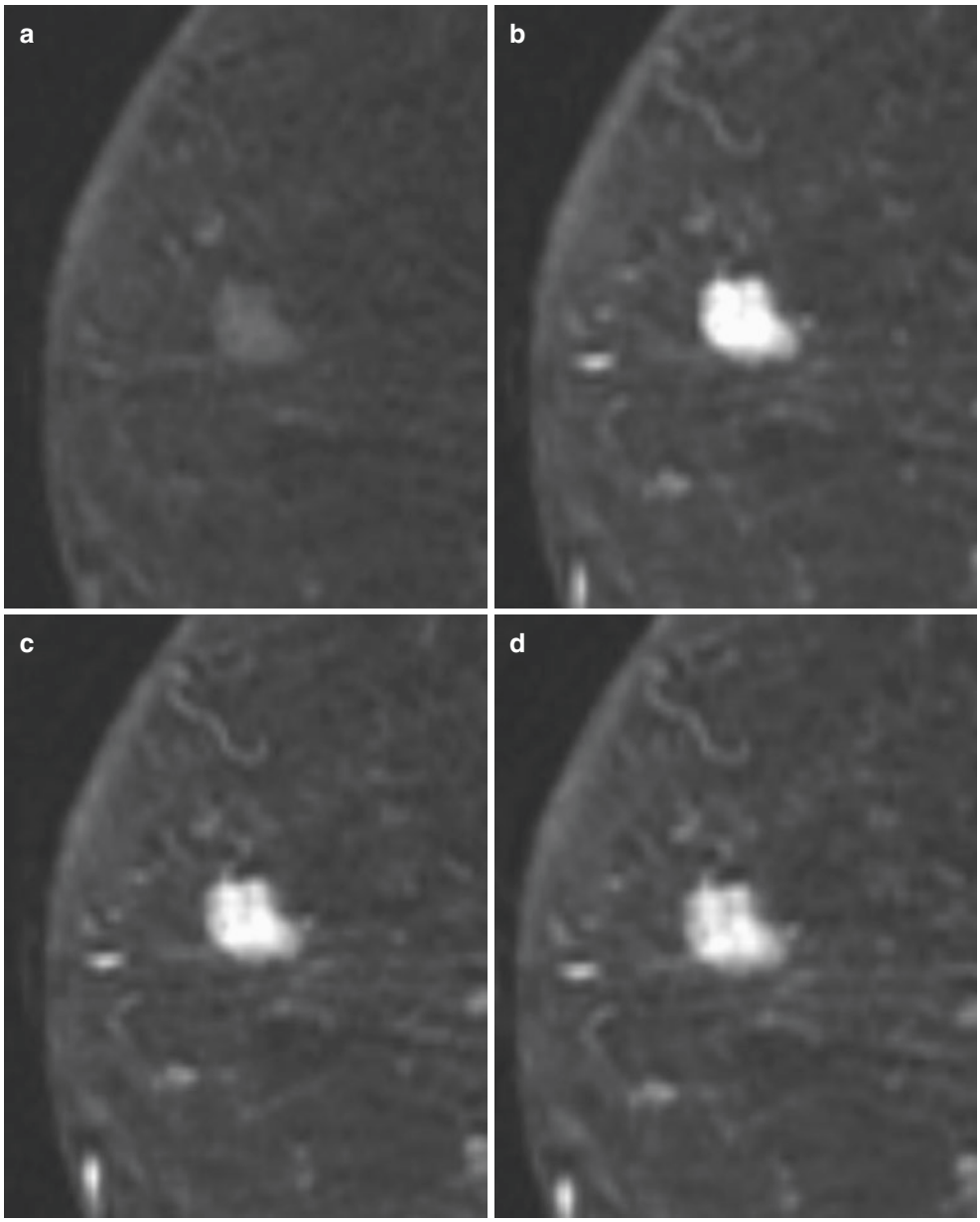

Fig. 1.18 Close-up evaluation of the mass (**a**) demonstrates the highest signal intensity of the mass on the first post-contrast image (**b**), with subsequent decrease in signal intensity on the delayed images (**c**, **d**). (**e**) Computer-generated curve of the signal intensity time course of the mass. (**f**) The pattern of washout is color-coded *red*

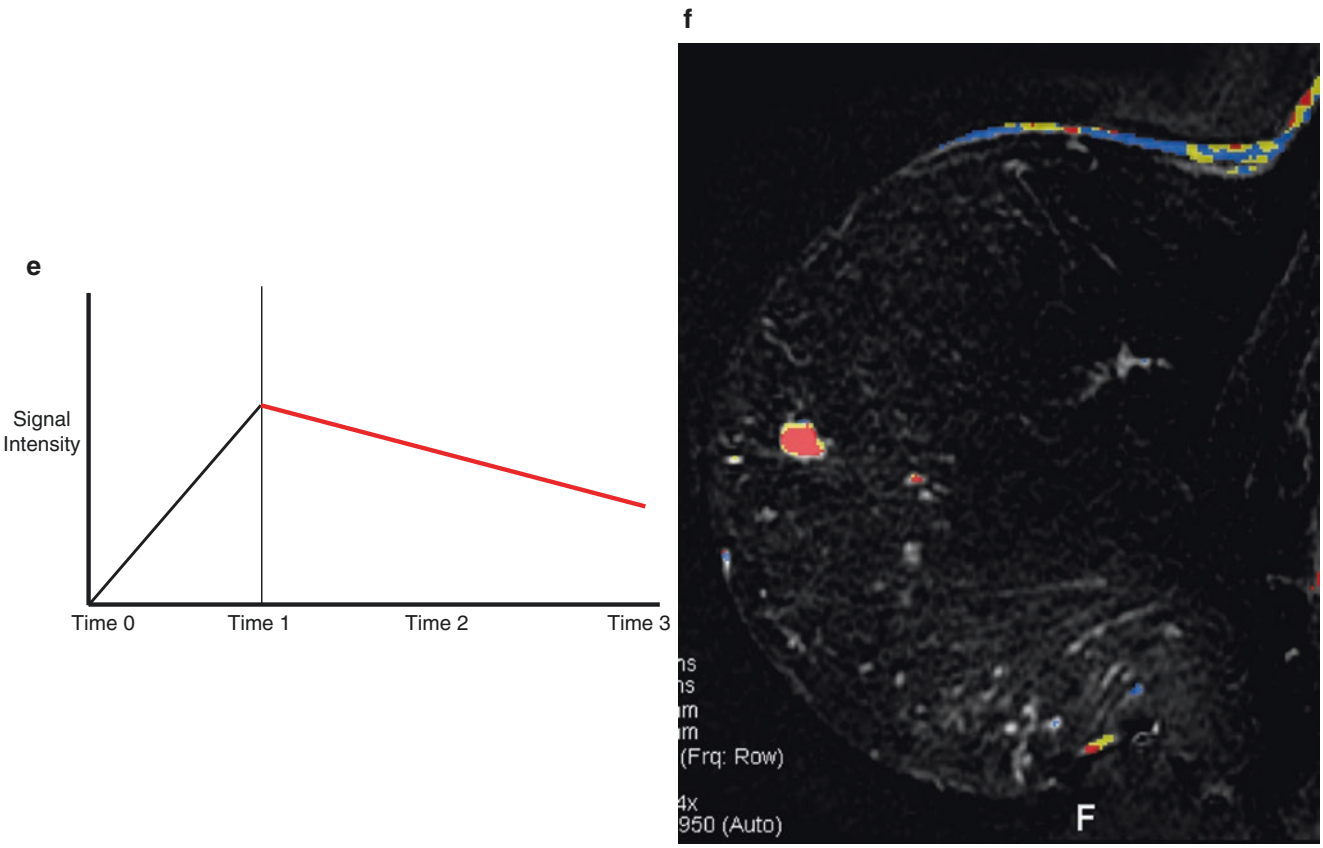

Fig. 1.18 (continued)

1.4 Computer-Aided Detection

Teaching Points In addition to the morphology assessment, the enhancement kinetics pattern can be analyzed by obtaining at least three post-contrast images. Typical breast tumor demonstrates intense and rapid uptake of contrast owing to increased angiogenesis and washout of contrast owing to increased capillary permeability and shunting. A study by Kuhl et al. (2005) showed kinetic analysis, specifically the signal intensity time course, to be specific for malignancy.

Three types of signal intensity time course (Fig. 1.19) can be identified:

- Type 1: Progressive
- Type 2: Plateau
- Type 3: Washout

When mixed enhancement is present, the worst curve is reported (Fig. 1.20).

Of note, the morphology assessment should outweigh the kinetics analysis in clinical decision making. Morphology has higher specificity for malignancy.

Image Findings

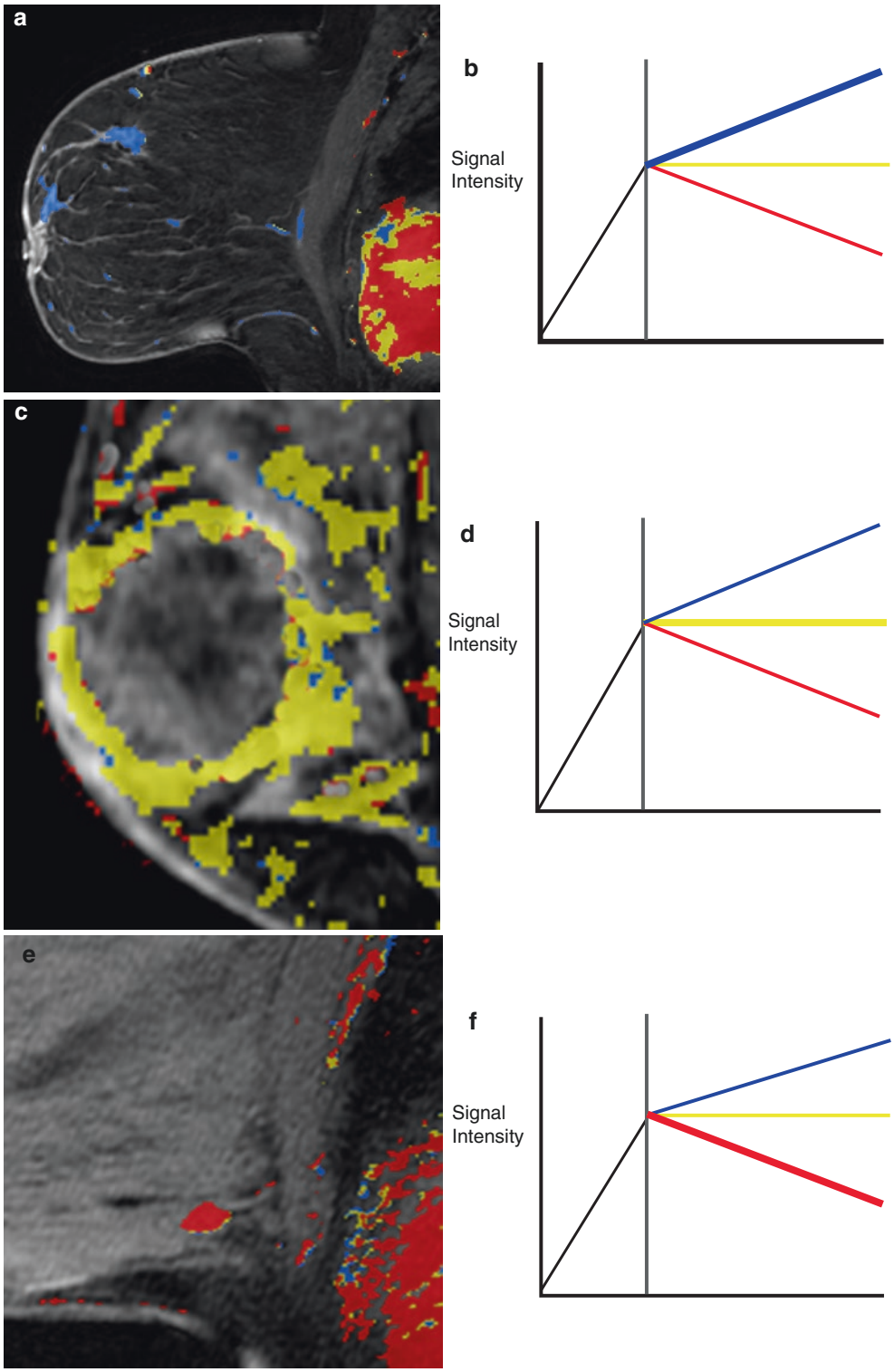

Fig. 1.19 Examples of MRI enhancement patterns. (**a**, **b**) Type I curve: progressive enhancement pattern. Continuous increase in signal intensity on subsequent post-contrast images. Color-coded blue. (**c**, **d**) Type II curve: plateau pattern. Delayed signal intensity is within 10 % of the initial post-contrast signal intensity. Color-coded *yellow*. (**e**, **f**) Type III curve: washout pattern. Relatively rapid uptake and high initial signal intensity followed by decreased enhancement on delayed phases. Color-coded *red*

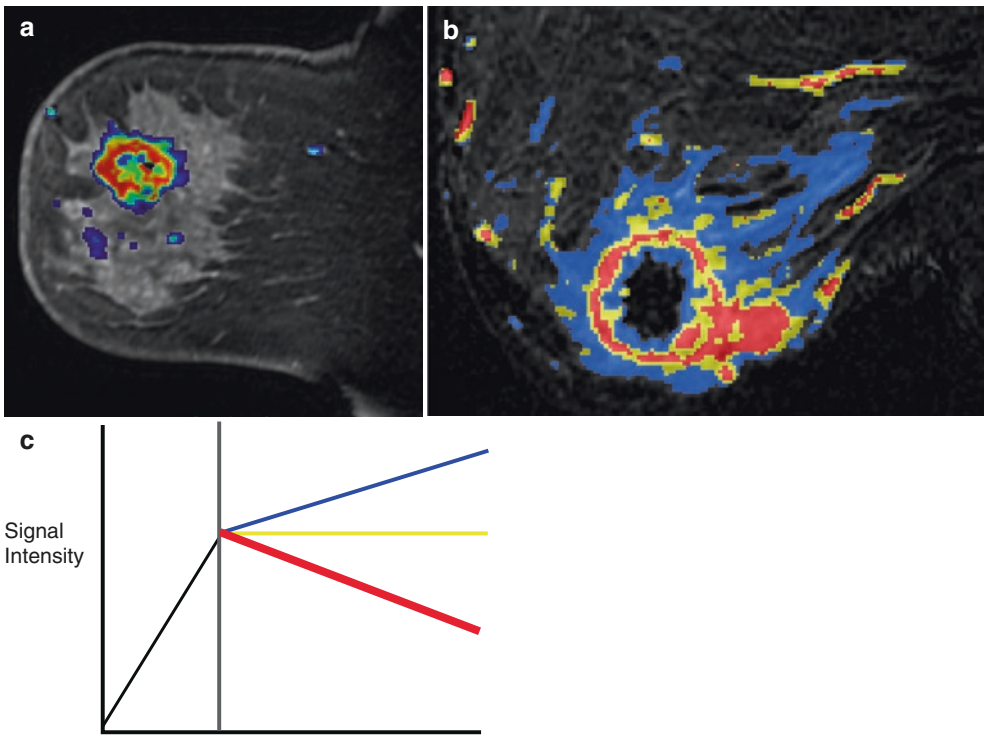

Fig. 1.20 (**a**, **b**) Two examples of irregular masses demonstrating mixed kinetics curves. (**c**) A type III washout curve is reported as the most suspicious enhancement pattern shown by the mass

1.5 History

31-year-old with recent diagnosis of pregnancy-associated breast cancer (Fig. 1.21).

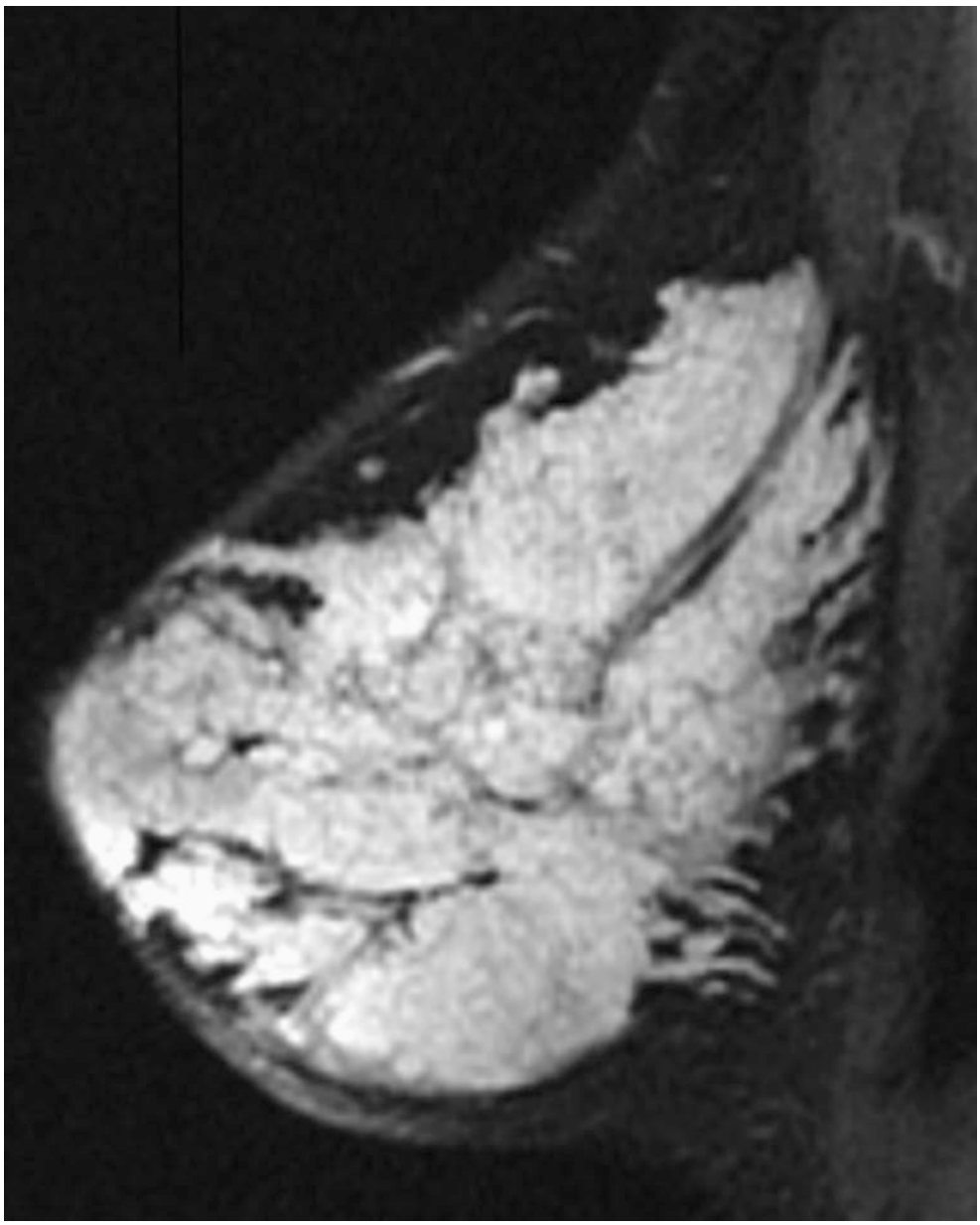

Fig. 1.21 Lactational changes: sagittal T2-weighted FSE sequence of the contralateral breast from a known cancer demonstrates diffuse high signal intensity involving all the fibroglandular tissue

1.5 T2-Weighted Sequence

Teaching Points In fat-saturated T2-weighted fast spin-echo (FSE) sequences (spectrally selective radiofrequency [RF] pulses), RF pulses are tailored to excite protons in a particular resonant frequency range. This range can be narrowed so that the RF pulse affects only water or only fat—unlike STIR (*below*), in which all magnetization is inverted. This technique is more effective at higher field strengths, in which these resonant frequencies are more separated. Good magnet (B0) homogeneity is required to make this frequency-selective excitation effective. Frequency-selective excitation is more effective over smaller fields of view.

The short inversion time inversion recovery (STIR) sequence is performed with short inversion times to eliminate signal from adipose tissue. The advantage of STIR is due to an increase in the relative signal intensity of fluid as a result of the additive T1 and T2 contrast effect. STIR images have greater contrast between fluid and other tissues than fat-suppressed T2-weighted images. The disadvantage of STIR sequences is that the images have relatively poor signal-to-noise ratios. STIR is often preferred when spectrally selective techniques may not be ideal (large fields of view, lower field strengths, areas of high magnetic susceptibility).

Adequate fat suppression is important in either sequence to differentiate true cystic from solid lesions. In addition, T2-weighted signal hyperintensity in the same portion of the lesion that appears enhanced on T1-weighted images is highly suggestive of benign entities such as these examples (Fig. 1.22):

- Fibrocystic disease, cysts, fibroadenoma
- Lymph nodes
- Pleural effusion
- Debris in ducts, blood vessels
- Postsurgical seroma or abscess
- Implants, saline and silicone
- Lactational changes

T2 hyperintensity can be associated with malignancy, however, as in these malignancy-associated T2-hyperintense findings (Fig. 1.23):

- Mucinous carcinoma
- Central necrosis, especially triple negative tumors
- Mucinous and papillary cancers
- Edema, skin thickening, necrotic lymph nodes

Image Findings

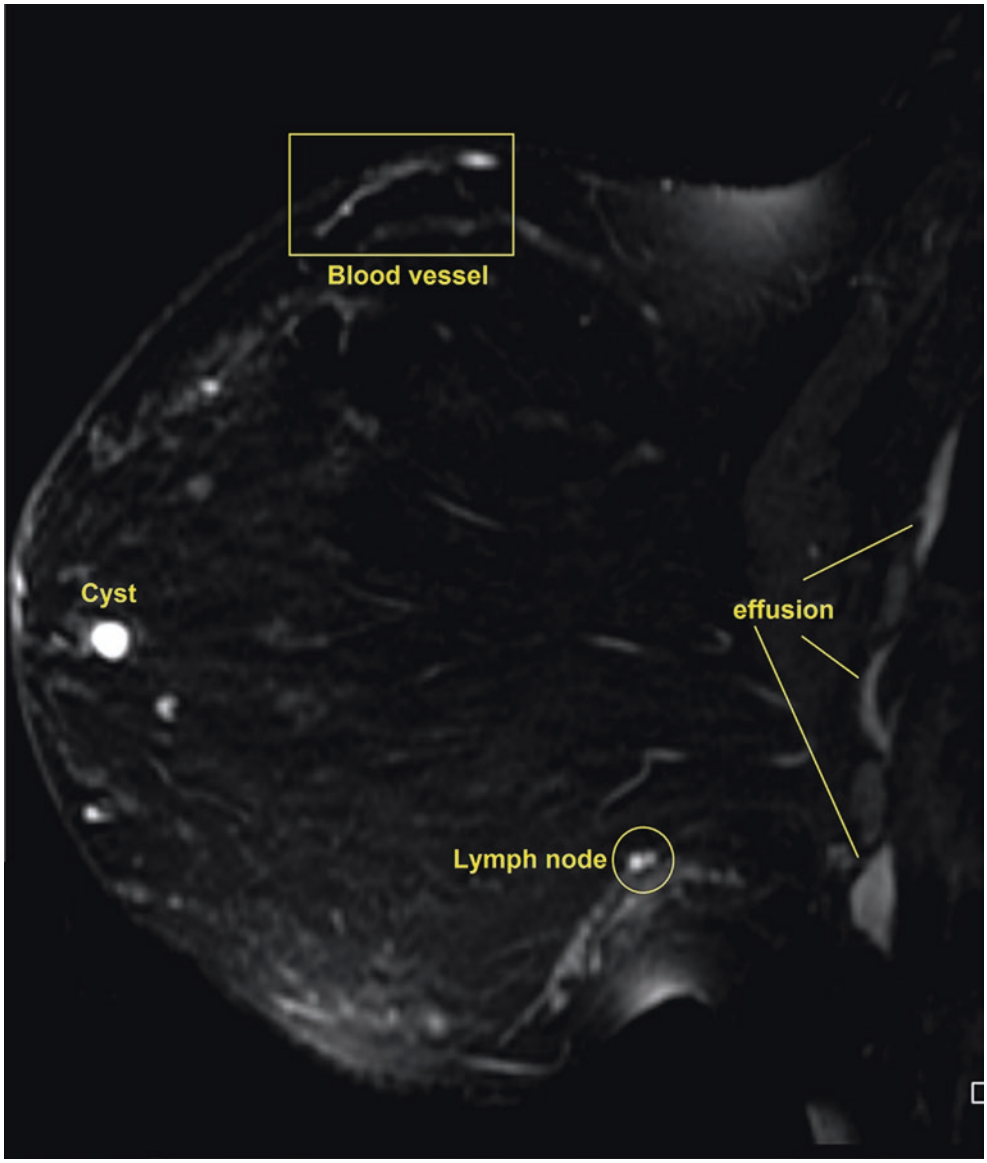

Fig. 1.22 Examples of some benign entities that are T2-hyperintense

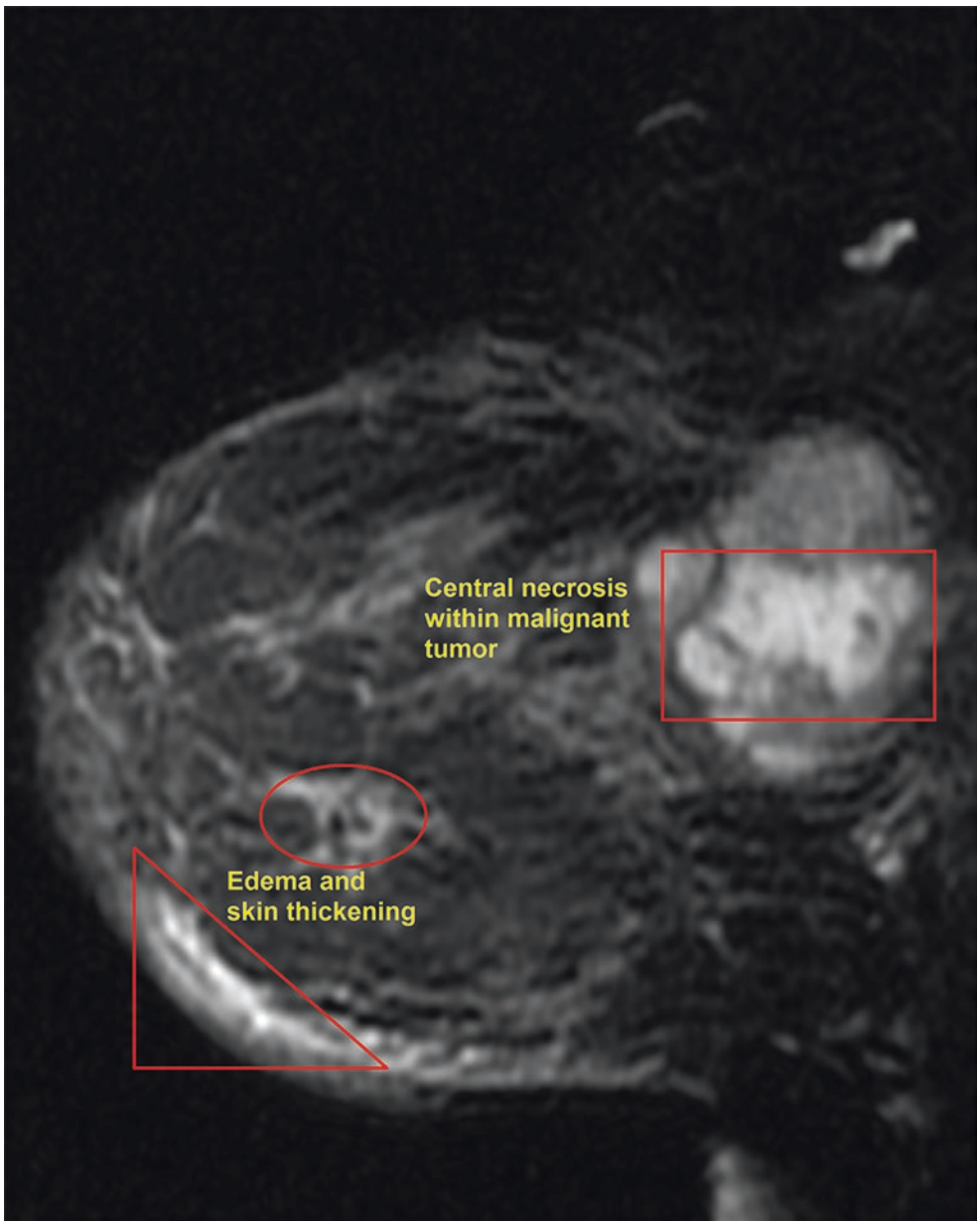

Fig. 1.23 T2 hyperintensity can be associated with malignancy. Examples of some malignancy-associated T2-hyperintense findings

1.6 History

49-year-old with newly diagnosed left breast cancer.

1.6 3D Maximum Intensity Projection

Teaching Points A three-dimensional (3D) maximum intensity projection (MIP) image can be constructed from the post-contrast images. The generalized view of the whole breast enables better delineation of locally advanced disease including multifocal or multicentric disease and tumors that involve the chest wall or skin, as illustrated in Fig. 1.24.

In addition, recent studies suggest a potential role for 3D MIP images in an abridged breast MRI protocol as a time-efficient and cost-effective screening tool for detecting breast cancer.

Image Findings

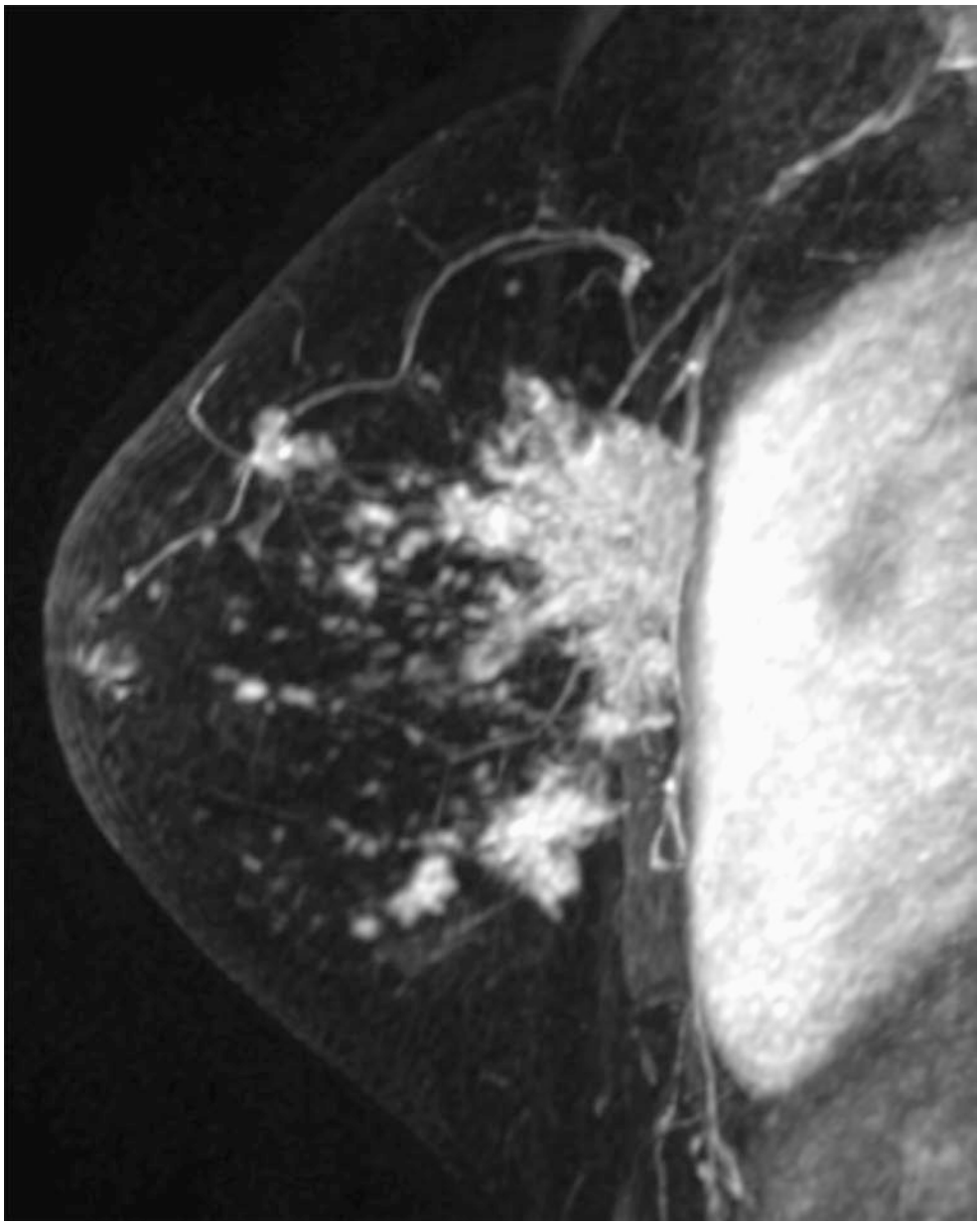

Fig. 1.24 Post-contrast 3D maximum intensity projection (MIP) demonstrates irregular masses involving the upper and lower left breast (*arrows*) and the chest wall, consistent with multicentric disease

1.7 History

67-year-old woman with newly diagnosed right breast malignancy (Figs. 1.25 and 1.26).

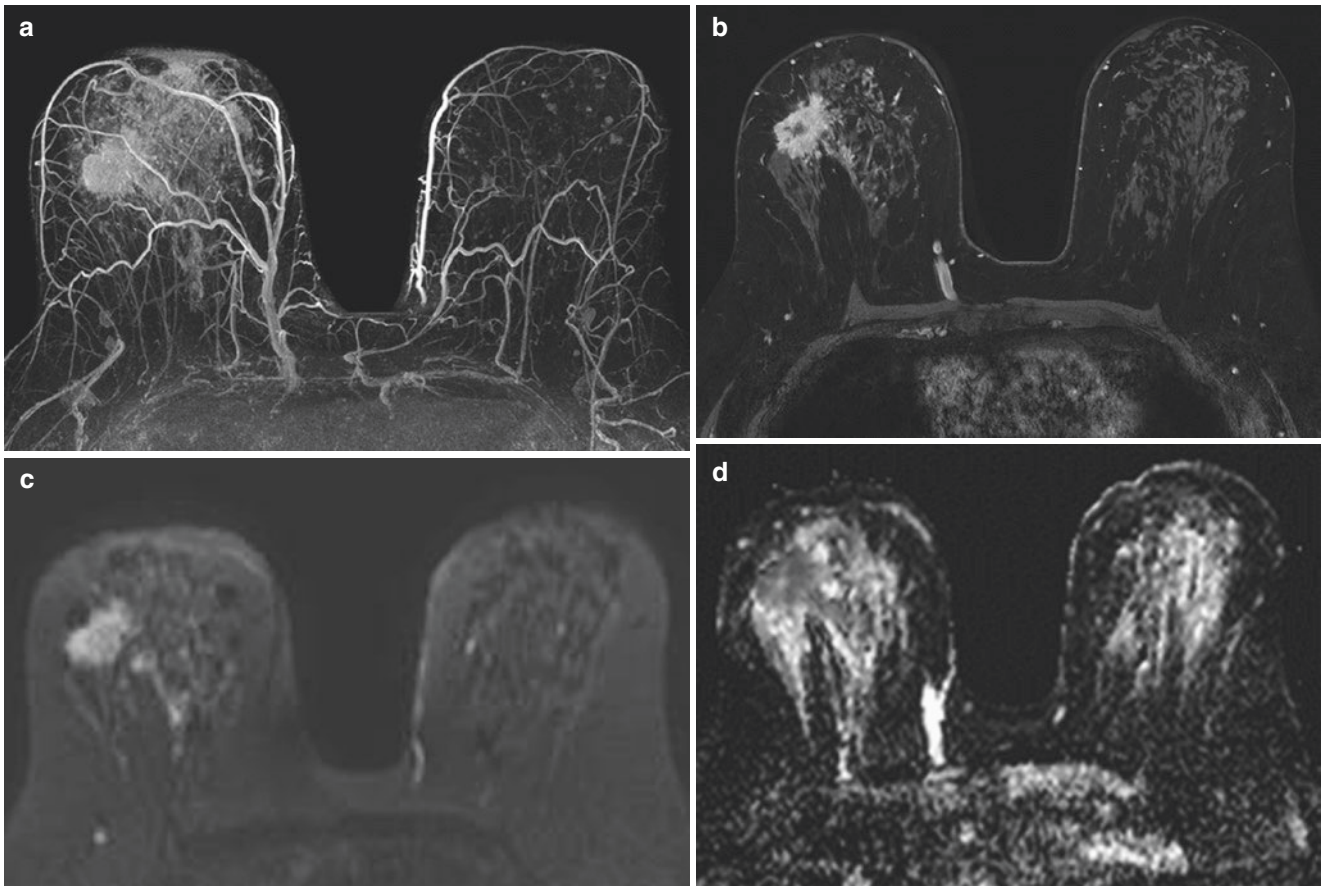

Fig. 1.25 (**a**) T1 post-contrast axial 3D MIP. (**b**) Selected axial T1 fat-saturated post-contrast image. (**c**) Diffusion-weighted imaging (DWI) ($b = 800$). (**d**) Apparent diffusion coefficient (ADC) map

1.7 Diffusion-Weighted Imaging

Teaching Points Diffusion-weighted imaging (DWI), an MRI technique that was originally developed for liver imaging, found its earliest widespread and accepted application in neuroradiology, beginning in 1985. It has been further applied to other areas of imaging, and the first diffusion-weighted breast images were published in 1997.

The physical basis of DWI is the relative restriction of the movement of water molecules in tissue. For example, the motion of water molecules in tissue can be restricted by intact cell membranes and increased cell density, so tissue with increased cellularity and intact cell membranes, such as breast cancer, will have more restricted diffusion than normal breast tissue or benign tumors with lower cellularity. Within breast cancers, cancers with relatively decreased cellularity, such as a mucinous carcinoma, will have less-restricted diffusion than other cancers.

Areas of restricted diffusion will appear bright on DWI, but because of the acquisition technique, the brightness may be due to the artifact of "T2 shine-through," so diffusion is more accurately described using information from images acquired at multiple b-values (a factor used to describe the strength and timing of the gradients used in the diffusion-weighted sequence). It is calculated and quantified by the apparent diffusion coefficient (ADC), measured in mm^2/s (units of area per unit of time). The result is visually displayed in an "ADC map" in which lower ADC values have darker pixels. The ADC of a region of interest is inversely proportional to the cellularity of the tissue. A lower ADC will correspond with higher tissue cellularity. Therefore, as in this case, the enhancing cancer is bright on the diffusion-weighted image and dark on the ADC map.

ADC values of tumors are dependent on technical factors including the type of scanner and chosen b-values, patient factors such as the ADC of the normal background breast parenchyma, and the operator's method of defining regions of interest. This variation has hindered the establishment of threshold values for what constitutes an ADC value consistent with malignancy. One meta-analysis noted a range of recommended maximum cutoff values for malignancy from 0.9 to 1.76×10^{-3} mm^2/s. Establishing standard protocols and cutoff values will aid the acceptance and use of DWI in routine clinical breast imaging. Awareness of false positive results (such as atypical ductal hyperplasia and intraductal papillomas) and false negative results (such as mucinous carcinoma and some intraductal carcinomas) will also be important if DWI is incorporated into a standard breast MRI protocol.

DWI has mostly been studied as a technique to improve upon the specificity of contrast-enhanced breast MRI in cancer detection, tumor characterization, and pre-therapy and post-therapy evaluation. There is, however, increasing study of its ability to support the use of unenhanced breast MRI in the screening setting, where the potential risks and costs of gadolinium administration are magnified in breast MRI screening of high-risk women.

Image Findings

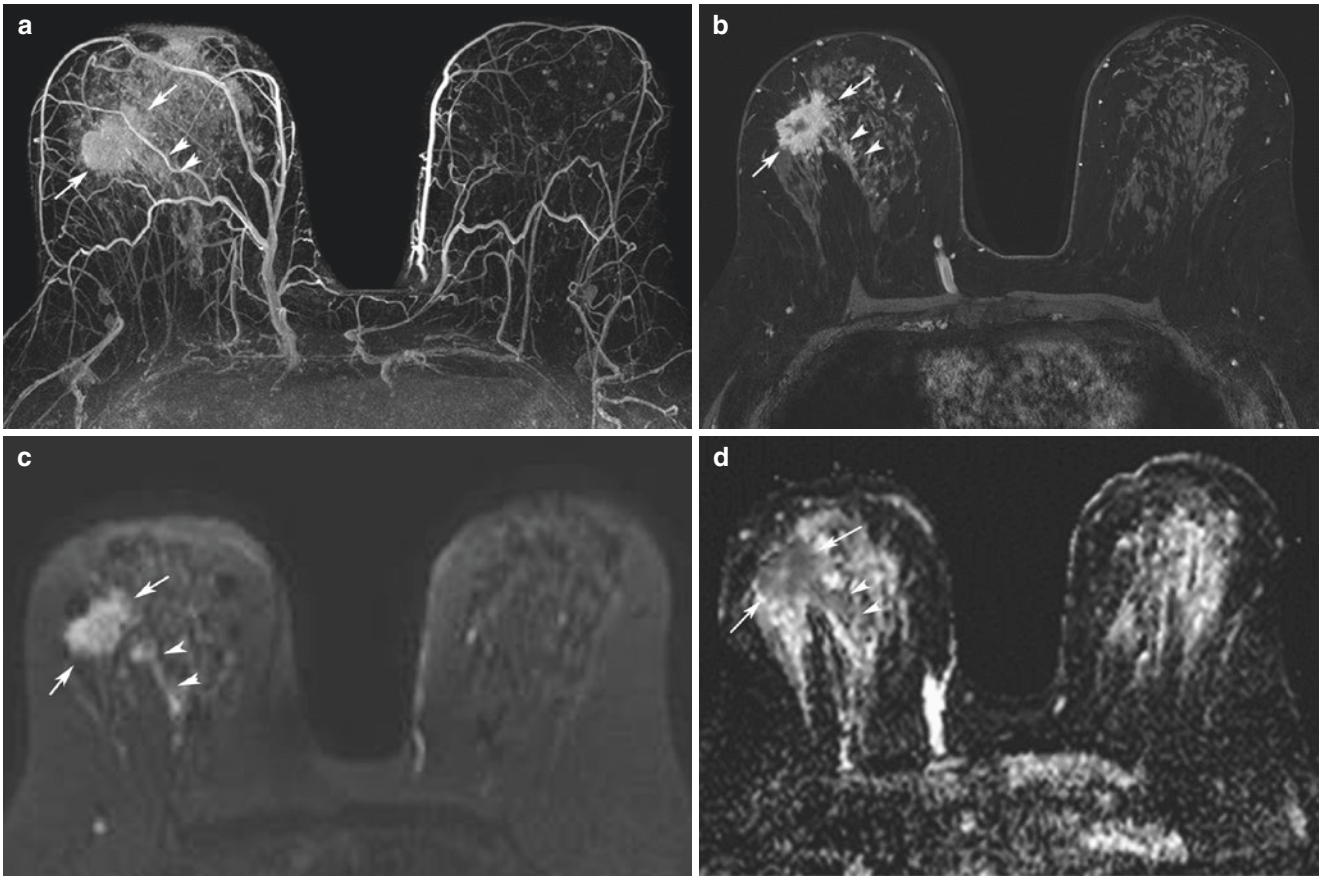

Fig. 1.26 Diffusion weighted imaging. (**a**) The 3D MIP image shows a mass (*arrows*) in the outer right breast with an associated linear non-mass enhancement (NME) extending posteriorly (*arrowheads*). (**b**) These are better delineated on the selected T1 post-contrast image. (**c**) DWI ($b = 800$) demonstrates high signal within the mass and the NME. (**d**) The low ADC values (ADC $= 0.9 \times 10^{-3}$ mm^2/s) are in the invasive malignancy range. Additional biopsies confirmed multicentric invasive and in situ disease

Suggested Reading

ACR BI-RADS®. Atlas/Breast MRI/reporting system. 5th ed. Reston: American College of Radiology (ACR); 2013.

Brandão AC, Lehman CD, Partridge SC. Breast magnetic resonance imaging: diffusion-weighted imaging. Magn Reson Imaging Clin N Am. 2013;21:321–36.

Castillo M. History and evolution of brain tumor imaging: insights through radiology. Radiology. 2014;273:S111–25.

Chen X, Li W, Zhang Y, Wu Q, Guo Y, Bai Z. Meta-analysis of quantitative diffusion-weighted MR imaging in the differential diagnosis of breast lesions. BMC Cancer. 2010;10:693.

Delfaut EM, Beltran J, Johnson G, Rousseau J, Marchandise X, Cotten A. Fat suppression in MR imaging: techniques and pitfalls. Radiographics. 1999;19:373–82.

Englander SA, Ulug AM, Brem R, Glickson JD, van Zijl PC. Diffusion imaging of human breast. NMR Biomed. 1997;10:348–52.

Giess CS, Yeh ED, Raza S, Birdwell RL. Background parenchymal enhancement at breast MR imaging: normal patterns, diagnostic challenges, and potential for false-positive and false-negative interpretation. Radiographics. 2014;34:234–47.

Hatakenaka M, Soeda H, Yabuuchi H, Matsuo Y, Kamitani T, Oda Y, et al. Apparent diffusion coefficients of breast tumors: clinical application. Magn Reson Med Sci. 2008;7:23–9.

Hendrick RE. High-quality breast MRI. Radiol Clin North Am. 2014;52:547–62.

King V, Brooks JD, Bernstein JL, Reiner AS, Pike MC, Morris EA. Background parenchymal enhancement at breast MR imaging and breast cancer risk. Radiology. 2011;260:50–60.

Kuhl CK, Schild HH, Morakkabati N. Dynamic bilateral contrast-enhanced MR imaging of the breast: trade-off between spatial and temporal resolution. Radiology. 2005;236:789–800.

Kuhl CK, Schrading S, Strobel K, Schild HH, Hilgers RD, Bieling HB. Abbreviated breast magnetic resonance imaging (MRI): first postcontrast subtracted images and maximum-intensity projection-a novel approach to breast cancer screening with MRI. J Clin Oncol. 2014;32:2304–10.

Macura KJ, Ouwerkerk R, Jacobs M. Patterns of enhancement on breast MR images: interpretation and imaging pitfalls. Radiographics. 2006;26:1719–34.

Mango VL, Morris EA, David Dershaw D, Abramson A, Fry C, Moskowitz CS, et al. Abbreviated protocol for breast MRI: are multiple sequences needed for cancer detection? Eur J Radiol. 2015;84:65–70.

Morris EA, Comstock CE, Lee CH, et al. ACR BI-RADS® Magnetic Resonance Imaging. In: ACR BI-RADS® Atlas, breast imaging reporting and data system. Reston: American College of Radiology; 2013.

Nie K, Chen JH, Chan S, Chau MK, Yu HJ, Bahri S, et al. Development of a quantitative method for analysis of breast density based on three-dimensional breast MRI. Med Phys. 2008;35:5253–62.

Palestrant S, Comstock CE, Moy L. Approach to breast magnetic resonance imaging interpretation. Radiol Clin North Am. 2014;52:563–83.

Parsian S, Rahbar H, Allison KH, Demartini WB, Olson ML, Lehman CD, Partridge SC. Nonmalignant breast lesions: ADCs of benign and high-risk subtypes assessed as false-positive at dynamic enhanced MR imaging. Radiology. 2012;265:696–706.

Partridge SC, DeMartini WB, Kurland BF, Eby PR, White SW, Lehman CD. Quantitative diffusion-weighted imaging as an adjunct to conventional breast MRI for improved positive predictive value. Am J Roentgenol. 2009;193:1716–22.

Partridge SC, McDonald ES. Diffusion weighted magnetic resonance imaging of the breast: protocol optimization, interpretation, and clinical applications. Magn Reson Imaging Clin N Am. 2013;21:601–24.

Pike MC, Pearce CL. Mammographic density, MRI background parenchymal enhancement and breast cancer risk. Ann Oncol. 2013;24:viii37–41.

Raza S, Birdwell RL, Ritner J, Gombos EC, Yeh ED, Odulate AS, et al. Specialty imaging. Breast MRI: a comprehensive imaging guide. Salt Lake City: Amirsys; 2010.

Saftlas AF, Hoover RN, Brinton LA, Szklo M, Olson DR, Salane M, Wolfe JN. Mammographic densities and risk of breast cancer. Cancer. 1991;67:2833–8.

Trimboli RM, Verardi N, Cartia F, Carbonaro LA, Sardanelli F. Breast cancer detection using double reading of unenhanced MRI including T1-weighted, T2-weighted STIR, and diffusion-weighted imaging: a proof of concept study. AJR Am J Roentgenol. 2014;203:674–81.

Woodhams R, Matsunaga K, Kan S, Hata H, Ozaki M, Iwabuchi K, et al. ADC mapping of benign and malignant breast tumors. Magn Reson Med Sci. 2005;4:35–42.

Benign Findings

2

Lauren Friedlander, Victoria Mango,
Rend Al-Khalili, and Richard Ha

L. Friedlander, MD
Director of Breast and Body Imaging Fellowship,
Division of Breast Imaging, Assistant Professor of Radiology,
Columbia University Medical Center, New York, NY, USA
e-mail: lf2386@columbia.edu;

V. Mango, MD
Director of Breast and Body Imaging Fellowship,
Breast Imaging Service, Memorial Sloan-Kettering Cancer Center,
Assistant Professor of Radiology, Weill Cornell Medical College,
New York, NY, USA
e-mail: vlm2125@columbia.edu

R. Al-Khalili, MD
Staff Radiologist, Washington Radiology Associates,
Fairfax, Virginia, VR, USA
e-mail: rendkhalili@gmail.com

R. Ha, MD (✉)
Director of Education and Research, Division of Breast Imaging,
Assistant Professor of Radiology, Columbia University Medical
Center, New York, NY, USA
e-mail: rh2616@cumc.columbia.edu

R. Ha et al. (eds.), Breast MRI Teaching Atlas, DOI 10.1007/978-1-4939-6409-3_2

2.1 History

A 39-year-old woman undergoing high-risk screening breast MRI (Figs. 2.1 and 2.2).

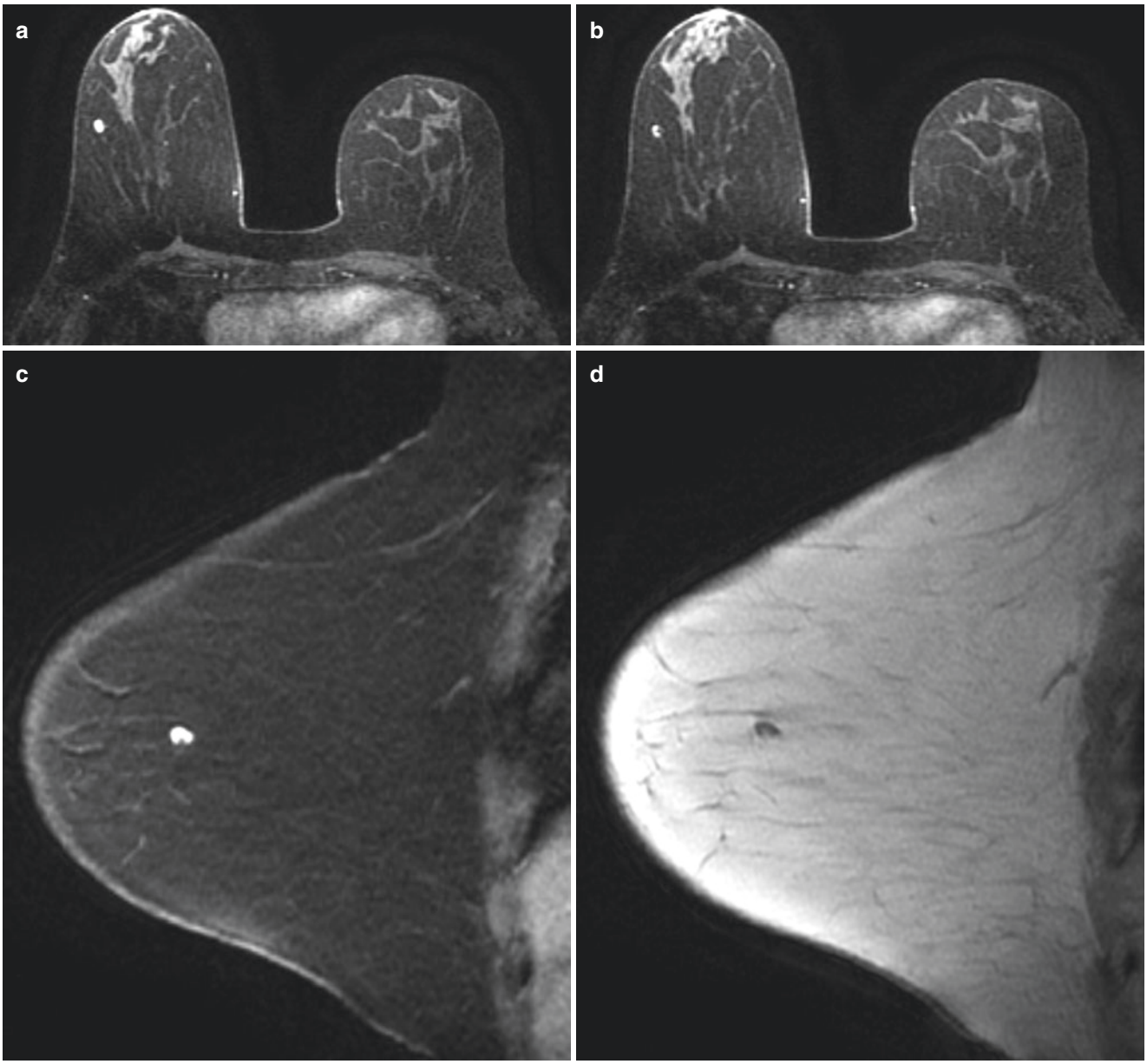

Fig. 2.1 (**a**, **b**) Sequential axial T1-weighted fat-suppressed post-contrast images of both breasts. Sagittal T1-weighted fat-suppressed post-contrast image (**c**), sagittal T1-weighted image (**d**), sagittal T2-weighted fat-suppressed image (**e**), and sagittal T1-weighted fat-suppressed image (**f**) with computer-aided detection (CAD) enhancement kinetics color overlay, all of the right breast

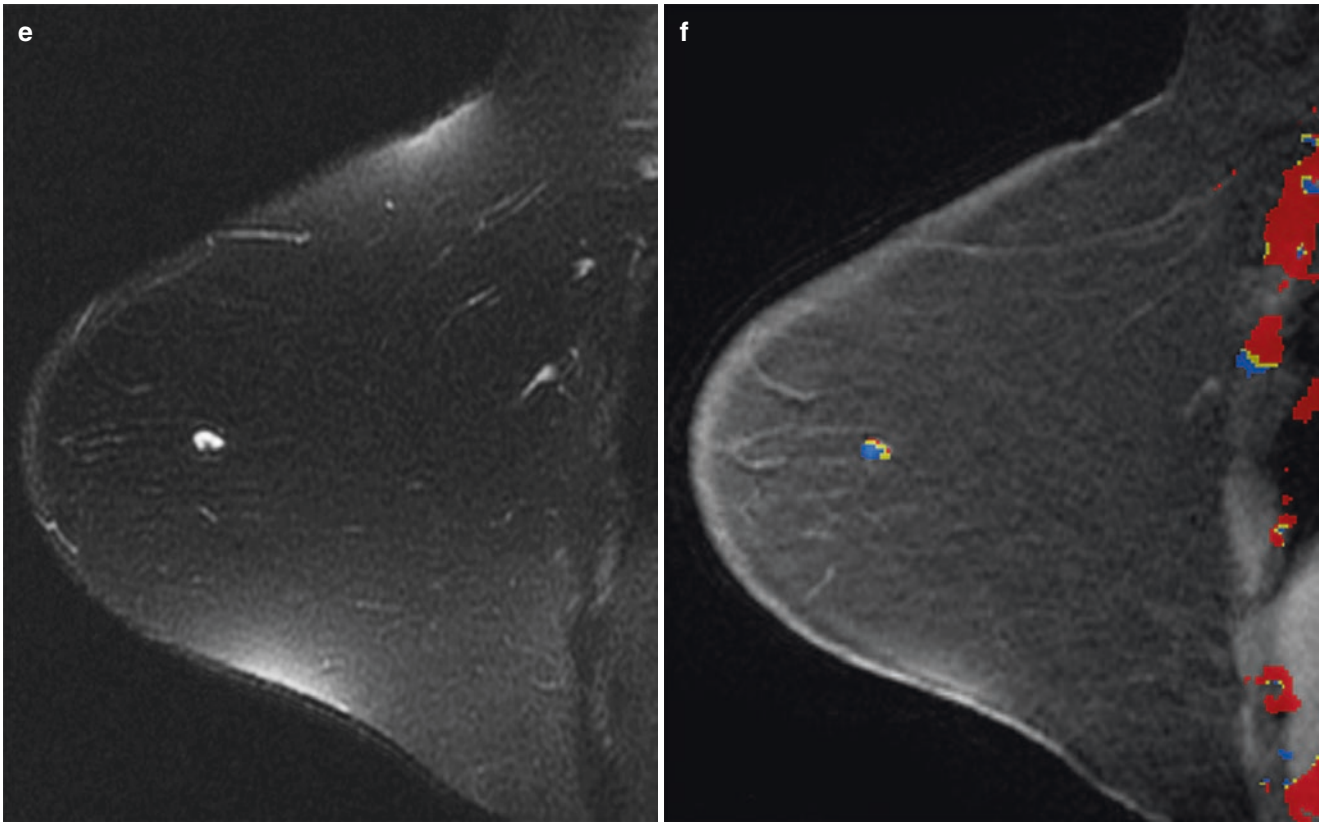

Fig. 2.1 (continued)

2.1 Intramammary Lymph Node 1

Teaching Points Intramammary lymph nodes are separate from axillary lymph nodes and are completely surrounded by breast tissue, typically in the upper outer quadrant. Approximately 5 % of patients undergoing mammography and up to 28 % of breast specimens will exhibit these lymph nodes. Characteristic features of a normal intramammary node include a fatty hilum, diameter less than 1 cm, and circumscribed margins. An intramammary lymph node may become abnormal and lose its hilum or enlarge secondary to hyperplasia, metastatic disease, or inflammation. A benign intramammary lymph node demonstrates reniform morphology with a fatty hilum on MRI. The cortex will be T1 hypointense and T2 hyperintense with rapid, homogeneous enhancement; a type III washout kinetic pattern can be seen, as demonstrated in this case.

Image Findings

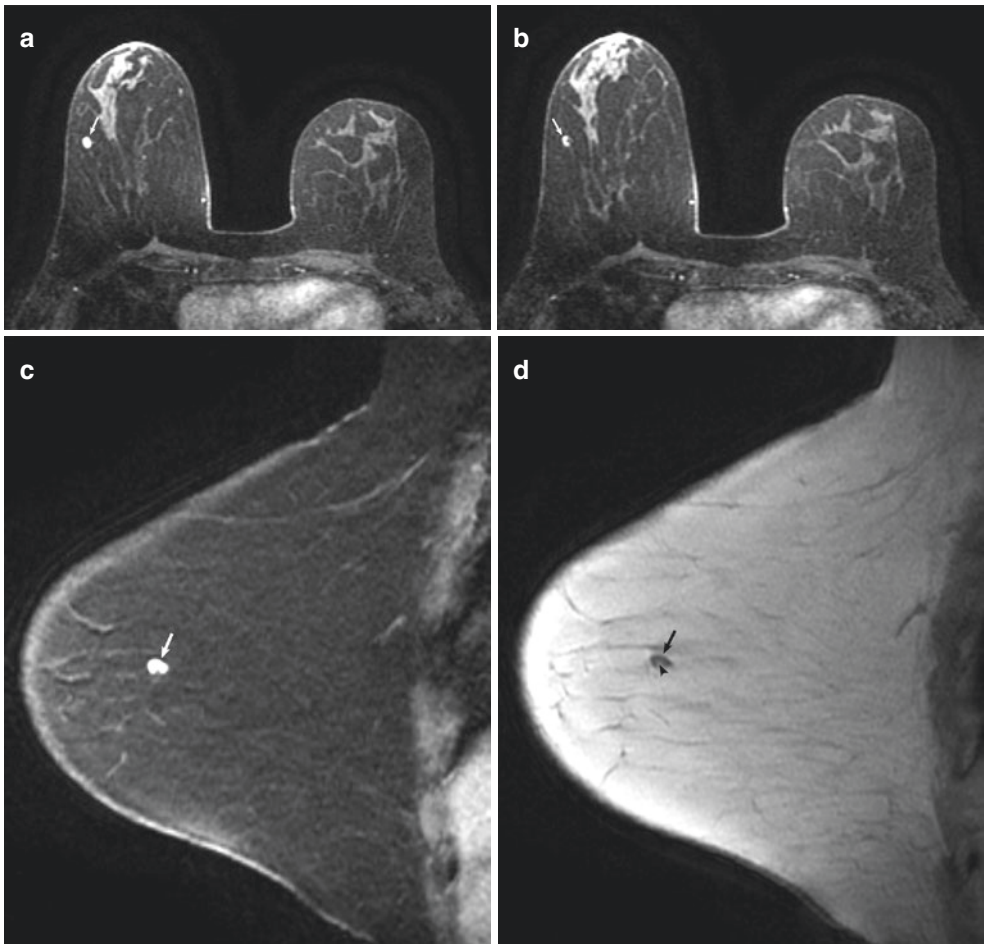

Fig. 2.2 Intramammary lymph node. (**a**, **b**) Sequential axial T1-weighted fat-suppressed post-contrast images demonstrate a homogeneously enhancing mass (*arrows*) in the outer right breast, which appears oval on one slice and reniform on the next. The reniform appearance is characteristic of a lymph node. (**c**) A sagittal T1-weighted fat-suppressed post-contrast image through the mass highlights its homogeneous enhancement and reniform shape (*arrow*). The lymph node (*arrows*) has low signal on the T1-weighted image (**d**) and high signal on the T2-weighted fat-suppressed image (**e**). Its central notch (*arrowheads*) is isointense to fat on both sequences. (**f**) CAD enhancement kinetics analysis demonstrates a color-coded mixed progressive (*yellow*) and washout (*red*) enhancement pattern

Fig. 2.2 (continued)

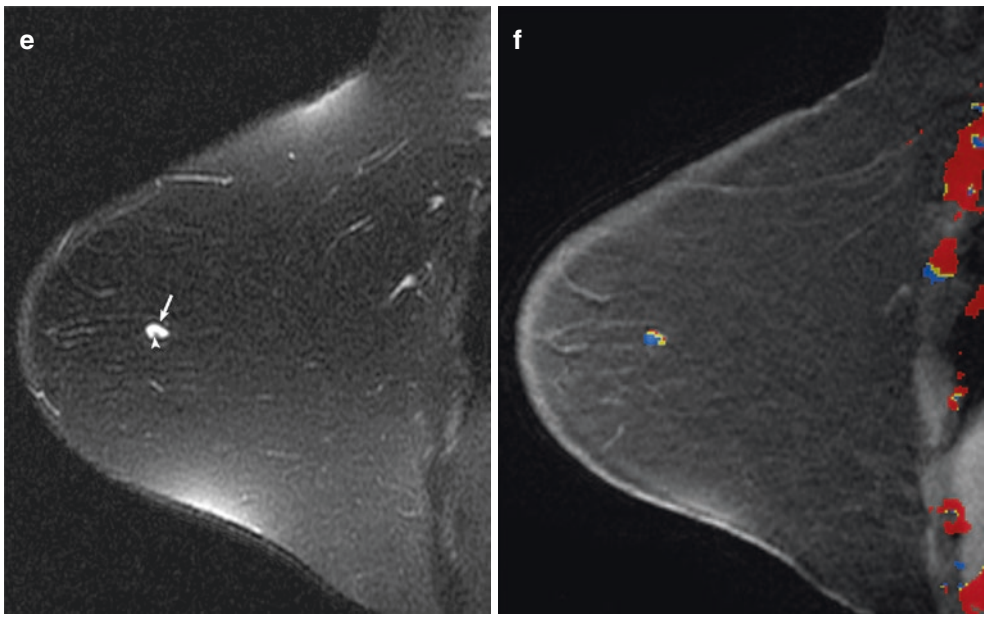

2.2 History

34-year-old women high-risk screening MRI (Fig. 2.2).

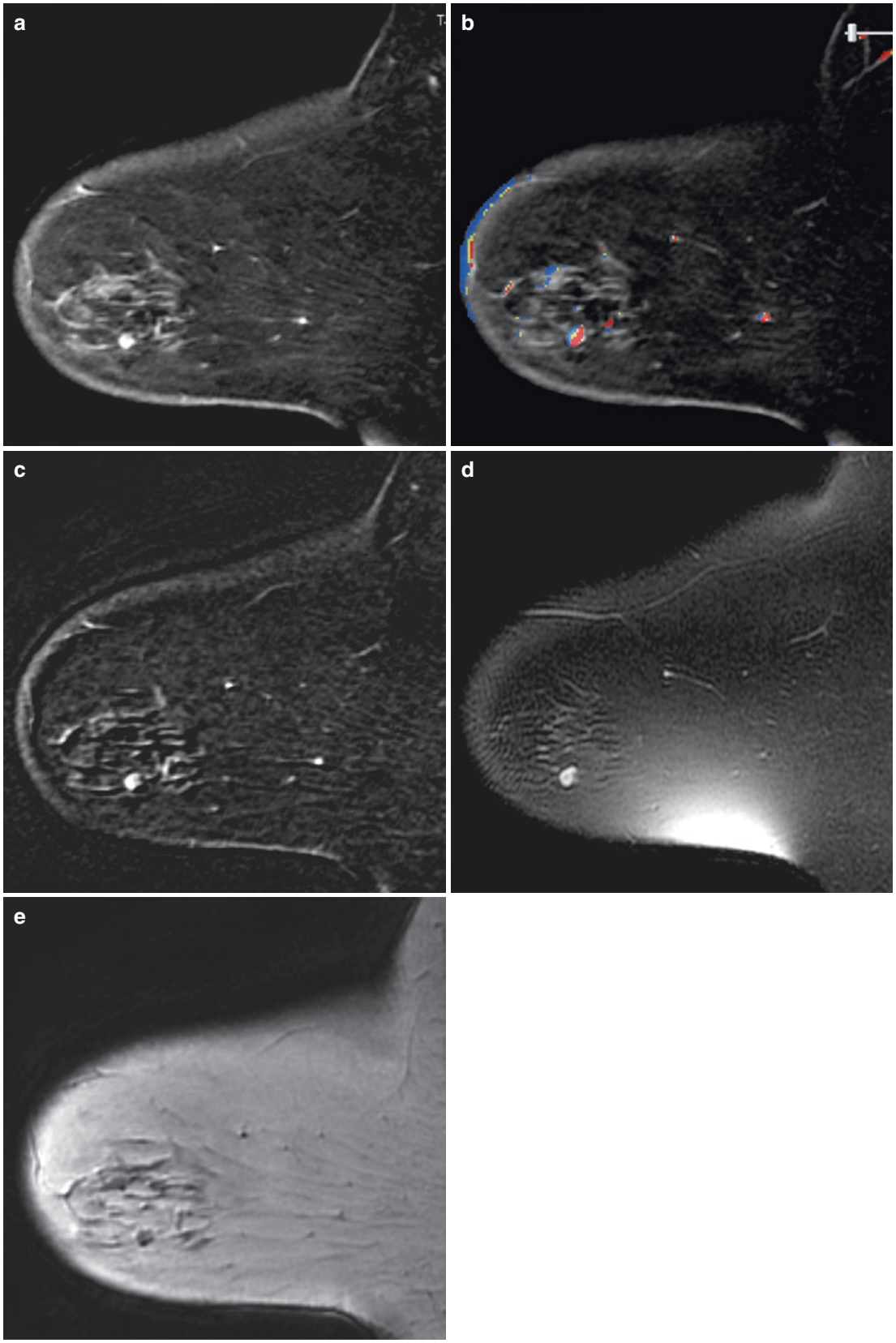

Fig. 2.3 (**a**) T1-weighted fat-saturated post-contrast sagittal image of the right breast with CAD kinetic analysis (**b**). (**c**) Post-contrast sagittal subtraction image. (**d**) Corresponding T2-weighted fat-saturated image. (**e**) T1-weighted sagittal image

2.2 Intramammary Lymph Node 2

Teaching Points Normal intramammary lymph nodes are usually seen as oval or reniform, smoothly marginated, fat-containing masses. They are often seen adjacent to vessels within the upper outer quadrant, although 28% of intramammary lymph nodes are found in other locations. They are usually nonpalpable and are found incidentally on breast MRI, where they appear hyperintense on T2-weighted images. They typically demonstrate homogenous enhancement with rapid initial and washout delayed kinetics. Non–fat-saturated T1-weighted images are usually helpful to confirm the presence of fat within the hilum. Biopsy can be avoided if the mass demonstrates classic characteristics of a benign lymph node (Figs. 2.3 and 2.4).

Image Findings

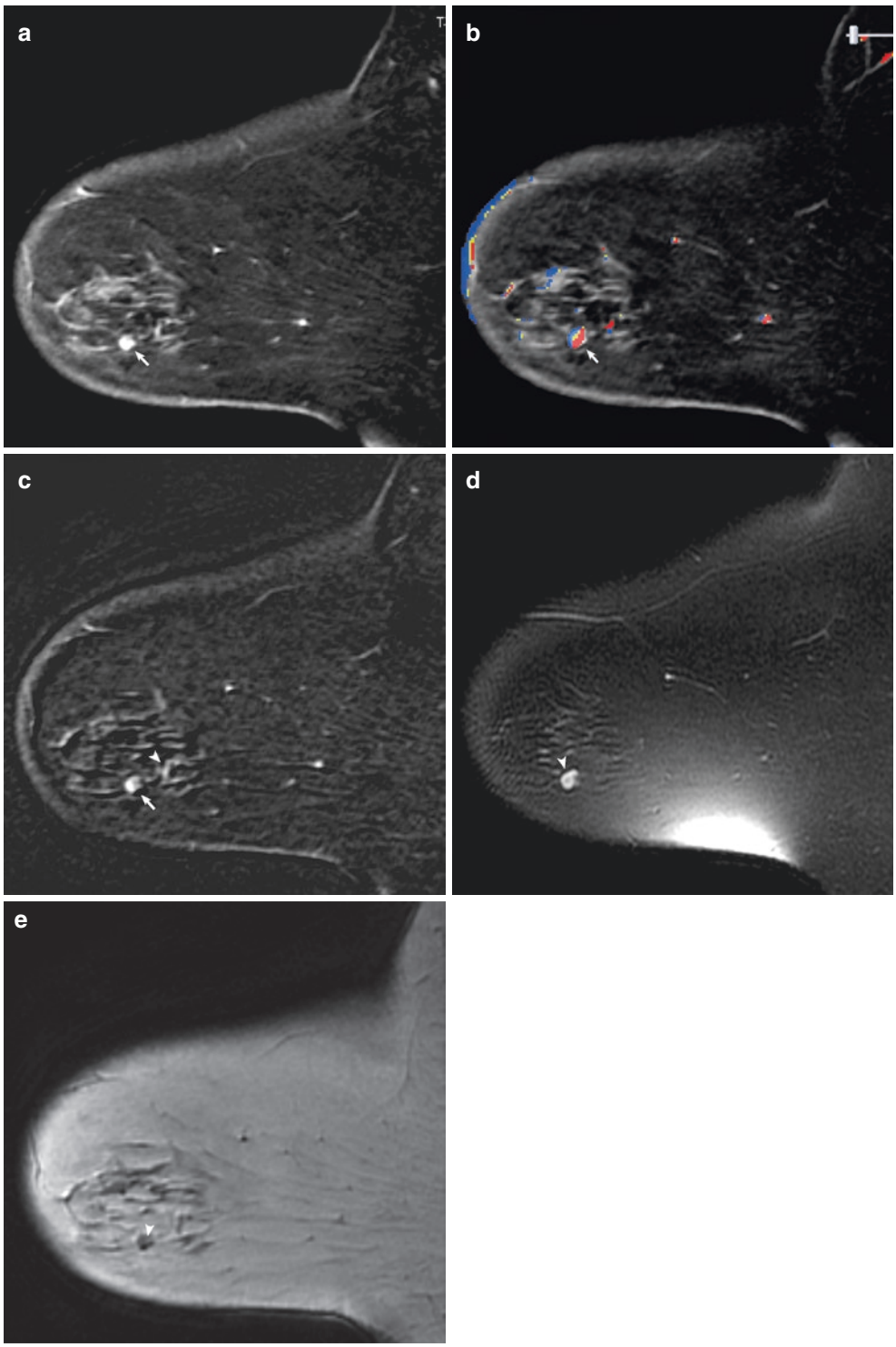

Fig. 2.4 Intramammary lymph node. (**a**) Sagittal T1-weighted fat-saturated post-contrast image of the right breast demonstrates a 4-mm focus of enhancement (*arrow*) in the lower outer anterior breast with a suspicious washout enhancement pattern (**b**) color-coded as red on CAD. (**c**) On the subtraction image, the morphology of the enhancement appears reniform (*arrow*) with an adjacent feeding vessel (*arrowhead*). (**d**) A sagittal T2-weighted fat-saturated image demonstrates peripheral hyperintensity (*arrowhead*), and a sagittal T1-weighted image (**e**) demonstrates central hyperintensity (*arrowhead*), compatible with a fatty hilum

2.3 History

37-year-old women high-risk screening MRI (Figs. 2.5 and 2.6).

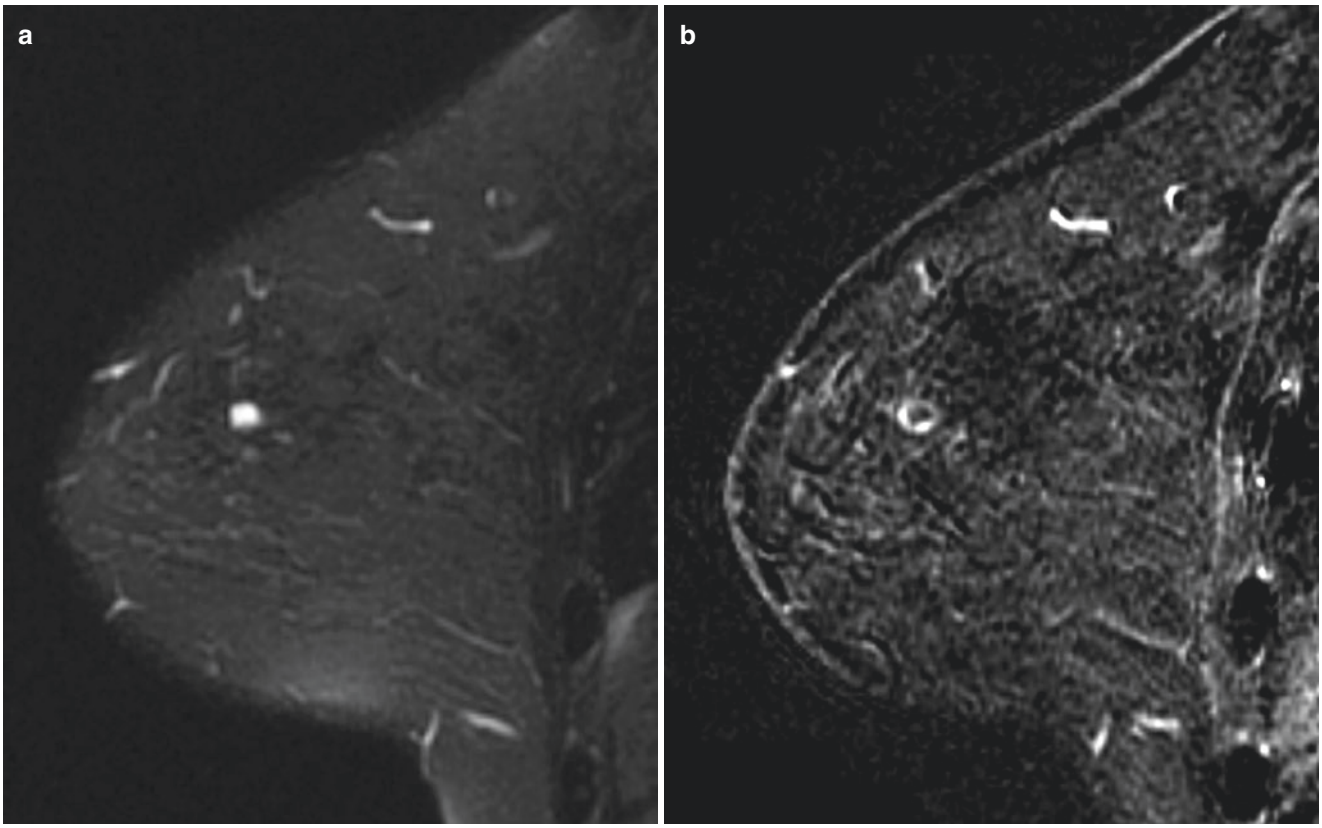

Fig. 2.5 Sagittal T2-weighted fat-saturated image (**a**) and corresponding sagittal T1-weighted post-contrast subtraction image (**b**) of the right breast

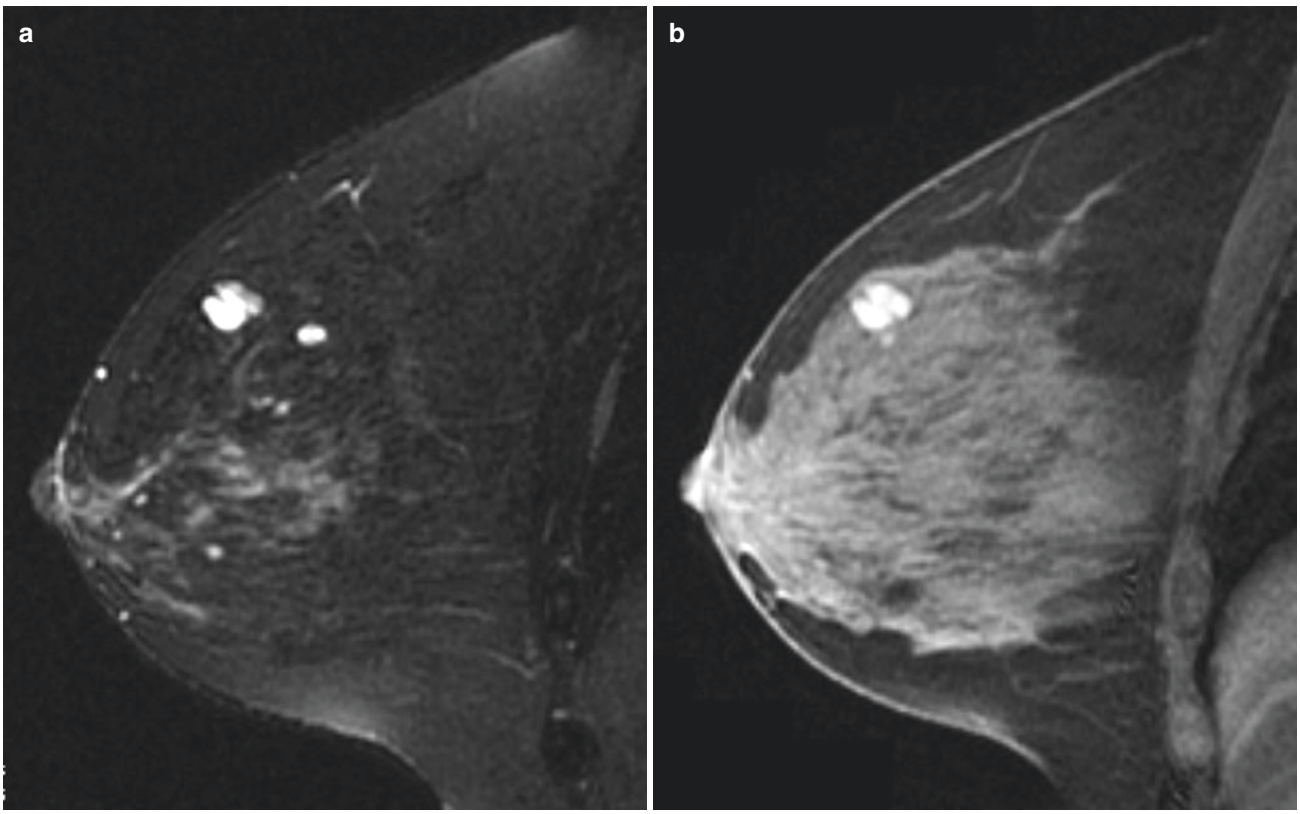

Fig. 2.6 Sagittal T2-weighted fat-saturated image (**a**) and corresponding sagittal T1-weighted fat-saturated pre-contrast image (**b**) of the left breast

2.3 Hemorrhagic and Inflamed Cyst

Teaching Points Simple cysts result from dilatation and effacement of the terminal duct lobular unit. They are commonly seen incidentally on MRI and follow fluid signal on all sequences (appearing very hyperintense on T2-weighted images and intermediate to hypointense on T1-weighted images). On post-contrast images, cysts typically do not enhance, but the periphery of the cyst may enhance if there is surrounding inflammation. Not infrequently, cysts may have intermediate or high signal on T1-weighted images owing to proteinaceous or hemorrhagic contents (Figs. 2.5, 2.6, 2.7, and 2.8).

Image Findings

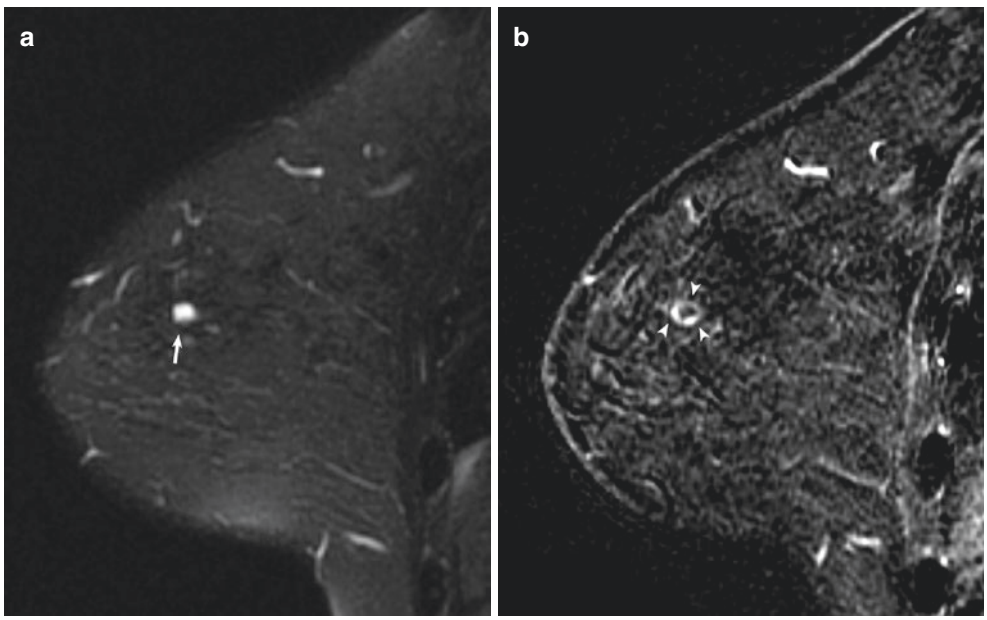

Fig. 2.7 Inflamed cyst. Sagittal T2-weighted fat-saturated image (**a**) and corresponding sagittal T1-weighted post-contrast subtraction image (**b**) of the right breast demonstrate a T2 hyperintense round mass (*arrow*) with rim enhancement (*arrowhead*) in the upper central breast

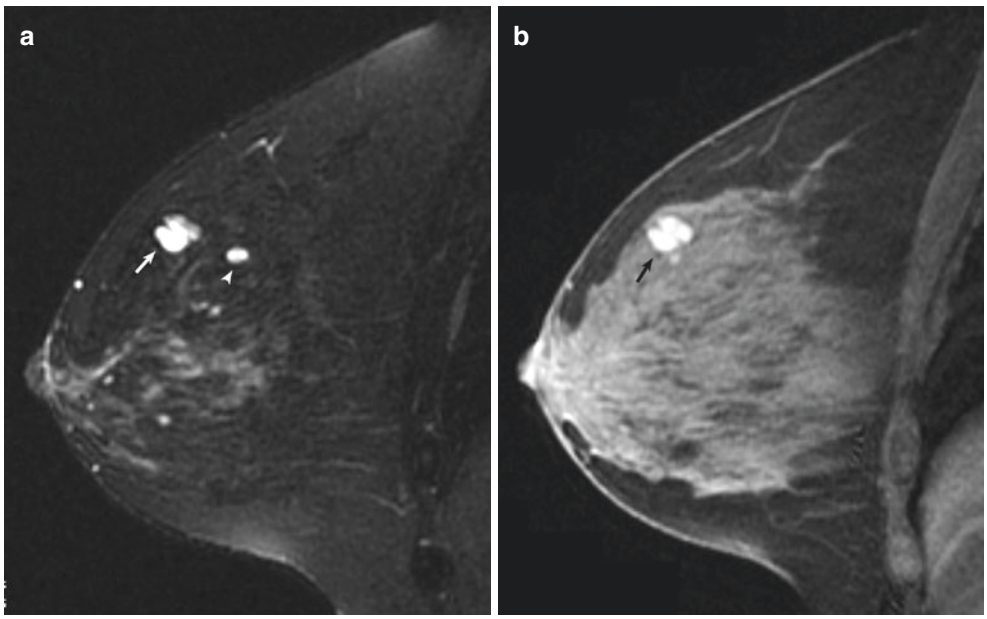

Fig. 2.8 Hemorrhagic/proteinaceous cyst. Sagittal T2-weighted fat-saturated image (**a**) and corresponding sagittal T1-weighted fat-saturated pre-contrast image (**b**) demonstrate a T1 and T2 hyperintense lobular mass in the upper central breast (*arrows*), compatible with a hemorrhagic cyst. For comparison, note the smaller, more posterior non-hemorrhagic cyst (*arrowhead*)

2.4 History

38-year-old woman undergoing high-risk screening MRI (Figs. 2.9 and 2.10).

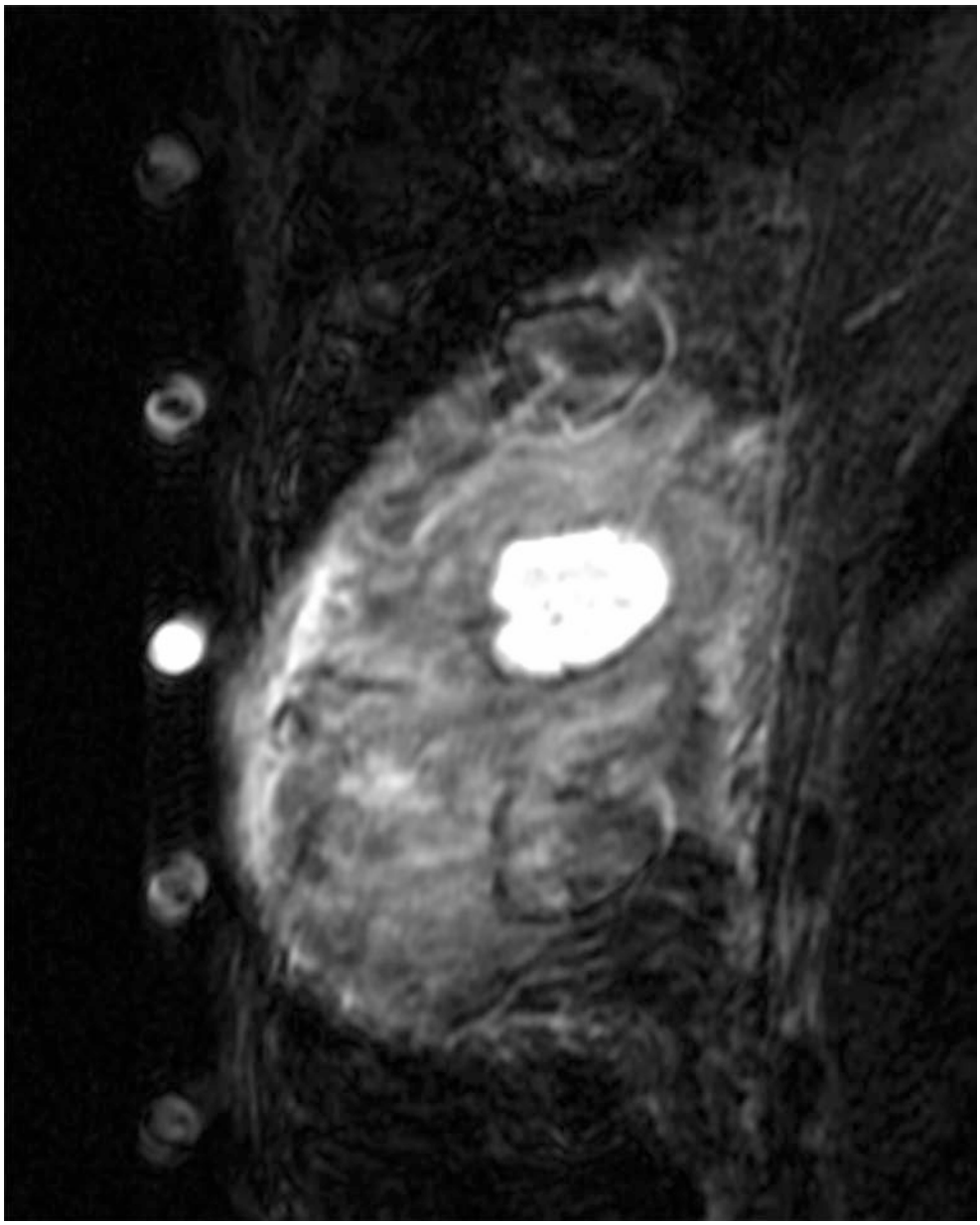

Fig. 2.9 Sagittal T2-weighted fat-saturated image of the left breast

2.4 Simple Cyst and Phase-Encoding Artifact

Teaching Points Phase-encoded motion artifact commonly seen in breast imaging is due to physical movement of the patient and manifests as ghosting in the direction of phase encoding, which is usually in the direction of the short axis. The spacing between the artifacts is related to the TR and frequency of the motion. Unlike Gibbs or truncation artifacts, the motion artifacts usually extend across the entire field of view. Possible solutions to phase-encoded motion artifact include cardiac/respiratory gating, switching phase and frequency encoding directions, increasing the number of signal averages, and shortening the scan time when patient motion is causing the artifact.

Image Findings

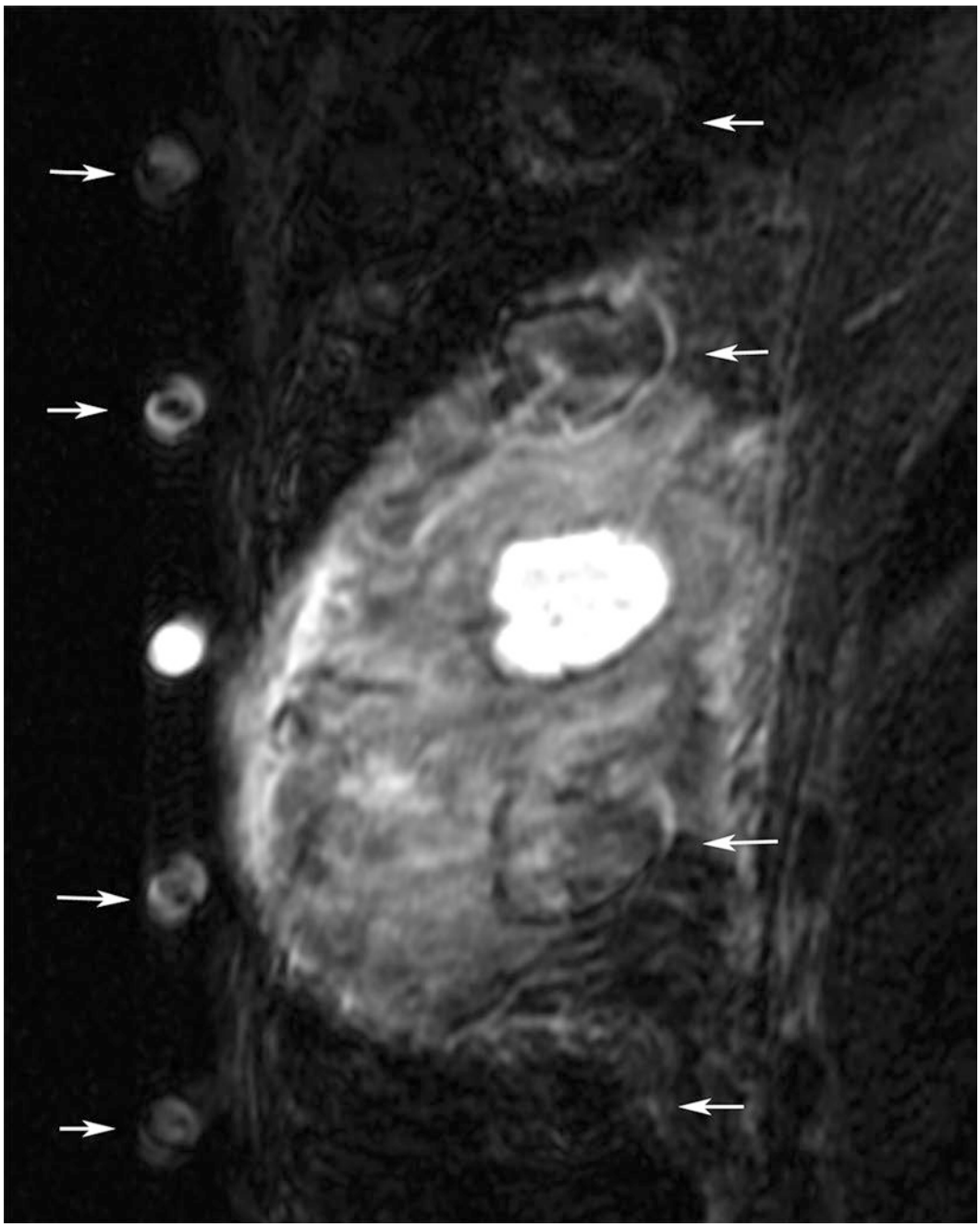

Fig. 2.10 Benign cyst and ghosting artifact. Sagittal T2-weighted fat-saturated image of the left breast shows a benign T2 hyperintense 3 cm cyst in the central breast. Ghosting artifact is seen superior and inferior to the cyst as well as superior and inferior to the separate T2 hyperintense nipple marker (*arrows*)

2.5 History

44-year-old women high risk screening MRI.

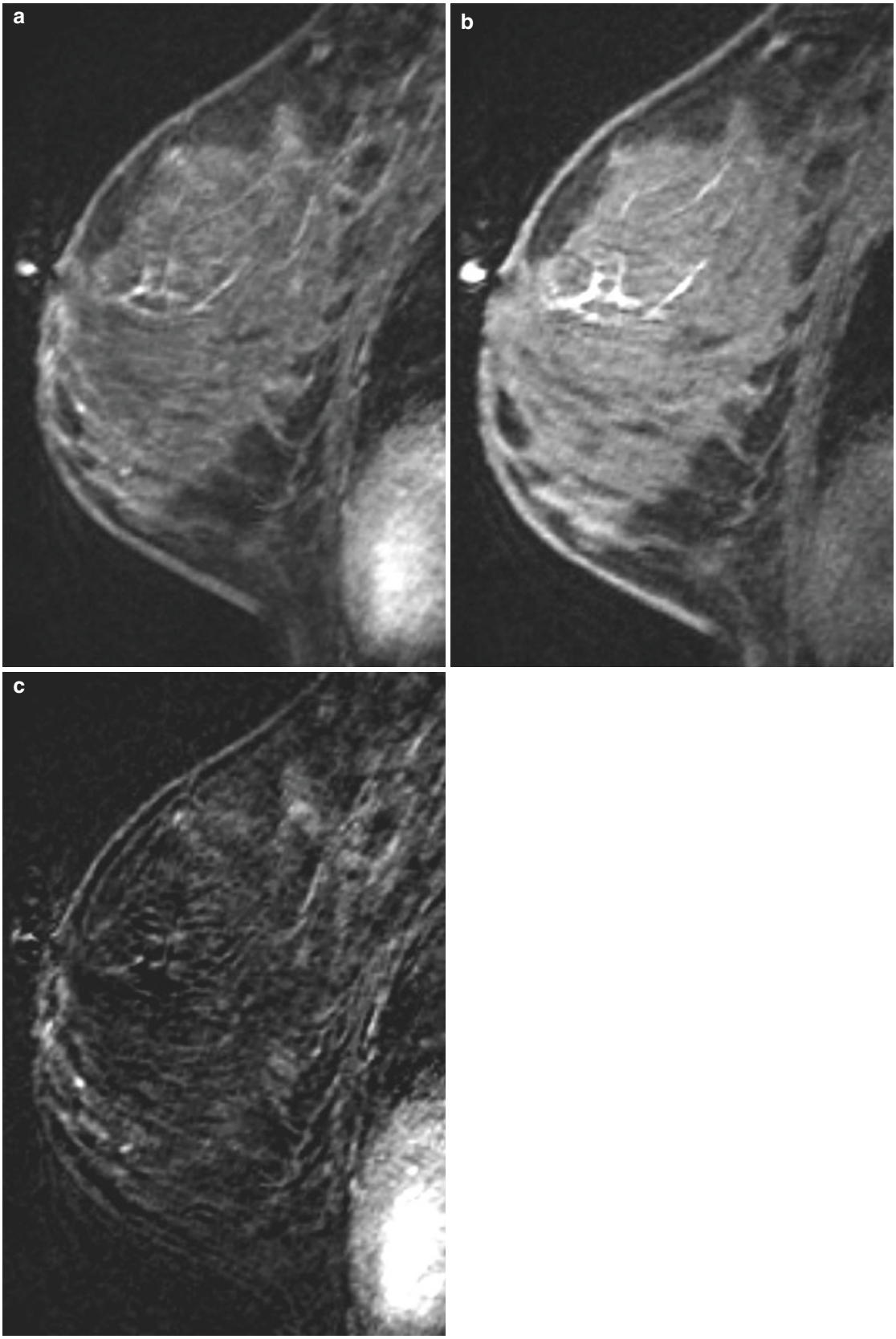

Fig. 2.11 Sagittal T1-weighted fat-saturated post-contrast (**a**) and pre-contrast (**b**) images. (**c**) Sagittal post-contrast subtraction

2.5 Dilated Duct

Teaching Points Normal ducts usually are not well visualized on breast MRI. In the setting of a chronic obstructive process, however, they become dilated and present as high-signal-intensity, branching tubular structures on T1-weighted images and as hypointense structures on T2-weighted images (owing to proteinaceous or hemorrhagic material). Dilated ducts do not typically enhance, but enhancement of the ductal wall may be seen because of underlying inflammation. It is important to remember that assessment of enhancement should not depend solely on the subtracted images, as misregistration artifact may occur (Figs. 2.11 and 2.12).

Image Findings

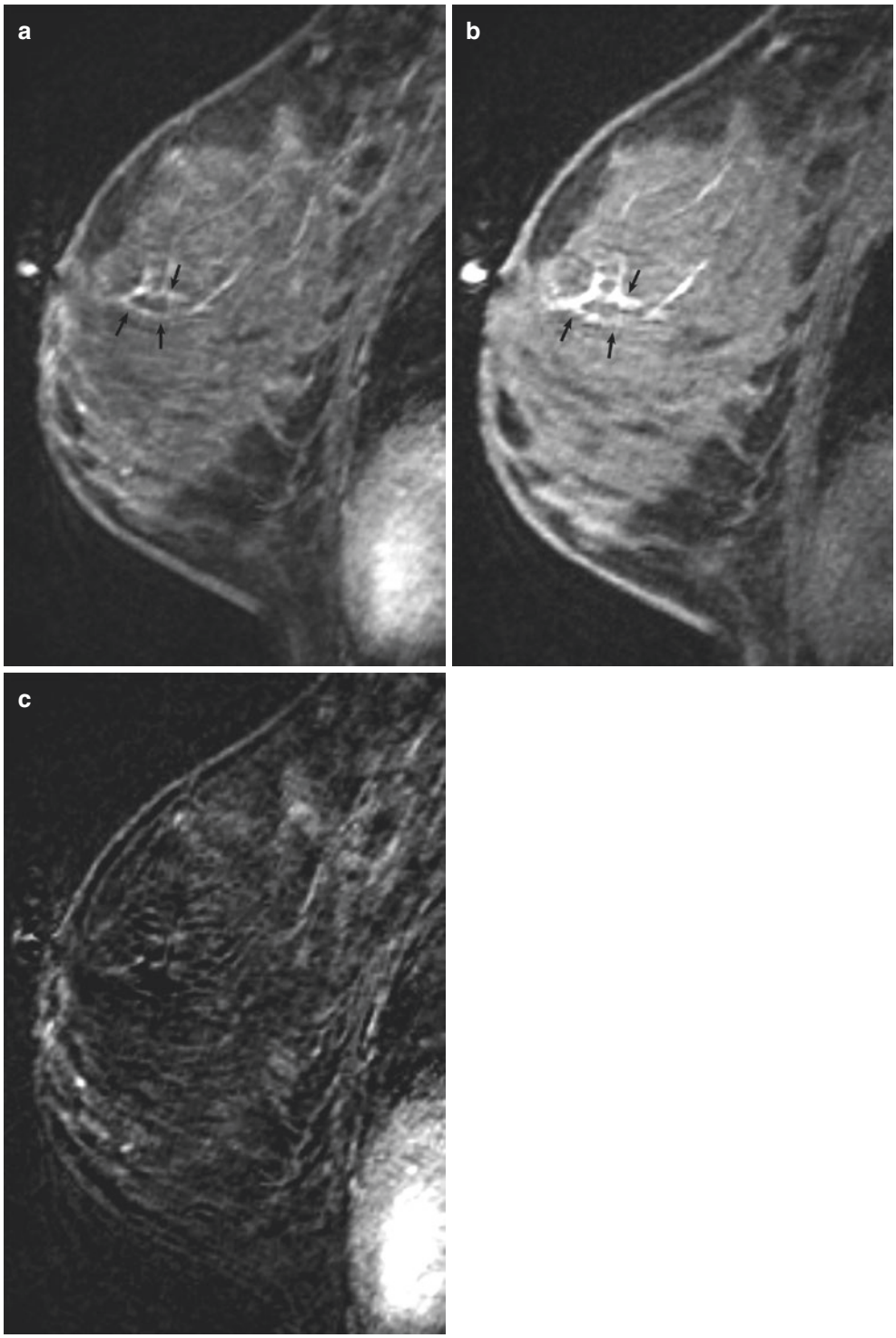

Fig. 2.12 Benign dilated ducts. (**a**) Sagittal T1-weighted fat-saturated post-contrast image of the left breast demonstrates linear hyperintensity (*arrows*) in the central middle third of the breast, which could represent non-mass enhancement. (**b**) The pre-contrast sequence demonstrates similar linear hyperintensity (*arrows*). (**c**) The sagittal post-contrast subtraction image demonstrates no enhancement in this location. Findings are consistent with proteinaceous or hemorrhagic material in the ducts

2.6 History

36-year-old woman with *BRCA1* mutation undergoing high-risk screening breast MRI.

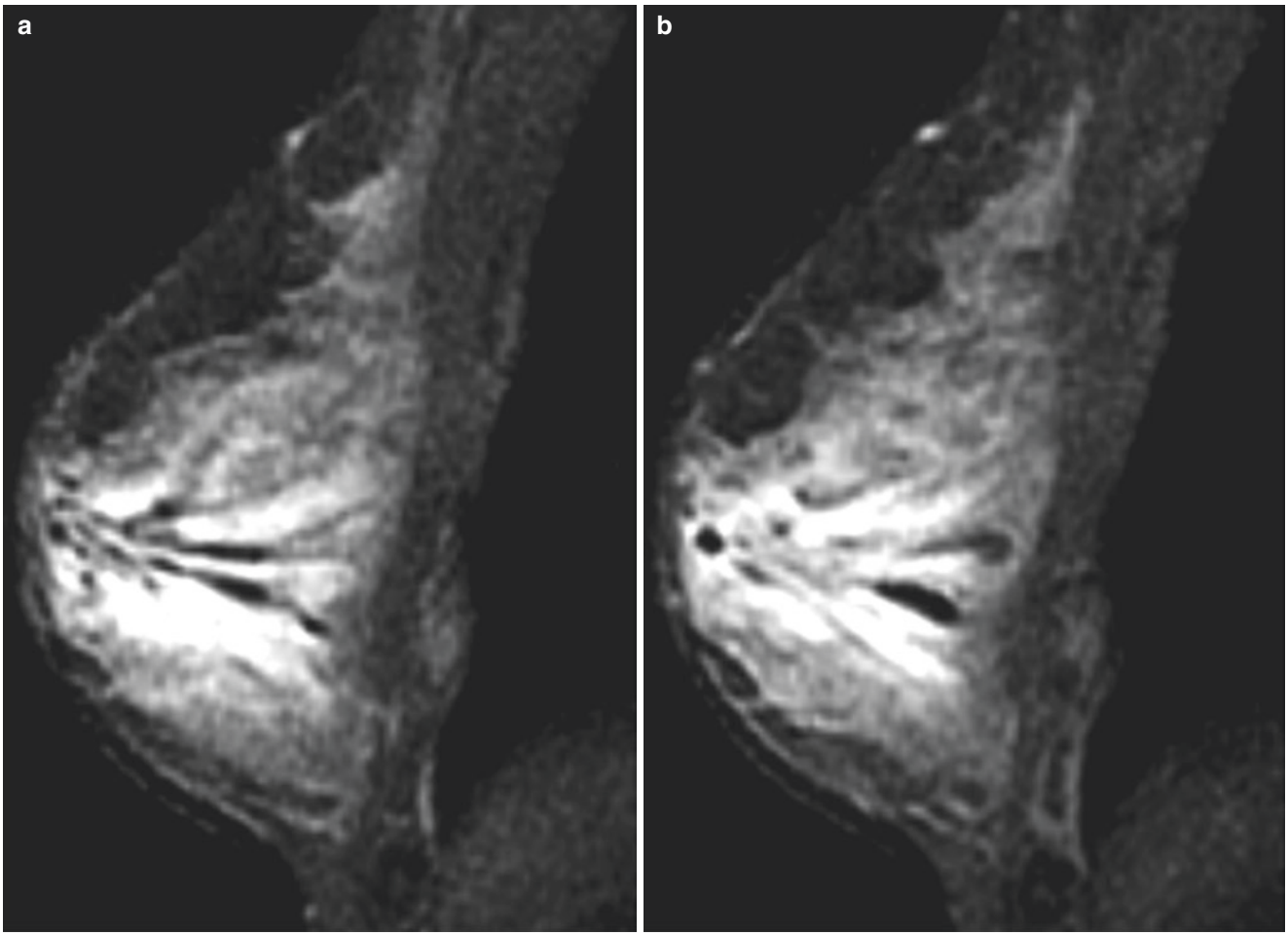

Fig. 2.13 (**a**, **b**) Sagittal T2-weighted fat-saturated images of the right breast. No suspicious enhancement was present on post-contrast images (*not shown*)

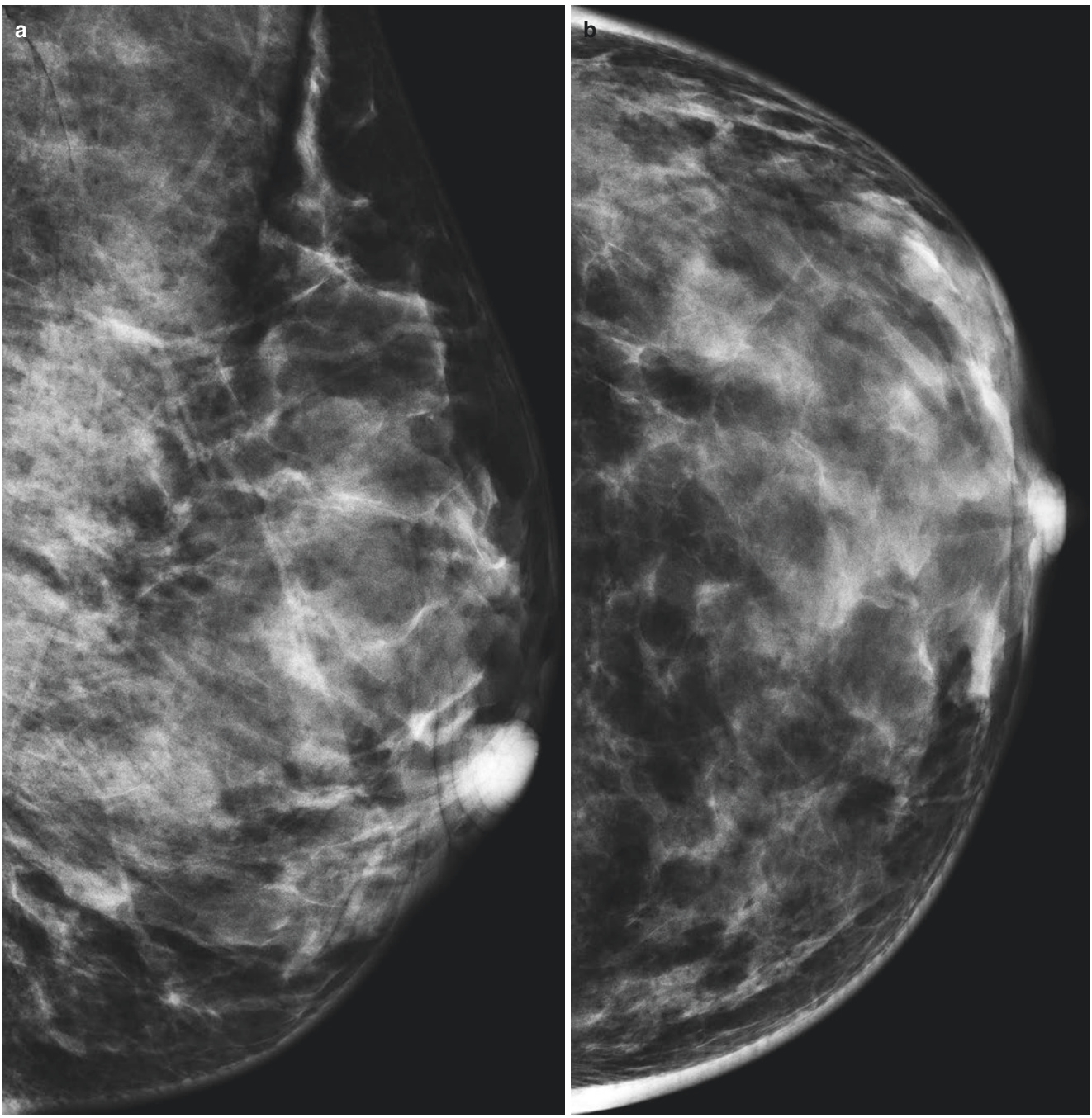

Fig. 2.14 Mediolateral oblique (MLO) (**a**) and craniocaudal (CC) mammographic (**b**) images of the right breast

2.6 Dilated Duct with Air

Teaching Points Signal void secondary to air can be seen on MR images on T1- and T2-weighted sequences (Figs. 2.13, 2.14, and 2.15). The etiology in healthy patients is unclear, but it is commonly iatrogenic (for example, following MRI-guided biopsy or ductography).

Image Findings

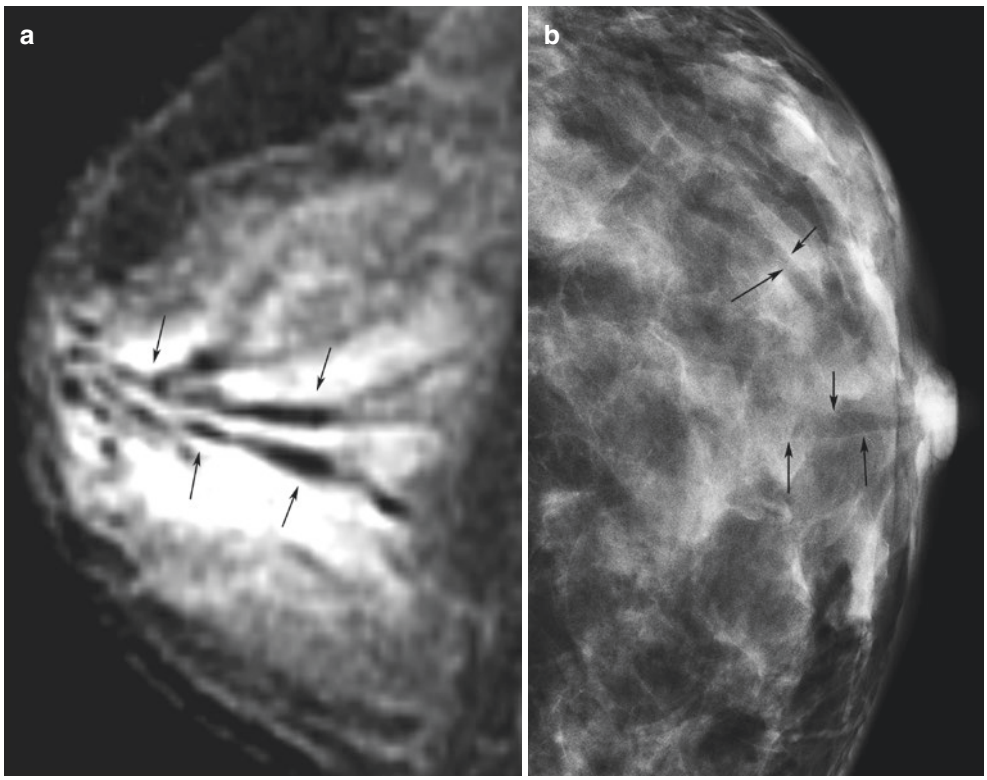

Fig. 2.15 Dilated duct with air. (**a**) Magnified sagittal T2-weighted fat-saturated MRI image of the right breast shows linear branching signal voids within subareolar ducts (*arrows*), representing air. (**b**) Magnified CC mammographic image of the right breast shows corresponding linear branching lucencies (*arrows*)

2.7 History

44-year-old woman undergoing high-risk screening breast MRI (Figs. 2.16 and 2.17).

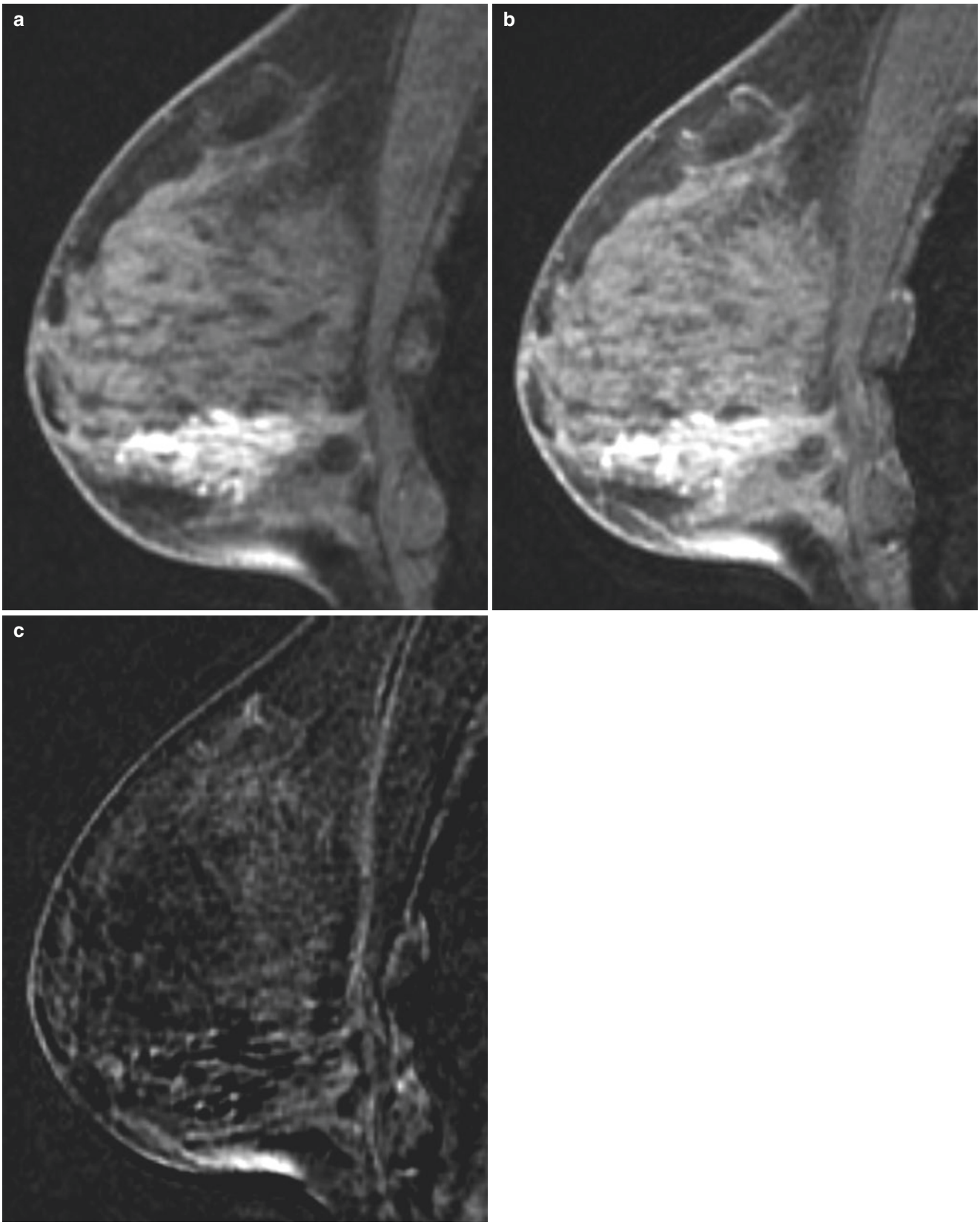

Fig. 2.16 Sagittal T1-weighted fat-suppressed pre-contrast (**a**), post-contrast (**b**), and post-contrast subtraction (**c**) images

2.7 Dilated Duct with Hemorrhage/ Proteinaceous Debris

Teaching Points Normal ducts usually are not seen on MR imaging, as they blend in with the background parenchyma. In cases of inflammation, infection, or obstruction, however, ducts filled with protein or blood will be visible on non-enhanced T1-weighted images as high-signal-intensity, branching tubular structures without associated enhancement. Therefore, subtraction images are very helpful when pre-contrast images demonstrate a hyperintense ductal pattern, to exclude abnormal enhancement. Otherwise, subtle areas of ductal wall enhancement may be overlooked, and a potential underlying carcinoma can be missed.

Image Findings

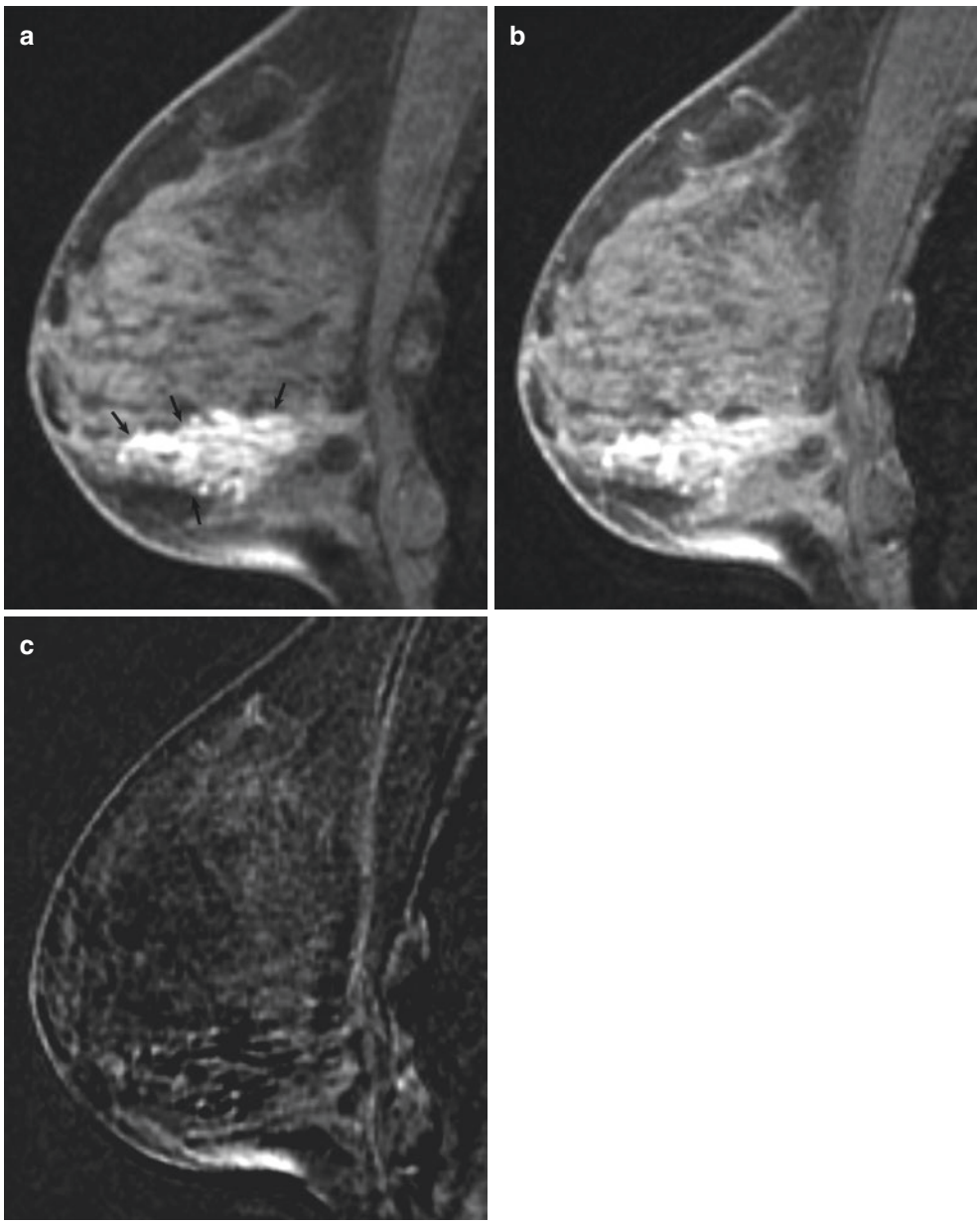

Fig. 2.17 Intraductal proteinaceous/hemorrhagic material. (**a**) Sagittal T1-weighted fat-suppressed pre-contrast image demonstrates segmentally distributed linear high signal (*arrows*) in the lower breast. Although one could mistake the high signal in this region on the sagittal T1-weighted fat-suppressed post-contrast image (**b**) for enhancement, the post-contrast subtraction image (**c**) shows that no enhancement is actually present

2.8 History

30-year-old women high risk screening MRI (Figs. 2.18 and 2.19).

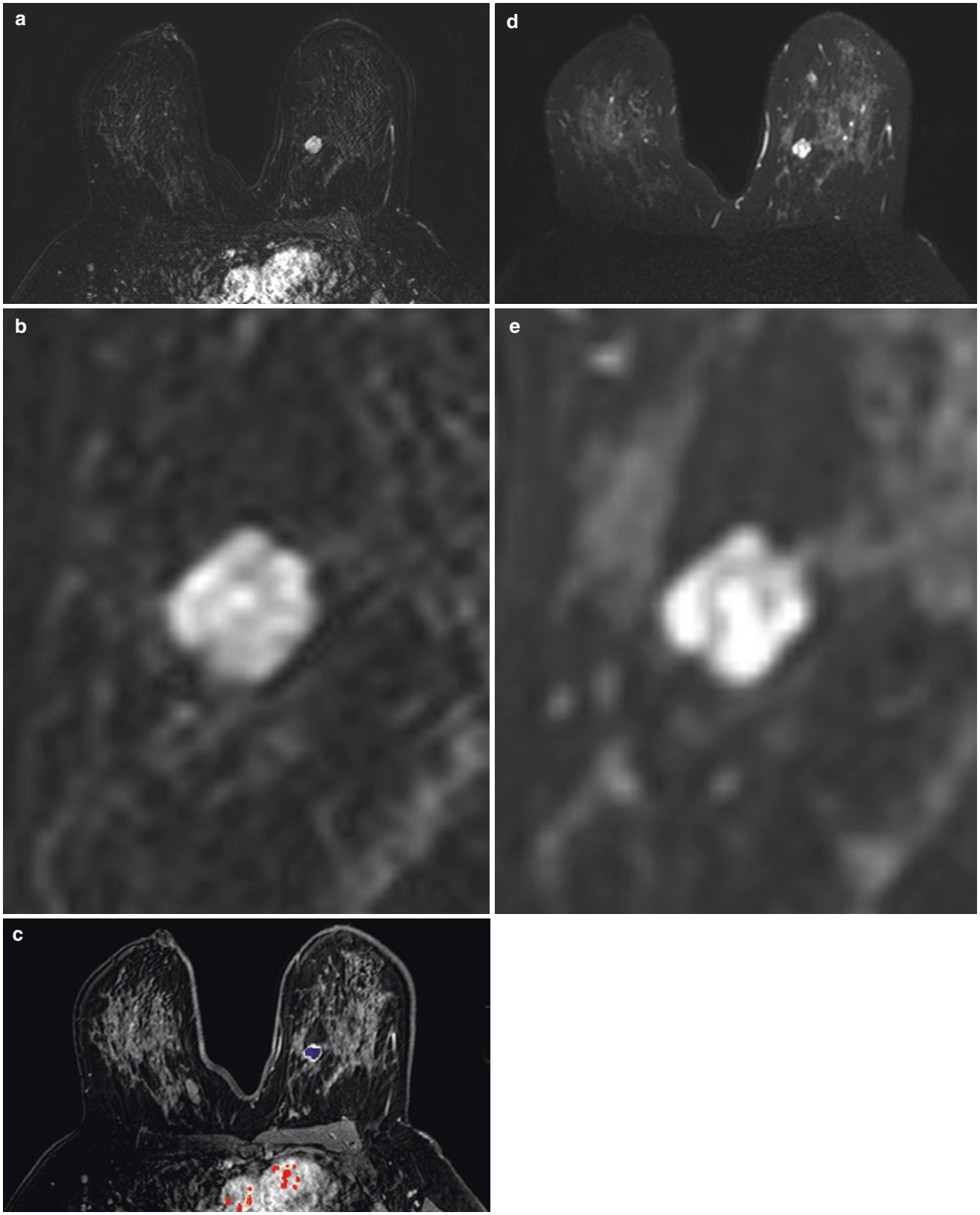

Fig. 2.18 (**a**) Axial post-contrast subtraction image of both breasts. (**b**) Magnified image of the left breast from **a**. (**c**) CAD overlay. (**d**) Axial T2-weighted fat-saturated image of both breasts. (**e**) Magnified image of the left breast from **d**

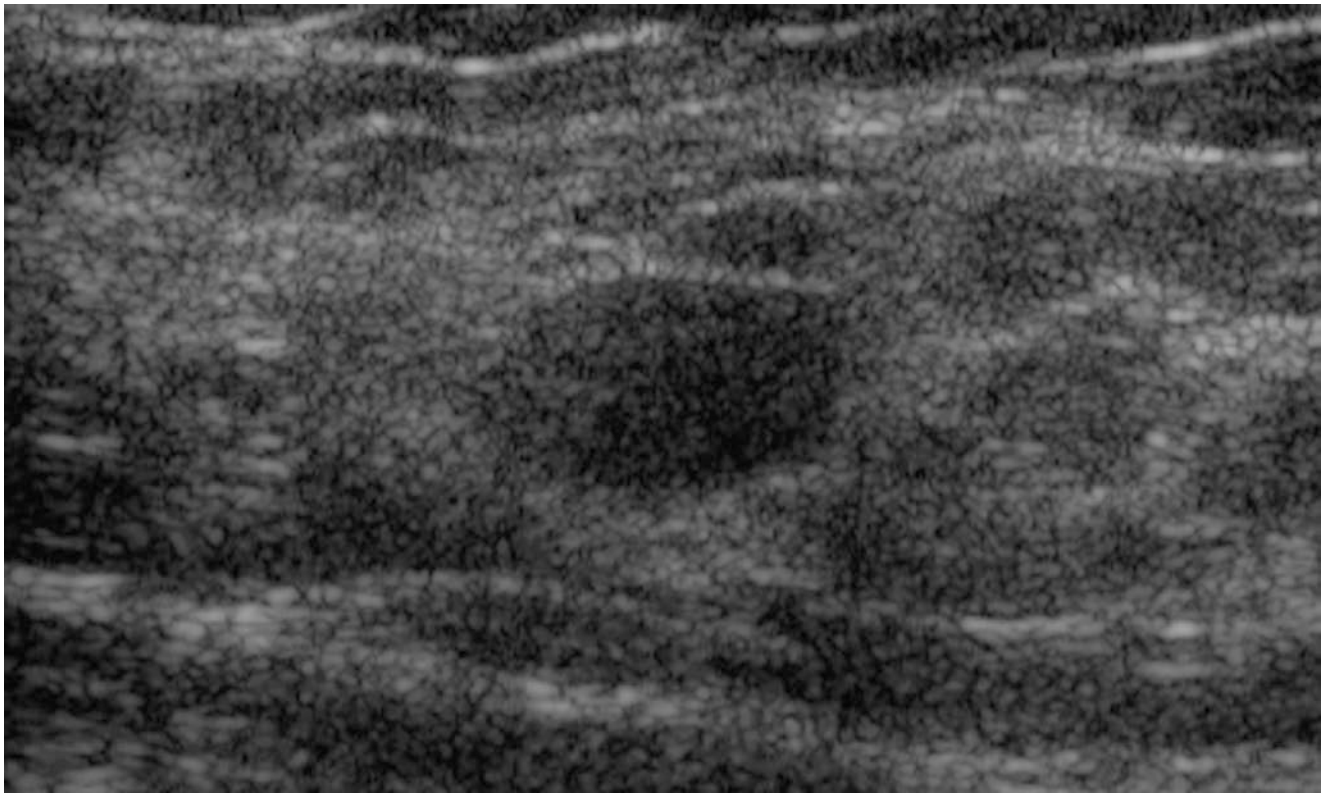

Fig. 2.19 Targeted second-look ultrasound image of the left breast

2.8 Fibroadenoma

Teaching Points Fibroadenomas are frequently seen on breast MRI and are best identified using morphologic features, classically a smooth margin with hypointense internal septa on T2-weighted images. Although less than 40 % of fibroadenomas demonstrate nonenhancing internal septations, if present they can be predictive of benignity (>95 %). MRI enhancement kinetics alone is neither specific nor sensitive because of the overlap in enhancement characteristics between benign and malignant lesions (Figs. 2.18, 2.19, 2.20, and 2.21).

Image Findings

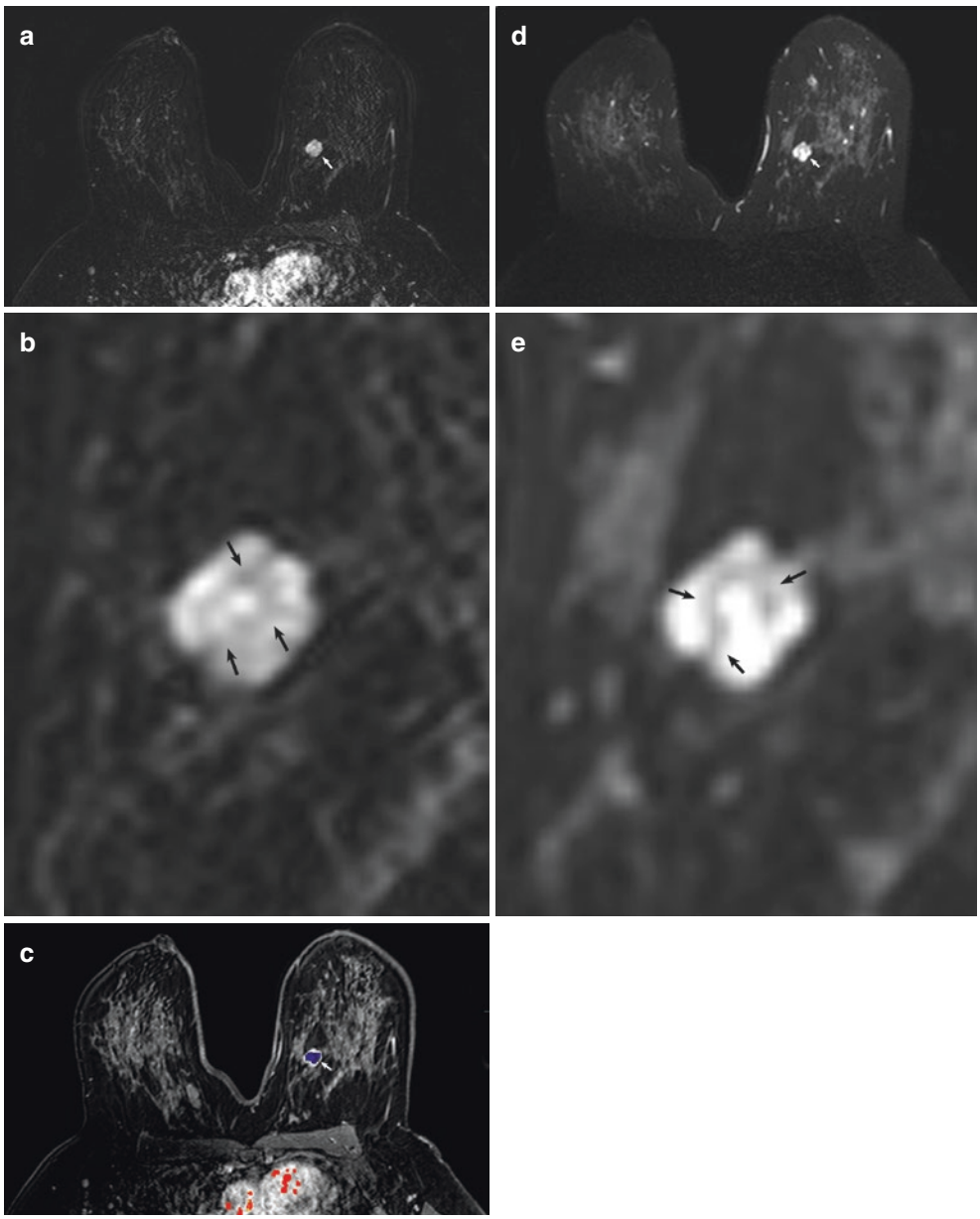

Fig. 2.20 Fibroadenoma on MRI. (**a**) Axial post-contrast subtraction image shows a homogeneously enhancing oval mass (*arrow*) along the 8:00 axis of the left breast. (**b**) The nonenhancing internal septations (*arrows*) are seen best on the close-up image. (**c**) CAD overlay demonstrates a progressive pattern of enhancement as evidenced by *blue color* assignment (*arrow*). Axial T2-weighted fat-saturated full-field (**d**) and close-up (**e**) images demonstrate a corresponding T2 hyperintense oval mass (*arrow*) with T2 hypointense internal septae (*arrows*)

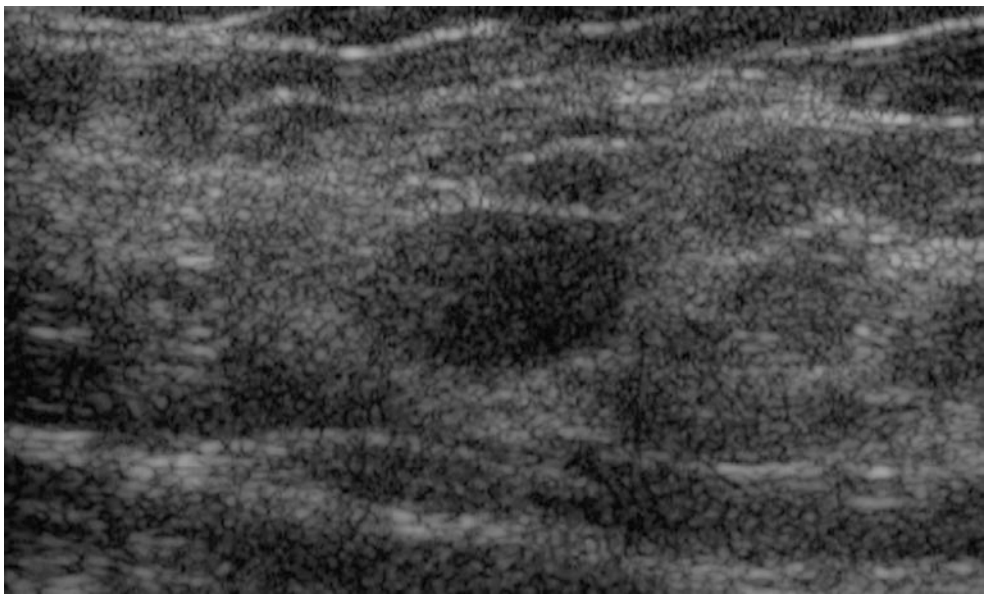

Fig. 2.21 Fibroadenoma on ultrasound. Second-look ultrasound was performed, demonstrating an oval, circumscribed, hypoechoic mass corresponding to the MRI mass

2.9 History

17-year-old girl with bilateral breast masses (Figs. 2.22, 2.23, 2.24, and 2.25).

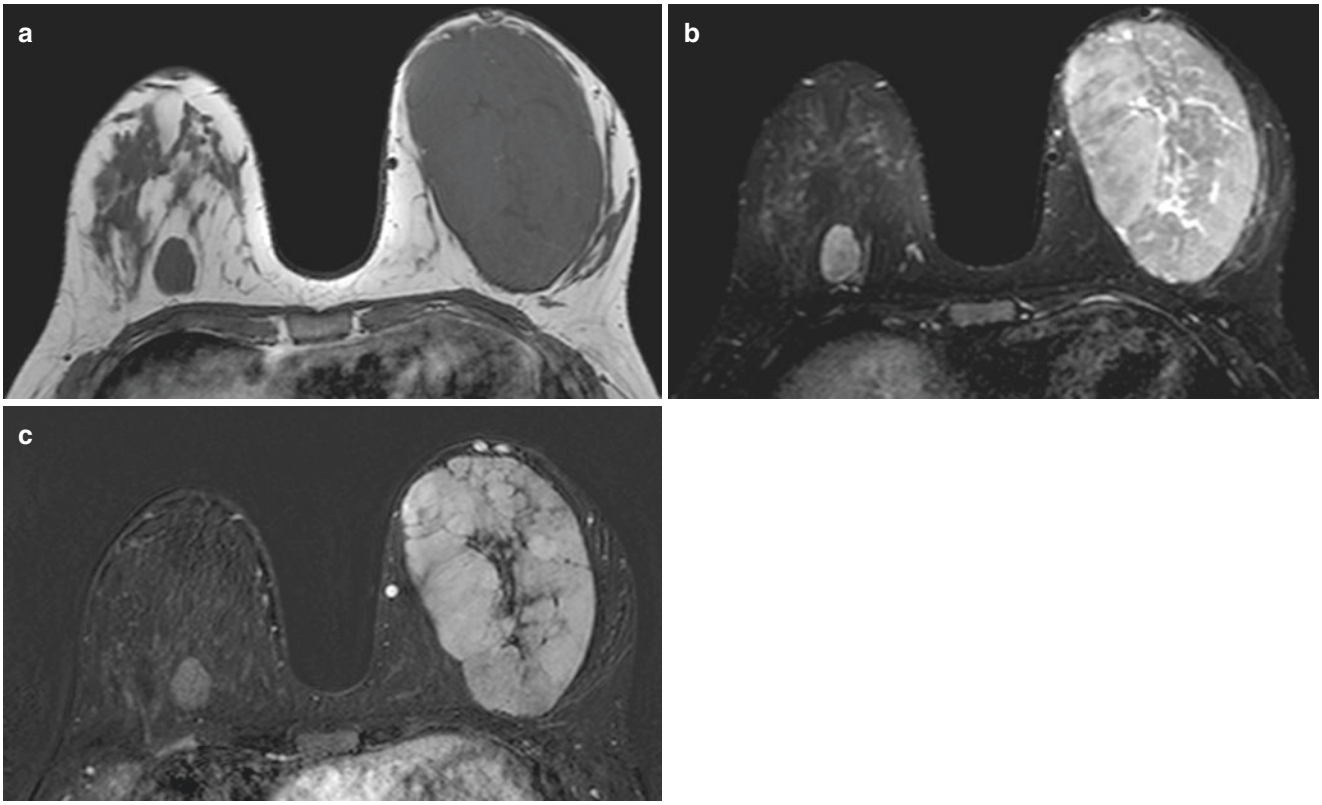

Fig. 2.22 (**a**) Axial T1-weighted image. (**b**) Corresponding axial T2-weighted fat-saturated image. (**c**) Corresponding axial post-contrast subtraction image

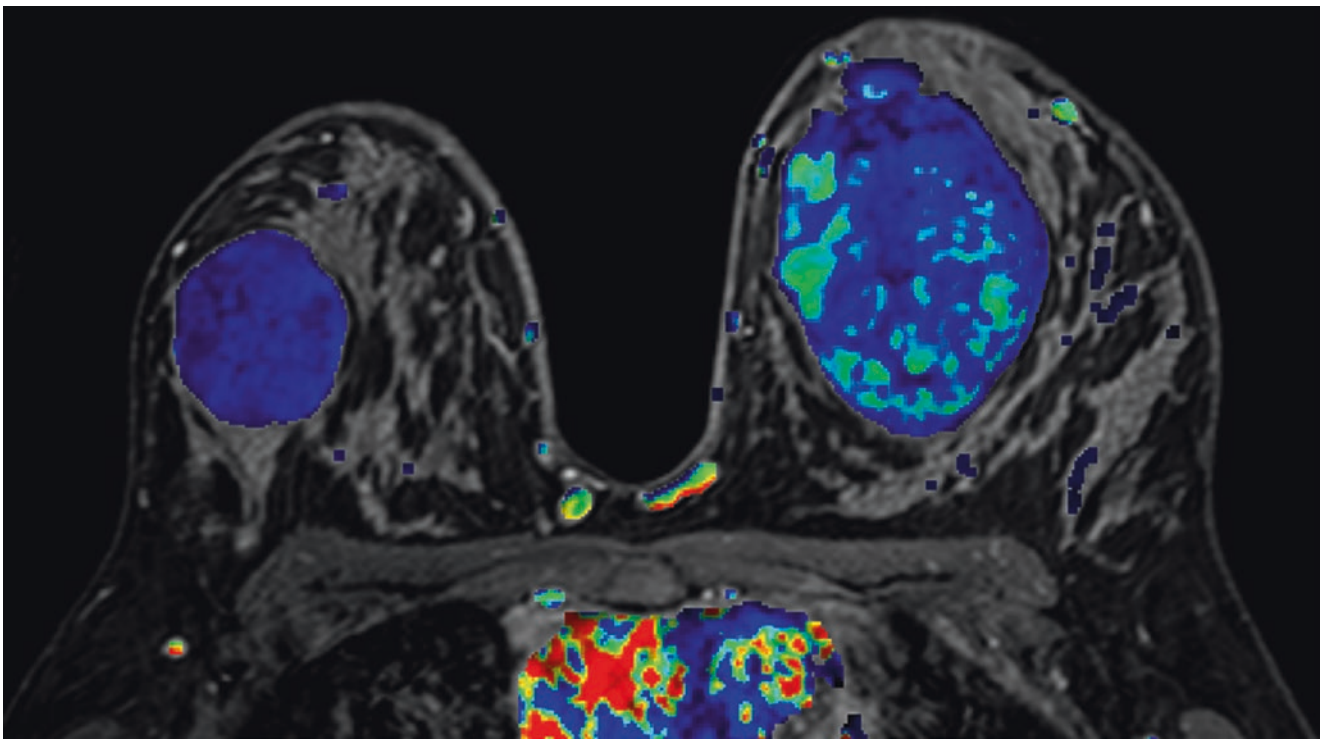

Fig. 2.23 More superior axial T1-weighted fat-saturated post-contrast image with CAD kinetics analysis color overlay

2.9 Juvenile Fibroadenomas

Teaching Points The patient underwent surgical excision of these masses, yielding juvenile fibroadenomas. MRI features in this case are typical for a fibroepithelial lesion, showing circumscribed masses with T1 hypointensity and T2 hyperintensity with nonenhancing septations. Juvenile or cellular fibroadenoma is an uncommon histologic variant of fibroadenoma that frequently undergoes markedly rapid growth. A fibroadenoma over 5–10 cm in diameter is termed a *giant fibroadenoma*. Approximately 10–25 % of patients with juvenile fibroadenomas have multiple or bilateral tumors at presentation.

Image Findings

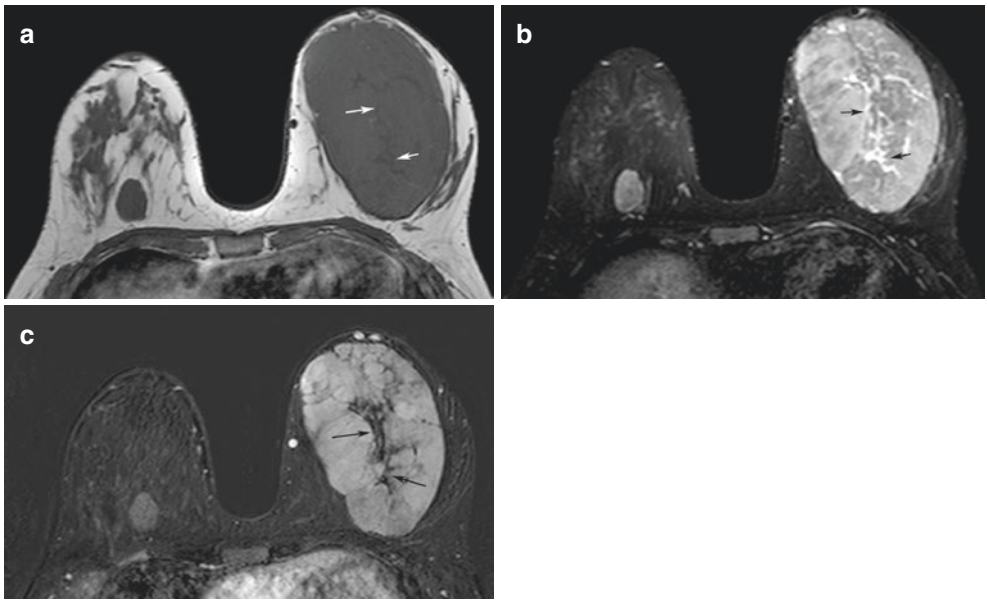

Fig. 2.24 Juvenile fibroadenoma. (**a**) Axial T1-weighted image shows a large, 9.5-cm circumscribed oval hypointense mass occupying most of the left breast. There are areas of linear lower signal intensity (*arrows*) within the mass, likely representing septations. A smaller 2.2-cm right breast mass with similar signal characteristics is noted. (**b**) These masses show corresponding T2 hyperintensity with areas of linear higher signal intensity (*arrows*) within the masses likely representing septations. (**c**) Axial post-contrast subtraction image shows intense homogeneous enhancement of both masses with central linear areas of nonenhancement corresponding to the T1 hypointense and T2 hyperintense septations

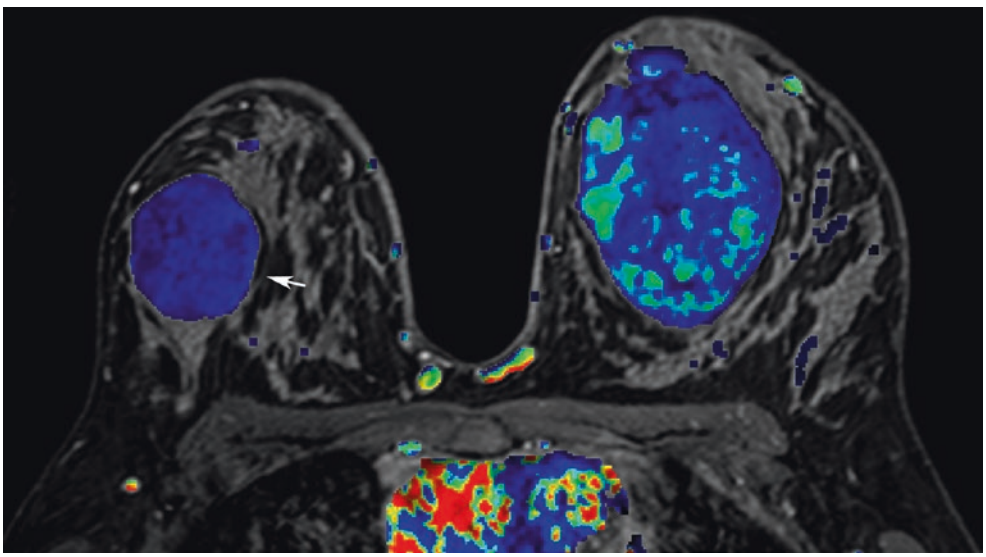

Fig. 2.25 More superior axial T1-weighted fat-saturated post-contrast image with CAD kinetics analysis shows a third mass (4.3 cm, *arrow*) in the right breast. Both masses demonstrate a predominantly persistent delayed enhancement pattern color-coded as *blue*

2.10 History

36-year-old with right breast palpable concern (Figs. 2.26, 2.27 and 2.28).

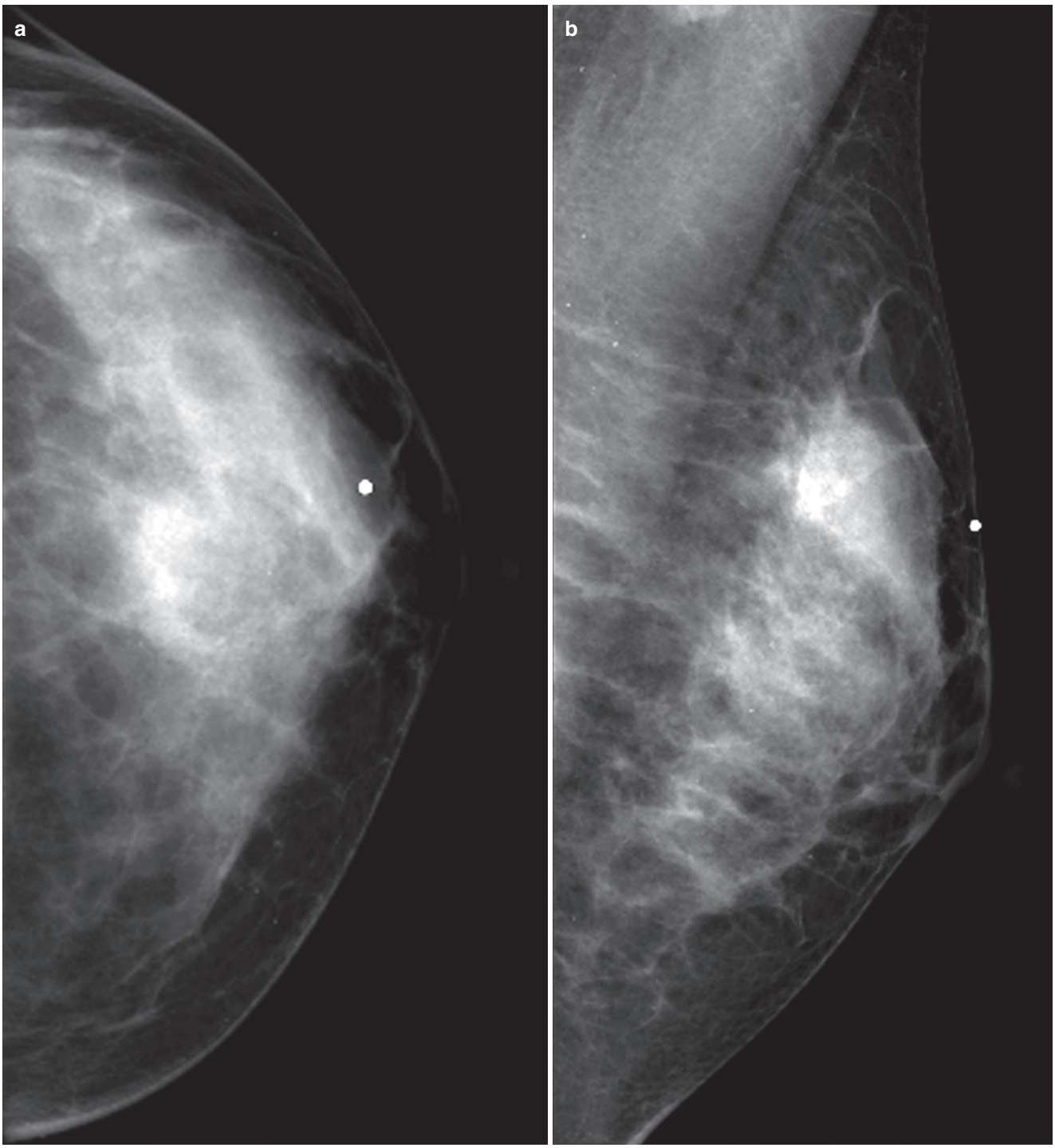

Fig. 2.26 36 Years old women high risk screening MRI. Mammographic images of the right breast. CC (**a**) and MLO (**b**) views with corresponding spot compression views (**c**, **d**) in a region of palpable abnormality

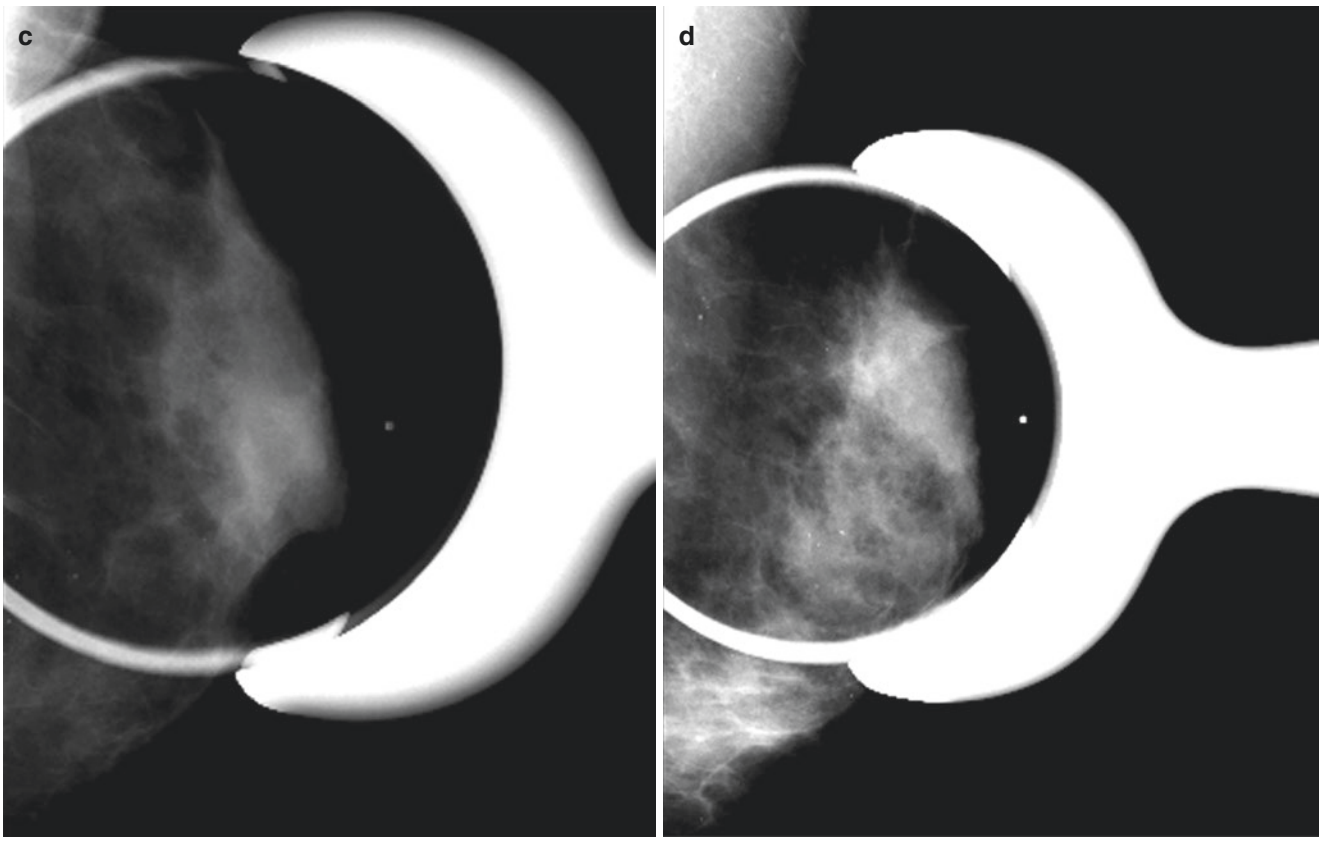

Fig. 2.26 (continued)

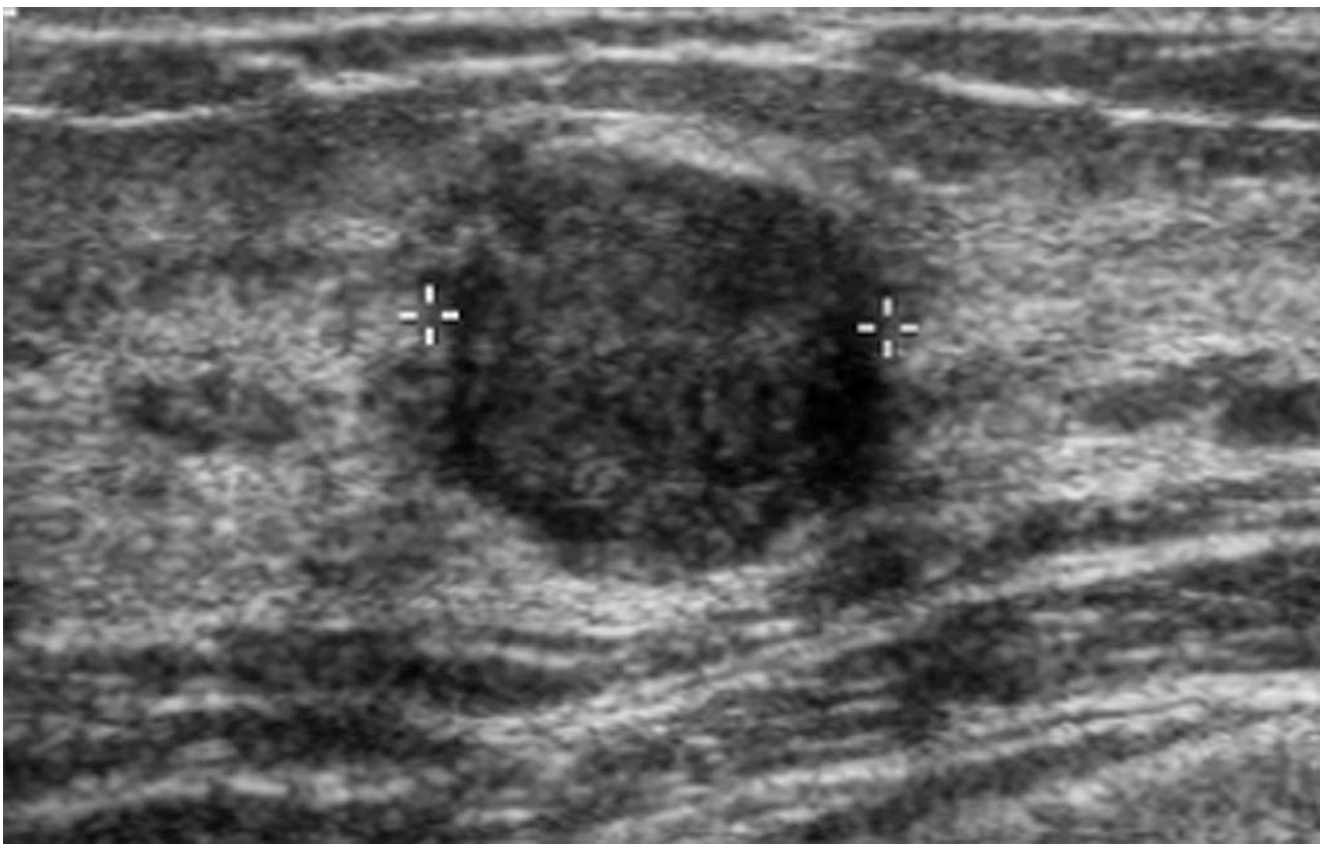

Fig. 2.27 A targeted right breast ultrasound

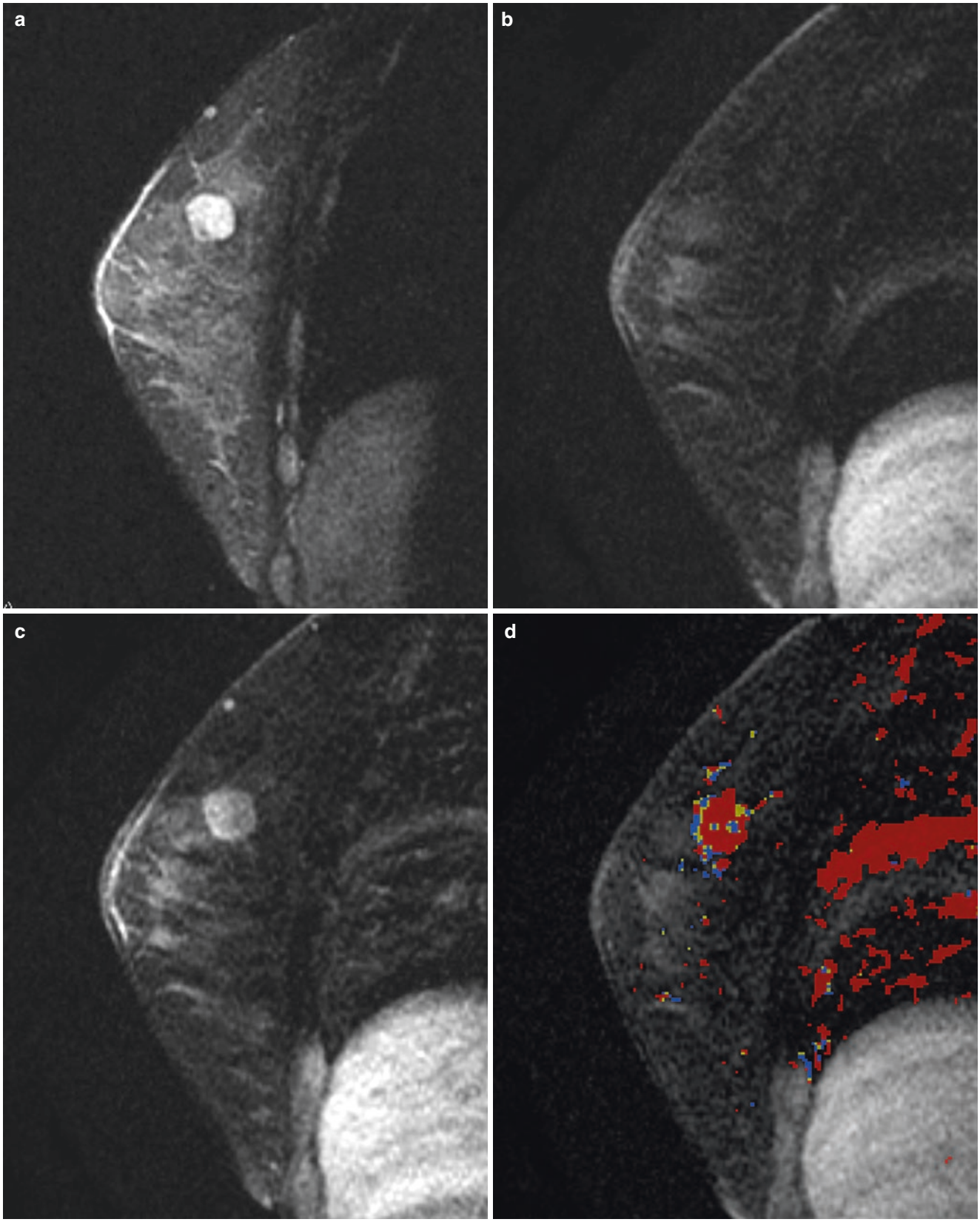

Fig. 2.28 Sagittal MRI images of the right breast. T2-weighted fat-saturated image (**a**) and T1-weighted fat-saturated pre-contrast image (**b**) and post-contrast image (**c**). CAD enhancement kinetics overlay (**d**)

2.10 Phyllodes Tumor

Teaching Points Phyllodes tumors are rare and constitute 0.3–1.0% of all breast tumors. They have a high incidence of local recurrence after surgery and potential for hematogenous metastases. Because of their rapid growth, phyllodes tumors tend to have circumscribed margins on mammography and sonography, so it is difficult to distinguish them from fibroadenomas on the basis of imaging. Large phyllodes tumors have a characteristic morphologic appearance on breast MRI, including smooth margins, internal cysts, and septations. They typically demonstrate low T1-weighted signal intensity and appear somewhat bright on T2-weighted images. Literature has shown that contrast enhancement pattern can be variable, so differentiation of phyllodes tumors and fibroadenomas on breast MRI remains unreliable (Figs. 2.26, 2.27, 2.28, 2.29, 2.30, and 2.31).

Image Findings

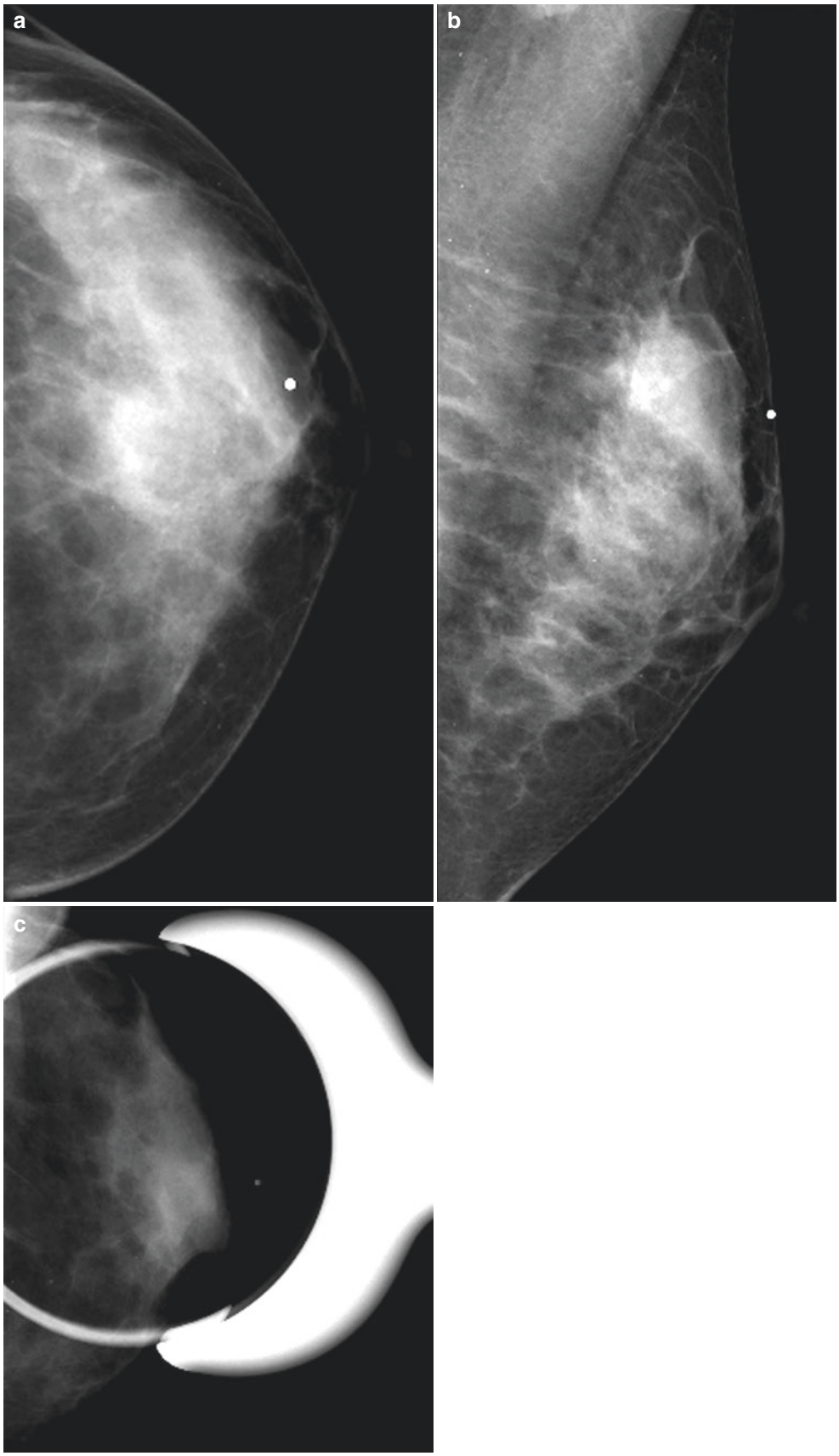

Fig. 2.29 Phyllodes tumor on mammography. Right CC (**a**) and MLO (**b**) views with corresponding spot compression view (**c**) of the region of palpable abnormality (marked by a BB) demonstrate extremely dense breast tissue without underlying abnormality

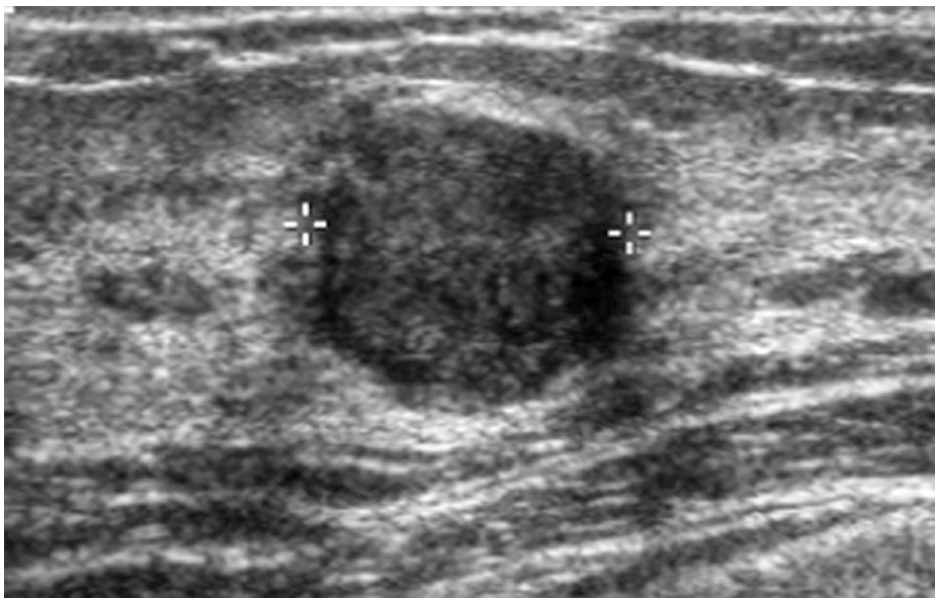

Fig. 2.30 Phyllodes tumor on ultrasound. Image from a targeted right breast ultrasound demonstrates a circumscribed, round, homogeneous, hypoechoic mass (between calipers)

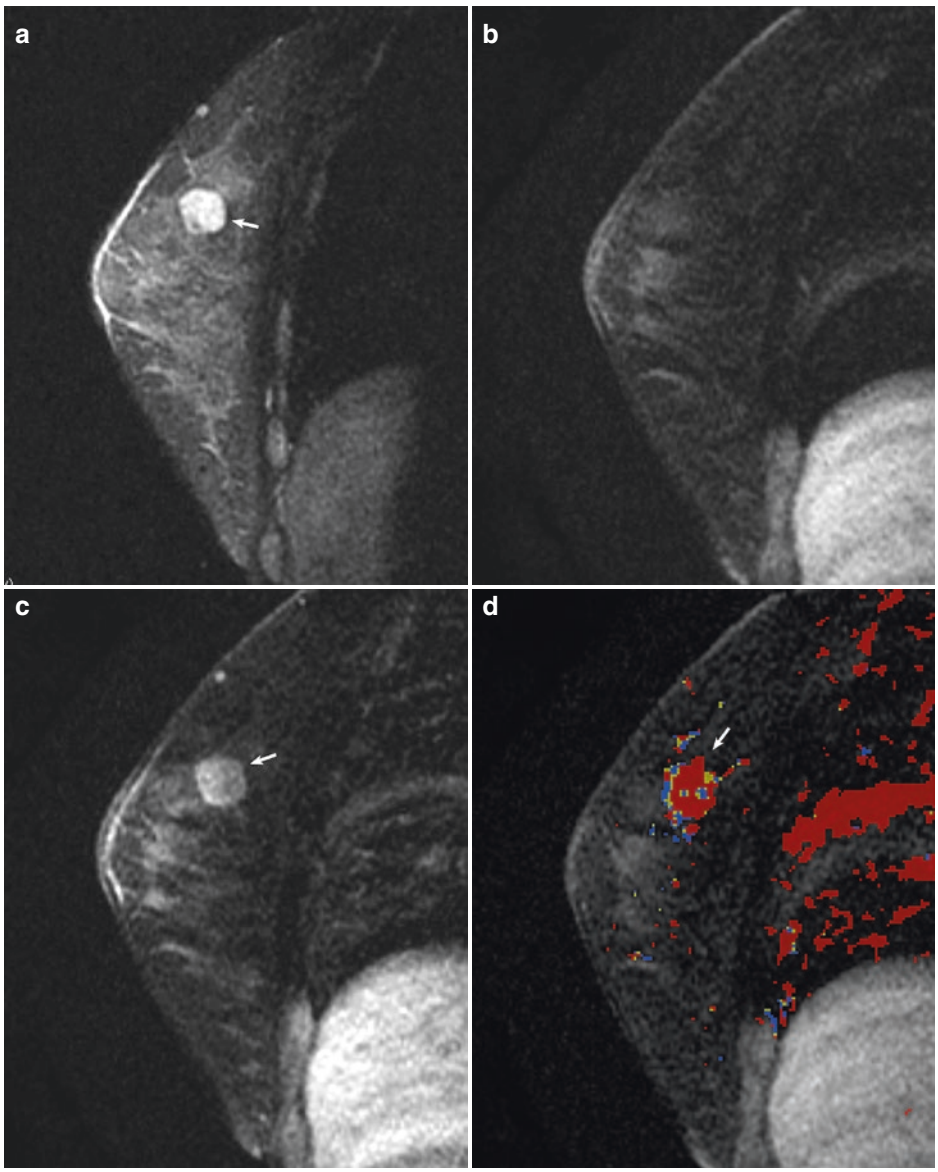

Fig. 2.31 Phyllodes tumor on sagittal MRI images. T2-weighted fat-saturated image (**a**) and T1-weighted fat-saturated pre-contrast image (**b**) and post-contrast image (**c**) demonstrate a round, homogeneously enhancing T1 isointense and T2 hyperintense mass (*arrows*). (**d**) CAD demonstrates mixed enhancement kinetics (*arrow*) with a predominant washout pattern

2.11 History

36-year-old woman with discordant biopsy result yielding mastitis (Figs. 2.32 and 2.33).

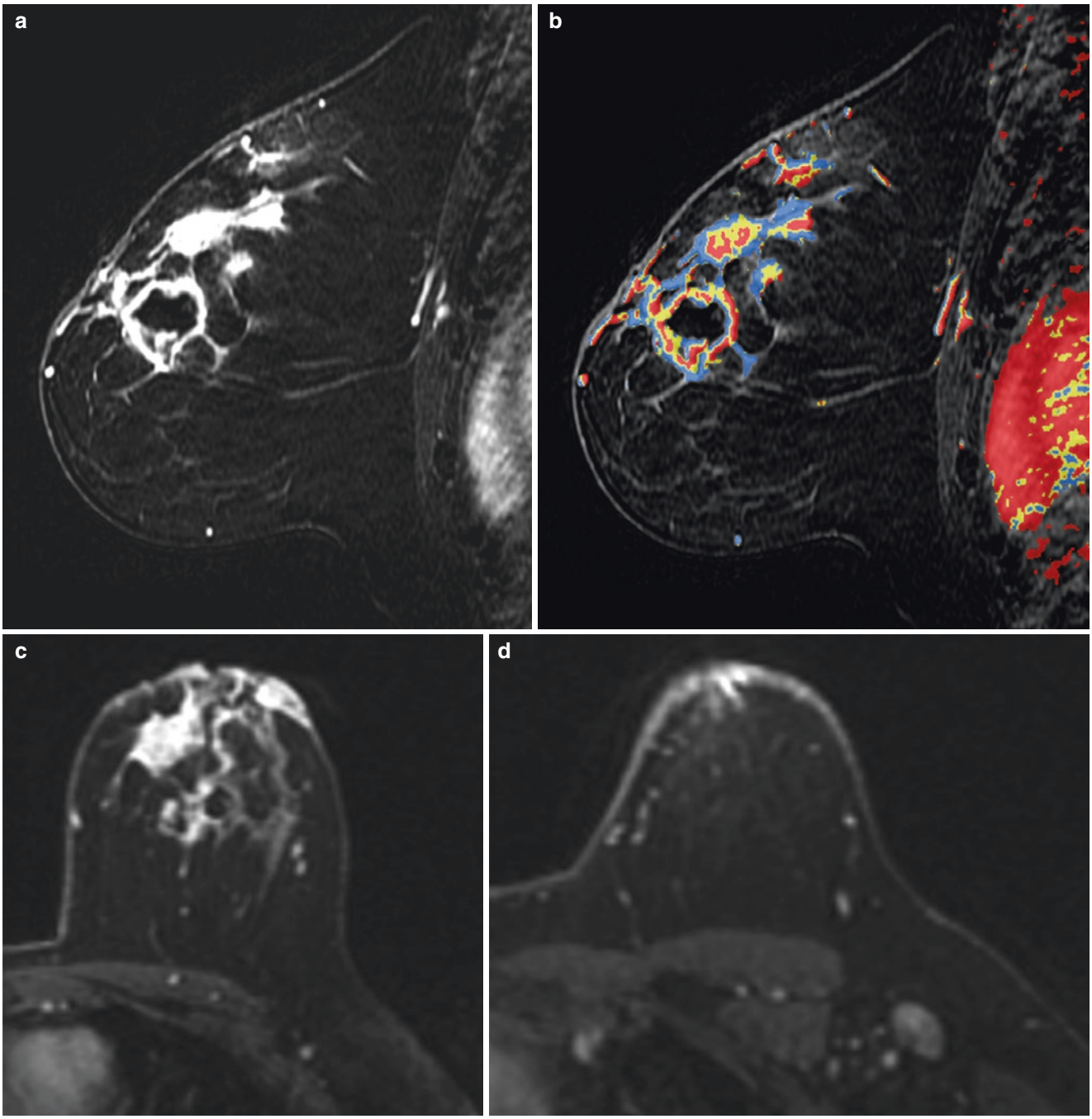

Fig. 2.32 (**a**) Selected sagittal T1-weighted post-contrast fat-saturated image of the left breast. (**b**) Corresponding CAD kinetics image. (**c**) Selected axial T1-weighted post-contrast fat-saturated image of the left breast. (**d**) Selected axial T1-weighted post-contrast fat-saturated image of the left axilla

2.11 Breast Abscess 1

Teaching Points Breast infection/abscess can result from unresolved local infection, obstruction of the duct near the nipple and acute, chronic or lactational mastitis. They are usually palpable, often associated with erythema, edema, and induration or overlying skin and pain. Depending on the water content of the collection, MR T2-weighted signal may vary. The overlying thickened skin may be intermediate or bright in signal depending on the degree of edema. Post-contrast T1-weighted images usually demonstrate a non-enhancing central, round, or irregular mass surrounded by an early, intensely enhancing rim. Abscess may be confused with malignancy due to the enhancement kinetics of the rim and overlying skin thickening, as illustrated in this case. In addition, focal skin thickening and axillary lymphadopathy can also be present. In case of persistent clinical concern with no resolution with antibiotics, surgical management may be appropriate.

Image Findings

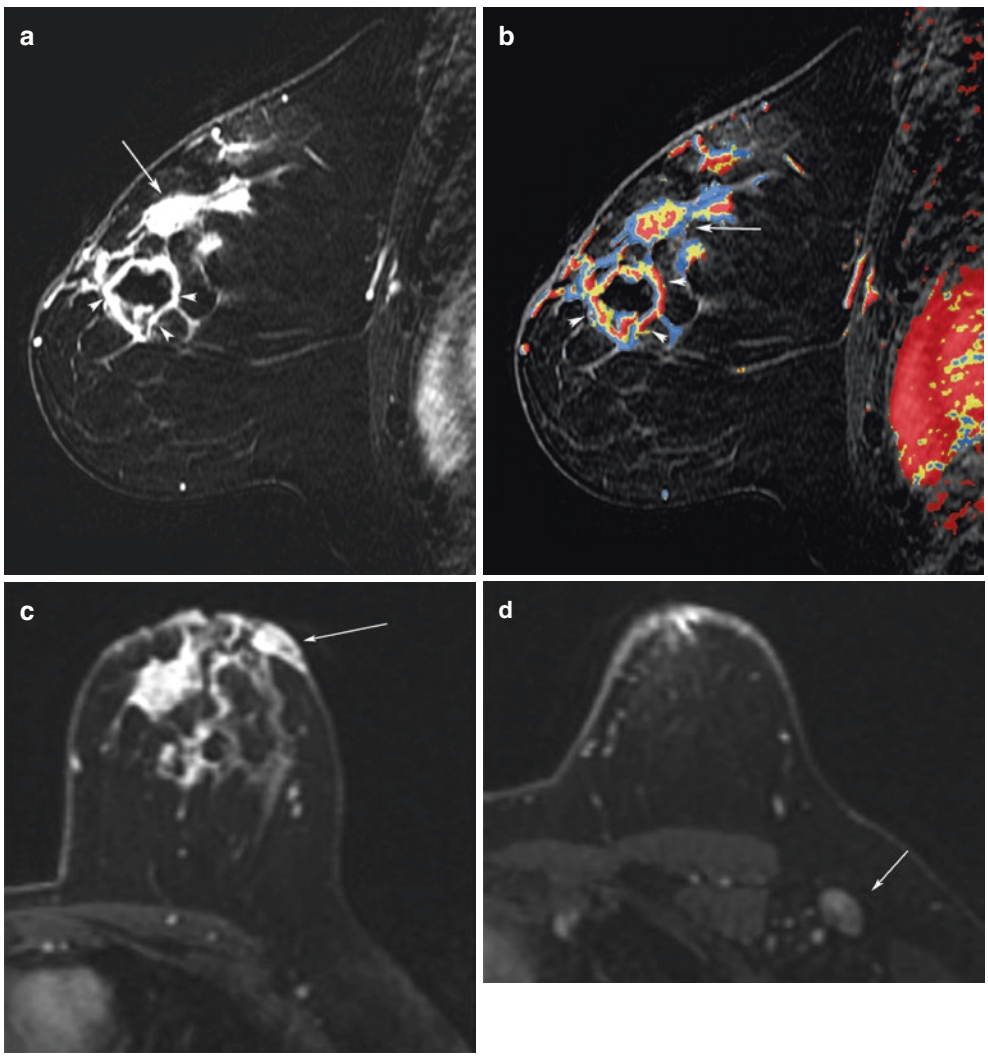

Fig. 2.33 Mastitis/abscess. (**a**) Sagittal image of the left breast shows irregular masses (spiculated mass; *arrow*) and rim-enhancing mass (*arrowheads*) in the upper breast. (**b**) Corresponding suspicious washout kinetics are present in the CAD images. (**c**) Focal nodular skin thickening is present in the outer anterior left breast (*arrow*) In the axilla, enlarged lymph node is present (*arrow* in **d**). Initial biopsy of the findings in the upper breast yielded inflammatory changes without evidence of malignancy. Following the MRI, surgical excision was performed yielding inflammatory changes without evidence of carcinoma

2.12 History

42-year-old patient with recurrent mastitis (Figs. 2.34 and 2.35).

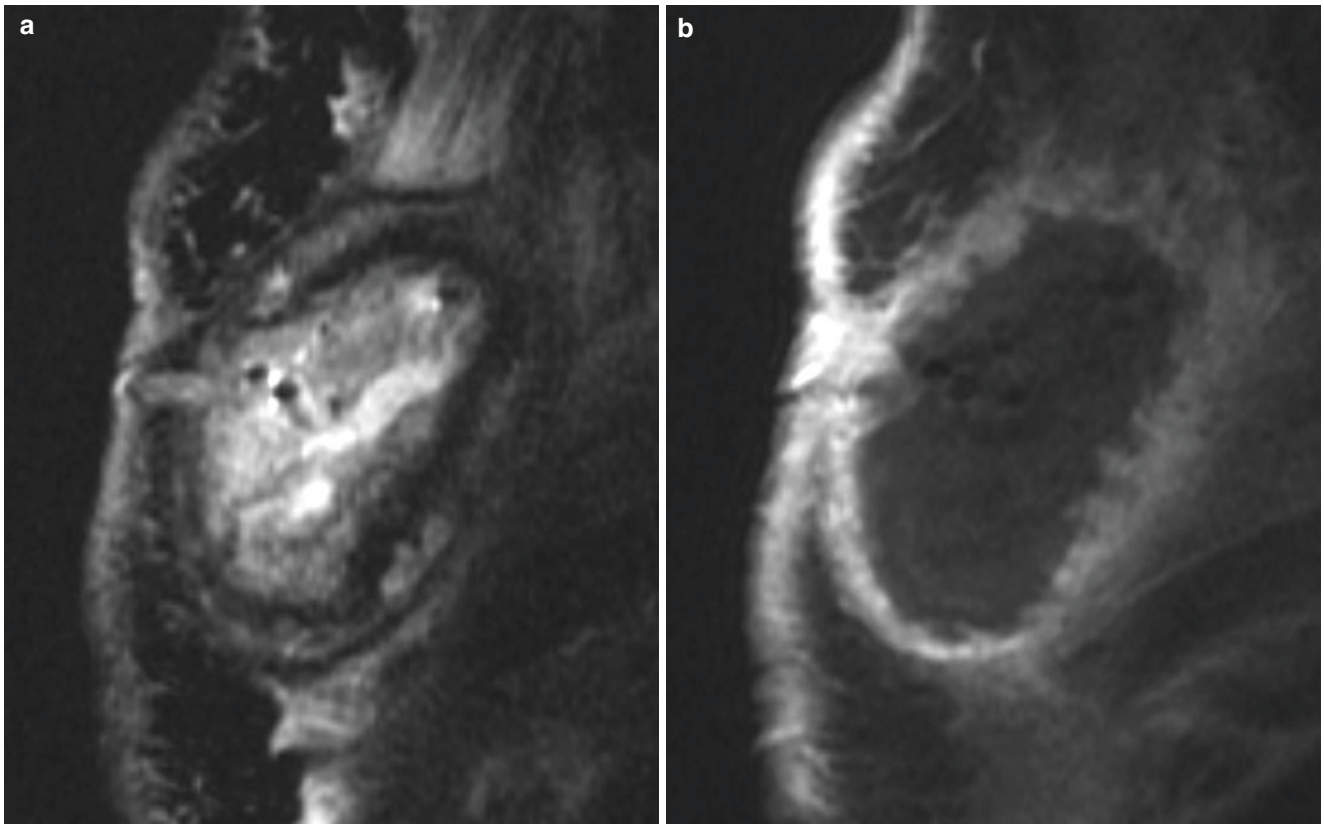

Fig. 2.34 (**a**) Selected sagittal T2-weighted fat-suppressed image of the right breast. (**b**) Corresponding sagittal T1-weighted post-contrast fat-suppressed image

2.12 Breast Abscess 2

Teaching Points Breast infection/abscess can result from unresolved local infection, iatrogenic in etiology, obstruction of the duct near the nipple, and acute, chronic or lactational mastitis. Depending on the water content of the collection, MR T2-weighted signal may vary but often is hyperintense. The overlying thickened skin may be intermediate or bright in signal depending on the degree of edema. Post-contrast T1-weighted images usually demonstrate a non-enhancing central, round, or irregular mass surrounded by an early, intensely enhancing rim. All these features are illustrated in this case.

Image Findings

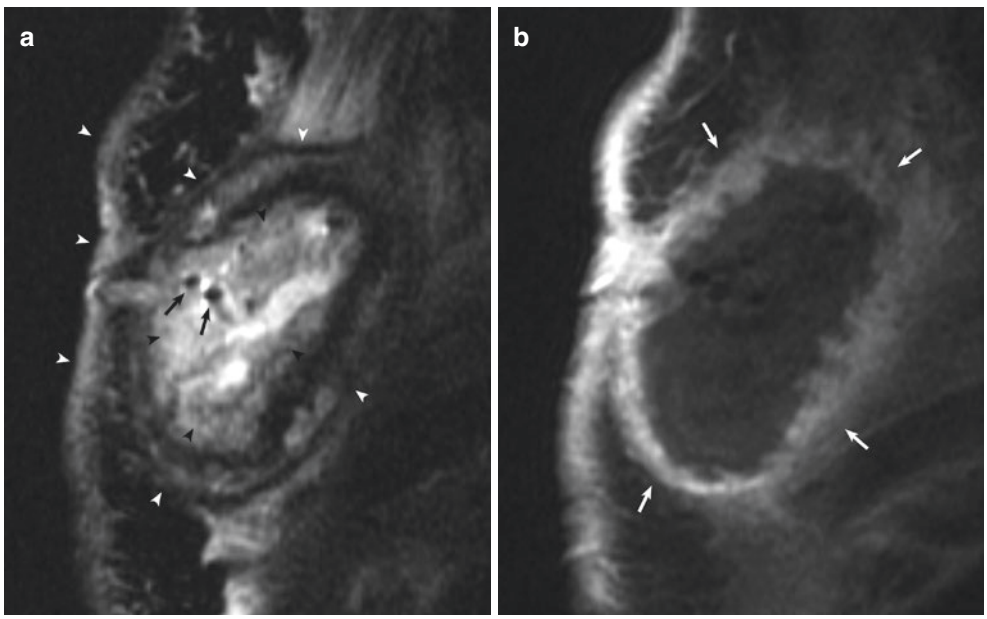

Fig. 2.35 Breast mastitis/abscess. (**a**) There is an irregular T2-weighted hyperintense collection (*black arrowheads*) with a thick heterogeneous signal rim (*white arrowheads*) and thickening and edema of the overlying skin (*white arrowhead*). Multiple punctate signal voids (*black arrows*) are present, reflecting gas bubbles. (**b**) Sagittal T1-weighted fat-suppressed post-contrast image demonstrates thick rim enhancement (*white arrows*)

2.13 History

36-year-old woman with a strong family history of breast cancer undergoing high-risk screening breast MRI (Figs. 2.36, 2.37, 2.38, and 2.39)

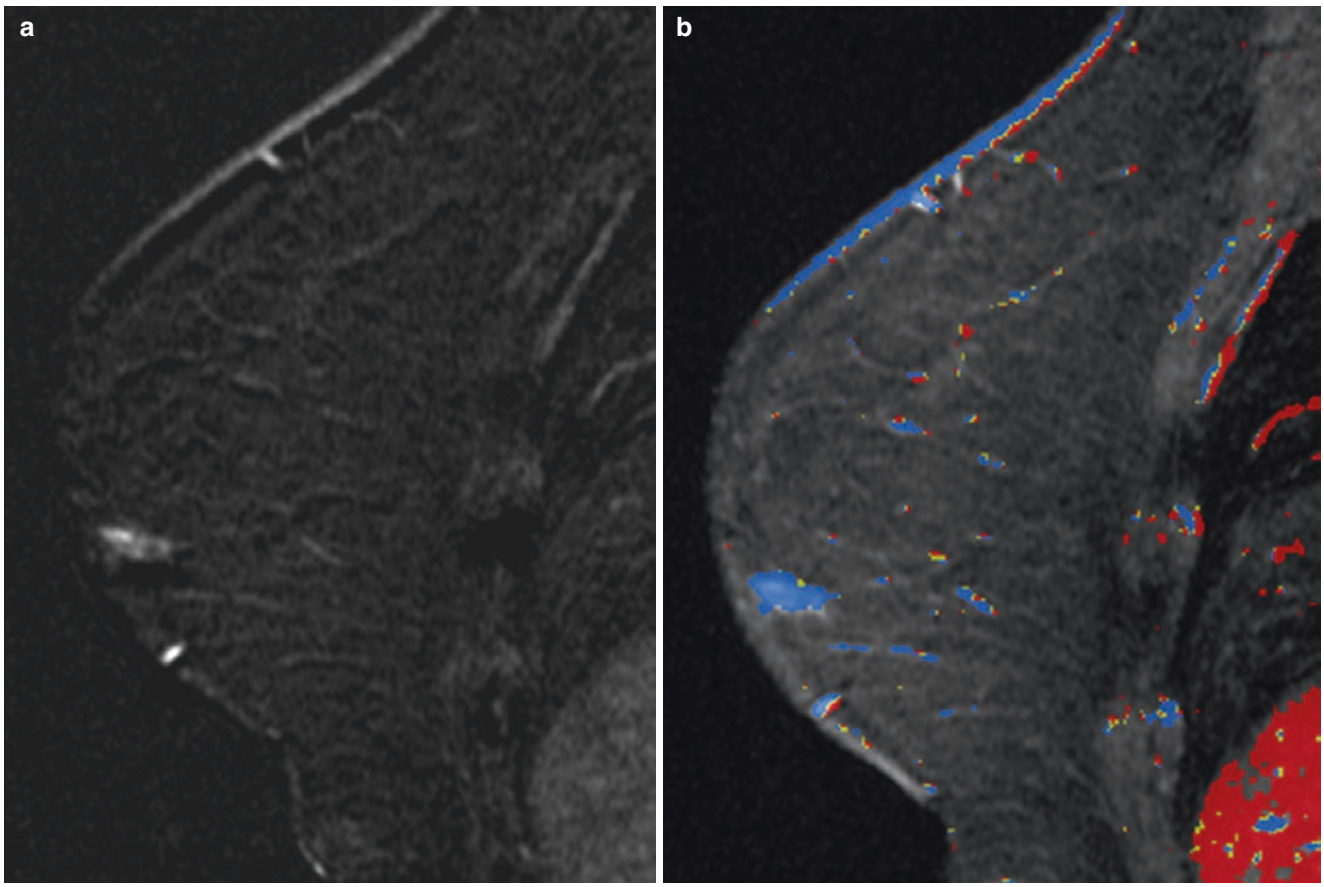

Fig. 2.36 (**a**) Sagittal post-contrast subtraction image of the left breast. (**b**) Corresponding sagittal T1-weighted fat-saturated post-contrast image with CAD kinetics analysis color overlay

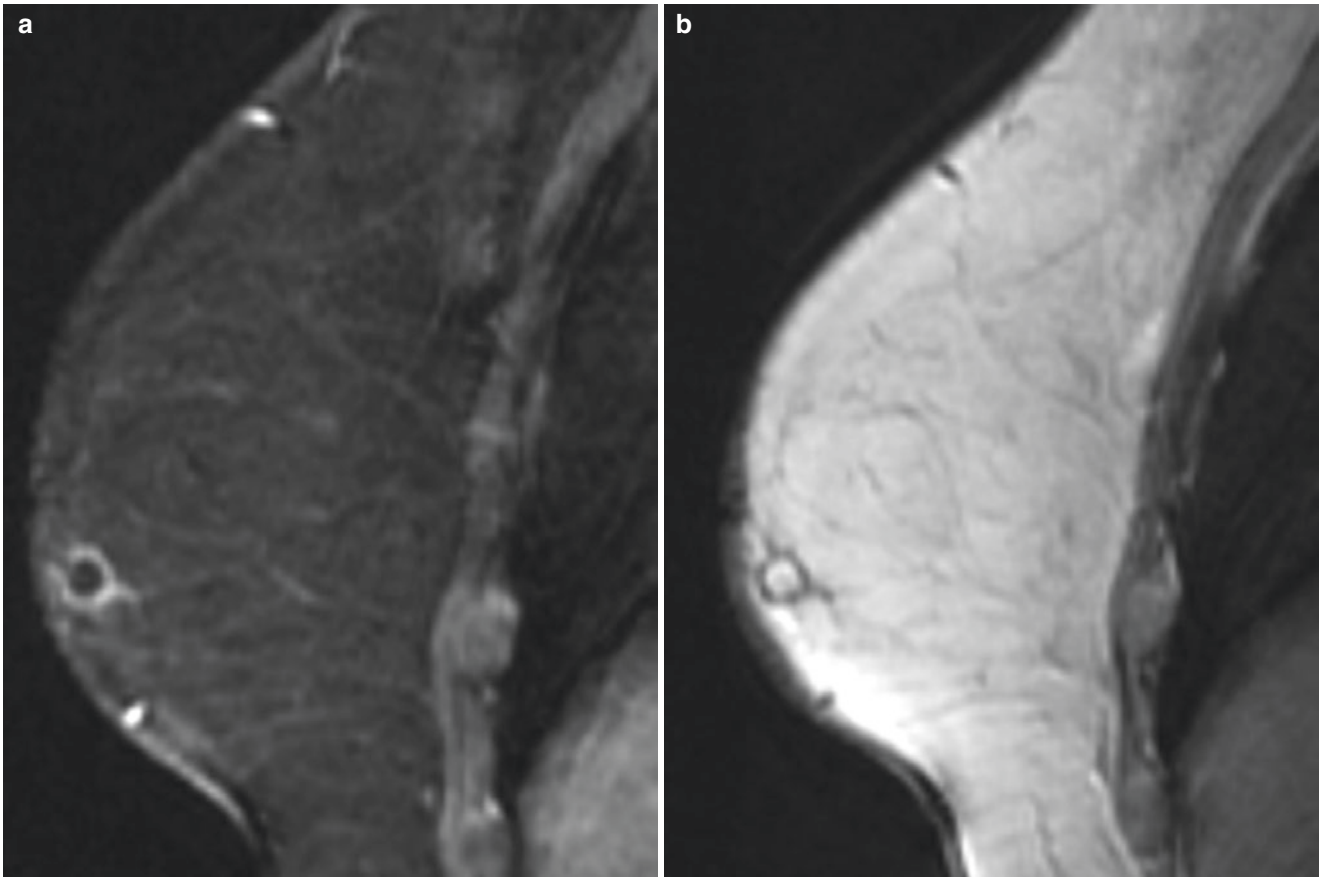

Fig. 2.37 Images from prior breast MRI performed at an outside institution provided for comparison. (**a**) Sagittal T1-weighted fat-saturated post-contrast image of the left breast. (**b**) Corresponding sagittal T1-weighted non–fat-saturated pre-contrast image

2.13 Fat Necrosis 1

Teaching Points Fat necrosis involves a cascade of cellular events starting with tissue injury resulting in liquefaction necrosis of fat cells, increased vascularization, and infiltration of fibroblasts, lymphocytes, and histiocytes. Subsequently, there is proliferation of foreign-body giant cells with fibrosis. Fat necrosis may be replaced with scar or persist as an oil cyst walled off by fibrous tissue. Fat necrosis of the breast is commonly seen secondary to breast procedures or surgery and may be palpable. Mammographically, oils cysts manifest as a thin rim of peripheral calcification creating the appearance of lucent "bubbles." Calcifications typically coarsen as fat necrosis evolves, but the imaging appearance of early fat necrosis and malignancy can overlap, with an ill-defined, spiculated, mass-like area and calcifications that mimic ductal carcinoma in situ (DCIS). Sonographically, the appearance of fat necrosis varies from a well-defined hypoechoic mass (likely representing an oil cyst) to an irregular hypoechoic mass. It is important to evaluate the sonographic images in the context of mammographic findings. On breast MRI, fat necrosis typically demonstrates peripheral enhancement surrounding central fat, best delineated on T1 non–fat-saturated images as illustrated in this case. The appearance of evolving fat necrosis can vary, however, and comparison with prior imaging and correlation with surgical history is important. When imaging features are indeterminate and clinical history is noncontributory, core biopsy is appropriate. Fat necrosis can be a benign concordant finding for most indeterminate MRI lesions and usually does not require surgical excision.

Image Findings

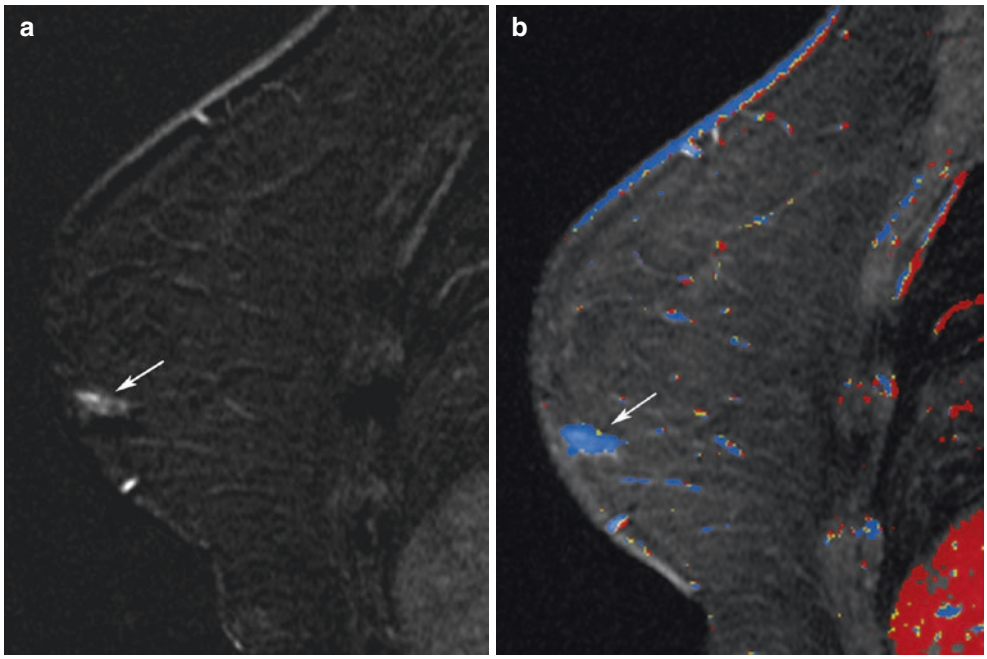

Fig. 2.38 Evolving fat necrosis. Sagittal post-contrast subtraction image (**a**) and corresponding CAD color overlay image (**b**) show 1.2 cm of linear nonmass enhancement in the retroareolar left breast, with a persistent delayed enhancement pattern color-coded as blue. The finding was considered indeterminate and second-look ultrasound and consideration of MRI-guided biopsy were recommended

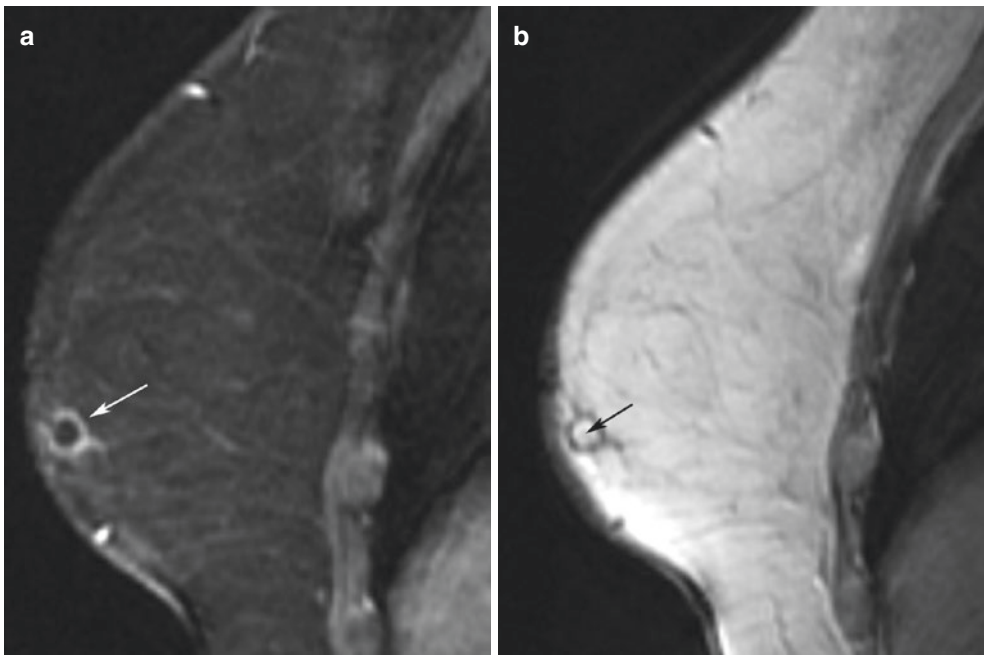

Fig. 2.39 Outside MRI images of the same region performed 12 months earlier demonstrate a round, rim-enhancing mass in the retroareolar left breast (**a**). On the T1-weighted non–fat-saturated image (**b**), central macroscopic fat is evident, consistent with benign fat necrosis. Final assessment was BI-RADS 2

2.14 History

Palpable right axillary lump in a patient with prior bilateral mastectomies and transverse rectus abdominis myocutaneous (TRAM) flap reconstructions (Figs. 2.40 and 2.41).

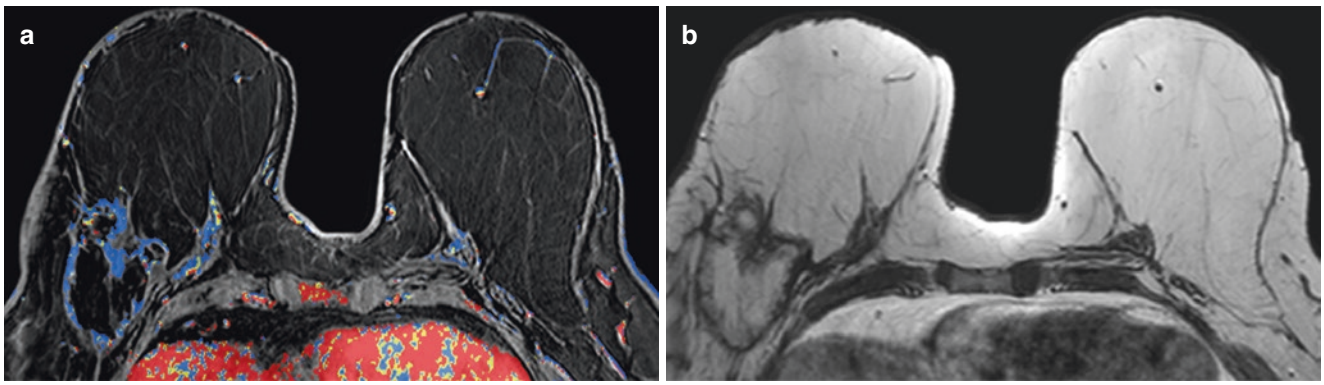

Fig. 2.40 (**a**) Axial T1-weighted fat-suppressed post-contrast image of lower reconstructed breasts with CAD kinetics analysis color overlay. (**b**) Corresponding axial T1-weighted non–fat-suppressed image

2.14 Fat Necrosis 2

Teaching Points Large areas of fat necrosis can present clinically as a palpable concern. A peripherally enhancing lesion with central macroscopic fat is consistent with benign fat necrosis. When these typical features are present, biopsy or short-term follow-up is not warranted. Large areas of fat necrosis are common in patients with extensive surgery such as breast reduction or mastectomies with TRAM flap reconstruction, as illustrated in this case.

Image Findings

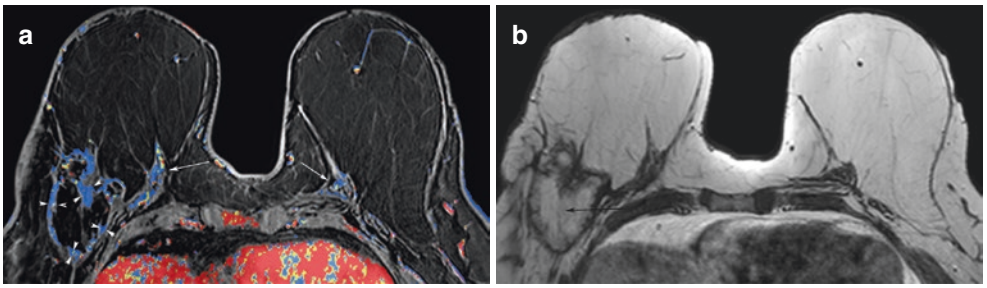

Fig. 2.41 Fat necrosis. (**a**) Axial T1-weighted fat-suppressed post-contrast image shows contiguous linear, heart-shaped enhancement (*arrowheads*) in the posterior lower outer breast with a persistent delayed enhancement pattern color-coded as blue. This area likely corresponds to the palpable concern. Enhancement of the TRAM (transverse rectus abdominis myocutaneous) flap's vascular pedicle is incidentally noted in the medial posterior reconstructed breast (*arrows*). (**b**) Corresponding axial T1-weighted non–fat-saturated image shows central focal fat within the heart-shaped rim of enhancement (*arrow*), consistent with benign fat necrosis

2.15 History

High-risk screening breast MRI. No history of trauma or breast procedures (Figs. 2.42, 2.43, 2.44, and 2.45).

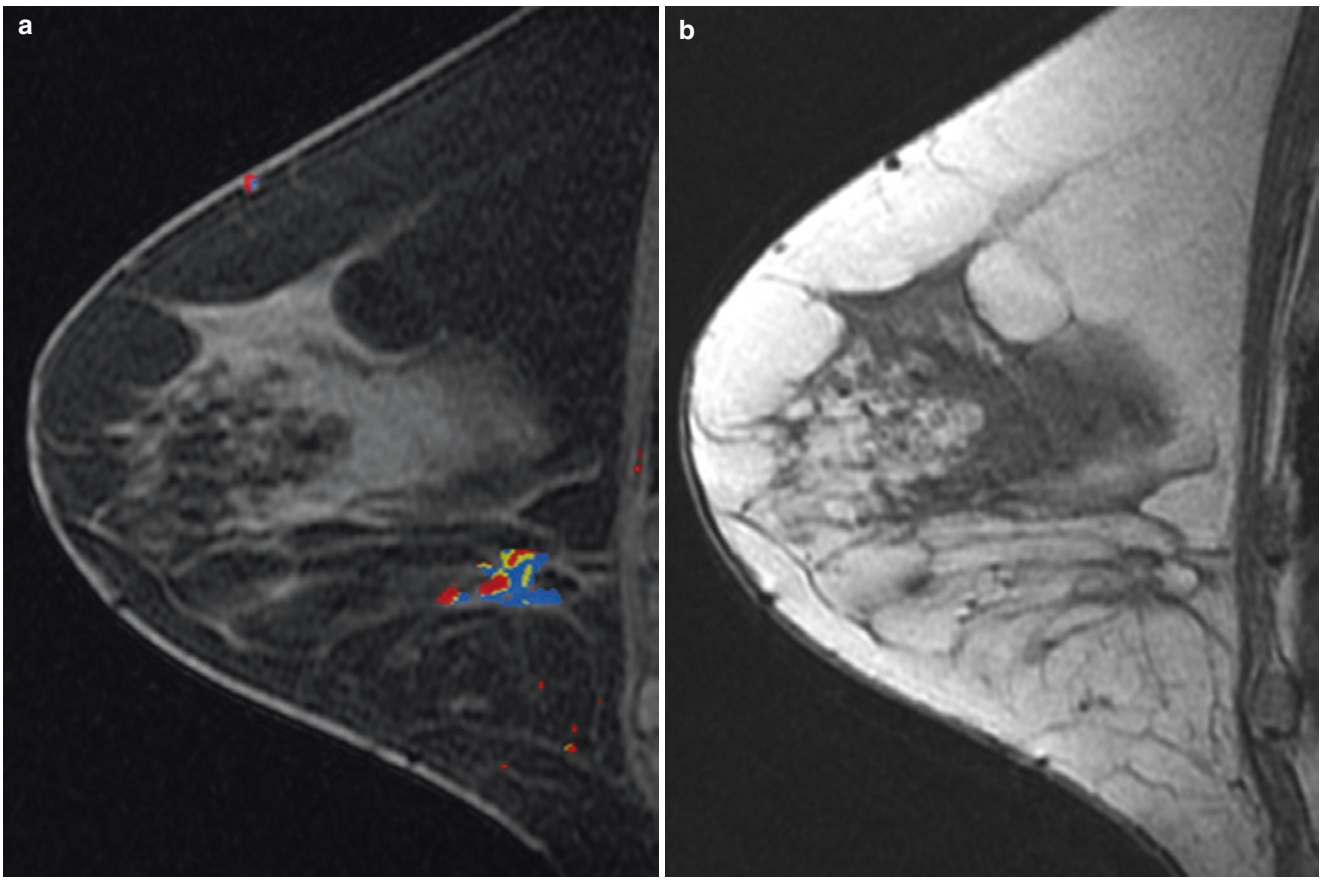

Fig. 2.42 (**a**) Sagittal T1-weighted fat-saturated post-contrast image of the left breast with CAD kinetics analysis color overlay. (**b**) Corresponding sagittal T1-weighted non–fat-saturated image

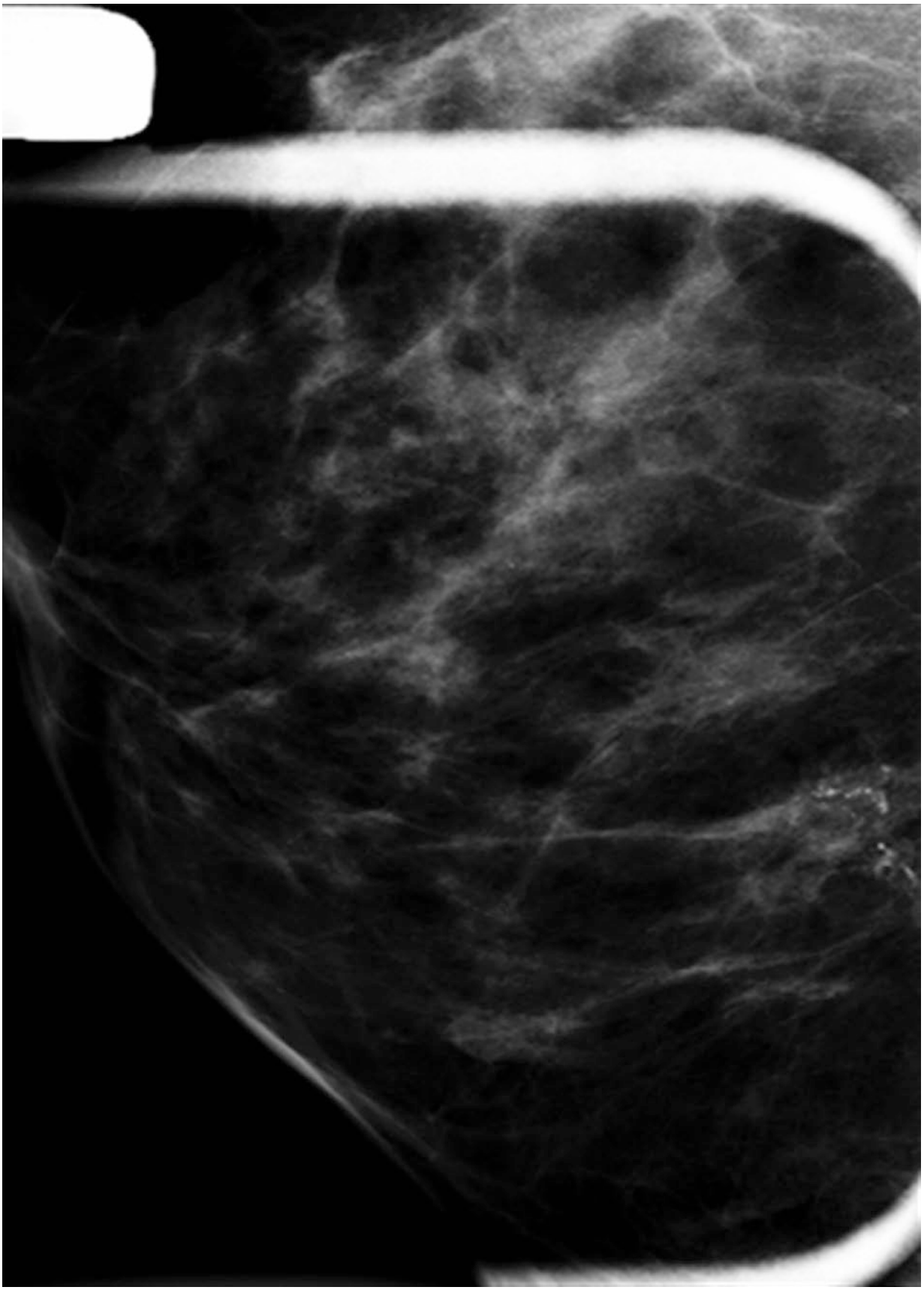

Fig. 2.43 Mediolateral (ML) mammographic magnification view of the left breast

2.15 Fat Necrosis 3

Teaching Points Because of asymmetric enhancement involving only the anterior aspect of the focal fat and suspicious mammographic calcifications, biopsy was recommended. The patient declined biopsy, and on subsequent breast MRIs there was a gradual decrease in enhancement consistent with benign fat necrosis. Not all patients with fat necrosis have a clinical history of trauma and all the typical imaging features, so when uncertain, core biopsy can be appropriate management.

Image Findings

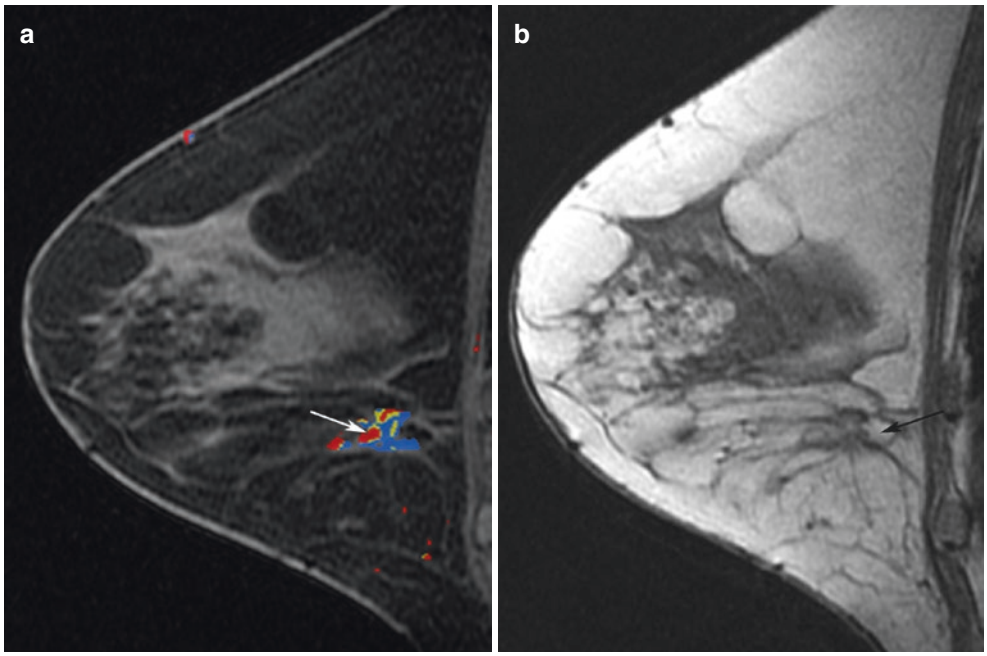

Fig. 2.44 (**a**) Sagittal T1-weighted fat-saturated post-contrast image shows a 1.5-cm area of irregular nonmass enhancement in the posterior lower outer left breast, which partially demonstrates a suspicious washout enhancement pattern (*arrow*). (**b**) Sagittal T1-weighted non–fat-saturated image shows adjacent focal fat (*arrow*) suggestive of fat necrosis

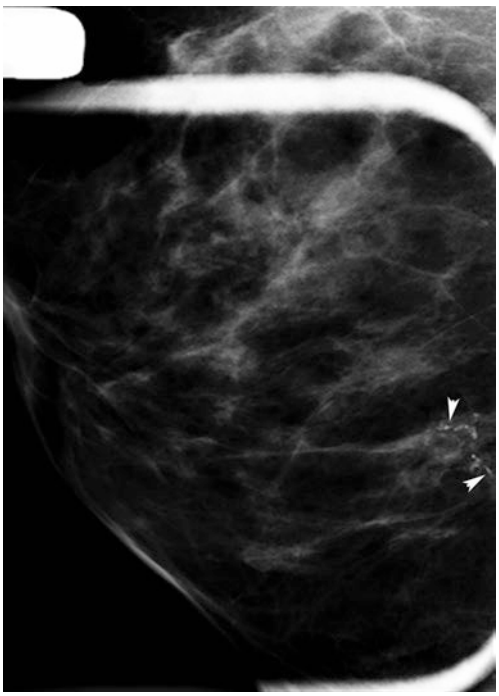

Fig. 2.45 Mammographic ML magnification view shows coarse heterogeneous calcifications correlating with the area of enhancement on MRI (*arrow heads*)

2.16 History

High-risk screening breast MRI due to family history. Patient reports motor vehicle accident 6 months prior with significant chest trauma (Figs. 2.46 and 2.47).

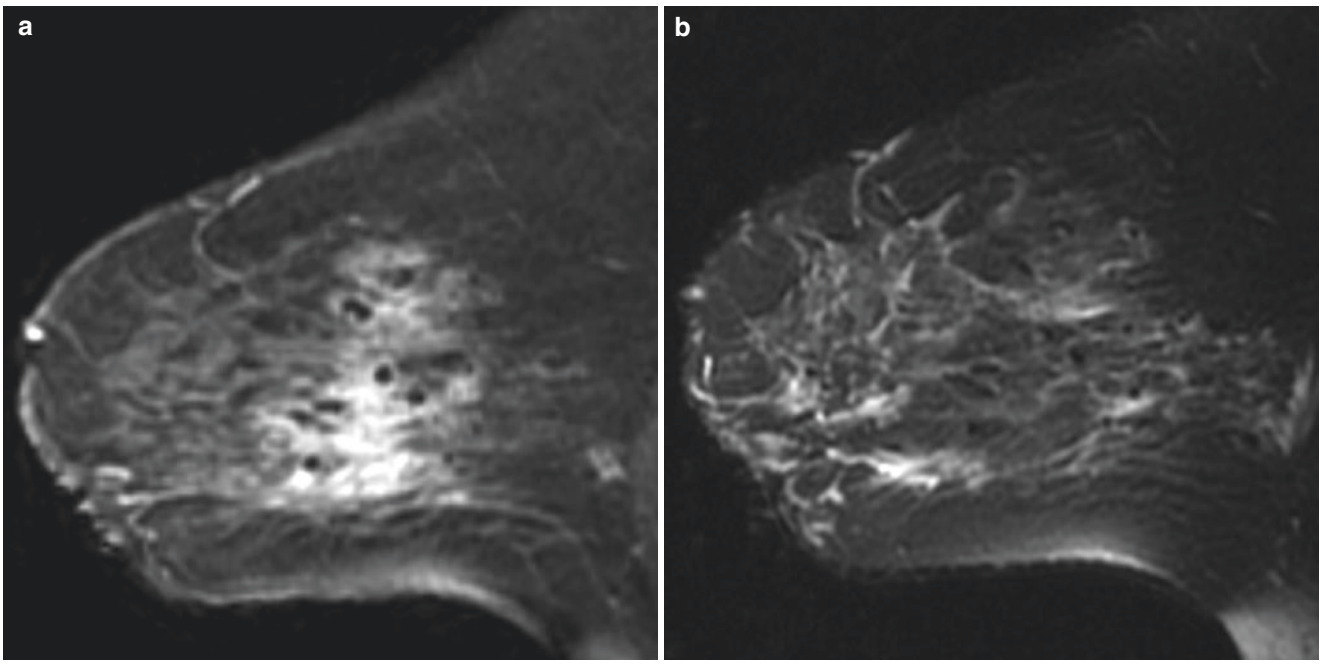

Fig. 2.46 (**a**) Sagittal T1-weighted fat-saturated post-contrast image of the right breast. (**b**) Corresponding sagittal T2-weighted fat-saturated image

2.16 Fat Necrosis 4

Teaching Points Fat necrosis has a variable appearance on MRI, and clinical history is important for correct diagnosis. The T1 dark and T2 dark foci in this case likely represent blood products containing hemosiderin. Calcifications can have a similar appearance on MRI but were not present on mammogram. The patient was managed conservatively with a short-term follow-up MRI, which showed a decrease in nonmass enhancement, likely indicating evolving fat necrosis with persistent dark foci.

Image Findings

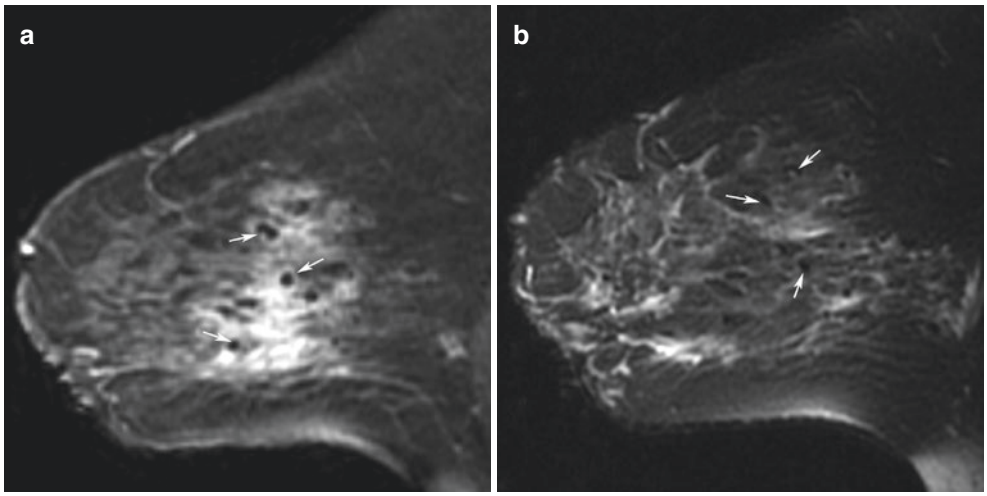

Fig. 2.47 Fat necrosis. (**a**) Sagittal T1-weighted fat-saturated post-contrast image shows intense nonmass enhancement involving the visualized parenchyma with several nonenhancing, scattered T1 dark foci (*arrows*) in the mid to posterior right breast. (**b**), Corresponding sagittal T2-weighted fat-saturated image shows that these foci (*arrows*) demonstrate marked T2 hypointensity. These dark foci persisted on non–fat-saturated images. A subsequent mammogram (*not shown*) showed no visible calcifications

2.17 History

34 year-old female, high-risk screening breast MRI (Figs. 2.48 and 2.49).

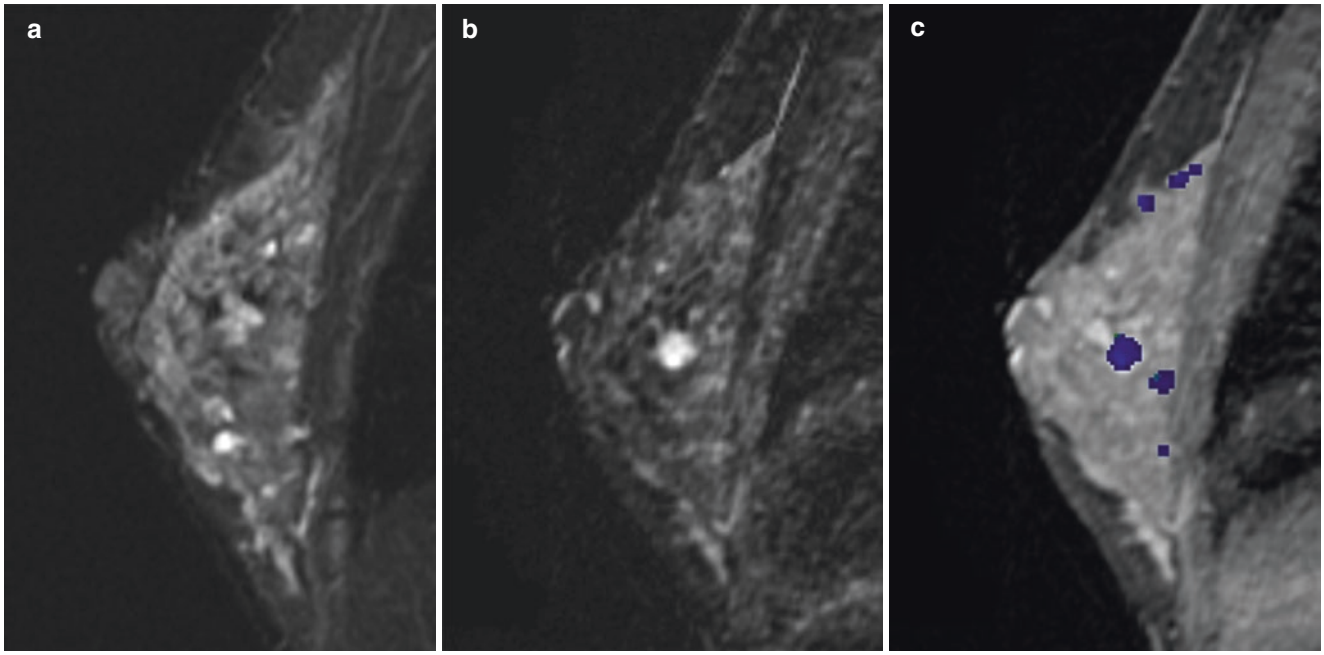

Fig. 2.48 Sagittal T2-weighted fat-saturated image (**a**), sagittal post-contrast subtraction image (**b**), and T1-weighted post-contrast image with CAD overlay (**c**)

2.17 Fibrocystic Change

Teaching Points Fibrocystic change (FCC) is a common benign condition, most often bilateral, that affects more than 50 % of women. Fibrocystic parenchyma, like normal parenchyma, has a variable imaging appearance dependent on the water and collagen content of the tissues. It may present as a discrete mass or an asymmetry mimicking tumor, in which case both mammography and sonography are considered unreliable. On breast MRI, fibrocystic change is usually difficult to distinguish from normal breast tissue on both T2-weighted and T1-weighted noncontrast images (Fig. 2.48). On dynamic contrast-enhanced images, however, it usually demonstrates scattered foci of regional enhancement with a progressive kinetic pattern (Fig. 2.49).

Image Findings

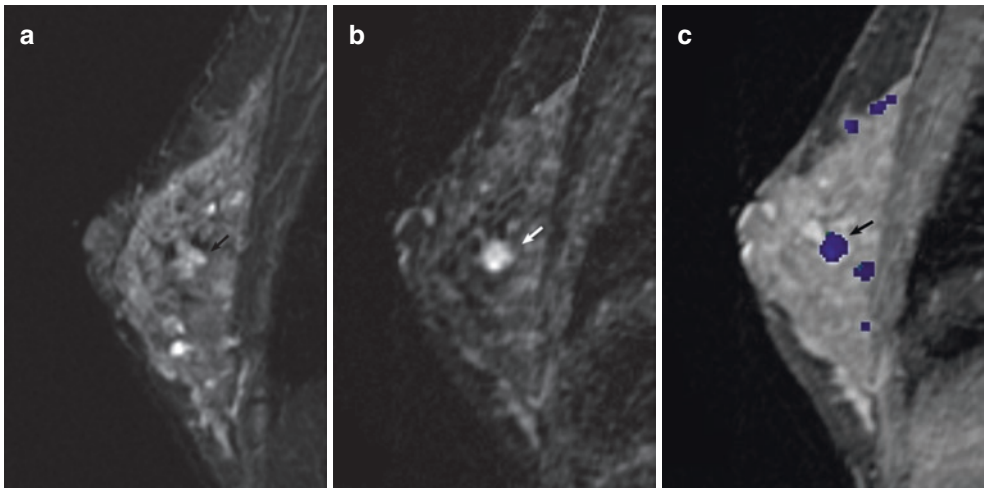

Fig. 2.49 Fibrocystic change. This sagittal T2-weighted fat-saturated image (**a**) and post-contrast subtraction image (**b**) demonstrate a mildly T2-hyperintense round mass (*arrows*) with progressive enhancement on CAD analysis (**c**). No sonographic correlate was identified, and subsequent MRI-guided core biopsy yielded fibrocystic change

2.18 History

36-year-old patient undergoing high-risk screening breast MRI (Figs. 2.50 and 2.51).

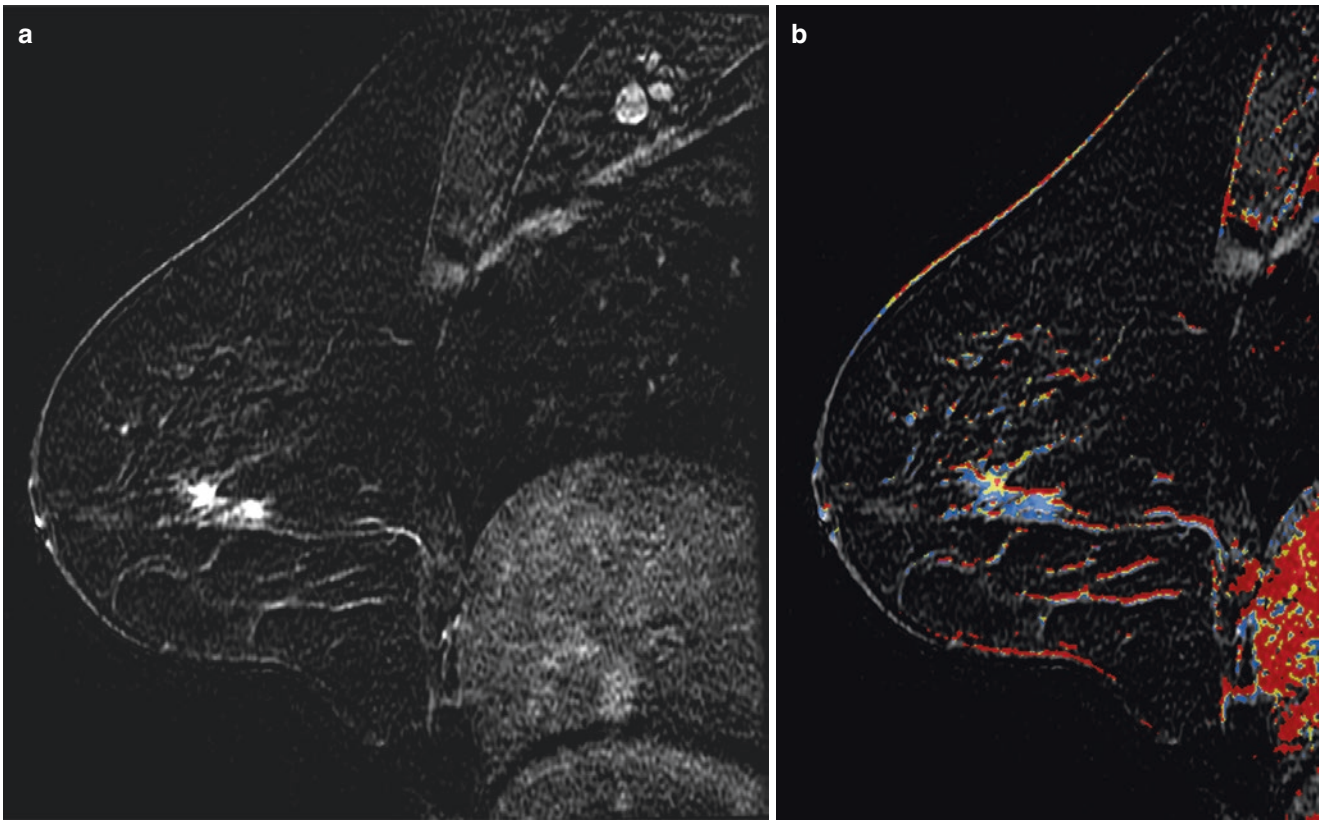

Fig. 2.50 Sagittal post-contrast subtraction images of the right breast without (**a**) and with (**b**) CAD color overlay

2.18 Stromal Fibrosis and Sclerosing Adenosis

Teaching Points Sclerosing adenosis (SA) and stromal fibrosis (SF) are benign entities known to mimic malignancy on clinical examination and radiologic imaging. SA is present in 12 % of benign surgical biopsies. It demonstrates increased numbers of distorted lobules usually accompanied by stromal fibrosis. Mammographically, SA typically presents as amorphous and pleomorphic calcifications, but it does not present distinctive features on contrast-enhanced MRI. Lesions may demonstrate ductal enhancement or a homogeneously enhancing oval or round mass with lobulated or angular margins showing rapid early enhancement and delayed persistent or washout kinetics.

SF, on the other hand, is defined as proliferation of fibrous tissue replacing normal connective tissue and causing obliteration and atrophy of mammary ducts and lobules. SF has a more variable mammographic and sonographic appearance. The most prevalent MRI features are round or oval shape, irregular or spiculated margins, rapid or medium rate of initial contrast uptake, and plateau or washout curves.

No further treatment is required for either diagnosis if the pathology is concordant with the imaging findings.

Image Findings

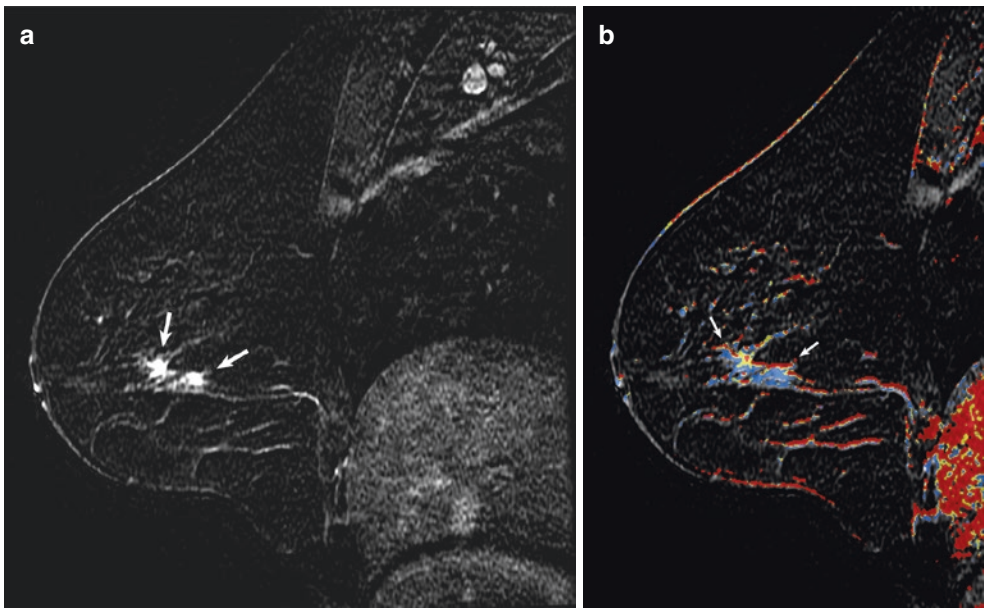

Fig. 2.51 Sclerosing adenosis and stromal fibrosis. Sagittal post-contrast subtraction images without (**a**) and with (**b**) CAD color overlay demonstrate two irregular masses (*arrows*) in the central right breast with mixed enhancement kinetics. No sonographic correlate was identified

2.19 History

A 39-year-old woman undergoing high-risk screening breast MRI (Figs. 2.52, 2.53, 2.54 and 2.55).

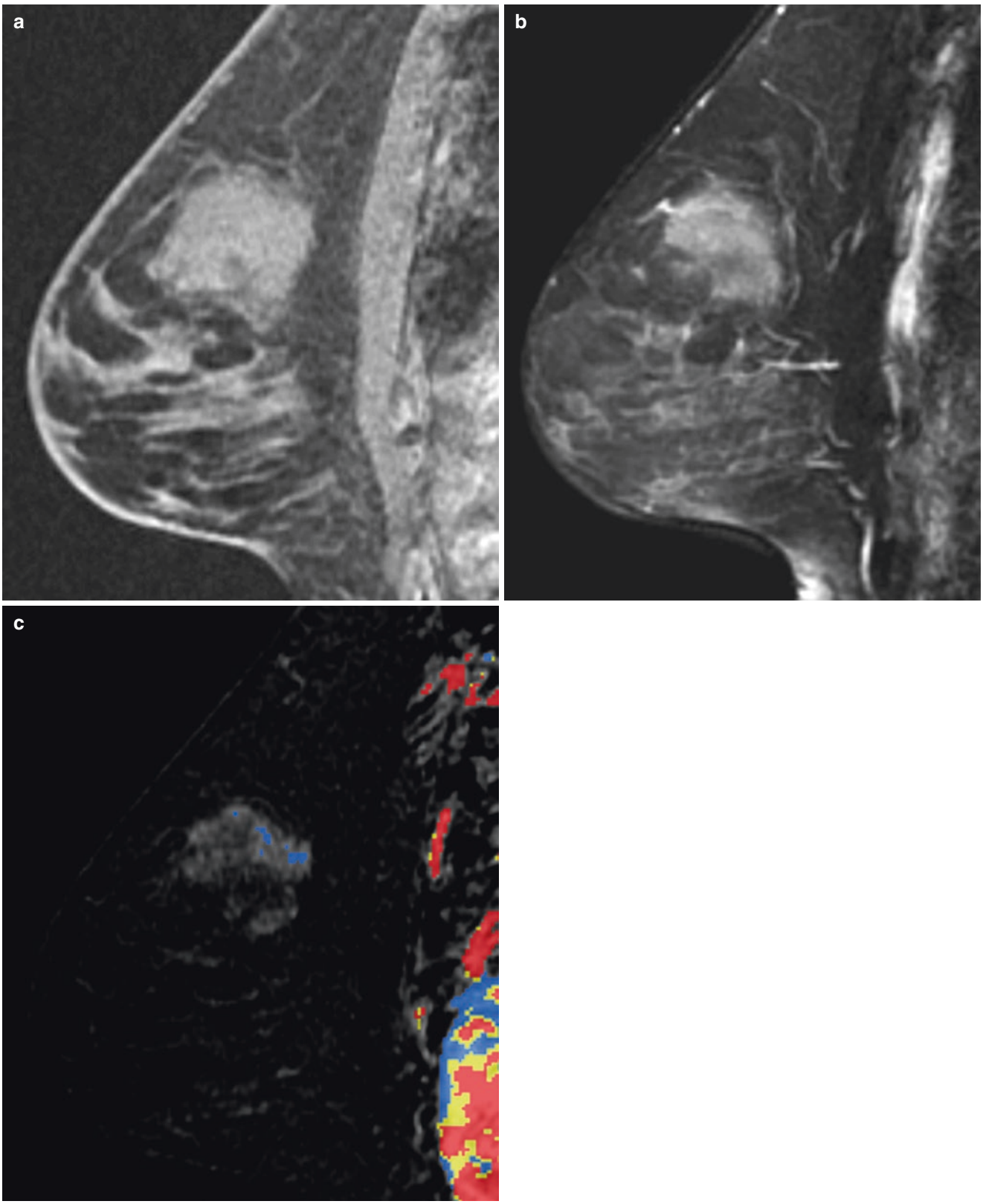

Fig. 2.52 (**a**) Sagittal T1-weighted fat-saturated image of the left breast. (**b**) Corresponding sagittal T2-weighted fat-saturated image. (**c**) Corresponding sagittal post-contrast subtraction image with CAD kinetics analysis color overlay

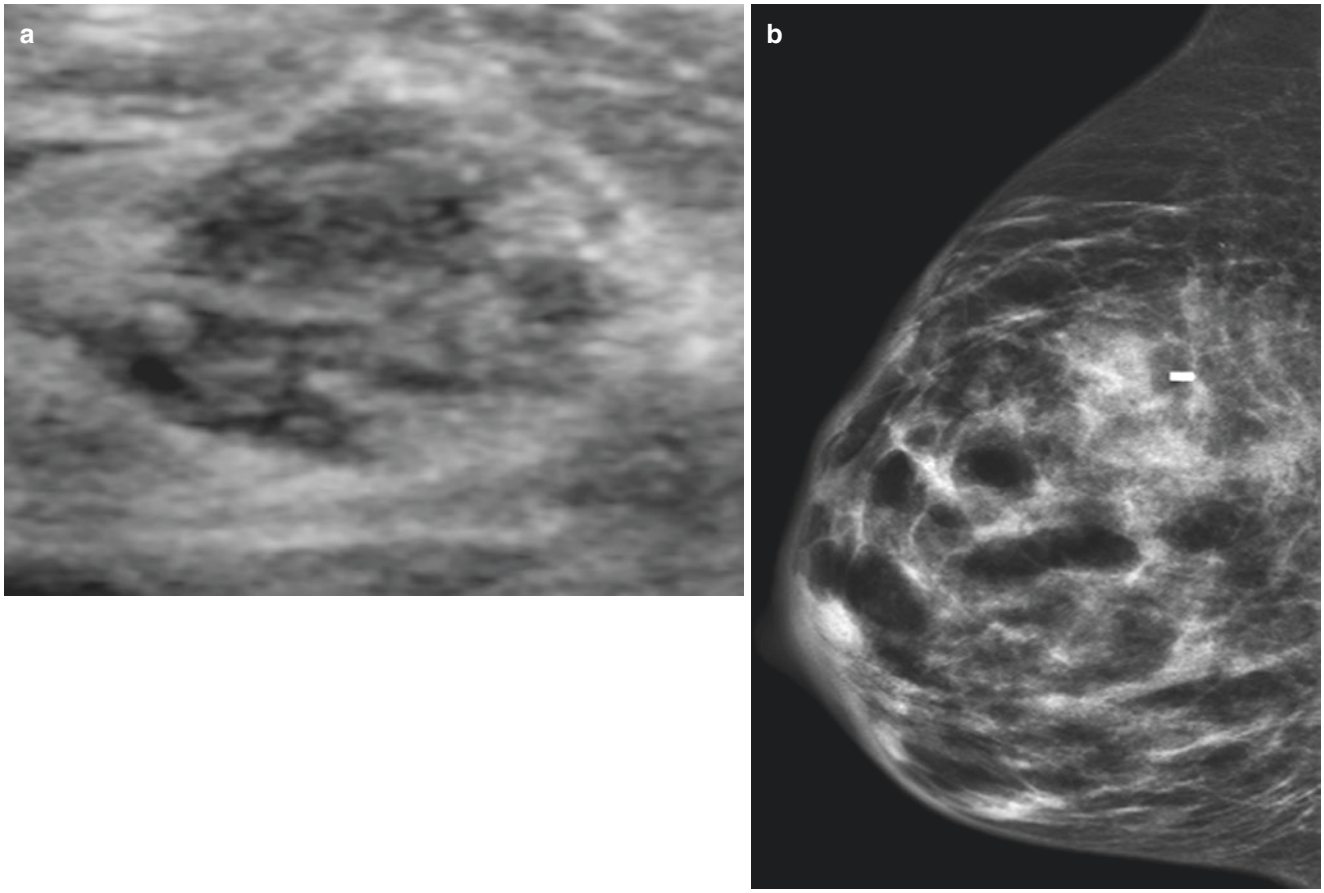

Fig. 2.53 (**a**) Second-look ultrasound image targeted to the MRI finding. (**b**) Lateromedial (LM) view from a post-biopsy left mammogram

2.19 Pseudoangiomatous Stromal Hyperplasia

Teaching Points Pseudoangiomatous stromal hyperplasia (PASH), a benign form of stromal (mesenchymal) overgrowth within breast tissue, typically affects women of reproductive age. Clinically, PASH can present as a palpable concern. On histology, it is characterized by the presence of open, slit-like spaces in dense collagenous stroma that are lined by a discontinuous layer of flat, spindle-shaped myofibroblasts with bland nuclei and contain complex, anastomosing spaces that may be confused with an angiosarcoma. PASH can be a focal microscopic incidental finding at breast biopsy, or it can be nodular (tumor-like). Mammographically, it commonly presents as a noncalcified, circumscribed or partially circumscribed mass. Asymmetric breast tissue or no imaging correlate has also been reported in cases of PASH. Sonographically, it commonly presents as a circumscribed, oval, hypoechoic mass, sometimes with a cystic component. Less commonly, ultrasound demonstrates a heterogeneously echogenic area with irregular or poorly defined borders, as illustrated in this case. On MRI, it has variable T1 and T2 signal intensity; both mass and nonmass enhancement have been reported, with persistent to plateau delayed enhancement pattern. Nodular PASH can grow over time, but it is not associated with malignancy and is not considered a premalignant lesion. Surgical excision is recommended only in discordant cases.

Image Findings

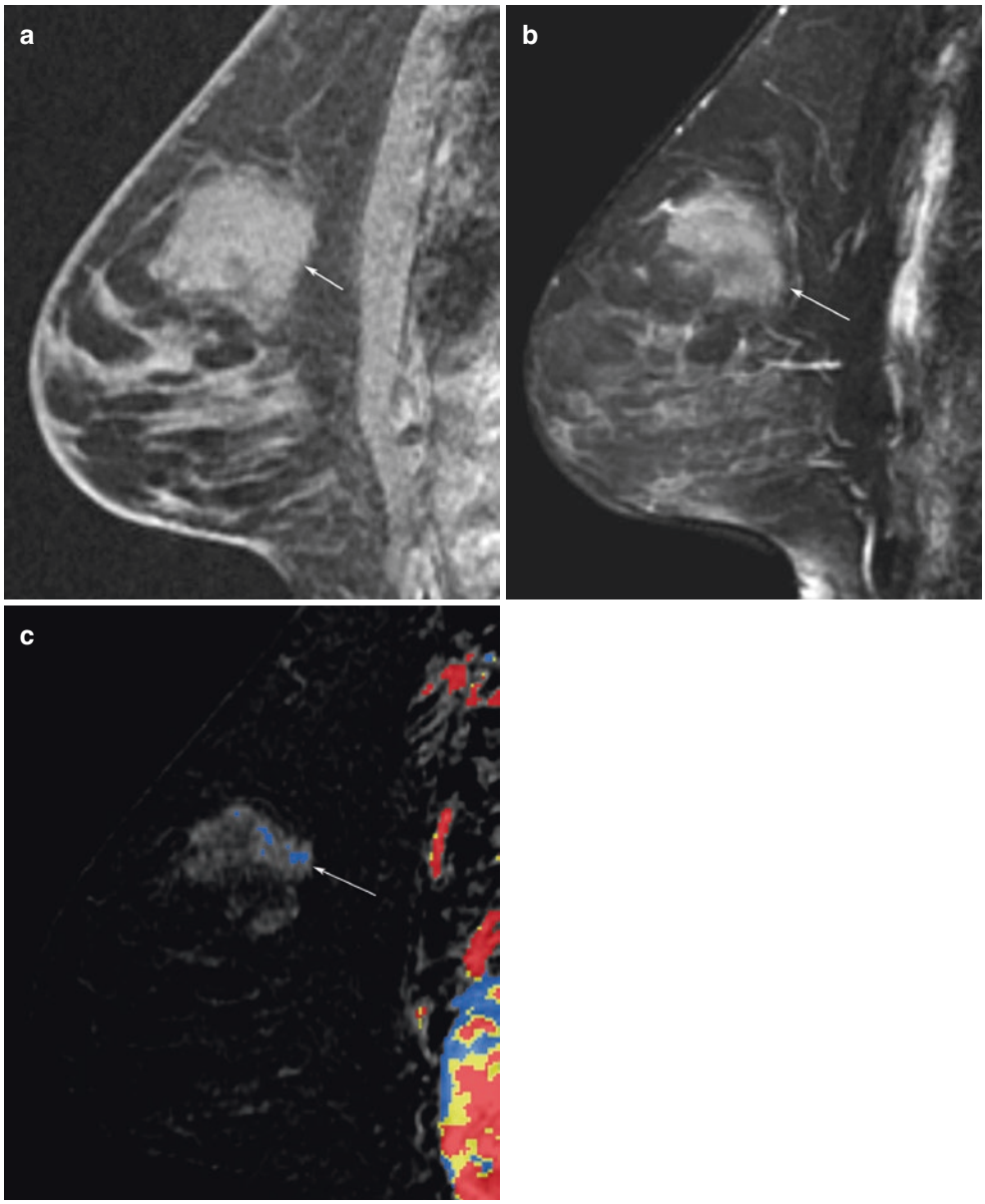

Fig. 2.54 Pseudoangiomatous stromal hyperplasia (PASH). Sagittal T1-weighted fat-saturated pre-contrast (**a**) and post-contrast (**b**) subtracted images demonstrate a 3.8-cm T1-hypointense and mildly T2-hyperintense irregular mass (*arrows*) in the upper, slightly outer, mid to posterior left breast. (**c**) The mass demonstrates mild enhancement with a persistent delayed enhancement pattern color-coded as blue (*arrow*) on the CAD color overlay

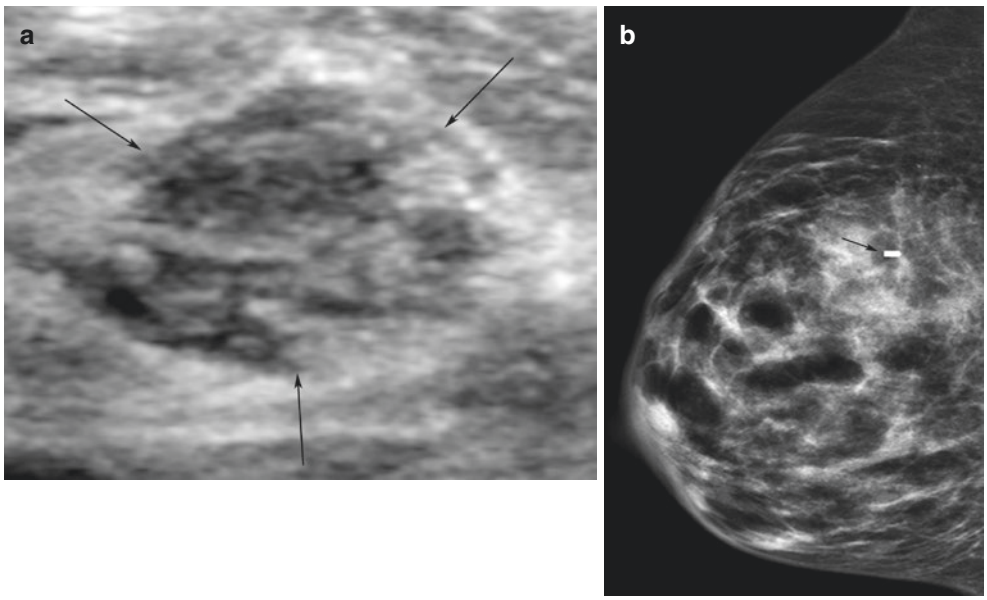

Fig. 2.55 (**a**) Targeted ultrasound of the left breast reveals a corresponding 3.5-cm mixed echogenic mass with indistinct borders (*arrows*). (**b**) The mass underwent ultrasound guided core biopsy yielding PASH. The post-biopsy mammogram shows a large, low-density mass in the upper outer left breast, with a centrally placed biopsy clip (*arrow*) corresponding to the sonographic and MRI masses

2.20 History

A 46-year-old woman with a palpable right breast lump and a negative mammographic and sonographic workup. MRI was performed for further evaluation (Figs. 2.57 and 2.58).

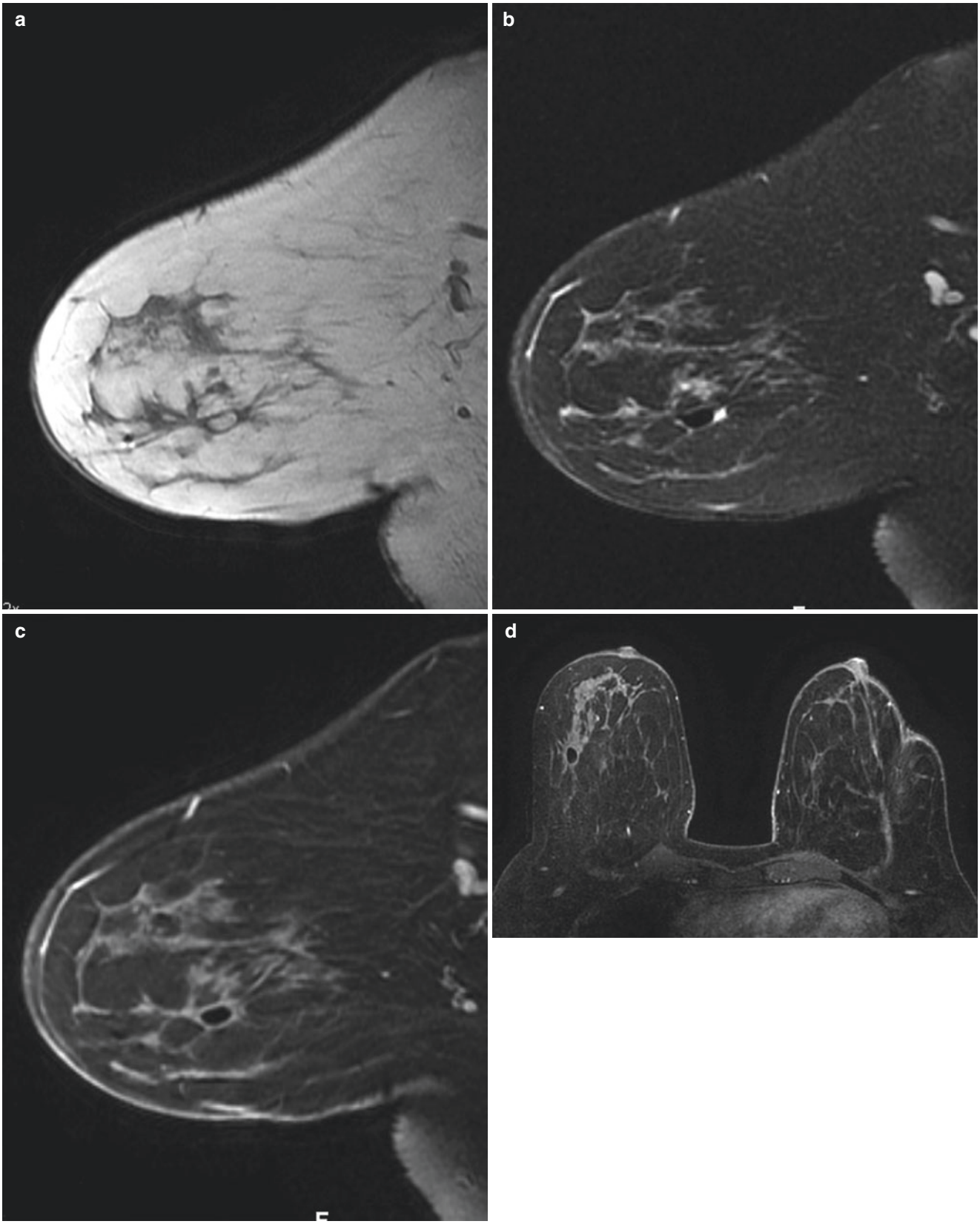

Fig. 2.56 Sagittal T1-weighted image (**a**), sagittal T2-weighted fat-suppressed image (**b**), and sagittal T1-weighted fat-suppressed post-contrast image (**c**) of the right breast. (**d**) Axial T1-weighted fat-suppressed post-contrast image of both breasts

2.20 Lipoma

Teaching Points Lipomas, one of the most common mesenchymal tumors, closely resemble fat and can occur in almost any part of the body. In addition to fat, lipomas may contain internal fibrous connective tissue. Lipomas are benign encapsulated masses occurring in 2.1 per 100 people. Clinically, lipomas are usually small and asymptomatic, but they may be large enough to present as a clinical mass or cause breast asymmetry and enlargement. Diagnostic dilemmas can arise, as lipomas may be difficult to appreciate in fatty breast tissue. Lipomas will typically be radiolucent on radiography and mammography, hyperechoic on ultrasound, and show fat attenuation on CT scans. On MRI, lipomas will mirror the signal intensity of fat on all pulse sequences and will not contrast enhance except for the surrounding fibrous capsule, as illustrated in this case.

Image Findings

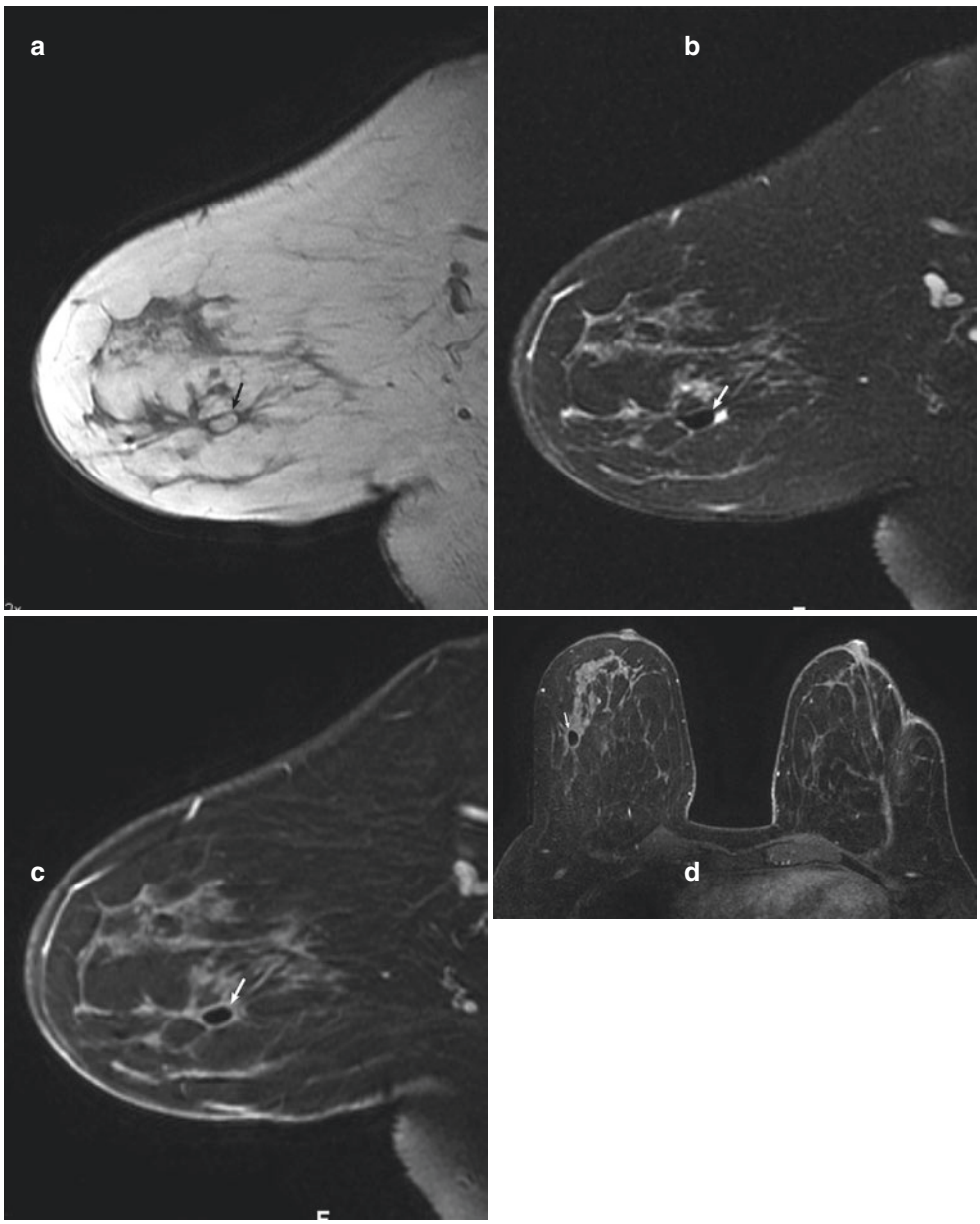

Fig. 2.57 (**a**) Sagittal T1-weighted image of the right breast shows an oval circumscribed mass (*arrow*) that is isointense to fat. The fat-suppressed images—the sagittal T2-weighted fat-suppressed image (**b**) and sagittal T1-weighted fat-suppressed post-contrast image (**c**)—and the axial T1-weighted fat-suppressed post-contrast image (**d**) all show the mass to be hypointense to the breast fat (*arrows*). Post-contrast images (**c**, **d**) show it to be nonenhancing. Post-lumpectomy changes are incidentally noted in the left breast

2.21 History

A 32-year-old woman undergoing high-risk screening breast MRI (Figs. 2.59, 2.60, and 2.61).

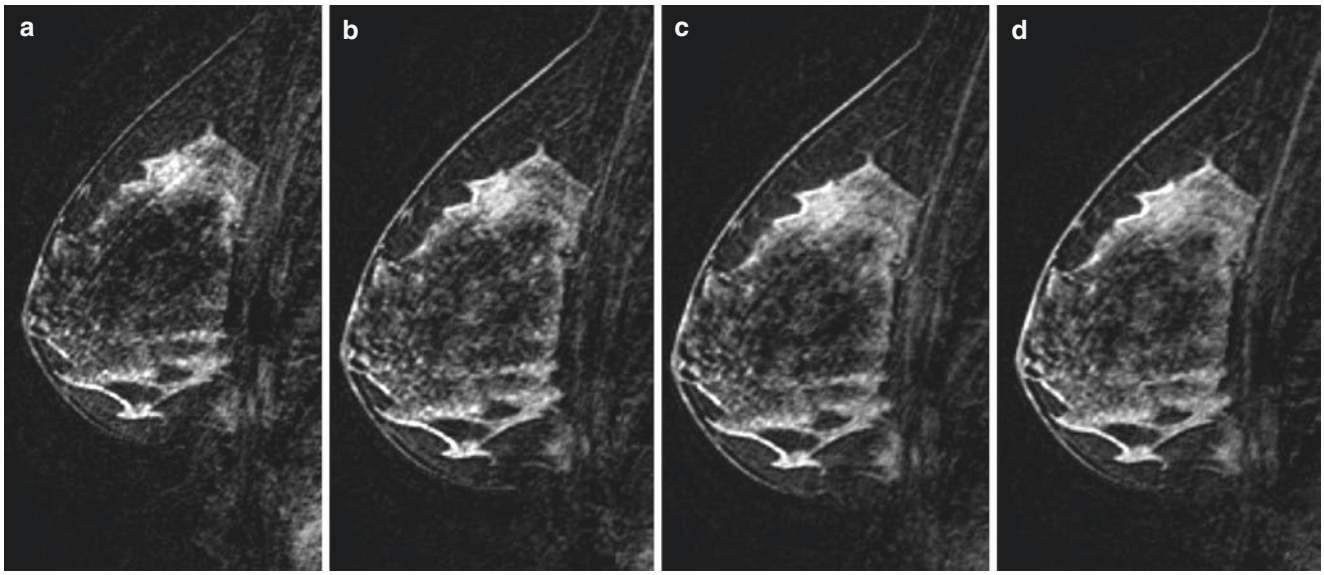

Fig. 2.58 (**a**–**d**) Sagittal post-contrast subtraction images of the right breast from early to late phases of enhancement

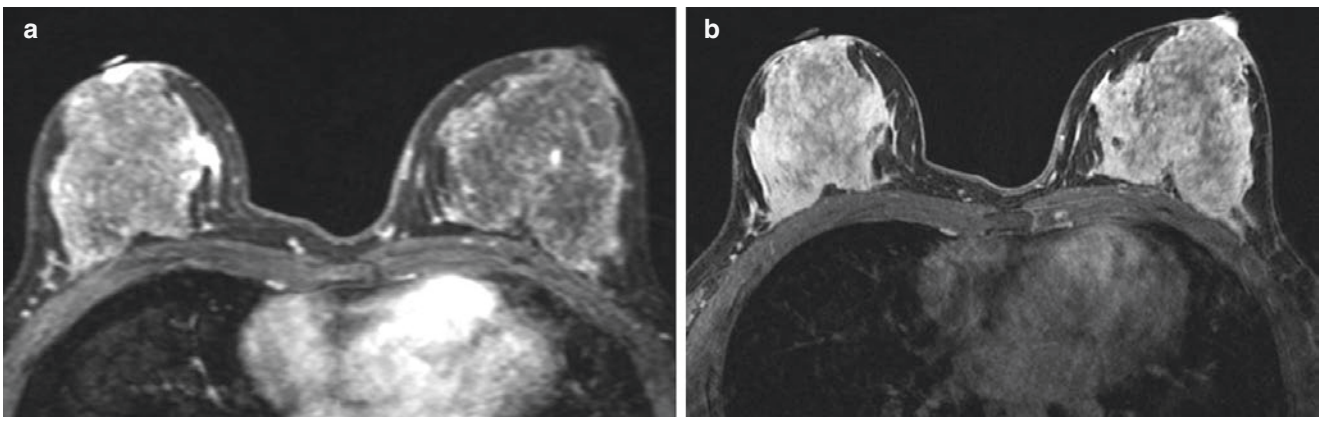

Fig. 2.59 Axial T1-weighted fat-saturated post-contrast images in early (**a**) and delayed (**b**) phases of enhancement

2.21 "Picture Frame" Background Parenchymal Enhancement

Teaching Points "Picture frame" enhancement is a type of background parenchymal enhancement (BPE) with preferential early enhancement of peripheral breast tissue with progressive centripetal and anterior enhancement. The term "vascular inflow" is also used because this variable enhancement of the breast parenchyma spatially and temporally is due to the breast's arterial supply entering peripherally through branches and perforators of the internal thoracic artery, thoracoacromial artery, lateral thoracic artery, and intercostal arteries. Individual variation in anatomy and cardiovascular status introduce further variation in this enhancement pattern. "Picture frame" enhancement is often appreciated on the earliest contrast images at the superior and inferior periphery of the breast on sagittal images or at the medial, lateral, and posterior peripheral aspects of the breast on axial images.

The fifth edition of the American College of Radiology BI-RADS (Breast Imaging Reporting and Data System) Atlas recommends that the amount of BPE should be categorized in the MRI report as "minimal," "mild," "moderate," or "marked" to describe its volume and intensity. A note should also be made of symmetry or asymmetry. The authors acknowledge variations in distribution and morphology of BPE, but they defer recommending description of these until more data become available. Research into the association of BPE with breast cancer risk or the effect of BPE on the performance of MRI has generally focused on the amount of BPE rather than its morphology or pattern. Any such additional reporting of the pattern of enhancement is considered optional.

Enhancement that is clearly ascribable to BPE based on the symmetry of the enhancement and the pattern of distribution, such as the "picture frame" enhancement in this case, may be considered benign.

Image Findings

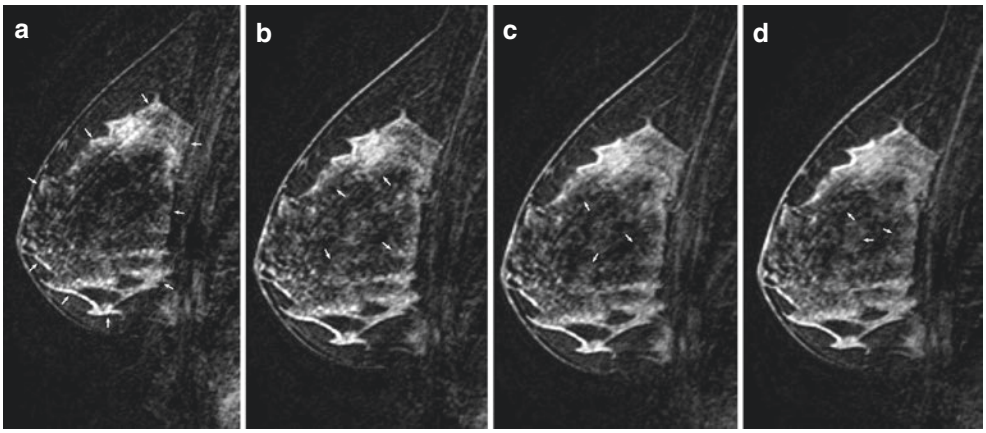

Fig. 2.60 Benign background parenchymal enhancement: "picture frame" variant. (**a**–**d**) Sagittal post-contrast subtraction images from early to delayed phases of enhancement demonstrate progressive centripetal enhancement (*arrows*) of the breast tissue from the periphery to the center

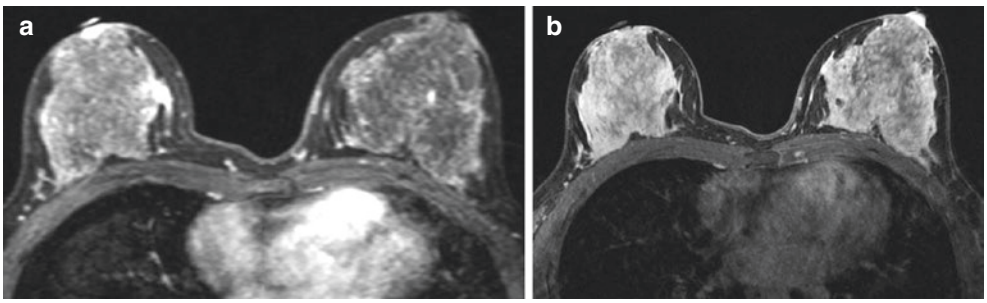

Fig. 2.61 Axial T1-weighted fat-saturated post-contrast images during the early (**a**) and delayed (**b**) phases of enhancement demonstrate progressive centripetal enhancement

2.22 History

29-year-old female undergoing high-risk screening breast MRI (Figs. 2.59, 2.60, 2.61, and 2.62).

2.22 Regional Background Parenchymal Enhancement

Teaching Points The fifth edition of the ACR BI-RADS (Breast Imaging Reporting and Data System) Atlas recommends that the amount of BPE be categorized in the MRI report as "minimal," "mild," "moderate," and "marked" to describe the volume and intensity of the BPE. A note should also be made about symmetry or asymmetry. This case illustrates BPE asymmetrically involving the lower breast. The authors acknowledge variations in distribution and morphology of BPE but they defer recommending description of these until more data become available. Research into the association of BPE with breast cancer risk or the effect of BPE on the performance of MRI has generally focused on the amount of BPE rather than morphology or BPE pattern. Any such additional reporting of the pattern of enhancement is considered optional.

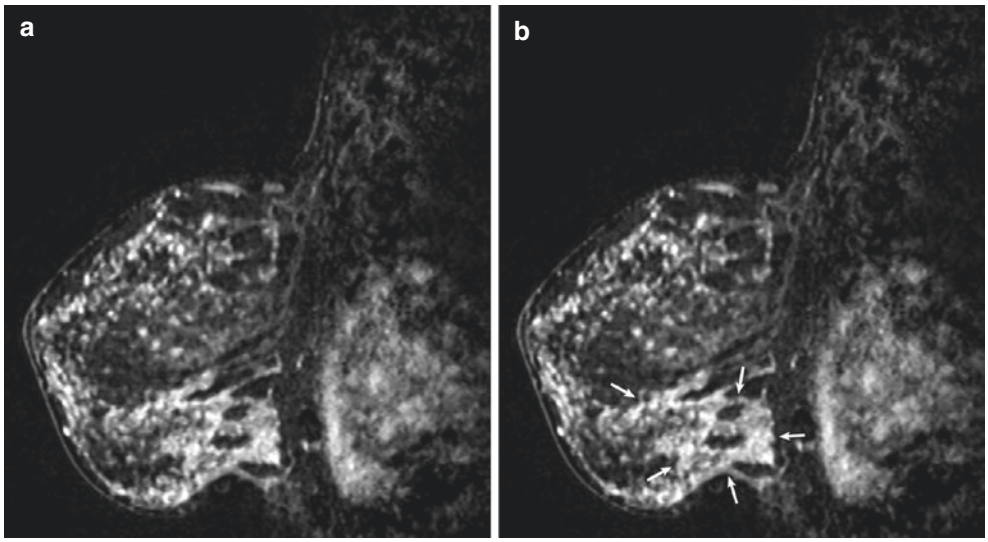

Fig. 2.62 (**a**) Selected sagittal T1-weighted post-contrast fat-saturated image. (**b**) Asymmetric geographic regions of background parenchymal enhancement. Selected sagittal image of the left breast demonstrate large area of non–mass enhancement involving the lower breast (*arrows*), likely representing asymmetric background parenchymal enhancement

2.23 History

22-year-old woman undergoing high-risk screening MRI (Figs. 2.64 and 2.65).

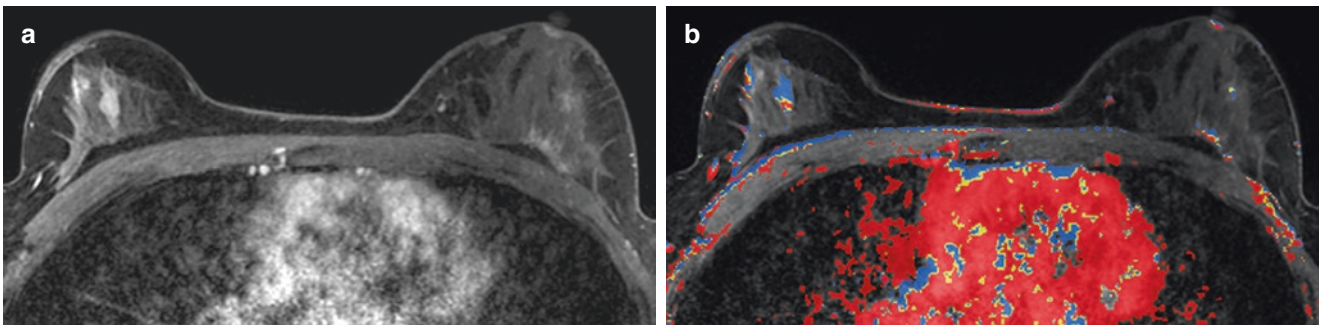

Fig. 2.63 (**a**) Selected axial T1-weighted post-contrast fat-saturated image of both breasts. (**b**) Corresponding CAD enhancement kinetics image

2.23 Focal Background Parenchymal Enhancement

Teaching Points When BPE is present symmetrically involving both breasts, it is unlikely that the enhancement pattern will lead to a false-positive imaging interpretation. However, when BPE is more focal or asymmetric in distribution, it has been associated with a higher likelihood of a BI-RADS 3 assessment with recommendation for short-interval follow-up. If the enhancement pattern is interpreted as focal NME or mass enhancement rather than as BPE, then further evaluation is necessary with a biopsy. Transient focal areas of BPE have been reported to be a major factor in the cancellation of MR-guided biopsy, as illustrated in this case.

Image Findings

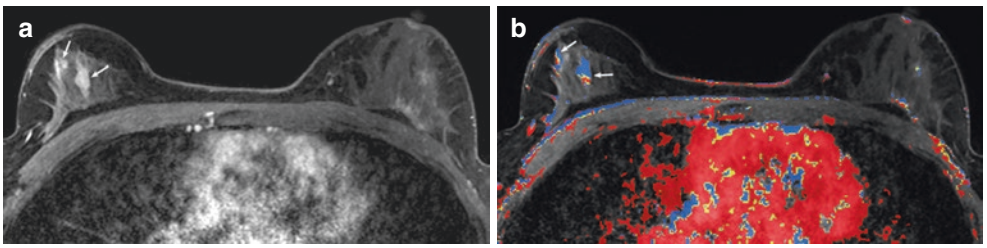

Fig. 2.64 Focal areas of background parenchymal enhancement in the right breast. (**a**) Axial image demonstrates two focal areas of enhancement involving the central and retroareolar right breast (*arrows*). (**b**) The CAD analysis shows the partly washout kinetics involving the central focal enhancement, which has an appearance of a mass. No corresponding sonographic correlate was identified and, on the day of the recommended MRI-guided biopsy, two focal areas of enhancement were no longer present, likely indicating resolved background parenchymal enhancement

2.24 History

A 40-year-old woman with a possible right breast mass identified on baseline screening mammogram. Breast MRI was performed for further evaluation (Figs. 2.66, 2.67, 2.68, and 2.69).

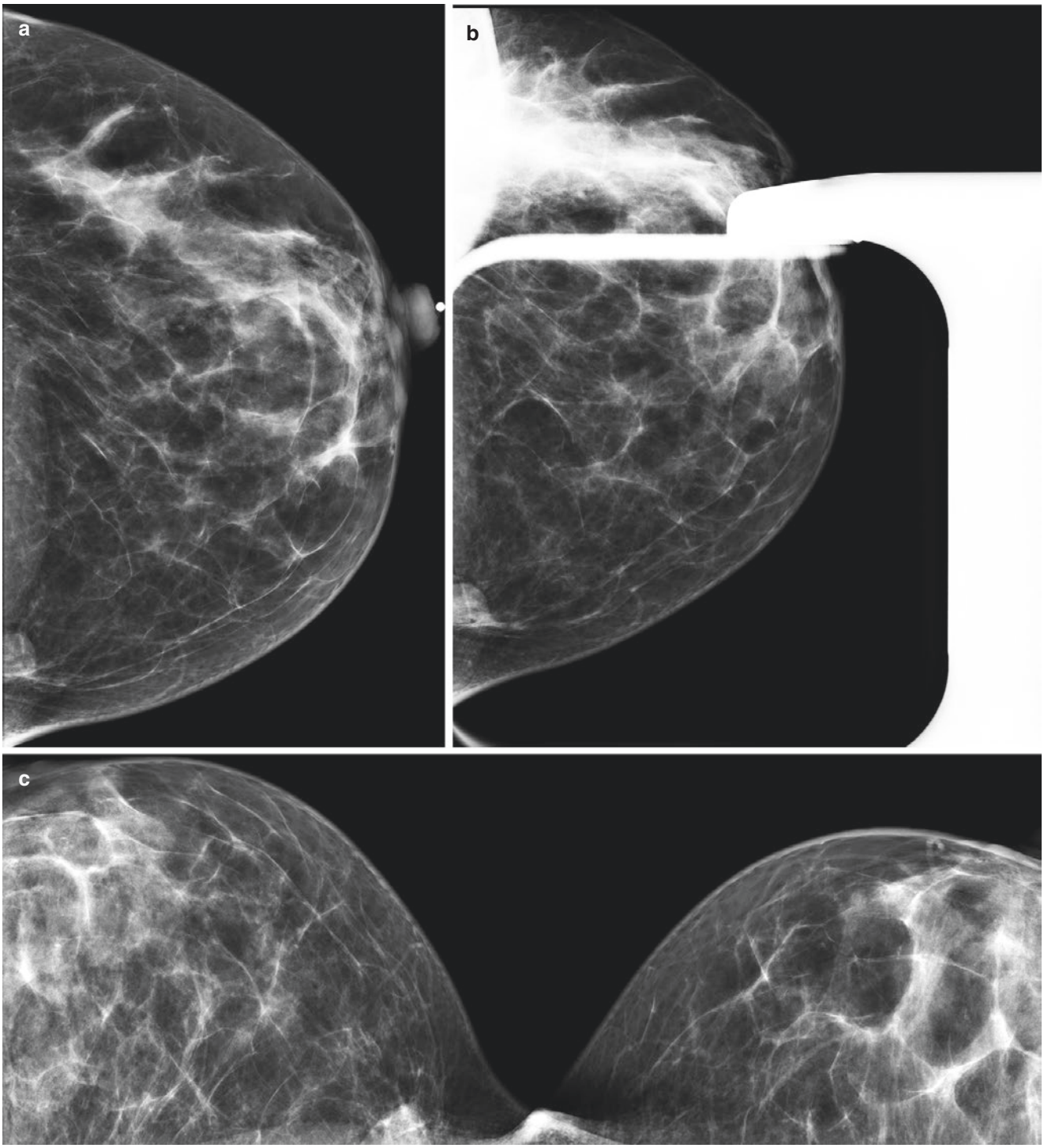

Fig. 2.65 Mammogram. Right CC view (**a**) and CC spot compression view (**b**). (**c**) Cleavage view

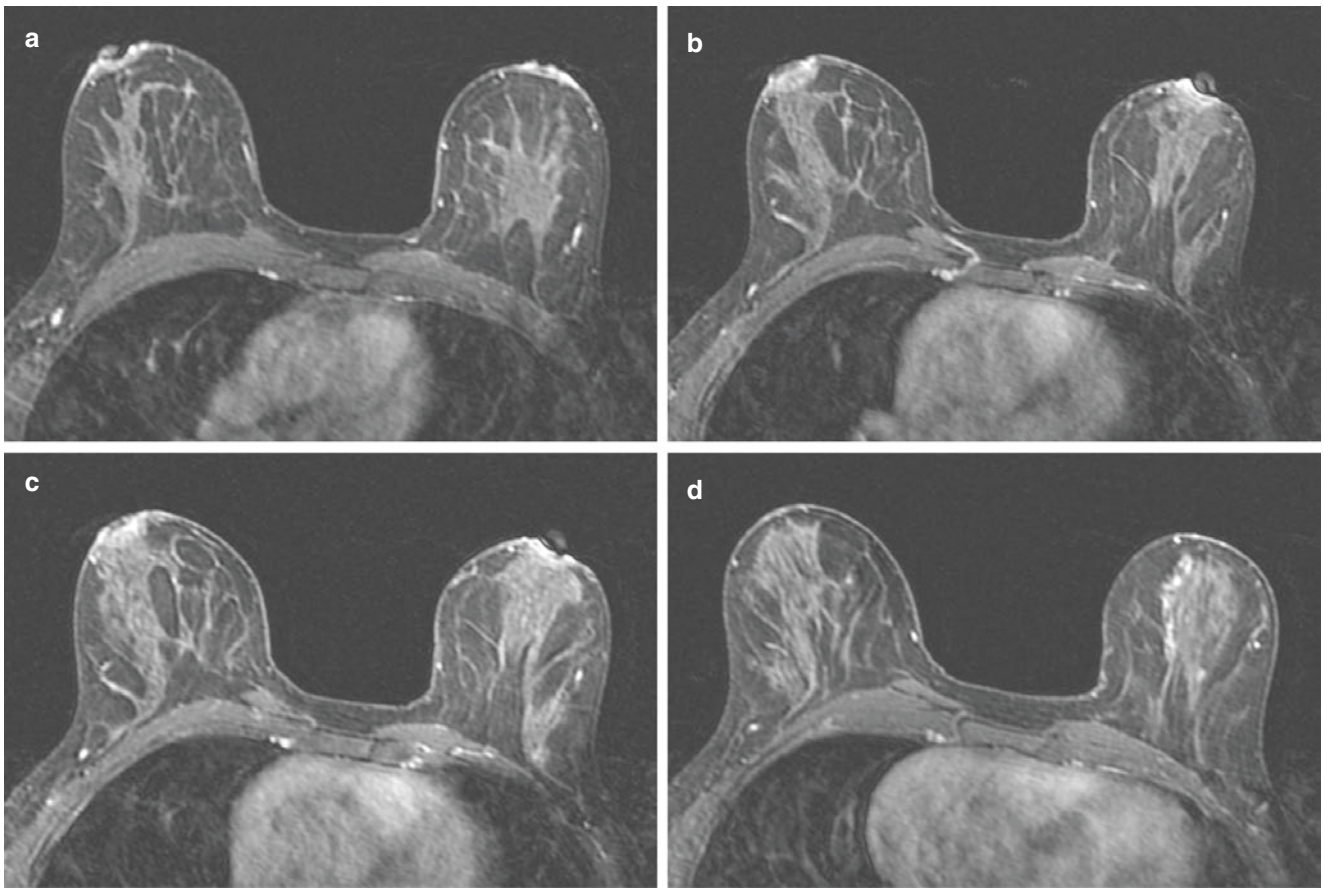

Fig. 2.66 (**a**–**d**) Serial axial T1-weighted post-contrast images of both breasts from superior to inferior

2.24 Sternalis

Teaching Points The sternalis muscle is a normal variant of the chest wall musculature. It may be visible as a rounded or irregular, flame-shaped asymmetry on the craniocaudal mammogram along the sternal edge. Radiologist awareness of this entity enables recognition of this finding as benign on the mammogram, but the appearance of the muscle can mimic malignancy, as illustrated in this case. This benign finding can be confirmed by the absence of a mass on ultrasound or on cross-sectional imaging such as CT or MR imaging if necessary.

Image Findings

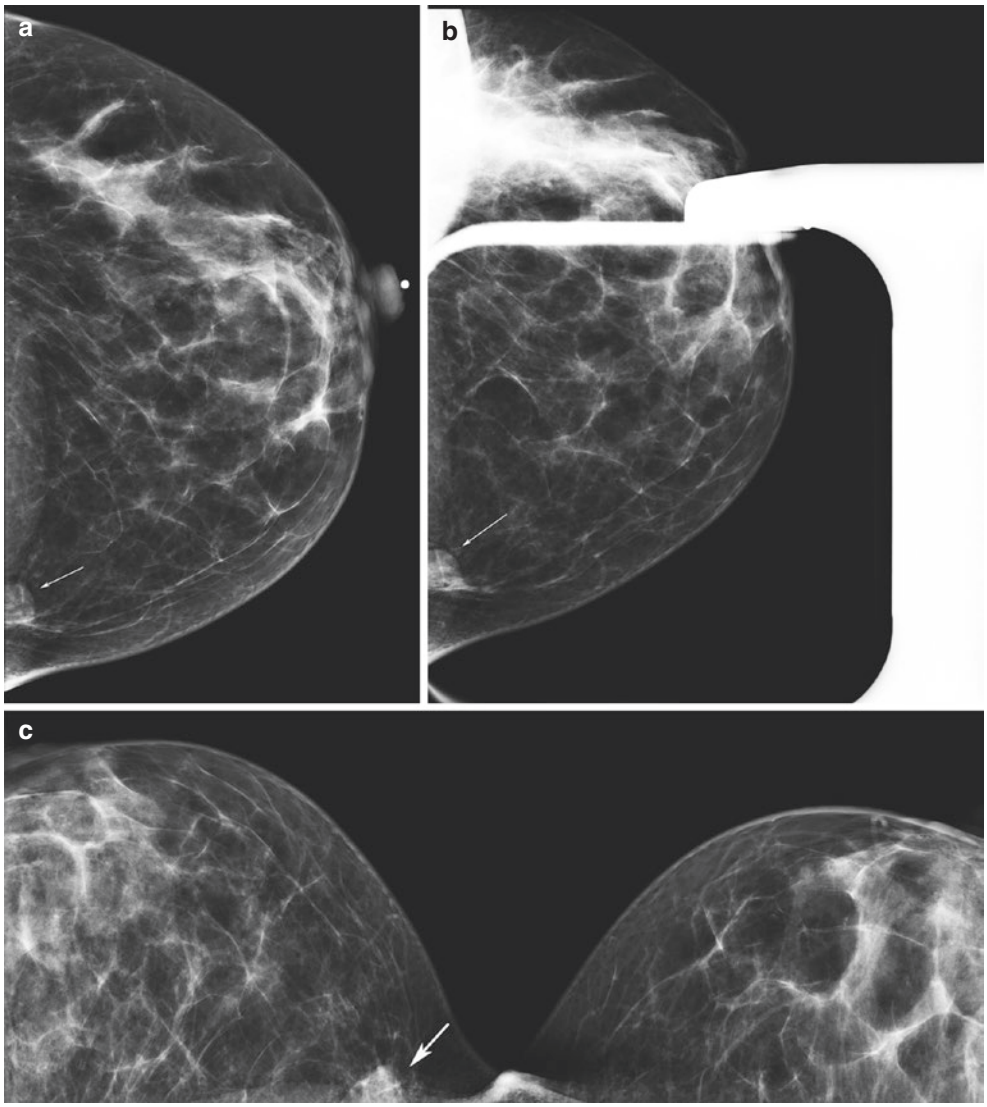

Fig. 2.67 Sternalis muscle. (**a**) Mammographic right CC view demonstrates a 1.2-cm asymmetry (*arrow*) in the far posterior medial breast, which persists on CC spot compression (**b**) and a cleavage view (**c**). No corresponding finding was present on the MLO view (*not shown*)

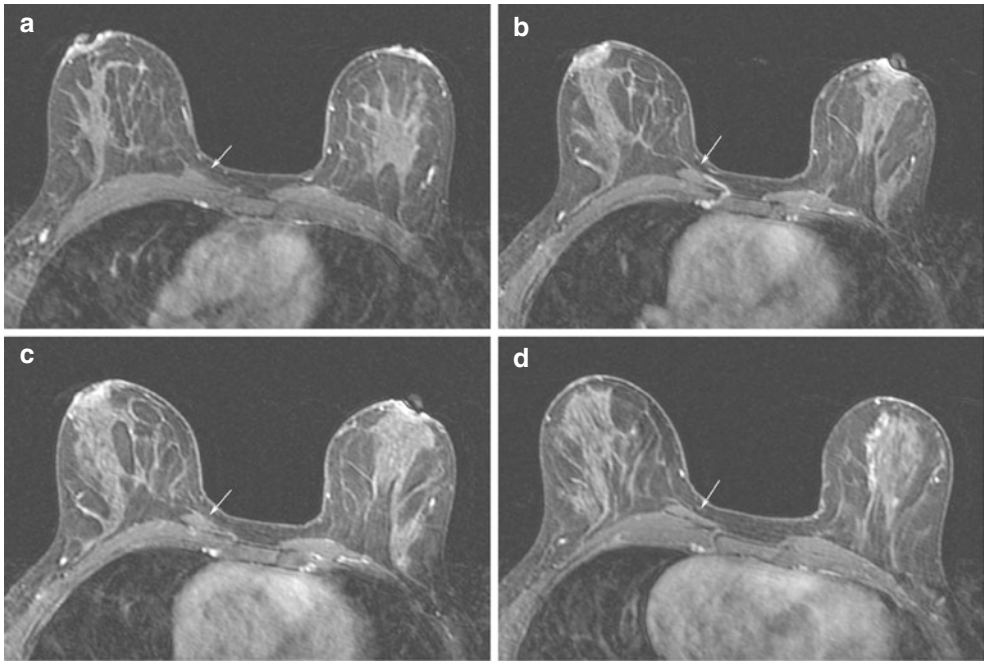

Fig. 2.68 (**a**–**d**) Serial axial T1-weighted post-contrast images from superior to inferior show a wedge-shaped mass (*arrows*) in the far posterior medial right breast with minimal enhancement and similar signal characteristics to the adjacent pectoralis musculature. This represents a sternalis muscle

2.25 History

A 48-year-old woman undergoing high-risk screening breast MRI (Figs. 2.70 and 2.71).

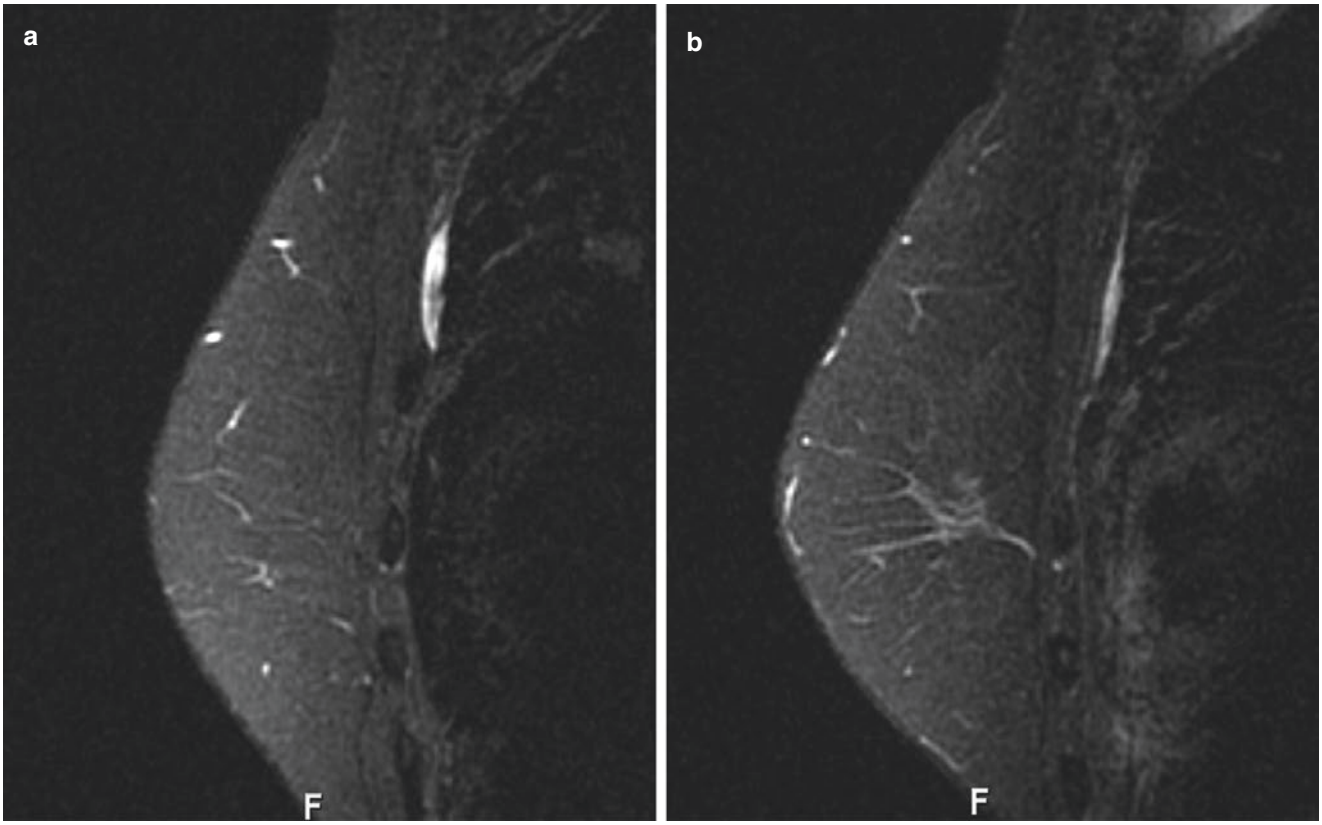

Fig. 2.69 (**a**, **b**) Selected sagittal T2-weighted fat-saturated images of the left breast. No suspicious enhancement is present on post-contrast images (*not shown*)

2.25 Pleural Effusion

Teaching Points A small amount of pleural fluid identified on MRI is likely to be physiologic and usually does not warrant additional evaluation.

Image Findings

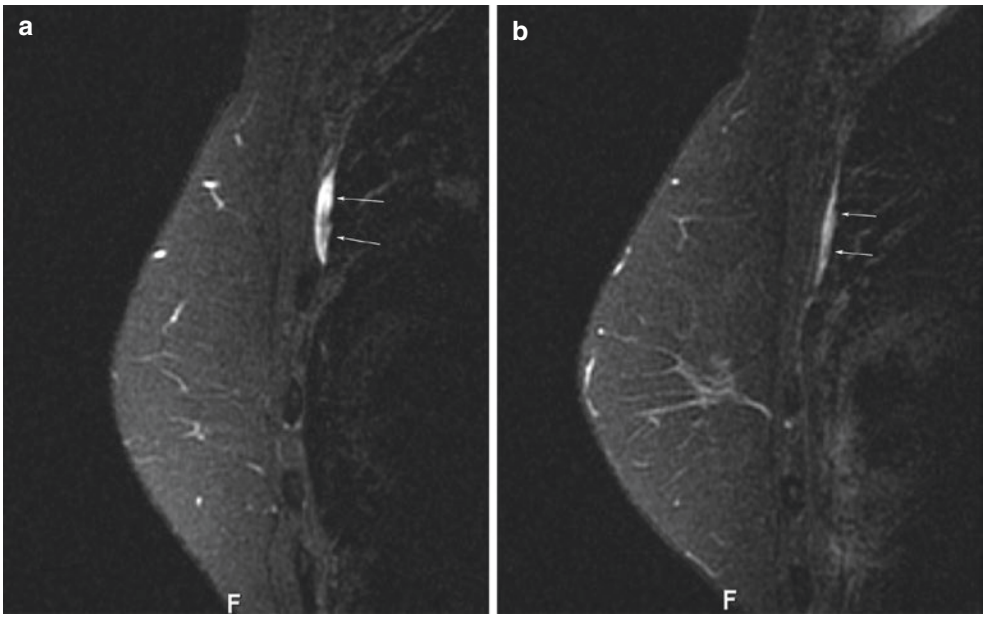

Fig. 2.70 Pleural fluid. (**a**, **b**) Sagittal T2-weighted fat-suppressed images show linear high signal intensity (*arrows*) along the dependent aspect of the thorax, consistent with trace pleural fluid

2.26 History

46-year-old patient undergoing high-risk screening breast MRI (Figs. 2.72, 2.73, and 2.74).

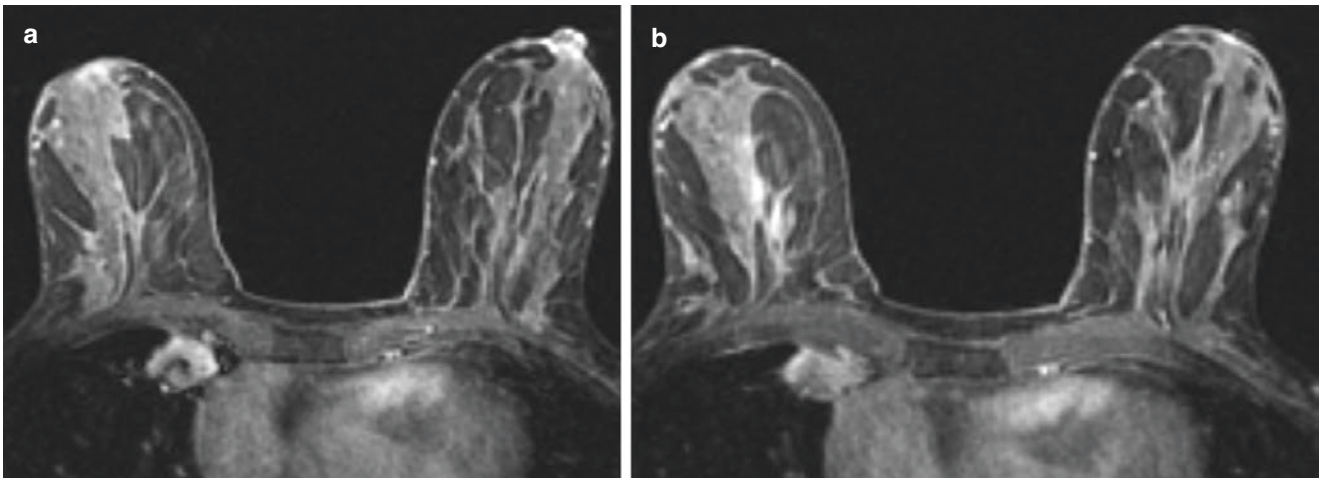

Fig. 2.71 (**a**, **b**) Sequential axial T1-weighted fat-suppressed post-contrast images

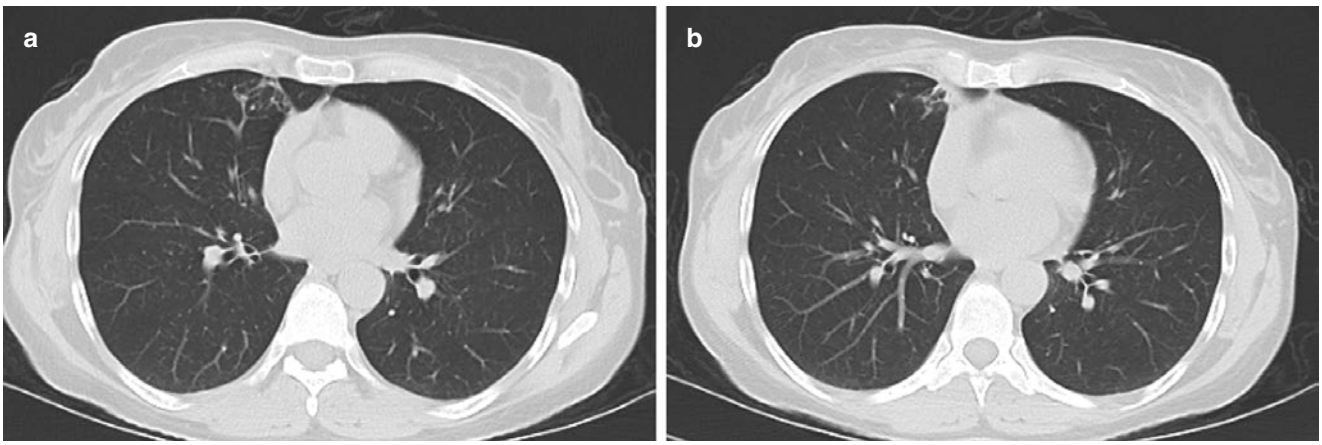

Fig. 2.72 (**a**, **b**) Corresponding axial CT images performed the following day

2.26 Round Atelectasis

Teaching Points Round atelectasis is an uncommon form of peripheral lung collapse that can be associated with asbestos exposure, exudative pleural effusions, prior cardiac surgery, or pneumothorax; it also can be idiopathic. Round atelectasis is usually asymptomatic, with minimal to no clinical findings, and is most often seen incidentally in a healthy patient or on long-term follow-up of an asbestos-exposed patient. The typical imaging appearance is a peripheral round, spindle-shaped, or wedge-shaped opacity with indistinct, irregular borders on radiography. On CT, it will appear as a peripheral round mass adjacent to thickened pleura. Variable contrast enhancement is noted, and a classic "comet-tail" sign may be appreciated, composed of swirling confluence of pulmonary vessels. On MRI, round atelectasis will be T1 hyperintense to muscle, T1 hypointense to fat, and T2 isointense to hypointense to fat, with contrast enhancement and a "comet-tail" sign similar to CT. This case illustrates round atelectasis with "comet-tail" sign on MRI, likely secondary to a combination of prior scarring in the right middle lobe and prone position. The finding resolved on CT performed the next day with the patient positioned supine, and only mild scarring was noted.

Image Findings

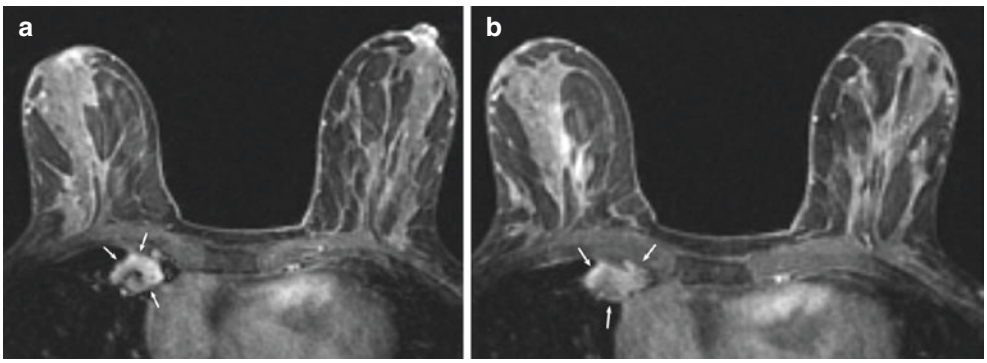

Fig. 2.73 Round atelectasis. (**a**, **b**) Sequential axial T1-weighted fat-suppressed post-contrast images obtained with the patient prone demonstrate an enhancing oval mass (*arrow*) in the right middle lobe. The mass demonstrates a swirling or comet tail appearance characteristic of round atelectasis

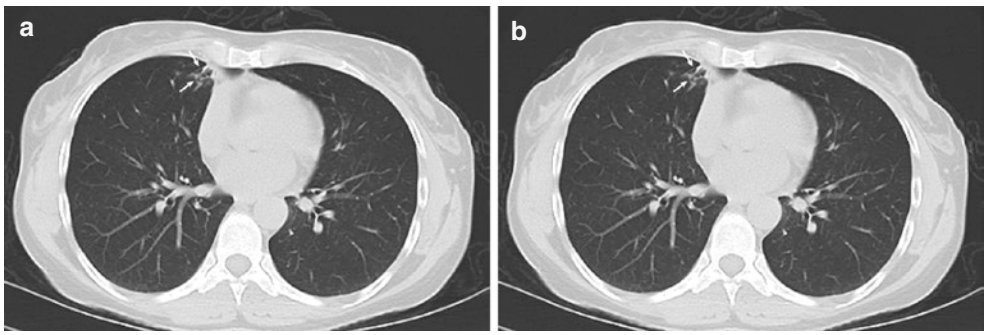

Fig. 2.74 (**a**, **b**) Corresponding supine CT images obtained the next day show resolution of the round atelectasis with some residual scarring (*arrows*)

2.27 History

50-year-old patient undergoing high-risk screening breast MRI (Figs. 2.75 and 2.76).

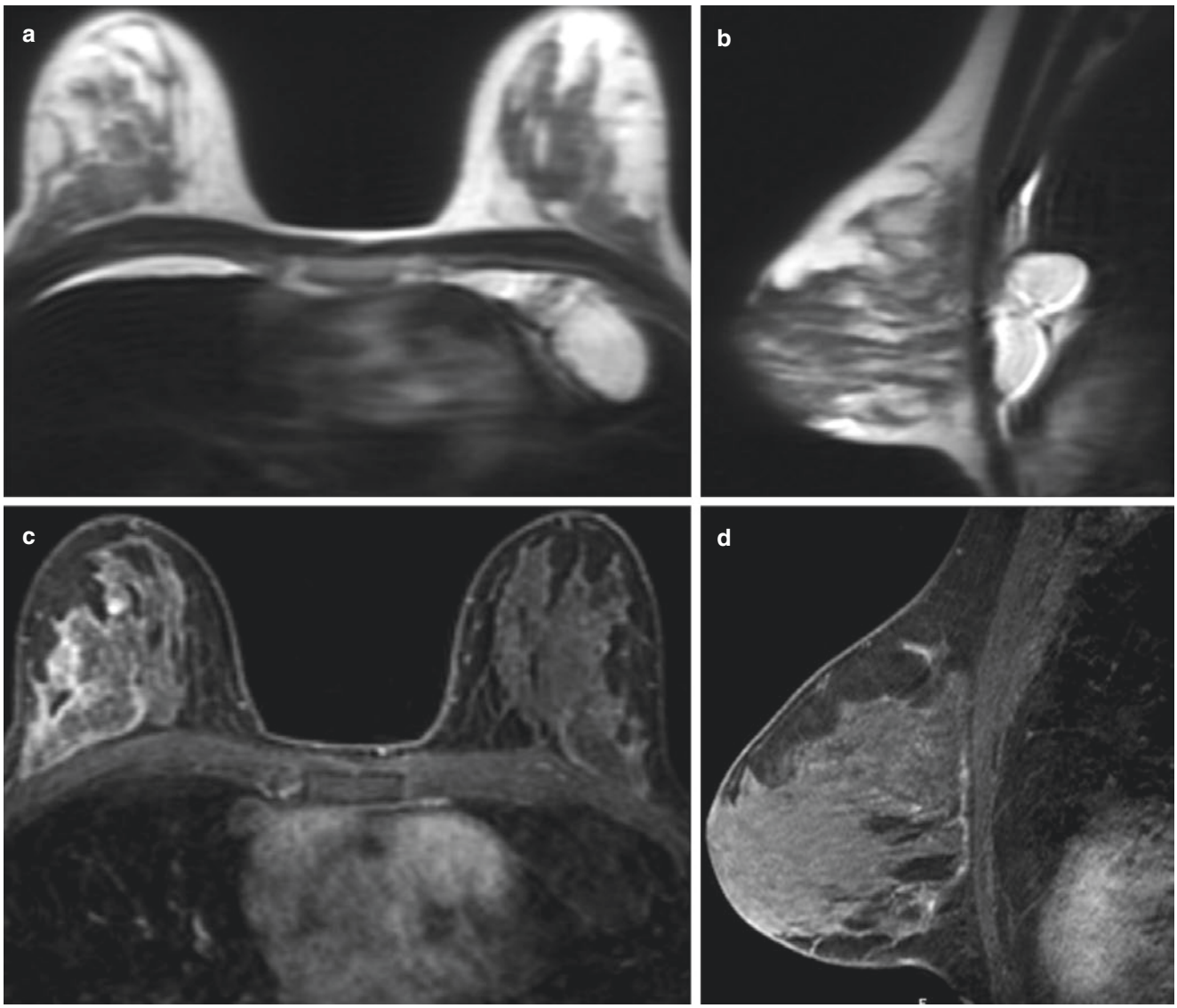

Fig. 2.75 (**a**) Axial T2-weighted image of both breasts. (**b**) Sagittal T2-weighted image of the left breast. (**c**) Axial T1-weighted fat-saturated post-contrast image of both breasts. (**d**) Sagittal T1-weighted fat-saturated post-contrast image of the left breast

2.27 Pericardial Cyst

Teaching Points When interpreting breast MRI, systematic evaluation of other anatomic structures and organs within the field of view is important. Incidental findings are not uncommon: about one in five patients will have an extramammary finding. Pericardial cysts are rare mediastinal cysts occurring with an incidence of 1 in 100,000. Most are asymptomatic and arise in the anterior cardiophrenic angle, more frequently on the right side. Mediastinal cystic lesions constitute about 3 % of all benign extramammary findings on breast MRI (Niell et al. 2015), for which no additional assessment is indicated.

Pericardial cyst, like any other mediastinal cyst, appears thin-walled with classic cystic features of low signal intensity on T1-weighted images (Fig. 2.75) and a homogenous, hyperintense signal on T2-weighted images (Fig. 2.76).

Image Findings

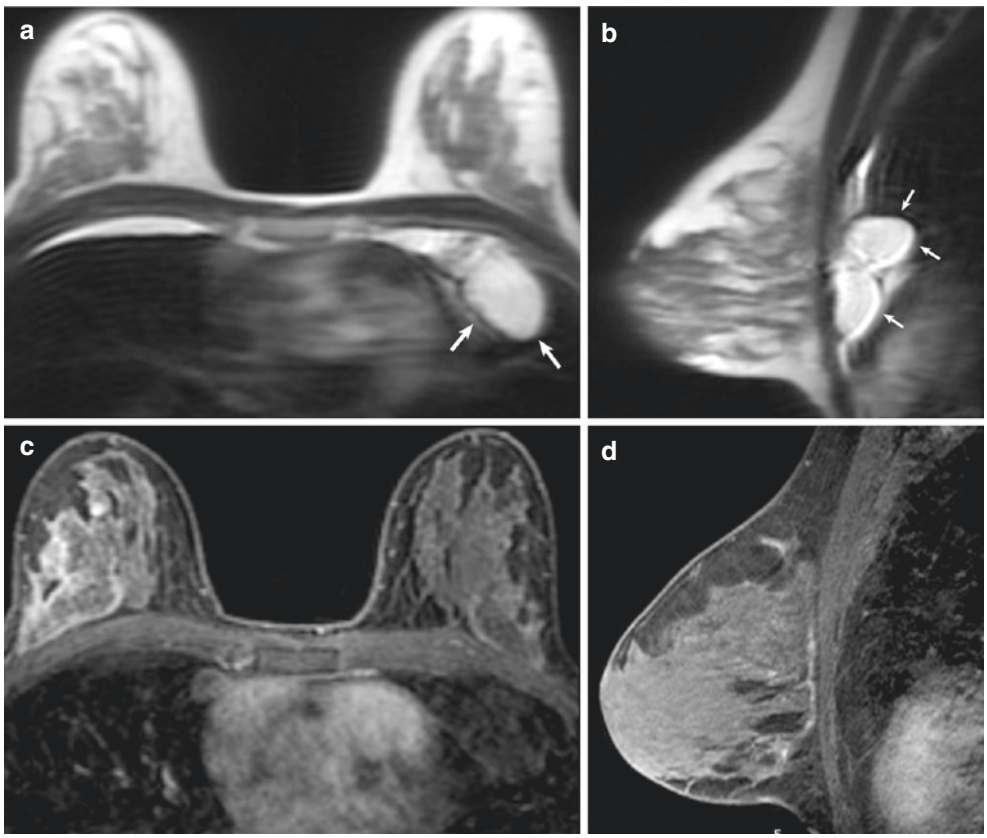

Fig. 2.76 Pericardial cyst. Axial (**a**) and sagittal (**b**) T2-weighted images demonstrate a lobulated, hyperintense structure (*arrows*) adjacent to the heart. Axial (**c**) and sagittal (**d**) T1-weighted fat-saturated post-contrast images demonstrate no enhancement of this structure, consistent with a cyst

2.28 History

29-year-old patient undergoing high-risk screening breast MRI (Figs. 2.77 and 2.78).

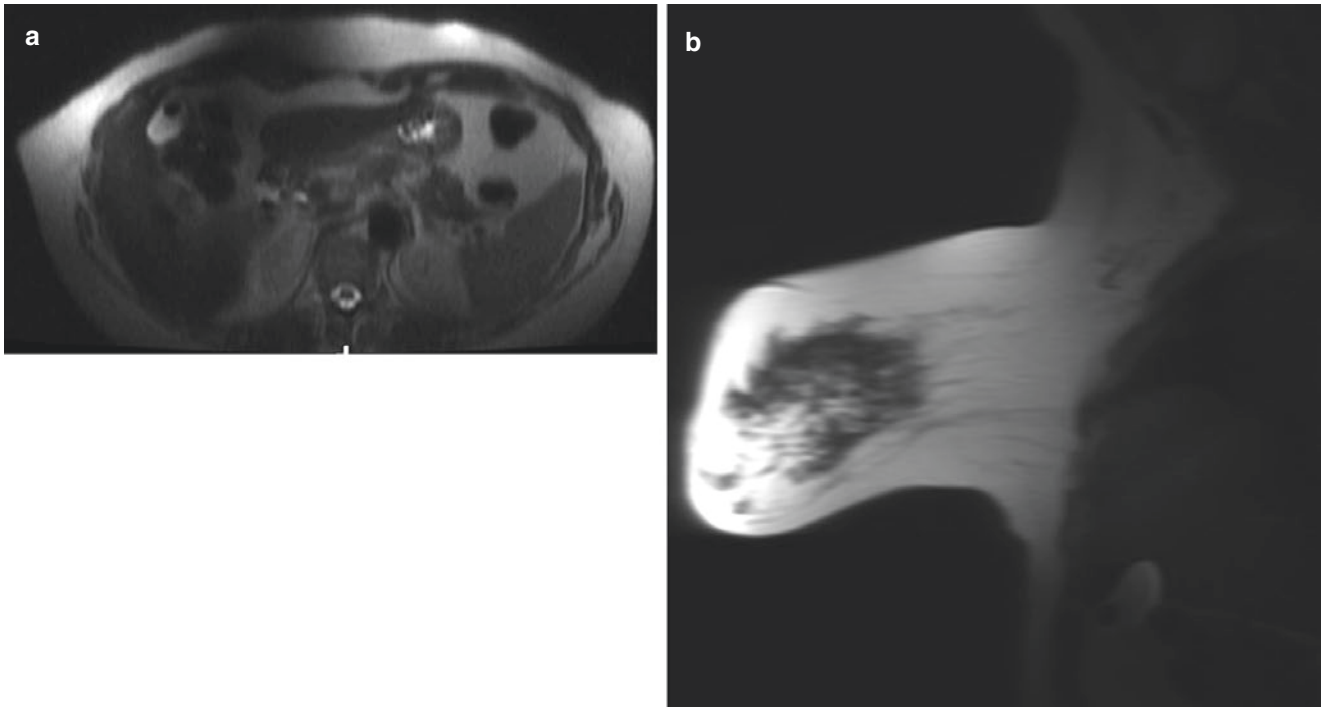

Fig. 2.77 Axial (**a**) and sagittal (**b**) localizing sequence images

2.28 Gallstone

Teaching Points When interpreting breast MRI, systematic evaluation of other anatomic structures and organs contained within the field of view is important. Incidental findings are not uncommon, with an extramammary finding in about one in five patients.

Gallstones are found in about 10 % of the general population and are twice as common in women as men. They are more prevalent with increasing age and are often detected incidentally. According to a recent study by Niell et al., gallstones were found to represent approximately 2 % of all benign extramammary findings that required no additional work-up. They are best appreciated on T2-weighted MR images and localizing sequences (Figs. 2.77 and 2.78).

Image Findings

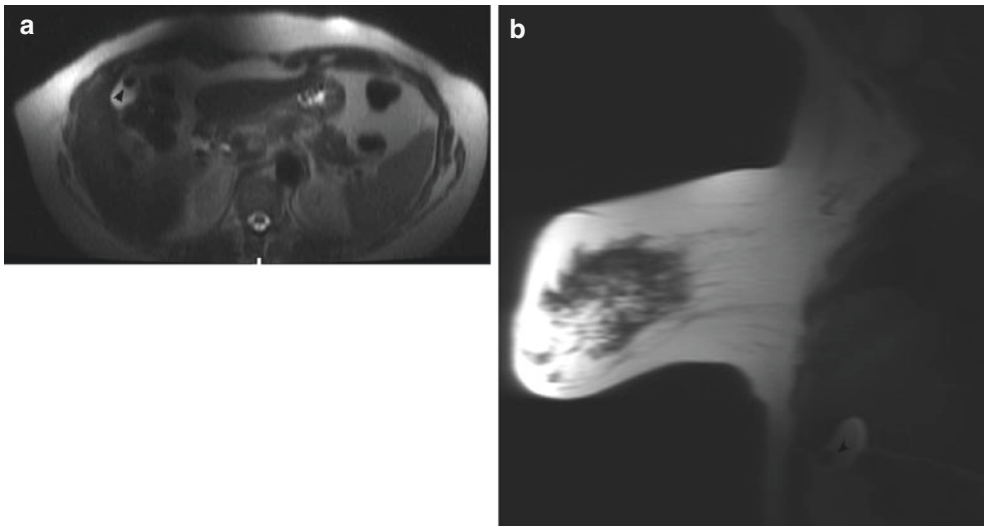

Fig. 2.78 Incidental gallstone. Axial (**a**) and sagittal (**b**) localizing images demonstrate a hypointense round structure (*arrowheads*) in the gallbladder, characteristic of a gallstone

Suggested Reading

ACR BI-RADS® Atlas/Breast MRI/Reporting System. 5th ed. Reston: American College of Radiology (ACR); 2013.

Ahuja A, Seth A. Juvenile fibroadenoma of breast. Indian Pediatr. 2005;42:72.

Bilgen IG, Ustun EE, Memis A. Fat necrosis of the breast: clinical, mammographic and sonographic features. Eur J Radiol. 2001;39:92–9.

Birdwell RL, Raza S, Odulate AS. NMLE: diffuse, background enhancement. In: Raza S, Birdwell RL, editors. Specialty imaging: breast MRI – a comprehensive imaging guide. Salt Lake City: Amirsys; 2010. p. II-3-84–II-3-99.

Bluemke DA, Gatsonis CA, Chen MH, DeAngelis GA, DeBruhl N, Harms S, et al. Magnetic resonance imaging of the breast prior to biopsy. JAMA. 2004;292:2735–42.

Bradley FM, Hoover Jr HC, Hulka CA, Whitman GJ, McCarthy KA, Hall DA, et al. The sternalis muscle: an unusual normal finding seen on mammography. AJR Am J Roentgenol. 1996;166:33–6.

Brennan SB, Sung JS, Dershaw DD, Liberman L, Morris EA. Cancellation of MR imaging-guided breast biopsy due to lesion nonvisualization: frequency and follow-up. Radiology. 2011;261(1):92–9.

Catalano OA, Sahani DV, Kalva SP, Cushing MS, Hahn PF, Brown JJ, Edelman RR. MR imaging of the gallbladder: a pictorial essay. Radiographics. 2008;28:135–55.

Chen JH, Liu H, Baek HM, Nalcioglu O, Su MY. Magnetic resonance imaging features of fibrocystic change of the breast. Magn Reson Imaging. 2008a;26:1207–14.

Chen JH, Nalcioglu O, Su MY. Fibrocystic change of the breast presenting as a focal lesion mimicking breast cancer in MR imaging. Magn Reson Imaging. 2008b;28:1499–505.

Cucci E, Santoro A, Di Gesù C, Di Cerce R, Sallustio G. Sclerosing adenosis of the breast: report of two cases and review of the literature. Pol J Radiol. 2015;80:122–7.

Daly CP, Jaeger B, Sill DS. Variable appearances of fat necrosis on breast MRI. AJR Am J Roentgenol. 2008;191:1374–80.

de Paredes ES. Atlas of mammography. 3rd ed. Philadelphia: Lippincott Williams & Wilkins; 2007.

Dinkel HP, Trusen A, Gassel AM, Rominger M, Lourens S, Müller T, Tschammler A. Predictive value of galactographic patterns for benign and malignant neoplasms of the breast in patients with nipple discharge. Br J Radiol. 2000;73:706–14.

Ecanow JS, Abe H, Newstead GM, Ecanow DB, Jeske JM. Axillary staging of breast cancer: what the radiologist should know. Radiographics. 2013;33:1589–612.

Ferris-James DM, Iuanow E, Mehta TS, Shaheen RM, Slanetz PJ. Imaging approaches to diagnosis and management of common ductal abnormalities. Radiographics. 2012;32:1009–30.

Fu P, Kurihara Y, Kanemaki Y, Okamoto K, Nakajima Y, Fukuda M, Maeda I. High-resolution MRI in detecting subareolar breast abscess. AJR Am J Roentgenol. 2007;188:1568–72.

Gallardo X, Sentís M, Castañer E, Andreu X, Darnell A, Canalías J. Enhancement of intramammary lymph nodes with lymphoid hyperplasia: a potential pitfall in breast MRI. Eur Radiol. 1998;8:1662–5.

García CJ, Espinoza A, Dinamarca V, Navarro O, Daneman A, García H, Cattani A. Breast US in children and adolescents. Radiographics. 2000;20:1605–12.

Giess CS, Raza S, Birdwell RL. Patterns of non-masslike enhancement at screening breast MR imaging of high-risk premenopausal women. Radiographics. 2013;33:1343–60.

Giess CS, Yeh ED, Raza S, Birdwell RL. Background parenchymal enhancement at breast MR imaging: normal patterns, diagnostic challenges, and potential for false-positive and false-negative interpretation. Radiographics. 2014;34:234–47.

Hambly NM, Liberman L, Dershaw DD, Brennan S, Morris EA. Background parenchymal enhancement on baseline screening breast MRI: impact on biopsy rate and short-interval follow-up. AJR Am J Roentgenol. 2011;196:218–24.

Hines N, Slanetz PJ, Eisenberg RL. Cystic masses of the breast. AJR Am J Roentgenol. 2010;194:W122–33.

Iglesias A, Arias M, Santiago P, Rodríguez M, Mañas J, Saborido C. Benign breast lesions that simulate malignancy: magnetic resonance imaging with radiologic-pathologic correlation. Curr Probl Diagn Radiol. 2007;36:66–82.

Jarzabkowski DC, Braunstein DB. Pericardial cyst: an incidental finding. J Am Osteopath Assoc. 1998;98:445–6.

Jeung MY, Gasser B, Gangi A, Bogorin A, Charneau D, Wihlm JM, et al. Imaging of cystic masses of the mediastinum. Radiographics. 2002;22:S79–93.

Jones K, Glazebrook K, Reynolds C. Pseudoangiomatous stromal hyperplasia: imaging findings with pathologic and clinical correlation. AJR Am J Roentgenol. 2010;195:1036–42.

King V, Brooks JD, Bernstein JL, Reiner AS, Pike MC, Morris EA. Background parenchymal enhancement at breast MR imaging and breast cancer risk. Radiology. 2011;260:50–60.

Kinoshita T, Fukutomi T, Kubochi K. Magnetic resonance imaging of benign phyllodes tumors of the breast. Breast J. 2004;10:232–6.

Kinoshita T, Yashiro N, Yoshigi J, Ihara N, Narita M. Fat necrosis of breast: a potential pitfall in breast MRI. Clin Imaging. 2002;26:250–3.

Lee SJ, Mahoney MC, Khan S. MRI features of stromal fibrosis of the breast with histopathologic correlation. AJR Am J Roentgenol. 2011;197:755–62.

Mercado CL, Naidrich SA, Hamele-Bena D, Fineberg SA, Buchbinder SS. Pseudoangiomatous stromal hyperplasia of the breast: sonographic features with histopathologic correlation. Breast J. 2004;10:427–32.

Meyer JE, Ferraro FA, Frenna TH, DiPiro PJ, Denison CM. Mammographic appearance of normal intramammary lymph nodes in an atypical location. AJR Am J Roentgenol. 1993;161:779–80.

Morris EA, Comstock CE, Lee CH, et al. ACR BI-RADS® Magnetic resonance imaging. In: ACR BI-RADS® atlas, breast imaging reporting and data system. Reston: American College of Radiology; 2013.

Morris EA, Liberman L, editors. Breast MRI: diagnosis and intervention. New York: Springer; 2005.

Murphey MD, Carroll JF, Flemming DJ, Pope TL, Gannon FH, Kransdorf MJ. From the archives of AFIP: benign musculoskeletal lipomatous lesions. Radiographics. 2004;24:1433–66.

Nguyen J, Nicholson BT, Patrie JT, Harvey JA. Incidental pleural effusions detected on screening breast MRI. AJR Am J Roentgenol. 2012;199:W142–5.

Niell BL, Bennett D, Sharma A, Gazelle GS. Extramammary findings on breast MR examinations: frequency, clinical relevance, and patient outcomes. Radiology. 2015;276:56–64.

Ojeda-Fournier H, Choe KA, Mahoney MC. Recognizing and interpreting artifacts and pitfalls in MR imaging of the breast. Radiographics. 2007;27:S147–64.

Piccoli CW, Feig SA, Palazzo JP. Developing asymmetric breast tissue. Radiology. 1999;211:111–7.

Ramirez-Montano L, Vargas-Tellez E, Dajer-Fadel WL, Maceda SE. Giant lipoma of the breast. Arch Plast Surg. 2013;40:244–6.

Raza S, Birdwell RL, Ritner J, Gombos EC, Yeh ED, Odulate AS, et al. Specialty imaging. Breast MRI: a comprehensive imaging guide. Salt Lake City: Amirsys; 2010.

Rosen PP. Rosen's breast pathology. Philadelphia: Lippincott-Raven; 1997.

Salvador R, Lirola JL, Dominguez R, Lopez M, Risueno N. Pseudoangiomatous stromal hyperplasia presenting as a breast mass: imaging findings in three patients. Breast. 2004;13:431–5.

Stathopoulos GT, Karamessini MT, Sotiriadi AE, Pastromas VG. Rounded atelectasis of the lung. Respir Med. 2005;99:615–23.

Svane G, Franzén S. Radiologic appearance of nonpalpable intramammary lymph nodes. Acta Radiol. 1993;34:577–80.

Taboada JL, Stephens TW, Krishnamurthy S, Brandt KR, Whitman GJ. The many faces of fat necrosis in the breast. AJR Am J Roentgenol. 2009;192:815–25.

Taşkin F, Köseoğlu K, Unsal A, Erkuş M, Ozbaş S, Karaman C. Sclerosing adenosis of the breast: radiologic appearance and efficiency of core needle biopsy. Diagn Interv Radiol. 2011;17:311–6.

Trop I, Dugas A, David J, El Khoury M, Boileau JF, Larouche N, Lalonde L. Breast abscesses: evidence-based algorithms for diagnosis, management, and follow-up. Radiographics. 2011;31:1683–99.

Uematsu T, Kasami M, Watanabe J. Does the degree of background enhancement in breast MRI affect the detection and staging of breast cancer? Eur Radiol. 2011;21:2261–7.

van den Bosch MA, Daniel BL, Mariano MN, Nowels KN, Birdwell RL, Fong KJ, et al. Magnetic resonance imaging characteristics of fibrocystic change of the breast. Invest Radiol. 2005;40:436–41.

Verslegers I, Van Goethem M, Hufkens G, Biltjes I, Parizel PM. Extramammary findings in T2-weighted MR breast images. Eur J Radiol. 2012;81:S181–2.

Wechselberger G, Schoeller T, Piza-Katzer H. Juvenile fibroadenoma of the breast. Surgery. 2002;132:106–7.

Westbrook C, Roth CK, Talbot J. MRI in practice. 4th ed. Chichester: Wiley-Blackwell; 2011.

Wurdinger S, Herzog AB, Fischer DR, Marx C, Raabe G, Schneider A, Kaiser WA. Differentiation of phyllodes breast tumors from fibroadenomas on MRI. AJR Am J Roentgenol. 2005;185:1317–21.

Yamaguchi T, Hayashi K, Ashizawa K, Mori M, Matsuoka Y, Kohzaki S, Uetani M. Magnetic resonance imaging of rounded atelectasis. J Thorac Imaging. 1997;12:188–94.

Young Lee B, Young Byun J, Hee Kim H, Sook Kim H, Mee Cho S, Hoon Lee K, et al. The sternalis muscles: incidence and imaging findings on MDCT. J Thorac Imaging. 2006;21:179–83.

Zhuo J, Gullapalli RP. AAPM/RSNA physics tutorial for residents: MR artifacts, safety, and quality control. Radiographics. 2006;26:275–97.

Breast Malignancy

3

Victoria Mango, Habib Rahbar, Lauren Friedlander,
Dustin Nguyen, and Richard Ha

V. Mango, MD
Director of Breast and Body Imaging Fellowship,
Breast Imaging Service, Memorial Sloan-Kettering Cancer Center,
Assistant Professor of Radiology, Weill Cornell Medical College,
New York, NY, USA
e-mail: vlm2125@columbia.edu

H. Rahbar, MD
Breast Imaging Section, Associate Professor of Radiology,
University of Washington School of Medicine,
Seattle, Washington, USA
e-mail: hrahbar@uw.edu

L. Friedlander, MD
Director of Breast and Body Imaging Fellowship,
Division of Breast Imaging, Assistant Professor of Radiology,
Columbia University Medical Center, New York, NY, USA
e-mail: lf2386@columbia.edu

D. Nguyen, DO
Staff Radiologist, Radiology Associates of North Texas,
Fort Worth, Texas, USA
e-mail: dustinguyen@gmail.com

R. Ha, MD (✉)
Director of Education and Research,
Division of Breast Imaging, Assistant Professor of Radiology,
Columbia University Medical Center, New York, NY, USA
e-mail: rh2616@cumc.columbia.edu

R. Ha et al. (eds.), Breast MRI Teaching Atlas, DOI 10.1007/978-1-4939-6409-3_3

3.1 History

Mammographically and sonographically occult low-grade DCIS on breast MRI (Figs. 3.1 and 3.2).

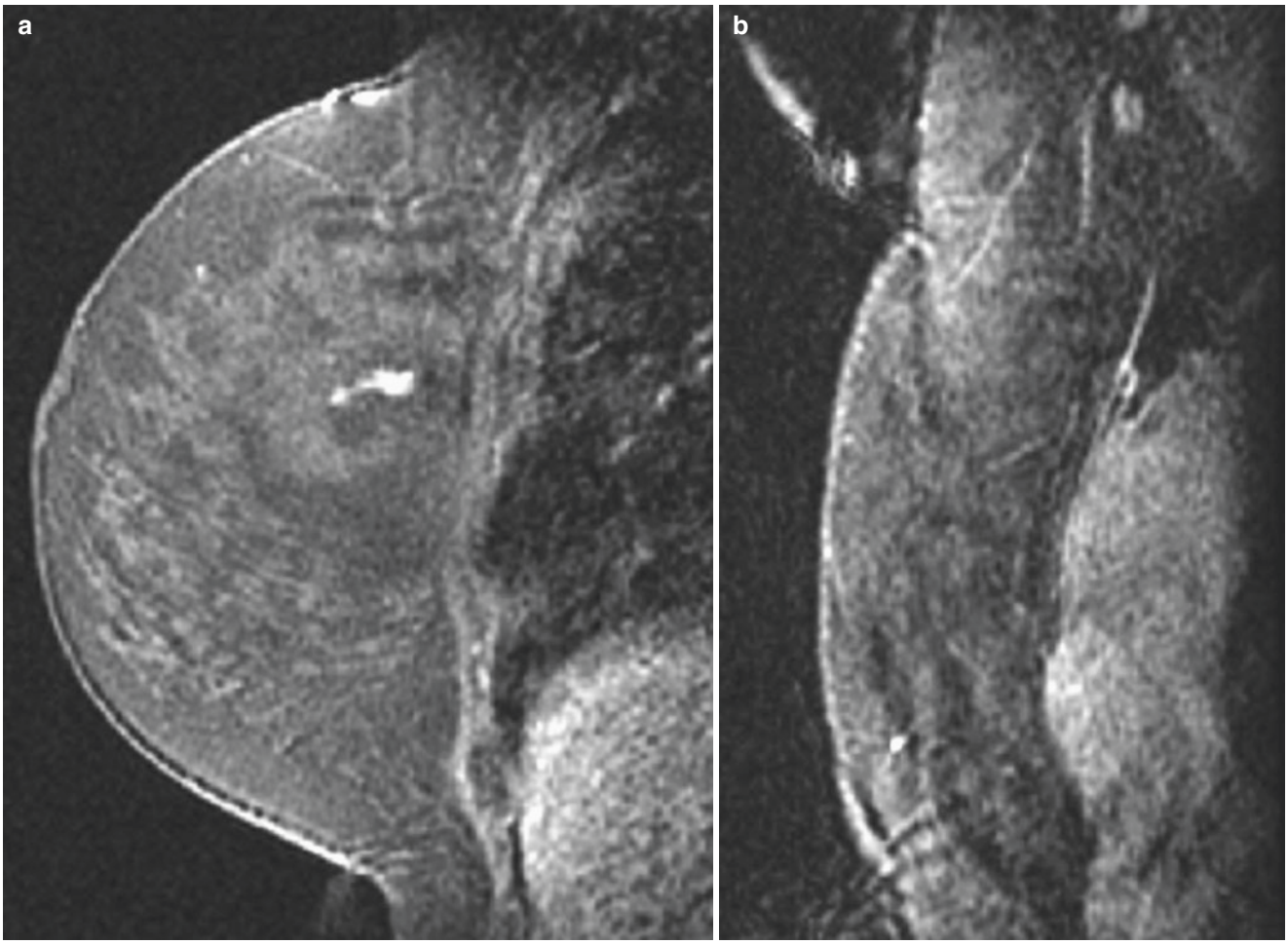

Fig. 3.1 Sagittal T1-weighted fat-suppressed post-contrast images through the right breast (**a**) and axilla (**b**)

3.1 Ductal Carcinoma In Situ (DCIS): Low Grade

Teaching Points MRI is more sensitive than mammography in detection of all grades of DCIS, with greater sensitivity for detection of high-grade and intermediate-grade DCIS than for low-grade DCIS. Mammographically, low-grade DCIS presents as amorphous calcifications and is more likely than high-grade DCIS to present as a mass or asymmetry. On MR imaging, nonmass enhancement is usually associated with all grades of DCIS (60–81 % of cases). Low-grade DCIS typically has benign blood flow enhancement kinetics, but no kinetic pattern has been demonstrated to predict DCIS grade.

Image Findings

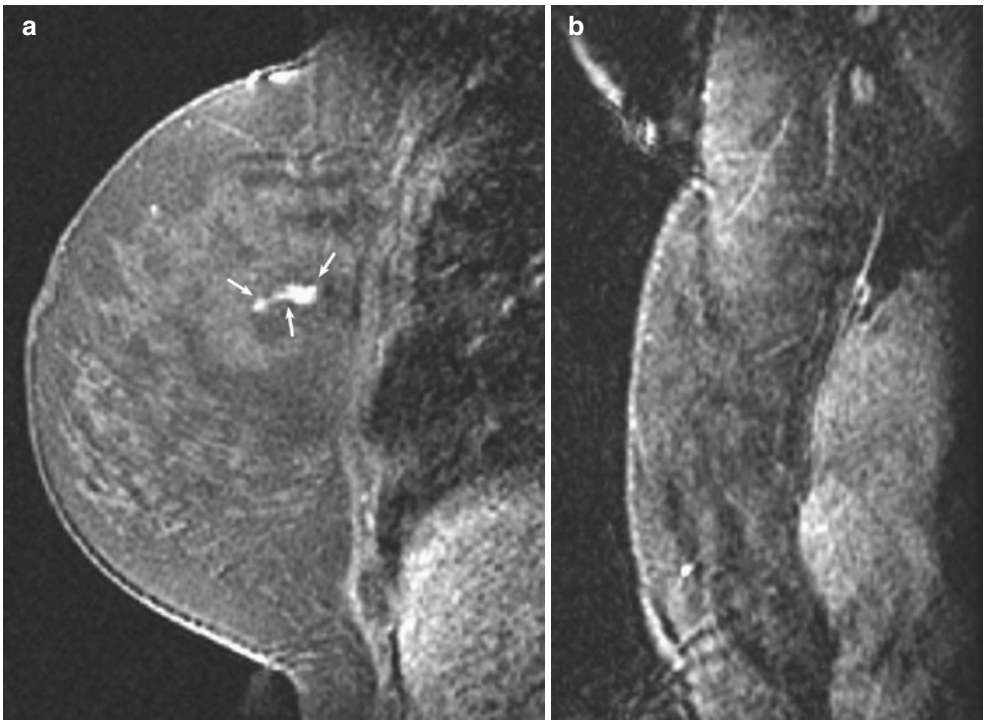

Fig. 3.2 (**a**) Sagittal T1-weighted fat-suppressed post-contrast image of the right breast demonstrates a 1.2-cm area of linear nonmass enhancement (*arrows*) along the right 10:00 axis. (**b**) Sagittal T1-weighted fat-suppressed post-contrast image of the right axilla shows no lymphadenopathy. The findings were mammographically and sonographically occult. MRI guided biopsy of the nonmass enhancement yielded low-grade ductal carcinoma in situ (DCIS)

3.2 History

32-year-old woman with high-grade DCIS for extent of disease evaluation (Figs. 3.3, 3.4, 3.5, 3.6, 3.7, 3.8, 3.9, and 3.10).

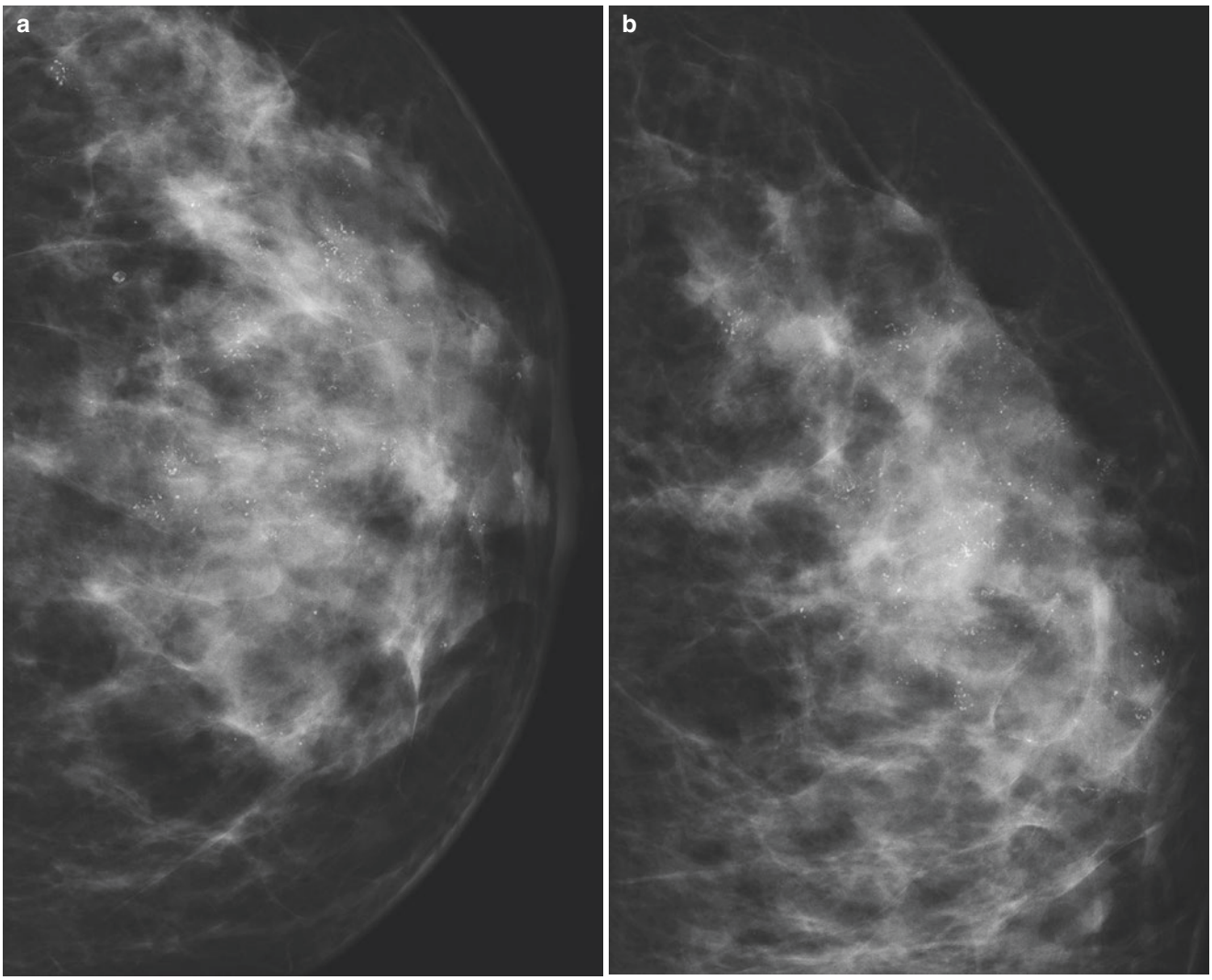

Fig. 3.3 Mammogram. Craniocaudal (CC) (**a**) and mediolateral (ML) (**b**) magnification views of the right breast

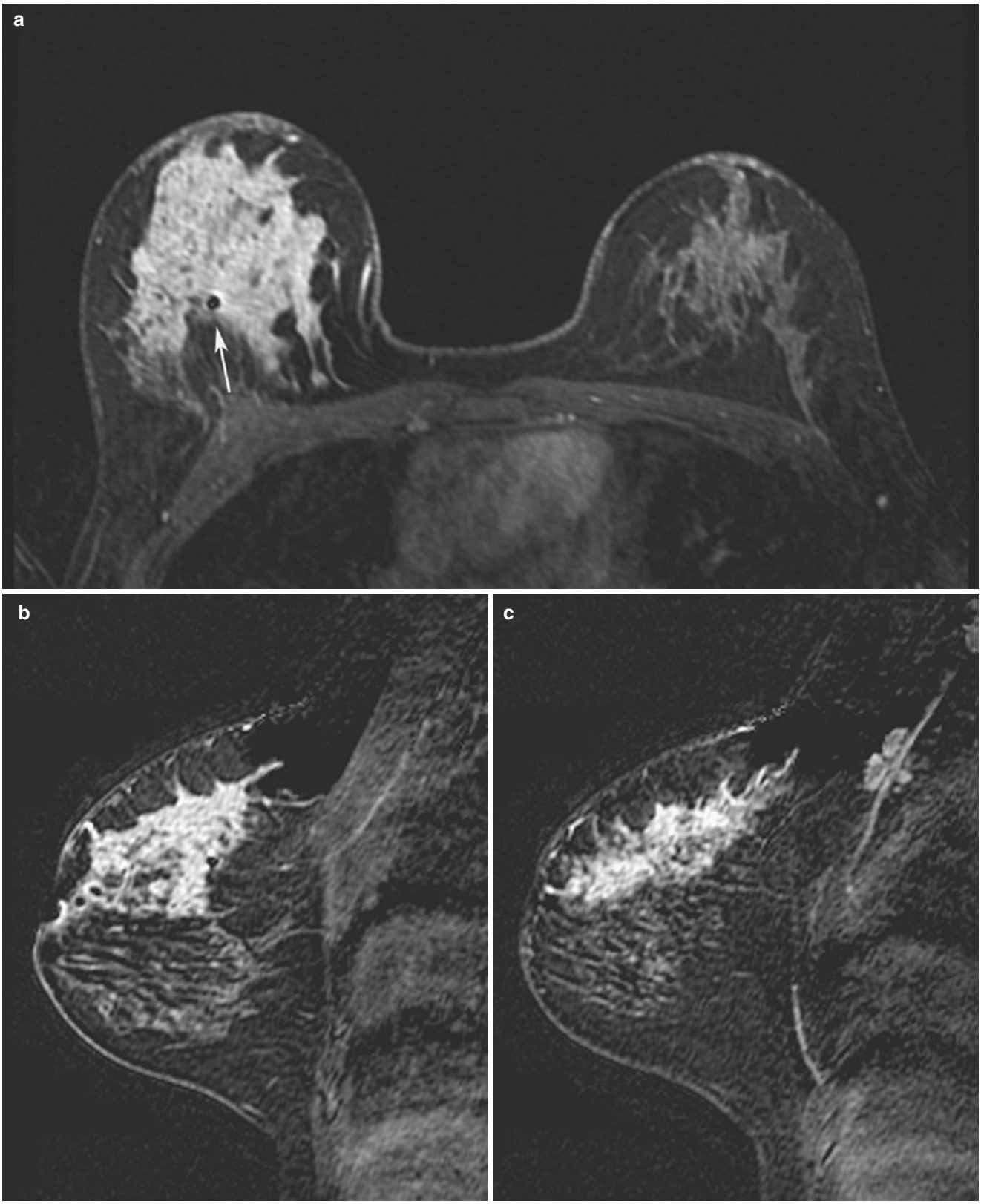

Fig. 3.4 Initial breast MRI. (**a**) Axial T1-weighted fat-suppressed post-contrast image of both breasts. (**b**, **c**) Sagittal T1-weighted fat-suppressed post-contrast images of the right breast

History: Same patient returns 11 months later after lost to follow up.

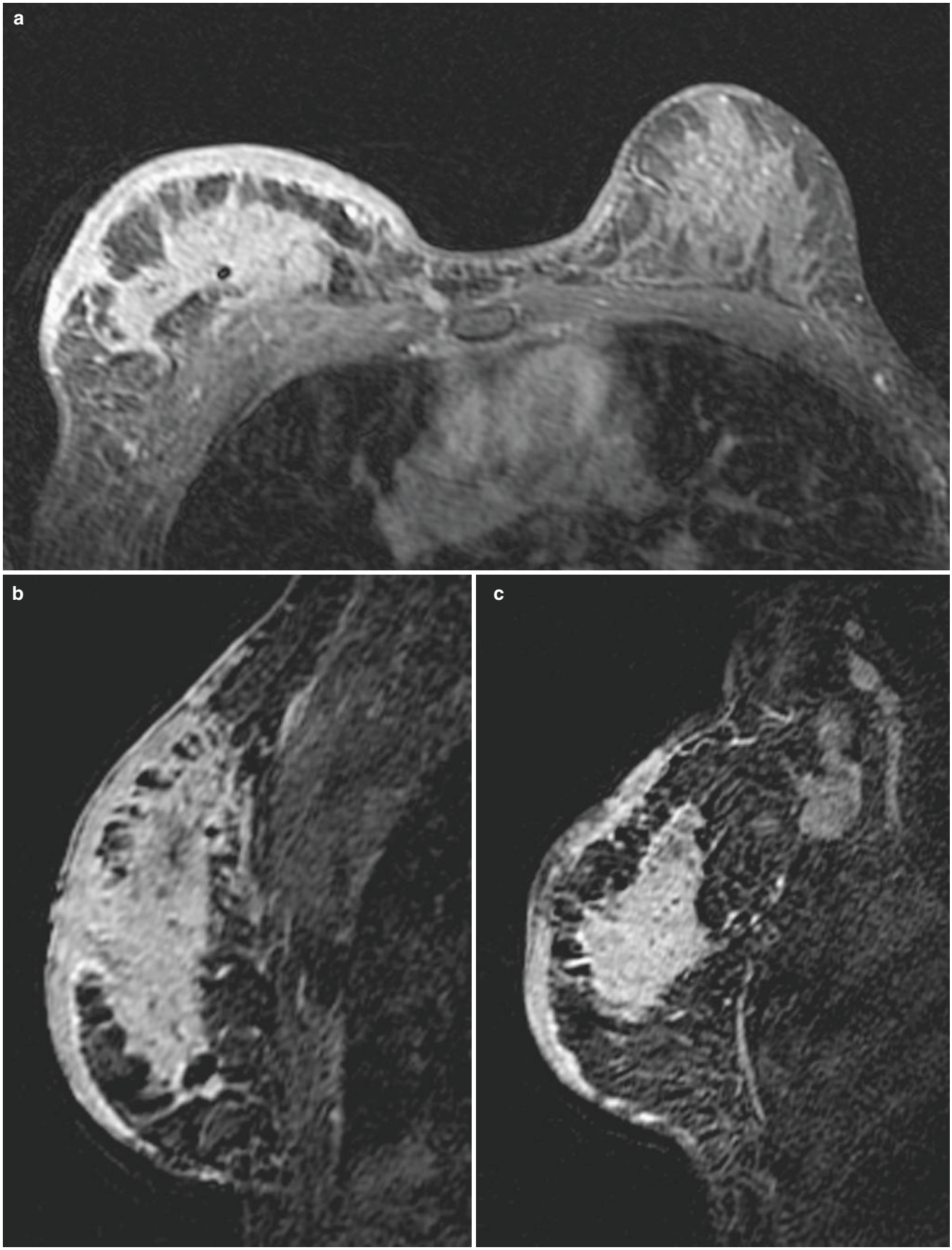

Fig. 3.5 Follow-up breast MRI performed 11 months later. (**a**) Axial T1-weighted fat-suppressed post-contrast image of both breasts. (**b**, **c**) Sagittal T1-weighted fat-suppressed post-contrast images of the right breast

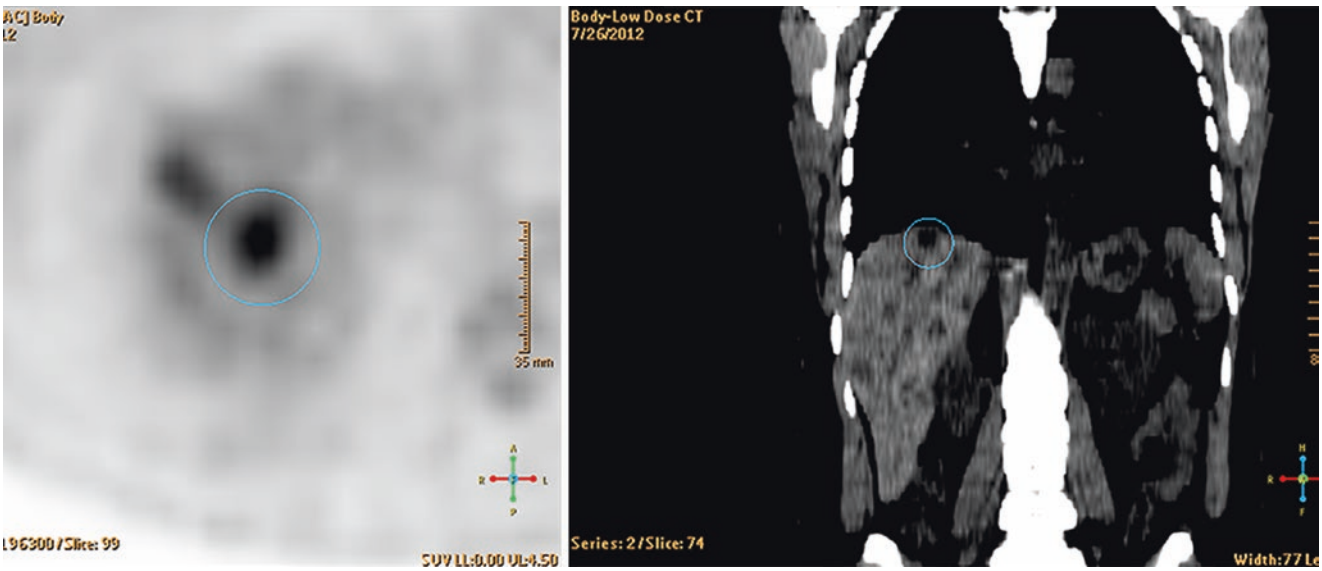

Fig. 3.6 Coned-down axial PET image of the liver and coronal fused PET-CT image of the chest and upper abdomen

3.2 DCIS: High Grade 1

Teaching Points DCIS is a heterogeneous disease varying in clinical presentation, morphology, and behavior. The published studies indicate that DCIS of all grades has the potential to progress to invasive ductal carcinoma, but high-grade DCIS has been shown to progress more rapidly than lower-grade lesions and is more likely to lead to metastatic disease with poor survival outcome. The MRI appearance of the natural progression of high-grade DCIS is illustrated in this case with dramatic increase in loco-regional disease with parenchymal spread of tumor, skin involvement, and axillary metastasis. Breast MRI is a sensitive modality for evaluating interval change of malignancy not only in patients with successful neoadjuvant therapy but also in cases of failed treatment.

Image Findings

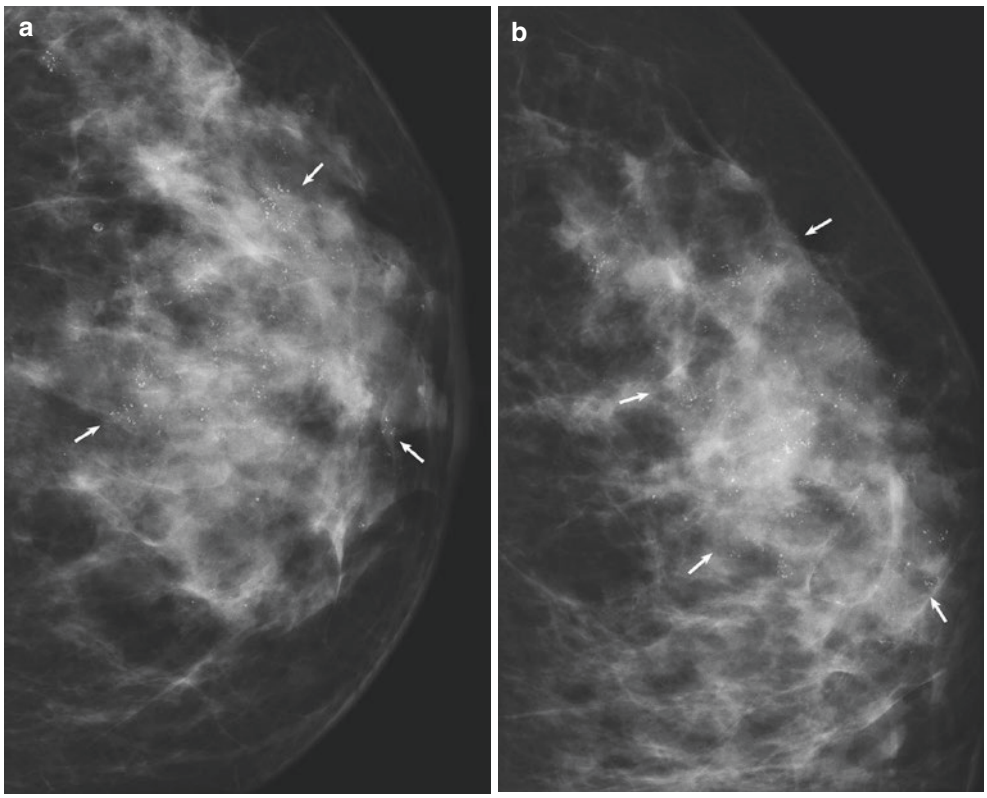

Fig. 3.7 Mammogram. CC (**a**) and ML (**b**) magnification views of the right breast demonstrate extensive suspicious pleomorphic calcifications (*arrows*) involving the upper outer breast. Stereotactic biopsy yielded high-grade DCIS

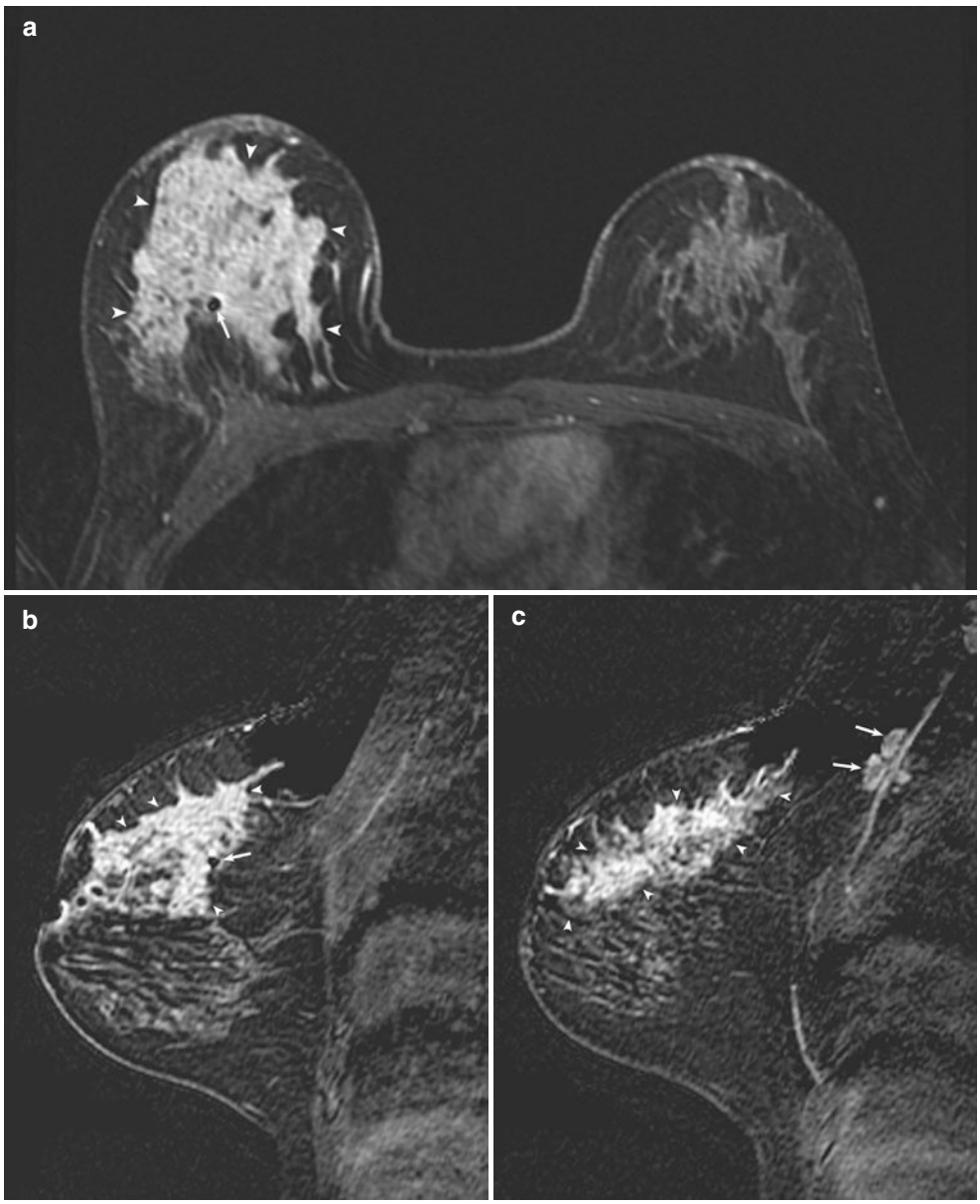

Fig. 3.8 Baseline breast MRI. (**a**) Axial T1-weighted fat-suppressed post-contrast image of both breasts reveals extensive nonmass enhancement (*arrowheads*) involving most of the right breast. (**b**) Sagittal T1-weighted fat-suppressed post-contrast image of the right breast shows extensive segmental nonmass enhancement (*arrowheads*) in the upper right breast. A breast biopsy clip artifact is seen (*arrow*). (**c**) Sagittal T1-weighted fat-suppressed post-contrast image of the right breast shows extensive segmental nonmass enhancement (*arrowheads*) in the upper right breast, as well as two enlarged axillary lymph nodes (*arrows*) suspicious for metastasis

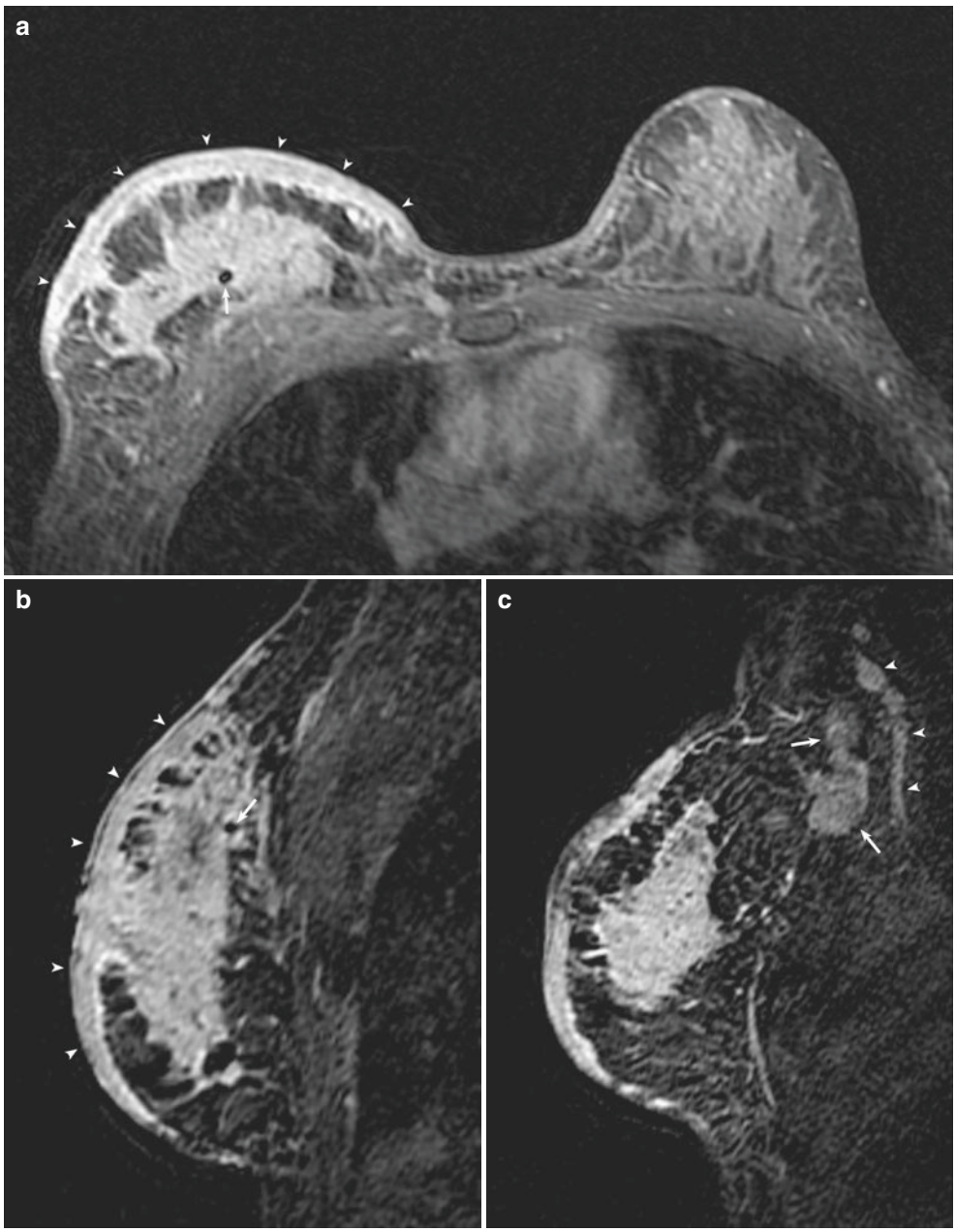

Fig. 3.9 Follow-up breast MRI performed after 11 months of nonconventional treatment. Axial (**a**) and sagittal (**b**) T1-weighted fat-suppressed post-contrast images at the level of the biopsy clip (*white arrow*) show increased extensive nonmass enhancement, now involving the entire right breast with associated diffuse and nodular skin thickening (*arrowheads*). (**c**) Sagittal T1-weighted fat-suppressed post-contrast image of the right breast demonstrates interval increase in enlarged axillary lymph nodes (*arrows*), which have a matted appearance adjacent to the axillary vasculature (*arrowheads*)

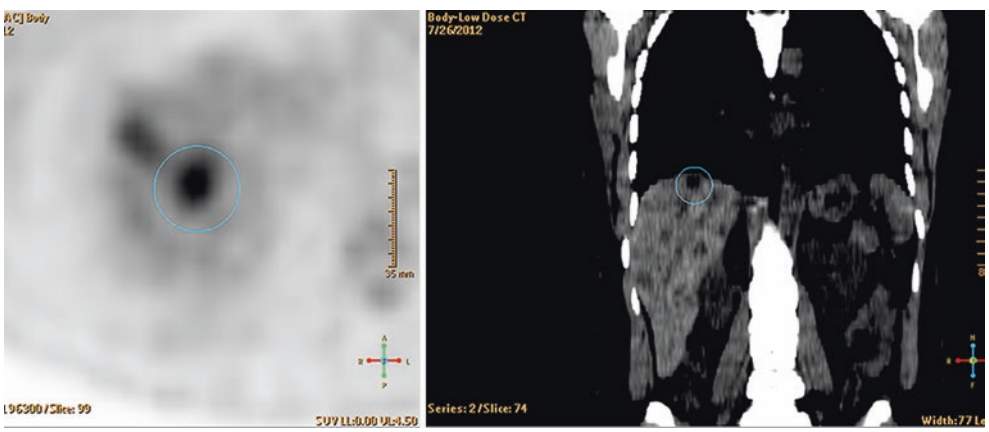

Fig. 3.10 PET/CT evaluation shows several FDG-avid irregular masses (teal circle) in the liver, suspicious for hepatic metastases

3.3 History

A 55-year-old woman with high-grade DCIS. Extent of disease evaluation (Figs. 3.11, 3.12, 3.13, and 3.14).

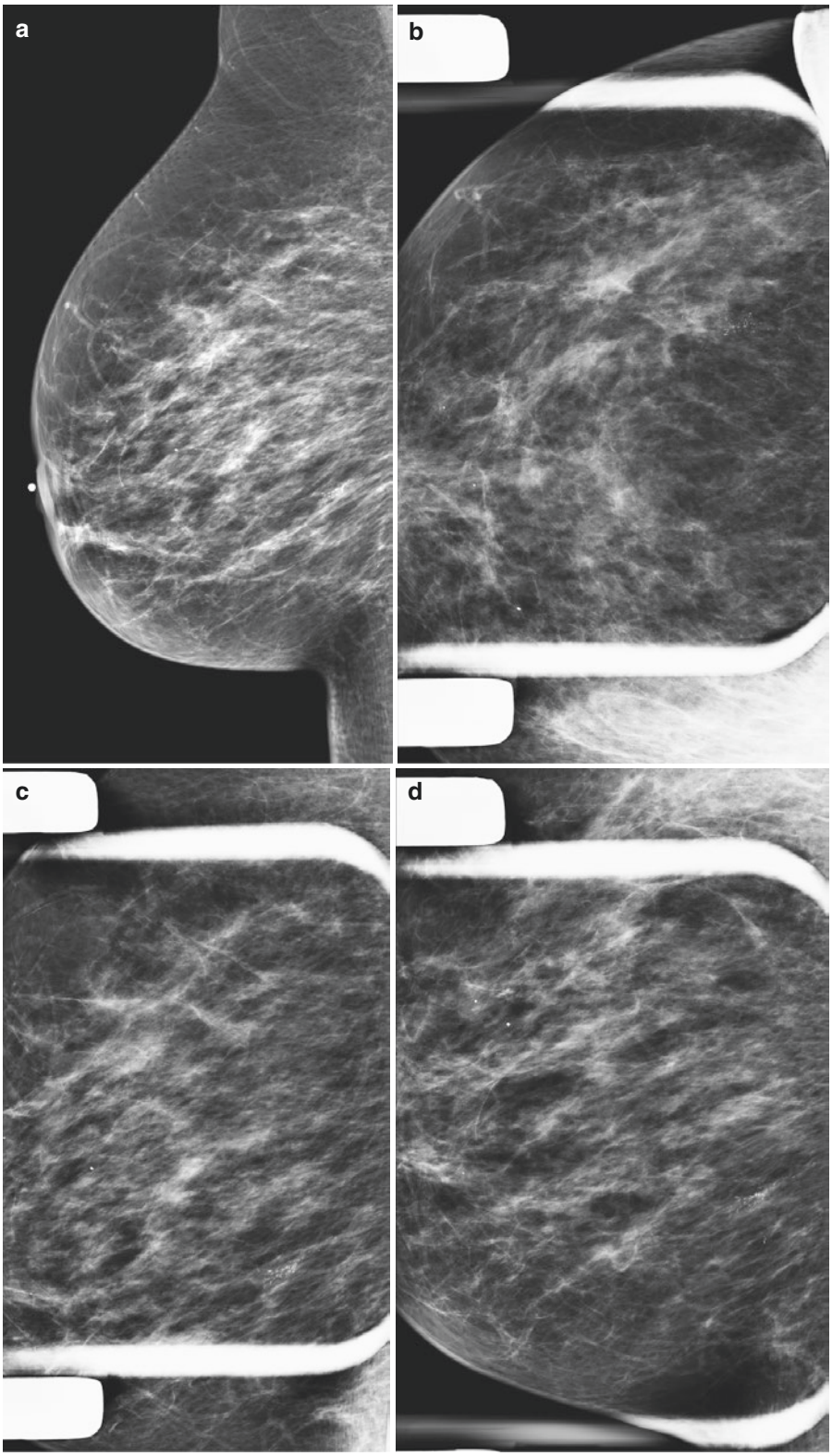

Fig. 3.11 Mammogram. ML view (**a**), CC spot magnification view (**b**), and ML spot magnification views (**c**, **d**) of the left breast

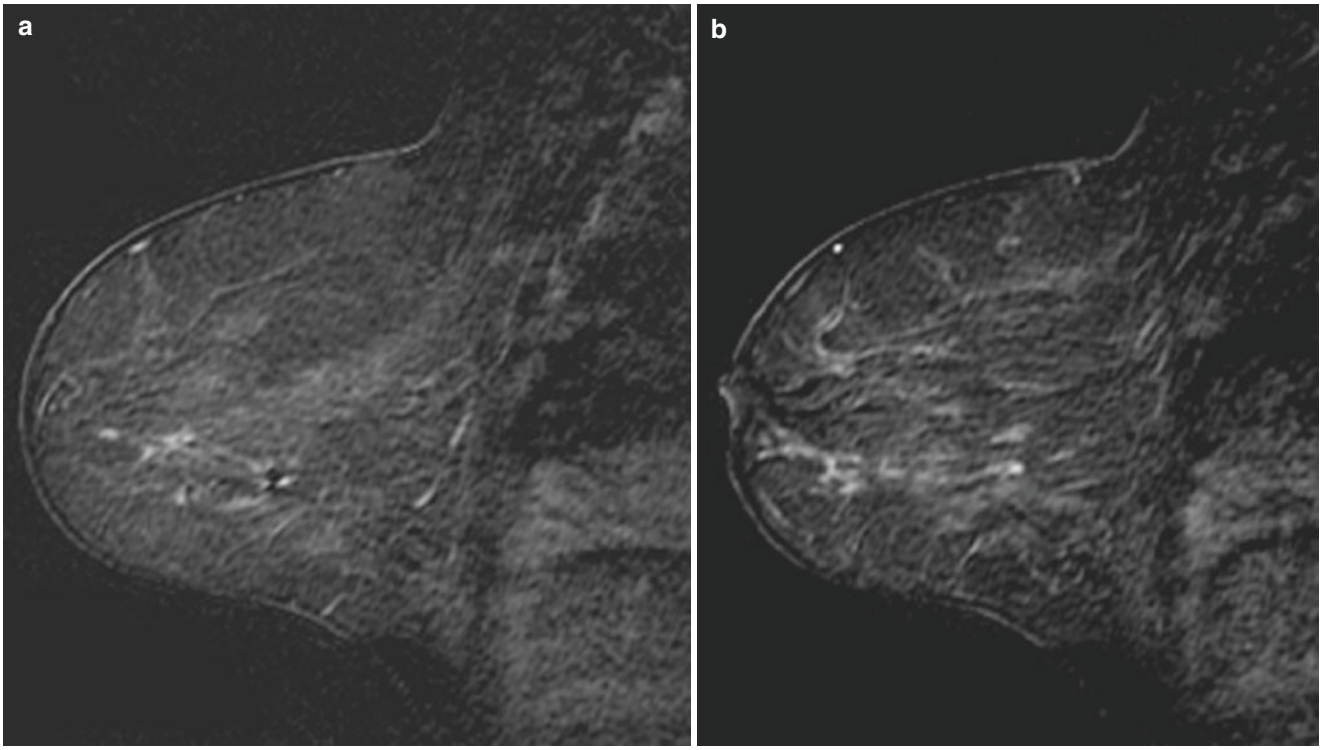

Fig. 3.12 (**a**, **b**) Sagittal post-contrast subtraction images of the left breast. High-grade DCIS with disease extent underestimated on mammography

3.3 DCIS: High Grade 2

Teaching Points Although mammography has been the mainstay for diagnosis of DCIS, there is a tendency to underestimate the extent of disease, especially in patients without microcalcifications or in those with dense breasts or breast implants. MRI is more sensitive than mammography in detecting pure DCIS. In many instances, MRI can reveal early-stage breast cancers, including DCIS and DCIS with small invasive carcinomas, that are mammographically, sonographically, and clinically occult. However, no differences in MR morphologic or kinetic features have been reported between low-grade and high-grade DCIS.

In our example, linearly distributed pleomorphic calcifications identified on mammography correspond to linear nonmass enhancement on the T1-weighted post-contrast images, a finding more likely to be associated with high-grade DCIS.

Image Findings

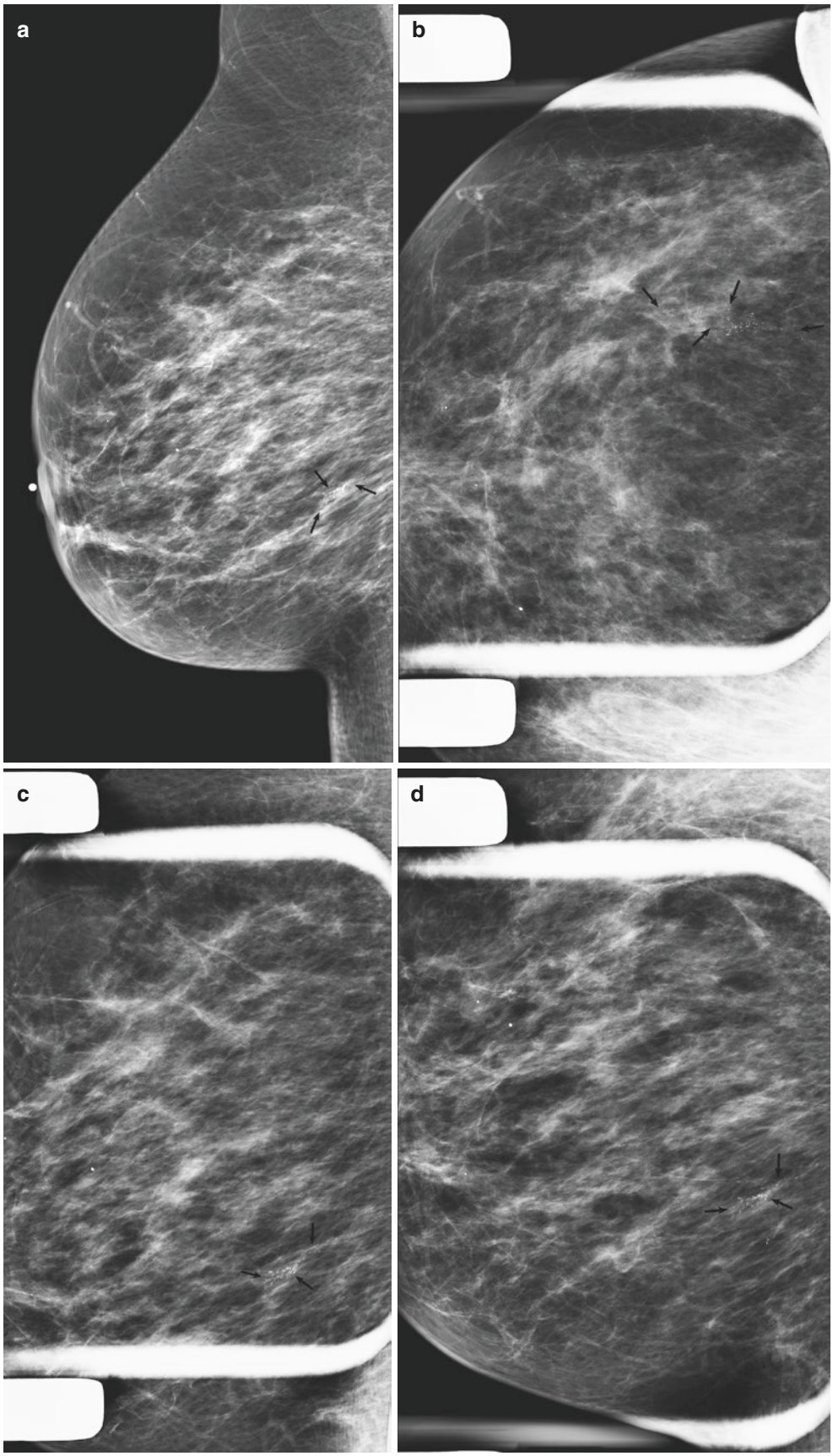

Fig. 3.13 Mammogram. ML view (**a**), CC spot magnification view (**b**), and ML spot magnification views (**c**, **d**) show pleomorphic calcifications in a linear distribution in the lower outer quadrant (*arrows*)

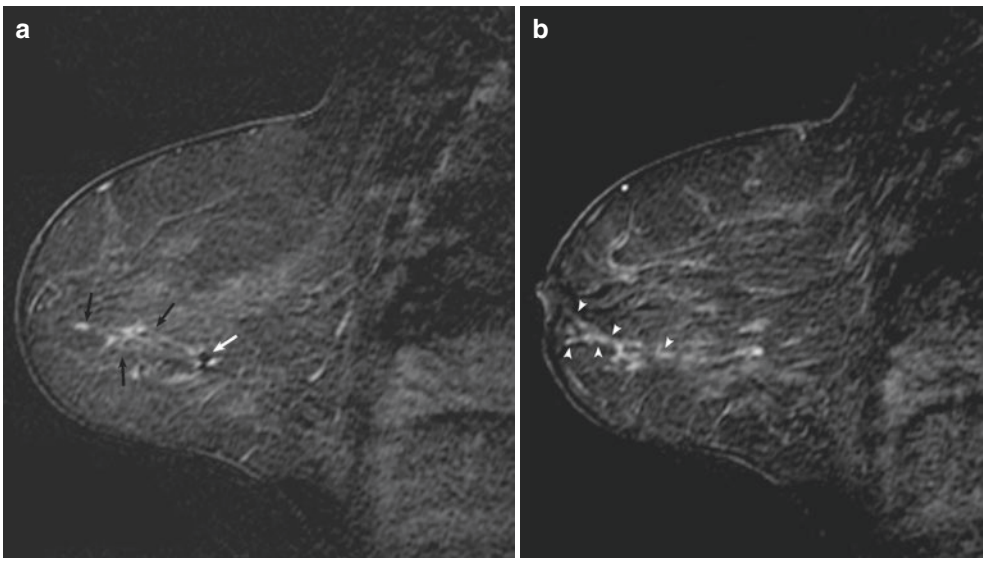

Fig. 3.14 (**a**) Sagittal post-contrast subtraction image shows linear nonmass enhancement (*black arrows*) corresponding to the pleomorphic calcifications on mammography. Biopsy clip artifact is seen (*white arrow*). (**b**) An additional sagittal post-contrast subtraction image reveals additional enhancement extending towards the nipple (*arrowheads*), for which there is no mammographic correlate

3.4 History

51-year-old woman with right nipple itchiness and erythema (Figs. 3.15, 3.16, 3.17, and 3.18).

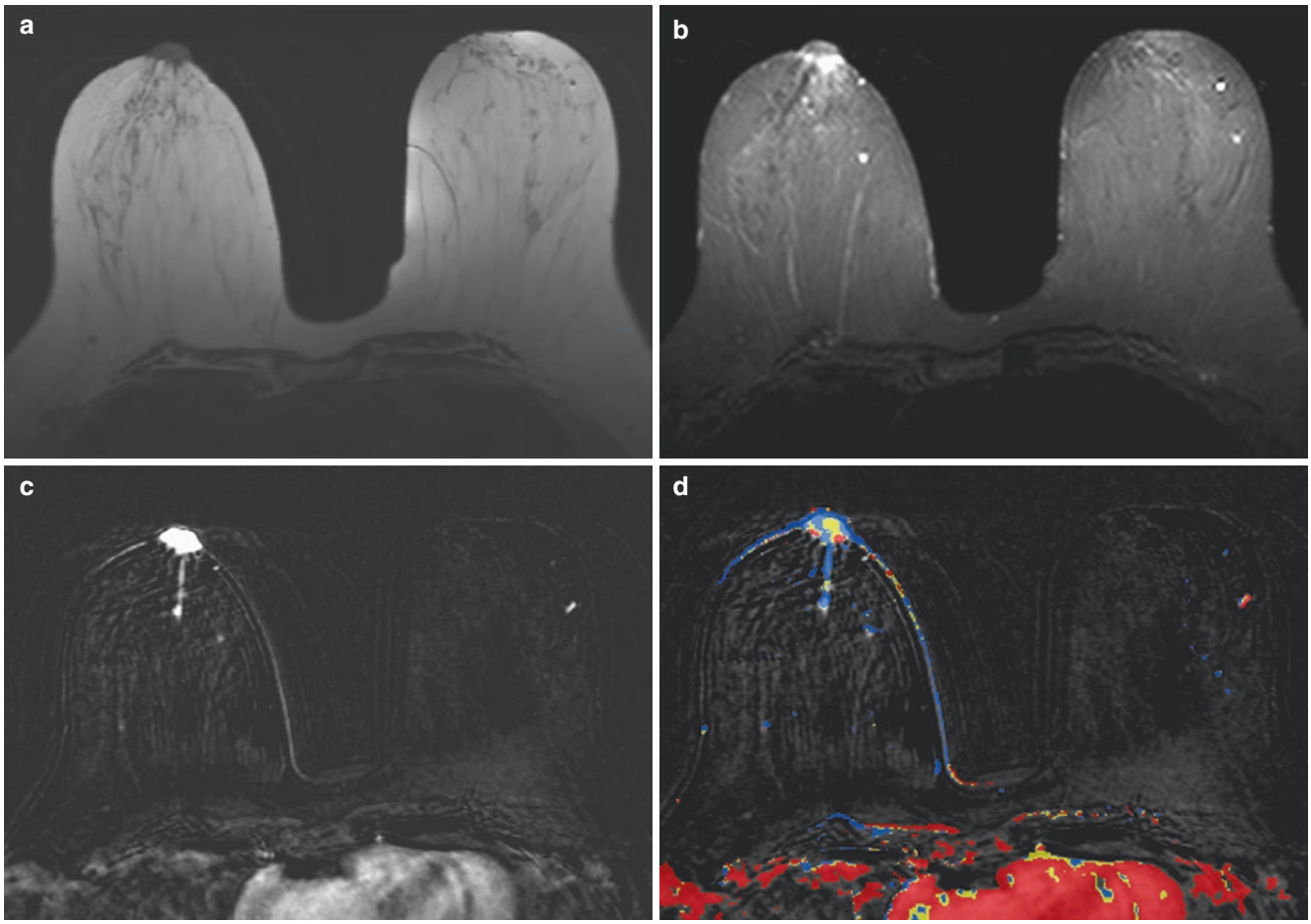

Fig. 3.15 Axial MR images of both breasts. (**a**) T1-weighted. (**b**) T2-weighted fat-saturated. (**c**) Post-contrast subtraction. (**d**) Corresponding computer-aided detection (CAD) images

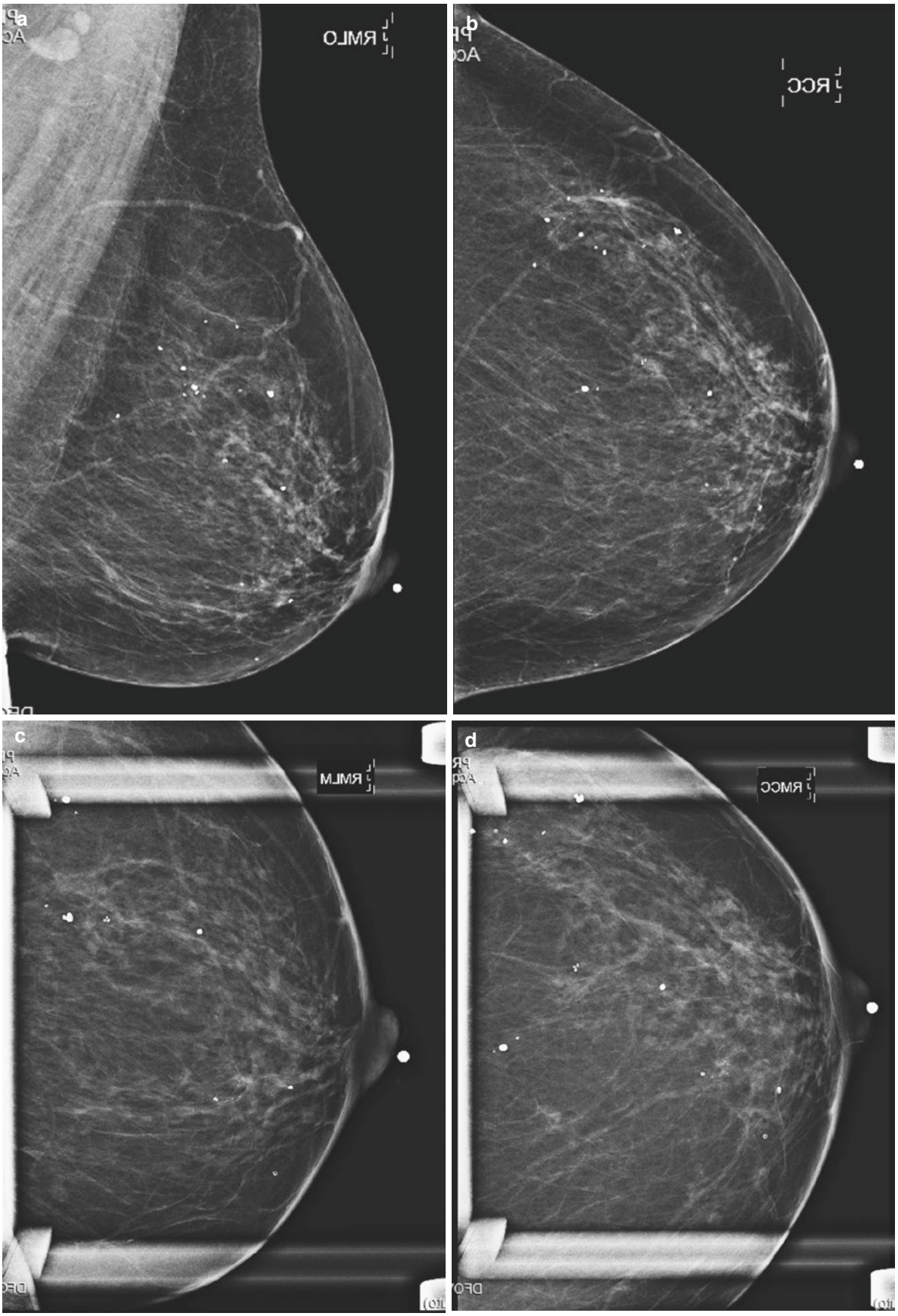

Fig. 3.16 Mammographic images of the right breast. Mediolateral oblique (MLO) view (**a**) and CC view (**b**) with corresponding retroareolar spot magnification views (**c**, **d**)

3.4 Paget's Disease

Teaching Points Paget's disease is a rare disease of the breast, accounting for 1–3% of all breast cancer cases. The disease is characterized by involvement of the nipple-areolar complex with malignant cells called Paget cells, manifested clinically by nipple/areolar itching, erythema, scaly skin, bloody nipple discharge, and nipple erosion, ulceration, or retraction. Diagnosis is usually made by a full-thickness punch biopsy of the nipple-areolar complex. Paget's disease of the breast is nearly always a sign of underlying breast malignancy, with most studies reporting the presence of a concurrent DCIS or invasive cancer in over 90% of patients. Approximately 50% of patients with Paget's disease also present with an associated palpable mass in the breast, 90% of whom are found to have invasive disease; a lesion without a palpable mass is usually associated with DCIS. On mammography, Paget's disease can be seen as nipple/areolar abnormalities such as skin thickening, malignant calcifications, or discrete lesions involving the nipple-areolar complex or breast parenchyma, but mammograms can appear normal in up to 50% of patients with Paget's disease, so correlation with clinical examination is critical. MR imaging is usually performed to detect underlying occult malignancy. Common MR findings of Paget's disease include asymmetric nipple enhancement and nodularity with or without associated features of DCIS and invasive carcinoma.

Image Findings

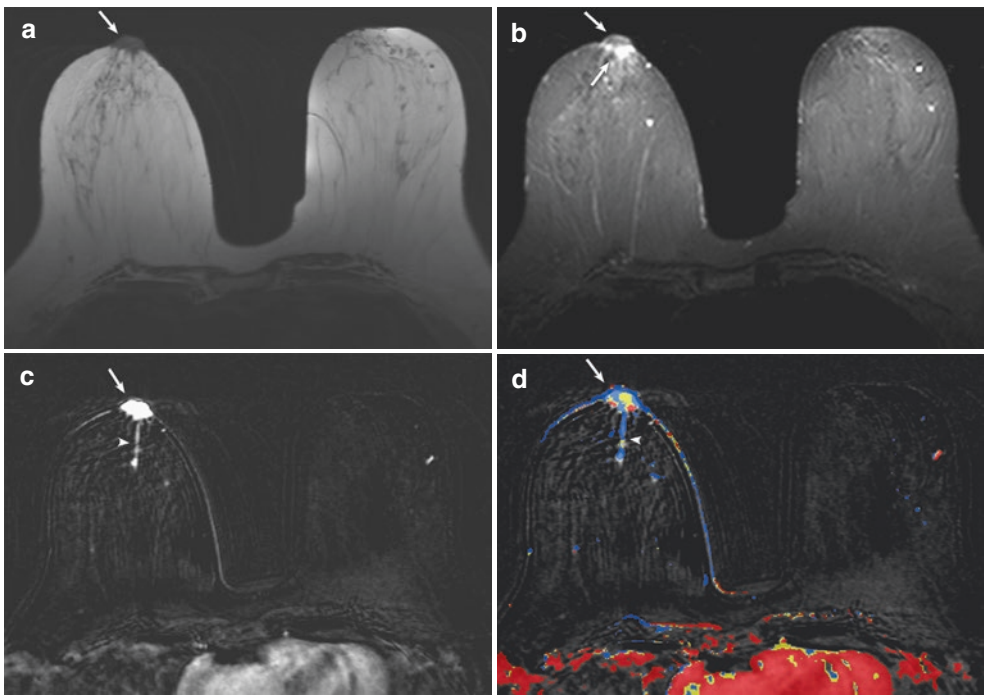

Fig. 3.17 Paget's disease with additional disease detected on MRI. Axial T1-weighted (**a**) and axial T2-weighted fat-saturated images (**b**) demonstrate T1 hypointensity and mild T2 hyperintensity of the right nipple (*arrow*), as well as marked retroareolar T2 hyperintensity (*arrow*). Axial post-contrast subtraction (**c**) with corresponding CAD images (**d**) demonstrate marked enhancement of the nipple (*arrow*) with mixed enhancement kinetics and additional linear nonmass enhancement posterior to the nipple (*arrowhead*)

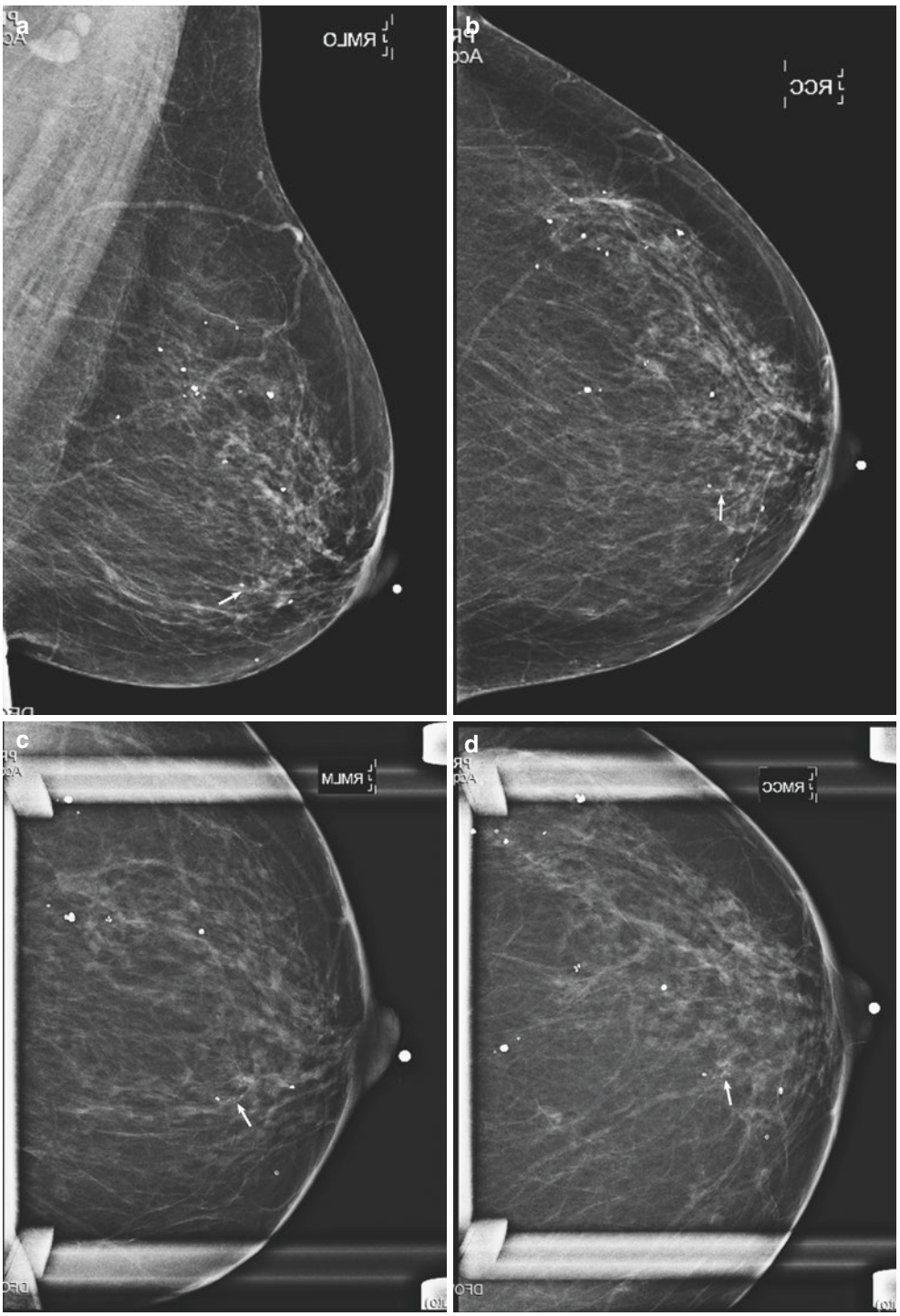

Fig. 3.18 Paget's disease on mammography. Right MLO (**a**) and CC (**b**) views with corresponding retroareolar spot magnification views (**c**, **d**) demonstrate a suspicious group of heterogeneous calcifications (*arrows*), which yielded DCIS on biopsy

3.5 History

49-year-old woman undergoing high-risk screening MRI (Figs. 3.19 and 3.20).

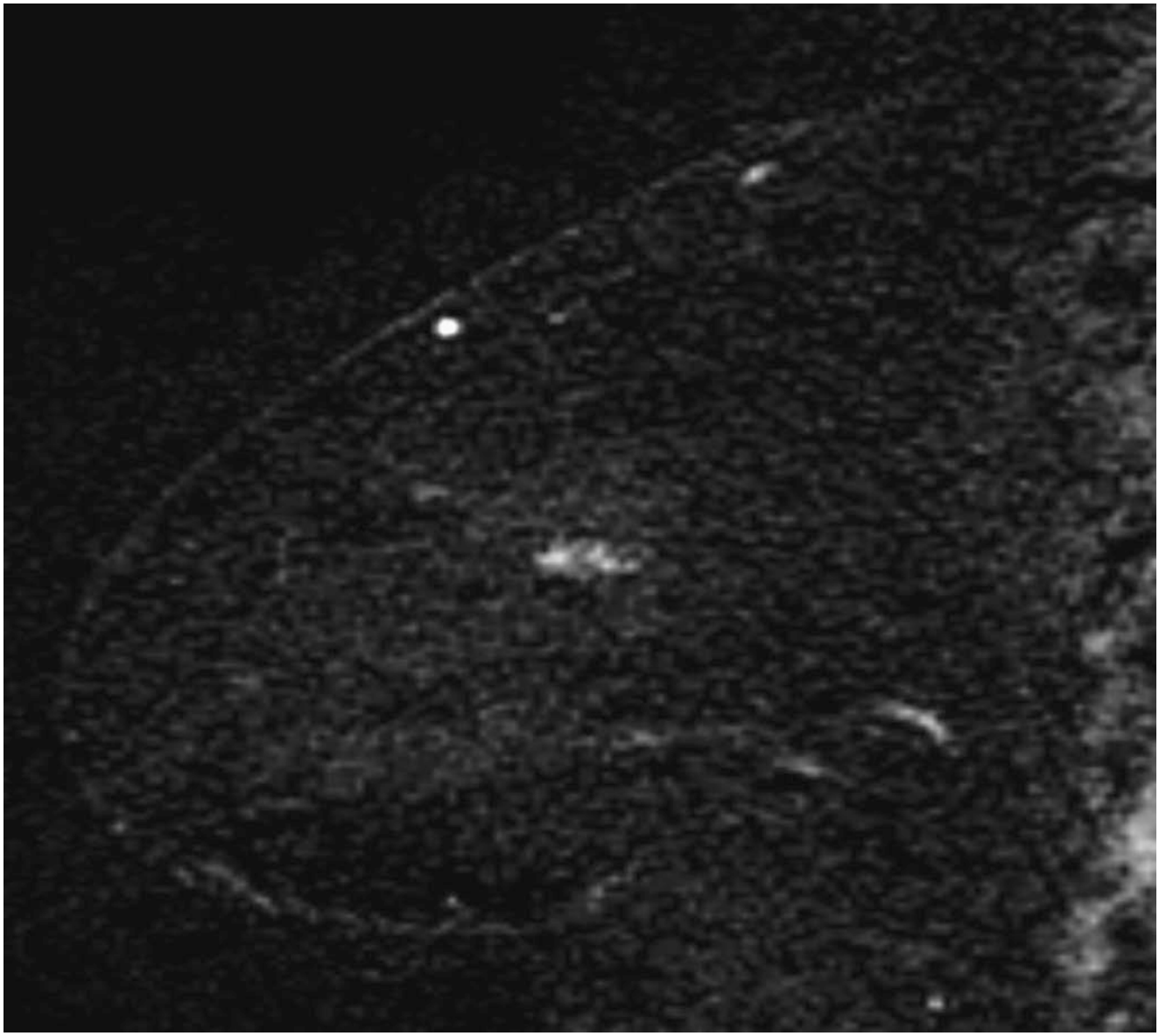

Fig. 3.19 Selected T1 post contrast fat-saturated image of the right breast

3.5 DCIS: Micropaillary

Teaching Points Ductal carcinoma-in-situ may be classified variably, taking into account architecture, nuclear pleomorphism, and the presence or absence of necrosis. Interest in classification stems in large part from the desire to use pathological features to help predict likelihood of recurrence, progression to invasive disease, and overall prognosis.

Micropapillary DCIS is an architectural subtype in which small club-like protuberances project into dilated ducts. Although some authors have associated micropapillary DCIS with lower nuclear grade and indolence, the micropapillary subtype has also been considered conversely to have negative implications for disease extent and prognosis, especially in more recent studies. It appears in several analyses as an independent risk factor for tumor recurrence.

The mammographic and sonographic features of both screen-detected and symptomatic DCIS have been well described, with mammography being the primary modality given its sensitivity for calcifications and sonography playing an adjunctive but important role, particularly in symptomatic patients and higher-grade disease. When used, MRI is the most sensitive examination for DCIS, which most frequently appears as non-mass enhancement, as illustrated in our case. Some unique aspects of the imaging of micropapillary DCIS have been revealed. Although most DCIS is detected mammographically through the presence of suspicious calcifications, the histologic extent of the disease is frequently greater than the extent of suspicious mammographic features. This discrepancy has been shown to be more pronounced in the architectural subtype of micropapillary DCIS. The imaging characteristics of micropapillary DCIS on mammography, sonography, and MRI were specifically reviewed by Lee et al. in a study of 42 tumors which were composed predominantly of micropapillary DCIS on pathology. Notably, the patient is often asymptomatic despite what may turn out to be extensive disease and, similarly, sonography is often negative. Pleomorphic calcifications were the most common imaging presentation. In this study, the infrequently used MRI showed non-mass enhancement in a segmental or regional distribution similar to other types of DCIS. Importantly, MRI was the only modality to accurately size the disease in the cases it was used. Debate on the appropriate preoperative use of breast MRI for both invasive or in-situ cancer is ongoing, but as the recommendations become more refined, consideration may be given to its use in the evaluation of micropapillary DCIS.

Image Findings

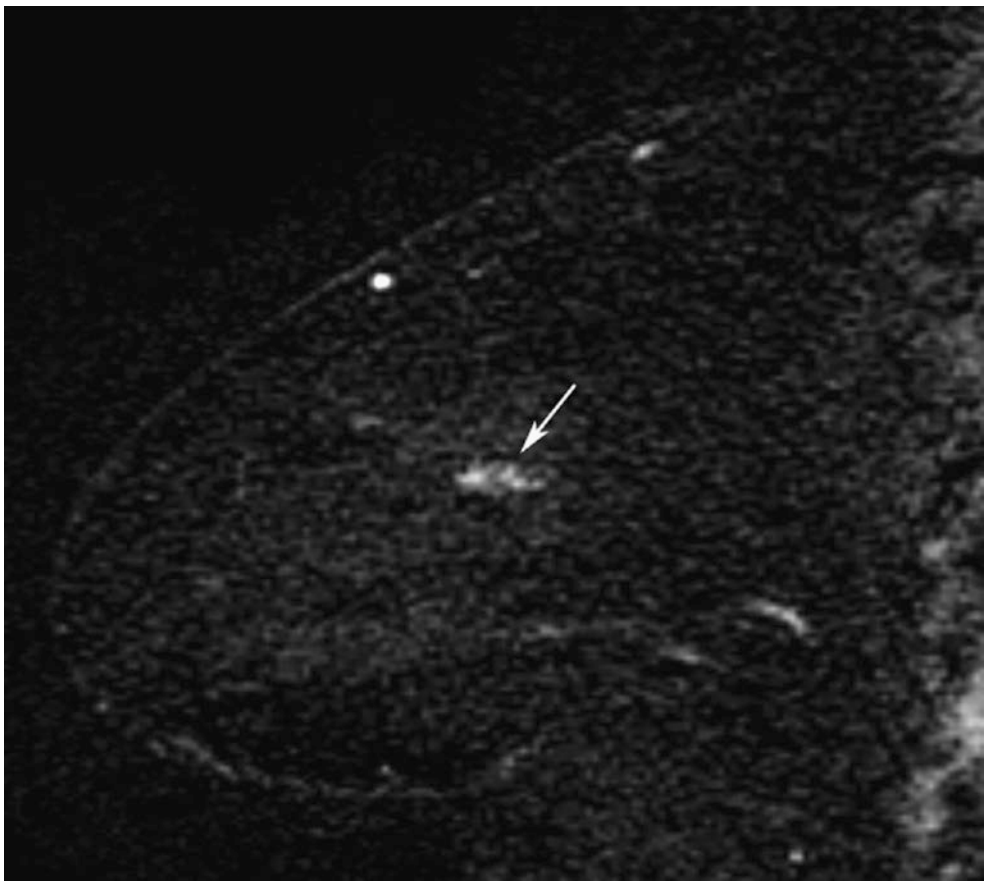

Fig. 3.20 Micropapillary DCIS. There is a 1.3 cm linear non-mass enhancement in the upper outer mid right breast. This area underwent MRI-guided biopsy, yielding micropapillary DCIS

3.6 History

67-year-old woman with newly diagnosed left breast IDC (Figs. 3.21, 3.22, 3.23, and 3.24).

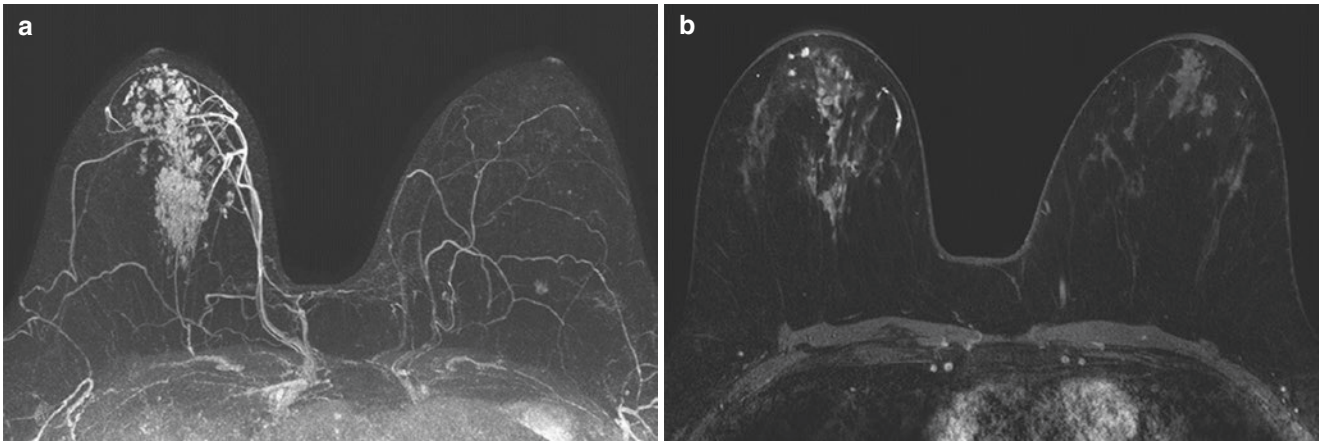

Fig. 3.21 (**a**) T1 post contrast axial 3D MIP. (**b**) Selected axial T1 post-contrast fat-saturated image

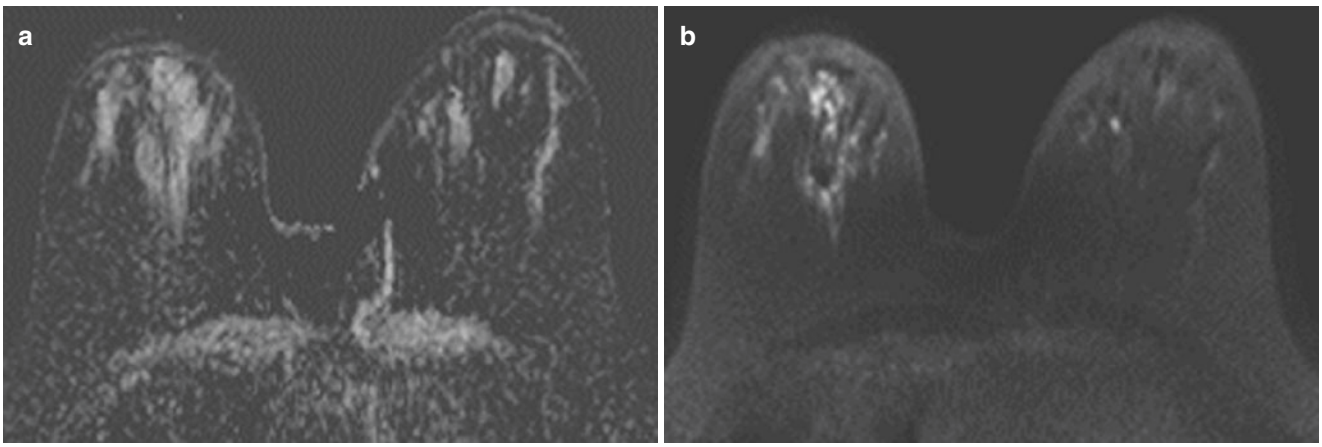

Fig. 3.22 (**a**) ADC. (**b**) DWI. DWI demonstrates high signal on $b = 800$ s/mm^2 corresponding to the non-mass enhancement representing

3.6 DCIS: DWI

Teaching Points The application of DWI for DCIS has to address several different questions including the following: (1) Can DCIS be distinguished from normal breast tissue and benign lesions? (2) Can DCIS be distinguished from invasive malignancy? (3) Can DCIS grades be differentiated?

Studies of DWI have demonstrated a mean apparent diffusion coefficient (ADC) value of DCIS that is intermediate between normal breast tissue and invasive disease. In three of these studies, the mean ADC of DCIS was shown to be 1.35–1.50×10^{-3} mm^2/s, compared to the mean ADC of normal breast tissue was 2.01–2.09×10^{-3} mm^2/s (sensitivity for DCIS was 91 % with an ADC value of $<1.81 \times 10^{-3}$ mm^2/s according to one study). The mean ADC of invasive disease investigated by two of these same authors was shown to be 1.2–1.29×10^{-3} mm^2/s. Woodhams et al. directly compared DCIS and invasive disease and found them statistical different. Concerns have been raised concerning the overlap of ADC values in malignant disease and benign lesions with potential false positives or false negatives depending on the threshold chosen.

High-nuclear grade (HNG) DCIS is considered more likely to progress to invasive cancer than lower-grade DCIS (non-HNG DCIS), and is considered more clinically significant. Using DWI to discriminate between grades of DCIS has had mixed results. Although Lim et al. in 2011 demonstrated statistically significant difference between the ADC values of grades of DCIS, other studies have not replicated that result. A 2012 study by Rahbar et al. did not demonstrate significant differences in the ADCs of HNG versus non-HNG DCIS. Further work is needed to determine the clinically applicability of DWI for assessing DCIS.

Image Findings

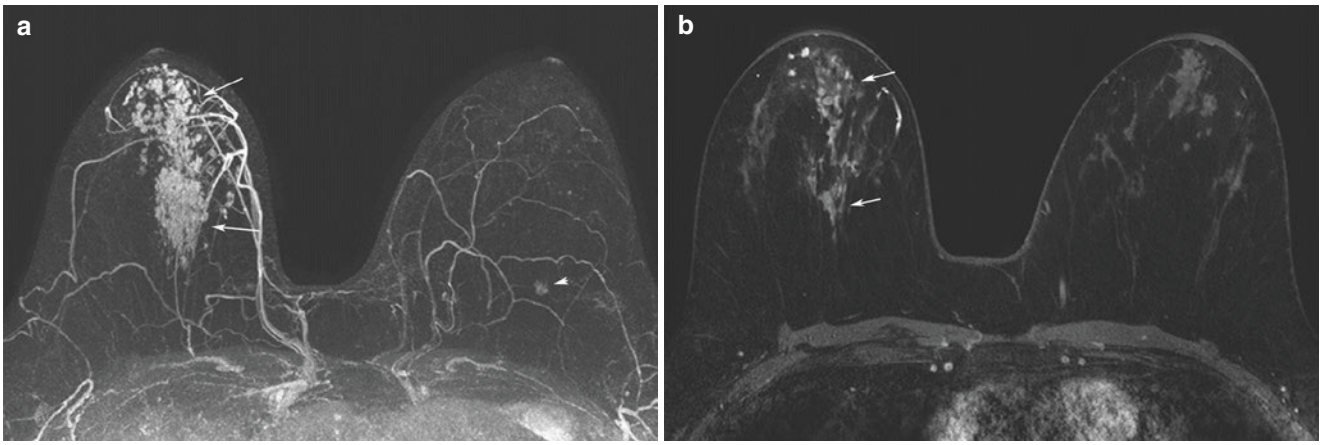

Fig. 3.23 (**a**) 3D MIP image demonstrates an 8 mm mass in the posterior left breast (*arrow head*) which underwent biopsy yielding IDC. (**b**) In the right breast segmentally distributed non mass enhancement is present spanning 9 cm

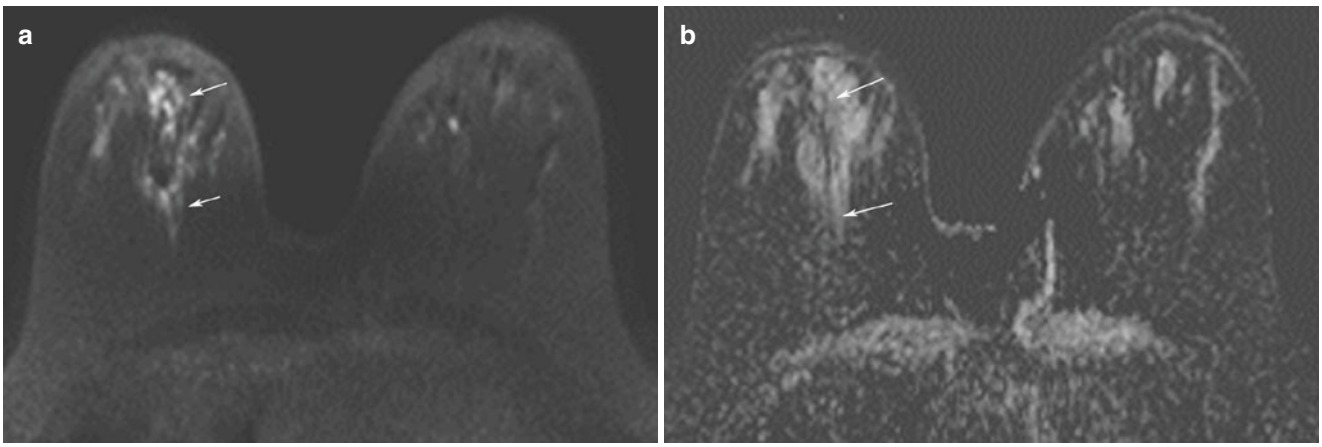

Fig. 3.24 (**a**) Low-grade DCIS. (**b**) ADC values are within the malignant range (1.35×10–3 mm^2/s), but higher than typical for invasive disease. Two site MR-guided biopsy demonstrated low nuclear-grade DCIS

3.7 History

42-year-old woman with recent diagnosis of left breast cancer. Breast MRI was performed to evaluate extent of disease (Figs. 3.25, 3.26, 3.27, and 3.28).

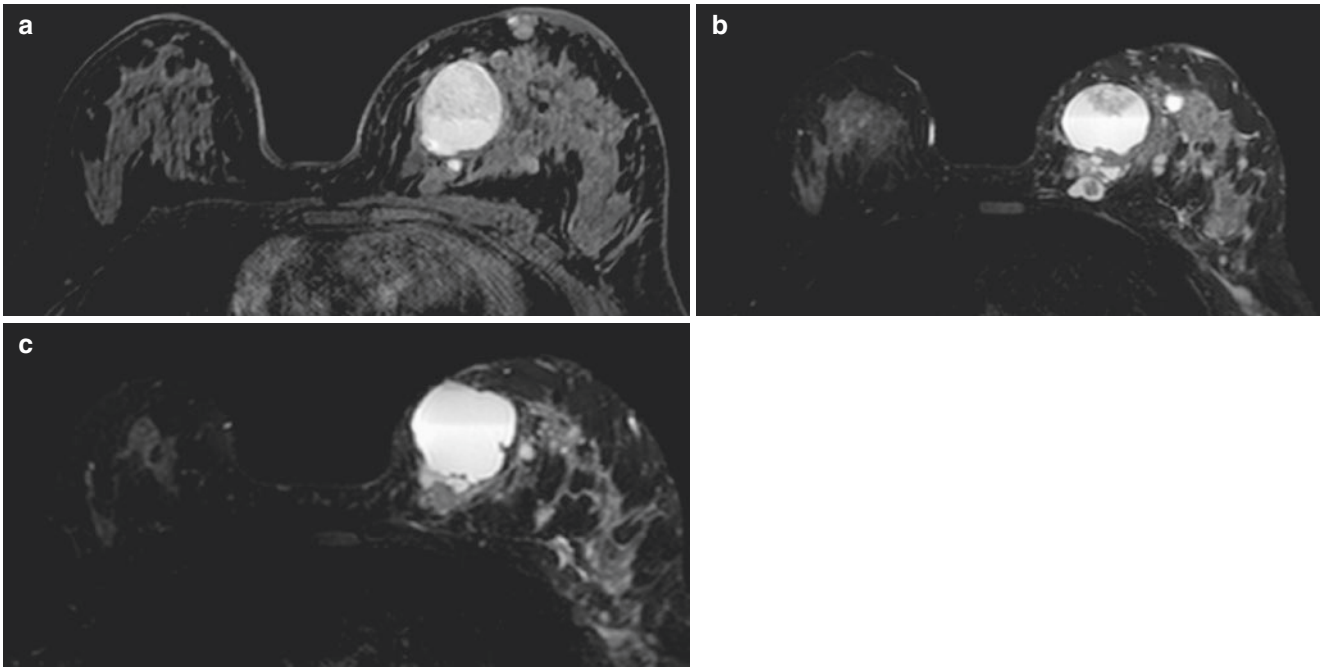

Fig. 3.25 (**a**) Axial T1-weighted fat-saturated image of both breasts. (**b**, **c**) Contiguous axial T2-weighted fat-saturated images of both breasts

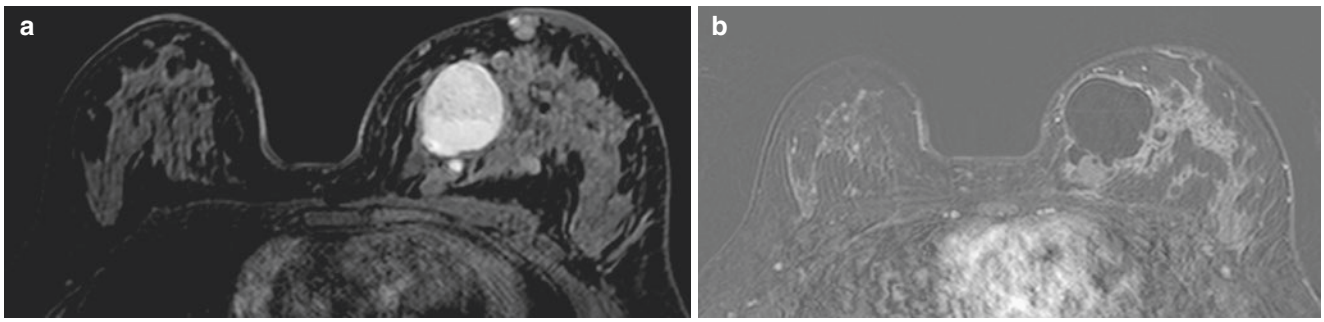

Fig. 3.26 (**a**) Axial T1-weighted fat-saturated post-contrast image of both breasts. (**b**) Corresponding axial post-contrast subtraction image

3.7 Invasive Ductal Carcinoma, Papillary

Teaching Points Papillary carcinoma of the breast is a rare type of invasive ductal carcinoma. It accounts for about 2 % of all breast cancers and usually occurs in post-menopausal women with an average age of 65 years. Clinically it can manifest as a palpable mass or nipple discharge and occurs most commonly in the retroareolar region. These lesions are classified as papillary DCIS, intracystic papillary carcinoma (ICPC) with or without invasion, or solid papillary carcinoma (if no cystic component is present). Invasive elements are typically detected at the periphery of the lesion. Histologically, it is characterized by a frond-like growth pattern on a fibrovascular core lacking a myoepithelial layer. Mammographically, papillary carcinoma can present as a round, oval, or lobulated mass, usually with a circumscribed margin. Sonographically, papillary carcinoma presents as a complex, cystic solid mass with posterior acoustic enhancement or as a hypoechoic solid mass. Increased vascularity is often present. On MRI, intracystic papillary carcinoma appears as complex, cystic solid mass or multicystic masses with heterogeneous internal composition with enhancing nodular masses and variable fluid content. Hemorrhagic contents can be hyperintense on both T1- and T2-weighted images and fluid-fluid levels may be seen, as illustrated in this case. Serous contents can show T1 hypointensity and T2 hyperintensity. Post-contrast images can show variable enhancement involving the cyst walls, septa, and mural nodules. Patients with papillary carcinoma have a more favorable prognosis than those with invasive ductal carcinoma–not otherwise specified (NOS).

Image Findings

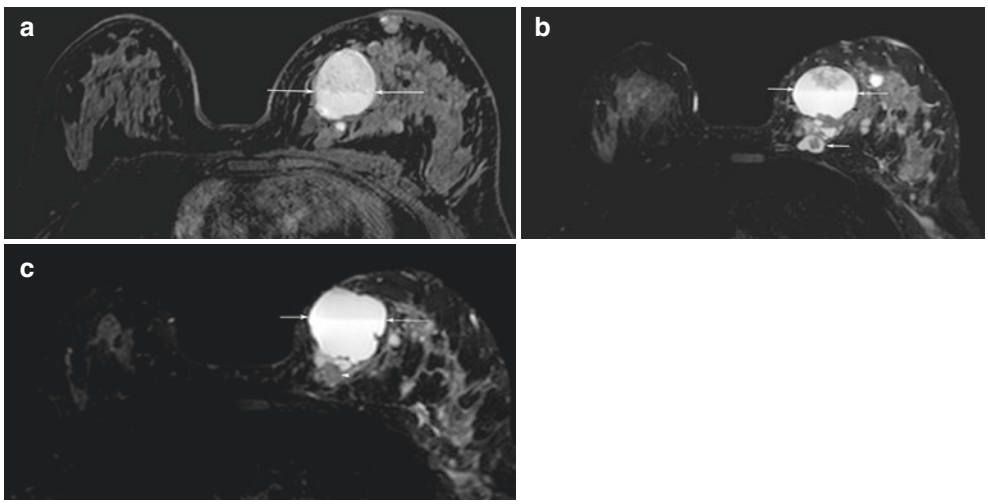

Fig. 3.27 Intracystic papillary carcinoma with surrounding DCIS. An axial T1-weighted fat-suppressed image (**a**) and axial T2-weighted fat-saturated images (**b**, **c**) show a complex, multicystic mass in the medial left breast with a fluid-fluid level (*arrows*) and T1- and T2-hyperintense layers reflecting hemorrhage (*arrowheads*). Additional T2-hyperintense cystic components are noted in the far posterior medial breast associated with a T1-hypointense mass (*arrowhead*)

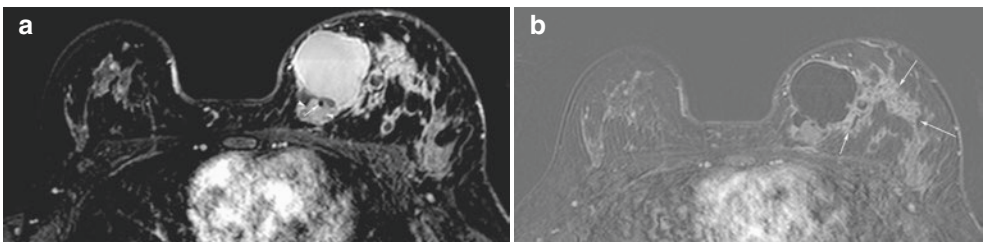

Fig. 3.28 (**a**) Axial T1-weighted fat-saturated post-contrast image shows a solid mass (*arrowheads*) within the posterior aspect of the multicystic mass. A clip artifact (*arrow*) within this solid component is from a biopsy, which yielded papillary carcinoma. (**b**) Axial post-contrast subtraction image reveals that the solid mass has mild enhancement. In addition, diffuse adjacent enhancement (*arrows*) is present in the central and outer breast, corresponding to an area of suspicious calcifications on mammography. Stereotactic biopsy of the calcifications yielded DCIS. The patient underwent left mastectomy, with final pathology revealing intracystic papillary carcinoma and extensive DCIS. No axillary lymph node metastases were present

3.8 History

59-year-old woman with newly diagnosed left breast malignancy with axillary metastasis. Breast MRI was performed to evaluate extent of disease (Figs. 3.29, 3.30, 3.31, 3.32, 3.33, 3.34, 3.35, 3.36, 3.37, 3.38, 3.39, and 3.40).

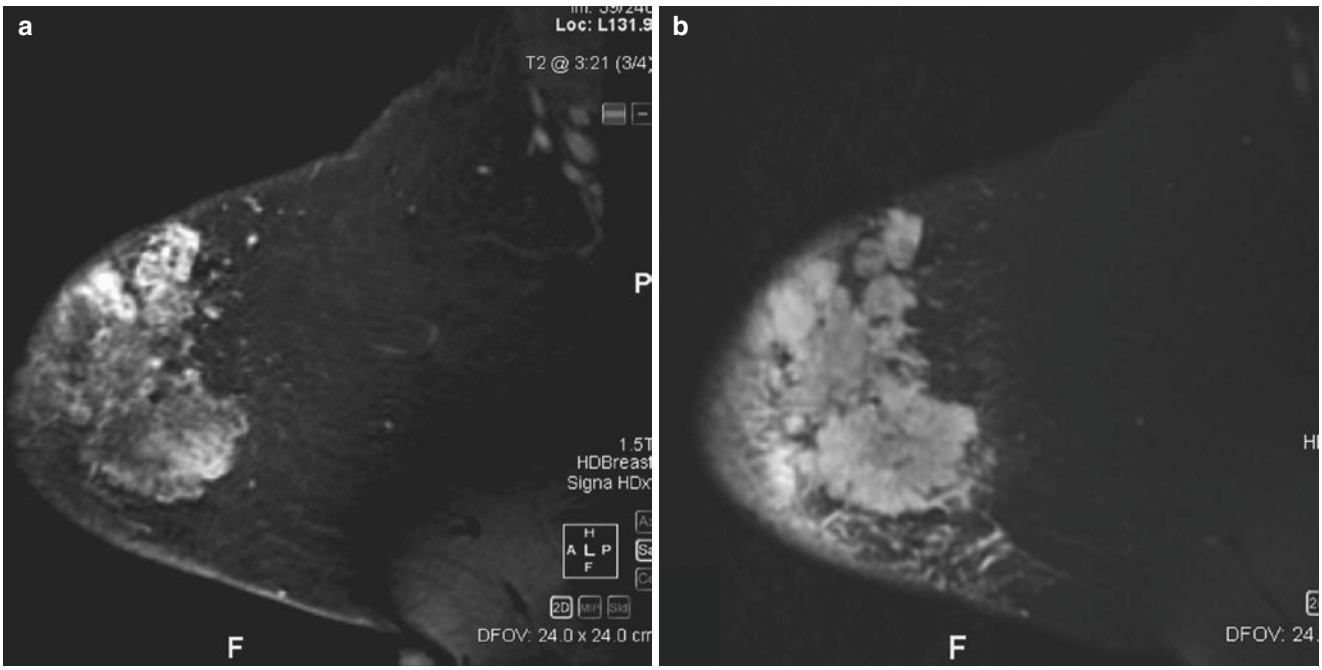

Fig. 3.29 (**a**) Sagittal T1-weighted fat-saturated post-contrast image of the mid left breast. (**b**) Corresponding sagittal T2-weighted fat-saturated image

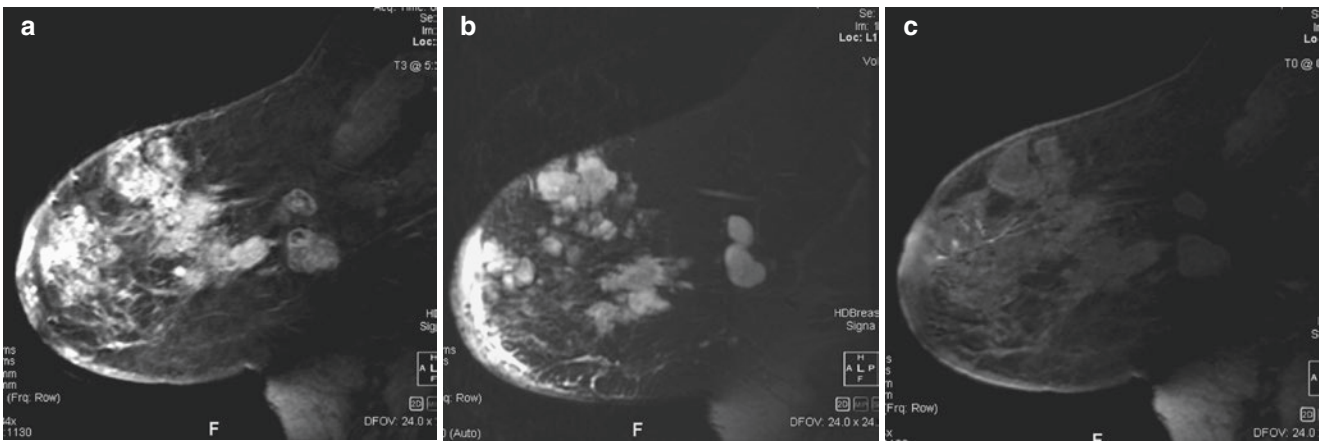

Fig. 3.30 (**a**) Sagittal T1-weighted fat-saturated post-contrast image of the outer left breast. (**b**) Corresponding sagittal T2-weighted fat-saturated image. (**c**) Corresponding sagittal T1-weighted fat-saturated pre-contrast image

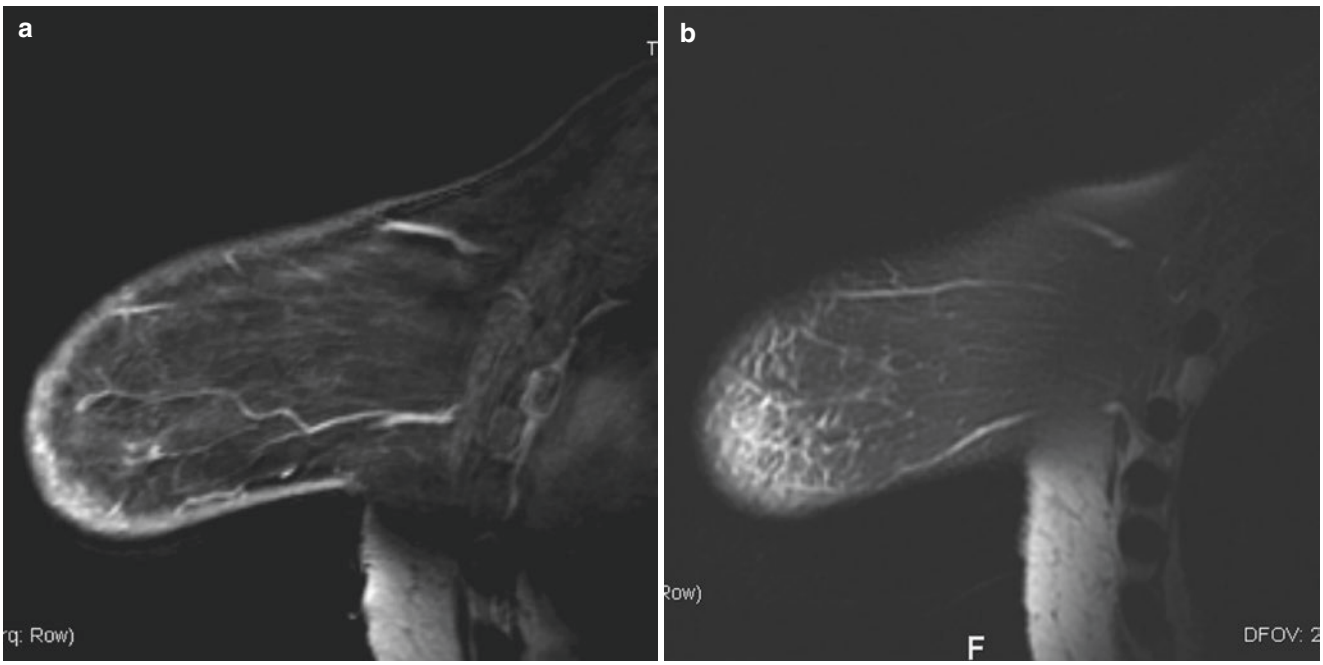

Fig. 3.31 (**a**) Sagittal T1-weighted fat-saturated post-contrast image of the medial left breast. (**b**) Corresponding sagittal T2-weighted fat-saturated image

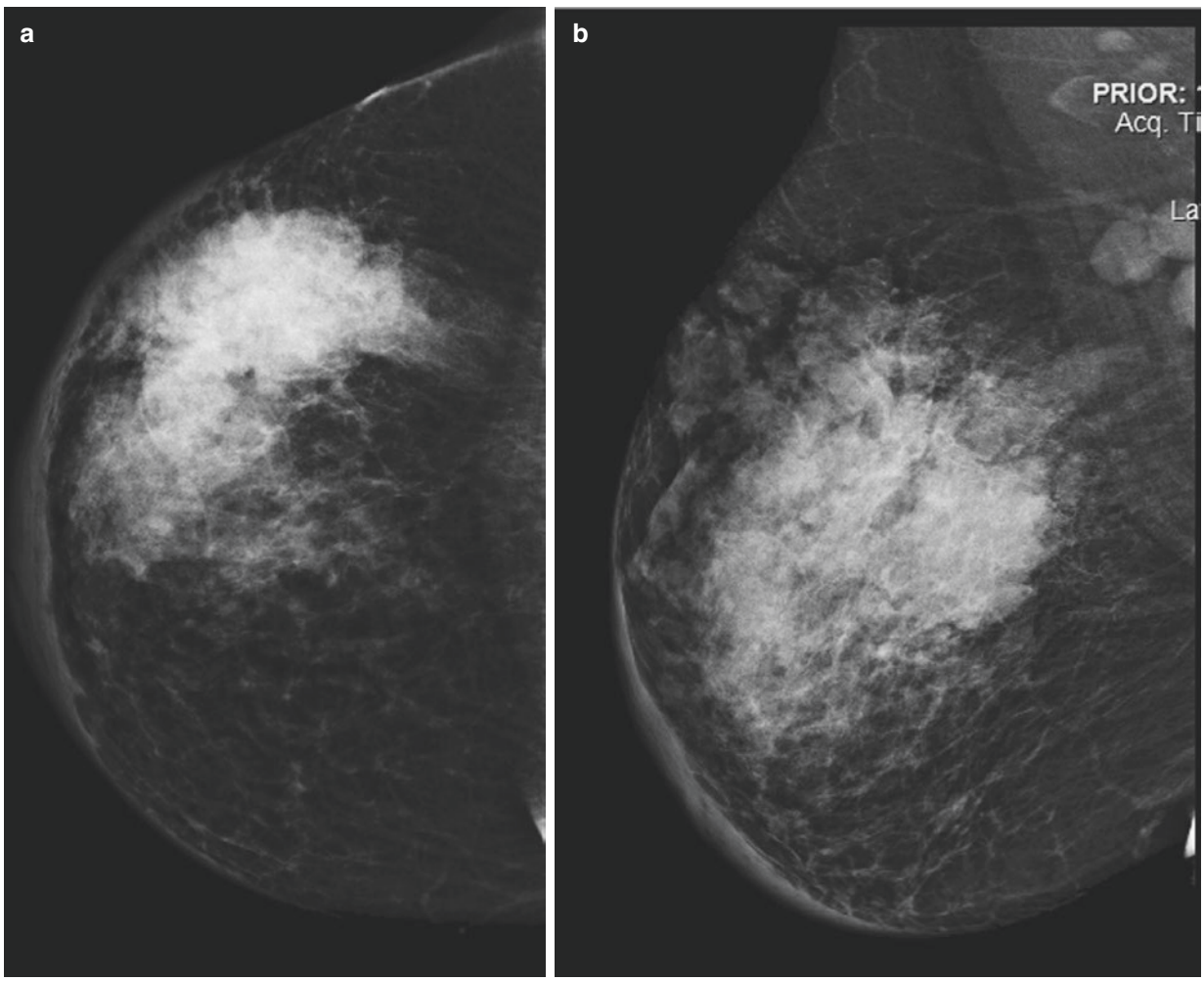

Fig. 3.32 Mammogram. Left breast CC view (**a**) and MLO view (**b**)

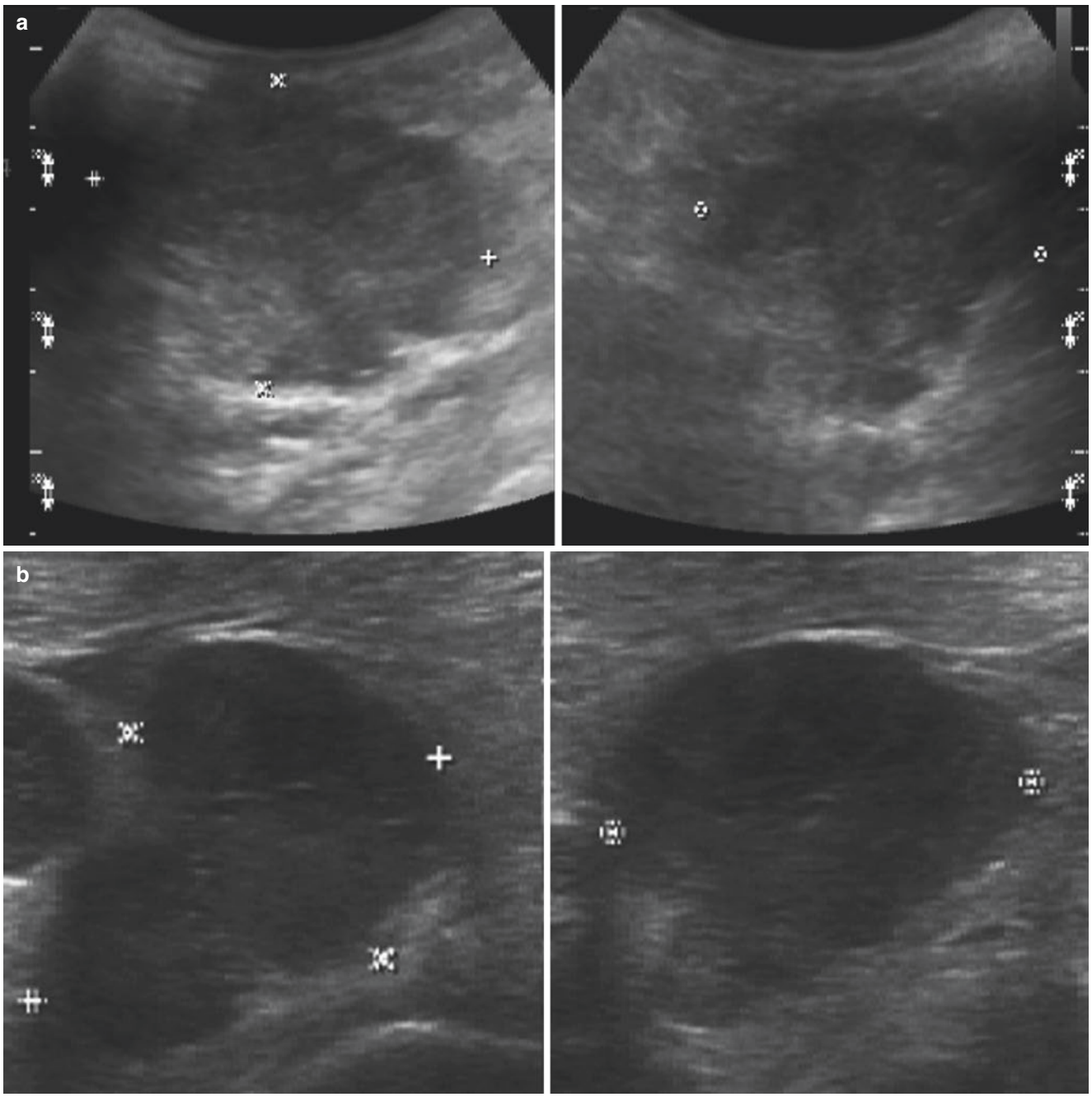

Fig. 3.33 Targeted ultrasound images of the left upper outer breast (**a**) and left axilla (**b**)

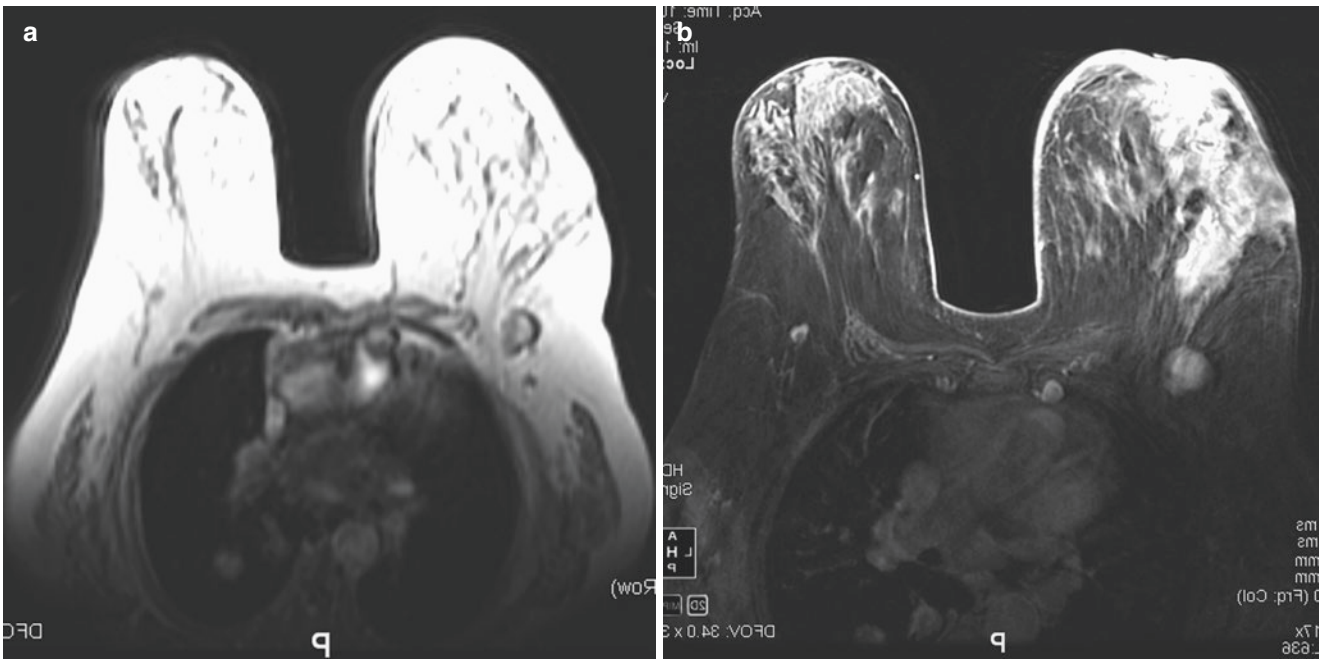

Fig. 3.34 (**a**) Axial localizer image. (**b**) Corresponding axial T1-weighted fat-saturated delayed post-contrast image

3.8 Invasive Ductal Carcinoma, Mucinous

Teaching Points Mucinous carcinoma of the breast, a form of invasive ductal carcinoma, is sometimes called colloid carcinoma. The tumor is made up of abnormal cells within pools of mucin, a key component in the slimy, slippery mucus. It can histologically be divided into pure mucinous breast cancer or mixed mucinous breast cancer. Mucinous carcinoma is extremely rare in men and in women (2 % of all breast cancers). It is more common after menopause, in the 60s or early 70s. Mammographically, the presence of mucin results in a low-density and well-defined lobular mass. Sonographically, mixed cystic and solid components, posterior acoustic enhancement, and micro-lobulated margins are commonly seen. On MRI, they can have very high signal intensity on T2-weighted images, as illustrated in this case, because of the water component in mucin. Post-contrast enhancement can be variable. Typically, a pure mucinous subtype carries a better prognosis than invasive ductal carcinoma NOS. Mixed mucinous carcinoma of the breast tends to demonstrate more aggressive behavior than the pure subtype, as illustrated in this case with distant metastasis.

Image Findings

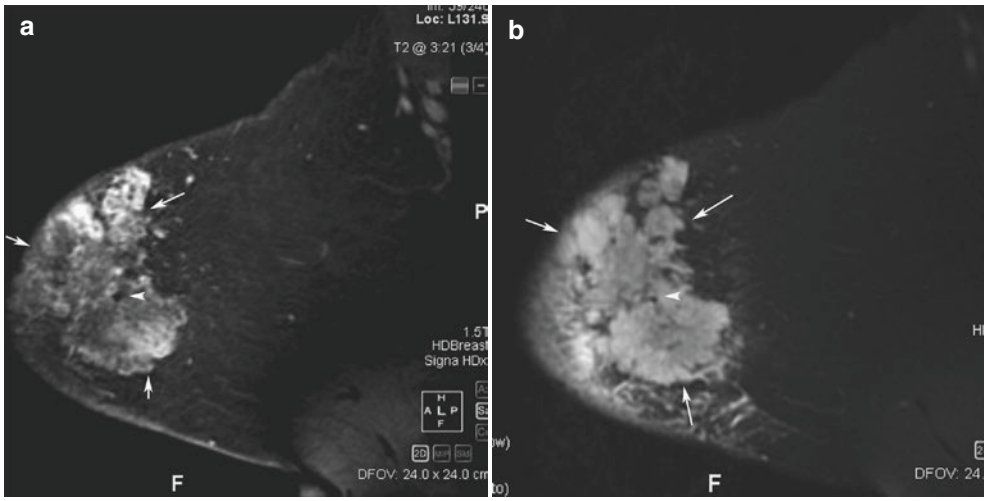

Fig. 3.35 Mucinous carcinoma. (**a**) Sagittal T1-weighted fat-saturated post-contrast image demonstrates several large, conglomerate, irregular masses (*arrows*) occupying most of the mid to anterior breast, with central clip artifact (*arrowhead*) from a biopsy that yielded invasive ductal carcinoma with mixed mucinous features. (**b**) Sagittal T2-weighted fat-saturated image shows these masses to have homogeneous high T2 signal, likely reflecting both the water content of mucin and areas of necrosis

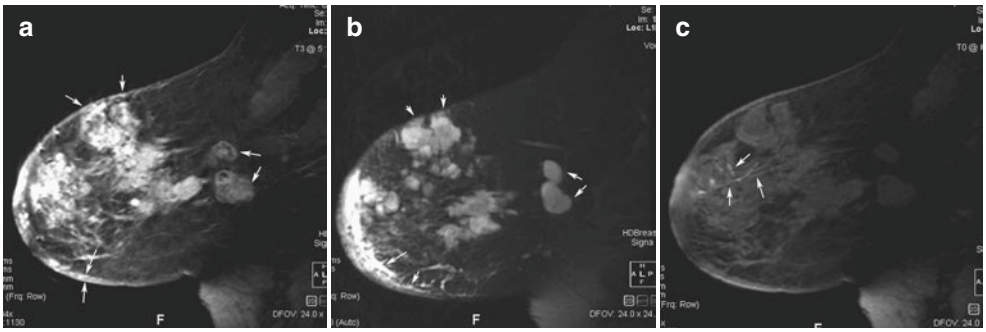

Fig. 3.36 (**a**) Sagittal T1-weighted fat-saturated post-contrast image of the outer breast shows the irregular masses extending into the outer breast and superficially to the skin (*arrows*). Posteriorly, enlarged low axillary lymph nodes are present, corresponding to the known metastases (*arrows*). (**b**) Sagittal T2-weighted fat-saturated image shows the masses and axillary lymph nodes to have homogeneous T2 hyperintensity (*arrows*). Both focal and diffuse skin enhancement and edema are present owing to the combination of direct skin invasion and secondary obstruction from axillary adenopathy. (**c**) Sagittal T1-weighted fat-saturated pre-contrast image shows subareolar linear branching high signal intensity (*arrows*), representing mildly dilated ducts containing hemorrhagic or proteinaceous debris

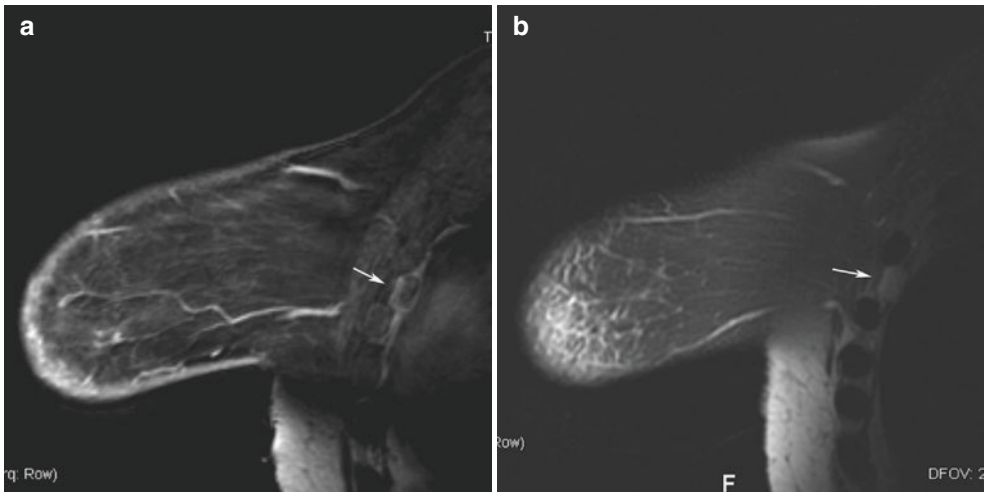

Fig. 3.37 Sagittal T1-weighted fat-saturated post-contrast image (**a**) of the medial breast demonstrates an enlarged left internal mammary lymph node (*arrow*) with peripheral enhancement and diffuse high T2 signal (**b**) (*arrow*). The peripheral enhancement pattern suggests central necrosis. PET/CT imaging (*not shown*) demonstrated focal FDG uptake involving the left internal mammary lymph node, suspicious for metastatic disease

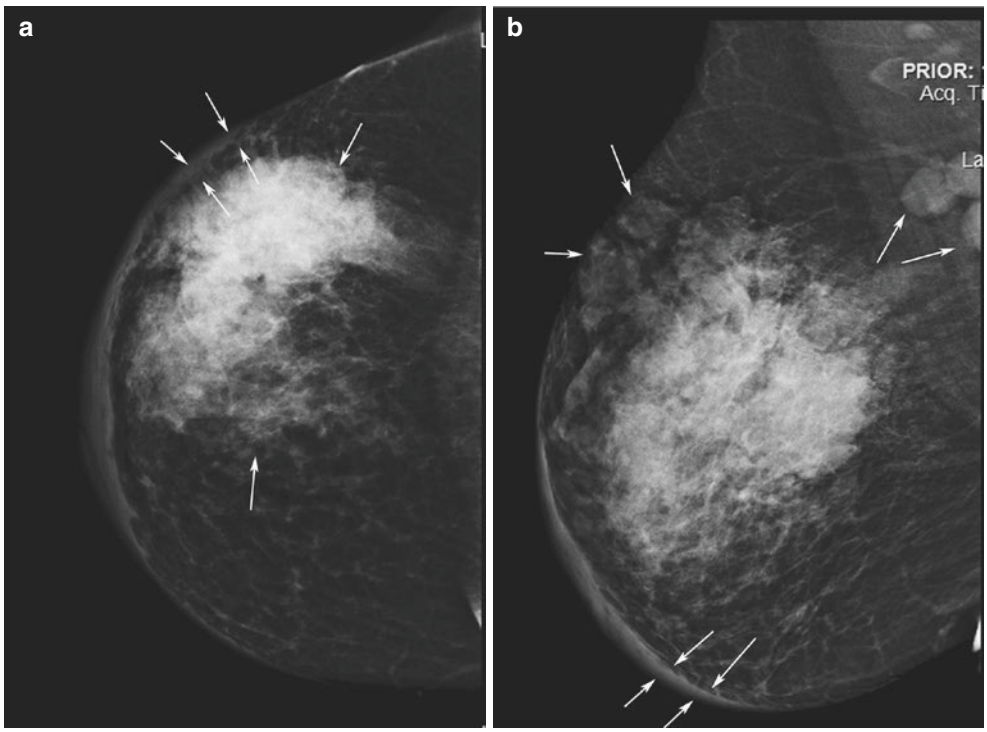

Fig. 3.38 CC (**a**) and MLO (**b**) mammographic images show large irregular masses occupying most of the upper outer left breast with associated diffuse skin thickening, axillary adenopathy, and cutaneous extension of the low-density mass involving the upper breast (*arrows*)

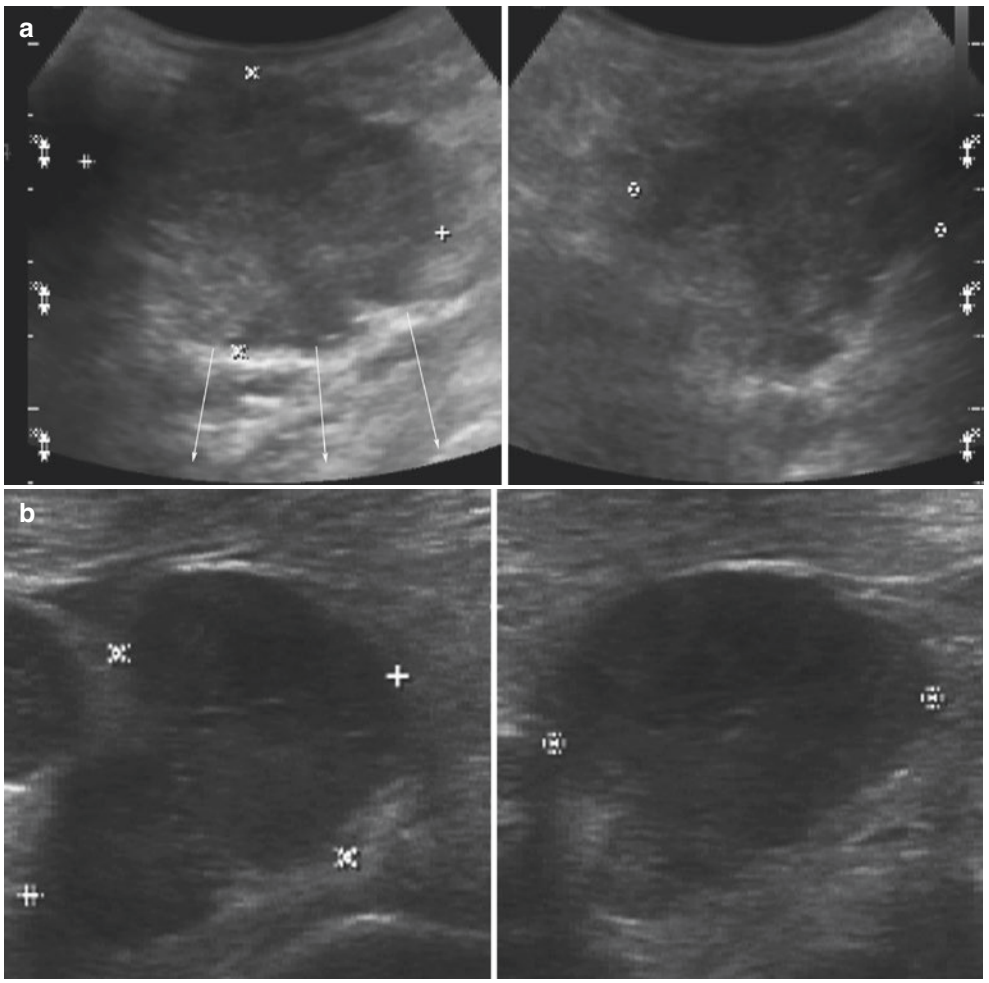

Fig. 3.39 (**a**) Sonography shows a partially imaged large hypoechoic mass with irregular margins in the upper outer left breast, corresponding to the known malignancy. Mild posterior acoustic enhancement is present (*arrows*). (**b**) Irregular large hypoechoic lymph nodes are sonographically evident in the low axilla, corresponding to the known metastatic disease

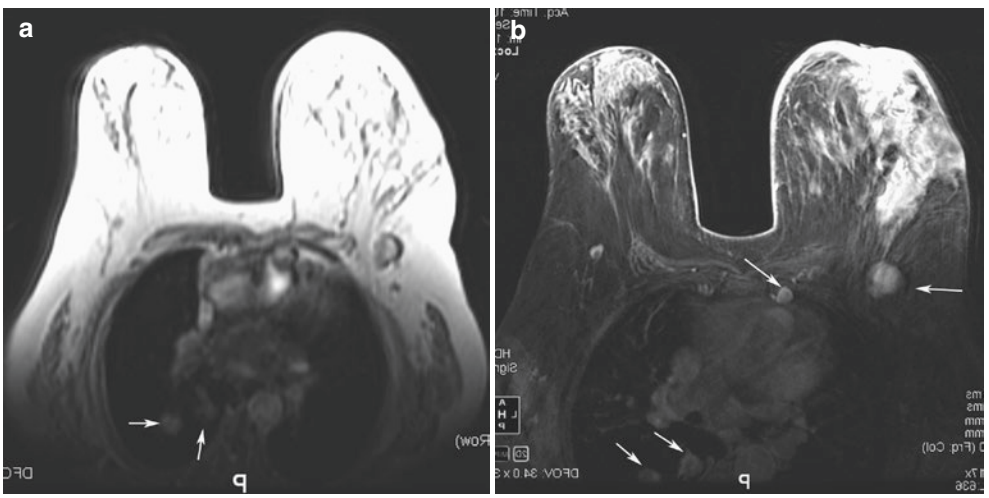

Fig. 3.40 (**a**) Axial localizer image shows T2 hyperintense lesions in the right lower lobe of the lung (*arrows*). (**b**) Corresponding axial T1-weighted fat-saturated post-contrast image shows enhancement of these lesions, suspicious for pulmonary metastases. In addition, enlarged left internal mammary and low axillary lymph nodes are seen (*arrows*). Subsequent biopsy confirmed metastatic disease

3.9 History

A 61-year-old woman with recently diagnosed left breast malignancy. Breast MRI was performed to evaluate extent of disease (Figs. 3.41, 3.42, 3.43, and 3.44).

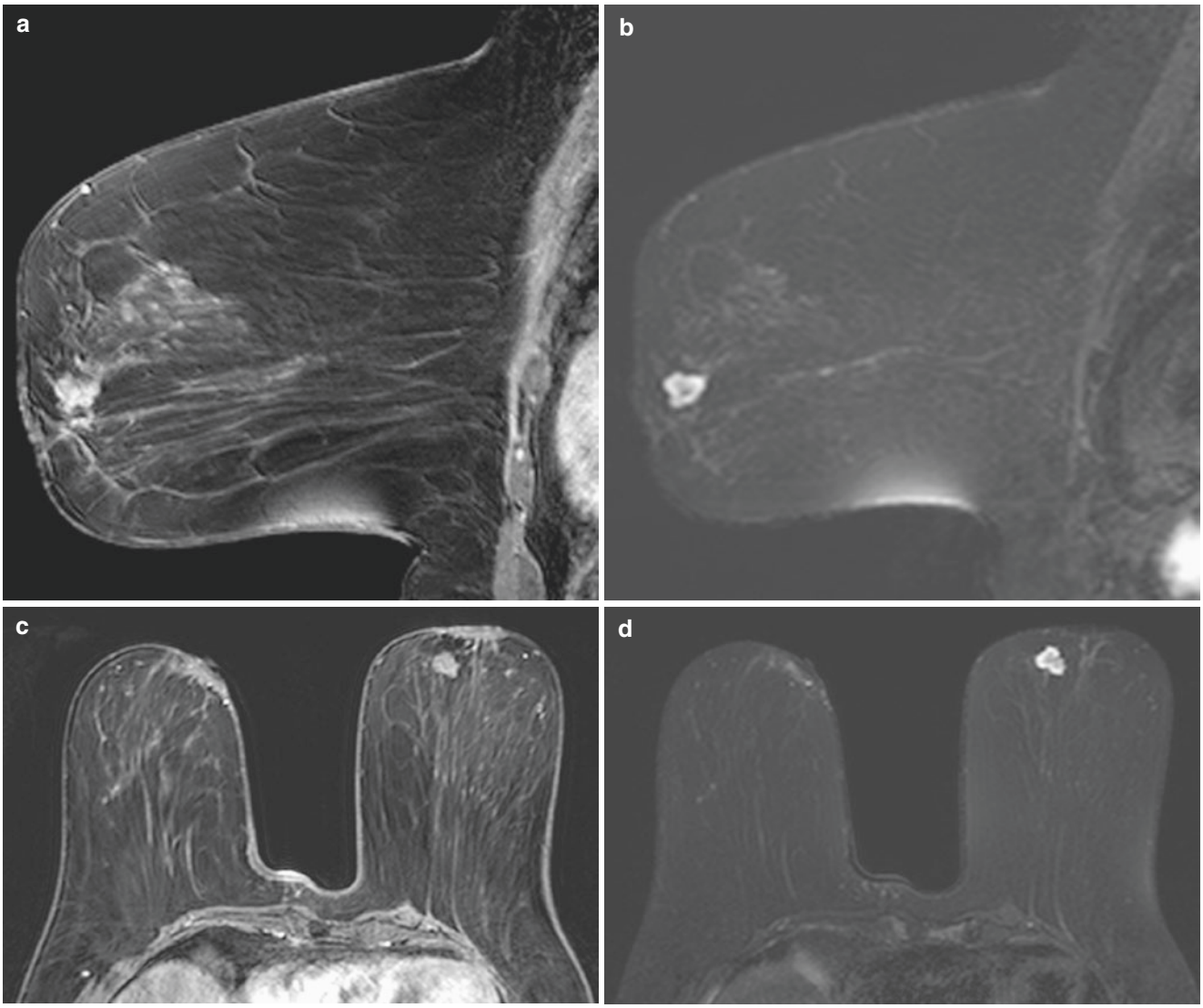

Fig. 3.41 (**a**) Sagittal T1-weighted fat-saturated post-contrast image of the left breast. (**b**) Corresponding sagittal T2-weighted fat-saturated image. (**c**) Axial T1-weighted fat-saturated post-contrast image of both breasts. (**d**) Corresponding axial T2-weighted fat-saturated image

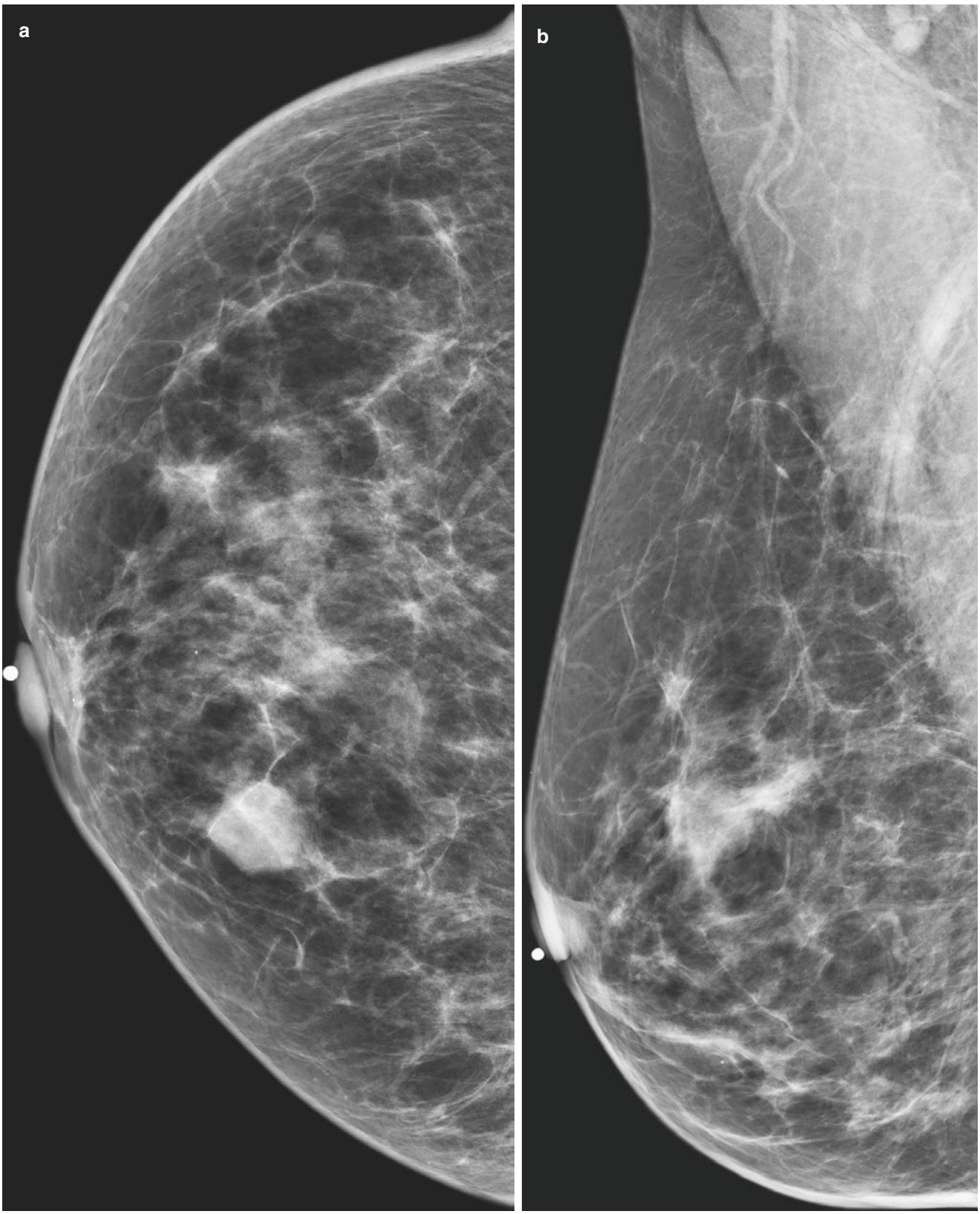

Fig. 3.42 Mammogram. CC image (**a**) and MLO image (**b**) of the left breast. CC spot compression image (**c**) and MLO spot compression image (**d**) of the left breast. (**e**) A targeted left breast ultrasound

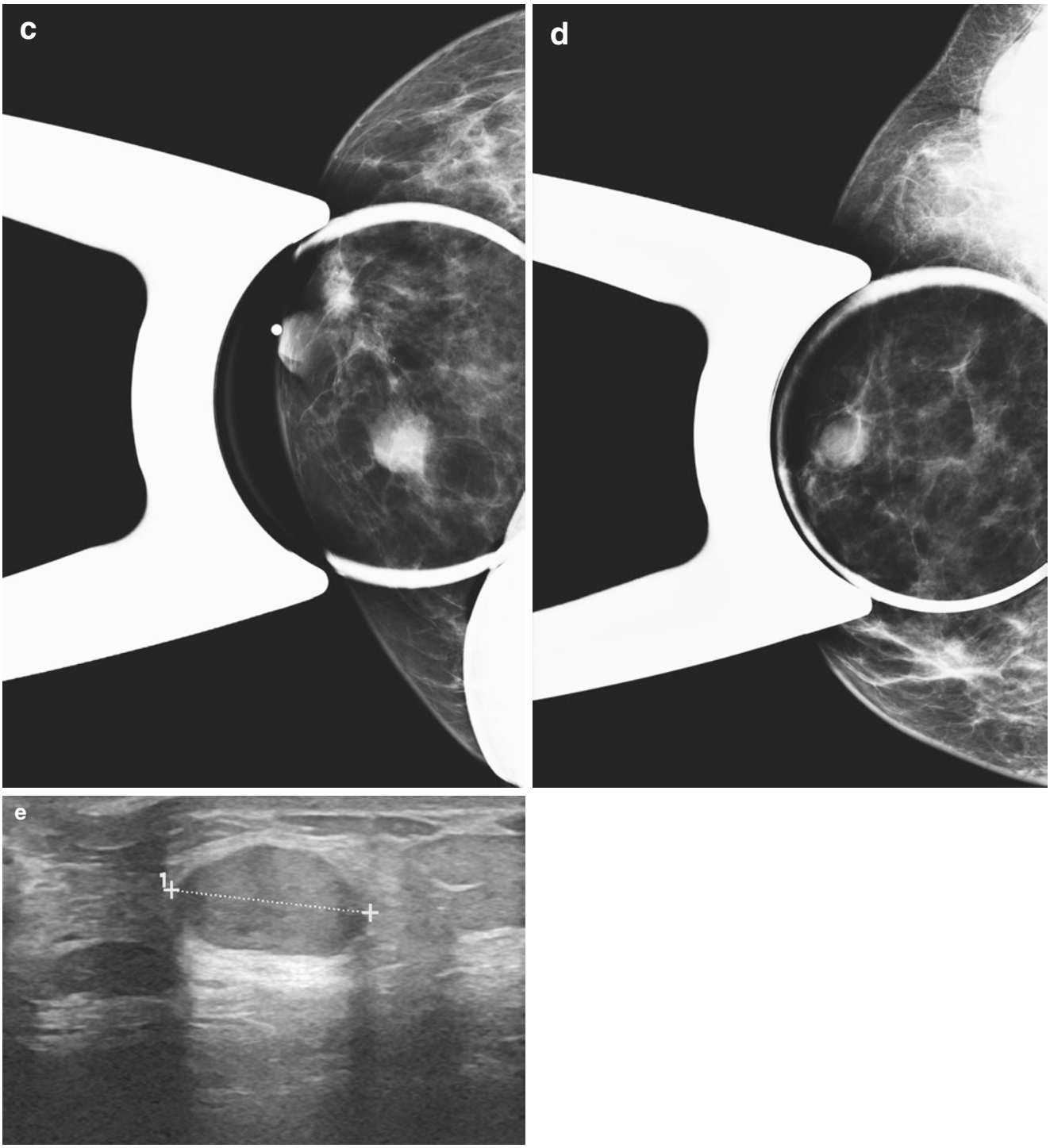

Fig. 3.42 (continued)

3.9 Invasive Ductal Carcinoma, Pure Mucinous 1

Teaching Points Mucinous carcinoma of the breast is a rare form of invasive ductal carcinoma. On mammography, the presence of mucin results in a low-density and relatively well-defined lobular mass. On sonography, a homogeneously hypoechoic mass is seen with posterior acoustic enhancement. On MRI, the masses can have very high signal intensity on T2-weighted images. All these imaging features are illustrated in this patient with a diagnosis of pure mucinous carcinoma. The pure mucinous subtype carries a better prognosis with a lower chance of axillary metastasis. The patient underwent breast conservation with final pathology of pure mucinous carcinoma, stage T1N0.

Image Findings

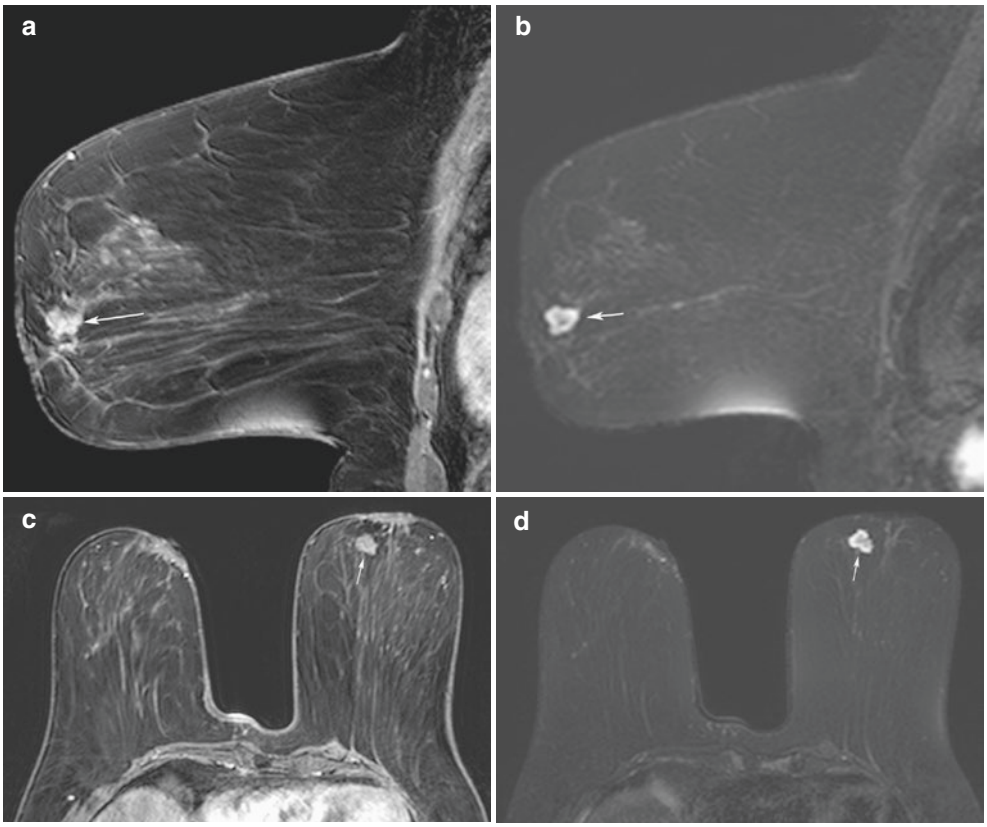

Fig. 3.43 Pure mucinous carcinoma. Sagittal (**a**) and axial (**b**) T1-weighted fat-saturated post-contrast images show a 1.6-cm irregular mass (*arrow*) in the retro-areolar left breast. Corresponding axial post-contrast (**c**) and axial T2-weighted fat-saturated (**d**) images show the mass (*arrow*) to have high T2 signal

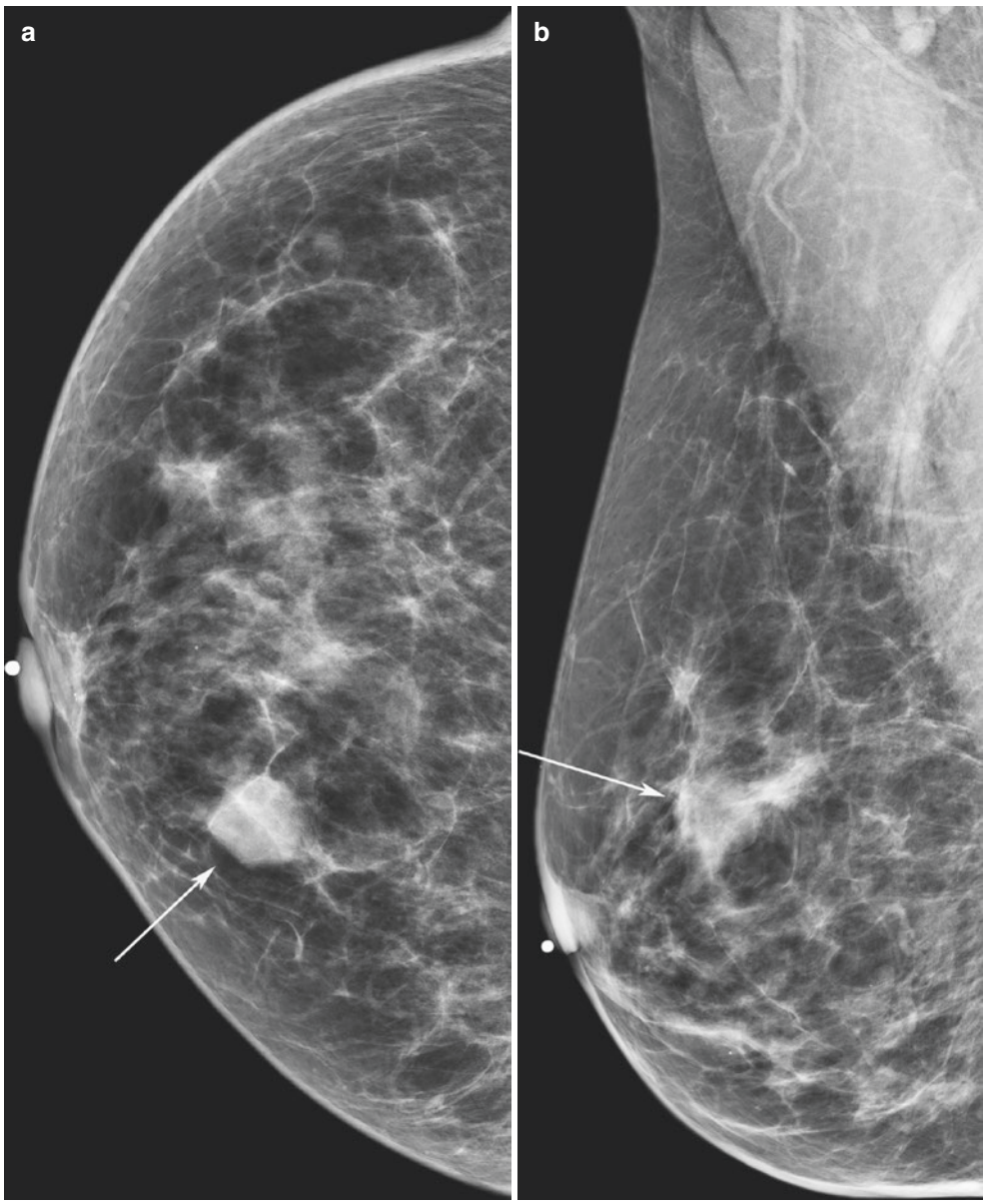

Fig. 3.44 CC (**a**) and MLO (**b**) mammography images of the left breast show a 1.5-cm partially circumscribed irregular mass (*arrow*) in the slightly medial subareolar left breast, which persists on spot compression views (**c**, **d**). (**e**) Targeted left breast ultrasound demonstrates a corresponding 1.5-cm oval circumscribed, homogeneously hypoechoic mass with posterior acoustic enhancement (*arrows*). The patient underwent ultrasound-guided core biopsy, yielding invasive ductal carcinoma, mucinous type

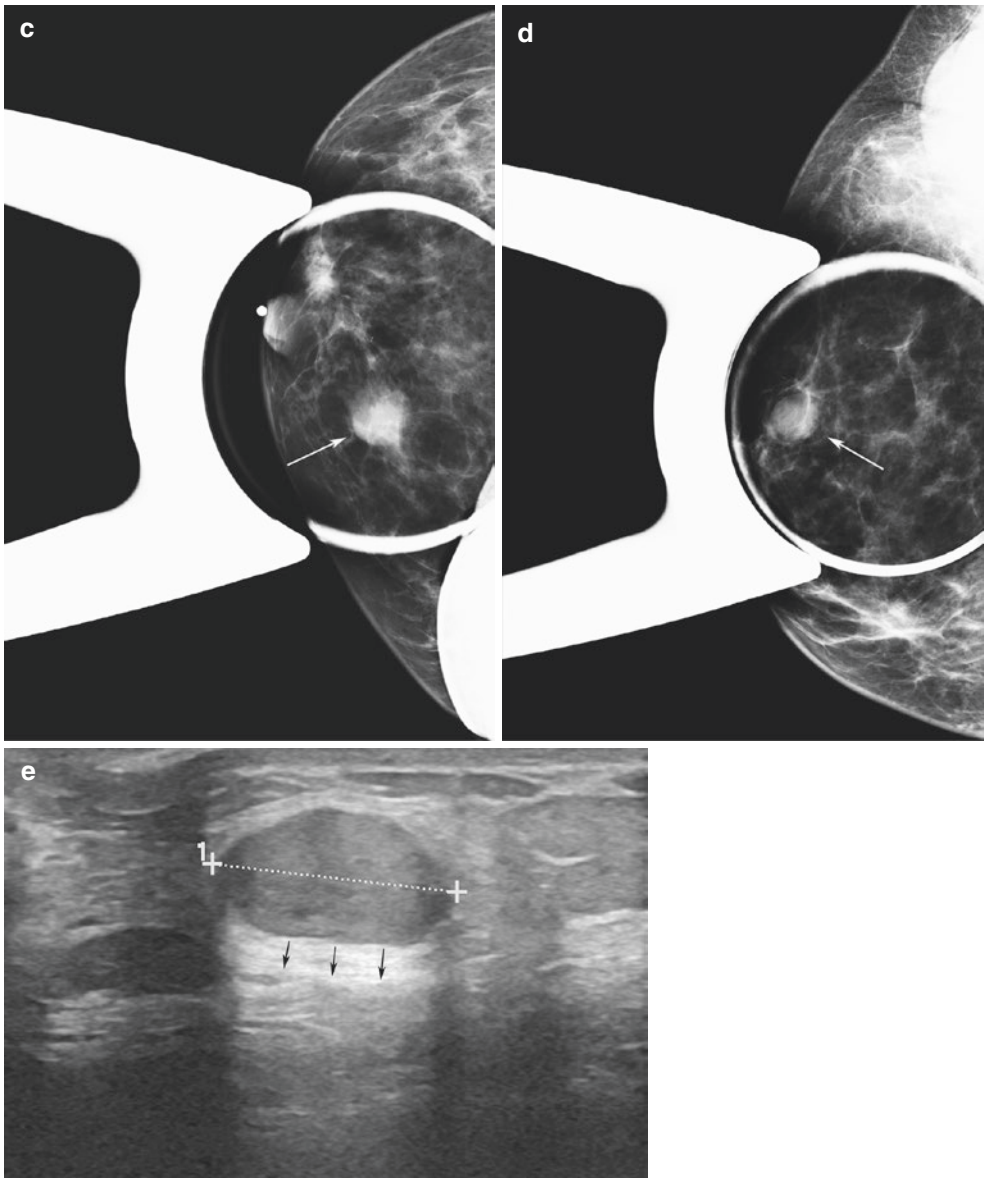

Fig. 3.44 (continued)

3.10 History

58-year-old woman with recently diagnosed left breast malignancy. Breast MRI was performed to evaluate extent of disease (Figs. 3.45 and 3.46).

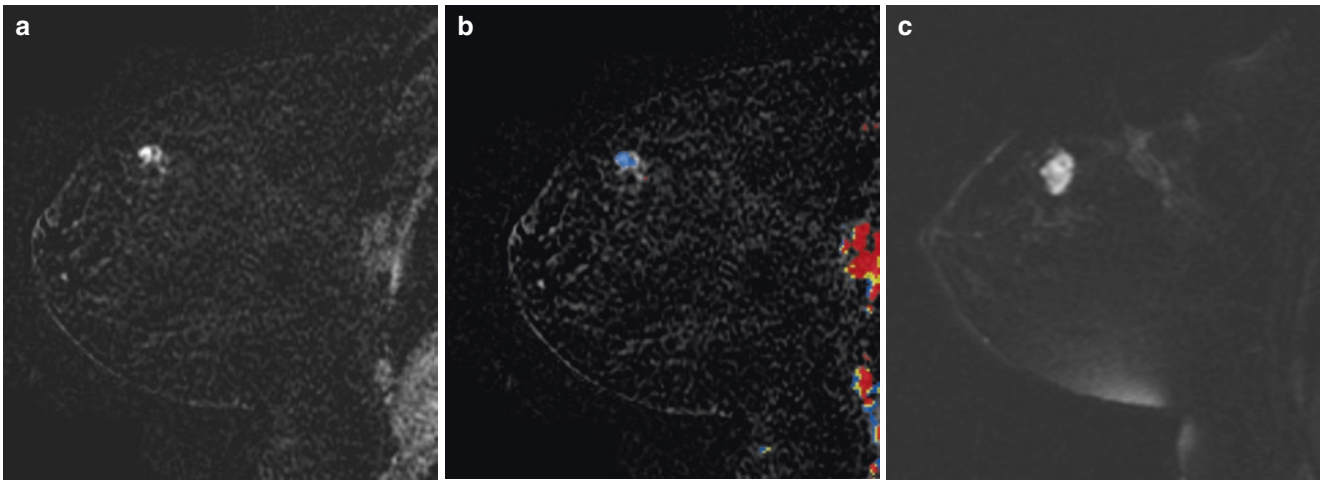

Fig. 3.45 Sagittal post-contrast subtraction image of the left breast (**a**) with CAD color overlay (**b**). (**c**) Corresponding sagittal T2-weighted fat-saturated image

3.10 Invasive Ductal Carcinoma, Pure Mucinous 2

Teaching Points Mucinous carcinoma of the breast is a rare form of invasive ductal carcinoma. On MRI, these tumors can have very high signal intensity on T2-weighted images, as illustrated in this case. In addition, post-contrast enhancement is variable; a benign-appearing, persistent enhancement pattern (as seen in this patient) may occur. The pure mucinous subtype carries a better prognosis than invasive ductal carcinoma NOS, with a lower chance of axillary metastasis. The patient underwent breast conservation, with final pathology yielding pure mucinous carcinoma, stage T1N0.

Image Findings

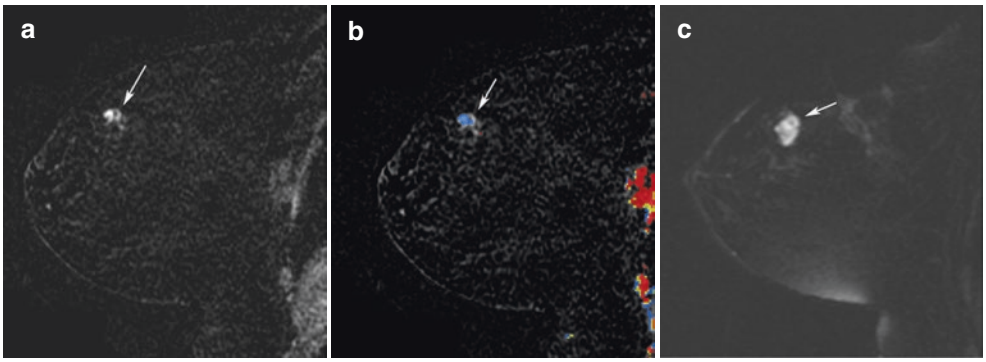

Fig. 3.46 Pure mucinous carcinoma. Sagittal post-contrast subtraction image (**a**) shows a 1.3-cm irregular mass (*arrow*) along the 12:00 axis of the left breast, demonstrating persistent enhancement color-coded as blue on CAD (**b**). (**c**) Corresponding sagittal T2-weighted fat-saturated image shows the T2-hyperintense mass (*arrow*) to be larger than the area of enhancement. The patient underwent ultrasound-guided core biopsy yielding invasive ductal carcinoma, mucinous type

3.11 History

Extent of disease evaluation (Figs. 3.47, 3.48, 3.49, and 3.50).

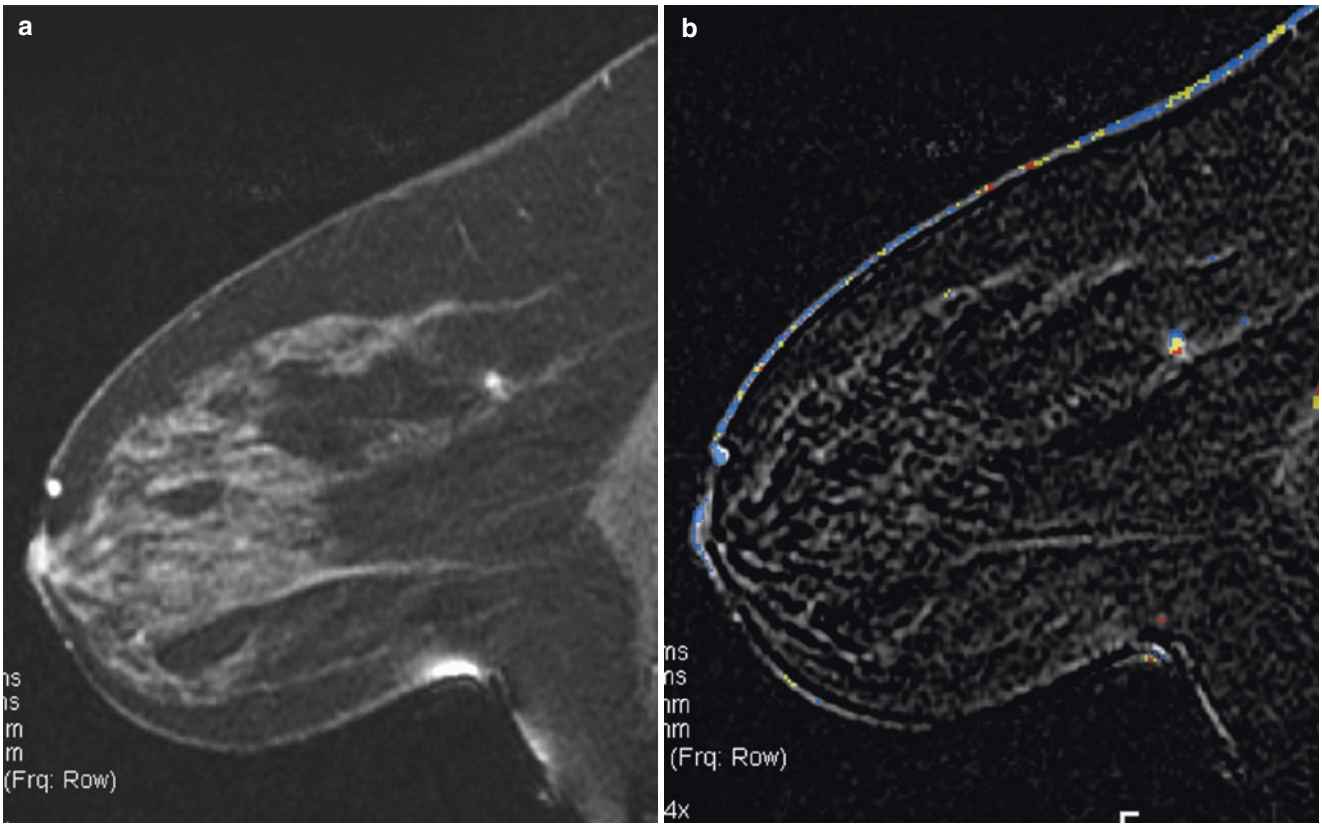

Fig. 3.47 Sagittal MRI images of the right breast. T1-weighted fat-saturated post-contrast image (**a**) and CAD color overlay on a post-contrast subtraction image (**b**)

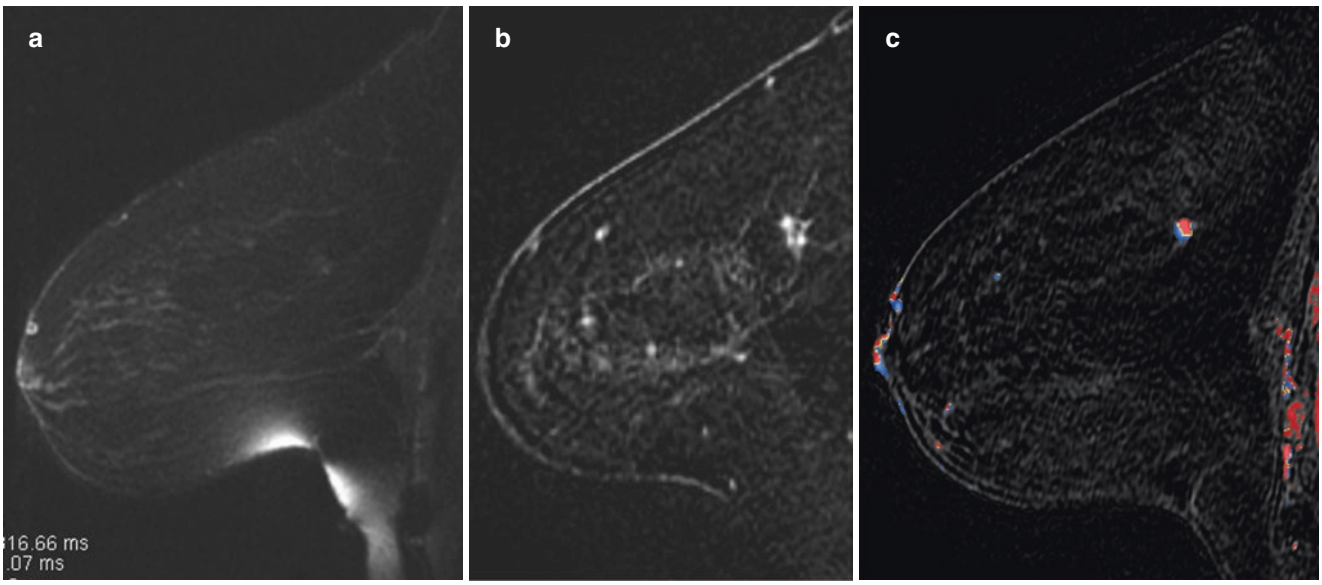

Fig. 3.48 Sagittal MRI images of the right breast obtained 12 months later: a T2-weighted fat-saturated image (**a**), post-contrast subtraction image (**b**), and post-contrast subtraction image with CAD color overlay (**c**)

3.11 Invasive Ductal Carcinoma, Tubular Carcinoma

Teaching Points Tubular carcinoma of the breast is a well-differentiated form of invasive ductal carcinoma. It typically occurs in younger women (middle to late 40s) and tends to have a more favorable prognosis than other breast cancers. Pure tubular carcinoma is rare and accounts for less than 2 % of all breast cancers. The diagnosis of tubular carcinoma requires a minimum percentage of tubular elements ranging from 75 to 90 %.

Tubular carcinoma is often detected as a small, spiculated mass on screening mammography, usually less than 1 cm, but it may be discovered as a palpable mass. The spiculations correspond to reactive stroma extending from the neoplasm. On MRI, tubular carcinoma appears similar to invasive ductal carcinoma NOS, with a variable kinetic enhancement pattern.

Image Findings

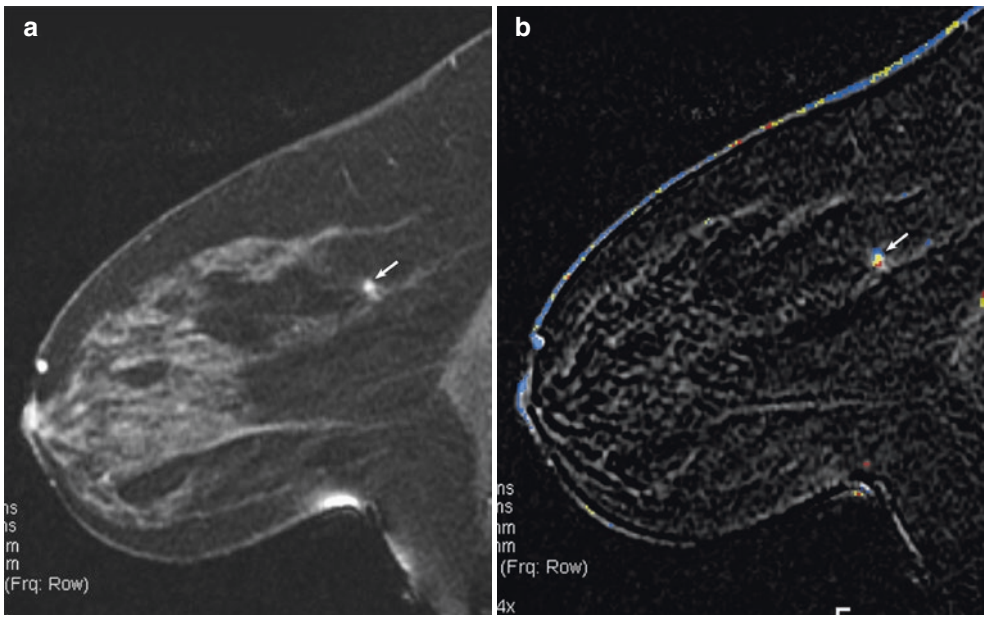

Fig. 3.49 Initial MRI images obtained in a patient with tubular carcinoma detected on high-risk screening MRI follow-up. (**a**) Sagittal T1-weighted fat-saturated post-contrast image shows a focus of enhancement along the posterior right 12:00 axis (*arrow*). (**b**) CAD enhancement kinetic analysis demonstrates a mixed pattern (*arrow*), with predominantly progressive and plateau kinetics

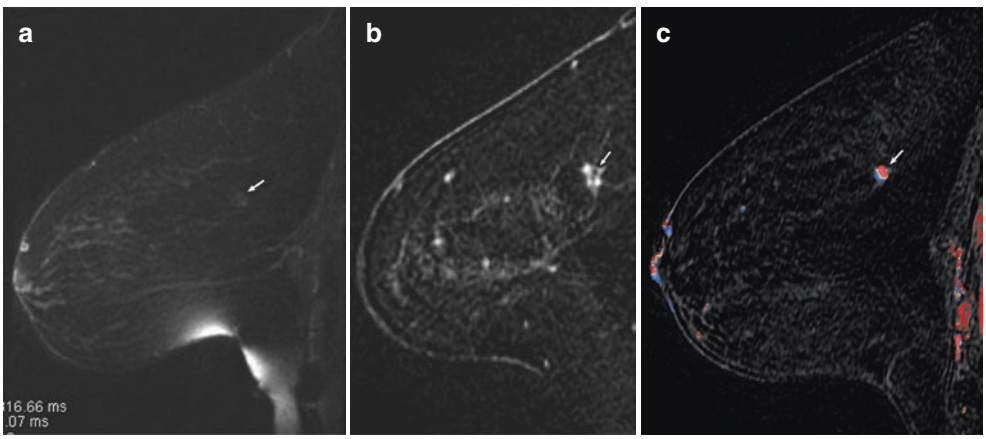

Fig. 3.50 12-month follow-up MRI images demonstrating tubular carcinoma. (**a**) Sagittal T2-weighted fat-saturated image of the right breast shows minimal T2 hyperintensity (*arrow*) in the posterior breast. (**b**) Sagittal post-contrast subtraction image shows interval enlargement of the previously seen enhancing focus, which is now a heterogeneously enhancing, irregular, spiculated mass (*arrow*) in the posterior right breast. (**c**) CAD enhancement kinetics analysis shows a mixed enhancement pattern, predominantly washout (*arrow*), suspicious for malignancy. Biopsy yielded tubular carcinoma

3.12 History

46-year-old woman with newly diagnosed left breast malignancy. Breast MRI was performed to evaluate extent of disease (Figs. 3.51, 3.52, 3.53, 3.54, 3.55, and 3.56).

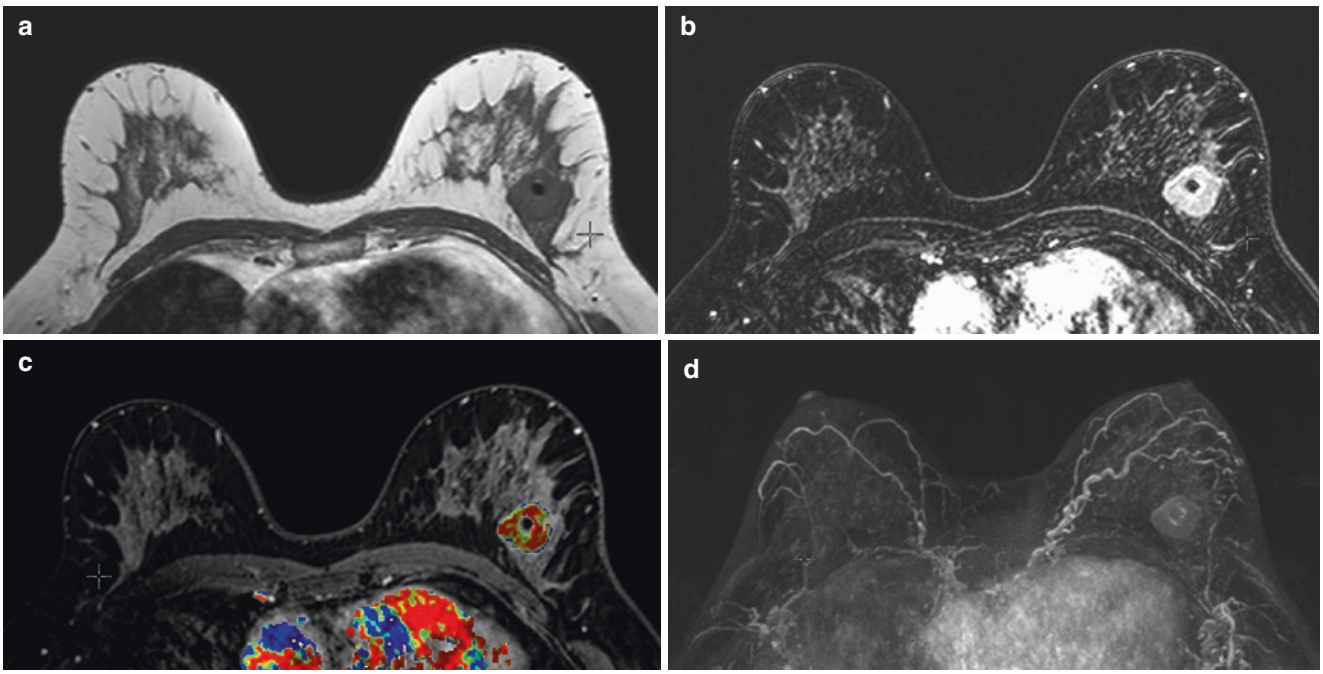

Fig. 3.51 (**a**) Axial T1-weighted image of both breasts. (**b**) Corresponding axial T2-weighted fat-saturated image. (**c**) Corresponding axial T1-weighted fat-saturated post-contrast image with CAD kinetic analysis color overlay. (**d**) Axial post-contrast 3D maximum intensity projection (MIP) image

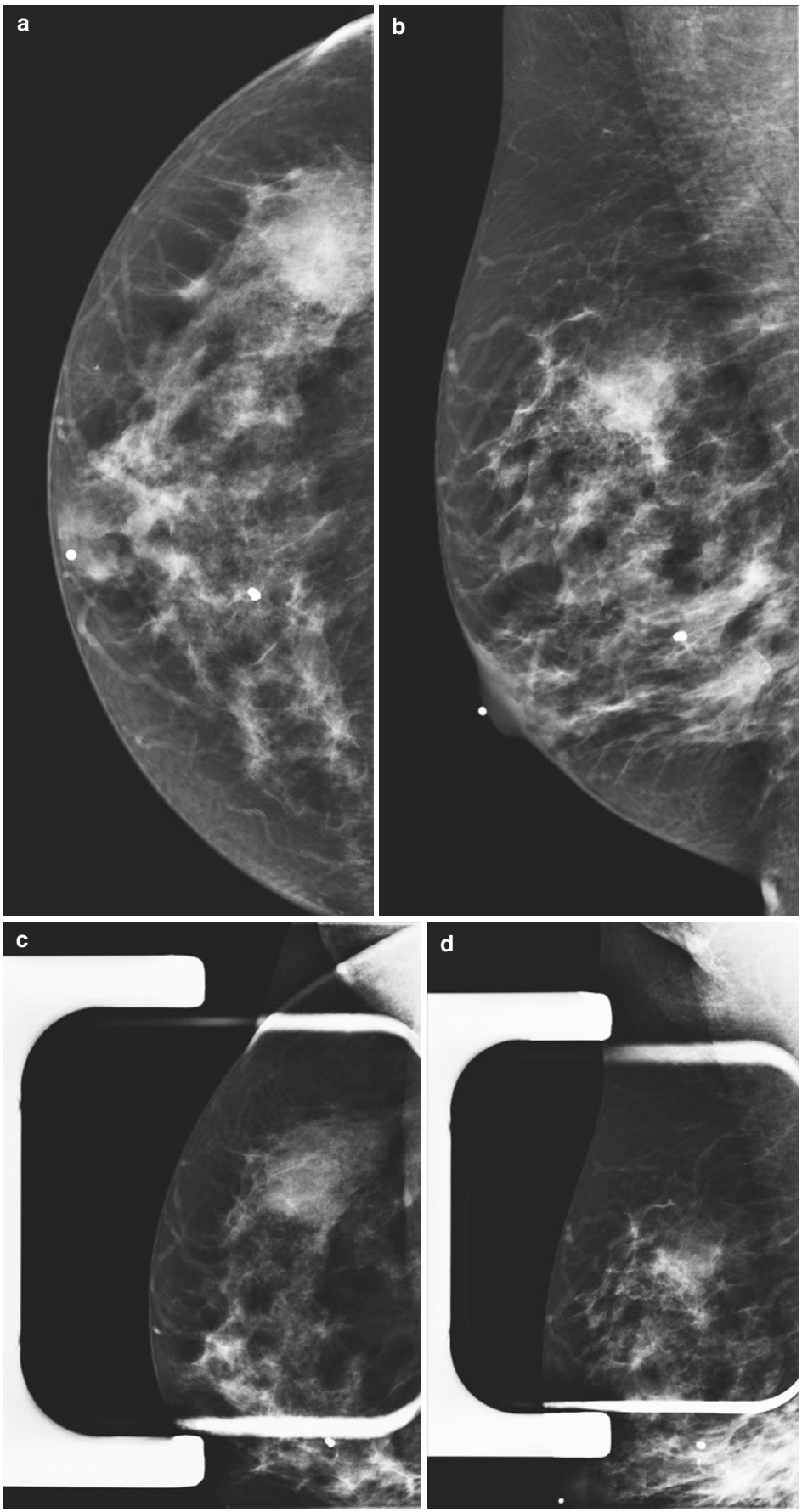

Fig. 3.52 Mammogram. CC view (**a**) and MLO view (**b**) of the left breast. CC (**c**) and MLO (**d**) spot compression views of the left breast

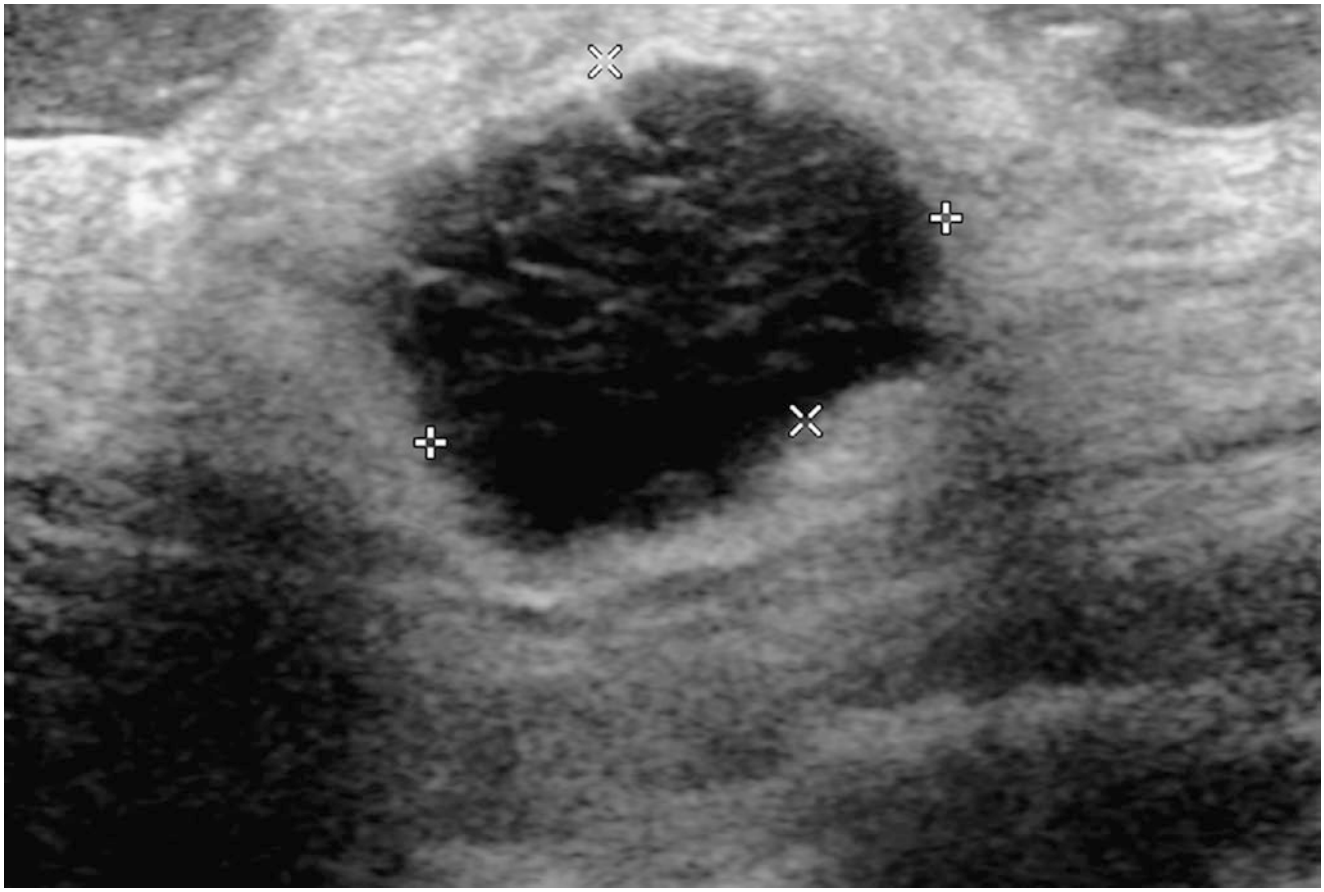

Fig. 3.53 Targeted left breast ultrasound image

3.12 Invasive Ductal Carcinoma, Medullary Carcinoma

Teaching Points Medullary carcinoma of the breast is a rare type of invasive ductal carcinoma that accounts for about 3 % of all breast cancers. This tumor can occur in younger women, including 10 % of cases in women under 35 years. On histology, medullary carcinomas have been classified as either typical or atypical. Atypical medullary carcinomas are now classified as invasive ductal carcinomas with medullary features. Patients with medullary carcinoma have a more favorable prognosis than those with atypical medullary carcinoma and nonmedullary carcinoma. The morphologic features of medullary carcinomas and fibroadenomas can overlap. Mammographically, medullary carcinoma is a round, ovoid, or lobular mass with ill-defined or circumscribed margins. On ultrasound, the mass can be either homogeneously hypoechoic or hypoechoic with mild heterogeneity. Posterior acoustic enhancement may be present. On MRI, medullary carcinomas appear as masses with an oval or lobular shape and circumscribed margins. The tumors are isointense or hypointense on T1-weighted images and isointense or hyperintense on T2-weighted images relative to the surrounding breast tissue. Kinetics curves demonstrate a rapid initial increase in enhancement and a washout or plateau delayed enhancement pattern. Many of the imaging features typical for medullary carcinoma were present in our case. The patient underwent breast conservation with final pathology showing typical medullary carcinoma, stage T2, N0.

Image Findings

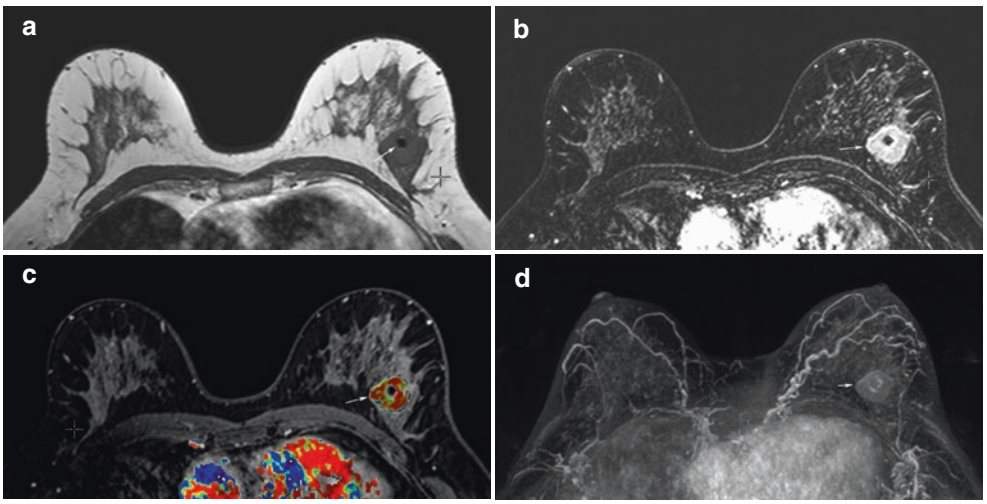

Fig. 3.54 Medullary carcinoma. Axial T1-weighted image (**a**) and fat-saturated T2-weighted image (**b**) demonstrate a 2.6-cm, T1-hypointense and T2-hyperintense round mass (*arrow*) in the posterior upper outer breast with central clip artifact from a biopsy, which yielded malignancy. (**c**) Corresponding axial T1-weighted fat-saturated post-contrast image with CAD kinetic analysis shows rapid uptake of contrast with delayed washout color-coded as red. (**d**) Axial post-contrast 3D MIP image shows the unifocal mass in the left breast. No other suspicious enhancement is present in ether breast or axilla

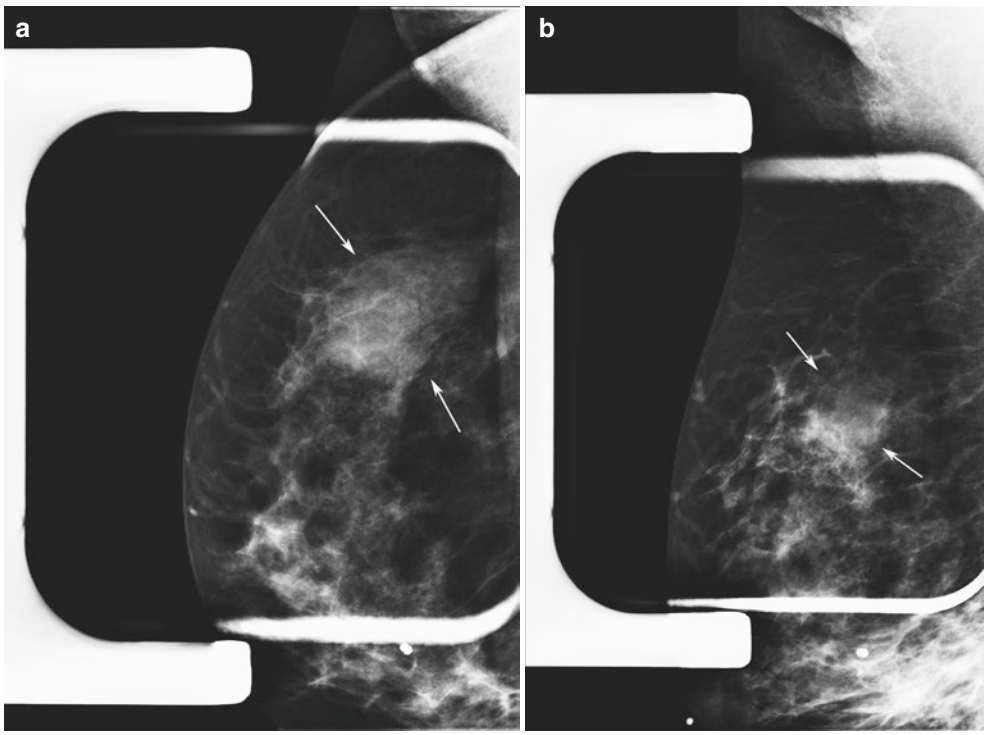

Fig. 3.55 (**a**, **b**) Mammography (spot compression views) shows a 2.5-cm partially obscured round mass (*arrows*) in the upper outer left breast

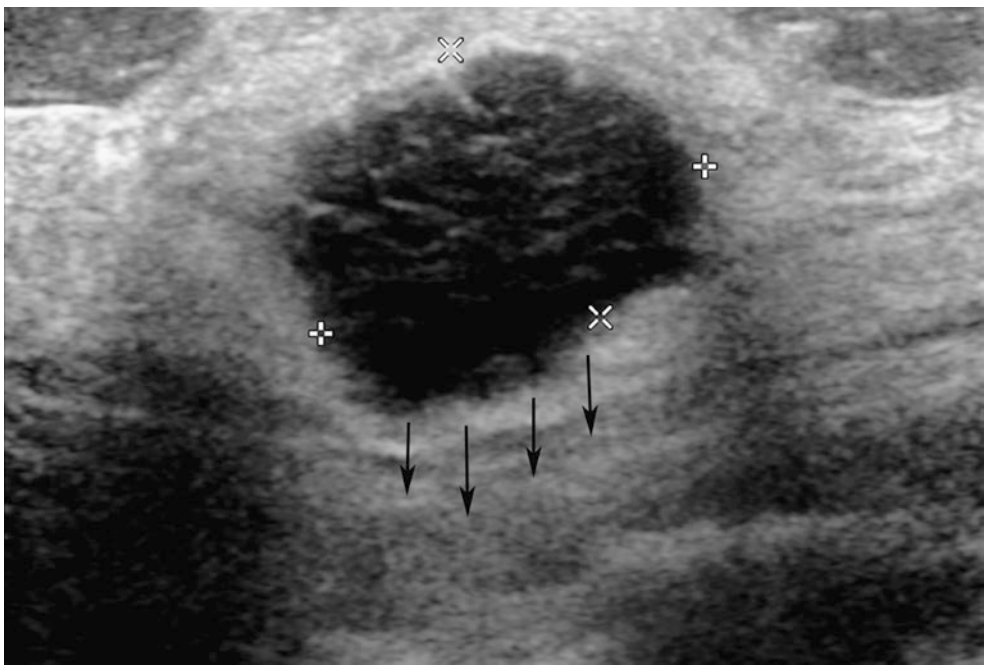

Fig. 3.56 Targeted ultrasound of the 2:00 axis of the left breast shows a partially circumscribed, round mass with some irregular margins and marked posterior acoustic enhancement (*arrows*), corresponding to the mammographic and MRI masses. The patient underwent ultrasound-guided core biopsy yielding medullary carcinoma

3.13 History

A 64-year-old woman with newly diagnosed left breast malignancy. Breast MRI was performed to evaluate extent of disease (Figs. 3.57, 3.58, 3.59, 3.60, and 3.61).

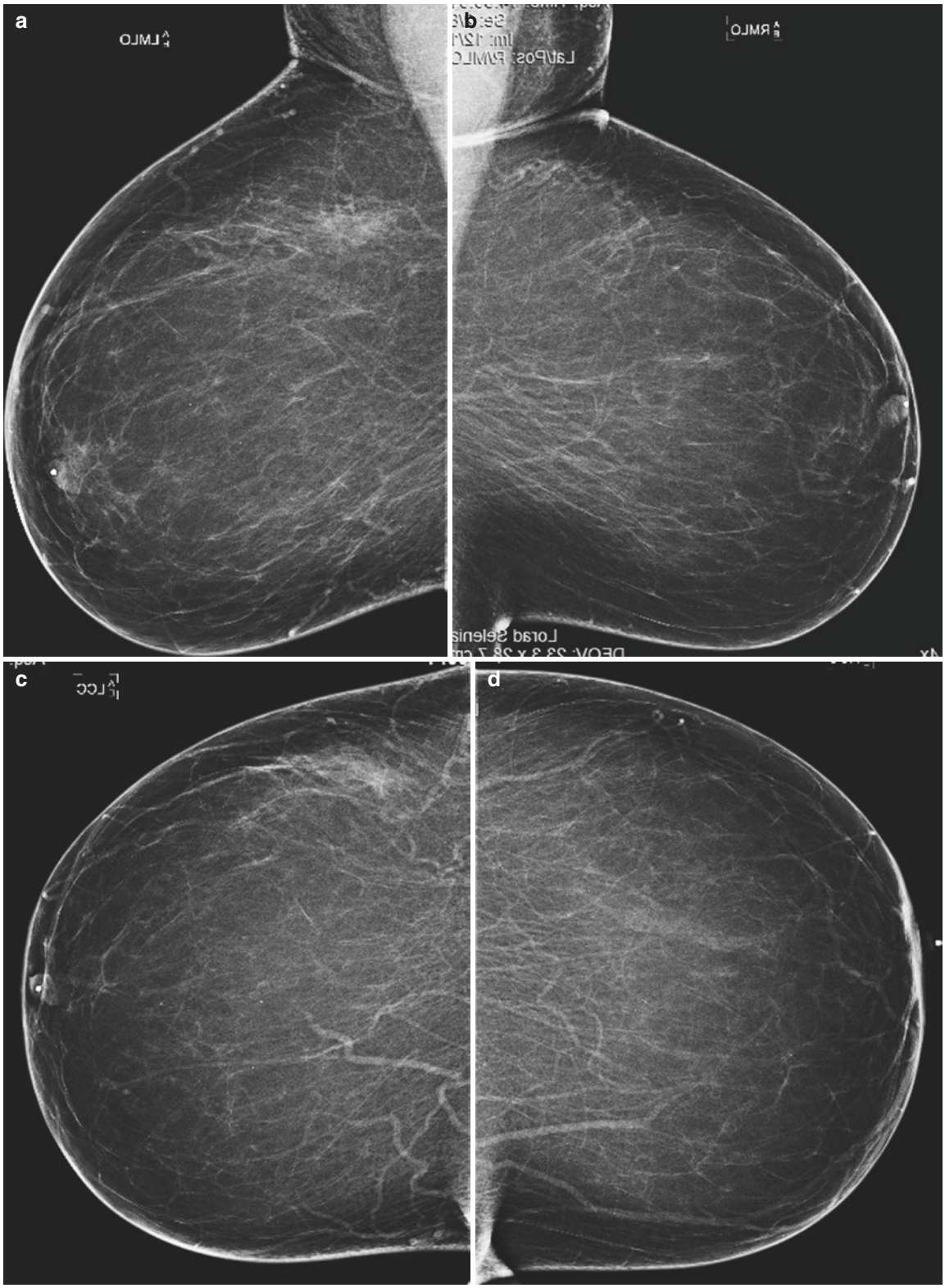

Fig. 3.57 Screening mammogram. Left (**a**) and right (**b**) MLO views. Left (**c**) and right (**d**) CC views

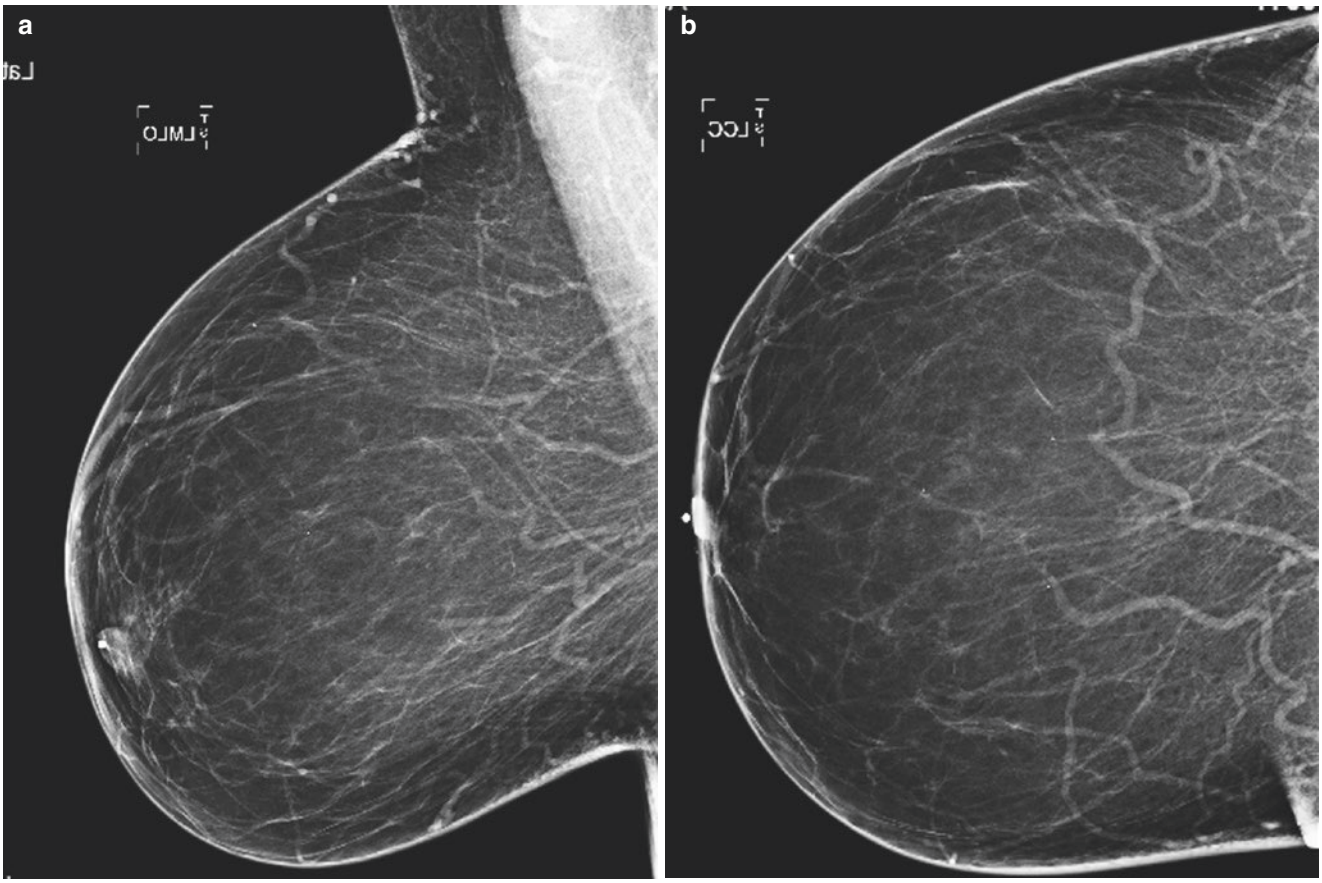

Fig. 3.58 Prior screening mammogram for comparison. Left MLO (**a**) and CC (**b**) views

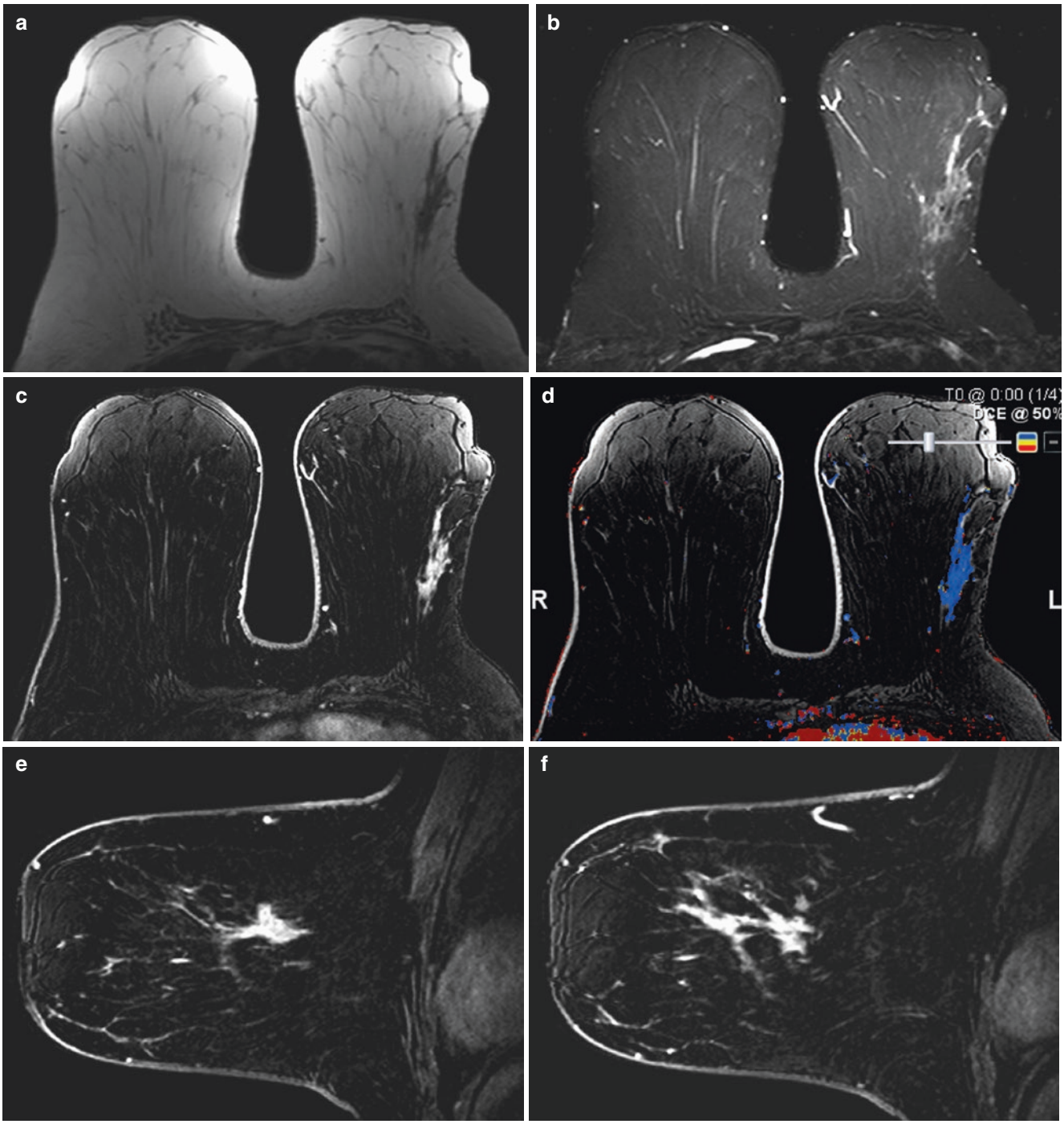

Fig. 3.59 (**a**) Axial T1-weighted image of both breasts. (**b**) Corresponding axial T2-weighted fat-saturated image. (**c**) Axial T1-weighted fat-saturated post-contrast image with (**d**) CAD kinetic analysis color overlay. (**e**, **f**) Contiguous sagittal T1-weighted fat-saturated post-contrast subtracted images of the outer left breast

3.13 Invasive Lobular Carcinoma 1

Teaching Points Breast MRI is commonly performed for extent of disease evaluation and preoperative planning, but its routine preoperative use is controversial because the long-term benefits for patient survival outcome are unclear, especially in the setting of adjuvant chemotherapy and radiation therapy. Breast MRI may be most important in patients who are relying only on surgery for their treatment. For patients with invasive lobular carcinoma (ILC), there is literature supporting preoperative MRI for better estimation of disease and additional findings, especially in patients with dense breasts. This patient underwent wide excision yielding 8.2 cm of disease with negative margins on final pathology. In this case, the breast MRI gave a more accurate estimation of disease than the mammogram. It is important to note that breast MRI can over-estimate disease extent owing to enhancement of tissue surrounding the tumor related to edema, inflammation, and desmoplastic reaction. The ILC in this case demonstrated a persistent, benign-appearing delayed enhancement pattern. This case illustrates the importance of utilizing morphology as the most important feature to be analyzed, as the kinetic enhancement pattern can be misleading.

Image Findings

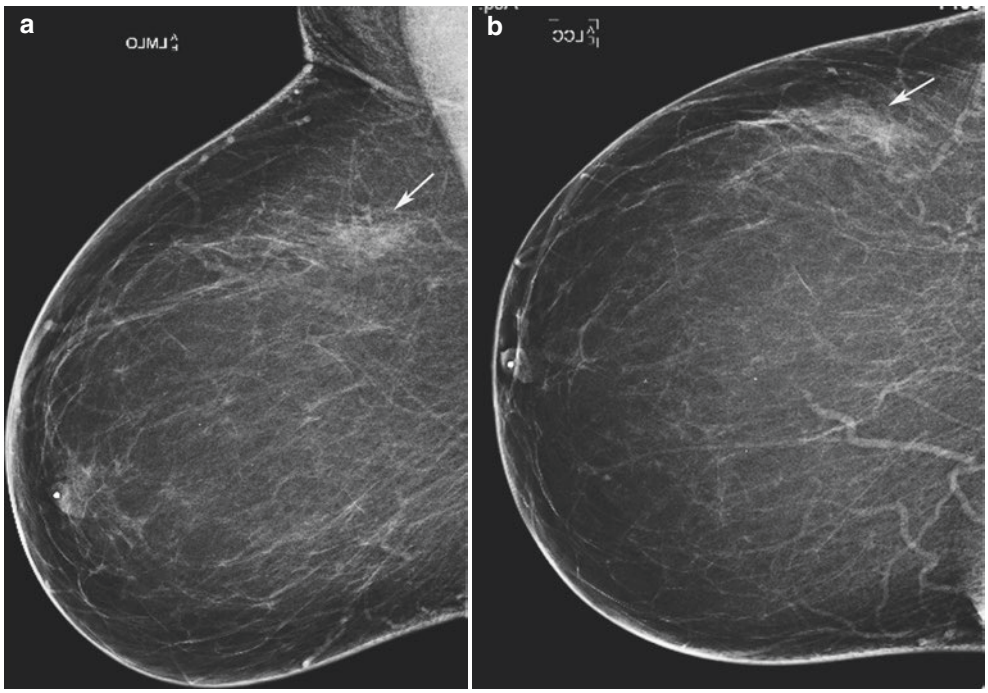

Fig. 3.60 Invasive lobular carcinoma (ILC). There is a new focal asymmetry in the upper outer posterior left breast (*arrow*), spanning 4 cm on the mammographic MLO view (**a**) and CC view (**b**). The focal asymmetry persisted on the spot compression views (*not shown*), but no definite sonographic correlate was reported. The focal asymmetry underwent stereotactic biopsy yielding ILC

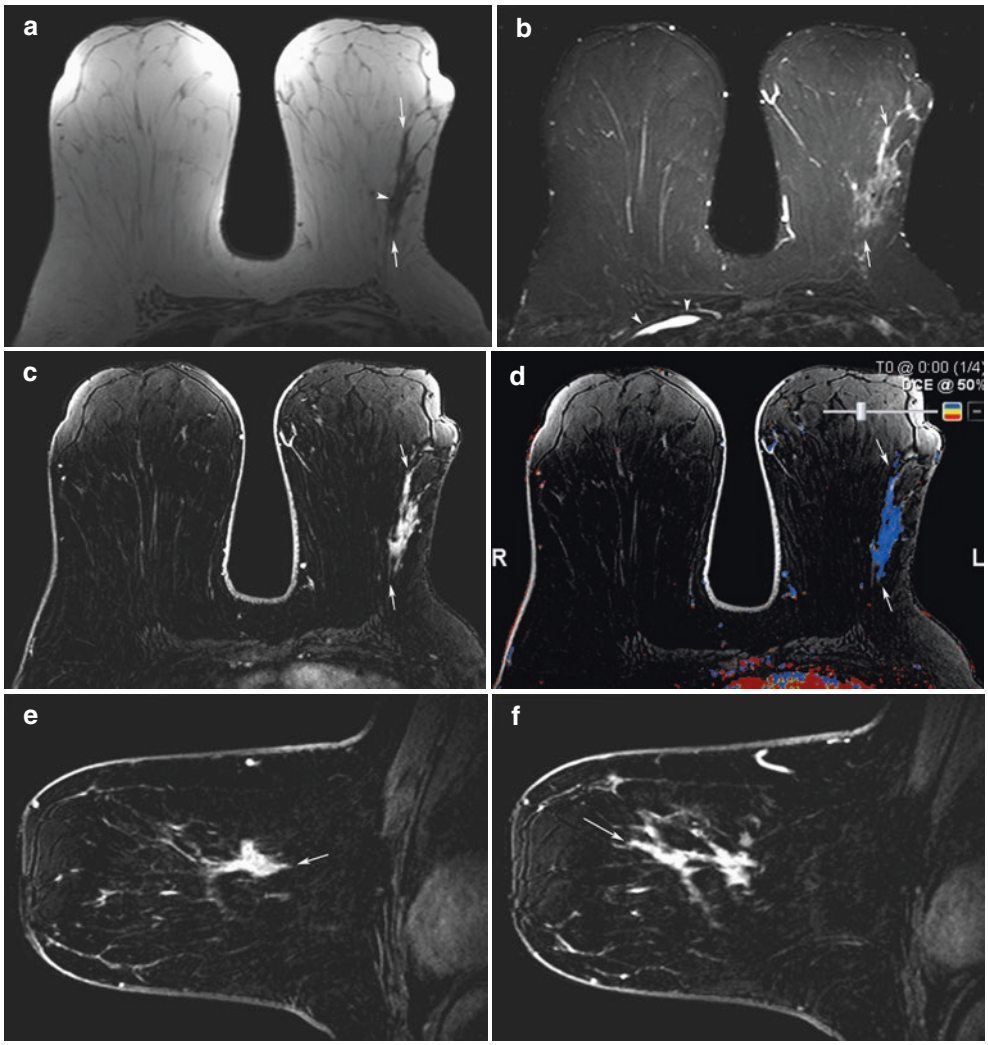

Fig. 3.61 Axial T1-weighted (**a**) and fat-saturated T2-weighted (**b**) images demonstrate a T1-hypointense and T2-mildly hyperintense irregular region (*arrows*) in the upper outer left breast, spanning at least 7.8 cm. Localizing clip artifact is seen within the medial aspect of this region (*arrowhead* on **a**), which yielded ILC at biopsy. Incidentally noted is curvilinear T2 hyperintensity (*arrowheads* on **b**) along the anterior right thorax, consistent with trace pleural fluid. (**c**) There is irregular nonmass enhancement (*arrows*) on the axial T1-weighted fat-saturated post-contrast image in the upper outer left breast. (**d**) Persistent enhancement is denoted by the color blue (*arrow*). (**e**, **f**) Sagittal T1-weighted fat-saturated post-contrast images further illustrate the disease extent (*arrows*)

3.14 History

A 49-year-old woman with newly diagnosed right breast malignancy. Breast MRI was performed to evaluate extent of disease (Figs. 3.62, 3.63, 3.64, 3.65, 3.66, 3.67, 3.68, and 3.69).

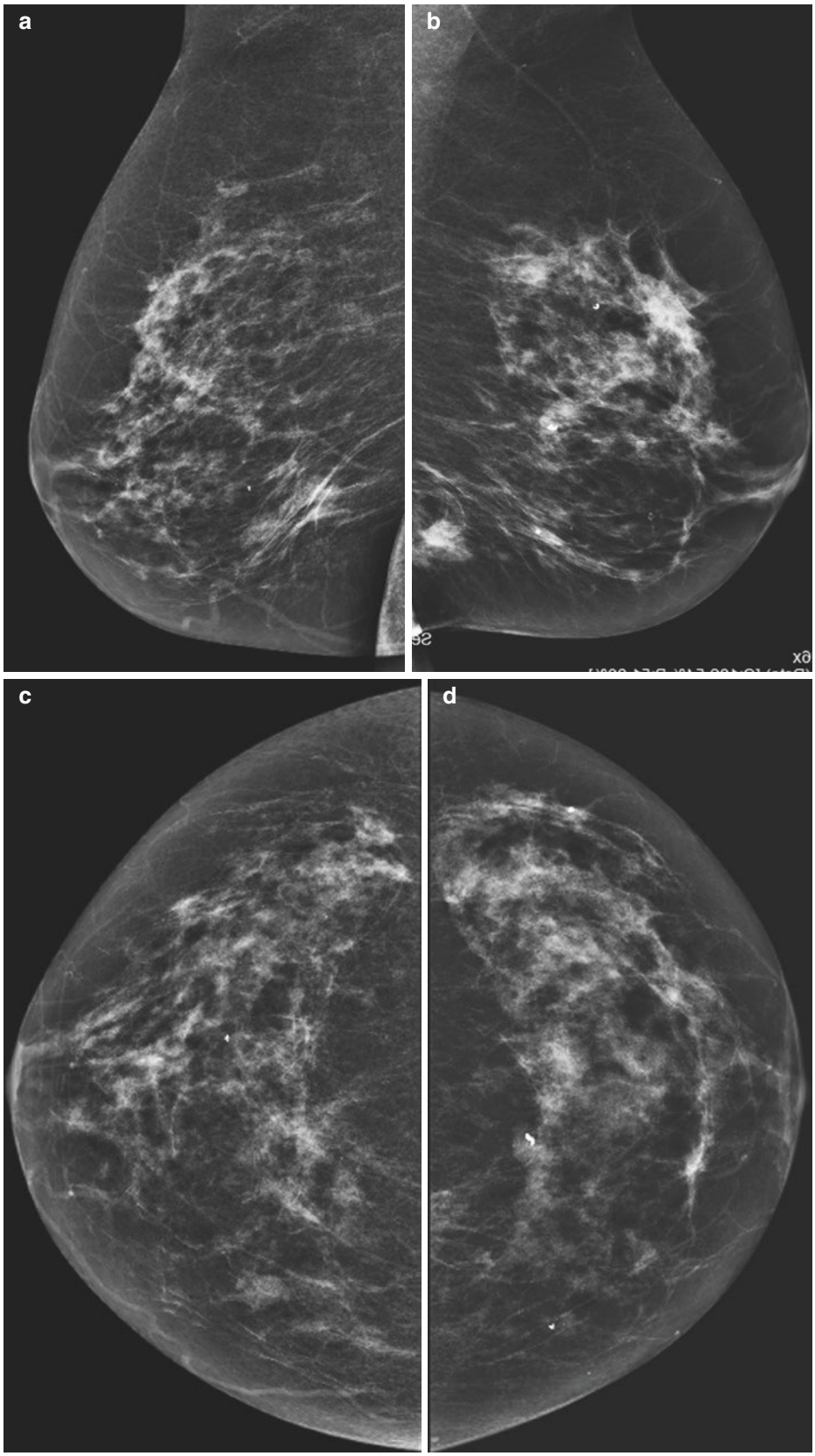

Fig. 3.62 Mammogram. Left (**a**) and right (**b**) MLO views. Left (**c**) and right (**d**) CC views

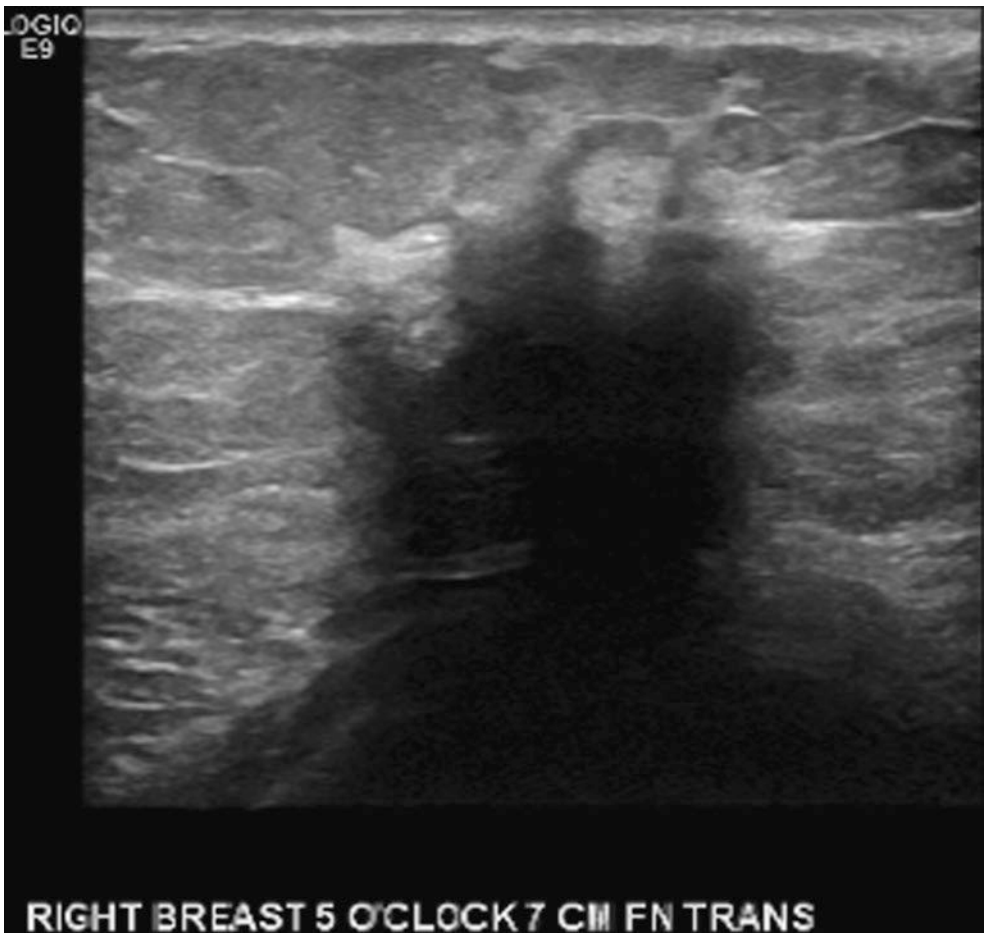

Fig. 3.63 Targeted ultrasound image of the right breast

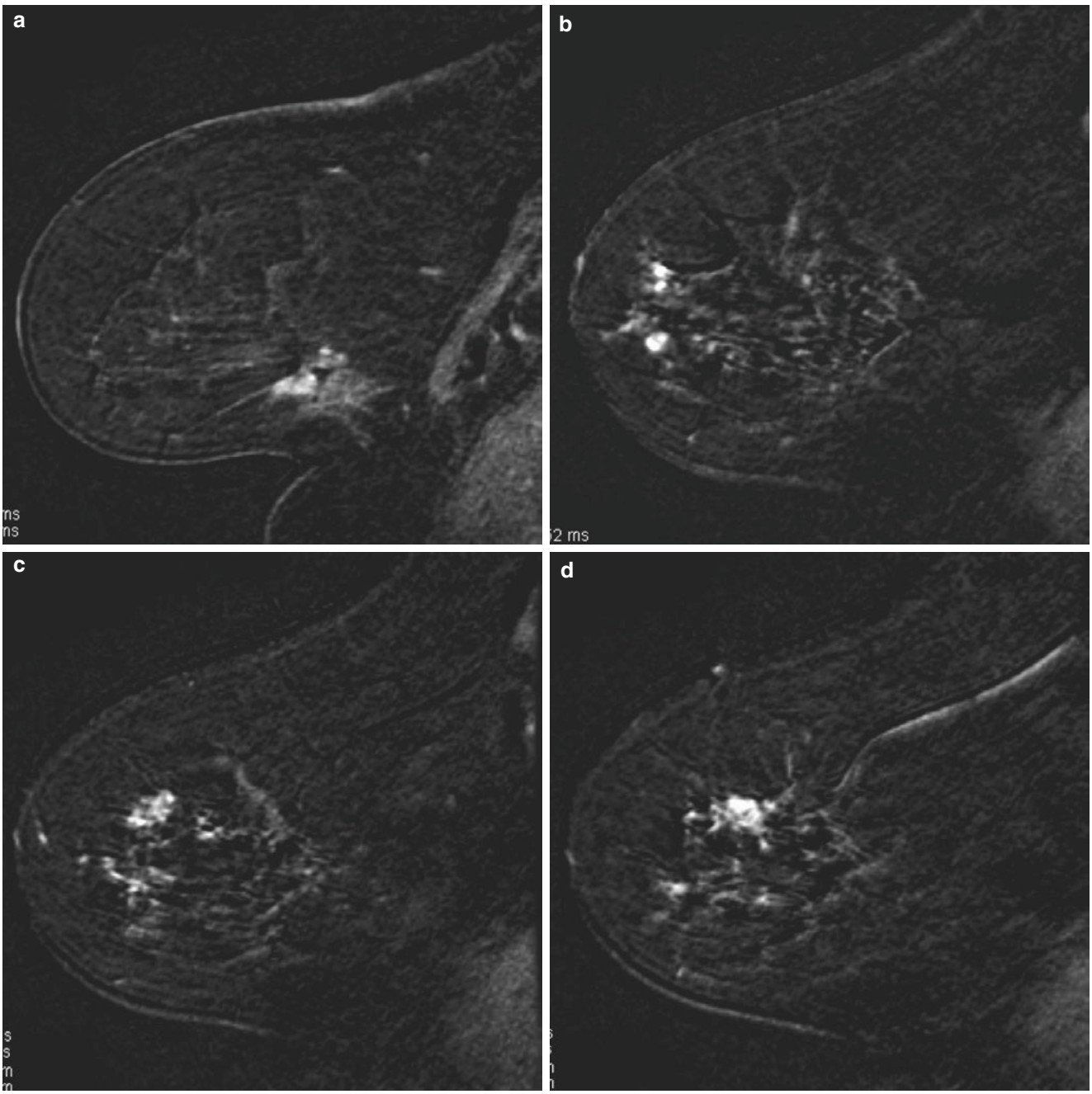

Fig. 3.64 Sagittal post-contrast subtraction images of the medial right breast (**a**), central right breast (**b**), and lateral right breast (**c**, **d**)

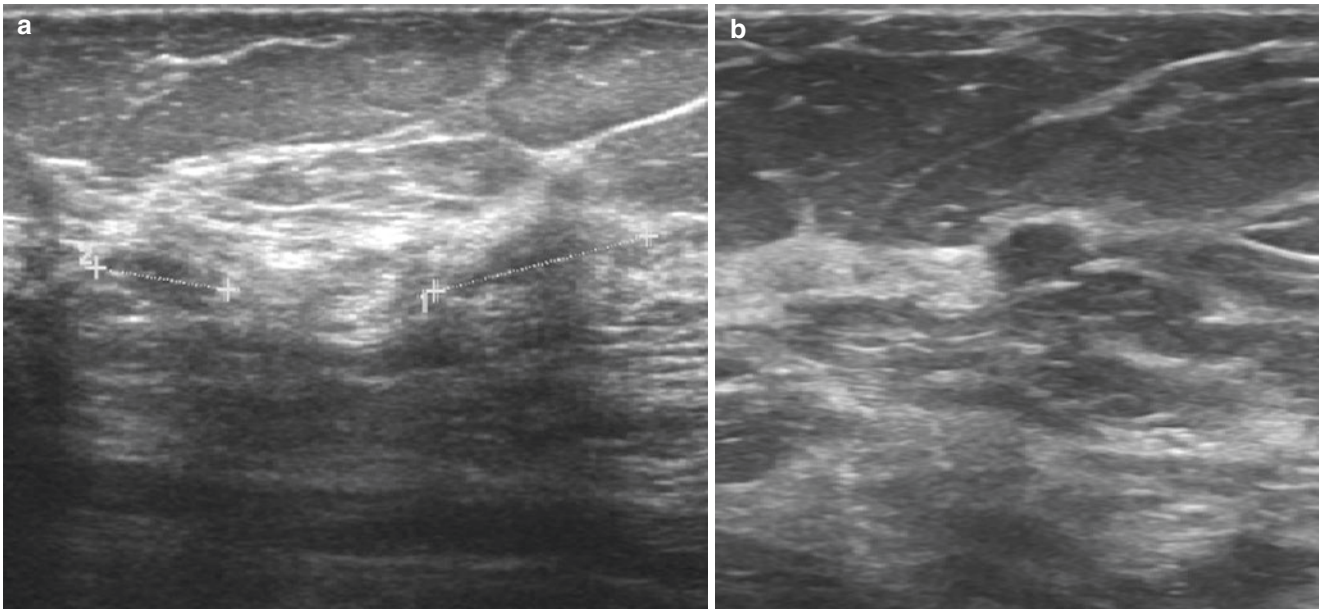

Fig. 3.65 Targeted ultrasound images of the upper outer right breast (**a**) and retroareolar right breast (**b**)

3.14 Invasive Lobular Carcinoma 2

Teaching Points Preoperative breast MRI can detect additional sites of disease in the ipsilateral breast in 20–30 % of cases and in the contralateral breast in 5 % of cases, especially in patients with invasive lobular cancer and dense breasts, as illustrated in this case. Such findings impact clinical management. It is important to note that pathology confirmation is needed to document multicentric disease despite the suspicious appearance of additional findings on MRI. Sonographic features of certain malignancies can be subtle, and breast MRI can help to direct ultrasound for localization of the finding, as shown in this case.

Image Findings

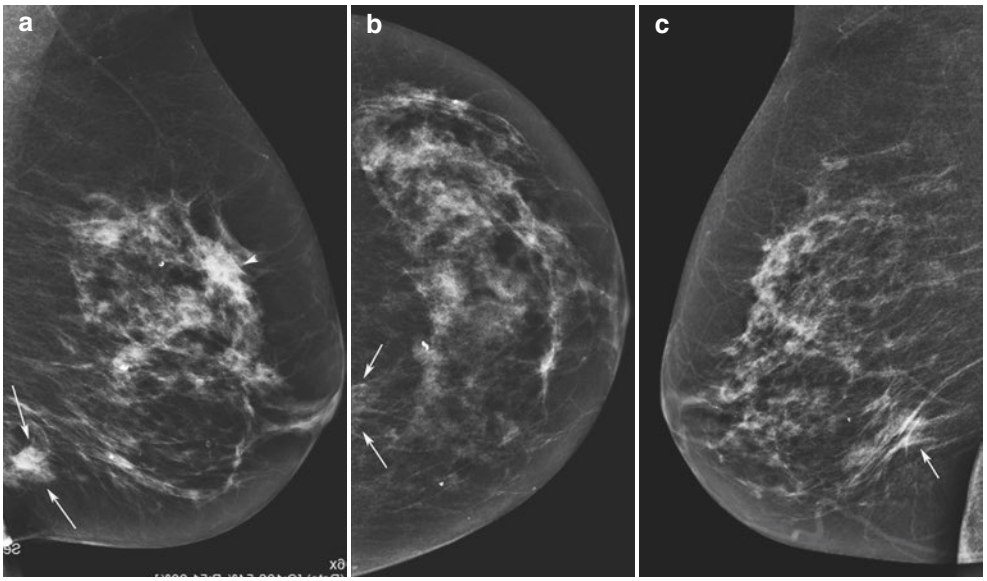

Fig. 3.66 Multicentric invasive lobular carcinoma. Mammography shows a focal asymmetry in the far posterior inferior and slightly medial right breast on MLO (**a**) and CC (**b**) views (*arrows*). The focal asymmetry persisted on spot compression views (*not shown*), and ultrasound was performed for further evaluation. The MLO view (**a**) also showed an asymmetry (*arrowhead*) in the upper right breast without a definite correlate on the CC view, and no sonographic correlate was reported. (**c**) An asymmetry (*arrow*) is noted in the posterior lower left breast without a definite correlate on the CC view. The appearance was similar to prior mammograms, and the finding was considered benign

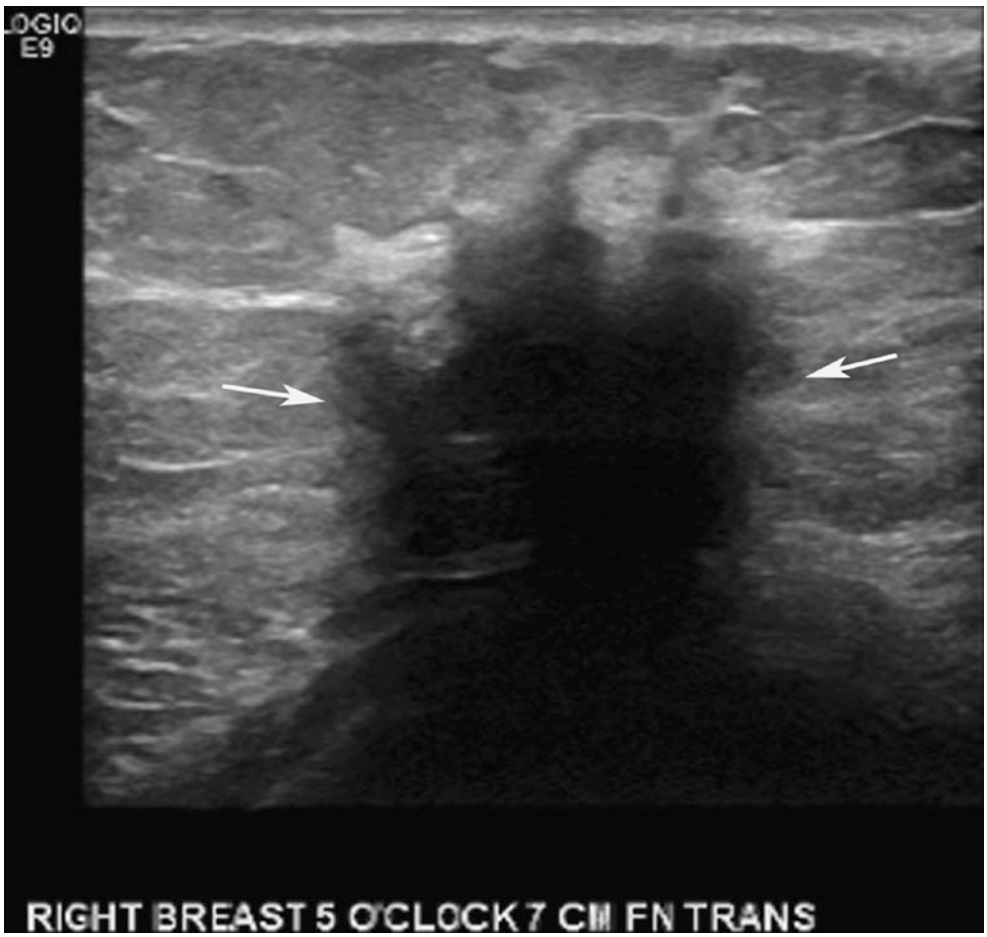

Fig. 3.67 Targeted right breast ultrasound demonstrates a 2.5-cm irregular hypoechoic mass along the 5:00 axis corresponding to the mammographic focal asymmetry. This mass underwent biopsy yielding ILC

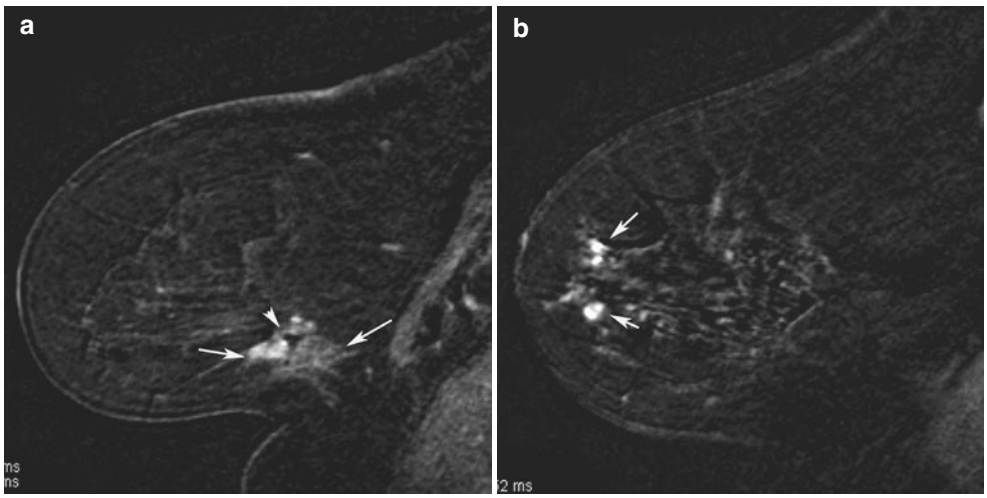

Fig. 3.68 Sagittal T1-weighted post-contrast subtraction images of the right breast demonstrate a 3.1-cm irregular mass (**a**, *arrows*) in the posterior 5:00 axis of the right breast with central localizing clip artifact (*arrowhead*), which yielded malignancy on biopsy. Additional suspicious enhancement is noted in the retroareolar right breast (**b**, *arrows*) and along the 10:00–10:30 axis (**c** and **d**, *arrows*)

Fig. 3.68 (continued)

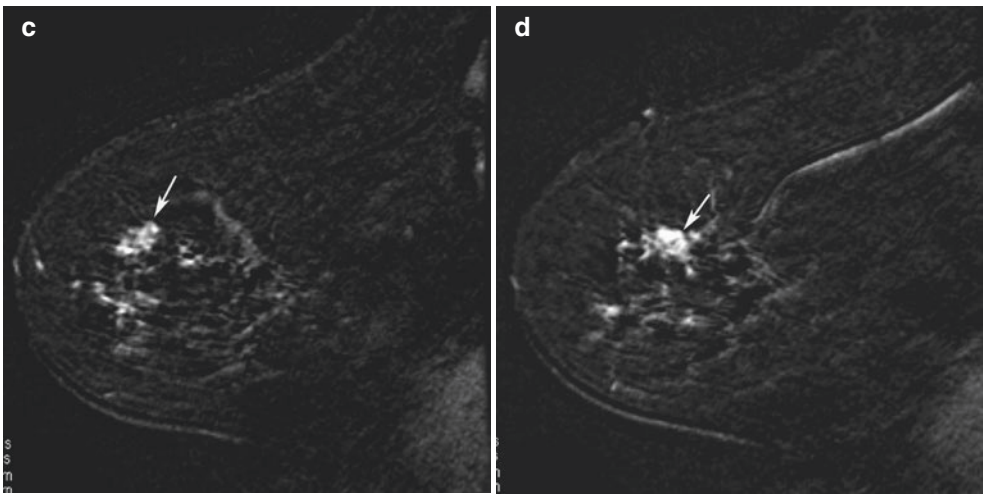

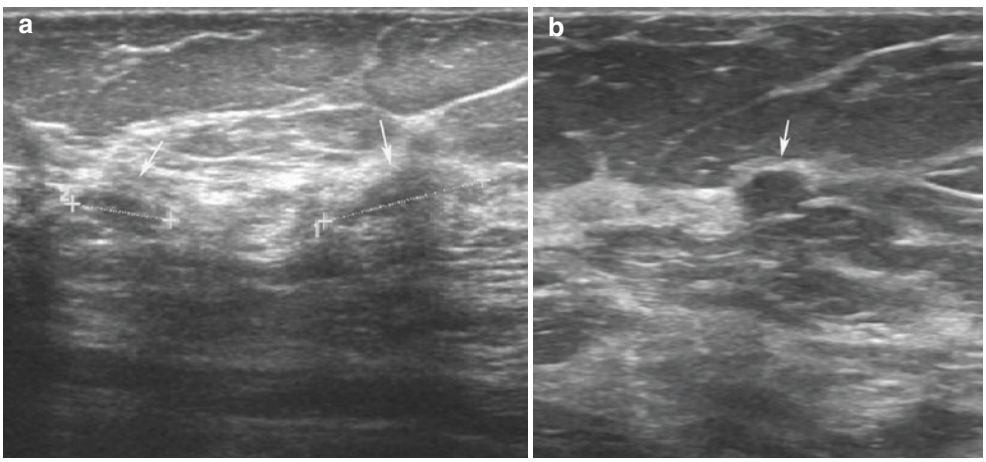

Fig. 3.69 Second-look ultrasound was performed for the additional MRI findings. (**a**) Targeted ultrasound of the upper outer right breast shows two adjacent mildly hypoechoic masses (*arrows*) likely corresponding to the areas of 10:00–10:30 MRI enhancement (and, in retrospect, to the mammographic asymmetry). (**b**) Targeted ultrasound of the retroareolar right breast demonstrates a hypoechoic mass (*arrow*) likely corresponding to the subareolar MRI enhancement. The 10:00 mass underwent ultrasound-guided biopsy yielding ILC. This proved multicentric disease, and the patient underwent mastectomy rather than lumpectomy

3.15 History

56-year-old patient newly diagnosed with breast cancer undergoing breast MRI extent of disease evaluation (Figs. 3.70, 3.71, 3.72, and 3.73).

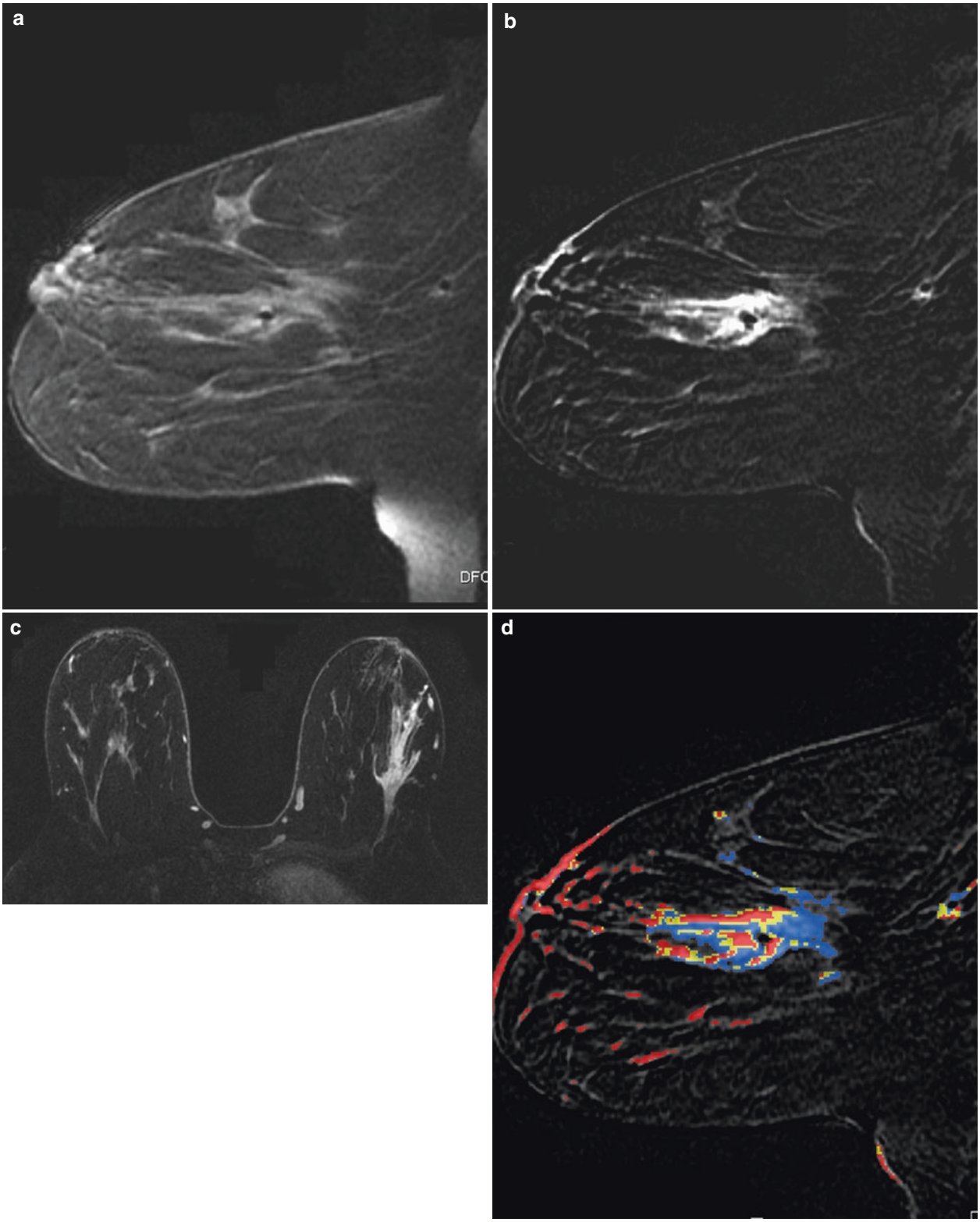

Fig. 3.70 (**a**) Sagittal T1-weighted fat-suppressed image of the left breast. (**b**) Sagittal post-contrast subtraction image of the left breast. (**c**) Axial T1-weighted fat-suppressed post-contrast image of both breasts. (**d**) Sagittal post-contrast subtraction image of the left breast with CAD color overlay

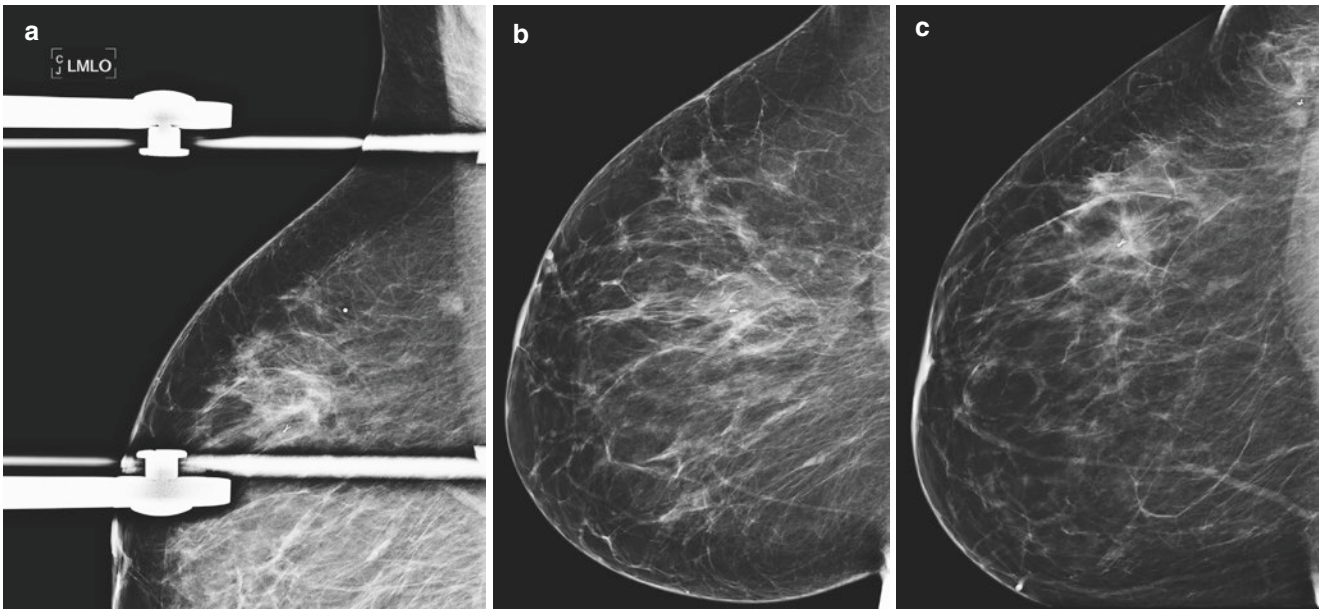

Fig. 3.71 Mammogram. (**a**) MLO spot compression view of the left breast. Post-biopsy ML view (**b**) and exaggerated lateral craniocaudal (XCCL) view (**c**) of the left breast

3.15 Invasive Lobular Carcinoma 3

Teaching Points Patient underwent mastectomy, which demonstrated the largest contiguous involvement of cancer to be 5.8 cm.

Invasive lobular carcinoma (ILC) is the second most common histologic type of breast carcinoma, accounting for approximately 10–15 % of all invasive breast cancers. Its mammographic manifestations may vary and can be vague, such as architectural distortion or asymmetry. Higher false-negative rates (up to 19 %) are reported for ILC than for other invasive cancers at mammography, because ILC is often difficult to diagnose mammographically and therefore disease extent may be underestimated.

Conversely, MR imaging tumor size correlates well with pathologic size of ILC. MR has additional value in patients with ILC, as otherwise-occult tumor foci are demonstrated in approximately one third of patients, changing management in 28 %. Detection of unsuspected contralateral carcinomas with MRI is seen in 7 % of patients with ILC, also impacting patient care.

Image Findings

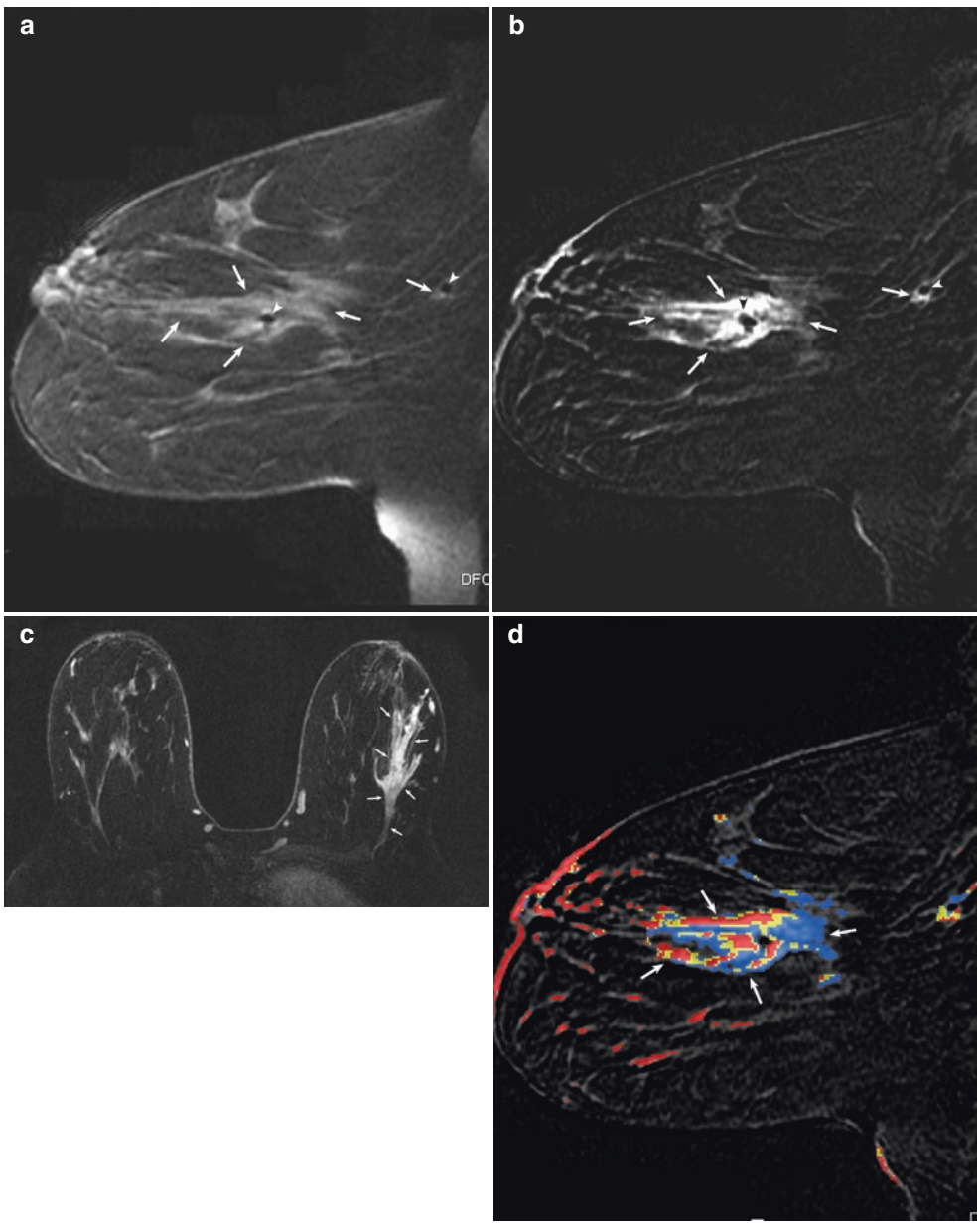

Fig. 3.72 (**a**) Sagittal T1 fat-suppressed pre-contrast image of the left breast demonstrates a dominant T1-intermediate region (*arrows*) with central clip artifact (*arrowhead*), as well as a more posterior T1-intermediate focus (*arrow*) with central clip artifact (*arrowhead*). Sagittal (**b**) and axial (**c**) T1 fat-suppressed post-contrast subtraction images demonstrate a large area of nonmass enhancement (*arrows*) spanning at least 6 cm with central clip artifact (*arrowhead*) in the 3:00 axis of the left breast; a biopsy yielded ILC. Also seen on the sagittal view (**b**), 2 cm posterior to the index lesion, is a 0.7-cm irregular enhancing mass (*arrow*) with central clip artifact (*arrowhead*), which also yielded ILC. No suspicious lymph node was present. (**d**) CAD enhancement kinetics analysis demonstrates washout as the worst curve

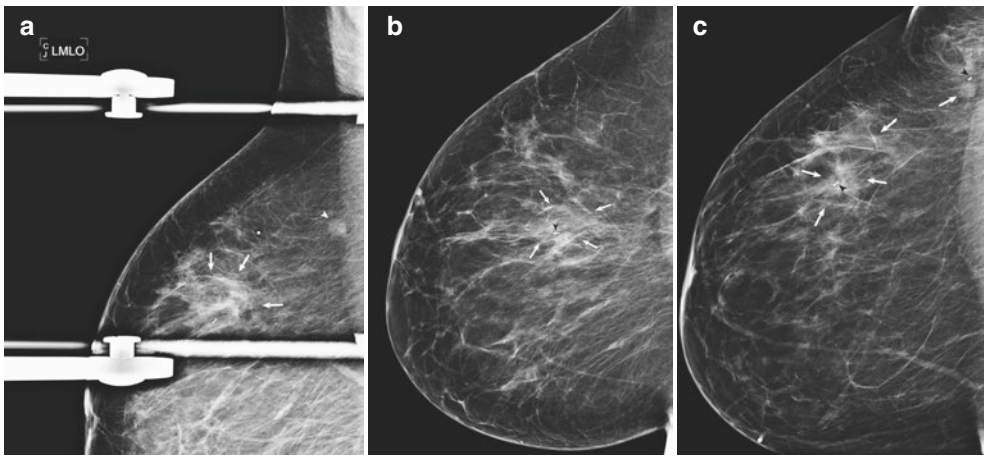

Fig. 3.73 Mammogram of same patient. (**a**) Spot compression MLO view of the left breast demonstrates an indistinct, mildly hyperdense irregular mass (*arrows*) at 2–3:00 mid left breast, spanning 3.5 cm, and a 0.7-cm small irregular mass (*arrowhead*) in the far posterior 2–3:00 axis. Post-biopsy ML (**b**) and XCCL (**c**) views of both of these areas (*arrows*) with clip placement (*arrowheads*) yielded ILC

3.16 History

A 44-year-old woman undergoing breast MRI to evaluate extent of disease (Figs. 3.74, 3.75, 3.76, and 3.77).

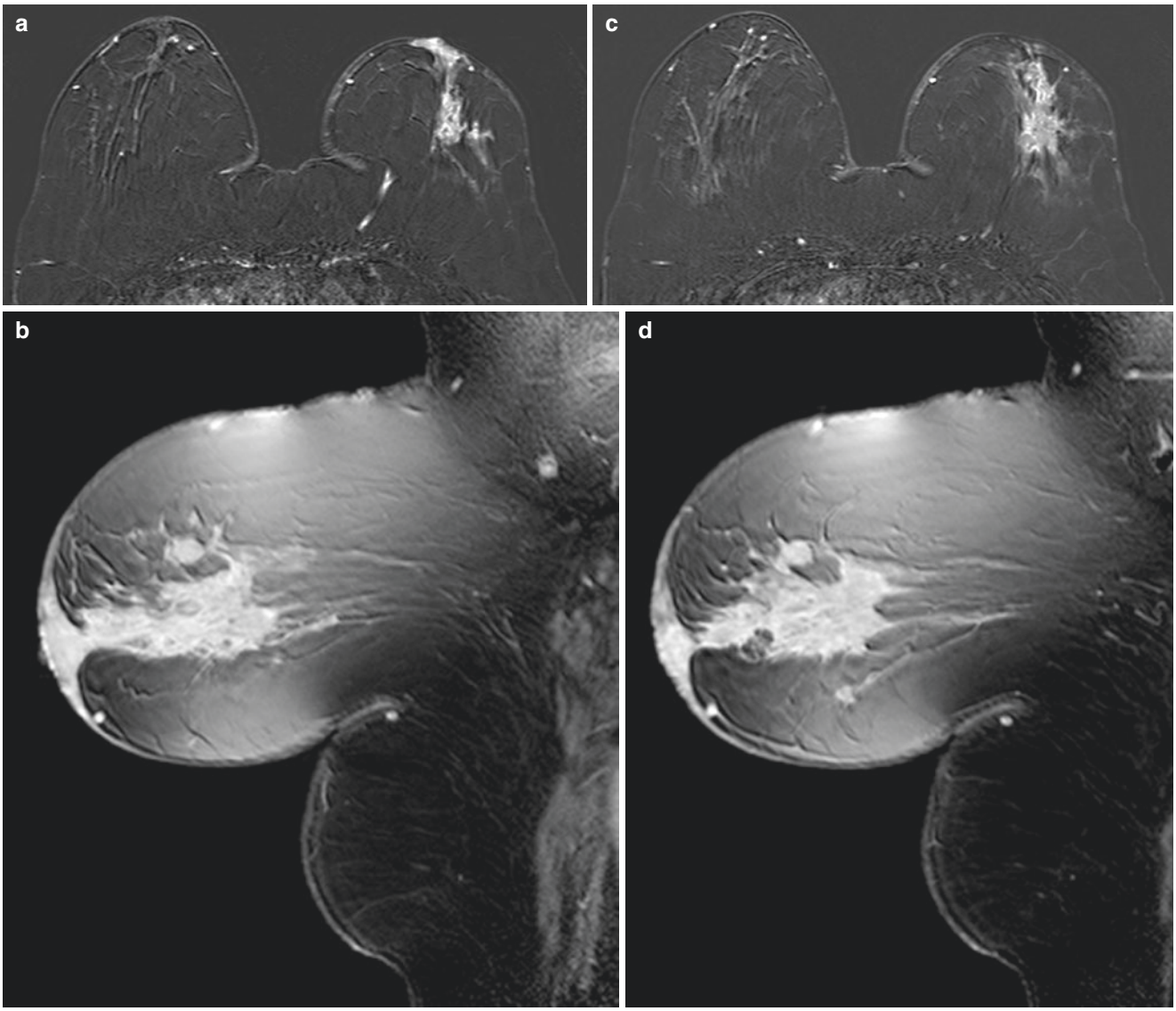

Fig. 3.74 (**a**, **c**) Axial post-contrast subtraction images of both breasts. (**b**, **d**) Sagittalt T1-weighted fat-suppressed post-contrast images of the left

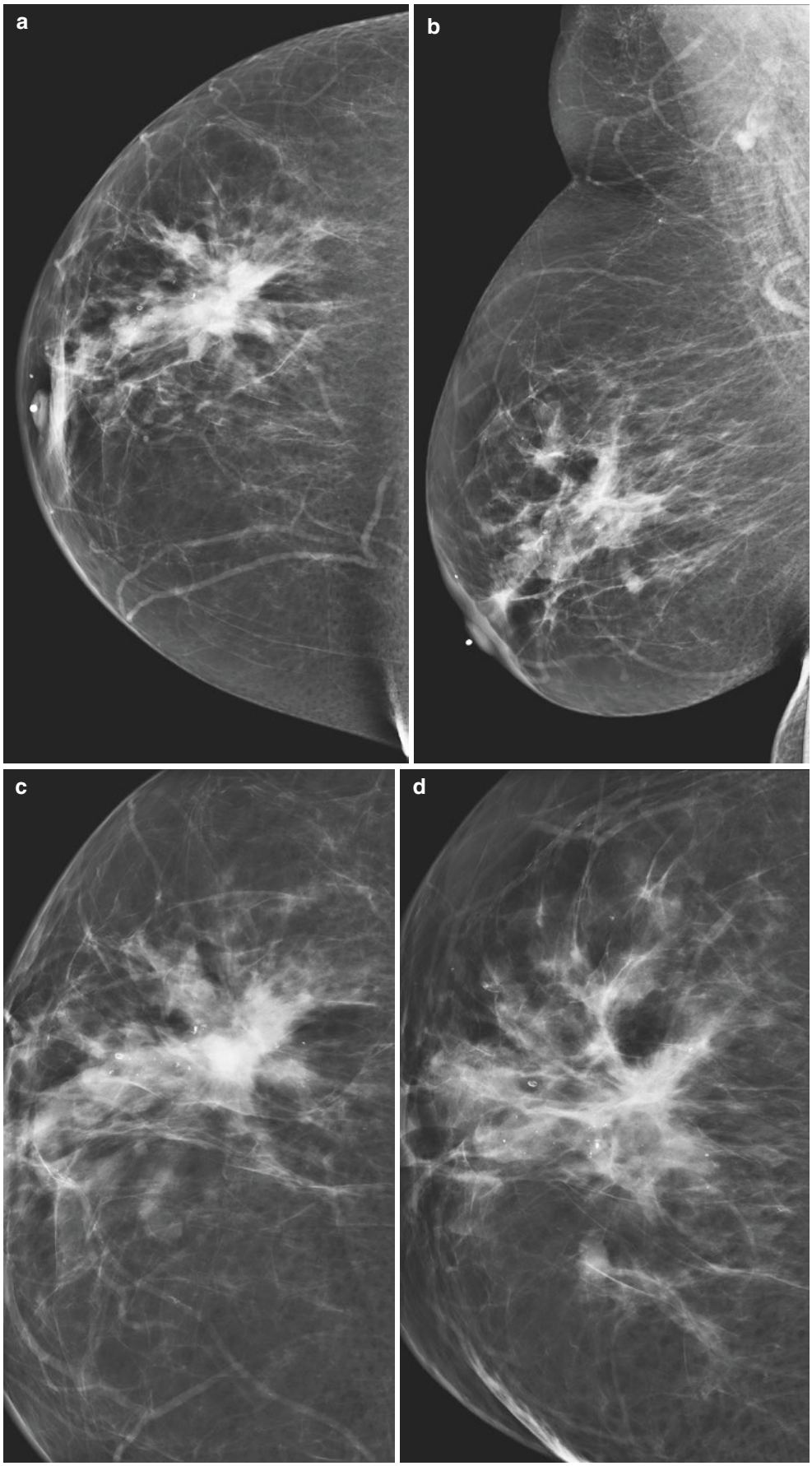

Fig. 3.75 Mammogram. CC (**a**), MLO (**b**), CC spot magnification (**c**), and ML spot magnification (**d**) views of the left breast

3.16 Nipple/Peri-areolar Involvement 1

Teaching Points MR imaging has been shown to affect clinical management in 50 % of patients with ILC, leading to changes in surgical management in 28 % of cases. Tumors less than 2 cm from the nipple or larger than 2 cm are significantly associated with nipple-areolar complex (NAC) involvement. Preoperative MR imaging can be performed to evaluate disease near the NAC and determine the patient's eligibility for nipple-sparing mastectomy.

Image Findings

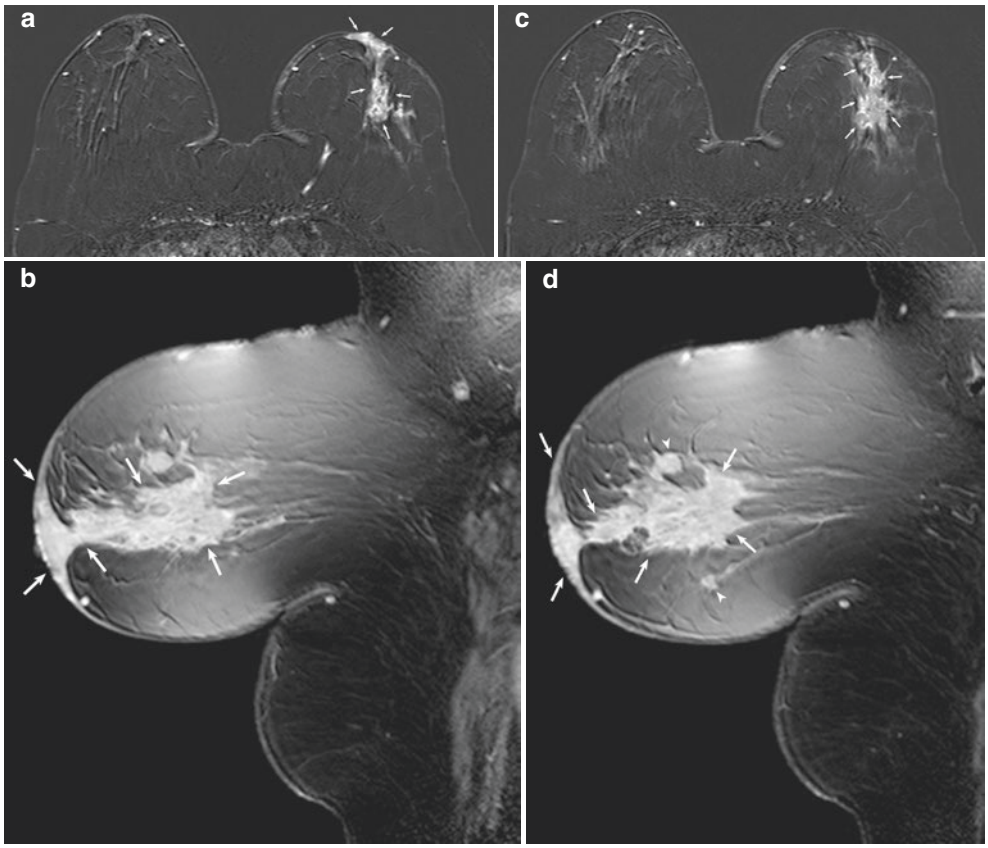

Fig. 3.76 Invasive lobular carcinoma involving the nipple. Axial post-contrast subtraction (**a**) and sagittal (**b**) T1-weighted fat-suppressed post-contrast images demonstrate a heterogeneously enhancing irregular mass (*arrows*) in the central left breast, extending to and involving the thickened, enhancing nipple-areolar complex (*arrows*). An axial post-contrast subtraction image (**c**) and a sagittal T1-weighted fat-suppressed post-contrast image (**d**) at a different level show to greater effect the heterogeneously enhancing spiculated mass (*arrows*) with additional satellite lesions (*arrowheads*) superior and inferior to it. Note the suboptimal positioning of the patient on the sagittal images, with infolding of the inframammary fold and incomplete fat suppression

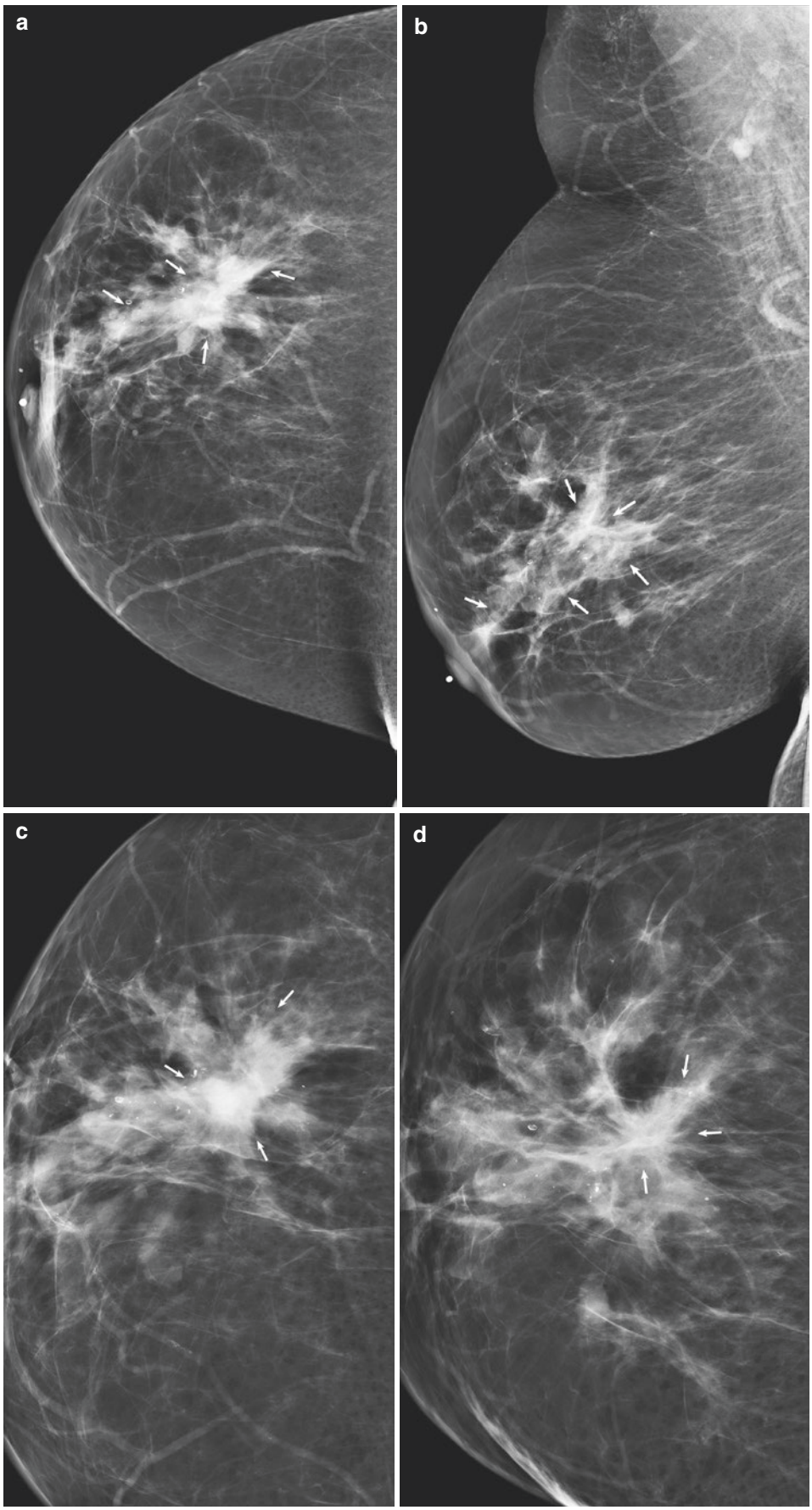

Fig. 3.77 CC (**a**), MLO (**b**), CC spot magnification (**c**), and ML magnification (**d**) mammographic views of the left breast demonstrate an irregular, spiculated mass (*arrows*) in the slightly lateral left breast, with associated architectural distortion and pleomorphic calcifications. Biopsy yielded ILC

3.17 History

Extent of disease evaluation (Figs. 3.78, 3.79, 3.80, 3.81, 3.82, and 3.83).

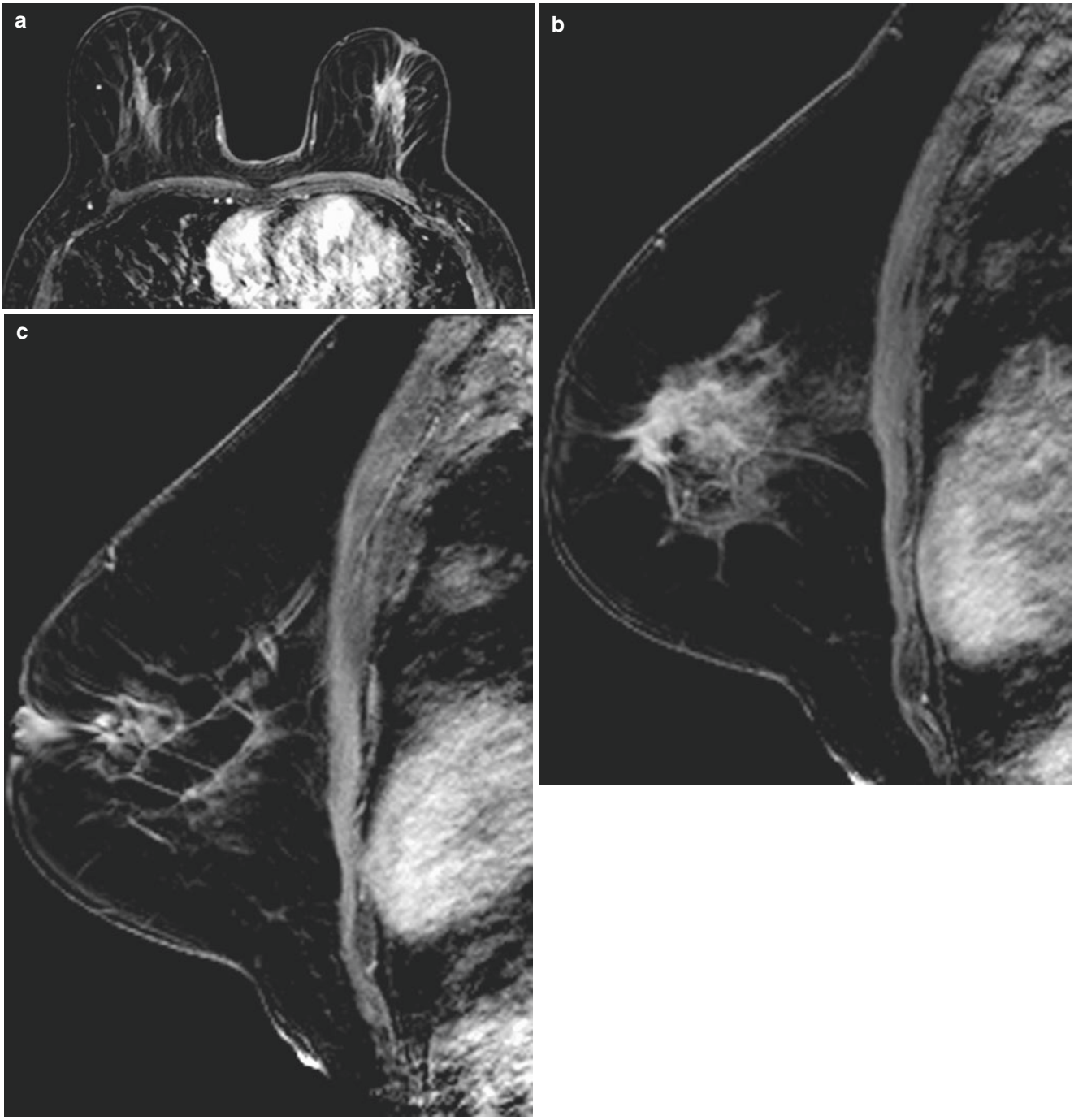

Fig. 3.78 (**a**) Axial post-contrast subtraction image of both breasts. (**b**, **c**) Sagittal post-contrast subtraction images of the left breast

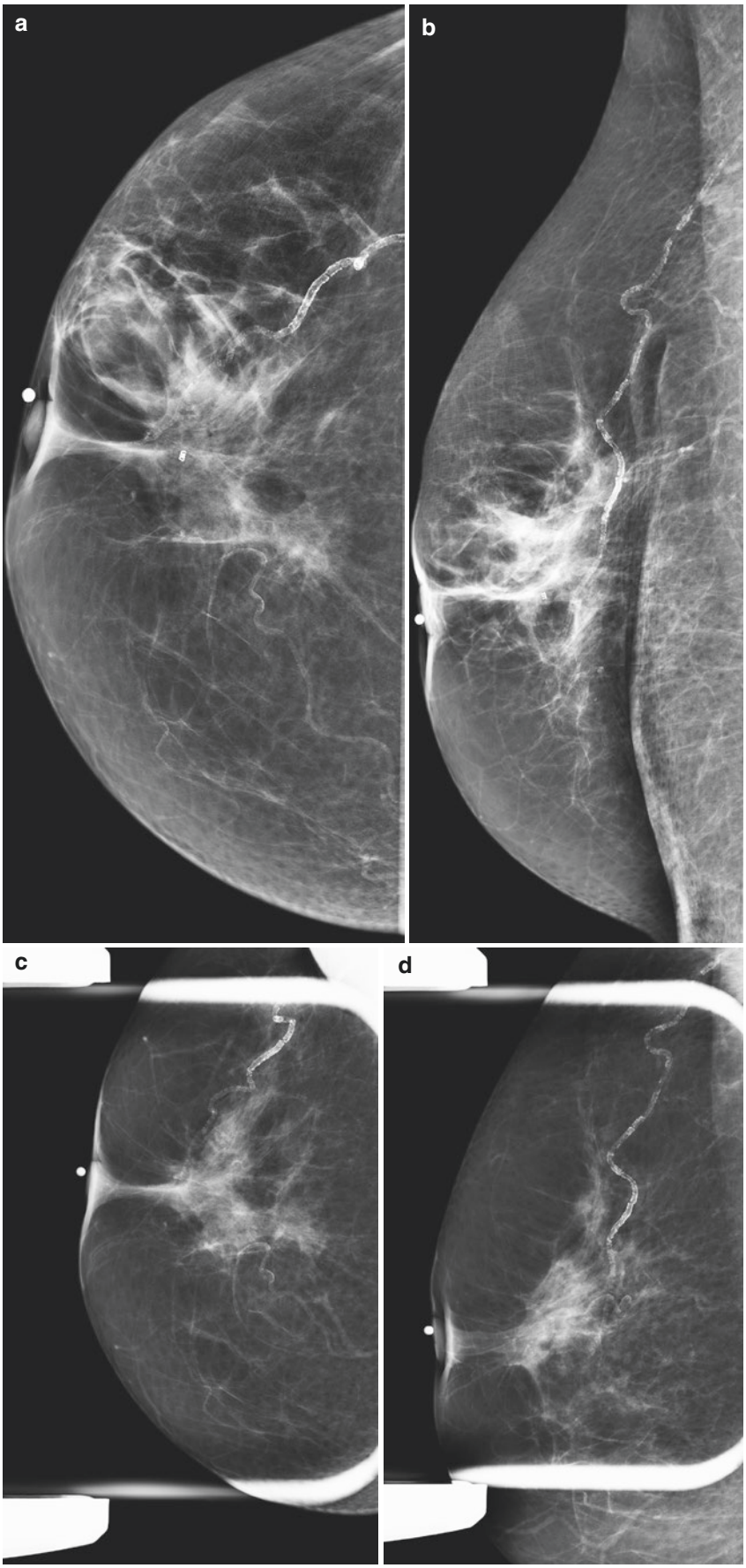

Fig. 3.79 Mammographic images of the left breast. CC (**a**), MLO (**b**), and spot compression CC (**c**) and ML views (**d**)

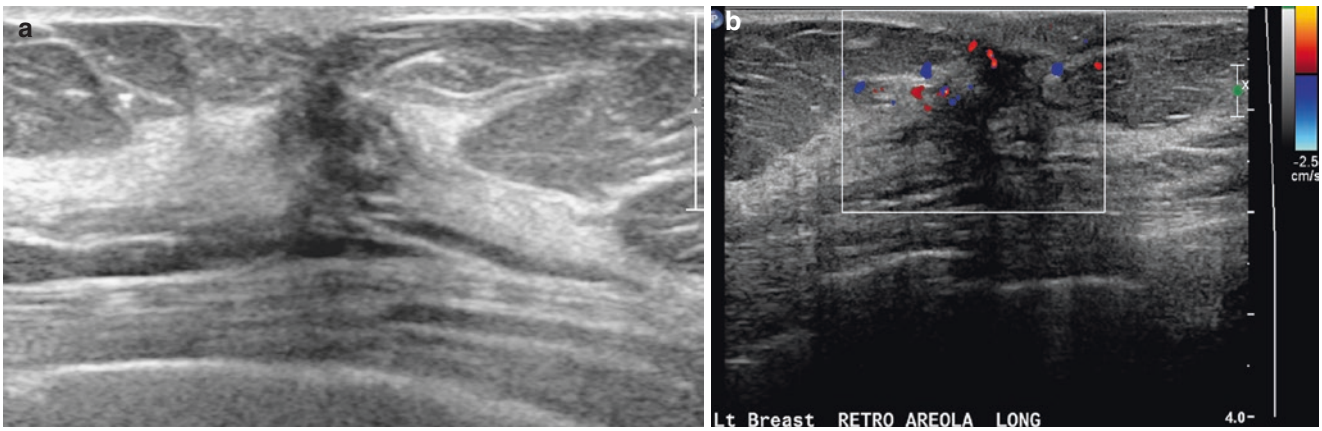

Fig. 3.80 Grayscale (**a**) and color Doppler (**b**) images from a targeted left breast ultrasound

3.17 Nipple/Peri-areolar Involvement 2

Teaching Points MR imaging has been shown to affect clinical management in up to 50 % of patients with ILC, leading to changes in surgical management in 28 % of cases. Several published studies indicate that preoperative MRI is helpful in identifying clinically occult tumor involvement of the NAC. Shorter MRI-measured distance from the NAC, larger tumor size, subareolar/central location (as illustrated in this case), and unilateral enhancement of the nipple with continuous enhancement from the index lesion are correlated with increased risk of NAC involvement.

Image Findings

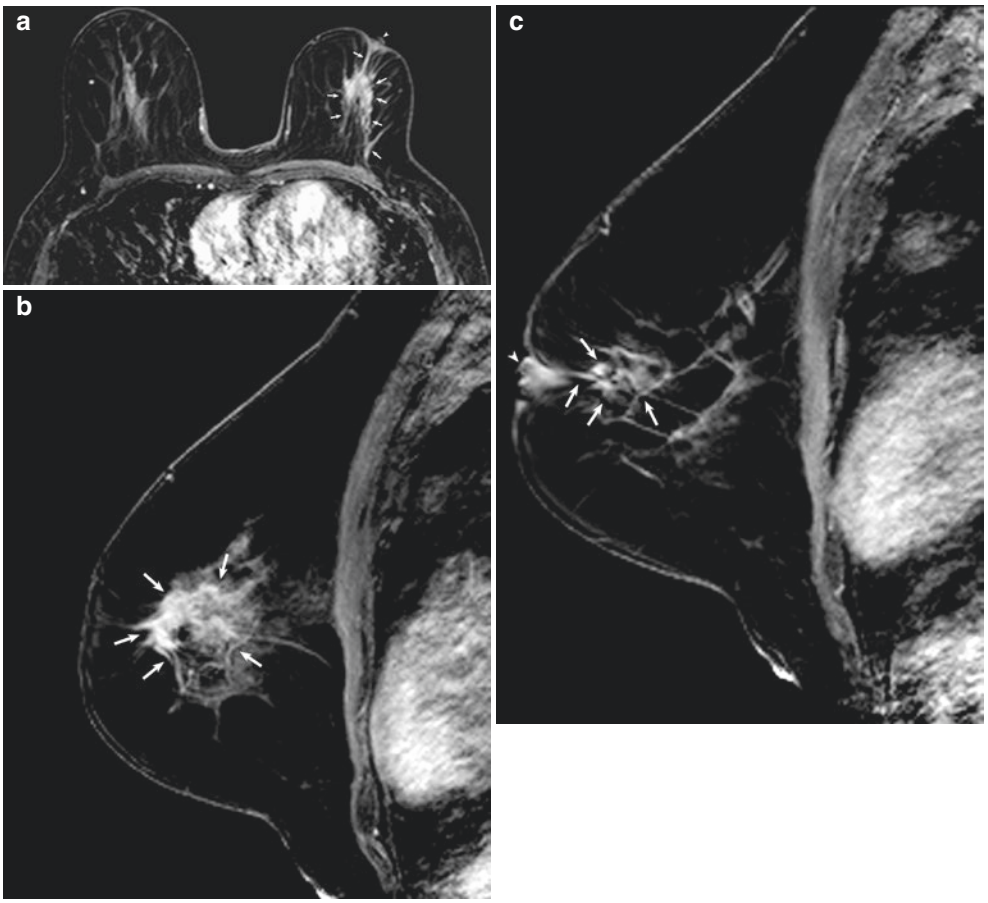

Fig. 3.81 MRI performed to evaluate disease extent in a patient with newly diagnosed left breast invasive lobular carcinoma. Axial post-contrast subtraction image (**a**) of both breasts and sagittal post-contrast subtraction images (**b** and **c**) of the left breast demonstrate a heterogeneously enhancing, irregular, spiculated retroareolar left breast mass (*arrows*) with extension to the nipple (*arrowheads*)

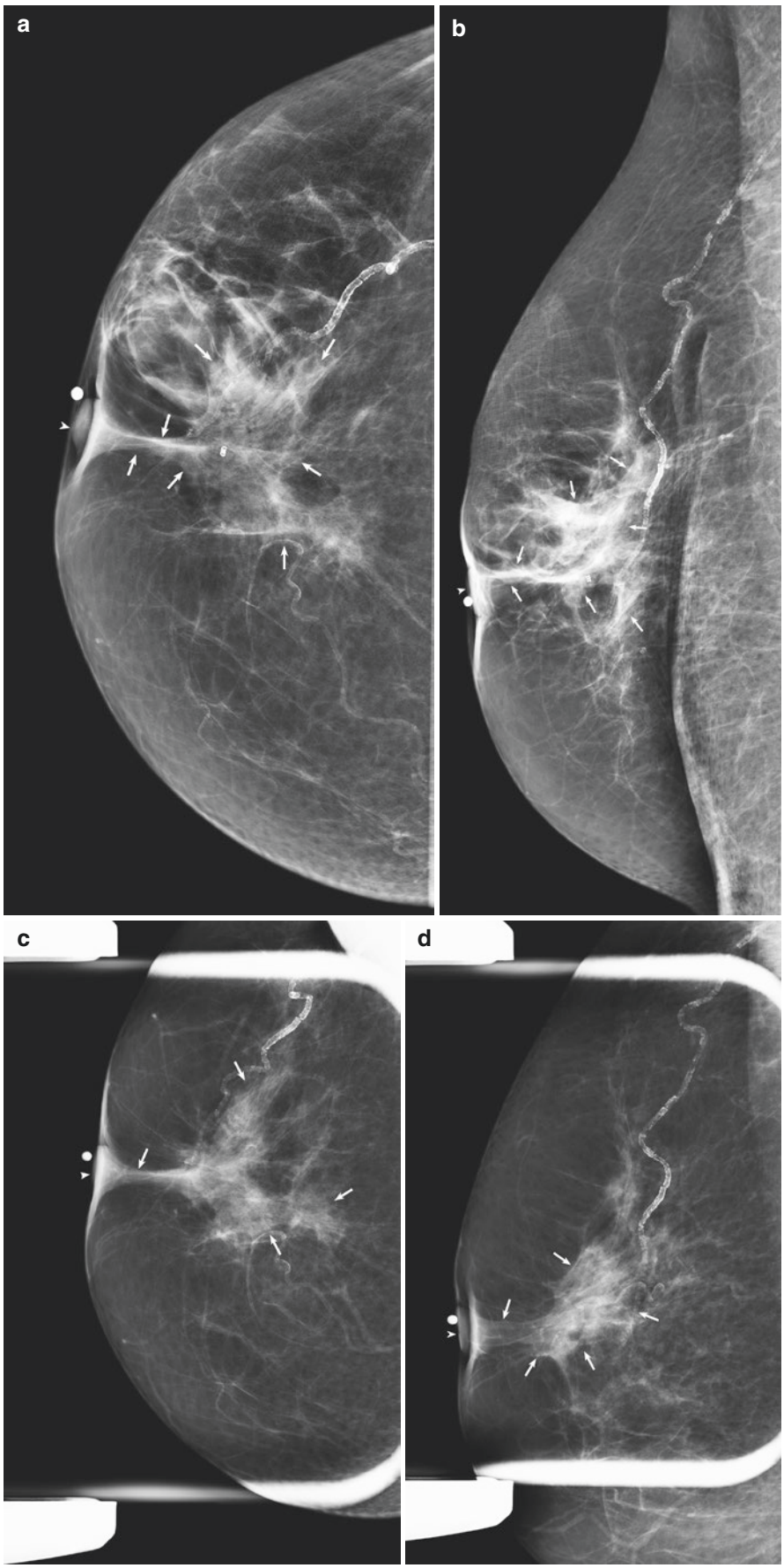

Fig. 3.82 Corresponding mammogram. Left CC (**a**) and MLO (**b**) views demonstrate an irregular, indistinct, hyperdense mass (*arrows*) in the retroareolar region with extension to the retracted nipple (*arrowhead*). Spot compression CC (**c**) and ML (**d**) views better depict the tumor extension (*arrows*) to the retracted nipple (*arrowhead*)

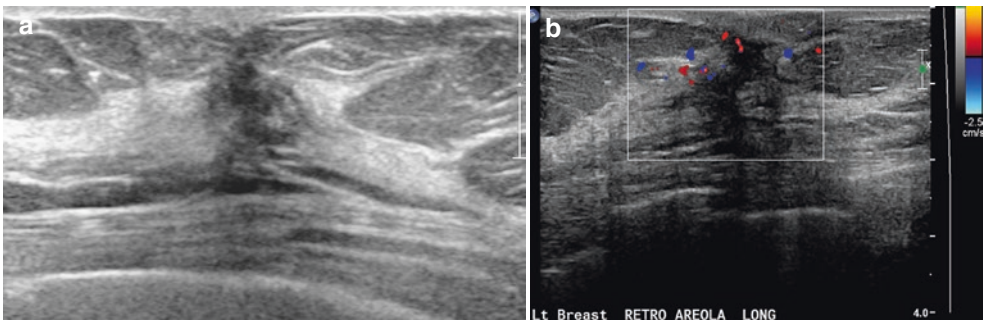

Fig. 3.83 Corresponding ultrasound. Grayscale (**a**) and color Doppler (**b**) images demonstrate a taller-than-wide, irregular, indistinct mass with posterior acoustic shadowing in the retroareolar left breast. Internal vascularity is noted

3.18 History

56-year-old woman undergoing breast MRI to evaluate extent of disease (Figs. 3.84 and 3.85).

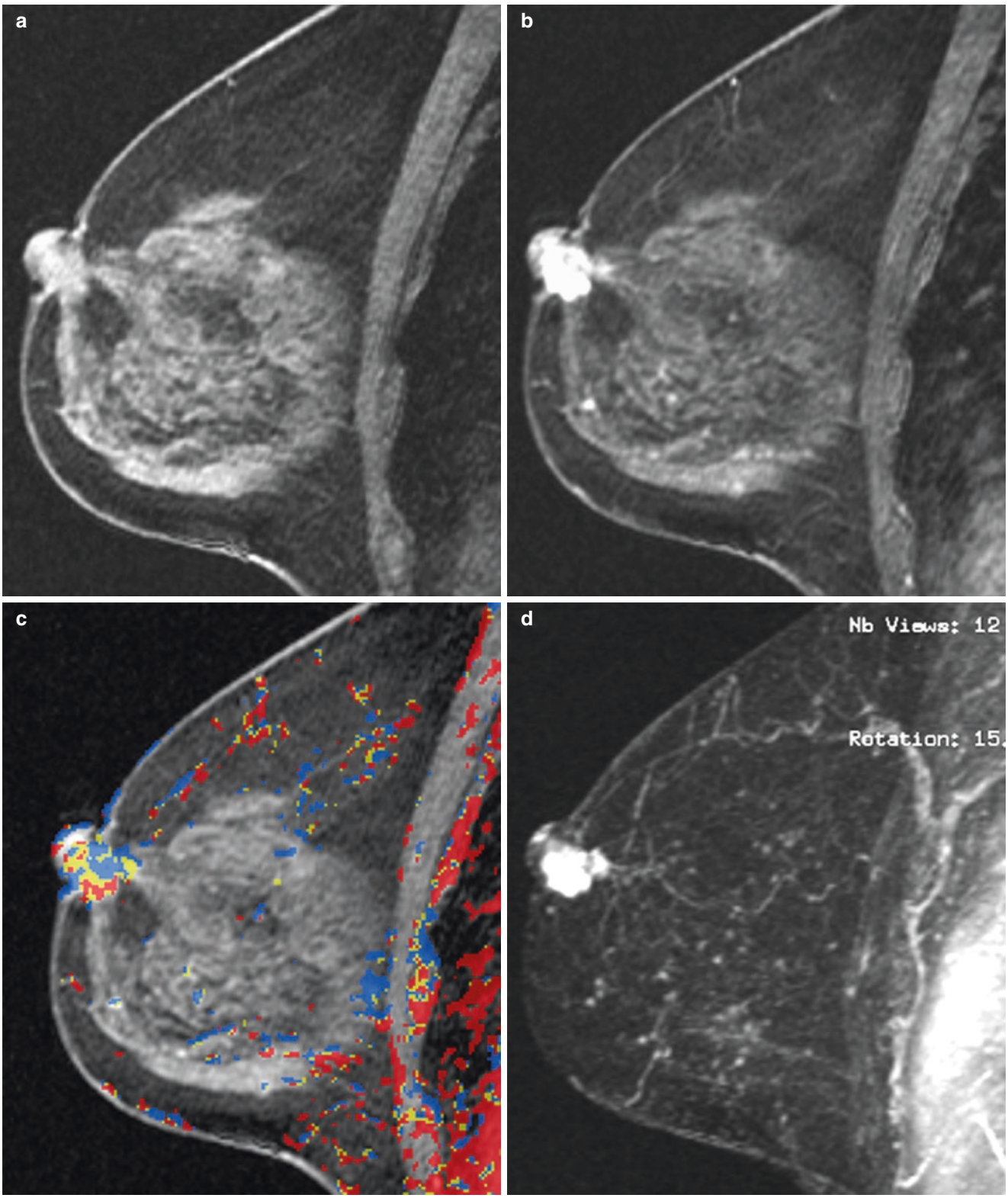

Fig. 3.84 Sagittal T1-weighted fat-suppressed pre-contrast image (**a**) and post-contrast image (**b**) of the right breast. (**c**) Sagittal T1-weighted fat-suppressed post-contrast image with CAD color overlay. (**d**) Sagittal post-contrast MIP image of the right breast

3.18 Nipple/Peri-areolar Involvement 3

Teaching Points The nipple may be involved by cancer via extension of underlying invasive ductal carcinoma, by ductal carcinoma in situ (DCIS), or by Paget cells within the epidermis. According to histopathologic examination of the nipple in mastectomy specimens, the prevalence of clinically occult nipple involvement by cancer is higher than previously thought. Therefore, it is important to rule out occult carcinoma within the nipple-areolar complex (NAC) in patients undergoing nipple-sparing mastectomy.

Greater MRI-measured tumor size and shorter distance from the NAC are correlated with increased risk of NAC involvement. Preoperative MRI is useful to predict extent of disease, including occult nipple invasion.

Image Findings

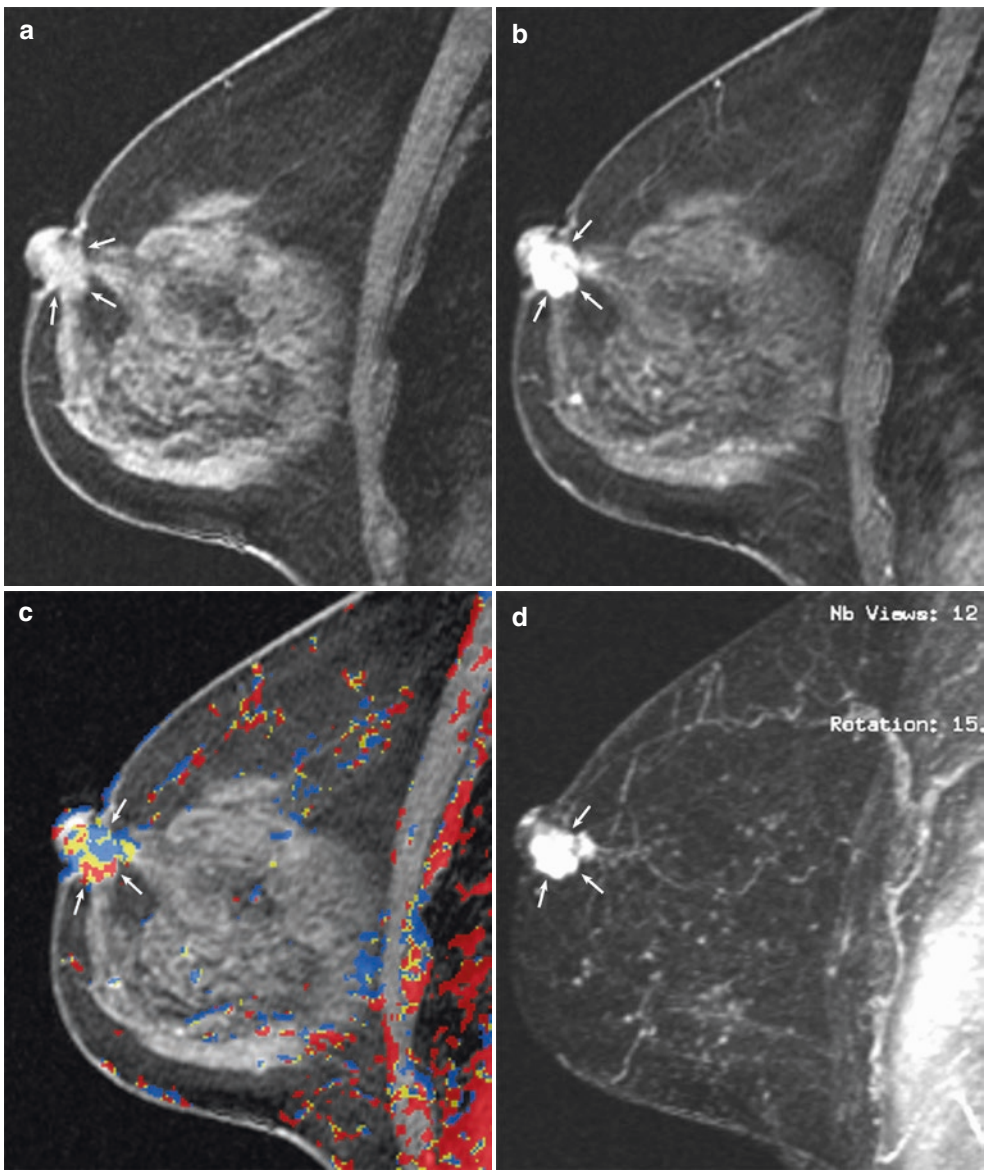

Fig. 3.85 Sagittal T1-weighted fat-suppressed pre-contrast image (**a**) and post-contrast image (**b**) of the right breast demonstrate a heterogeneously enhancing, irregular T1-isointense retroareolar mass (*arrows*) involving the nipple. (**c**) CAD enhancement kinetics analysis demonstrates a mixed enhancement pattern. (**d**) Post-contrast 3D MIP image shows the enhancing retroareolar mass (*arrows*) involving the nipple

3.19 History

Extent of disease evaluation (Figs. 3.86 and 3.87).

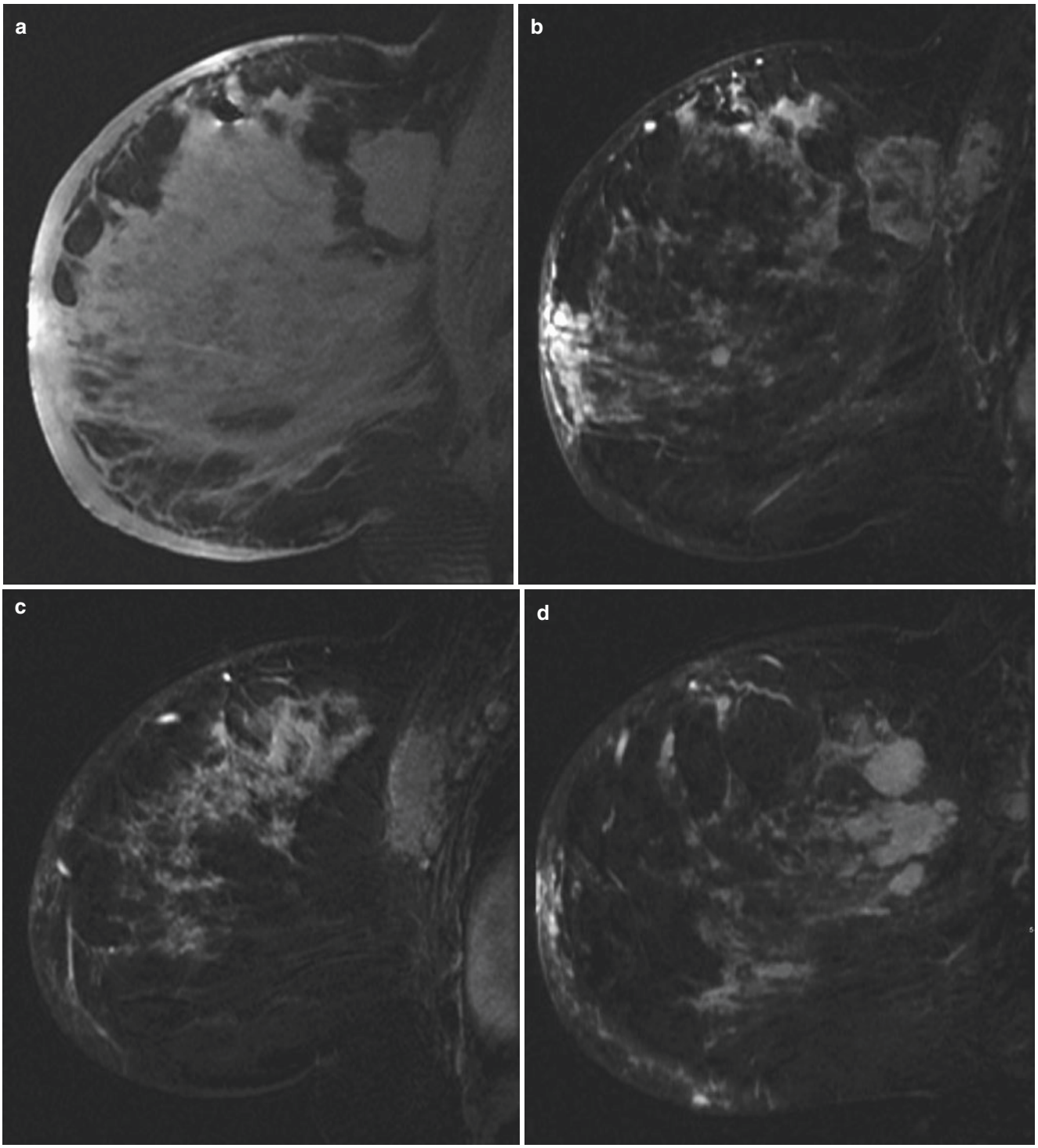

Fig. 3.86 Sagittal MRI images of the left breast. (**a**) T1-weighted fat-saturated. (**b–d**) Post-contrast subtraction at three locations

3.19 Pectoralis Involvement

Teaching Points MRI evaluation of breast carcinoma prior to surgical treatment may be useful in both mastectomy and breast conservation candidates, to define the relationship of the tumor to the fascia and possible extension into the pectoralis major and chest wall. Tumor invasion of the pectoralis muscle is either infiltrative or mass-like and should be easily distinguishable from baseline muscle enhancement. Obliteration of the fat plane between tumor and muscle alone does not indicate muscle involvement; there must be associated focal muscle enhancement.

The patient with tumor extension into the chest wall is usually considered stage T4 according to TNM classification and stage IIIB, which requires chest wall resection. Invasion of the pectoralis major muscle alone does not affect staging and may require only muscle resection at the time of surgery.

Image Findings

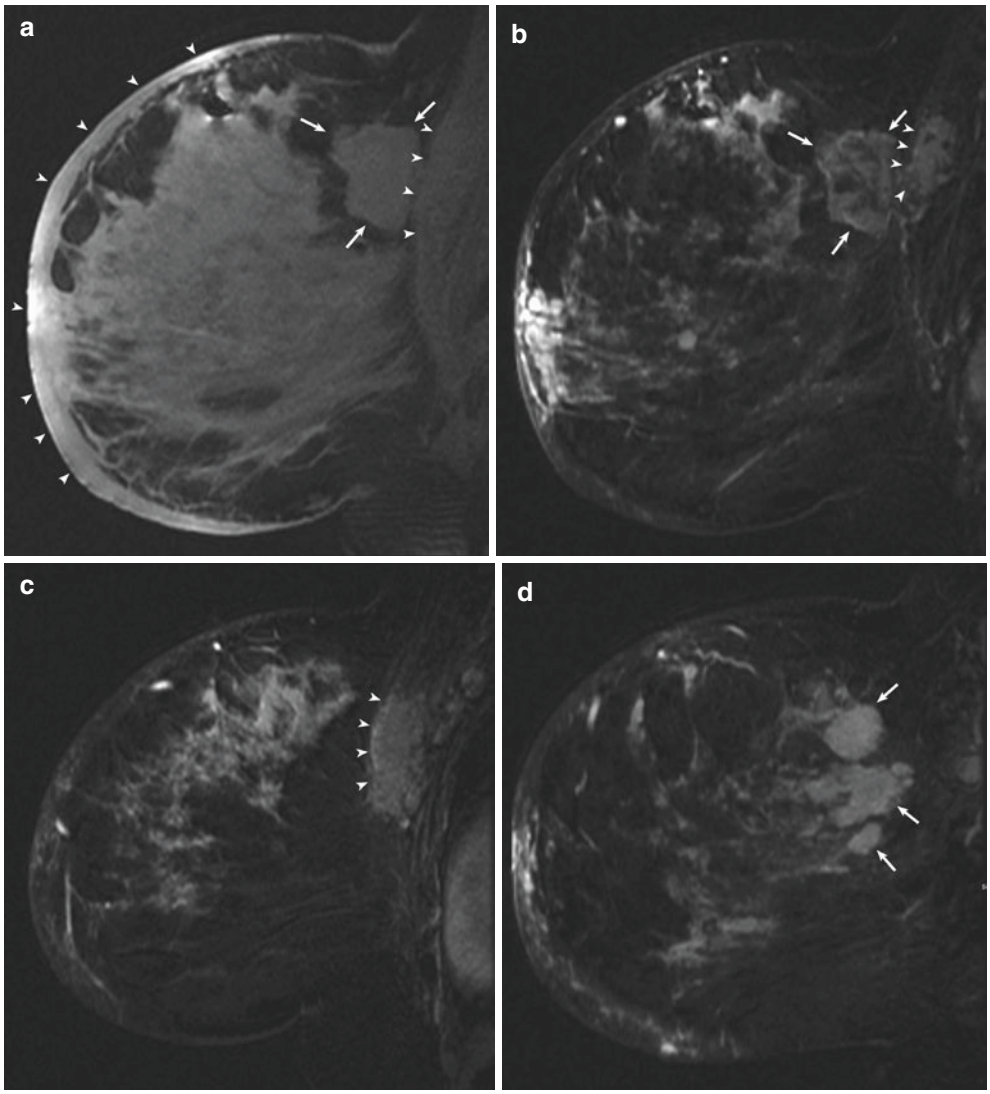

Fig. 3.87 Left breast cancer with pectoralis muscle involvement. (**a**) Sagittal T1-weighted fat-saturated image demonstrates an irregular mass (*arrows*) abutting the pectoralis major muscle (*arrowheads*). Skin thickening is noted (*arrowheads*). (**b**–**d**) Selected sagittal post-contrast subtraction images demonstrate irregular, homogeneously and heterogeneously enhancing masses (*arrows*) in the posterior third of the breast, some of which abut the expanded, enhancing pectoralis major muscle (*arrowheads*)

3.20 History

58-year-old woman with chest pain.

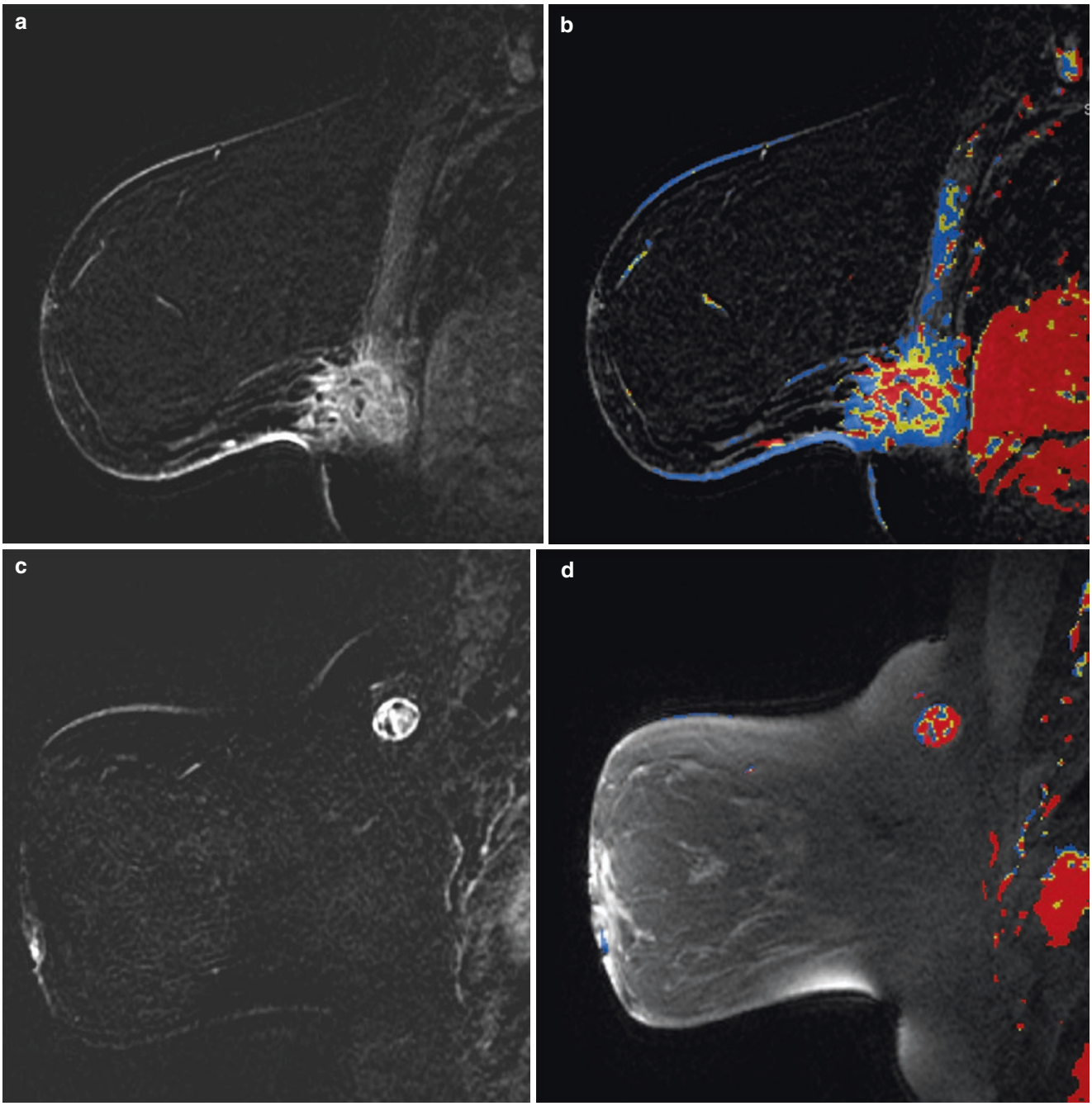

Fig. 3.88 Sagittal MRI images of the left breast. Post-contrast subtraction image (**a**) with corresponding CAD color overlay (**b**). (**c**) Post-contrast subtraction image through the right axilla. (**d**) T1-weighted fat-saturated post-contrast image with CAD color overlay

3.20 Chest Wall Involvement

Teaching Points Teaching points: companion case to 3.17 (Figs. 3.88 and 3.89).

Image Findings

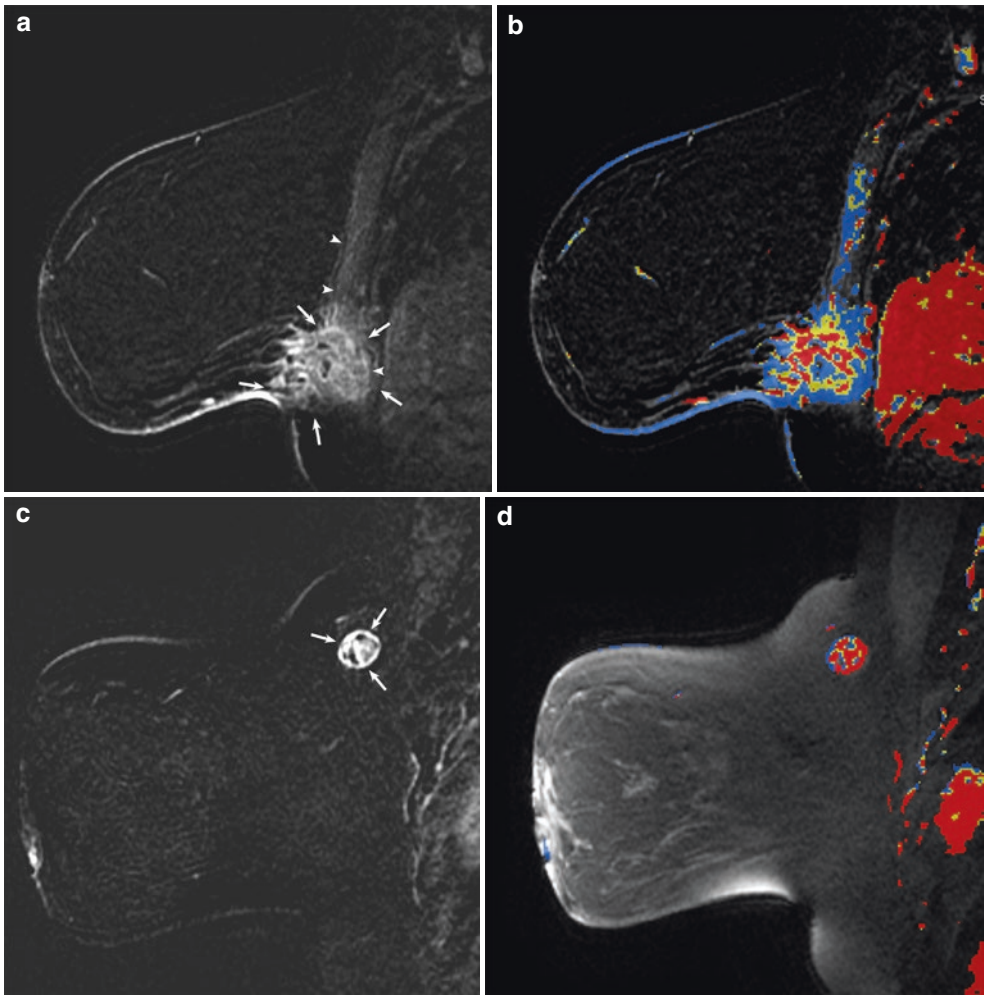

Fig. 3.89 Bilateral breast MRI was performed on a patient with a history of left breast malignancy with worsening left chest pain 5 years after lumpectomy. (**a**) Sagittal post-contrast subtraction image of the left breast shows a highly suspicious, heterogeneously enhancing mass (*arrows*) in the posterior left breast involving the chest wall (*arrowheads*) and possibly the pleura. (**b**) CAD kinetic enhancement analysis demonstrates a mixed pattern with central washout. (**c**) Sagittal post-contrast subtraction image through the right axilla shows an abnormally enlarged lymph node (*arrows*) with predominant washout kinetics on CAD enhancement kinetics analysis (**d**), suspicious for metastasis. Biopsy of the left chest wall mass and contralateral axillary lymph node yielded recurrent invasive ductal carcinoma with metastasis to the contralateral lymph node

3.21 History

38-year-old with palpable left breast lump (Figs. 3.90, 3.91, 3.92, 3.93, 3.94, and 3.95).

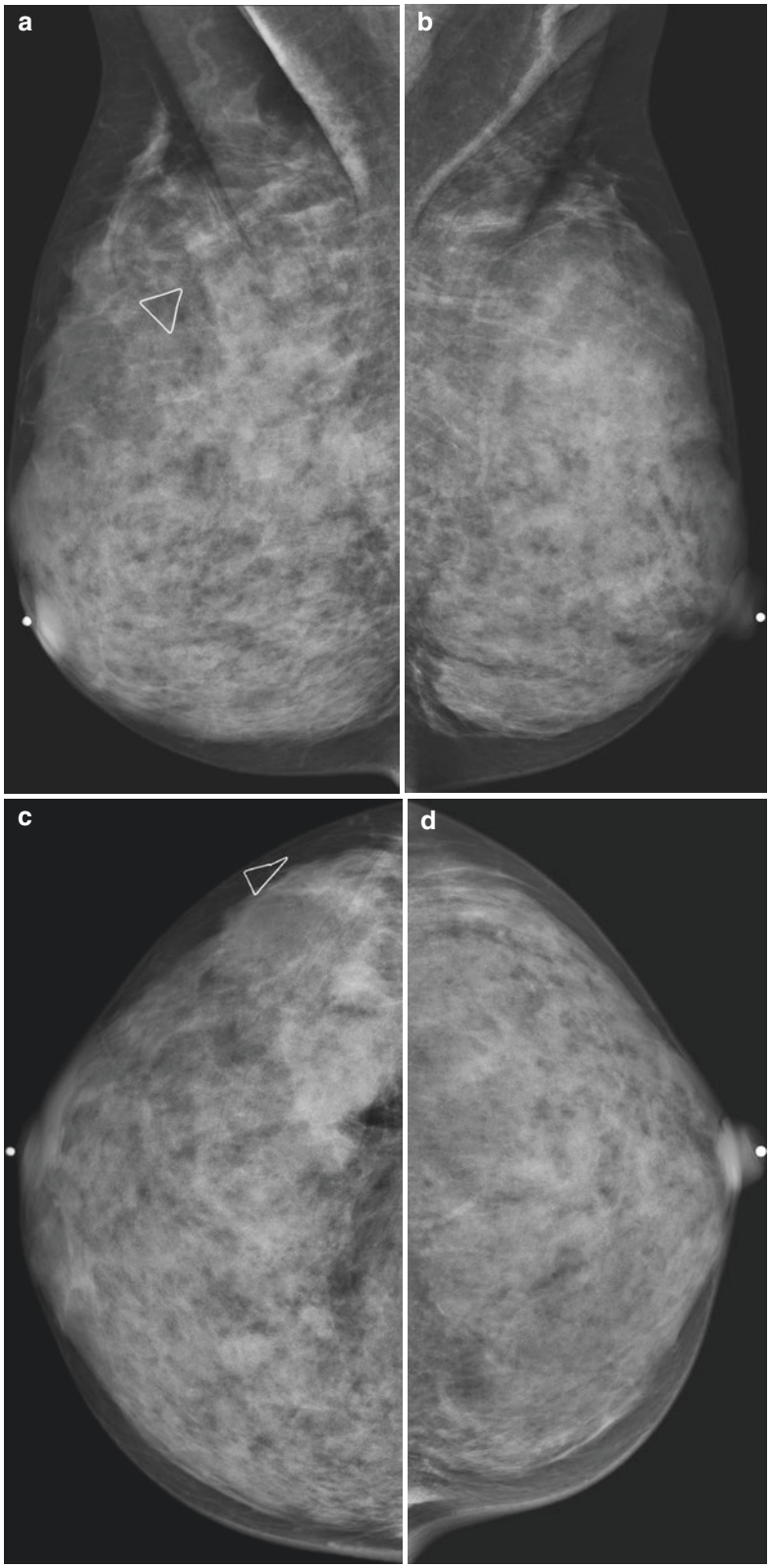

Fig. 3.90 Mammogram. Bilateral MLO (**a**, **b**) and CC views (**c**, **d**). Left spot compression CC (**e**) and MLO (**f**) views

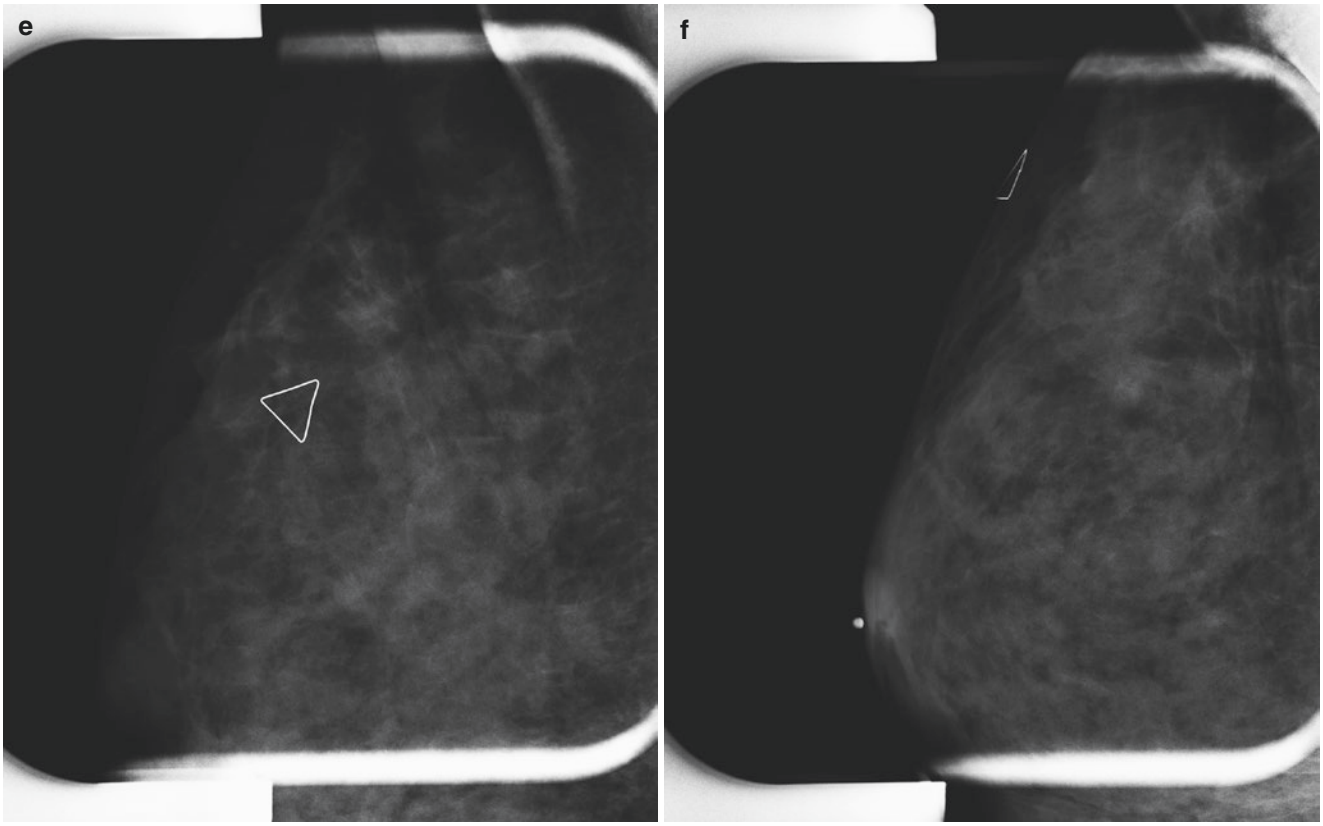

Fig. 3.90 (continued)

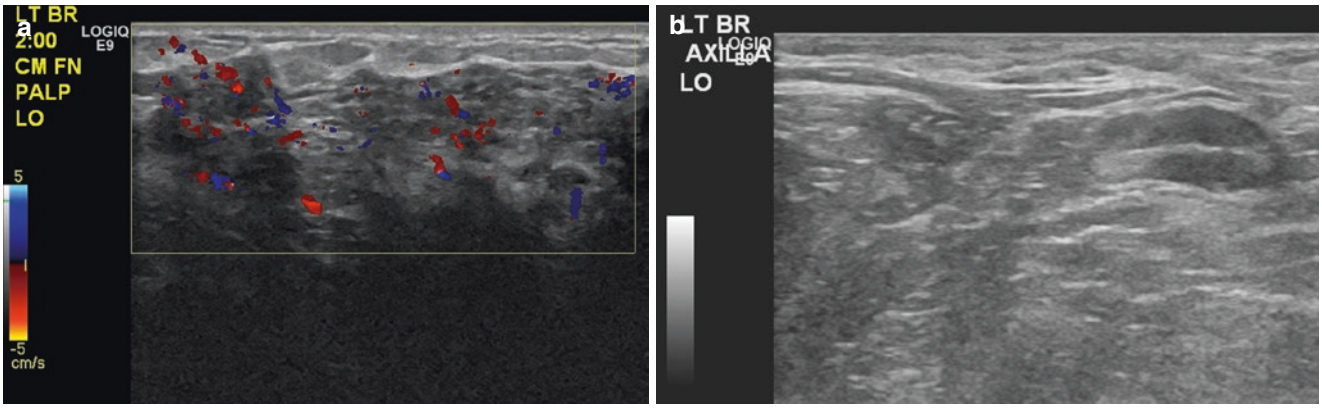

Fig. 3.91 Ultrasound. (**a**) Color Doppler image of the outer left breast. (**b**) Grayscale image of the left axilla

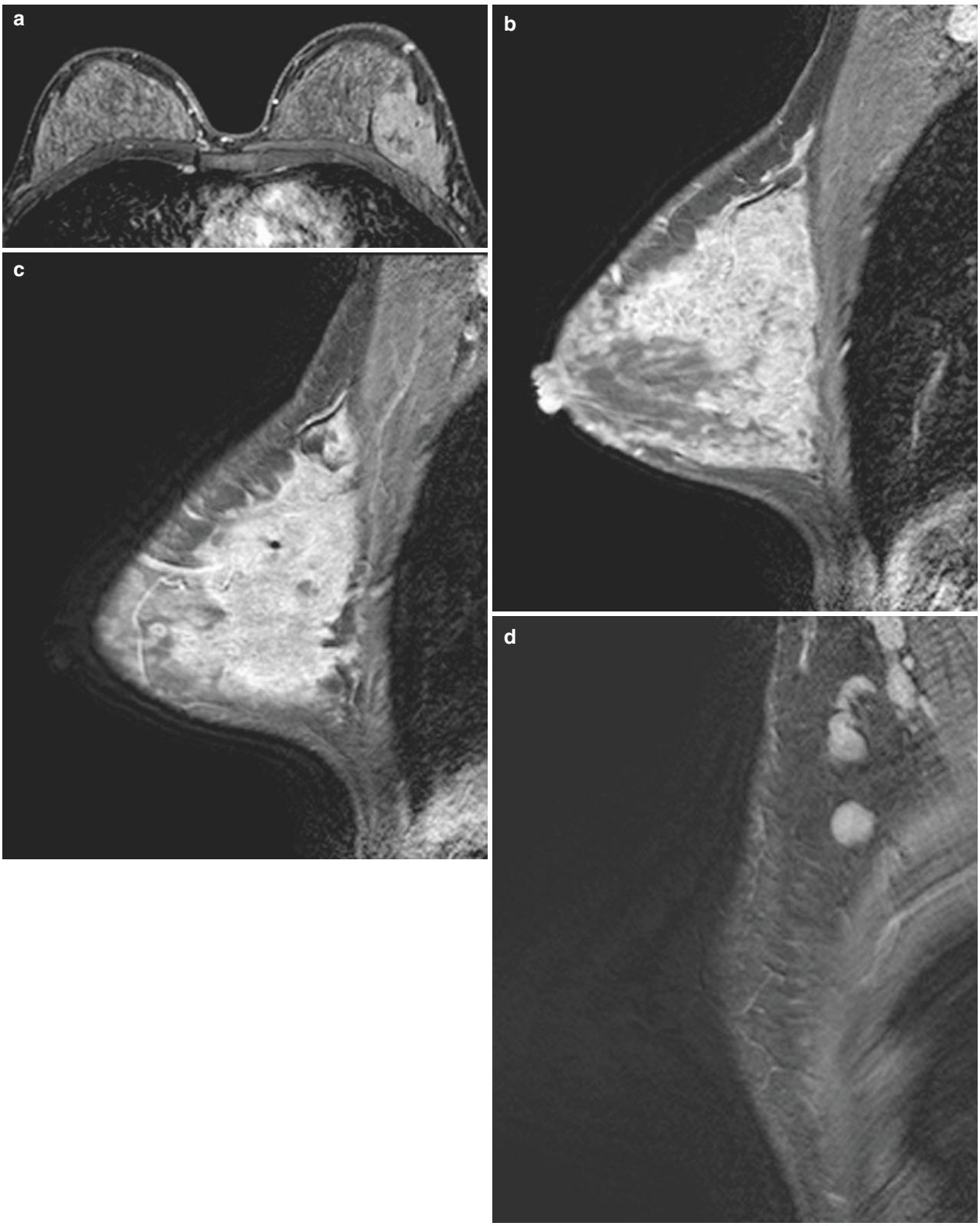

Fig. 3.92 (**a**) Axial T1-weighted fat-saturated post-contrast image of both breasts. Selected sagittal T1-weighted fat-saturated post-contrast images of the outer left breast (**b**, **c**) and of the axilla (**d**)

3.21 Dense Breast

Teaching Points There is literature support for preoperative breast MRI in patients with extremely dense and heterogeneously dense breasts and newly diagnosed breast carcinoma. As illustrated in this case, the extent of disease can be better delineated on MRI than in the mammogram in the setting of dense breasts. In addition, the sonographic findings in this case were vague, limiting the measurement of disease extent. The mastectomy specimen in this case confirmed the extent of disease best delineated by the breast MRI. It is important to note that breast MRI can also overestimate disease because of nontumoral enhancement of the surrounding tissue from inflammation and edema.

Image Findings

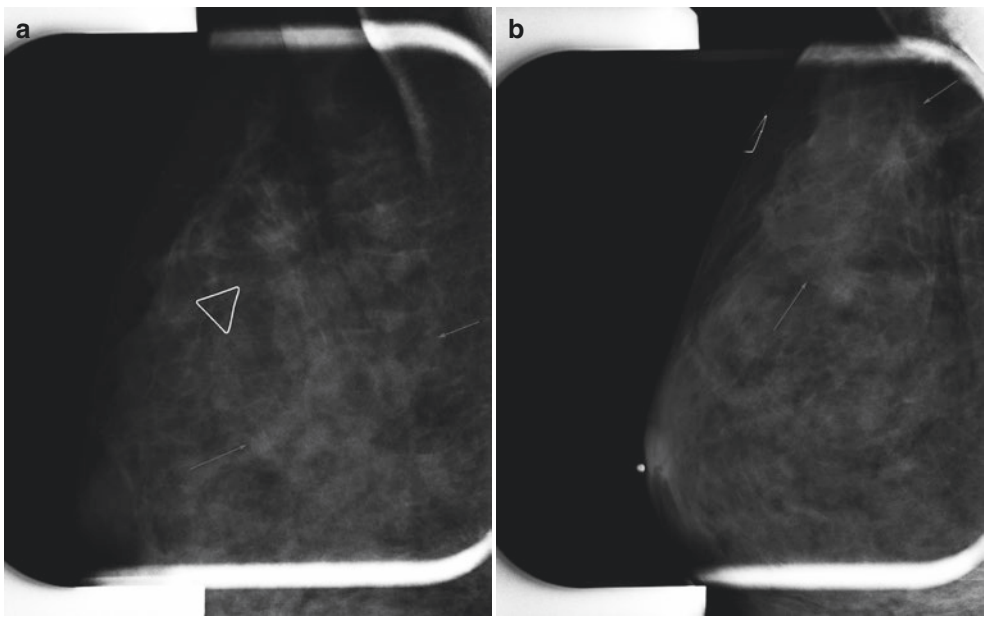

Fig. 3.93 Extensive malignancy better appreciated on MRI in a patient with dense parenchyma. A vague asymmetry is present underlying the palpable marker (*triangle*) in the upper outer left breast, better delineated on the CC spot compression view (**a**, *arrows*) than on the MLO spot compression view (**b**, *arrows*)

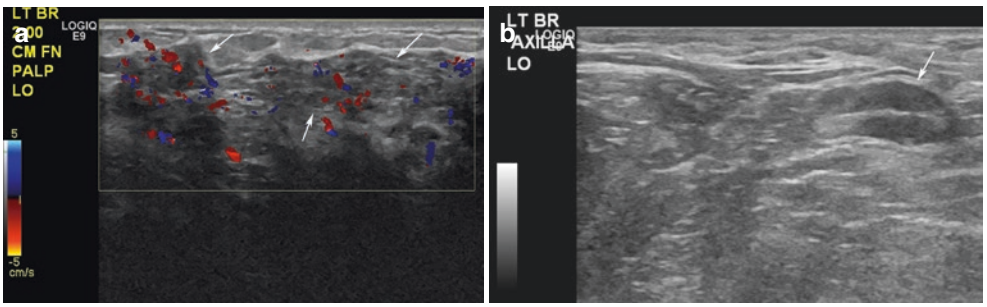

Fig. 3.94 (**a**) Targeted ultrasound of the upper outer left breast shows vague hypoechoic areas (*arrows*) with increased vascularity likely corresponding to the mammographic finding. (**b**) Abnormal left axillary lymph nodes were also identified. A representative area in the left breast and an axillary lymph node underwent ultrasound-guided biopsy yielding invasive ductal carcinoma not otherwise specified, with axillary metastasis

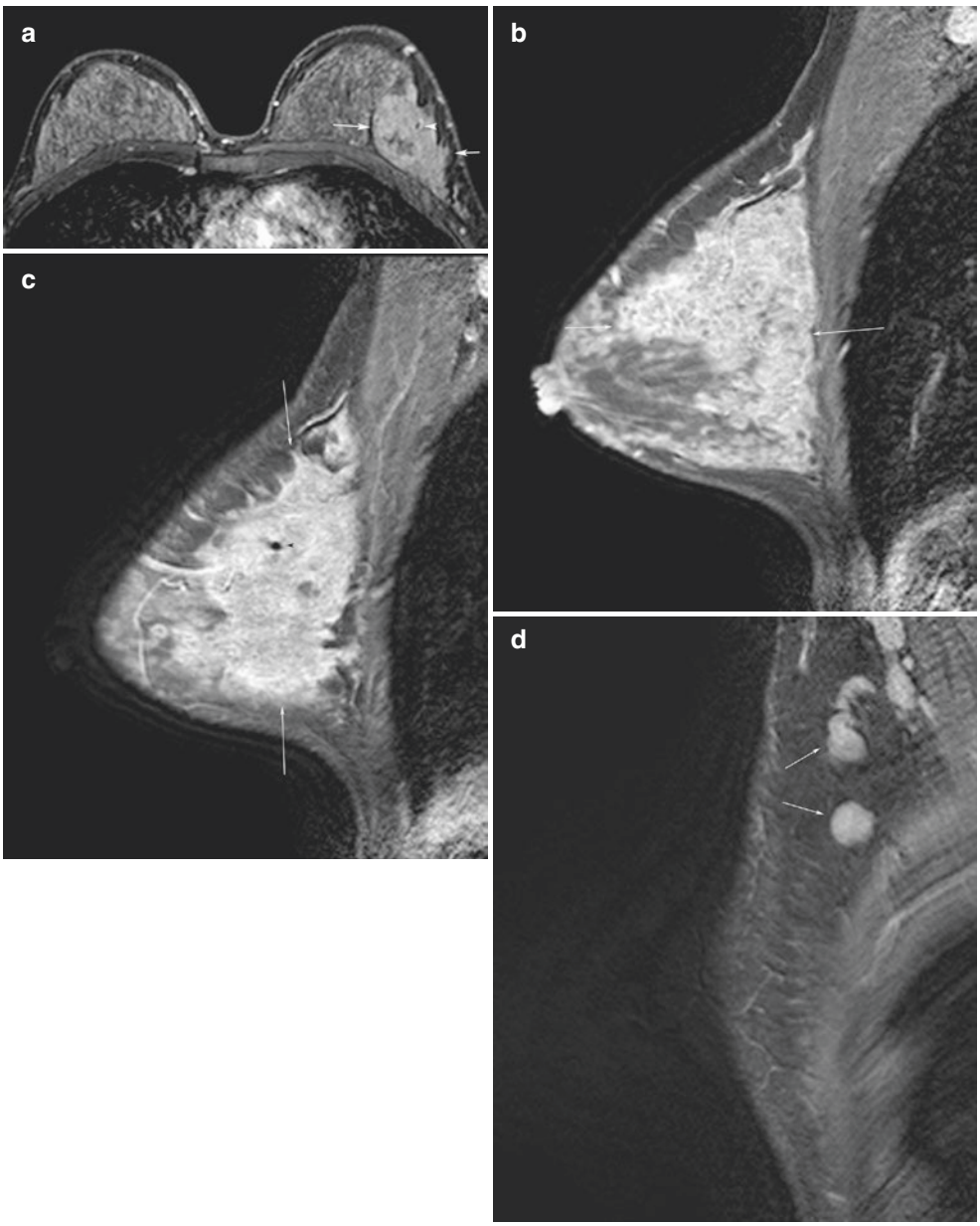

Fig. 3.95 (**a**) Axial T1-weighted fat-saturated post-contrast image shows a large irregular mass (*arrows*) in the outer mid to posterior left breast spanning 4.2 cm in transverse dimension. Localizing clip artifact (*arrowhead*) is noted in the outer aspect of the mass. (**b**, **c**) The mass (*arrows*) spans 7.2 cm in anteroposterior (AP) dimension and 9.8 cm in CC dimension on the sagittal T1-weighted fat-saturated post-contrast images. Localizing clip artifact (*arrowhead*) is noted in the upper aspect of the mass. No adjacent pectoralis muscle enhancement is present to suggest involvement. (**d**) Two enlarged axillary lymph nodes (*arrows*) are present on a sagittal T1-weighted fat-saturated post-contrast image, one of which (inferior) likely corresponds to the known metastatic disease. No suspicious finding was present in the contralateral breast (*not shown*). The patient underwent left mastectomy, with final pathology showing 9.3 cm of disease and three positive axillary lymph nodes

3.22 History

32-year-old postpartum woman with a right breast palpable concern (Figs. 3.96, 3.97, 3.98, 3.99, 3.100, and 3.101).

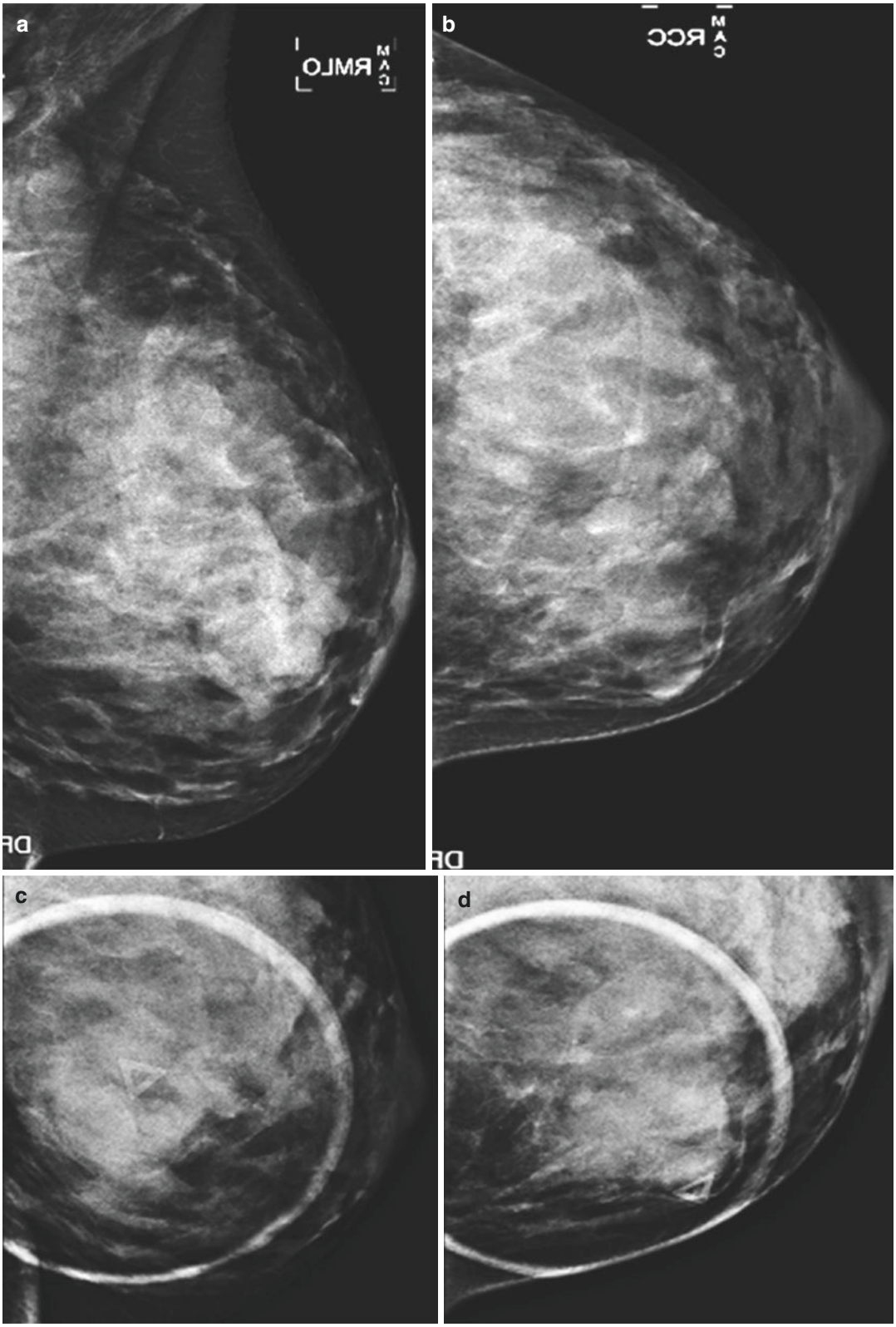

Fig. 3.96 Mammographic images of the right breast. MLO view (**a**) and CC view (**b**) with corresponding spot compression views (**c**, **d**)

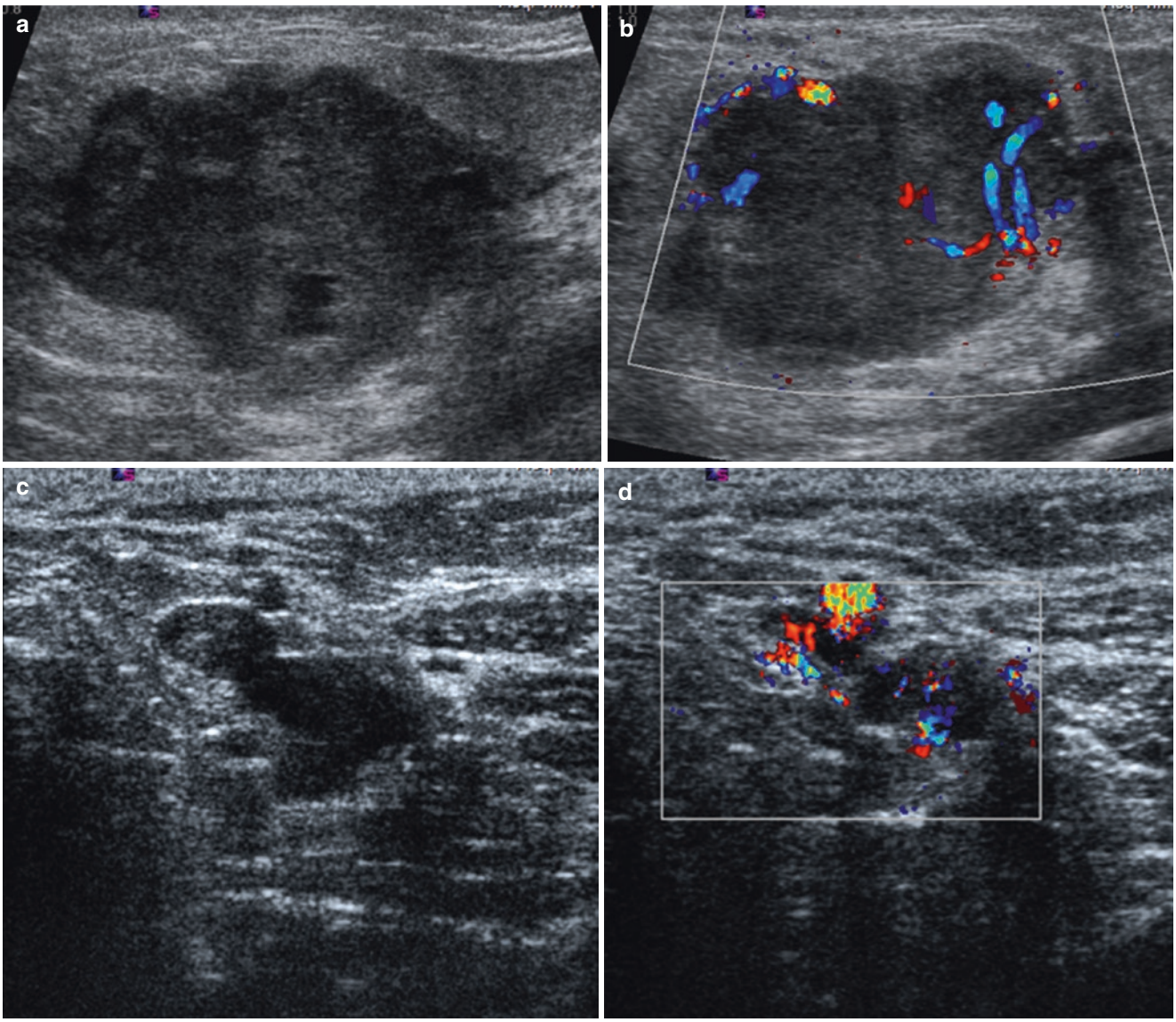

Fig. 3.97 Images from a targeted right breast ultrasound. Grayscale image (**a**) and color Doppler image (**b**) of the right breast. Grayscale image (**c**) and color Doppler image (**d**) of the right axilla

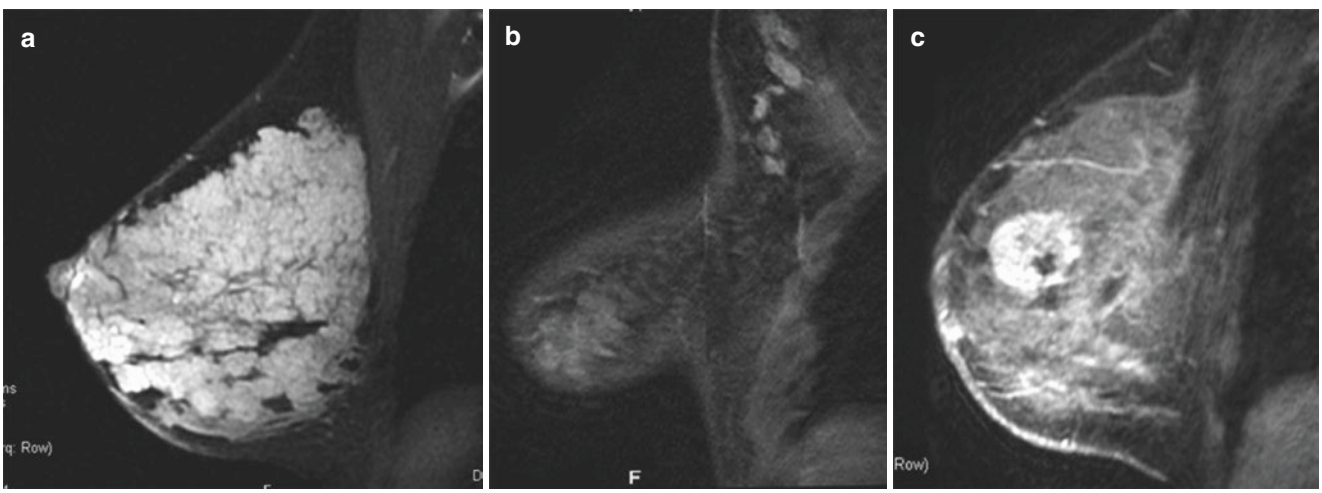

Fig. 3.98 Sagittal MR images of the right breast. T2-weighted fat-saturated image (**a**) and selected T1-weighted fat-saturated post-contrast images (**b**, **c**)

3.22 Pregnancy-Associated Breast Cancer

Teaching Points Pregnancy-associated breast carcinoma (PABC) is a rare occurrence, with an estimated frequency of 2.3 cases per 100,000 deliveries; it represents up to 3 % of all breast malignancies. A breast cancer diagnosis during pregnancy is challenging for the patient and clinician because it involves both the mother and the fetus. The hormone-induced changes that occur in breast tissue during pregnancy and lactation is a major cause of delayed diagnosis of PABC, resulting in poorer outcome. Given its high sensitivity compared with mammography and the lack of radiation, ultrasound is usually the initial imaging test in symptomatic pregnant or lactating women. However, mammography almost always should be performed as an adjunct to ultrasound in the setting of suspicious sonographic findings, to evaluate for additional features of malignancy such as microcalcifications. The radiologic features of PABC are similar to those of non-PABC. MR imaging in pregnant women should not be used routinely, although there is no known adverse effect of MRI on the fetus.

In lactating women, the breast parenchyma shows diffuse increased signal intensity on the T2-weighted images due to water in milk. Following contrast administration, lactational parenchyma demonstrates an initial rapid enhancement and a subsequent early plateau of enhancement. Tumors can be well visualized on the T2W sequence is these patients.

Image Findings

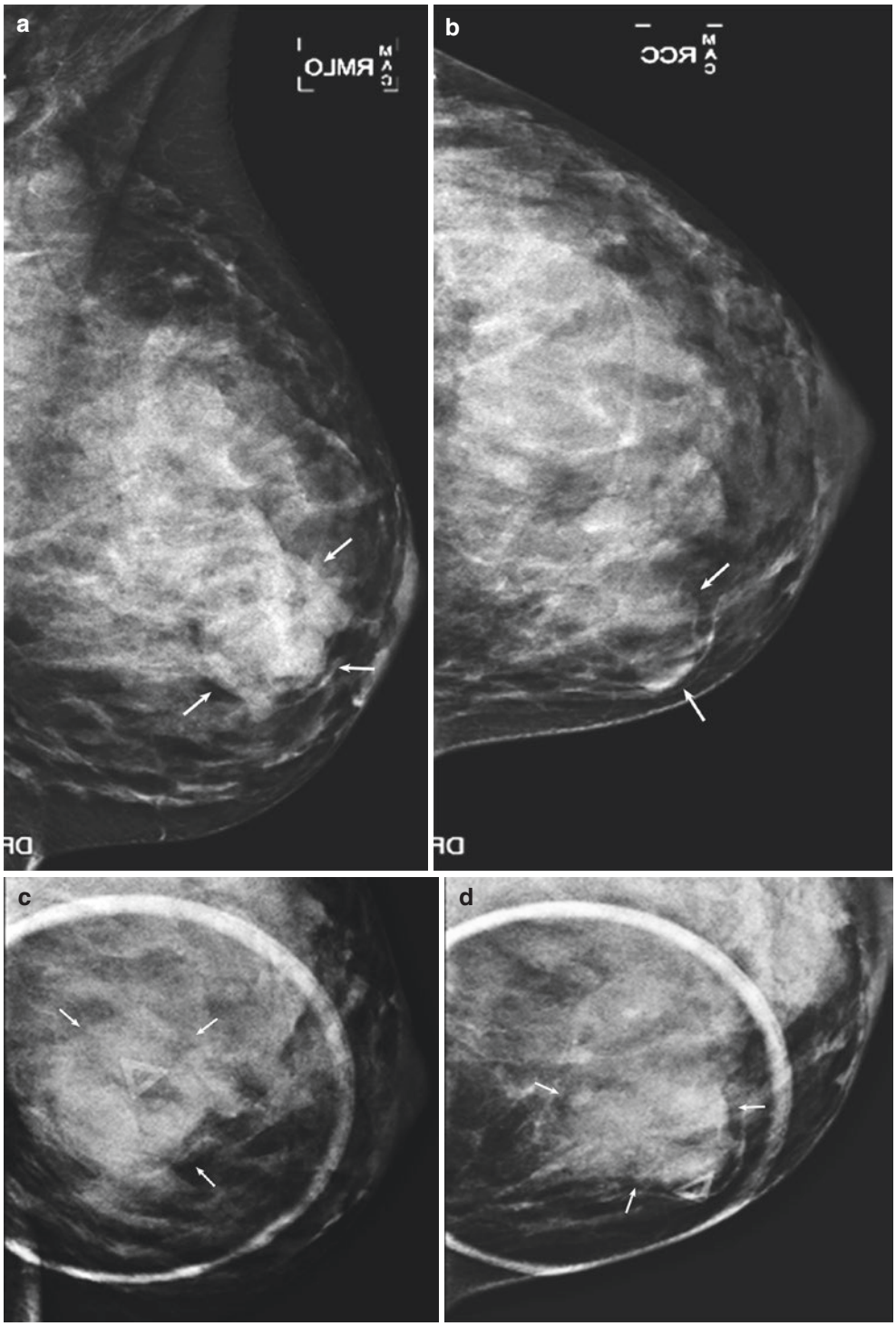

Fig. 3.99 Invasive ductal carcinoma (IDC) in a pregnant patient on mammography. MLO (**a**), CC (**b**), and spot compression (**c**, **d**) views of the right breast demonstrate an obscured mass in the medial right breast (*arrows*)

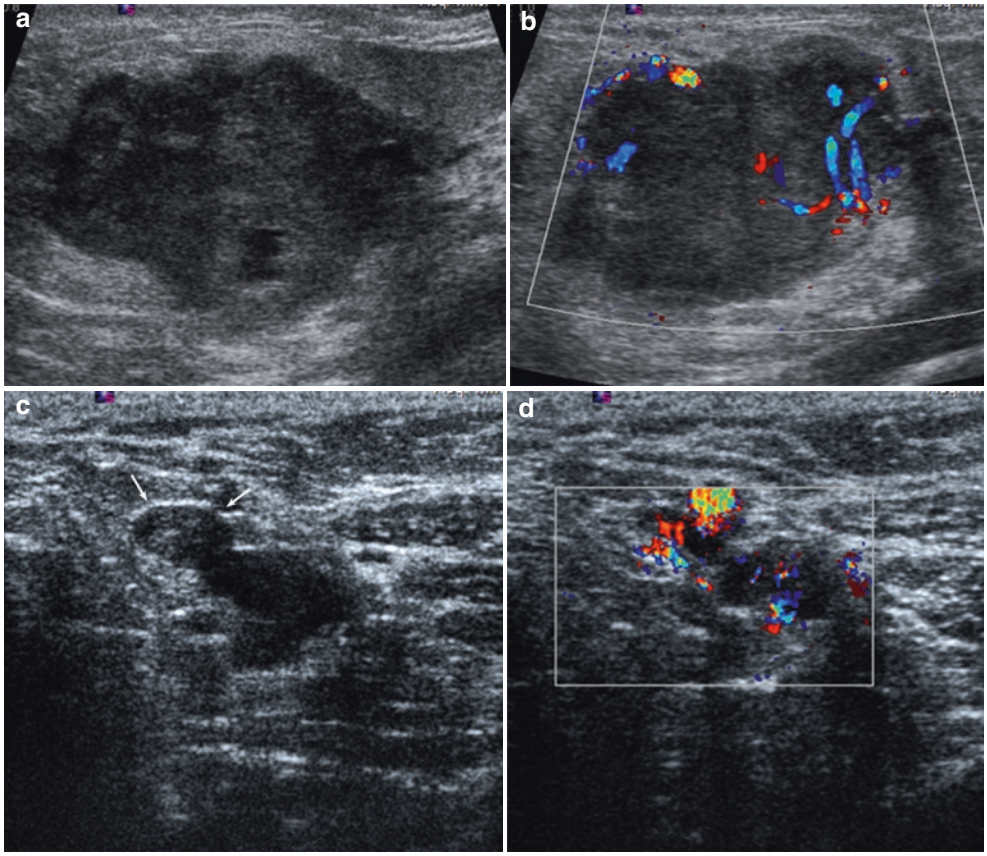

Fig. 3.100 IDC on ultrasound in a post-partum patient. Grayscale (**a**) and color Doppler (**b**) evaluation of the right breast demonstrates an irregular, hypoechoic mass with internal vascularity corresponding to the mammographic and palpable abnormality. (**c**, **d**) Prominent lymph nodes (*arrows*) with thickened cortices were identified in the axilla on grayscale and color Doppler images. Biopsy was performed on the mass and lymph node under ultrasound, yielding invasive ductal carcinoma (IDC), NOS, poorly differentiated with axillary metastasis

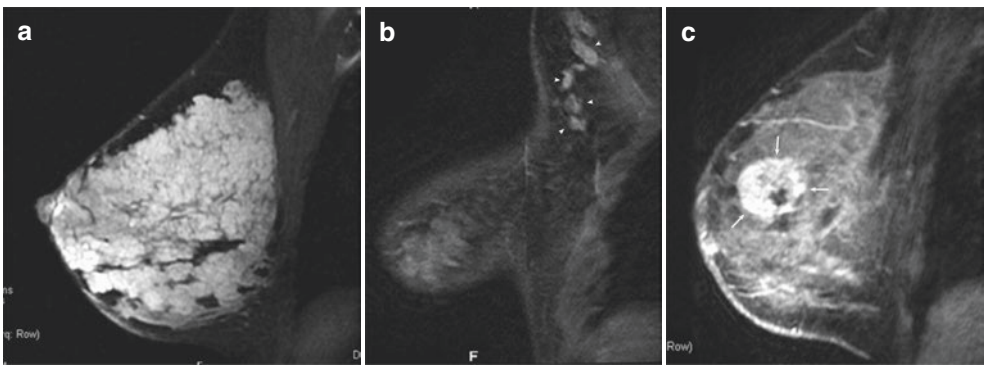

Fig. 3.101 IDC in a pregnant patient, with MRI performed for extent of disease evaluation. (**a**) Sagittal T2-weighted fat-saturated image demonstrates marked hyperintensity of the glandular tissue related to lactation. (**b**, **c**) Sagittal T1-weighted fat-saturated post-contrast images demonstrate enlarged right axillary lymph nodes (*arrowheads* on **b**) and an irregular round necrotic mass (*arrows* on **c**) corresponding to the known malignancy, with washout kinetics on CAD analysis (*not shown*)

3.23 History

66-year-old woman with newly diagnosed left axillary metastatic disease with unknown primary. Mammogram and ultrasound evaluation were negative (Figs. 3.102 and 3.103).

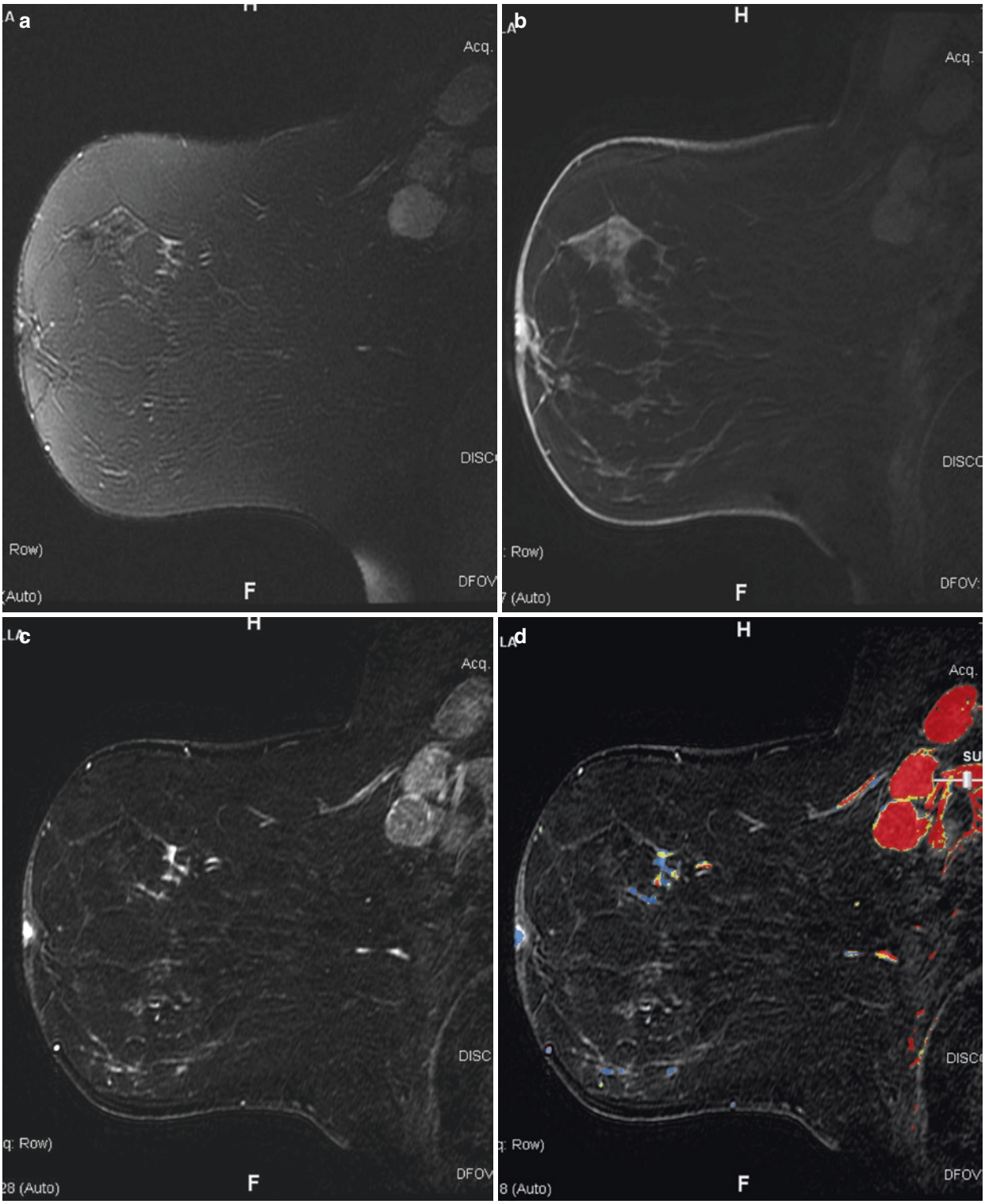

Fig. 3.102 (**a**) Sagittal T2-weighted fat-saturated image of the left breast. (**b**) Corresponding sagittal T1-weighted fat-saturated image. (**c**) Corresponding sagittal post-contrast subtraction image with CAD kinetics analysis color overlay (**d**)

3.23 Axillary Nodal Metastasis from Carcinoma of Unknown Primary 1

Teaching Points Breast MRI is the most sensitive imaging modality for the detection of otherwise occult breast cancer in patients with malignant axillary adenopathy. Breast MRI can detect an otherwise mammographically and sonographically occult breast cancer in over 60 % of patients; this detection is therefore an accepted clinical indication for breast MRI. Routine application of breast MRI in occult breast cancer can impact clinical management, including the possibility of breast-conserving surgery.

Image Findings

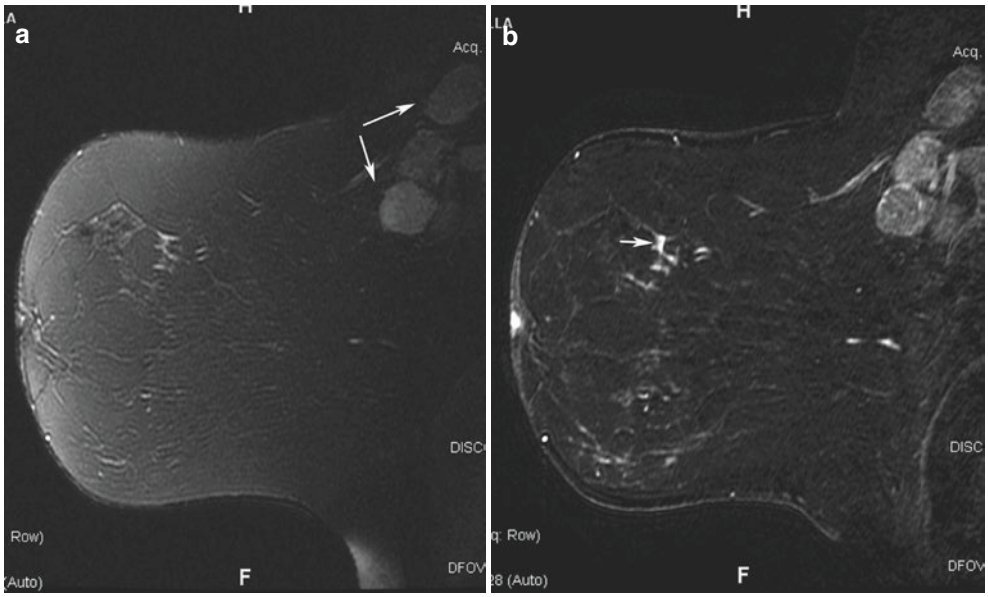

Fig. 3.103 Metastatic axillary lymph nodes with occult primary malignancy. (**a**) Sagittal T2-weighted fat-suppressed image of the left breast shows several T2-hyperintense enlarged axillary lymph nodes (*arrows*) corresponding to the known malignancy. (**b**) Sagittal post-contrast subtraction image shows a 1.2-cm irregular enhancing mass in the mid left breast, suspicious for malignancy. Subsequent MRI-guided biopsy yielded invasive ductal carcinoma

3.24 History

55-year-old patient with axillary lymph node metastasis of unknown primary malignancy (Figs. 3.104, 3.105, 3.106, 3.107, and 3.108).

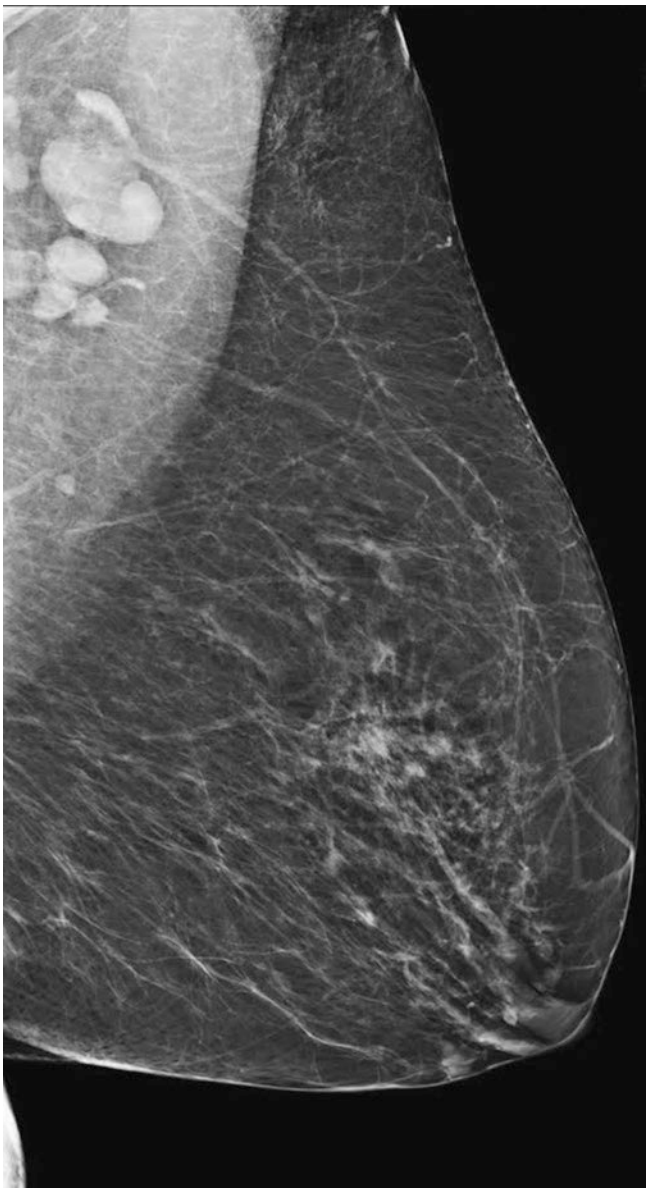

Fig. 3.104 Screening mammogram. MLO view of the right breast

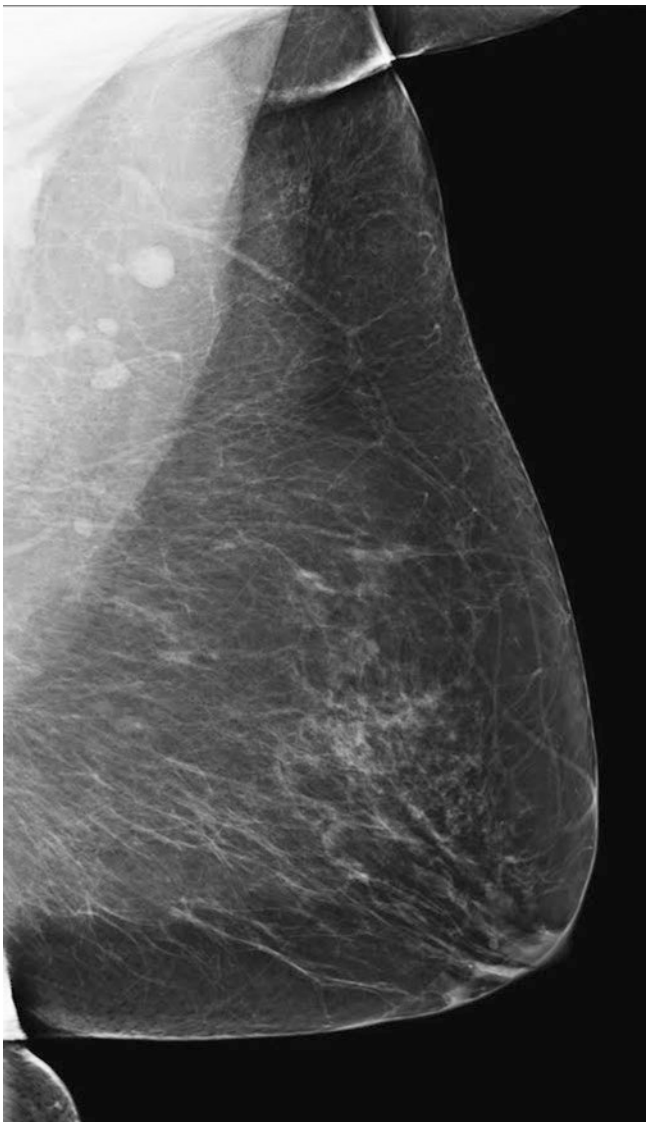

Fig. 3.105 Screening mammogram, 3 years prior. MLO view of the right breast

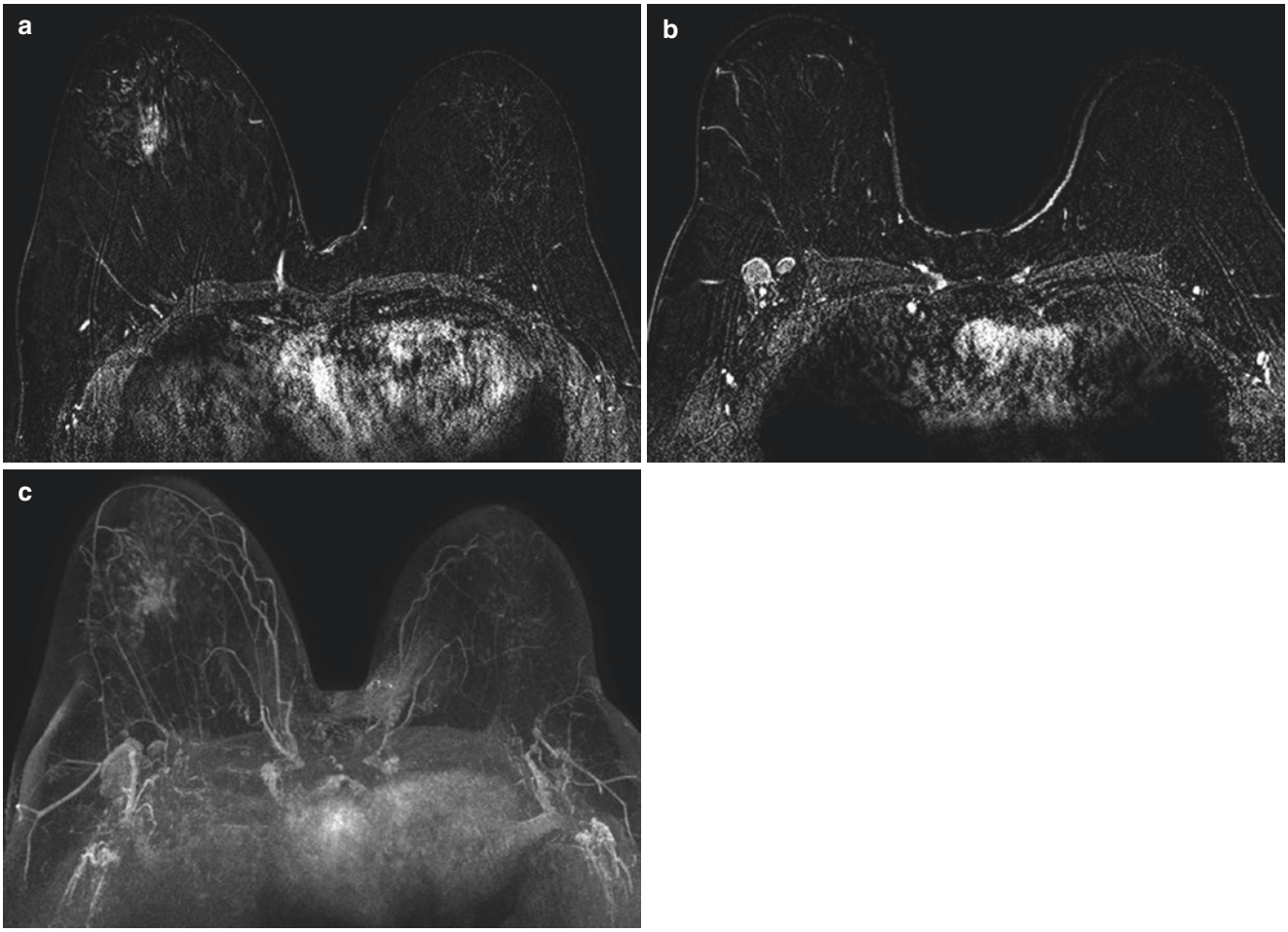

Fig. 3.106 Axial post-contrast subtraction images (**a**, **b**) and an axial post-contrast 3D MIP image (**c**) of both breasts

3.24 Axillary Nodal Metastasis from Carcinoma of Unknown Primary 2

Teaching Points Breast MRI is the most sensitive imaging modality for the detection of clinically occult breast cancer in patients with malignant axillary adenopathy. Breast MRI can detect an otherwise mammographically and sonographically occult breast cancer in over 60 % of patients. Utilization of breast MRI to evaluate for occult breast cancer can impact clinical management, including the possibility of breast-conserving surgery, and therefore is one of the generally accepted clinical indications for breast MRI.

Image Findings

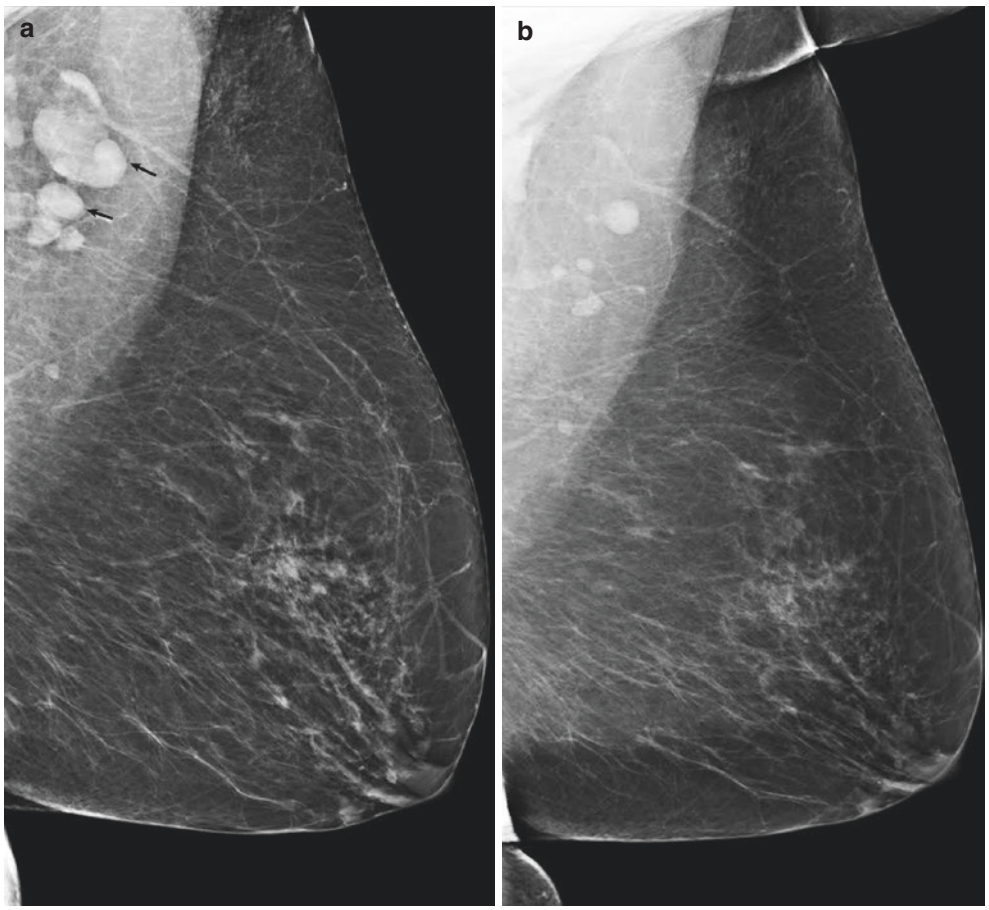

Fig. 3.107 Mammographically occult breast cancer presenting with axillary adenopathy. The MLO view of the right breast (**a**) demonstrates new enlarged axillary lymph nodes (*arrows*). Otherwise the mammogram was interpreted to be negative. The axillary lymph node underwent ultrasound evaluation, and subsequent biopsy yielded metastatic invasive ductal carcinoma (**b**)

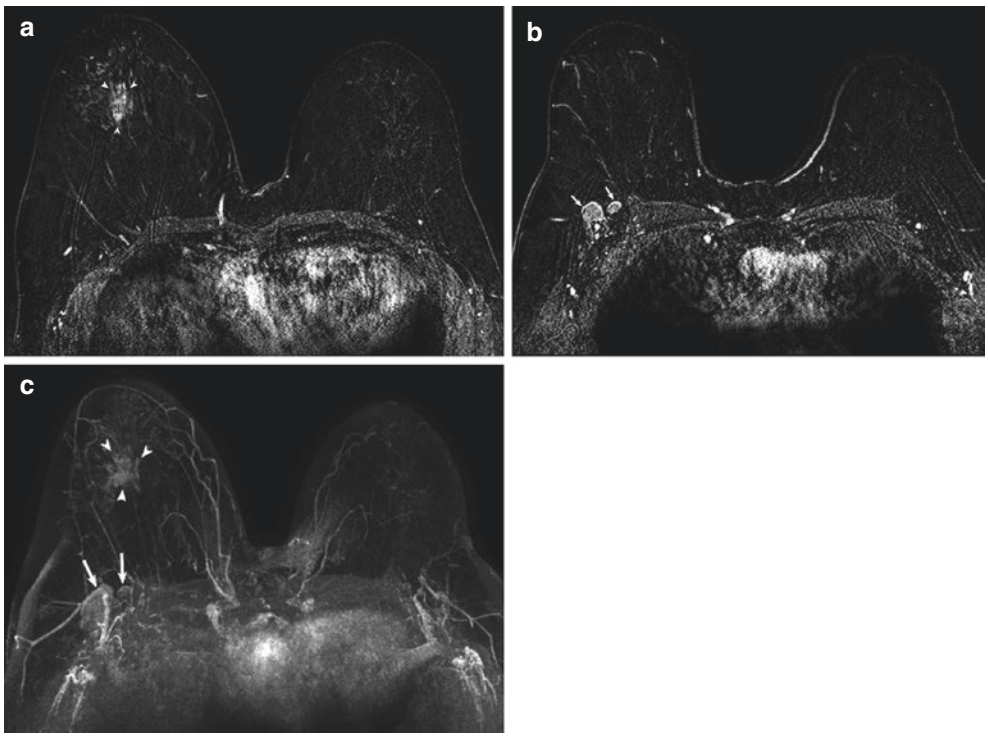

Fig. 3.108 Axial post-contrast subtraction images (**a**, **b**) and an axial post-contrast 3D MIP image (**c**) show a heterogeneously enhancing irregular mass (*arrowheads*) in the central right breast with axillary lymphadenopathy (*arrows*). The irregular mass in the central right breast underwent biopsy yielding invasive ductal carcinoma. Slightly increased density with distortion can be seen in the central right breast on retrospective review of the mammogram

3.25 History

Extent of disease evaluation (Figs. 3.109 and 3.110).

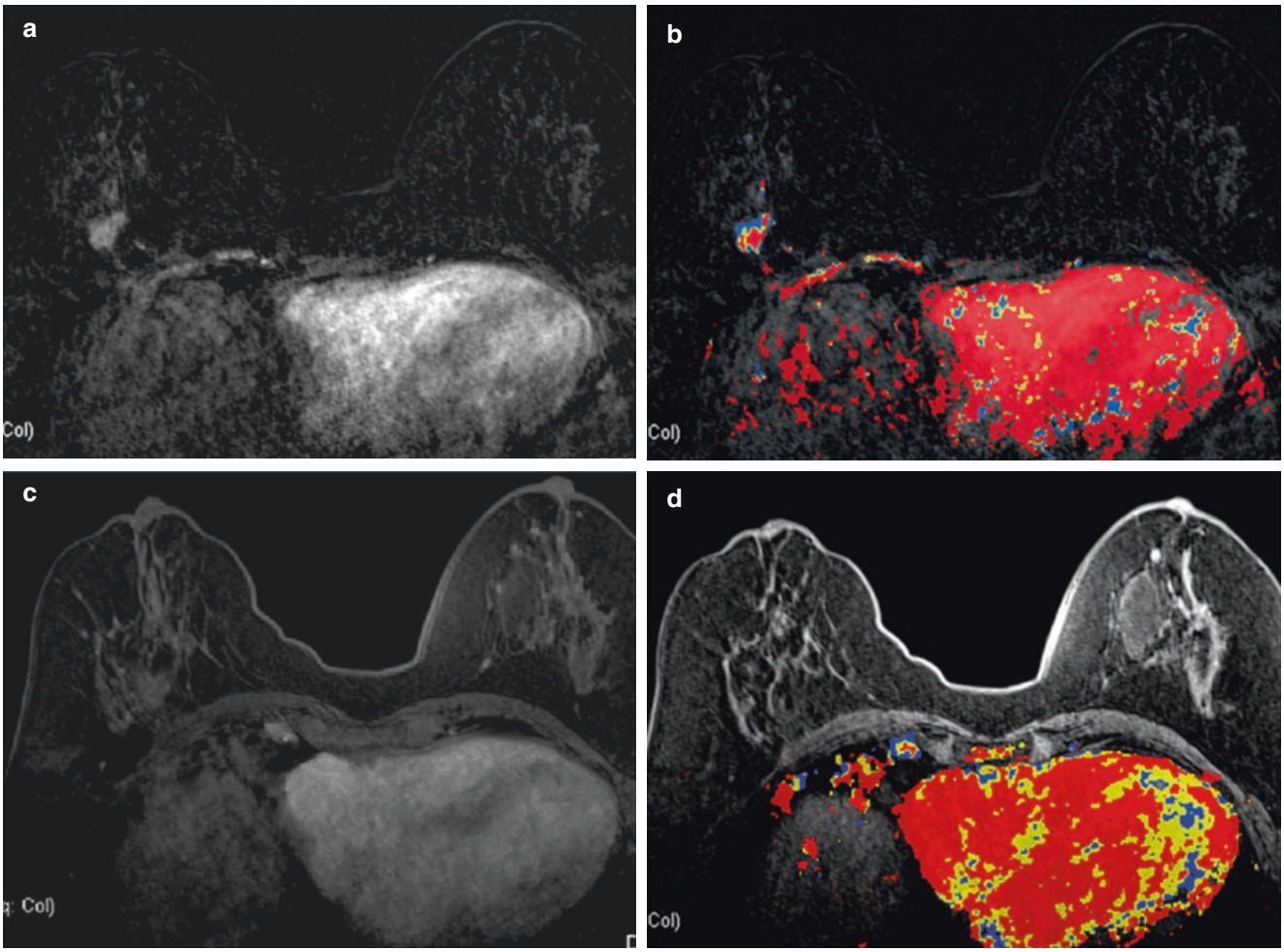

Fig. 3.109 Axial MRI images of both breasts. Post-contrast subtraction image (**a**) and corresponding image with CAD color overlay (**b**). T1-weighted fat-saturated post-contrast image (**c**) and corresponding image with CAD color overlay (**d**)

3.25 N2 Status

Teaching Points Lymph node status and tumor size are the most important prognostic indicators. Appropriate evaluation of regional lymph node status (N) is important for staging, treatment planning, and prognosis.

According to the seventh edition of the American Joint Committee on Cancer (AJCC) TNM classification, metastases to fewer than four nonmatted, moveable level I or level II nodes is considered N1 disease. N2 disease, as we see in our case example, is defined as involvement of the ipsilateral internal mammary node in the absence of axillary metastases. This usually occurs in cases of deep or medial breast tumors and may occur in 1–5 % of breast cancers; it can impact radiation treatment planning.

Image Findings

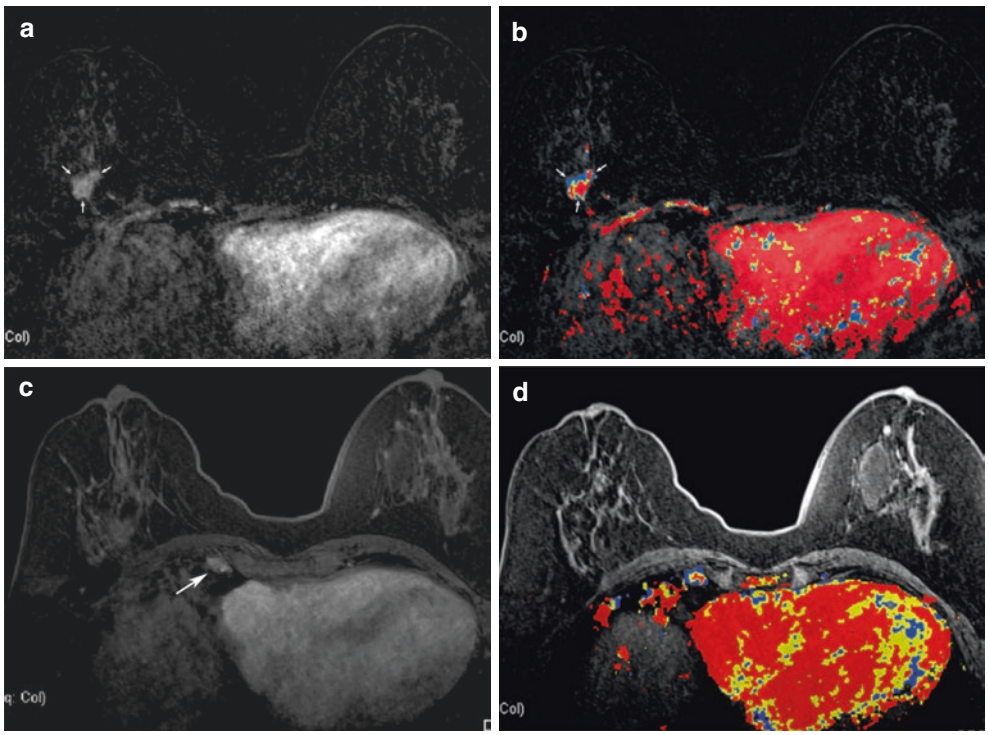

Fig. 3.110 Breast MRI was performed for extent of disease evaluation in a patient with recently diagnosed right breast cancer. A post-contrast axial subtraction image (**a**) demonstrates an enhancing, irregular spiculated mass in the posterior right breast (*arrows*) with central washout on CAD enhancement kinetics analysis (**b**). This corresponds to the known malignancy. (**c**) A more inferior T1-weighted fat-saturated post-contrast image shows a prominent right internal mammary lymph node (*arrow*) with mixed enhancement kinetics on CAD analysis (**d**). Subsequently, the right internal mammary lymph node was identified on ultrasound, and fine-needle aspiration (FNA) was performed, yielding adenocarcinoma, compatible with breast cancer metastasis

3.26 History

Extent of disease evaluation (Figs. 3.111, 3.112, 3.113, and 3.114).

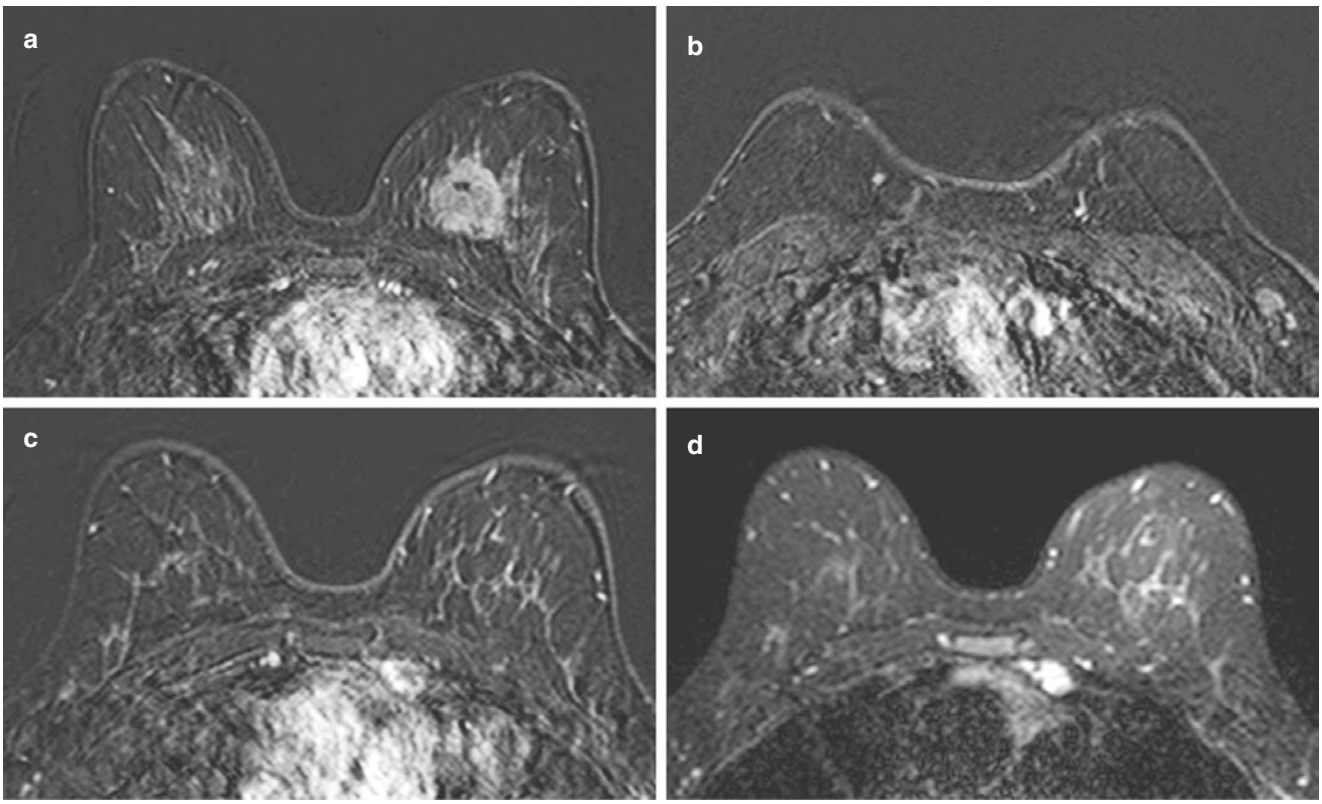

Fig. 3.111 Axial MR images of both breasts. (**a**–**c**) Multiple post-contrast subtraction images at different levels. (**d**) T2-weighted fat-saturated image

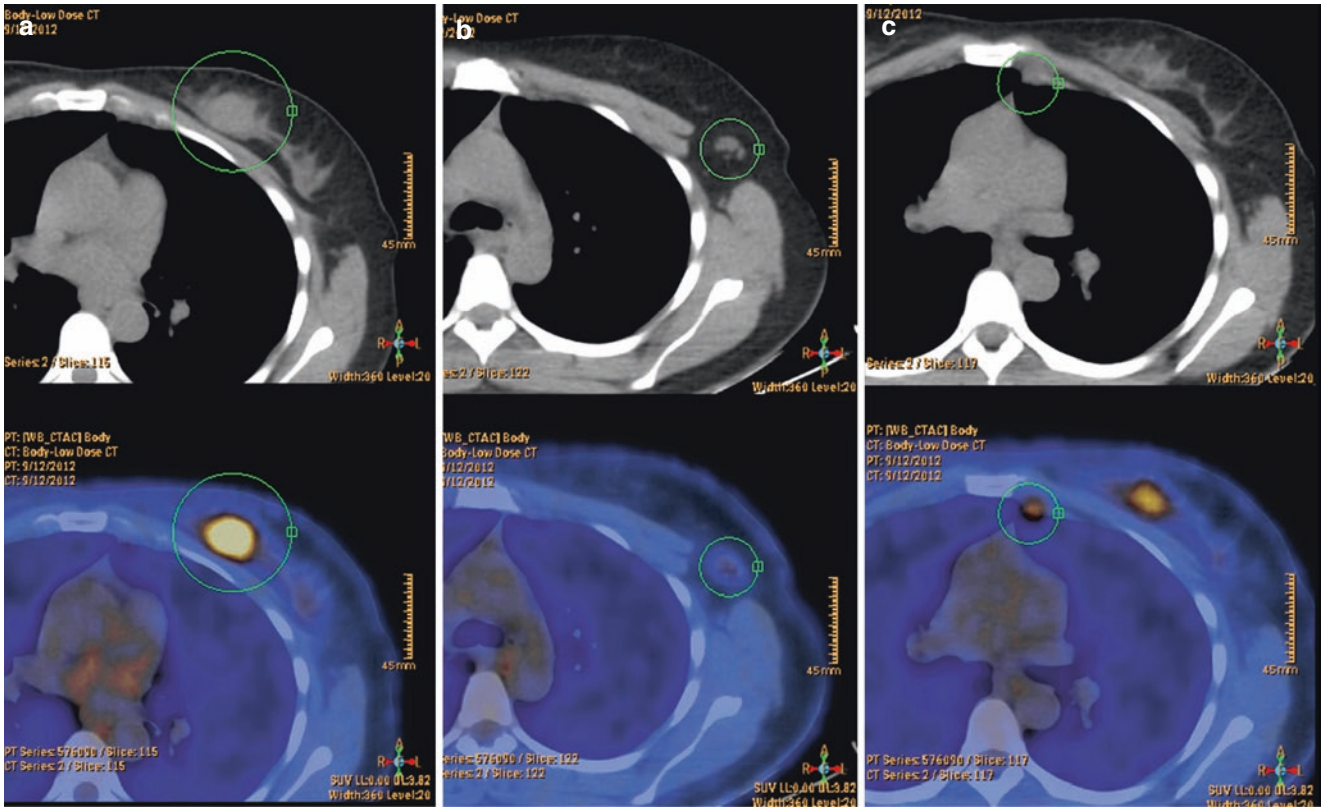

Fig. 3.112 Axial PET/CT images. (**a**–**c**) CT and fused PET/CT images at three levels

3.26 N3 Status

Teaching Points Breast MRI can identify abnormal internal mammary lymph nodes that can impact clinical staging and radiation therapy planning (i.e., a wide field of irradiation). The N3 category, which includes metastases to level III (infraclavicular) and supraclavicular nodal stations, is subdivided into subcategories N3a, N3b, and N3c. N3a includes metastases in the ipsilateral infraclavicular nodes with or without level I–II axillary involvement; N3b, ipsilateral internal mammary lymph node metastases with level I–II axillary nodal involvement; and N3c, ipsilateral supraclavicular lymph node involvement with or without level I–II axillary involvement.

In this case, the patient had a presumed metastatic internal mammary lymph node in addition to level I and II axillary lymph node involvement consistent with category N3b.

Image Findings

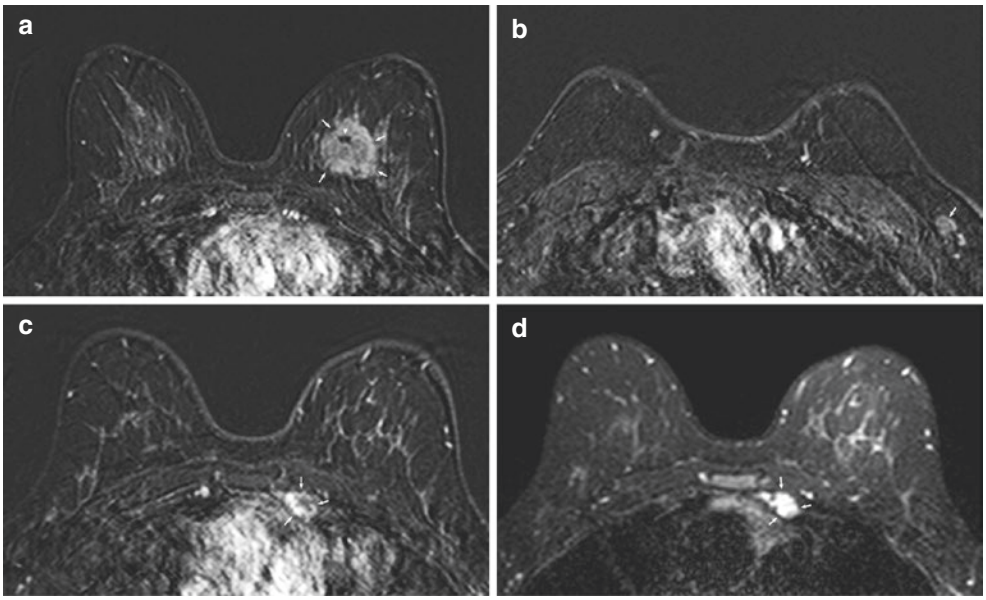

Fig. 3.113 Breast MRI performed for extent of disease evaluation in a patient with newly diagnosed left breast invasive ductal carcinoma. (**a**) Axial post-contrast subtraction image shows an irregular 3.5-cm heterogeneously enhancing left breast mass (*arrows*) with central clip artifact (*arrowhead*), which yielded invasive ductal carcinoma on biopsy. (**b**) A more superior axial post-contrast subtraction image shows a mildly enlarged left axillary lymph node (*arrow*), which underwent FNA yielding metastasis. (**c**) An axial post-contrast subtraction image at another level shows a 1.9-cm heterogeneously enhancing left internal mammary lymph node, with areas of hyperintensity on the T2-weighted fat-saturated image (**d**) consistent with necrosis

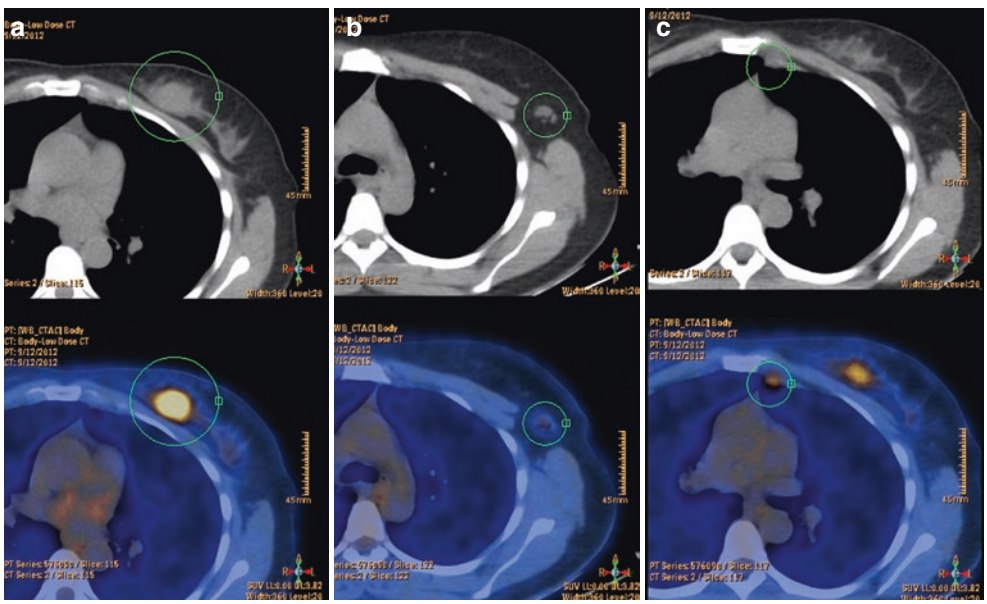

Fig. 3.114 Corresponding axial CT and fused PET/CT images show the hypermetabolic index left breast mass (**a**, *green circle*), the malignant left axillary lymph node (**b**, *green circle*) and the hypermetabolic left internal mammary lymph node (**c**, *green circle*)

3.27 History

Extent of disease evaluation (Figs. 3.115, 3.116, 3.117, 3.118, 3.119, and 3.120).

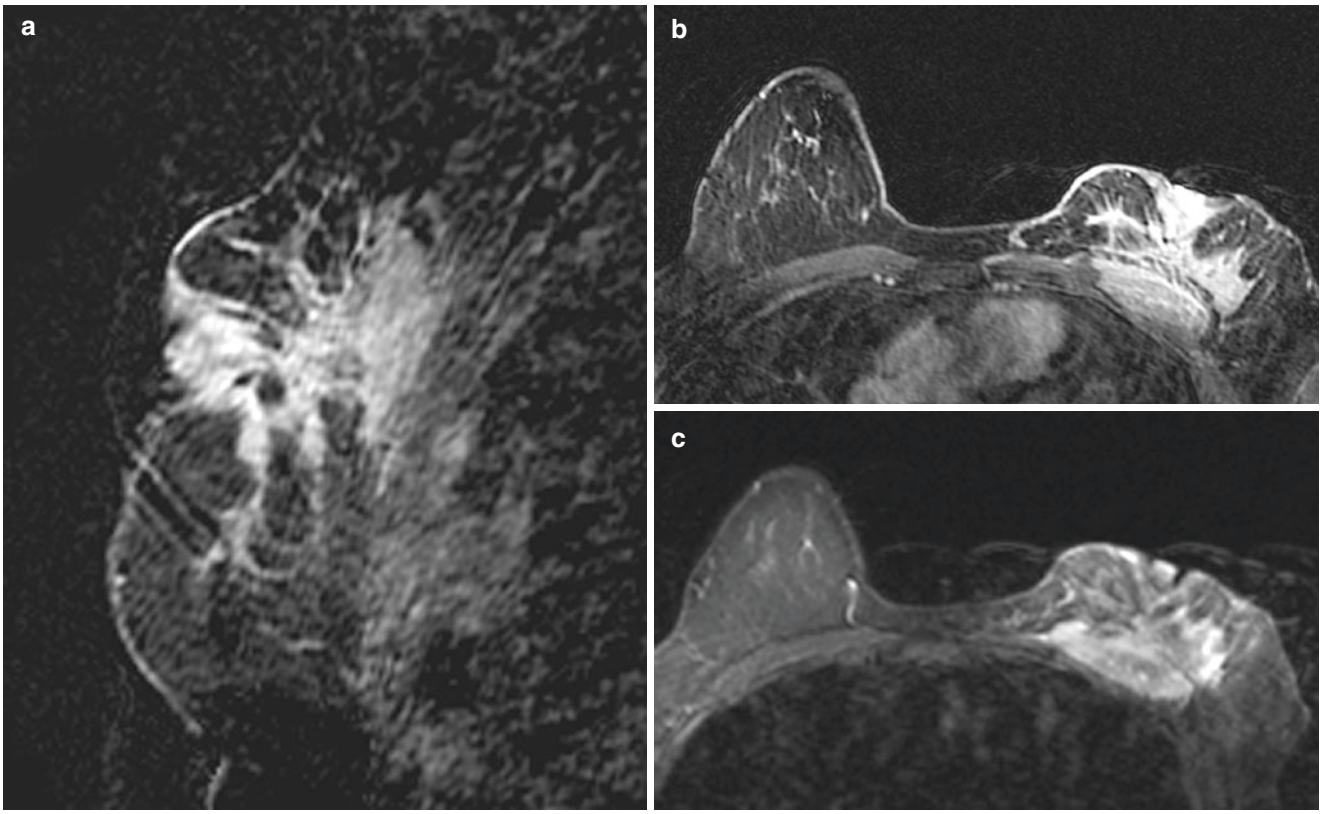

Fig. 3.115 (**a**) Sagittal post-contrast subtraction image of the left breast. (**b**) Axial T1-weighted fat-saturated post-contrast image. (**c**) Axial T2-weighted fat-saturated image

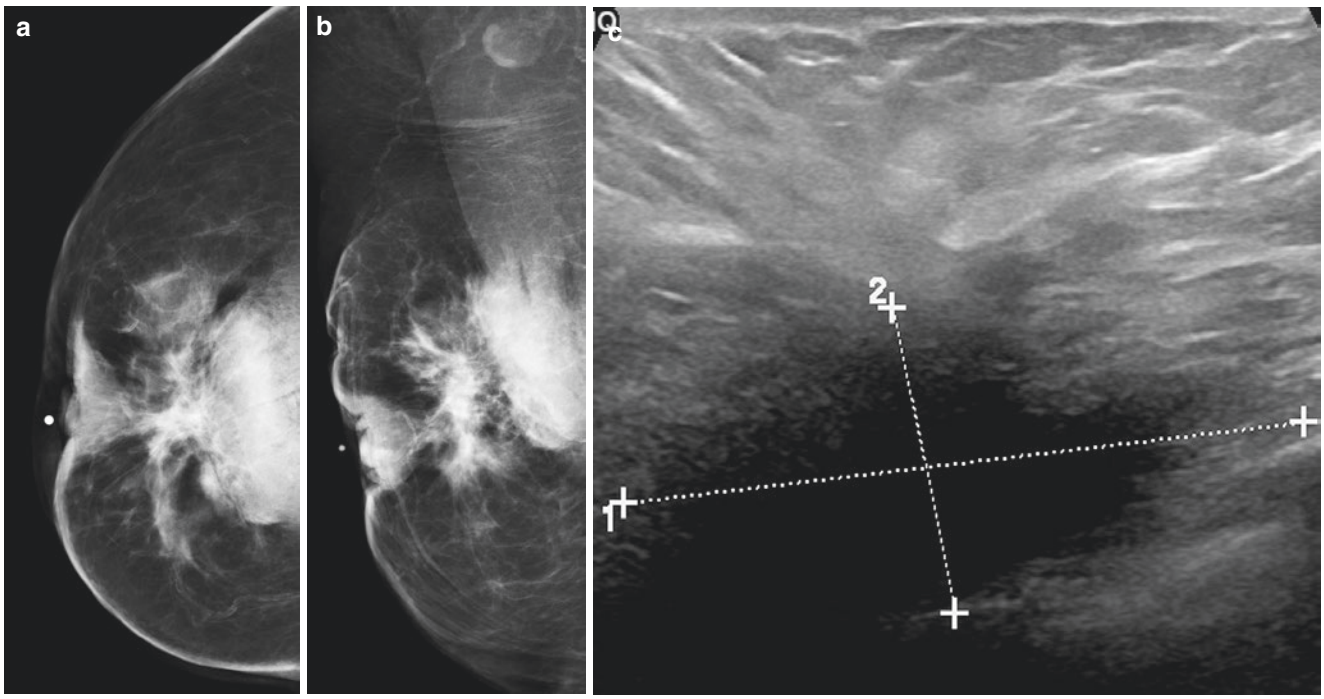

Fig. 3.116 Mammographic CC (**a**) and MLO (**b**) views of the left breast. (**c**) Targeted ultrasound image of the left breast

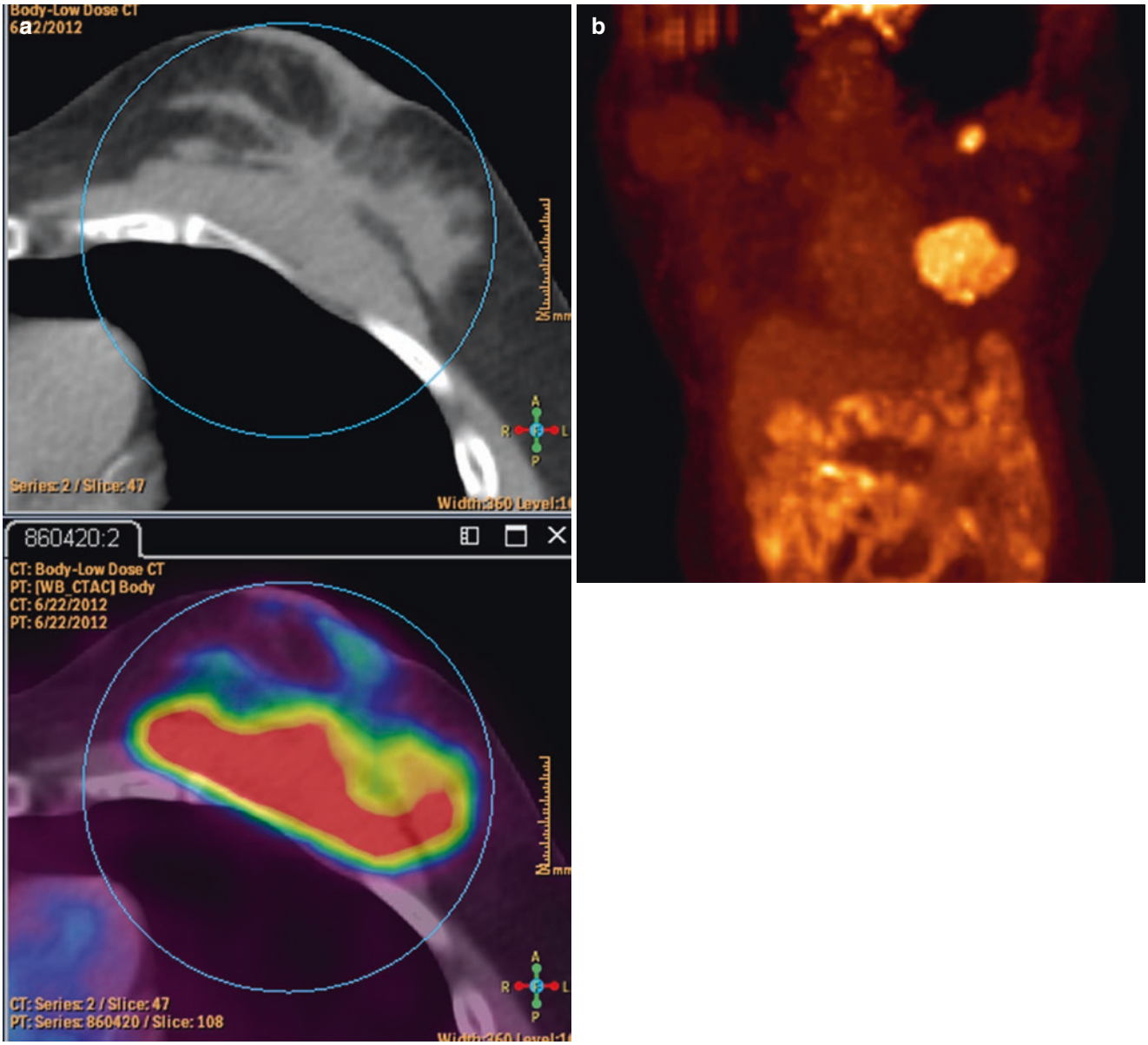

Fig. 3.117 PET/CT images. (**a**) Axial CT and fused PET/CT images of the left breast. (**b**) Coronal PET MIP of the thorax and upper abdomen

3.27 Stage 3C

Teaching Points Two patterns of pectoralis muscle involvement by breast carcinoma have been noted: (1) an infiltrative enhancement pattern with preservation of muscular architecture, and (2) a mass-like enhancement that expands the pectoralis major muscle with loss of muscle striations. As discussed earlier, invasion of the pectoralis major muscle alone does not affect staging and may require only muscle resection at the time of surgery. In this case, however, the spiculated mass extends posteriorly into the pectoralis muscles and the chest wall. Given the positive ipsilateral supraclavicular lymph node, the final stage was IIIC which is a nonoperable with N3c classification.

Image Findings

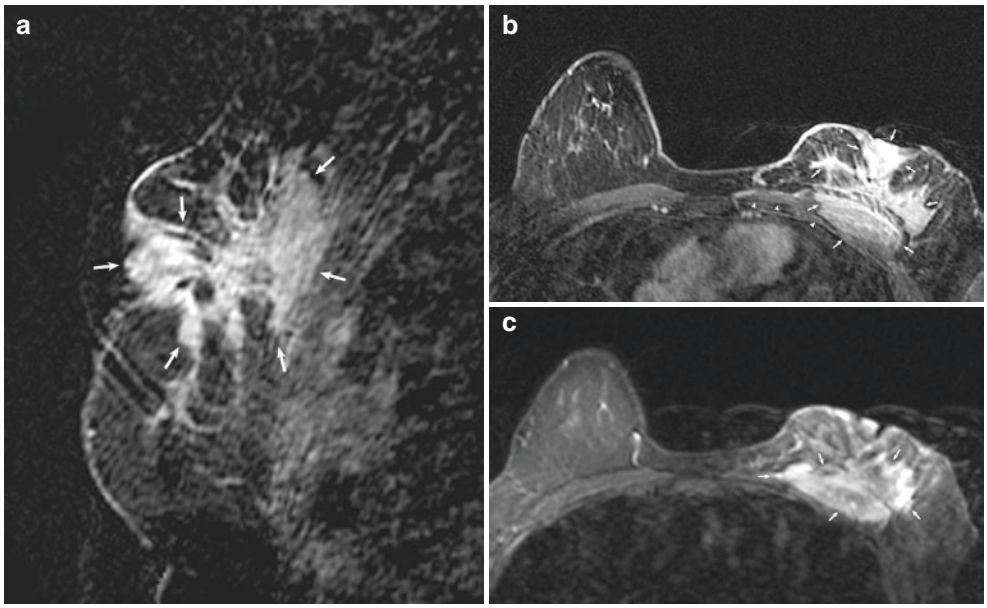

Fig. 3.118 MRI performed to evaluate extent of disease in a patient with newly diagnosed left breast invasive ductal carcinoma. Sagittal post-contrast subtraction image of the left breast (**a**), axial T1-weighted fat-saturated post-contrast image of both breasts (**b**), and axial T2-weighted fat-saturated image (**c**) of both breasts demonstrate a mildly T2-hyperintense, heterogeneously enhancing, irregular, spiculated mass (*arrows*) extending anteriorly to the skin surface with nipple retraction and posteriorly to the pectoralis muscle and chest wall (*arrowheads*). This was staged as T4c according to the TNM classification system

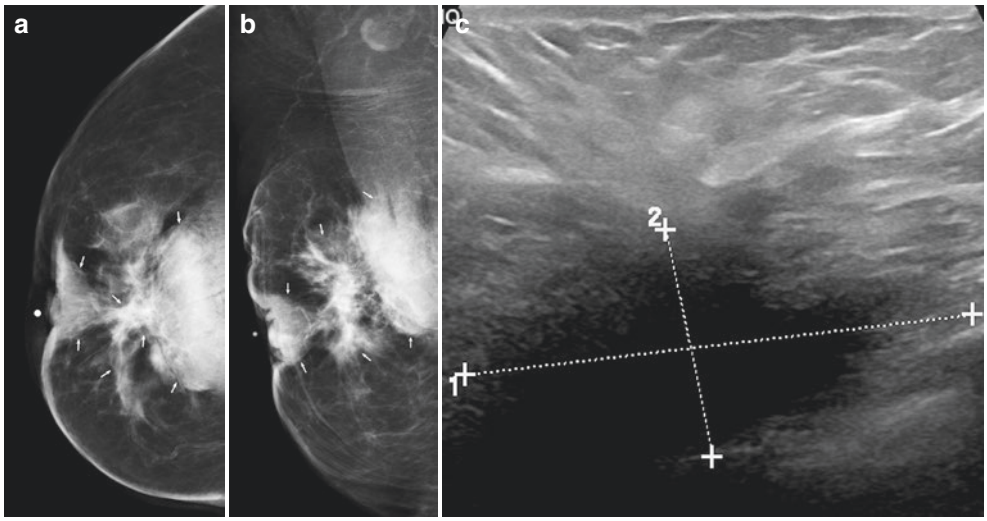

Fig. 3.119 Corresponding left mammogram and ultrasound images. CC (**a**) and MLO (**b**) views demonstrate an irregular, spiculated, dense mass (*arrows*) in the central left breast with associated architectural distortion. (**c**) Left breast ultrasound shows a shadowing irregular hypoechoic mass (calipers) corresponding to the mass shown on MRI and mammography

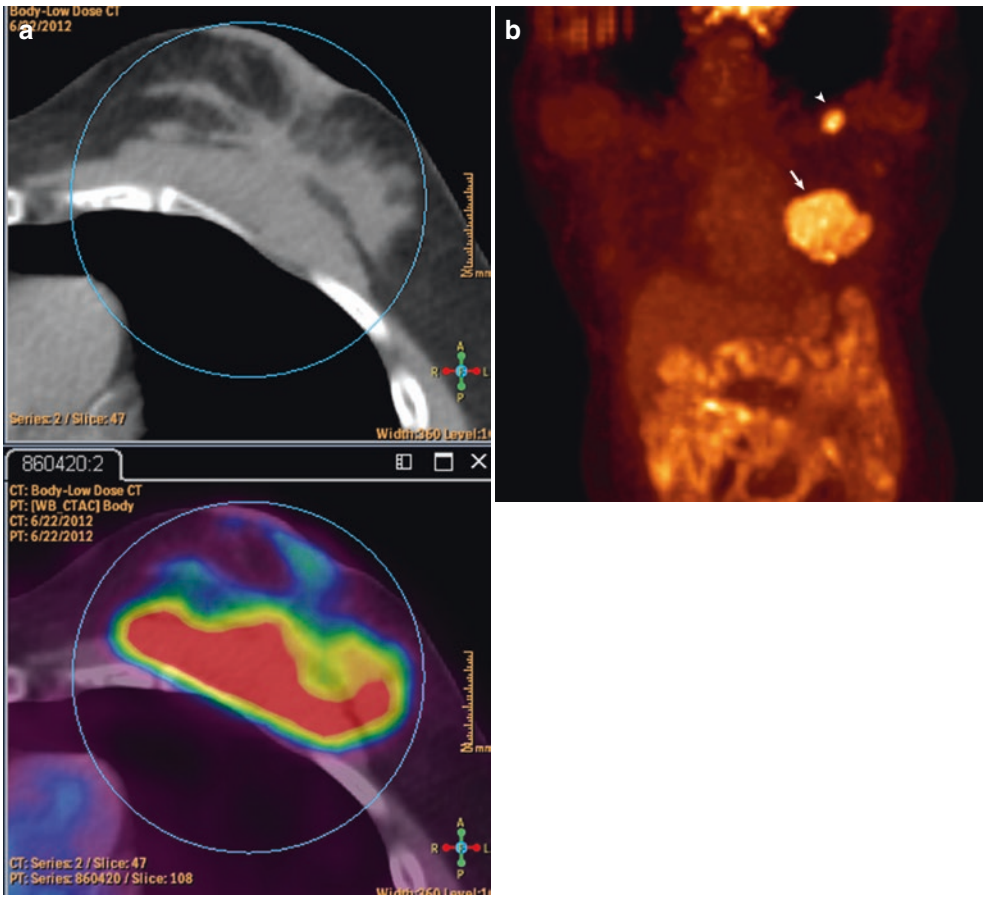

Fig. 3.120 Corresponding PET/CT images. (**a**) Axial CT and fused PET/CT images corroborate the findings with a large hypermetabolic left breast mass (*teal circle*) shown involving the underlying pectoralis major muscle. (**b**) Coronal PET MIP image shows both the hypermetabolic left breast mass (*arrow*) and a hypermetabolic ipsilateral supraclavicular lymph node (*arrowhead*). This was classified as N3c

3.28 History

42-year-old MRI extent of disease evaluation.

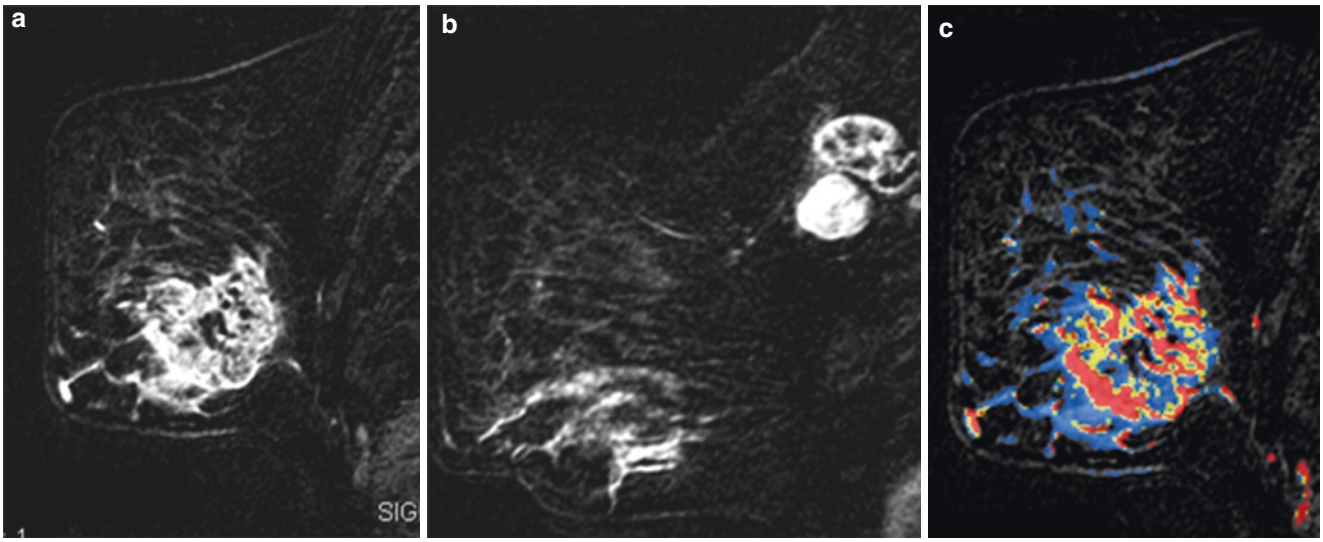

Fig. 3.121 (**a**, **b**) Sagittal MRI post-contrast subtraction images of the right breast. (**c**) CAD color overlay image corresponding to **a**

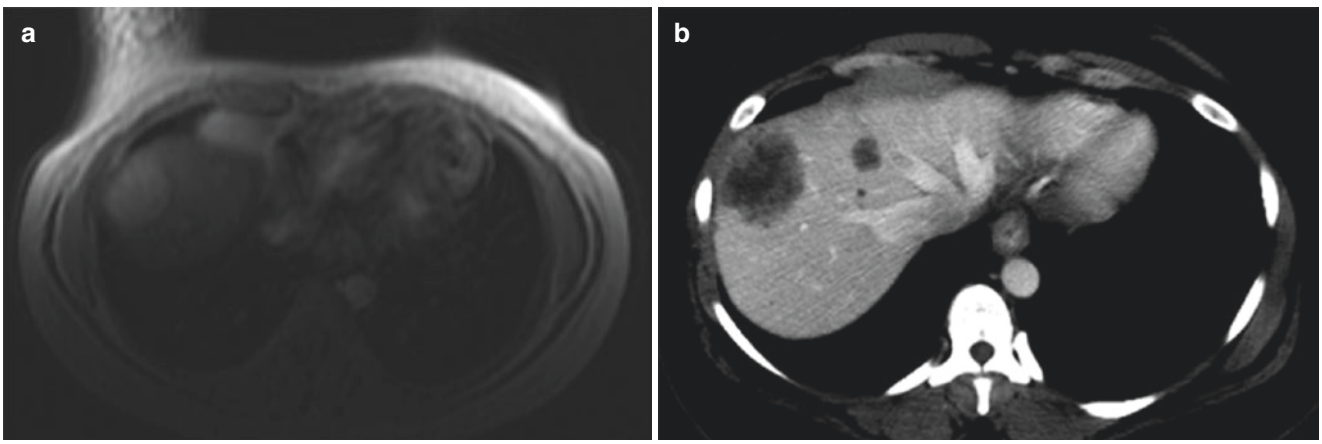

Fig. 3.122 (**a**) Axial localizer image from MRI. (**b**) Axial CT image

3.28 Stage 4, Liver Metastasis

Teaching Points Approximately 4 % of patients with breast cancer will have distant metastases at the time of presentation. Breast MRI localizer images with a large field of view can sometimes indicate possible distant metastasis, as illustrated in this case, prompting additional dedicated imaging and confirmation biopsy. The most common sites of distant metastasis for breast cancer are bone, lung, brain, and liver. Regardless of tumor size and nodal status, the presence of distant metastases at the time of diagnosis indicates stage IV disease which has a 5-year survival rate of approximately 22 % (Figs. 3.121, 3.122, 3.123, and 3.124).

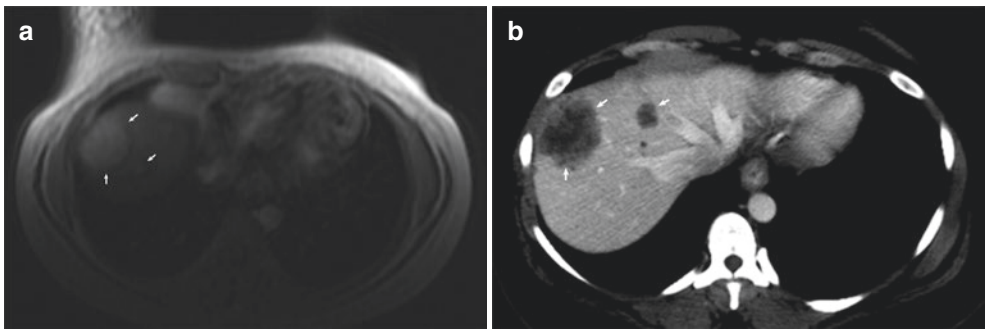

Fig. 3.124 Axial MRI localizer image (**a**) and corresponding axial CT image (**b**) demonstrate metastatic lesions within the liver (*arrows*)

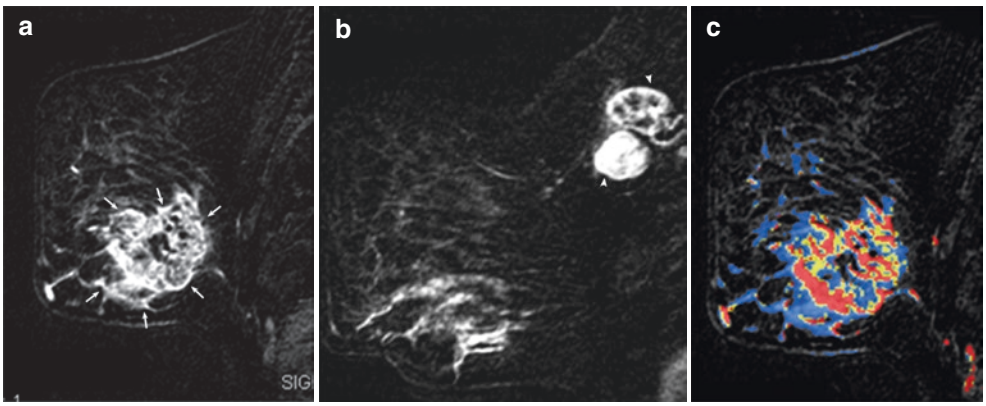

Fig. 3.123 MRI and CT performed to evaluate for extent of disease in a patient with biopsy-proven right breast invasive ductal carcinoma. (**a**, **b**) Sagittal post-contrast subtraction images demonstrate an irregular, heterogeneously enhancing mass (*arrows*) with central necrosis. Enlarged axillary lymph nodes (*arrowheads* on **B**) are noted. (**c**) CAD enhancement kinetics analysis demonstrates a predominant washout pattern within the mass

3.29 History

Extent of disease evaluation (Figs. 3.125, 3.126, 3.127, and 3.128).

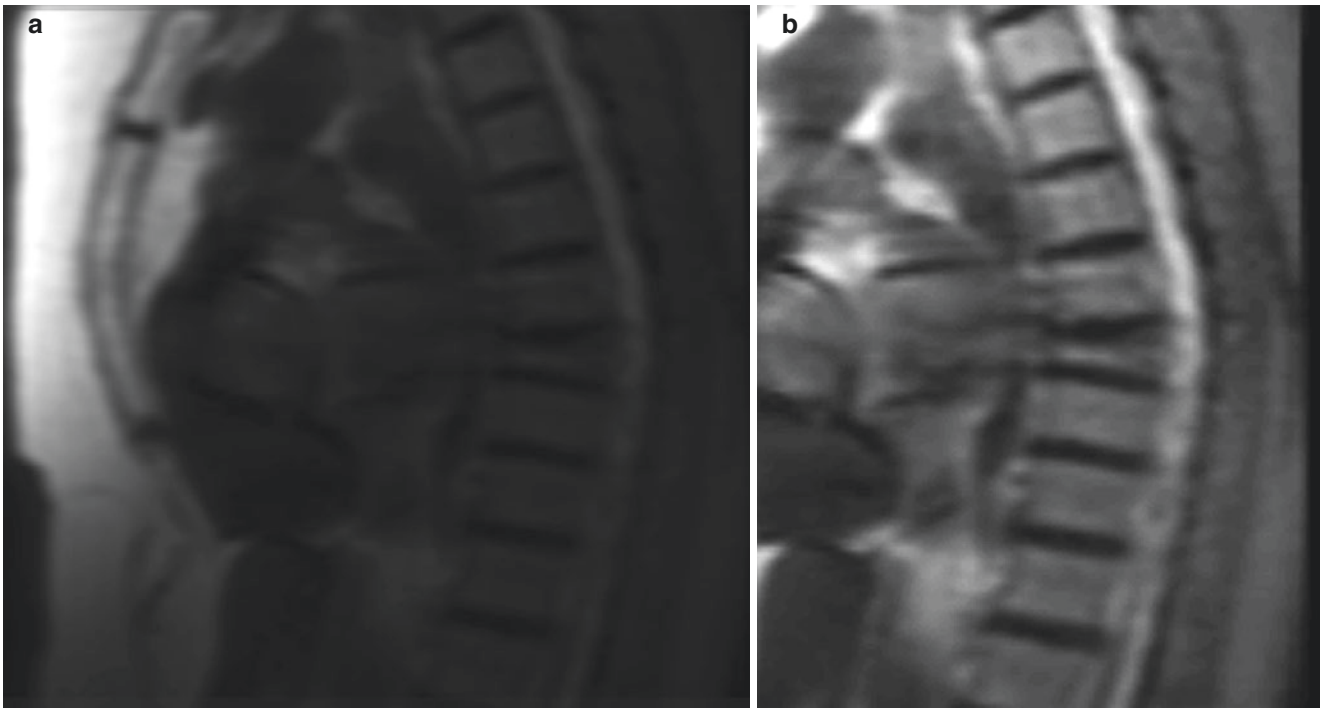

Fig. 3.125 Full-field (**a**) and magnified (**b**) sagittal localizer images from a breast MRI

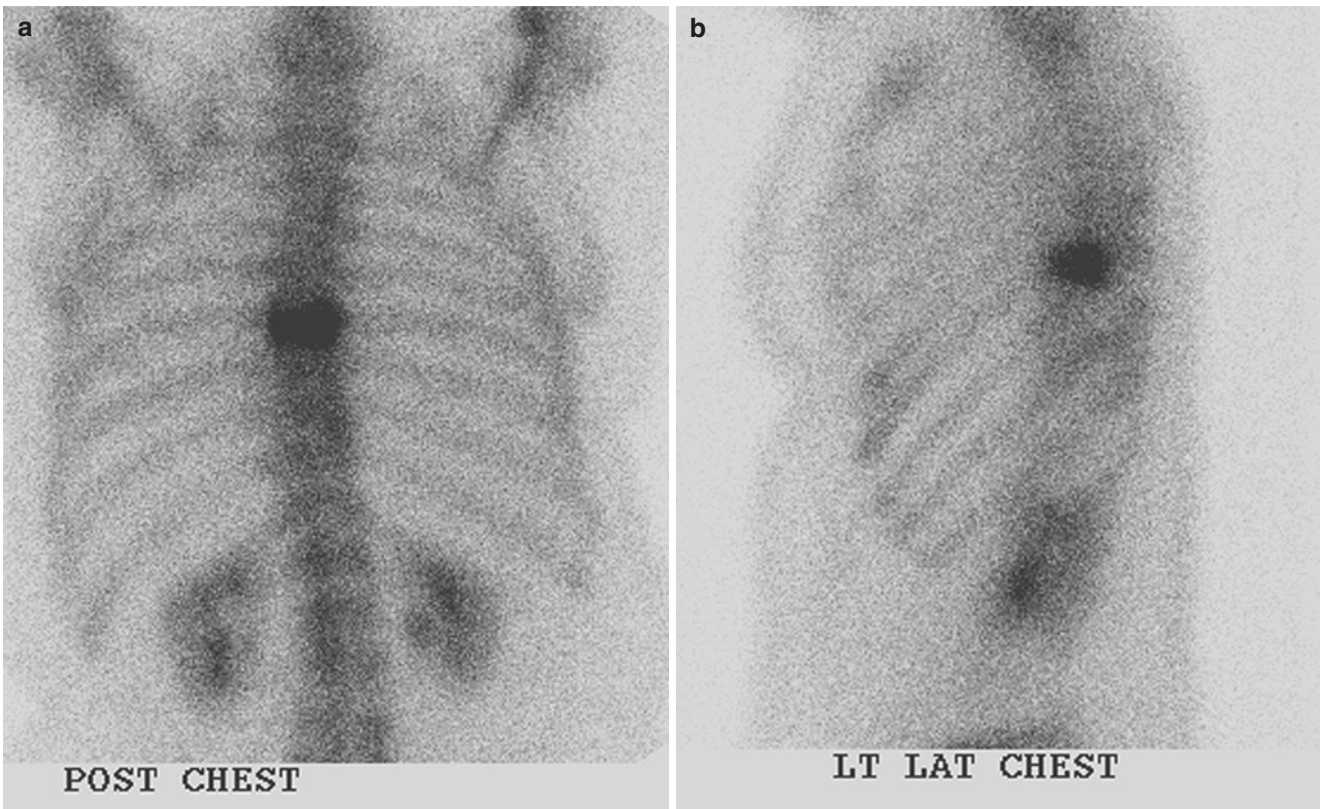

Fig. 3.126 Anterior (**a**) and lateral (**b**) Tc99m-MDP bone scan delayed images

3.29 Stage 4, Osseous Metastasis

Teaching Points MR localizing images of the breast, performed in the axial, coronal, and sagittal planes, are done to evaluate for optimal positioning and to ensure full coverage of both breasts and axillae. Portions of the lungs, mediastinum, chest wall, spine, and upper abdomen can be visualized and evaluated on these images. A large spectrum of abnormalities may be seen, from benign pleural effusion, with no effect on the clinical management, to extensive metastatic involvement of lymph nodes, bone, or organs, which has significant impact on diagnostic workup and disease management. This case is an example of a high-risk screening MRI with a T8 compression fracture on the localizing scout images, confirmed to be pathologic on subsequent biopsy.

Image Findings

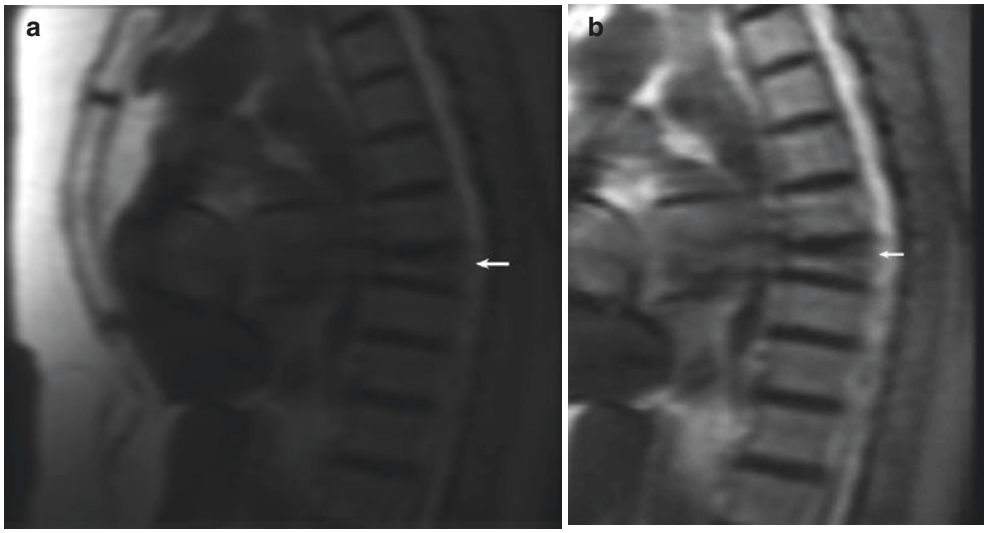

Fig. 3.127 Incidental T8 vertebral compression fracture detected on breast MRI localizer images. Full-field (**a**) and magnified (**b**) sagittal localizer images from a breast MRI demonstrate loss of height of the T8 vertebral body (*arrows*)

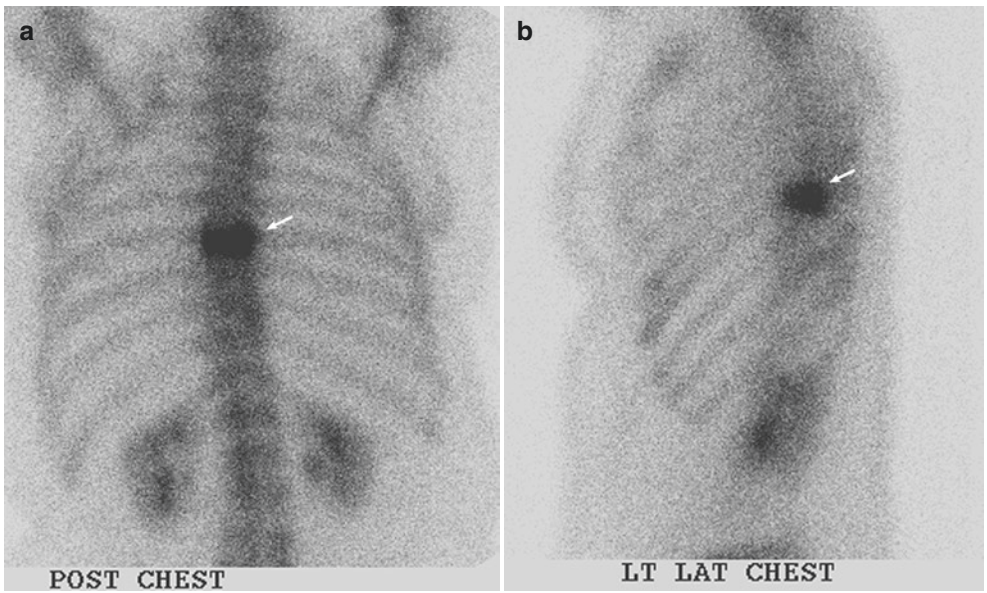

Fig. 3.128 Incidental T8 vertebral compression fracture on bone scan. Anterior (**a**) and lateral (**b**) Tc99m-MDP bone scan delayed images demonstrate increased radiotracer uptake in T8 (*arrows*) correlating with the MRI finding, compatible with acute or subacute fracture

3.30 History

32-year-old woman with biopsy-proven malignancy undergoing breast MRI to evaluate disease extent (Figs. 3.129, 3.130, 3.131, 3.132, 3.133, 3.134, 3.135, and 3.136).

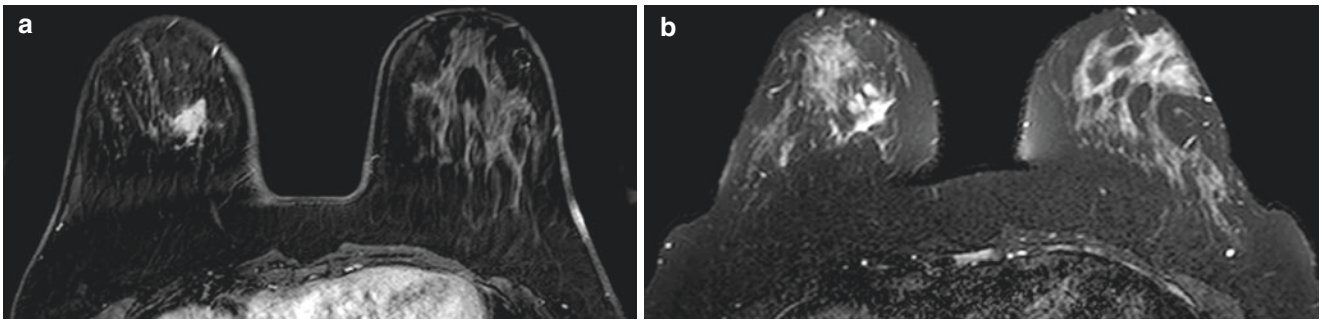

Fig. 3.129 Axial T1-weighted fat-suppressed post-contrast image of both breasts (**a**) and corresponding T2-weighted fat-suppressed image (**b**)

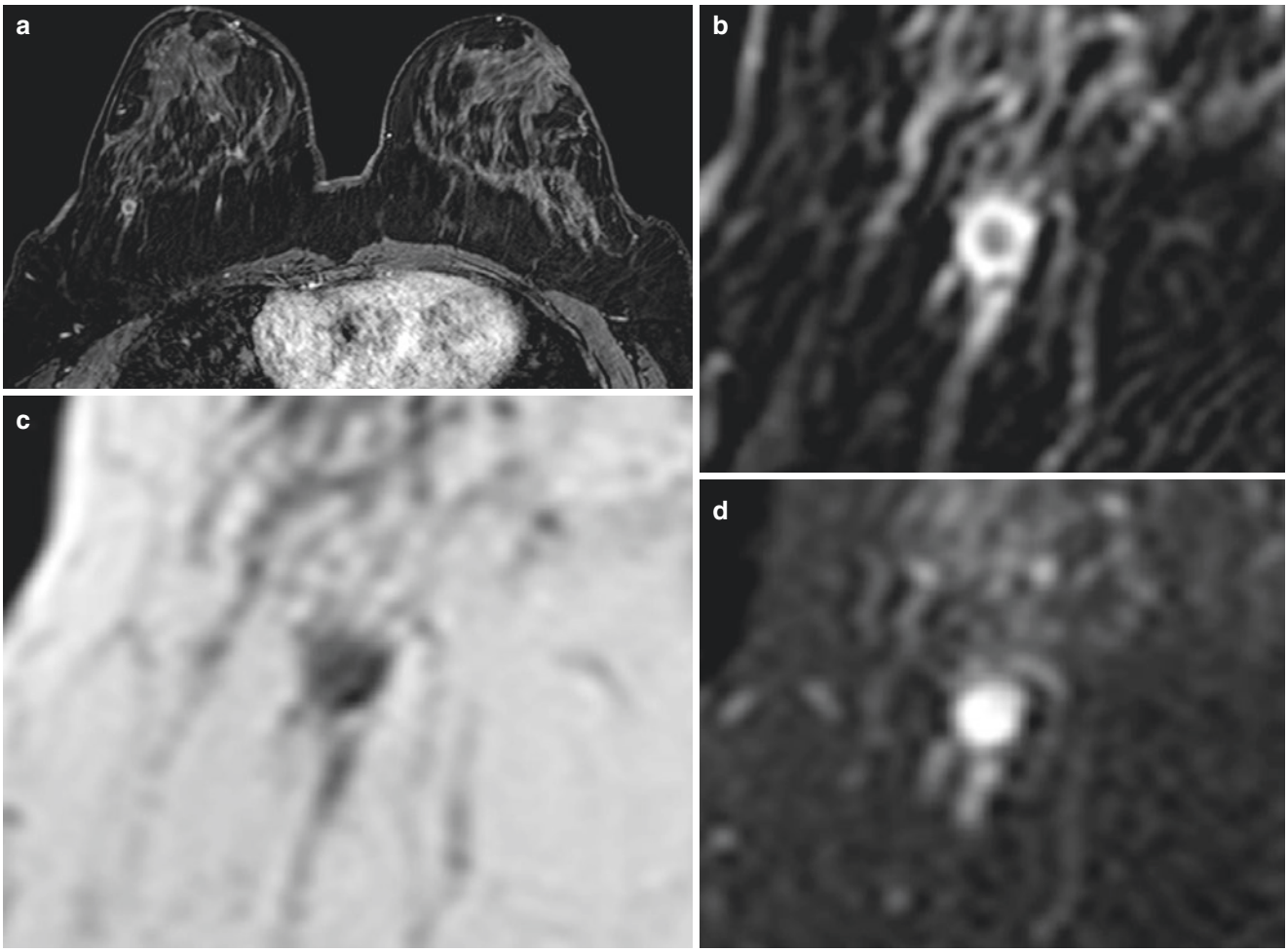

Fig. 3.130 (**a**) Axial T1-weighted fat-suppressed post-contrast image of the more inferior breasts. (**b**) Coned-down, magnified axial T1-weighted fat-suppressed post-contrast image of the finding. (**c**, **d**) Axial T1-weighted and T2-weighted fat-suppressed images of the finding

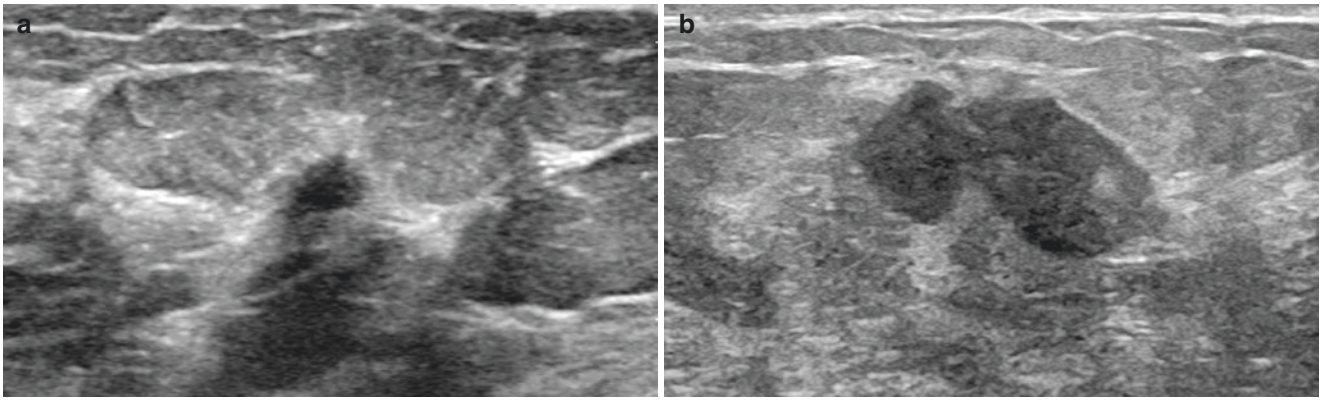

Fig. 3.131 Ultrasound. (**a**) Grayscale image of the right breast 8:00 axis. (**b**) Grayscale image of the right breast 5:00 axis

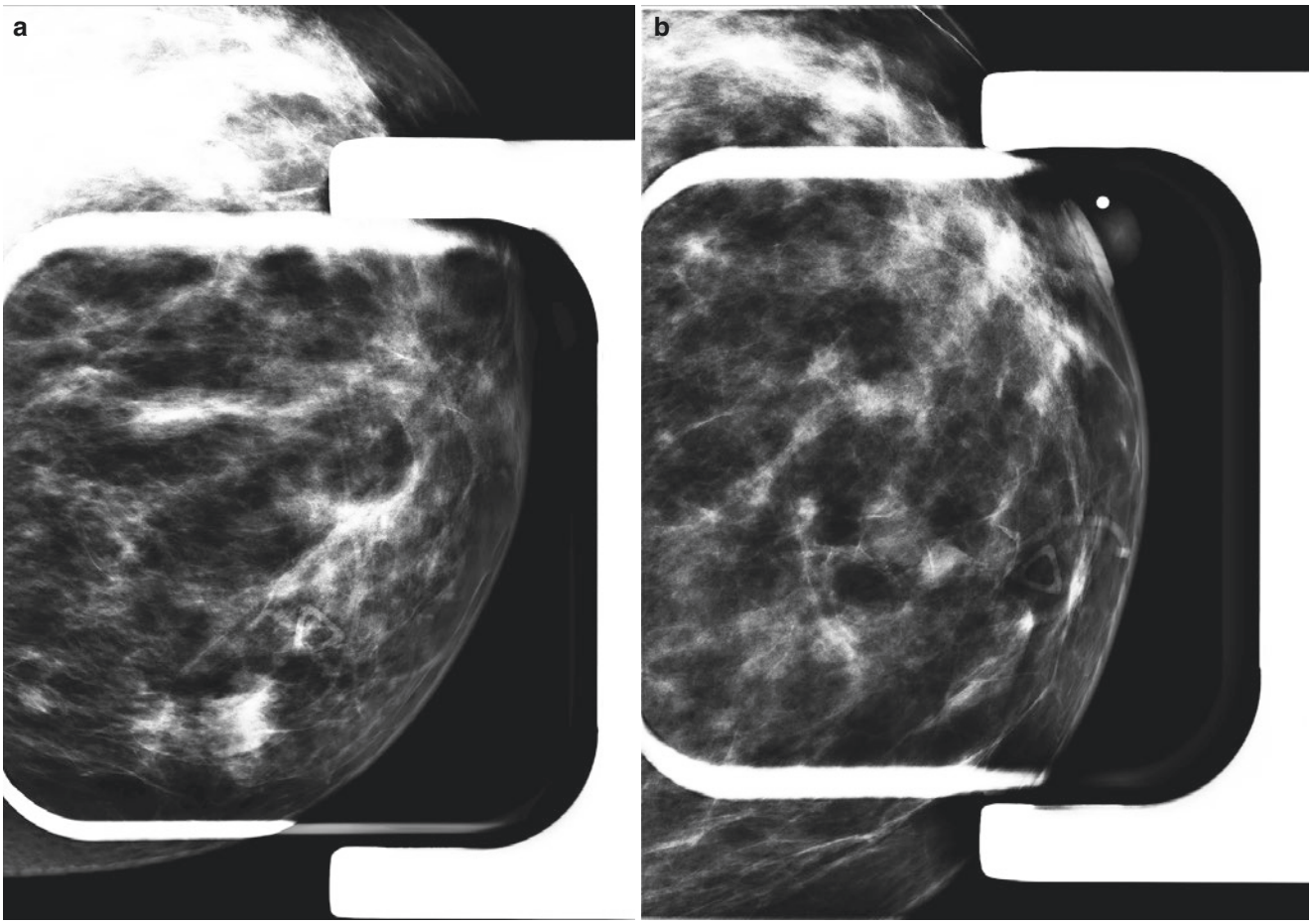

Fig. 3.132 Mammogram. CC (**a**) and MLO (**b**) spot compression views of the right breast performed in an area of palpable abnormality as part of an initial diagnostic workup

3.30 HER2 (ErbB2) Cancer

Teaching Points Multicentric disease (MCD) is defined as two or more tumor areas in different quadrants of the same breast. Studies have reported the ability of MRI to identify additional cancer sites that otherwise would have remained undetected on the basis of clinical assessment and conventional imaging, thereby changing surgical planning. Data suggest that MCD may be more common in patients with certain molecular subtypes (luminal B and human epidermal growth factor receptor 2 [HER2]). Immunohistochemical staining can be used as a substitute to categorize molecular subtypes. The illustrated case of IDC was found to be positive for HER2 and estrogen receptor (ER) but negative for progesterone receptor (PR), corresponding to luminal B tumor.

It is important for the radiologist to review the pre-contrast non–fat-saturated T1-weighted images for the presence of fat within rim-enhancing lesions to help differentiate fat necrosis from malignant lesions.

Image Findings

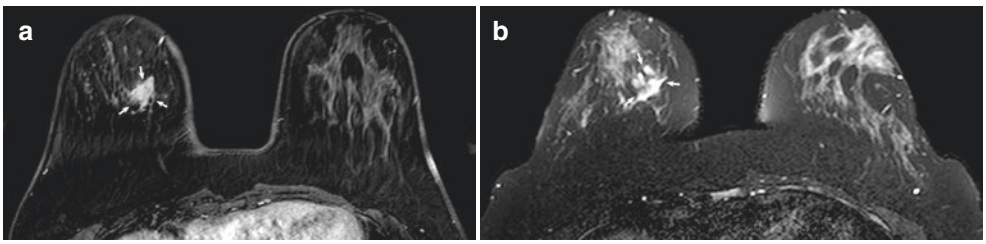

Fig. 3.133 Multicentric invasive ductal carcinoma (HER2+, ER+, PR−). (**a**) Axial T1-weighted fat-suppressed post-contrast image of both breasts demonstrates a 2.3-cm heterogeneously enhancing irregular mass (*arrows*) along the 5:00 axis of the right breast, representing known invasive ductal carcinoma. (**b**) Axial T2-weighted fat-suppressed image shows areas of T2 hyperintensity (*arrows*) within the mass, representing necrosis

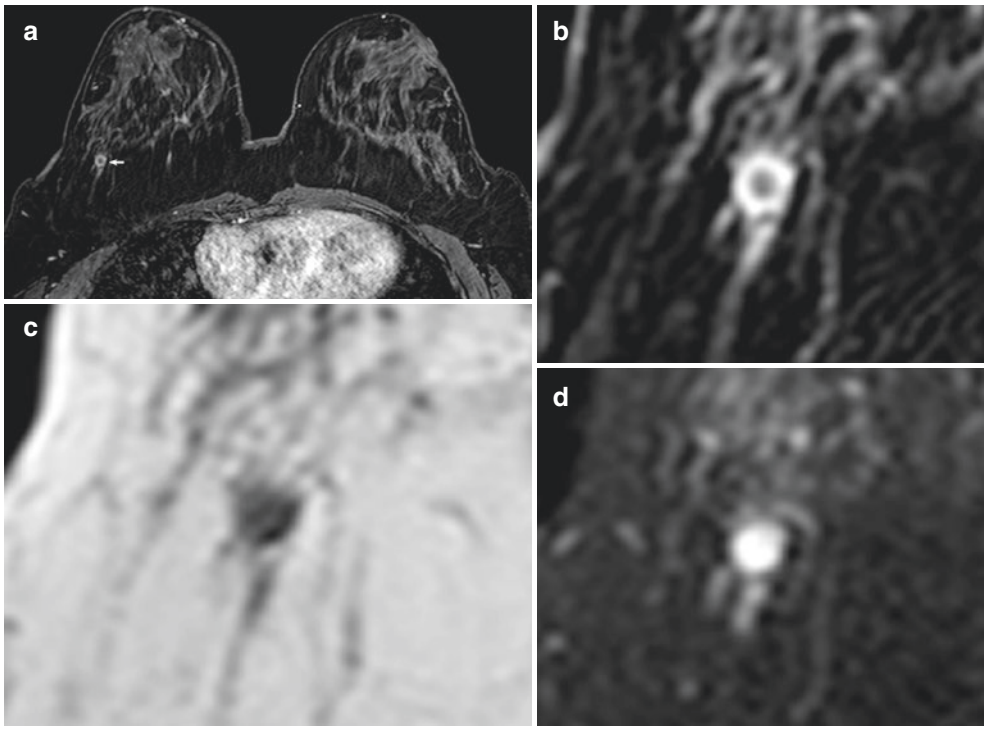

Fig. 3.134 (**a**) Axial T1-weighted fat-suppressed post-contrast image of the more inferior breasts demonstrates an additional 1-cm, rim-enhancing round mass (*arrow*) along the 8:00 axis of the right breast. (**b**) Coned-down magnified axial T1-weighted fat-suppressed post-contrast image of the mass highlights the rim enhancement. (**c**) T1-weighted fat-suppressed image of the mass highlights the lack of central T1 high signal, to indicate fat necrosis. (**d**) T2-weighted fat-suppressed image of the mass highlights the T2 high signal

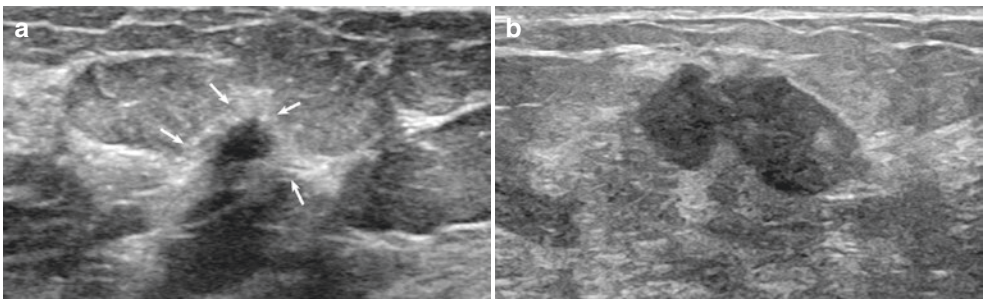

Fig. 3.135 Second-look ultrasound to evaluate for the 5:00 mass (known malignancy) and 8:00 mass (newly identified on MRI). (**a**) Grayscale image of the right 8:00 axis demonstrates an irregular hypoechoic mass with angular margins and echogenic halo (*arrows*), corresponding to the unsuspected MRI mass. Ultrasound-guided core biopsy yielded IDC. (**b**) Grayscale image of the right 5:00 axis demonstrates a deceptively circumscribed mass corresponding to the known malignancy

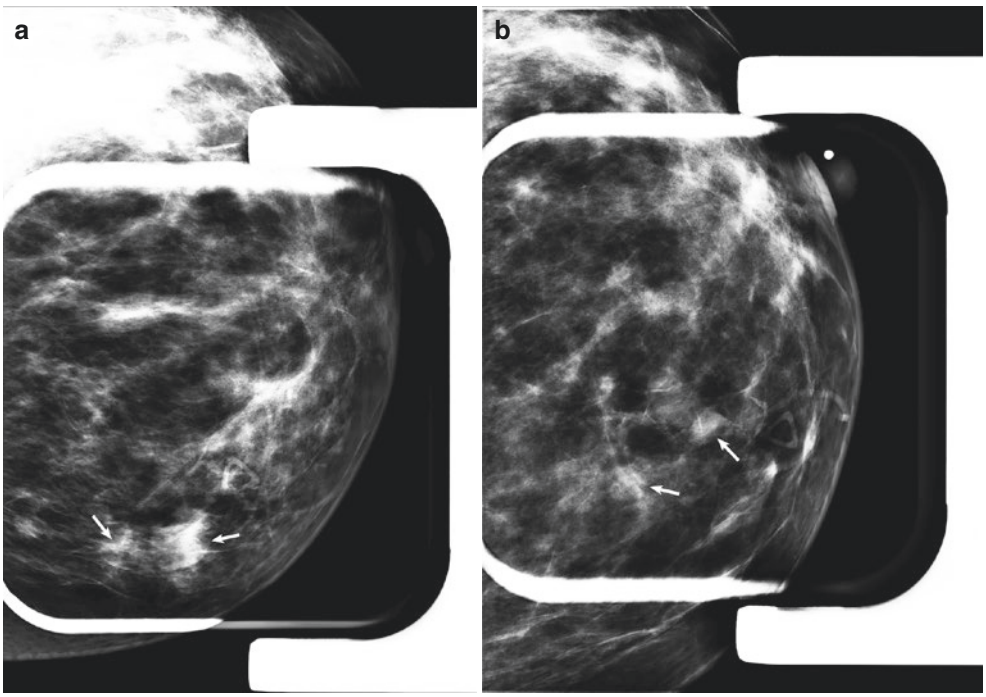

Fig. 3.136 Initial diagnostic right breast mammogram. CC (**a**) and MLO (**b**) spot compression views performed in an area of palpable abnormality demonstrate vague nodular asymmetries (*arrows*) that partially efface. Ultrasound and MRI findings are more diagnostic

3.31 History

Extent of disease evaluation (Figs. 3.137, 3.138, 3.139, 3.140, 3.141, and 3.142).

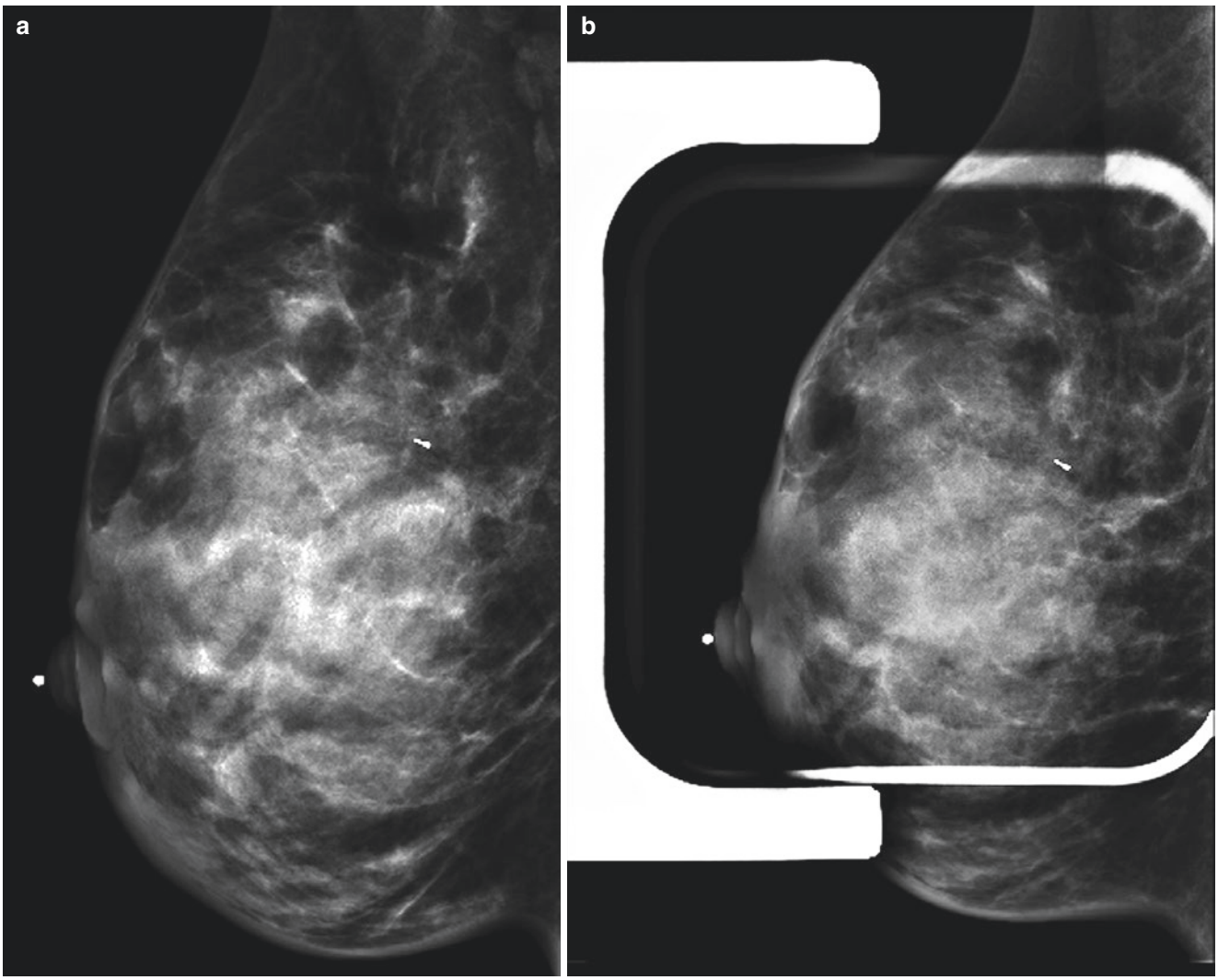

Fig. 3.137 MLO (**a**) and MLO spot (**b**) compression mammographic views of the left breast

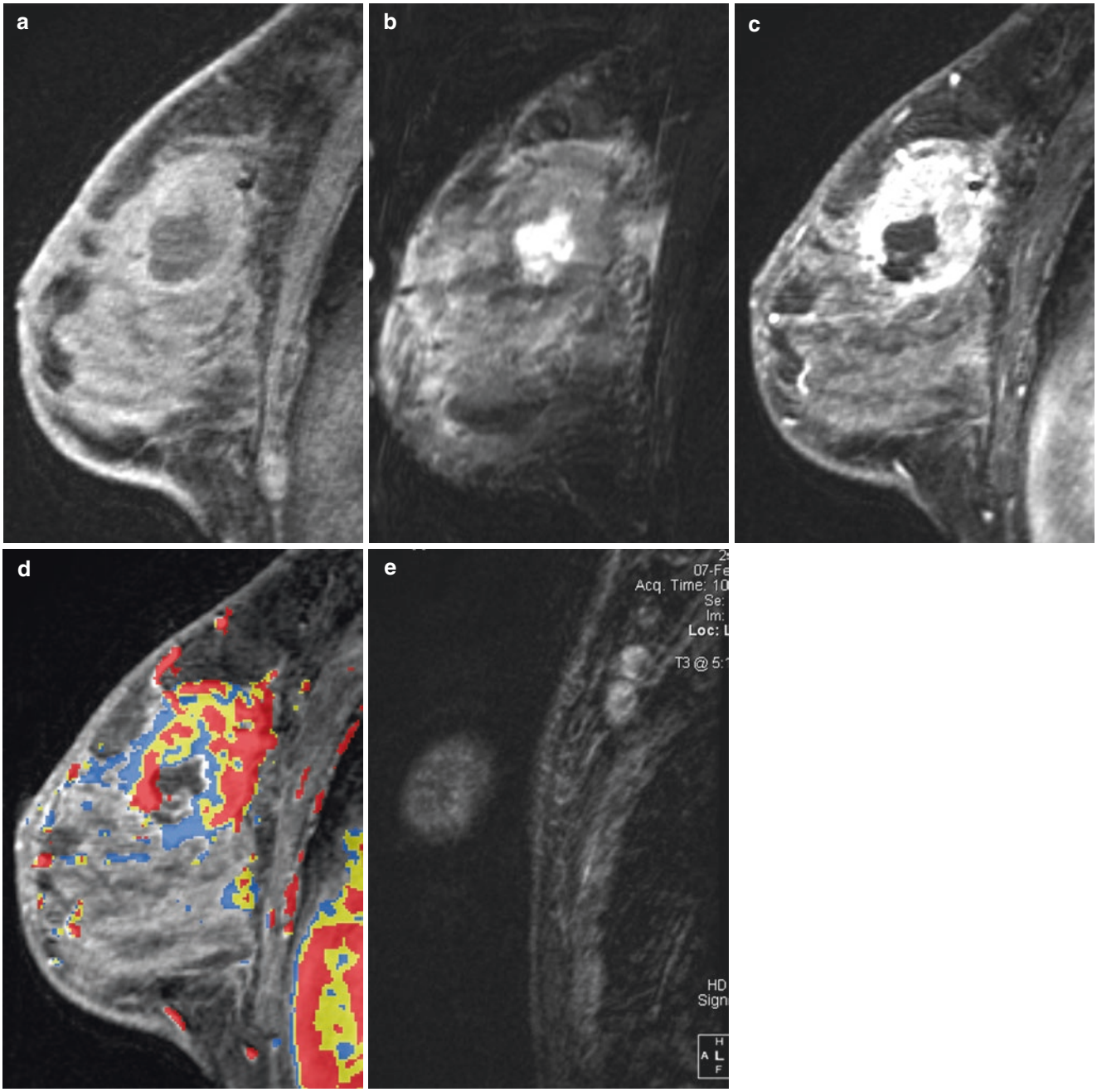

Fig. 3.138 Sagittal MRI images of the left breast. T1-weighted fat-saturated (**a**), T2-weighted fat-saturated (**b**), T1-weighted fat-saturated post-contrast (**c**), and corresponding image with CAD color overlay (**d**). (**e**) T1-weighted fat-saturated post-contrast image through the left axilla

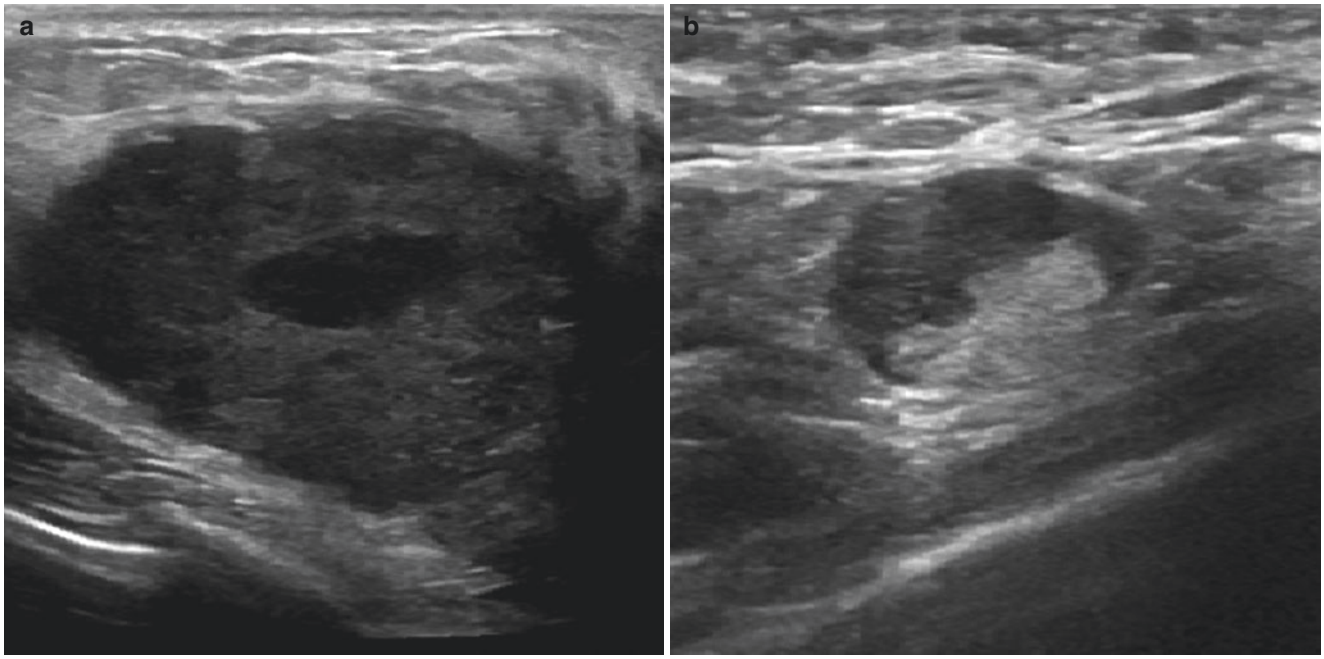

Fig. 3.139 Targeted ultrasound images of the left breast (**a**) and left axilla (**b**)

3.31 Triple-Negative (Basal) Cancer

Teaching Points Triple-negative breast cancer is a distinct subgroup of breast cancer that is negative for estrogen receptor (ER), progesterone receptor (PR), and HER2, accounting for 11–20 % of all breast cancers. It is used as immunohistochemistry (IHC) substitute for basal molecular subtype. Patients with triple-negative tumors have poorer clinical outcomes, with higher rates of recurrence and distant metastasis.

Sonographically, triple-negative tumors can mimic a benign fibroadenoma or a complicated cyst. On MR imaging, these tumors usually present as a unifocal necrotic mass with heterogeneous rim enhancement and central T2 hyperintensity consistent with central necrosis, as in this case.

Image Findings

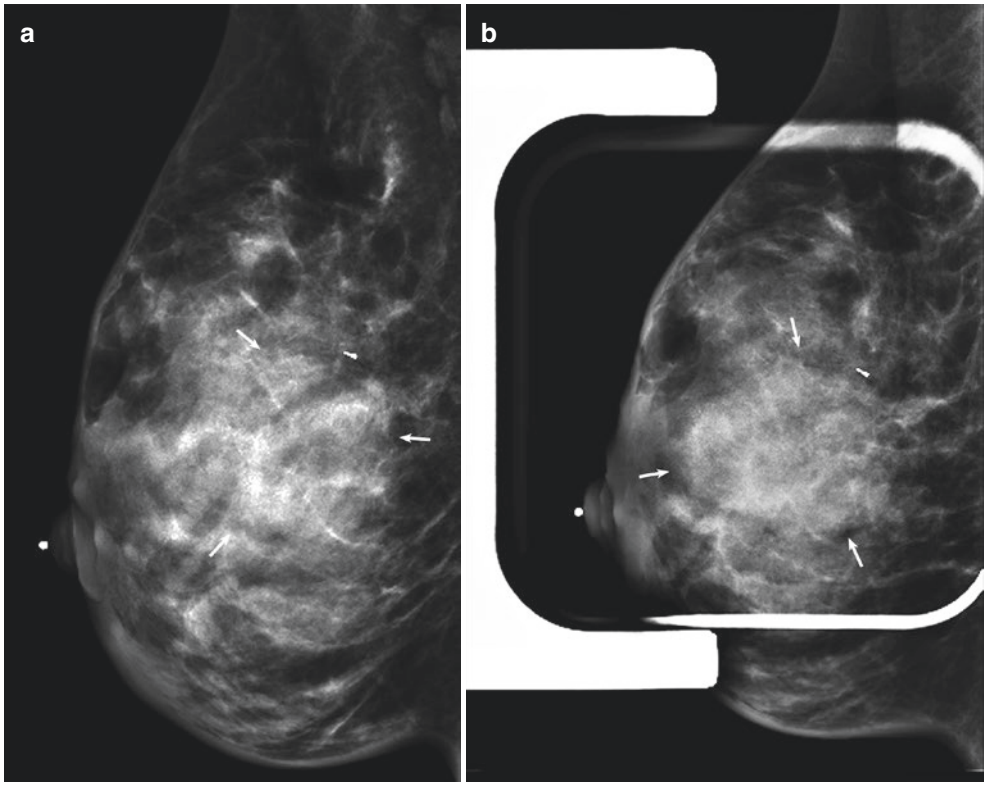

Fig. 3.140 Triple-negative infiltrating ductal carcinoma (IDC) on mammography. Left MLO view (**a**) demonstrates an obscured oval mass (*arrows*) at the superior aspect of the breast, middle depth; the mass is seen better on spot compression (**b**)

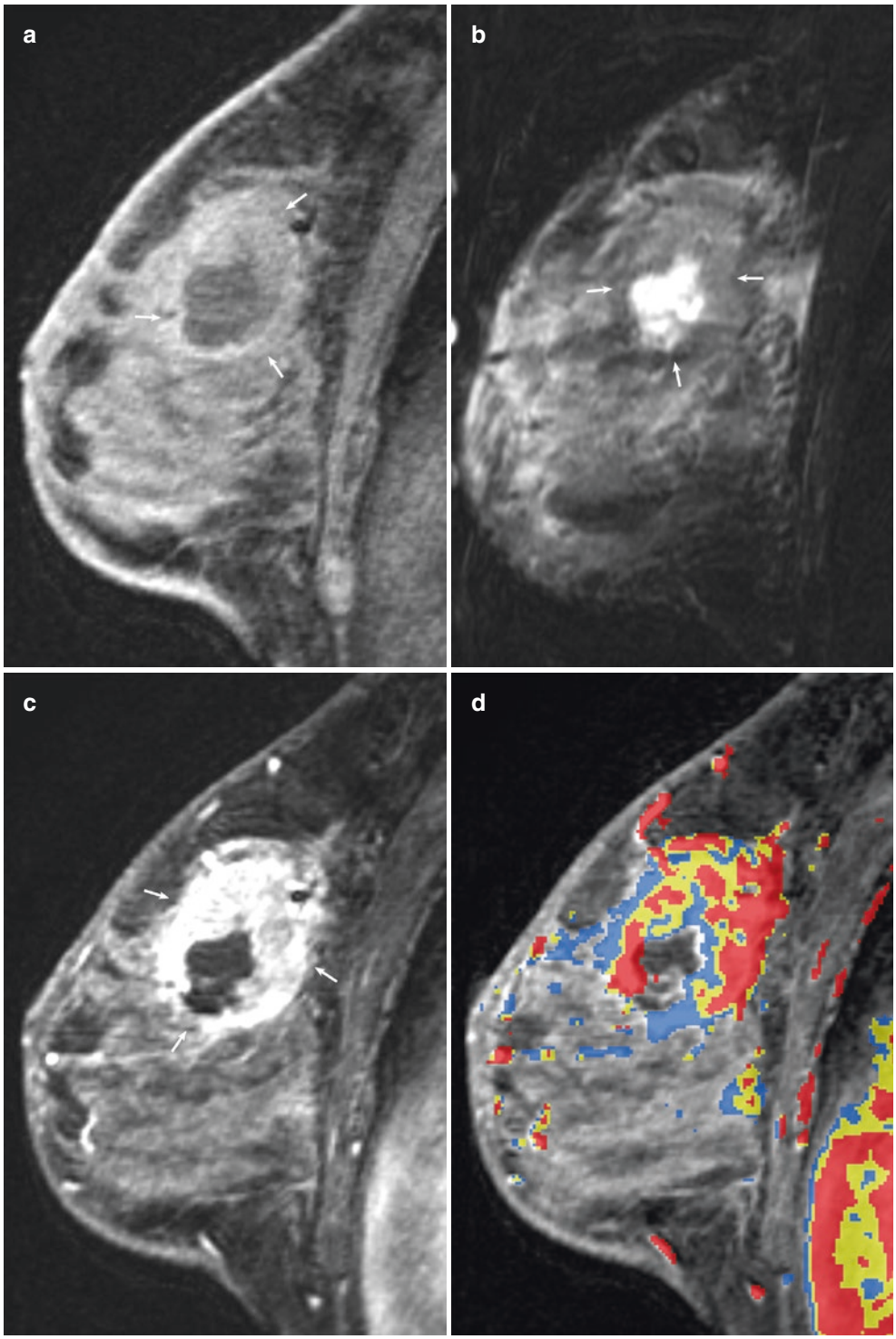

Fig. 3.141 Triple-negative IDC on MRI. (**a**) Sagittal T1-weighted fat-saturated image shows an oval lobulated heterogeneous mass (*arrows*) in the superior aspect of the breast. (**b**) Corresponding T2-weighted fat-saturated image shows T2 isointensity and central T2 hyperintensity. Metallic artifact from a biopsy clip is best appreciated on the T1 image. (**c**) Sagittal T1-weighted fat-saturated post-contrast image shows thick, heterogeneous rim enhancement (*arrows*) with inferocentral nonenhancement corresponding to the T2 hyperintensity, signifying central necrosis. (**d**) CAD analysis demonstrates mixed enhancement kinetics with a predominant washout pattern in the viable portions of the tumor and nonenhancement in the central necrotic portion. (**e**) Sagittal T1-weighted fat-saturated post-contrast image of the left axilla shows axillary lymphadenopathy (*arrows*)

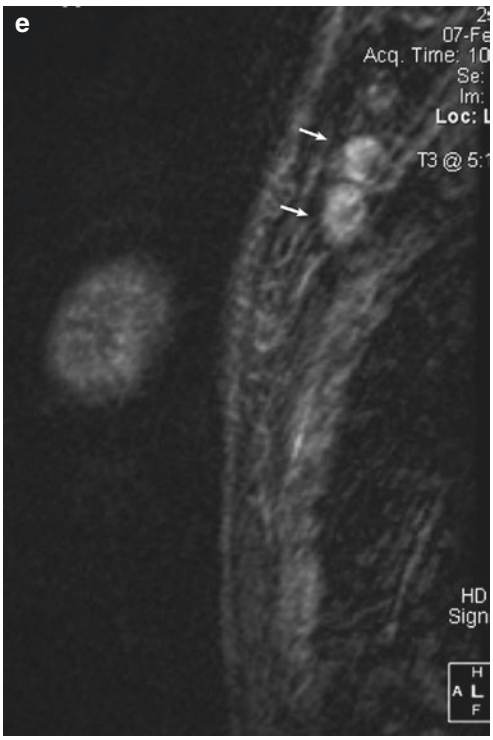

Fig. 3.141 (continued)

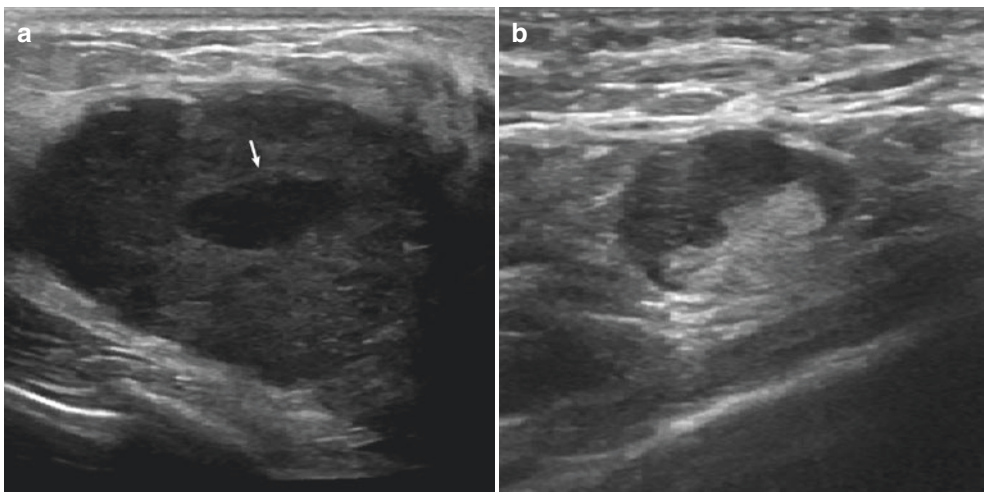

Fig. 3.142 Triple-negative IDC on ultrasound. (**a**) Targeted ultrasound of the left breast mass shows an oval, hypoechoic mass with a central anechoic region (*arrow*), correlating with the central necrosis on MRI. (**b**) Targeted ultrasound of the left axilla shows an abnormal lymph node with irregular cortical thickening

3.32 History

48-year-old woman with newly diagnosed right breast invasive ductal carcinoma NOS with axillary metastasis. Breast MRI was performed to evaluate extent of disease.

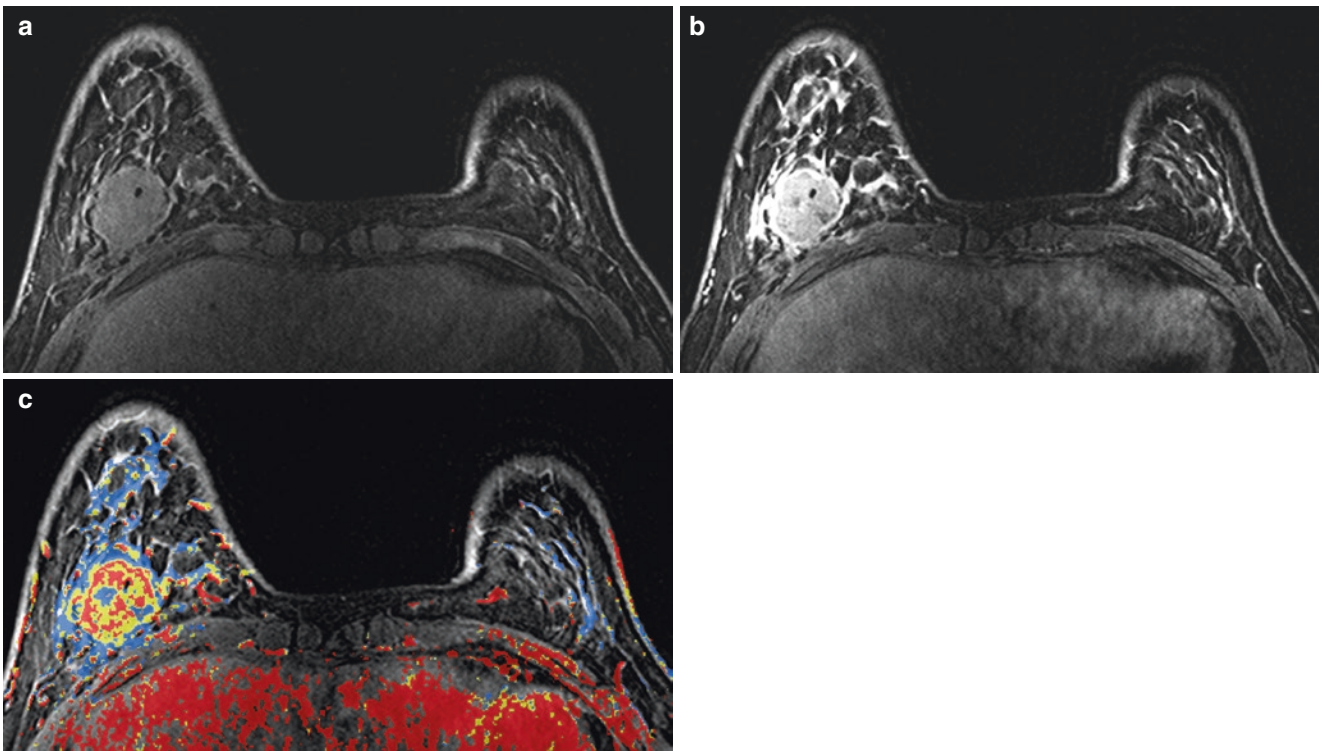

Fig. 3.143 Axial T1-weighted fat-saturated pre-contrast (**a**) and post-contrast (**b**) images of the lower breasts with CAD kinetic analysis color overlay (**c**)

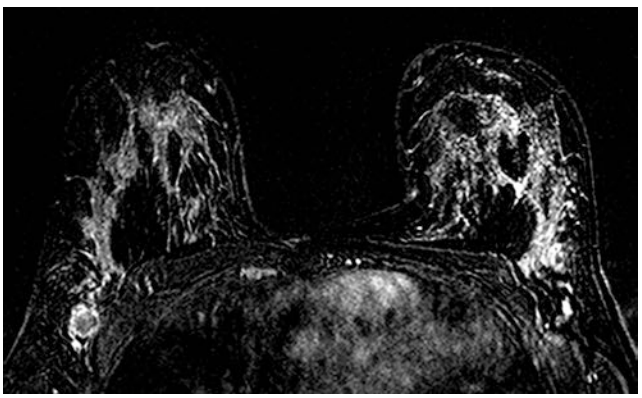

Fig. 3.144 Axial post-contrast subtraction image at the level of the axillae

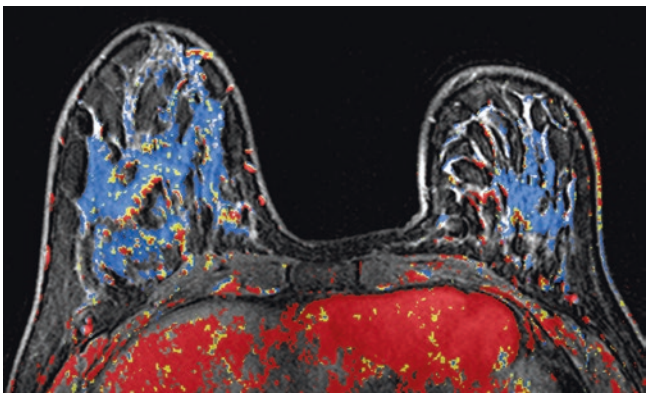

Fig. 3.145 Axial T1-weighted fat-saturated post-contrast image at the level of the nipples with CAD kinetic analysis color overlay

History: Same patient status post neoadjuvant chemotherapy.

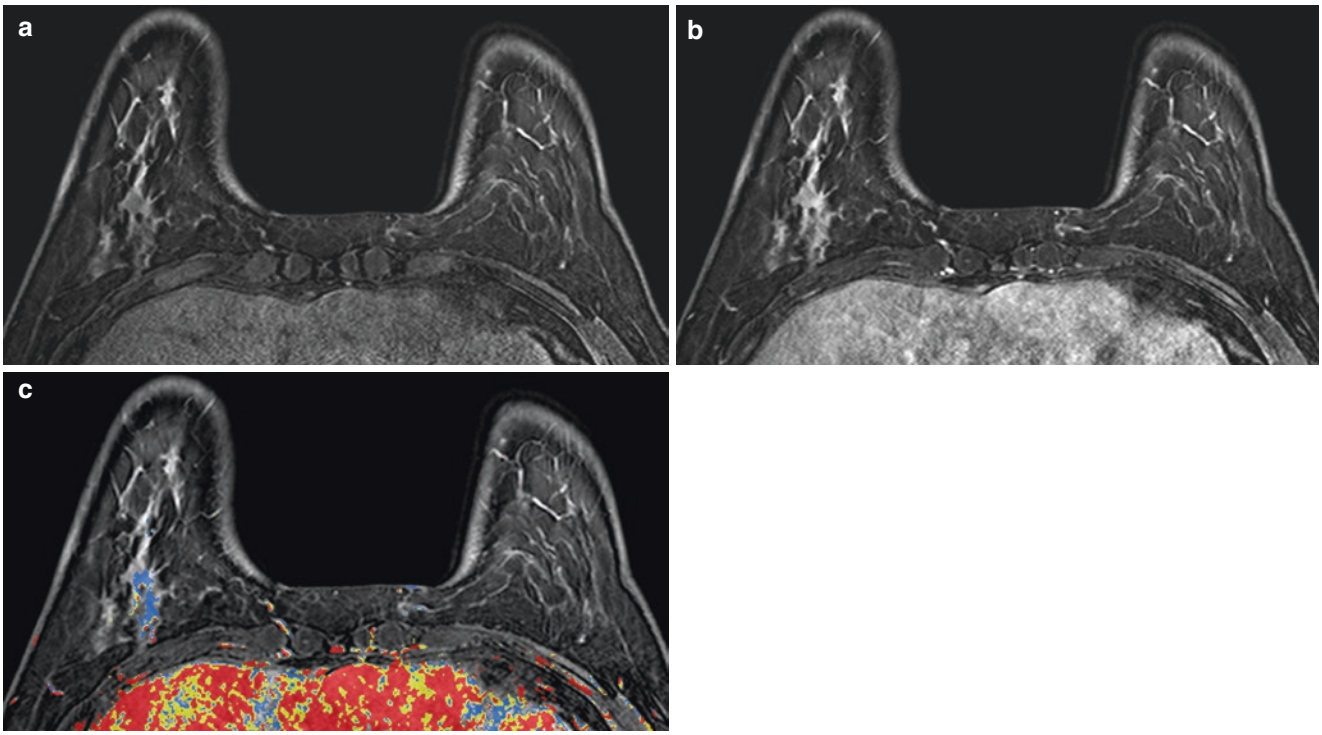

Fig. 3.146 Axial T1-weighted fat-suppressed pre-contrast (**a**) and post-contrast (**b**) images of the lower breasts with CAD kinetic analysis color overlay (**c**)

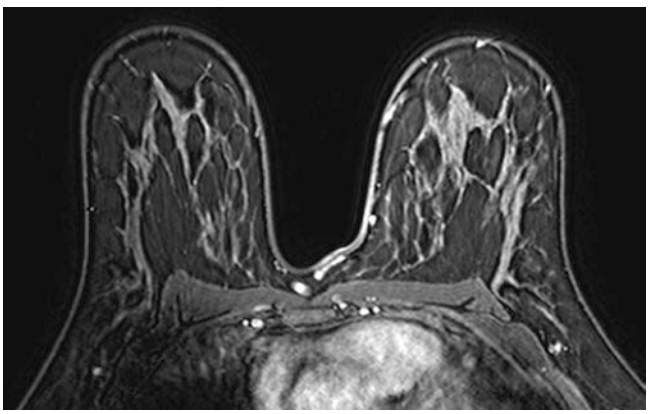

Fig. 3.147 Axial T1-weighted fat-saturated post-contrast image at the level of the axillae

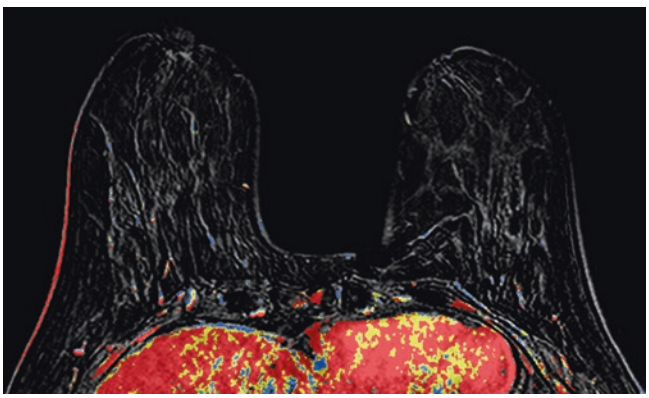

Fig. 3.148 Axial post-contrast subtraction image at the level of the nipples with CAD kinetic analysis color overlay

3.32 Neoadjuvant Therapy 1

Teaching Points Baseline images (Figs. 3.143, 3.144, and 3.145).

Images obtained 4 months later (Figs. 3.146, 3.147, and 3.148).

Partial treatment response of invasive ductal carcinoma following neoadjuvant chemotherapy (Figs. 3.149, 3.150, 3.151, 3.152, 3.153, and 3.154).

In patients undergoing neoadjuvant therapy, breast MRI provides better correlation with final surgical pathology than physical examination, mammography, or sonography. This clinical scenario is therefore one of the accepted indications for breast MRI evaluation, but MRI may overestimate (6 %) or underestimate (23 %) residual disease.

The Response Evaluation Criteria In Solid Tumors (RECIST) guideline for tumor response lists several levels:

- Complete Response (CR): Disappearance of all target lesions
- Partial Response (PR): At least a 30 % decrease in the sum of the longest diameter (LD) of target lesions
- Stable Disease (SD): Neither sufficient shrinkage to qualify for PR nor sufficient increase to qualify for PD
- Progressive Disease (PD): At least a 20 % increase in the sum of the LD of target lesions

The patient in our case demonstrates partial response to neoadjuvant therapy and on final surgical pathology showed a 1.9-cm residual tumor and two positive axillary lymph nodes. Neoadjuvant treatment can be effective in reducing locally advanced tumor, and in certain cases breast conservation (rather than mastectomy) can become a surgical treatment option.

In patients with a good response, in addition to tumor size reduction, a change in enhancement pattern (to persistent from washout) and overall decreased background parenchymal enhancement have been noted, as illustrated in this case.

Image Findings

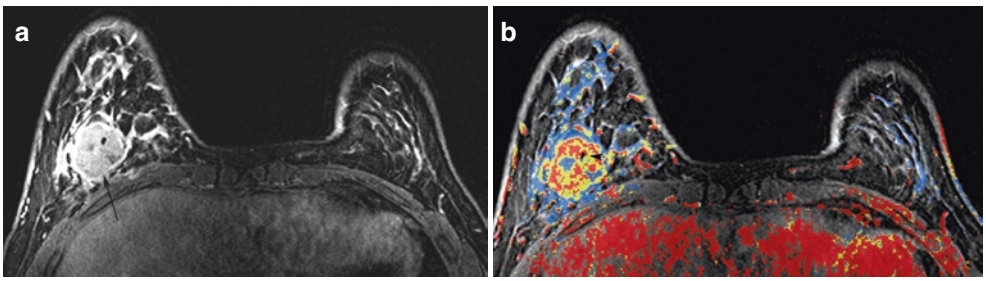

Fig. 3.149 Baseline axial T1-weighted fat-saturated post-contrast image (**a**) demonstrates a 3.1-cm round, enhancing mass (*arrow*) with suspicious delayed washout color-coded red on CAD color overlay (**b**). An *arrowhead* identifies central clip artifact from a biopsy, which yielded malignancy. No other suspicious finding was noted in either breast

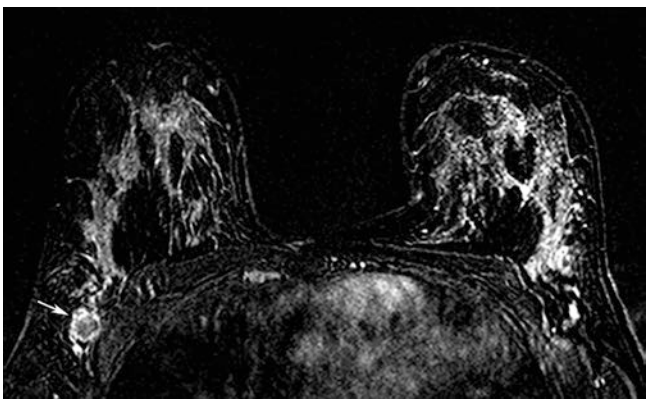

Fig. 3.150 Axial post-contrast subtraction image shows an ipsilateral irregular, enlarged axillary lymph node (*arrow*) corresponding to known metastatic disease at baseline

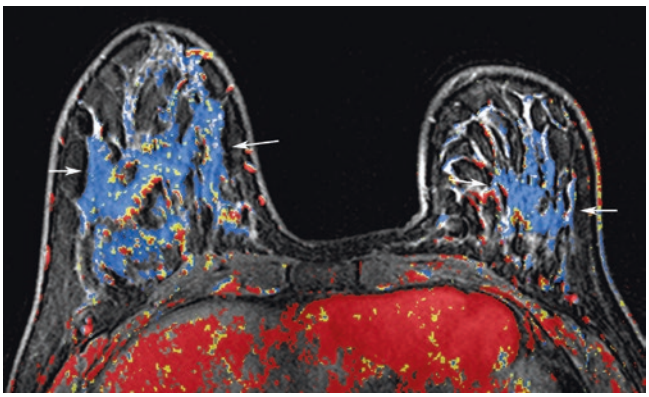

Fig. 3.151 Axial T1-weighted fat-saturated post-contrast image with CAD kinetic analysis shows marked background parenchymal enhancement at baseline

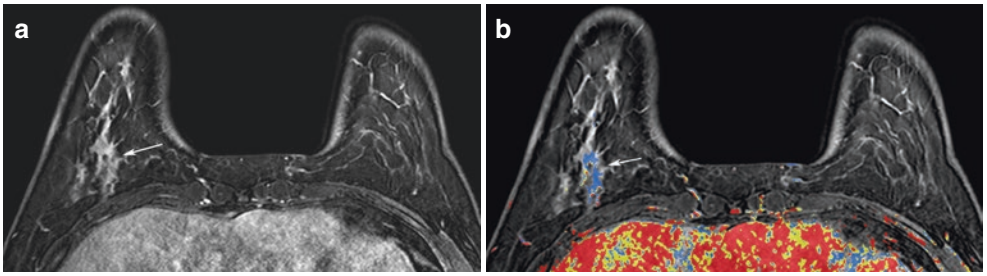

Fig. 3.152 (**a**) Following neoadjuvant chemotherapy, the axial T1-weighted fat-saturated post-contrast image shows a decrease in the known right breast malignancy, with a residual 1.5-cm area of less distinct nonmass enhancement (*arrow*). (**b**) Corresponding CAD color overlay shows a persistent delayed enhancement pattern color-coded blue. Findings are consistent with a partial response to chemotherapy

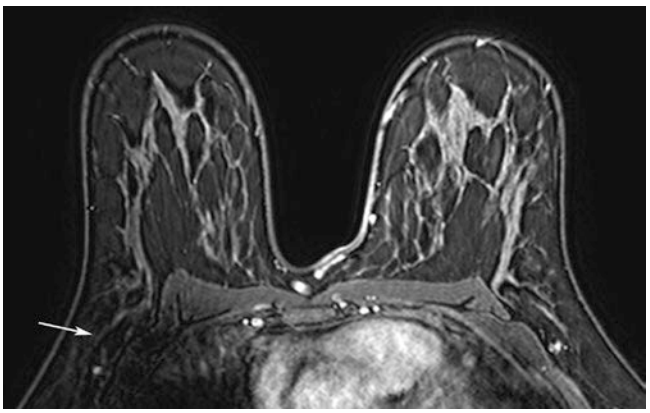

Fig. 3.153 Axial T1-weighted fat-saturated post-contrast image demonstrates interval resolution of right axillary lymphadenopathy

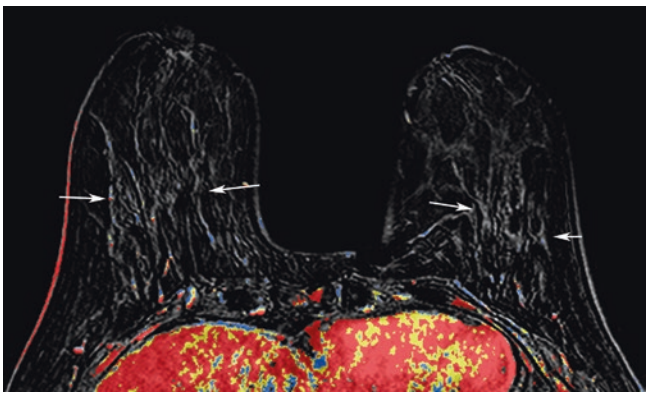

Fig. 3.154 Axial post-contrast subtraction image with CAD color overlay shows a marked decrease in background parenchymal enhancement (*arrows*) following neoadjuvant chemotherapy

3.33 History

41-year-old woman for follow-up MRI status after neoadjuvant therapy (Figs. 3.155, 3.156, 3.157, and 3.158).

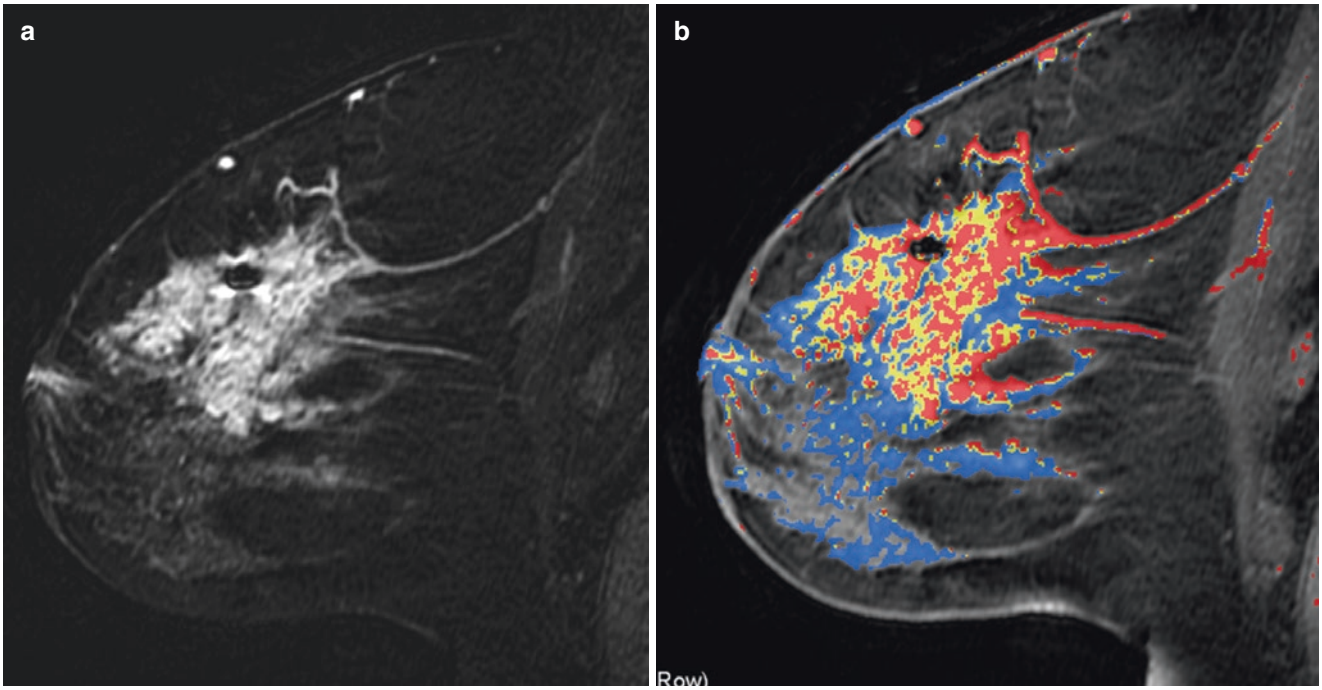

Fig. 3.155 Initial sagittal MR images of the left breast. (**a**) Post-contrast subtraction image. (**b**) T1-weighted fat-saturated post-contrast image with CAD overlay

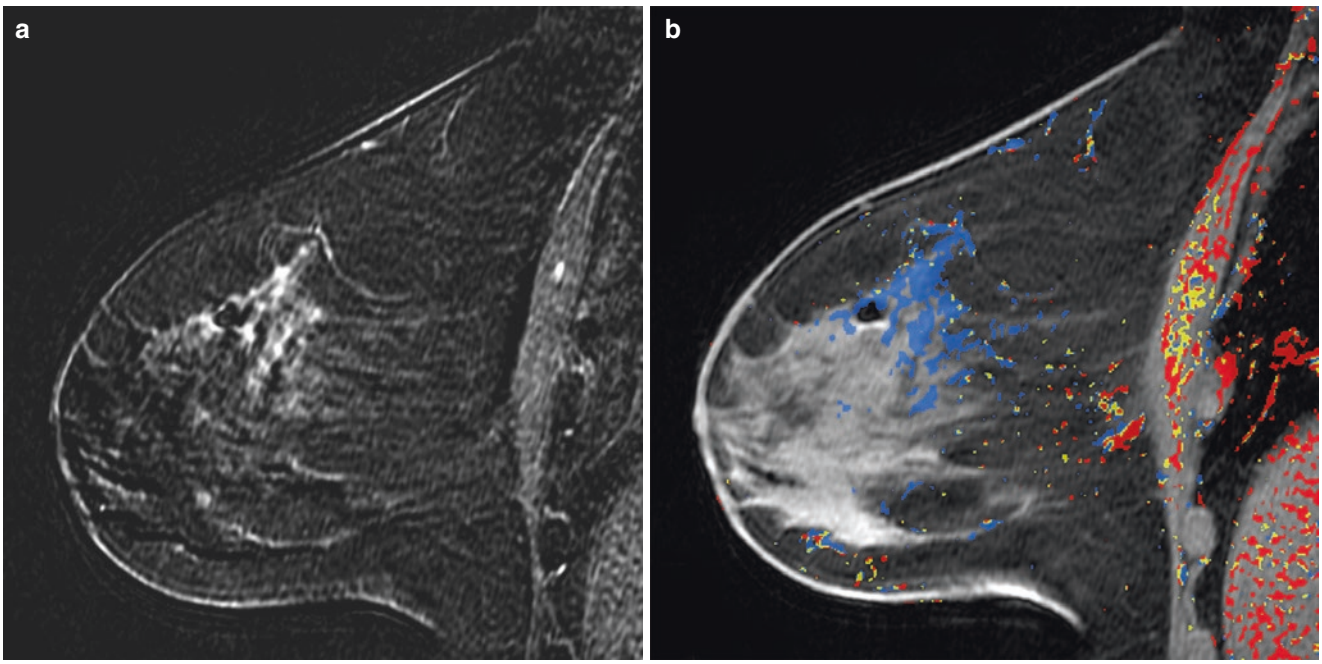

Fig. 3.156 Follow-up sagittal MRI images of the left breast performed 5 months after the initial exam. (**a**) Post-contrast subtraction image. (**b**) T1-weighted fat-saturated post-contrast iamge with CAD overlay

3.33 Neoadjuvant Therapy 2

Teaching Points In patients undergoing neoadjuvant therapy, breast MRI provides better correlation with final surgical pathology than physical examination, mammography, or sonography. Neoadjuvant therapy is one of the accepted indications for breast MRI evaluation, but MRI may overestimate or underestimate residual disease in approximately 29 % of the patients. Neoadjuvant treatment can be effective in reducing locally advanced tumor, and in certain cases breast conservation can become a surgical treatment option, rather than mastectomy. In patients with a good response, in addition to the reduction in tumor size, a change in enhancement pattern to persistent from washout and overall decreased background parenchymal enhancement have been noted, as illustrated in this case.

Image Findings

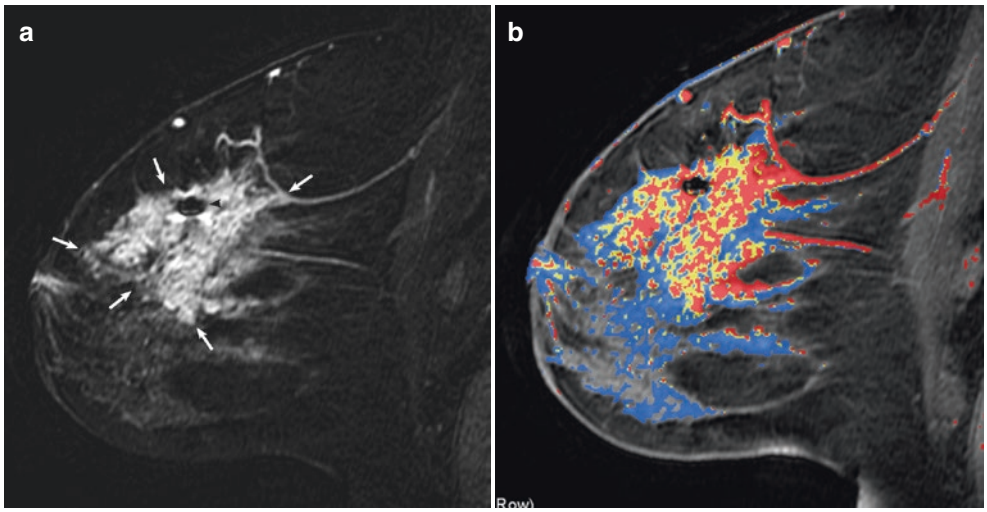

Fig. 3.157 MRI of newly diagnosed left breast invasive ductal carcinoma with axillary lymph node metastases. (**a**) Sagittal post-contrast subtraction image of the left breast demonstrates segmental nonmass enhancement (*arrows*) measuring up to 6.2 cm in the upper left breast with associated localizing clip artifact (*arrowhead*) from a biopsy, which yielded invasive ductal carcinoma. (**b**) This area is predominantly colored red on the corresponding CAD enhancement kinetics overlay, indicating rapid uptake and washout

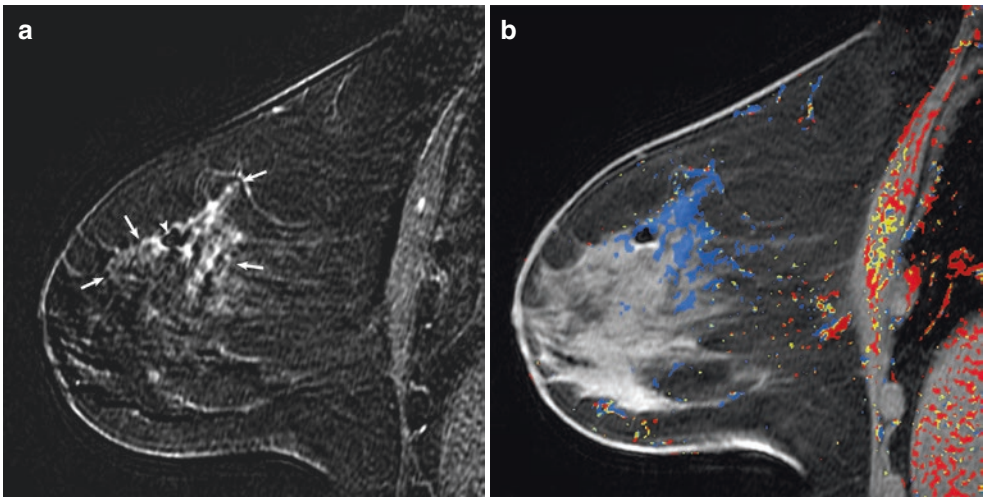

Fig. 3.158 5-month follow-up MRI after neoadjuvant chemotherapy. (**a**) Sagittal post-contrast subtraction image of the left breast at the location of the localizing clip (*arrowhead*) shows reduction of nonmass enhancement (*arrows*), now measuring up to 2.8 cm. (**b**) The CAD enhancement kinetics overlay now shows the area to be predominantly blue, indicating mild uptake and progressive enhancement. Enlarged axillary lymph nodes from known metastatic disease had also decreased in size and resumed their normal morphology (*not shown*). Surgical pathology at the time of lumpectomy showed residual tumor measuring up to 2.5 cm and two positive axillary lymph nodes

3.34 History

57-year-old woman with personal history of breast cancer undergoing screening MRI (Figs. 3.159 and 3.160).

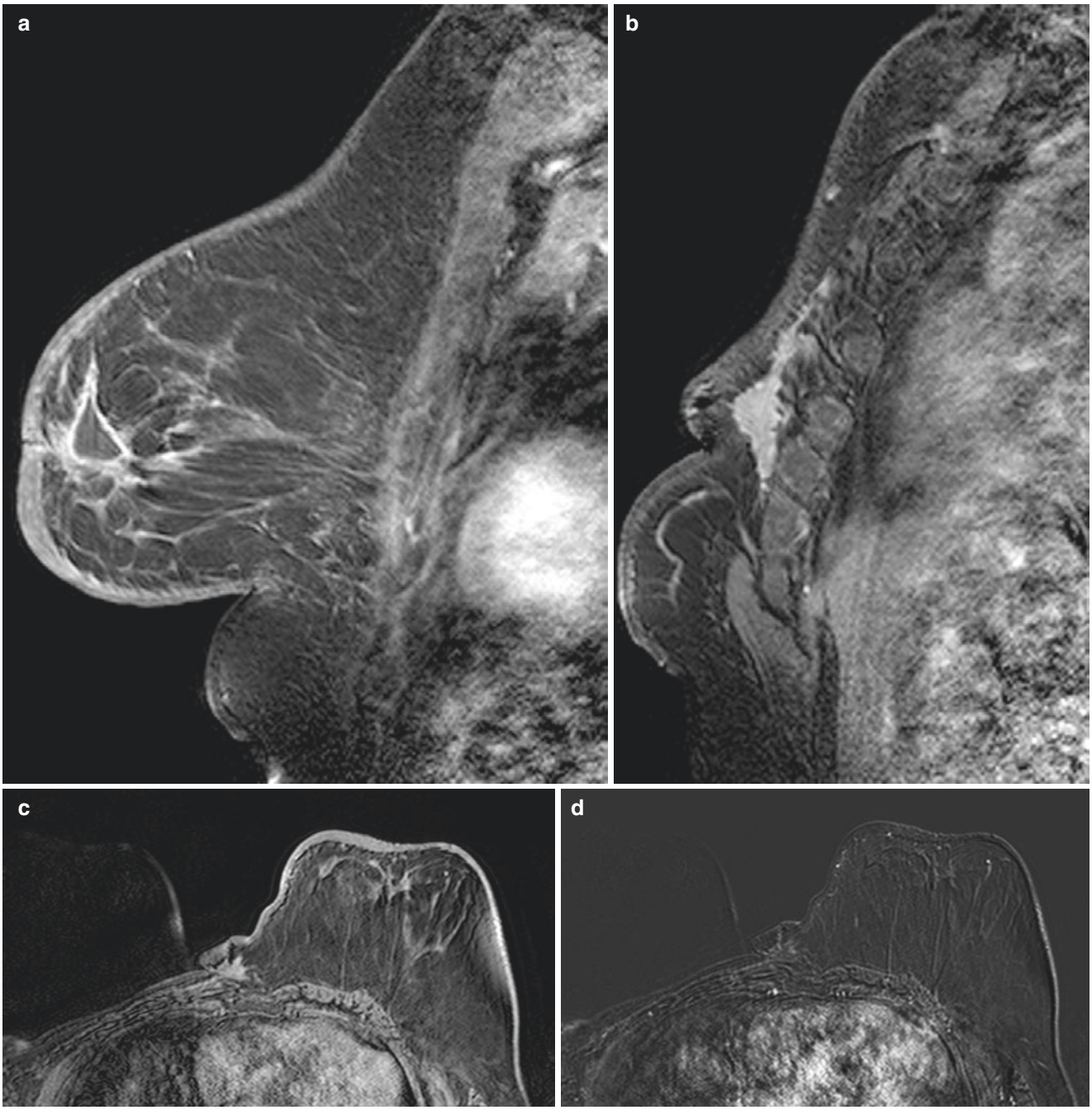

Fig. 3.159 (**a**) Sagittal T1-weighted fat-saturated post-contrast image of the left breast. Sagittal (**b**) and axial (**c**) T1-weighted fat-saturated post-contrast images of the right mastectomy site. (**d**) Axial post-contrast subtraction image of the right mastectomy site

3.34 Post-Surgical Breast

Teaching Points Breast MRI is an adjunct imaging tool in pre-surgical planning for the identification of mammographically occult additional disease and the evaluation of residual disease in patients whose pathology specimens demonstrate close or positive margins. In breast-conserving surgery, positive margins have been reported in 32–63 % of cases of breast cancer and are associated with increased long-term risk of cancer recurrence in the ipsilateral breast. The outcome of patients with close margins at excision remains controversial, however. This case illustrates normal expected appearance of the post-surgical cavity without associated suspicious enhancement. Screening MRI in patients with a personal history of cancer can yield additional breast cancer detection, but this has not been generally accepted as an indication for screening MRI.

Image Findings

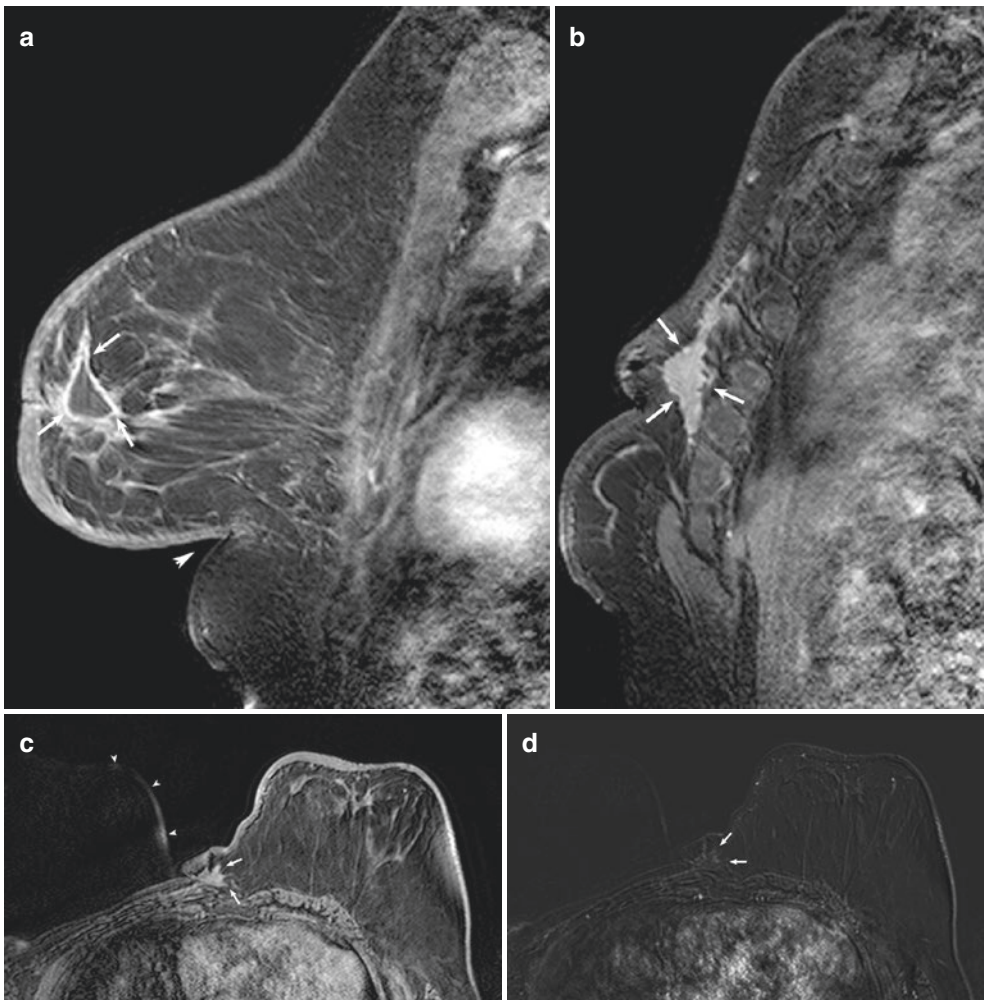

Fig. 3.160 Post-surgical scar. Sagittal T1-weighted fat-saturated post-contrast image (**a**) of the left breast demonstrates rim enhancement outlining the surgical cavity (*arrows*) without suspicious enhancement to indicate recurrent disease. Note the protruding inframammary fold (*arrowheads*) secondary to suboptimal coil positioning. (**b**, **c**) Sagittal and axial T1-weighted fat-saturated post-contrast images of the medial right mastectomy site demonstrate an apparent irregular mass (*arrows*). Note the ghosting artifact of the left breast (*arrowheads* in **c**). (**d**) Corresponding axial post-contrast subtraction image demonstrates no significant enhancement in this region, consistent with benign mastectomy scar (*arrows*)

3.35 History

48-year-old woman status post lumpectomy with positive margin. Post-surgical evaluation breast MRI (Figs. 3.161 and 3.162).

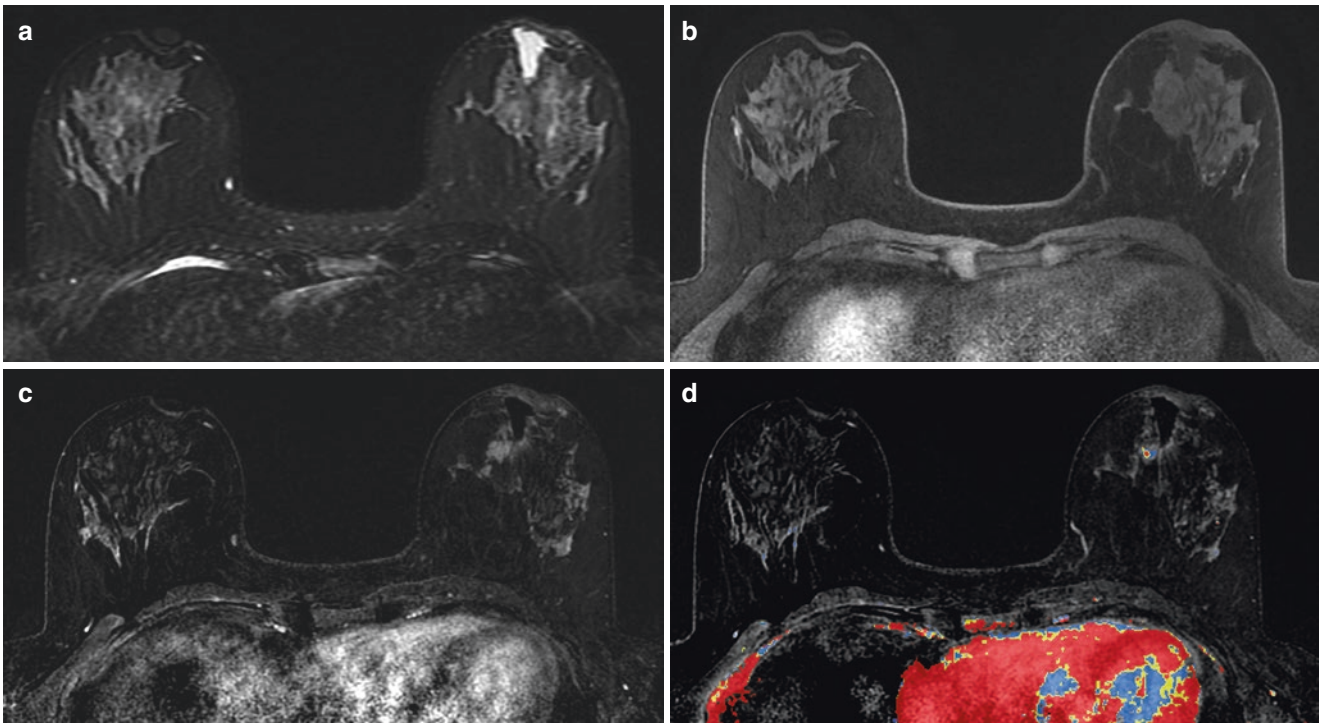

Fig. 3.161 Axial MRI images of both breasts. (**a**) T2-weighted fat-saturated image. (**b**) T1-weighted fat-saturated image. (**c**, **d**) Post-contrast subtraction and corresponding CAD color overlay image

3.35 Residual Disease 1

Teaching Points In breast-conserving surgery, positive margins have been reported in 32–63 % of cases. Breast MRI has been shown to be helpful in identifying residual disease, which can guide appropriate surgical management, as illustrated in this case. This patient underwent wide posterior re-excision with subsequent negative margin on pathology.

Image Findings

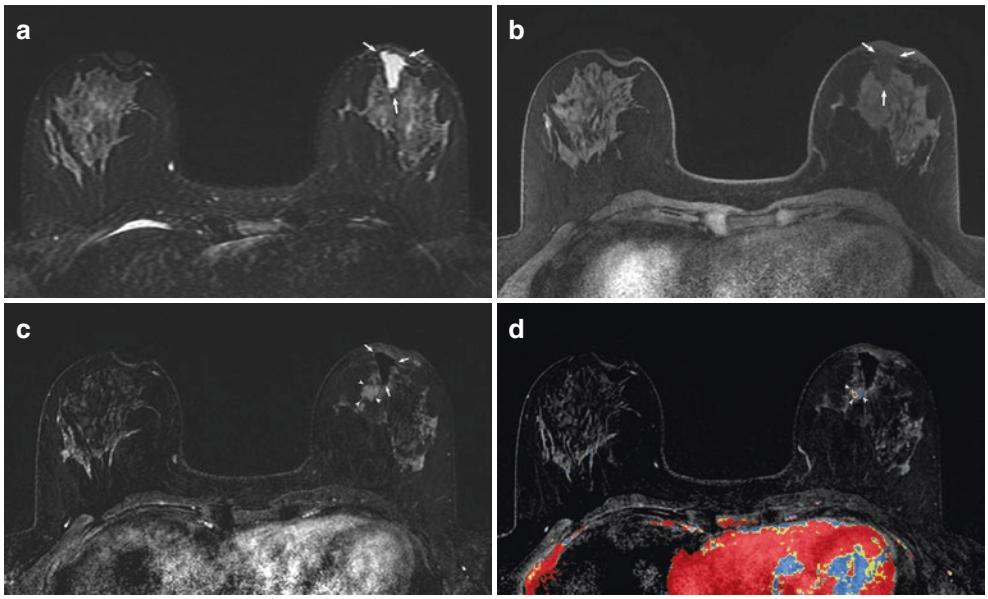

Fig. 3.162 Residual disease. Axial T2-weighted fat-saturated image (**a**) and T1-weighted fat-saturated pre-contrast image (**b**) demonstrate a T2-hyperintense and T1-hypointense lumpectomy cavity (*arrows*) in the retroareolar left breast. (**c**) Axial post-contrast subtraction image demonstrates a thin rim of enhancement outlining the lumpectomy cavity (*arrows*), as well as irregular enhancing masses (*arrowheads*) posterior and medial to the lumpectomy cavity with washout kinetics (**d**) on CAD analysis

3.36 History

61-year-old woman status post lumpectomy with positive margin. Post-surgical evaluation breast MRI (Figs. 3.163 and 3.164).

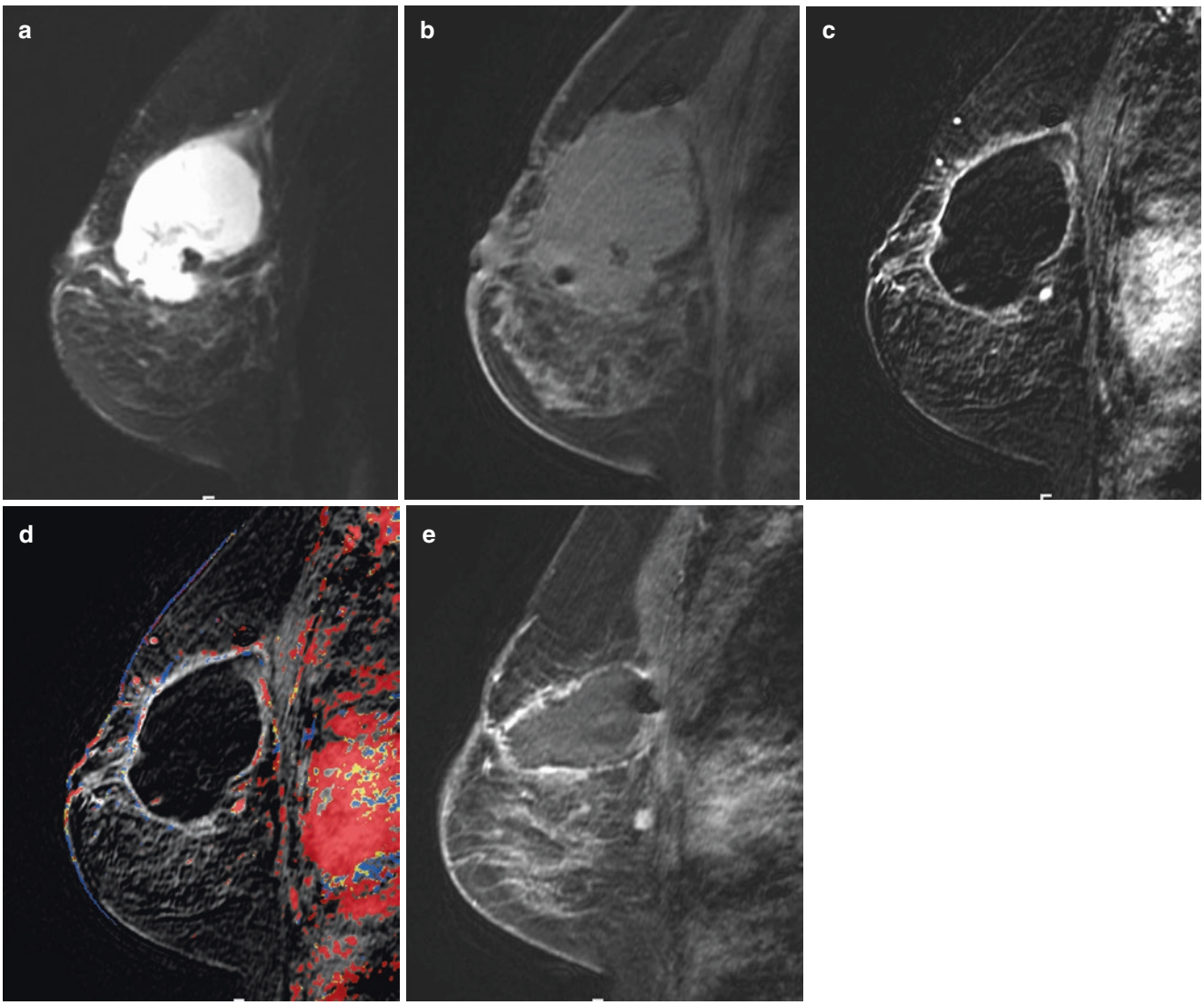

Fig. 3.163 Sagittal MR images of the left breast. (**a**) T2-weighted fat-saturated image. (**b**) T1-weighted fat-saturated image. (**c**) Post-contrast subtraction image. (**d**) Corresponding image with CAD color overlay. (**e**) T1-weighted fat-saturated post-contrast image of the more lateral aspect of the breast

3.36 Residual Disease 2

Teaching Points Breast MRI has been shown to be helpful in identifying post-operative residual disease, which can guide appropriate surgical management. This case illustrates not only residual disease near the lumpectomy cavity but also unsuspected additional ipsilateral disease that is occult on other imaging modalities.

Image Findings

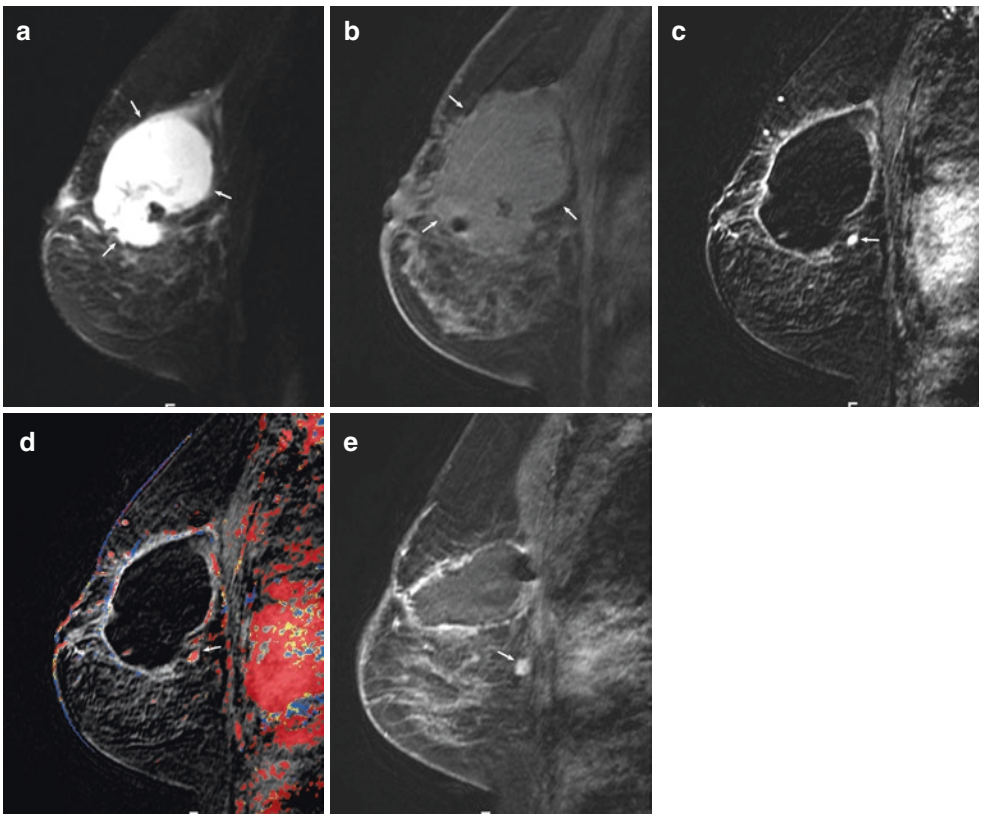

Fig. 3.164 Residual disease. Sagittal T2-weighted fat-saturated image (**a**) and T1-weighted fat-saturated pre-contrast image (**b**) demonstrate a T2-hyperintense and T1-isointense surgical cavity (*arrows*) at the 12:00 axis of the left breast. (**c**) Sagittal post-contrast subtraction image demonstrates an oval enhancing mass (*arrow*) along the posterior inferior margin of the surgical cavity with washout kinetics (**d**) on CAD analysis, suspicious for residual disease. In addition, a sagittal T1-weighted fat-saturated post-contrast image (**e**) of the more lateral left breast demonstrates a separate 0.8-cm enhancing round mass (*arrow*) along the far posterior 3:00 axis, with ultrasound correlate (*not shown*) and subsequent biopsy yielding IDC. The patient underwent mastectomy with additional disease identified on surgical pathology, including areas corresponding to the findings on MRI

3.37 History

61-year-old woman after right mastectomy with TRAM reconstruction undergoing screening MRI (Figs. 3.165 and 3.166).

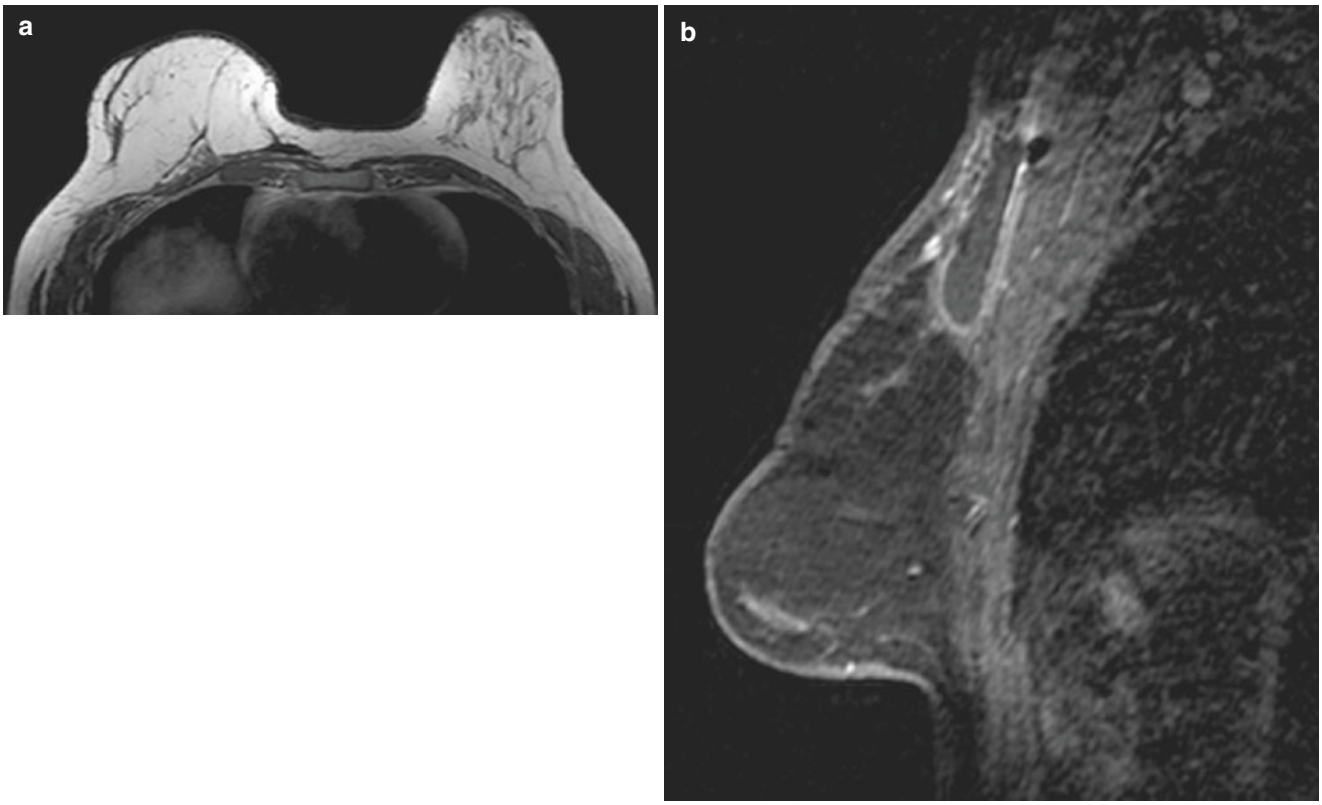

Fig. 3.165 (**a**) Selected axial T1 pre-contrast non-fat saturated image. (**b**) Selected sagittal T1 post-contrast fat saturated image

3.37 TRAM Recurrence

Teaching Points Transverse rectus abdominis muscle (TRAM) flap reconstruction is the most common reconstruction with a low (2–4 %) incidence of local tumor recurrence, therefore, routine MRI screening is not typically warranted in asymptomatic patients with a history of breast cancer and myocutaneous flap. With the increasing use of breast MRI for high-risk screening in patients with a personal history of breast cancer, the reconstructed side should be included in the evaluation with particular attention to the contact zone. In the case above, recurrent invasive ductal carcinoma was detected along the contact zone between the TRAM flap and the native breast tissue incidentally detected on a routine high-risk screening MRI of the breast in an asymptomatic patient with a history of breast cancer.

Image Findings

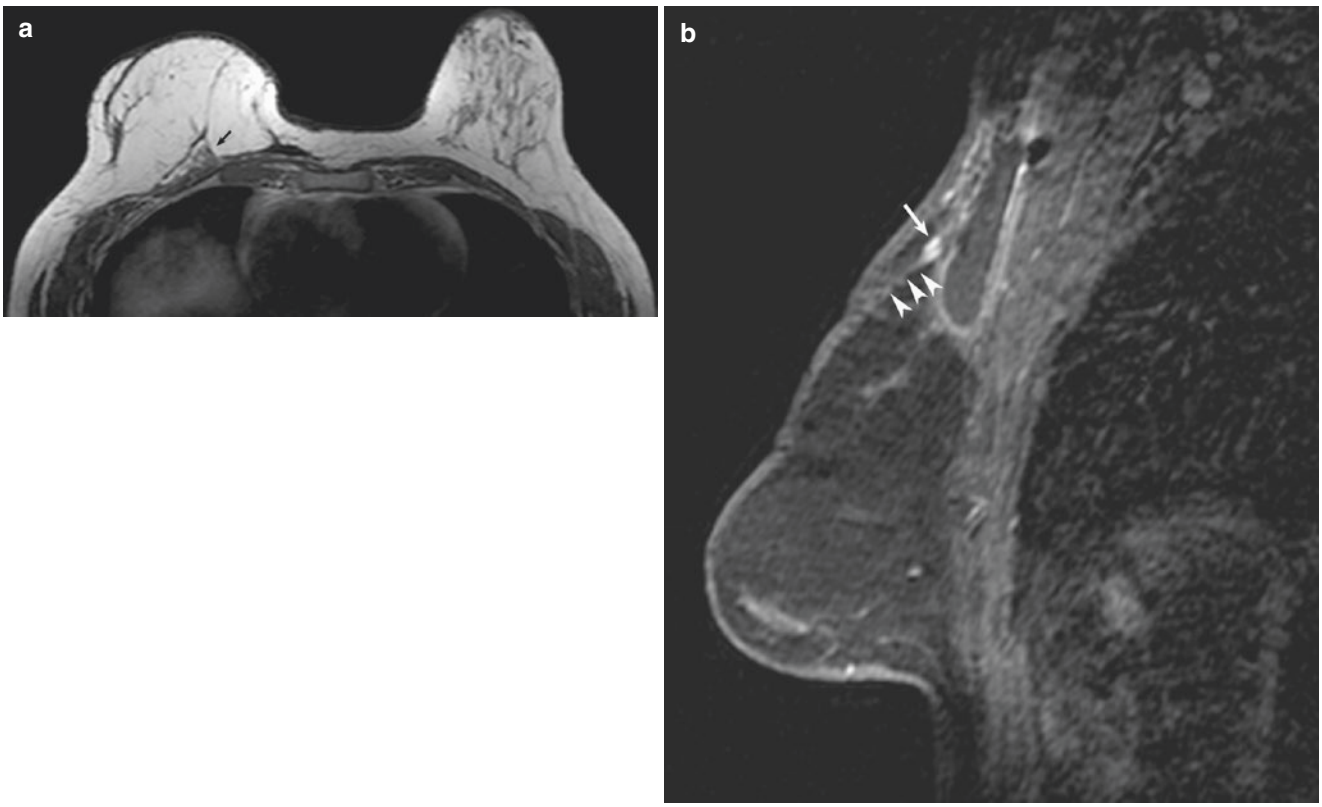

Fig. 3.166 TRAM flap cancer recurrence. (**a**) Selected axial image demonstrates a right TRAM flap reconstruction with a vascular pedicle (*arrow*). (**b**) Sagittal image of the right reconstructed breast demonstrates a new 5 mm mass in the upper breast (*arrow*) along a linear tissue plane separating the TRAM flap from native tissue. This mass was identified on ultrasound and subsequent biopsy yielded IDC. Incidental unresolved long standing post-surgical seroma is noted in the upper posterior breast

3.38 History

63-year-old with newly diagnosed left breast cancer (Figs. 3.167, 3.168, and 3.169).

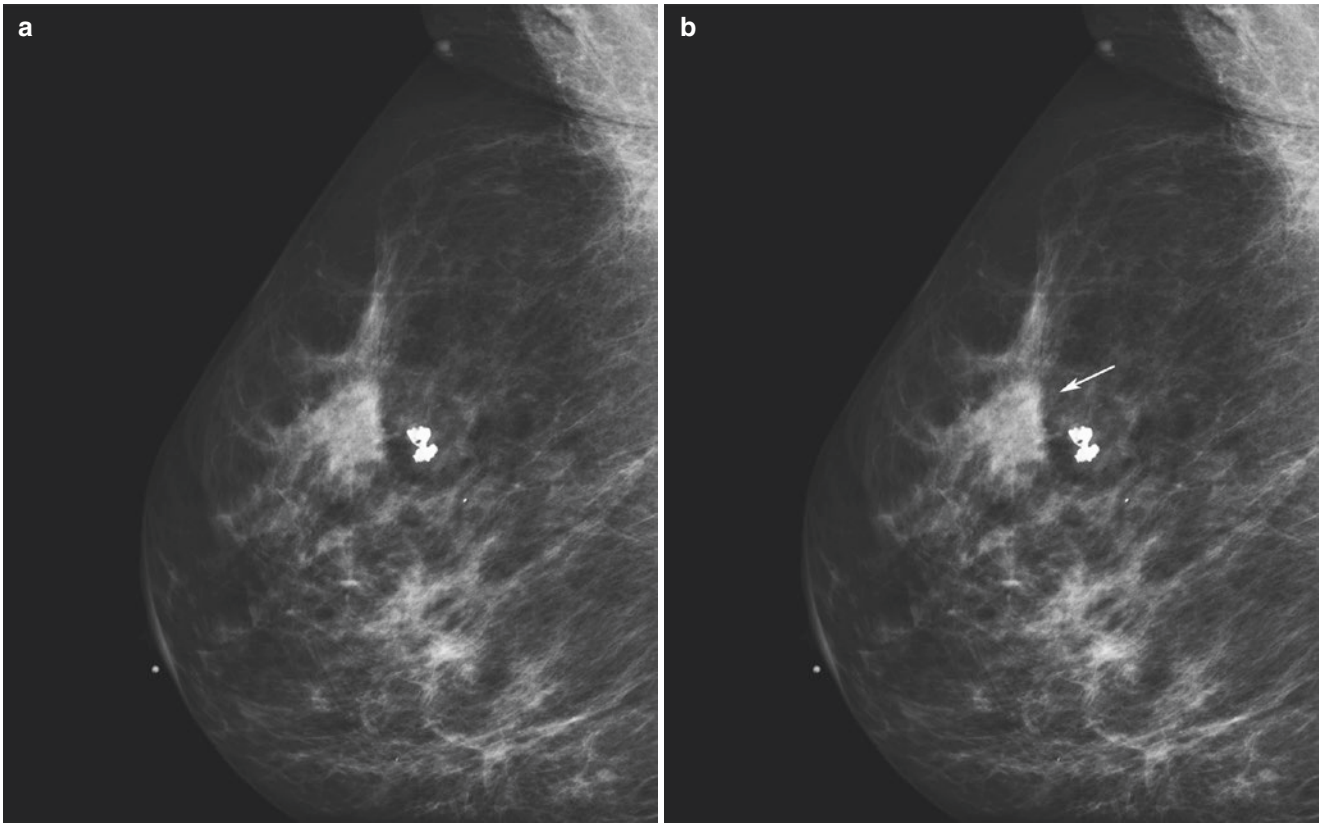

Fig. 3.167 (**a**) ML view (mammogram) of the left breast. (**b**) Multifocal IDC; preoperative MRI for surgical planning. There is a 1.8 cm irregular dense mass (*arrow*) in the upper mid left breast, which underwent biopsy yielding invasive ductal carcinoma

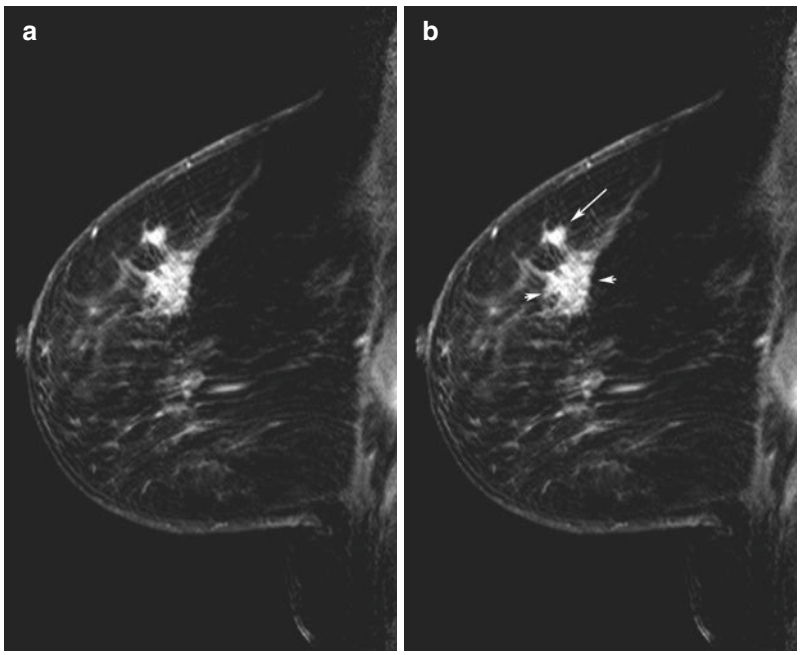

Fig. 3.168 (**a**) Selected sagittal T1 post-contrast MRI image of the left breast. (**b**) Corresponding MRI image demonstrates 1.8 cm irregular enhancing mass (*arrowheads*) in the upper mid breast. Additional 7 mm irregular mass (*arrow*) is noted 1 cm superior to the index mass suspicious for multifocal disease

3.38 Pre-operative Planning

Teaching Points Pre-operative breast MRI can identify 10–30 % of additional cancers that are mammographically occult. Multifocal disease is defined as additional cancer(s) occurring within the same quadrant, usually in close proximity to the index mass. These patients can still undergo breast conservation. Breast MRI can be helpful in pre-operative planning to include the additional areas of concern as illustrated in this case.

Image Findings

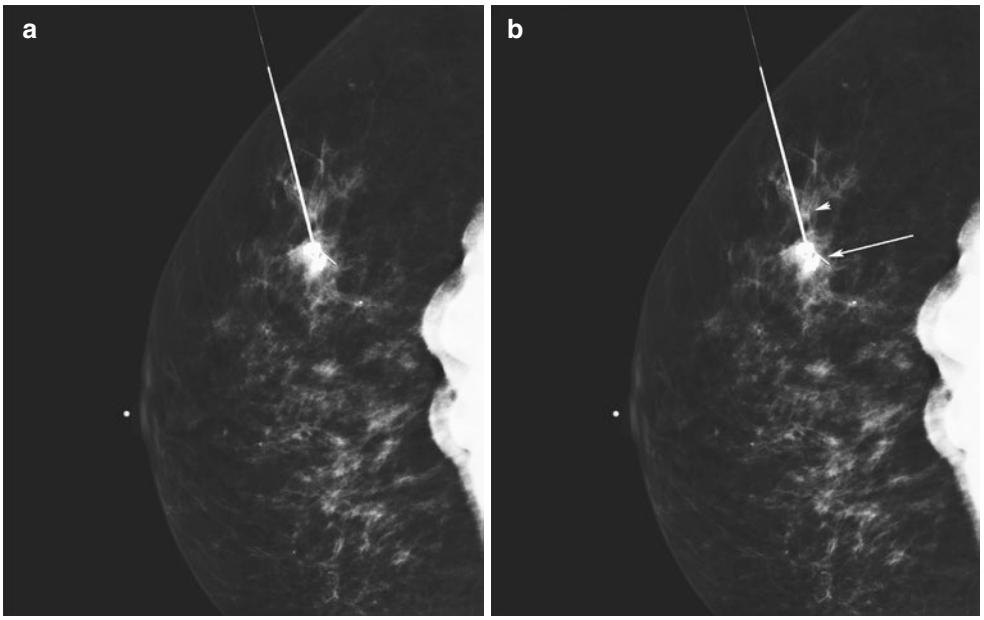

Fig. 3.169 (**a**) Ml view (mammogram) of the left breast from preoperative needle localization. (**b**) Superior approach was used for pre-operative wire placement to include the additional area of enhancement (*arrowhead*) identified on MRI and the tip of the wire at the known cancer (*arrow*). Surgical pathology yielded 1.9 cm IDC and additional 0.9 IDC, likely corresponding to the imaging findings

3.39 History

33-year-old patient undergoing MRI-guided biopsy (Figs. 3.170 and 3.171).

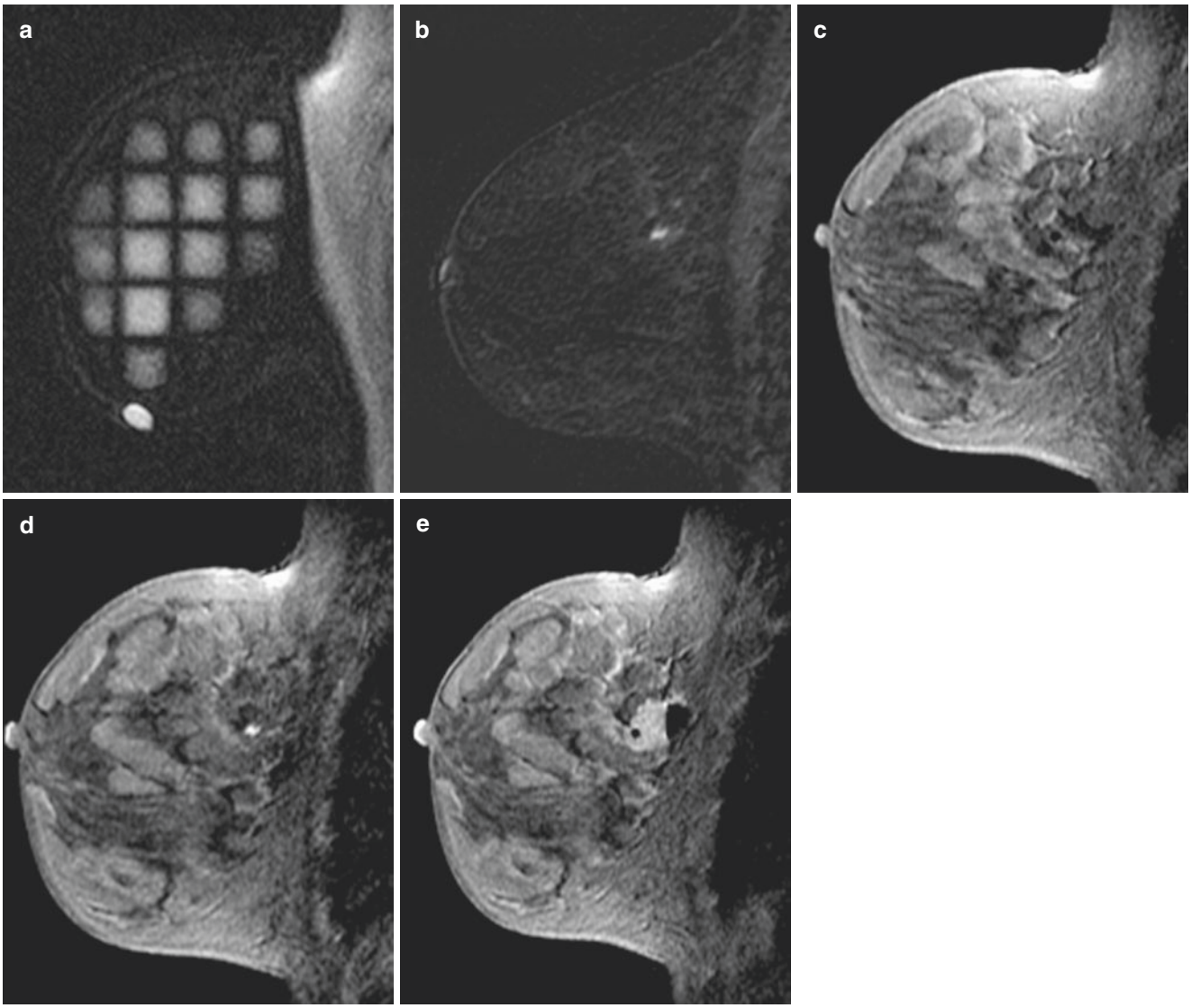

Fig. 3.170 (**a**) Sagittal image of the peripheral left breast at the level of the localizing grid. (**b**) Sagittal T1 post-contrast subtracted image at the level of the biopsy target. (**c**–**e**) Sagittal T1 post-contrast image at the level of the superficial breast and at the level of the biopsy target during the biopsy

3.39 MRI-Guided Biopsy

Teaching Points MRI-guided core biopsy technique has evolved over the past years. Currently, the most widely used system utilizes a vacuum-assisted devise and a localizing grid. Biopsy in this case was performed with a commercially available 9-gauge vacuum-assisted MRI-compatible biopsy system (ATEC Breast Biopsy System; Suros Surgical Systems, Indianapolis, IN). A vitamin E marker is taped on the skin of the breast/grid and its position is marked on a transparency diagram for localizing purposes. Post-contrast images are reviewed and a cursor is placed over the targeted lesion on the monitor. The x-axis and y-axis coordinates of the target were calculated on the basis of the spatial relationship between the lesion, vitamin E marker, and grid lines. The z-axis (depth) of the lesion was determined by calculating the distance between the lesion and the skin surface. The obturator is placed inside the white introducer, and the depth stop is set to the calculated depth. The tip of the obturator, which is visualized as a round signal void, is placed in close proximity to the targeted lesion. The tip of the obturator marks the center of the biopsy collection device. After tissue sampling is complete, the device is removed, the obturator reinserted, and post-biopsy MRI is performed to determine if the appropriate area underwent biopsy, which is noted with an absent area of enhancement and replacement with hematoma cavity. The biopsy site is marked with a titanium clip and post-biopsy MRI may be obtained to assess for clip deployment.

Image Findings

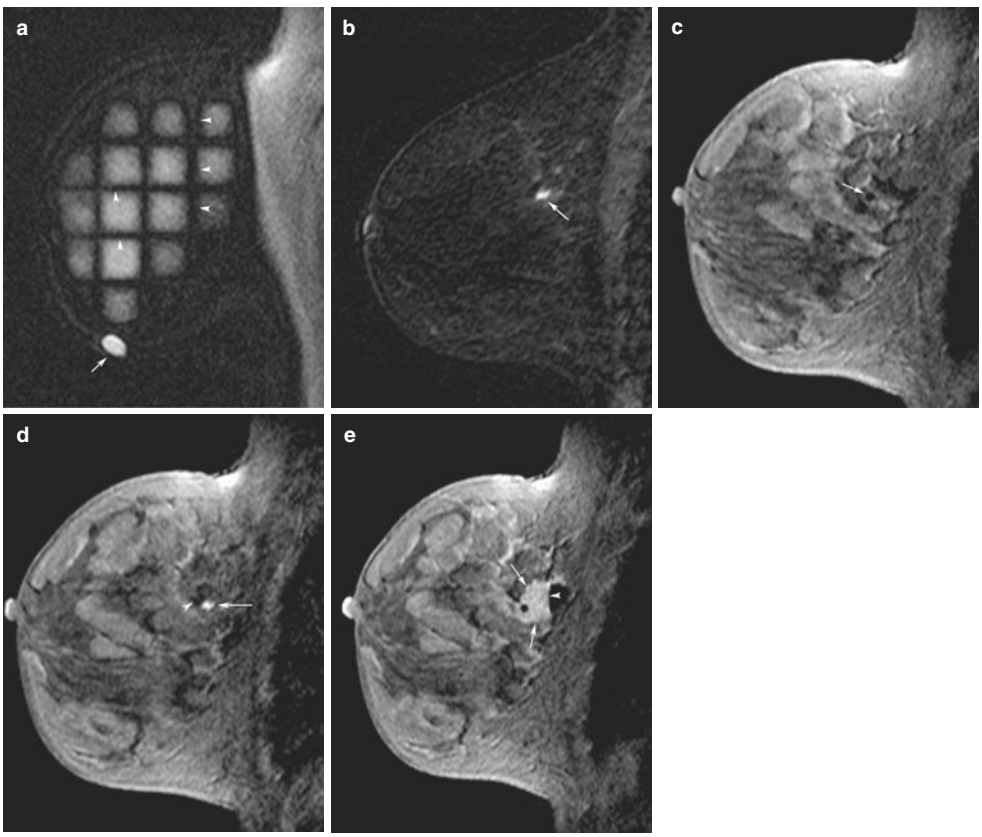

Fig. 3.171 MRI guided core biopsy. (**a**) Sagittal image of the peripheral breast demonstrates the grid (*arrowheads*) and vitamin E marker (*arrow*) used as a fiducial marker. (**b**) Post-contrast image demonstrates a 5 mm mass (*arrow*) in the posterior upper breast. (**c**) Select sagittal image demonstrates a round signal void (*arrow*) corresponding to the obturator entering the superficial breast. (**d**) Sagittal image at the level of the targeted mass (*arrow*) shows appropriate adjacent position of the obturator tip (*arrowhead*). (**e**) Post-biopsy sagittal image demonstrates non-visualization of the targeted enhancement at the same level denoted by the obturator tip with the presence of a layering hemorrhage (*arrows*) with an air fluid level (*arrowhead*)

3.40 History

45-year-old woman with newly diagnosed right breast ILC (Figs. 3.172 and 3.173).

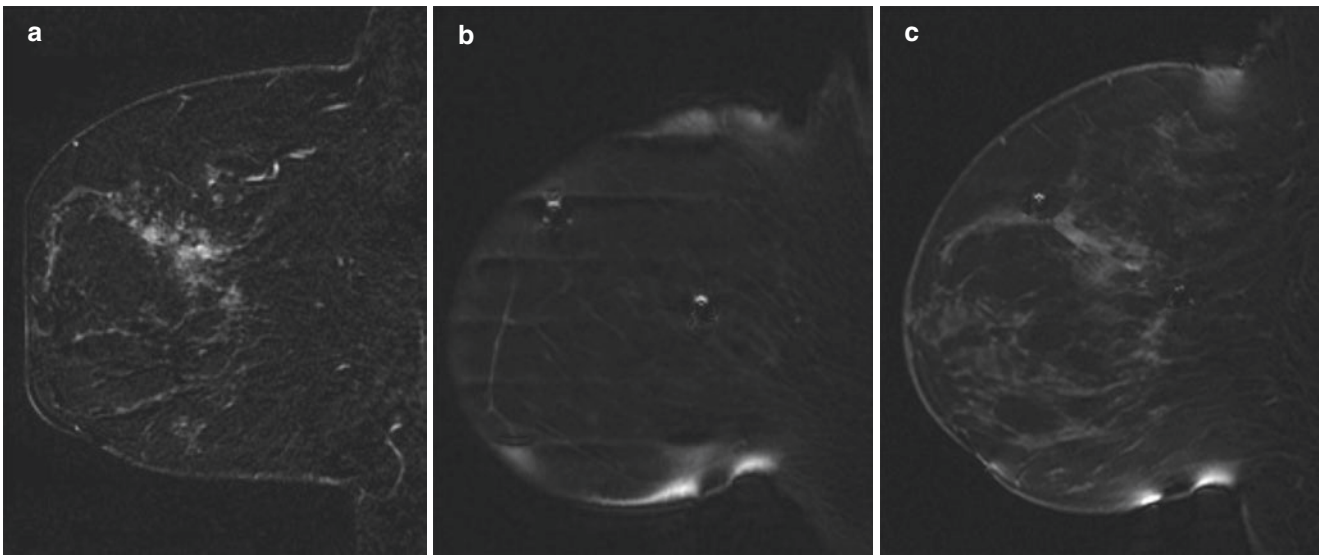

Fig. 3.172 (**a**) Selected sagittal T1 post-contrast subtracted image of the right breast at the level of the known cancer. (**b**) Selected image of the right breast at the level of the localizing grid. (**c**) Selected sagittal T1 post-contrast subtracted image of the right breast at the level of the known cancer with bracketing needles

3.40 MRI-Guided Wire Localization

Teaching Points MRI-guided needle localization including bracketing as illustrated in this case can be performed quickly and safely with commercially available equipment. This is most useful for localizing cancers best delineated on MRI such as ILC. The positive predictive value of MRI-guided needle localization was comparable to the mammographically guided needle localization.

Image Findings

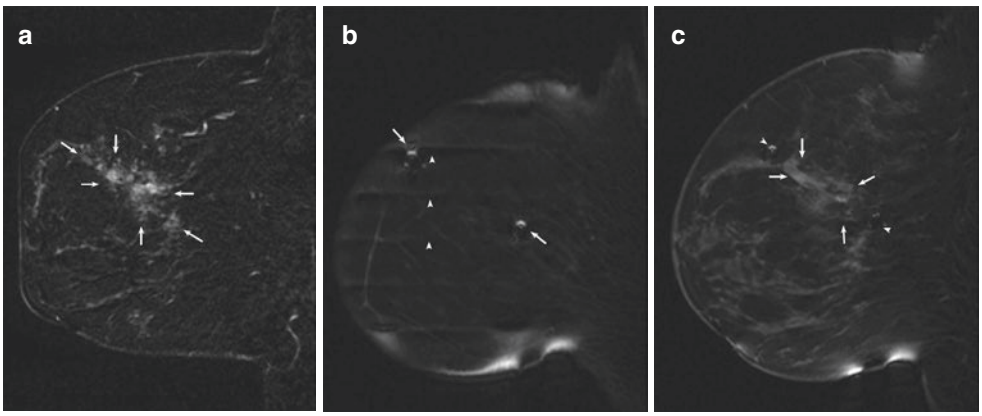

Fig. 3.173 MR-guided needle bracketed localization of invasive lobular carcinoma best seen on MRI. (**a**) Sagittal T1 post-contrast subtraction image of the right breast demonstrating a 4 cm region of heterogeneous non-mass enhancement in the upper breast (*arrows*) likely corresponding to ILC. (**b**) Select sagittal image demonstrating the localizing grid (*arrowheads*) and susceptibility artifact from two MR-compatible needles (*arrows*) used for bracketed needle localization. (**c**) Select sagittal image demonstrates the needles (*arrowhead*) bracketing the anterior and posterior extent of the non-mass enhancement (*arrows*)

Suggested Reading

American College of Radiology. ACR practice parameter for the performance of contrast enhanced magnetic resonance imaging (MRI) of the breast. Amended 2014 (Resolution 39).

Ballard LJ, Ballard GR. High-grade ductal carcinoma in situ: an overview for the radiologist. J Am Osteopath Coll Radiol. 2013;2:18–25.

Brandão AC, Lehman CD, Partridge SC. Breast magnetic resonance imaging: diffusion-weighted imaging. Magn Reson Imaging Clin N Am. 2013;21(2):321–36.

Behjatnia B, Sim J, Bassett LW, Moatamed NA, Apple SK. Does size matter? Comparison study between MRI, gross, and microscopic tumor sizes in breast cancer in lumpectomy specimens. Int J Clin Exp Pathol. 2010;3:303–9.

Castellano I, Marchiò C, Tomatis M, Ponti A, Casella D, Bianchi S, et al. Micropapillary ductal carcinoma in situ of the breast: an interinstitutional study. Mod Pathol. 2010;23(2):260–9.

Chan S, Chen JH, Agrawal G, Lin M, Mehta RS, Carpenter PM, et al. Characterization of pure ductal carcinoma in situ on dynamic contrast-enhanced MR imaging: do nonhigh grade and high grade show different imaging features? J Oncol. 2010. doi:10.1155/2010/431341.

Córdoba O, Llurba E, Saura C, Rubio I, Ferrer Q, Cortés J, Xercavins J. Multidisciplinary approach to breast cancer diagnosed during pregnancy: maternal and neonatal outcomes. Breast. 2013;22:515–9.

D'Alonzo M, Martincich L, Biglia N, Pisacane A, Maggiorotto F, Rosa GD, et al. Clinical and radiological predictors of nipple-areola complex involvement in breast cancer patients. Eur J Cancer. 2012;48:2311–8.

de Bresser J, de Vos B, van der Ent F, Hulsewé K. Breast MRI in clinically and mammographically occult breast cancer presenting with an axillary metastasis: a systematic review. Eur J Surg Oncol. 2010;36:114–9.

Devon RK, Rosen M, Mies C, Orel S. Breast reconstruction with a transverse rectus abdominis myocutaneous flap: spectrum of normal and abnormal MR imaging findings. Radiogaphics. 2004;24:1287–99.

Ecanow JS, Abe H, Newstead GM, Ecanow DB, Jeske JM. Axillary staging of breast cancer: what the radiologist should know. Radiographics. 2013;33:1589–612.

Elson BC, Helvie MA, Frank TS, Wilson TE, Adler DD. Tubular carcinoma of the breast: mode of presentation, mammographic appearance, and frequency of nodal metastases. AJR Am J Roentgenol. 1993;161:1173–6.

Fischer U, Vosshenrich R, Döler W. MR imaging-guided breast intervention: experience with two systems. Radiology. 1995;195(2):533–8.

Fisher ER, Land SR, Saad RS, Fisher B, Wickerham DL, Wang M, et al. Pathologic variables predictive of breast events in patients with ductal carcinoma in situ. Am J Clin Pathol. 2007;128(1):86–91.

Greenwood HI, Heller SL, Kim S, Sigmund EE, Shaylor SD, Moy L. Ductal carcinoma in situ of the breasts: review of MR imaging features. Radiographics. 2013;33:1569–88.

Holland R, Schuurmans Stekhoven JH, Hendriks JHC, Verbeek ALM, Mravunac M. Extent, distribution, and mammographic/histological correlations of breast ductal carcinoma in situ. Lancet. 1990;335(8688):519–22.

Howard MA, Polo K, Pusic AL, Cordeiro PG. Breast cancer local recurrence after mastectomy and TRAM flap reconstruction: incidence and treatment options. Plastic Reconstr Surg. 2006;117(5):1381–6.

Iima M, Le Bihan D, Okumura R, Okada T, Fujimoto K, Kanao S, et al. Apparent diffusion coefficient as an MR imaging biomarker of low-risk ductal carcinoma in situ: a pilot study. Radiology. 2011;260(2):364–72.

Jaffer S, Bleiweiss IJ. Histologic classification of ductal carcinoma in situ. Microsc Res Tech. 2002;59(2):92–101.

Jeong SJ, Lim HS, Lee JS, Park MH, Yoon JH, Park JG, Kang HK. Medullary carcinoma of the breast: MRI findings. AJR Am J Roentgenol. 2012;198:W482–7.

Kawashima M, Tamaki Y, Nonaka T, Higuchi K, Kimura M, Koida T, et al. MR imaging of mucinous carcinoma of the breast. AJR Am J Roentgenol. 2002;179:179–83.

Kim HS, Seok JH, Cha ES, Kang BJ, Kim HH, Seo YJ. Significance of nipple enhancement of Paget's disease in contrast enhanced breast MRI. Arch Gynecol Obstet. 2010;282:157–62.

Kitagawa K, Sakuma H, Ishida N, Hirano T, Ishihara A, Takeda K. Contrast-enhanced high-resolution MRI of invasive breast cancer: correlation with histopathologic subtypes. AJR Am J Roentgenol. 2004;183:1805–9.

Lauby-Secretan B, Scoccianti C, Loomis D, Benbrahim-Tallaa L, Bouvard V, Bianchini F, et al. Breast-cancer screening--viewpoint of the IARC Working Group. N Engl J Med. 2015;372(24):2353–8.

Lee SC, Jain PA, Jethwa SC, Tripathy D, Yamashita MW. Radiologist's role in breast cancer staging: providing key information for clinicians. Radiographics. 2014;34:330–42.

Lee YS, Mathew J, Dogan BE, Resetkova E, Huo L, Yang WT. Imaging features of micropapillary DCIS: correlation with Clinical and Histopathological Findings. Acad Radiol. 2011;18(7):797–803.

Lehman C, Aikawa T. MR-guided vacuum-assisted breast biopsy: accuracy of targeting and success in sampling in a phantom model. Radiology. 2004;232(3):911–4.

Lehman CD, Gatsonis C, Kuhl CK, Hendrick RE, Pisano ED, Hanna L, et al.; ACRIN Trial 6667 Investigators Group. MRI evaluation of the contralateral breast in women with recently diagnosed breast cancer. N Engl J Med. 2007;356:1295–303.

Leonard GD, Swain SM. Ductal carcinoma in situ, complexities and challenges. J Natl Cancer Inst. 2004;96:906–20.

Liberman L, Feng TL, Susnik B. Case 35: intracystic papillary carcinoma with invasion. Radiology. 2001;219:781–4.

Lim HS, Jeong SJ, Lee JS, Park MH, Kim JW, Shin SS, et al. Paget disease of the breast: mammographic, US, and MR imaging findings with pathologic correlation. Radiographics. 2011;31:1973–87.

Linda A, Zuiani C, Girometti R, Londero V, Machin P, Brondani G, Bazzocchi M. Unusual malignant tumors of the breast: MRI features and pathologic correlation. Eur J Radiol. 2010;75:178–84.

Lopez JK, Bassett LW. Invasive lobular carcinoma of the breast: spectrum of mammographic, US, and MR imaging findings. Radiographics. 2009;29:165–76.

Mann RM. The effectiveness of MR imaging in the assessment of invasive lobular carcinoma of the breast. Magn Reson Imaging Clin N Am. 2010;18:259–76.

Mann RM, Hoogeveen YL, Blickmann JG, Boetes C. MRI compared to conventional diagnostic work-up in the detection and evaluation of invasive lobular carcinoma of the breast: a review of existing literature. Breast Cancer Res Treat. 2008;107:1–14.

Mann RM, Loo CE, Wobbes T, Bult P, Barentsz JO, Gilhuijs KG, Boetes C. The impact of preoperative breast MRI on the re-excision rate in invasive lobular carcinoma of the breast. Breast Cancer Res Treat. 2010;119:415–22.

Memis A, Ozdemir N, Parildar M, Ustun EE, Erhan Y. Mucinous (colloid) breast cancer: mammographic and US features with histologic correlation. Eur J Radiol. 2000;35:39–43.

Meyer JE, Amin E, Lindfors KK, Lipman JC, Stomper PC, Genest D. Medullary carcinoma of the breast: mammographic and US appearance. Radiology. 1989;170:79–82.

Monzawa S, Yokokawa M, Sakuma T, Takao S, Hirokaga K, Hanioka K, Adachi S. Mucinous carcinoma of the breast: MRI features of pure and mixed forms with histopathologic correlation. AJR Am J Roentgenol. 2009;192:W125–31.

Moon JY, Chang YW, Lee EH, Seo DY. Malignant invasion of the nipple-areolar complex of the breast: usefulness of breast MRI. AJR Am J Roentgenol. 2013;201:448–55.

Morris E, Liberman L, Dershaw DD, Kaplan JB, LaTrenta LR, Abramson AF, et al. Preoperative MR imaging-guided needle localization of breast lesions. AJR Am J Roentgenol. 2002;178(5):1211–20.

Morris EA, Schwartz LH, Drotman MB, Kim SJ, Tan LK, Liberman L, et al. Evaluation of pectoralis major muscle in patients with posterior breast tumors on breast MR images: early experience. Radiology. 2000;214:67–72.

Morris EA. Should we dispense with preoperative breast MRI? Lancet. 2010;375:528–30.

Morrow M. Magnetic resonance imaging in breast cancer. One step forward, two steps back? JAMA. 2004;292:2779–80.

Muttarak M, Siriya B, Kongmebhol P, Chaiwun B, Sukhamwang N. Paget's disease of the breast: clinical, imaging and pathologic findings: a review of 16 patients. Biomed Imaging Interv J. 2011;7:e16.

Neal CH, Daly CP, Nees AV, Helvie MA. Can preoperative axillary US help exclude N2 and N3 metastatic breast cancer? Radiology. 2010;257:335–41.

Olson Jr JA, Morris EA, Van Zee KJ, Linehan DC, Borgen PI. Magnetic resonance imaging facilitates breast conservation for occult breast cancer. Ann Surg Oncol. 2000;7:411–5.

Orel SG, Weinstein SP, Schnall MD, Reynolds CA, Schuchter LM, Fraker DL, Solin LJ. Breast MR imaging in patients with axillary node metastases and unknown primary malignancy. Radiology. 1999;212:543–9.

Partridge SC, McDonald ES. Diffusion weighted magnetic resonance imaging of the breast: protocol optimization, interpretation, and clinical applications. Magn Reson Imaging Clin N Am. 2013;21(3):601–24.

Peng C, Chang B, Tso H, Flowers C. MRI appearance of tumor recurrence in myocutaneous flap reconstruction after mastectomy. Am J Roentgenol. 2011;196:W471–5.

Peters NH, van Esser S, van den Bosch MA, Storm RK, Plaisier PW, van Dalen T, et al. Preoperative MRI and surgical management in patients with nonpalpable breast cancer: the MONET – randomised controlled trial. Eur J Cancer. 2011;47:879–86.

Pilewskie M, Olcese C, Eaton A, Patil S, Morris E, Morrow M, et al. Perioperative breast MRI is not associated with lower locoregional recurrence rates in DCIS patients treated with or without radiation. Ann Surg Oncol. 2014;21(5):1552–60.

Rahbar H, Partridge SC, DeMartini WB, Gutierrez RL, Allison KH, Peacock S, et al. In vivo assessment of ductal carcinoma in situ grade: a model incorporating dynamic contrast-enhanced and diffusion-weighted breast MR imaging parameters. Radiology. 2012;263(2):374–82.

Rahbar H, Partridge SC, Eby PR, Demartini WB, Gutierrez RL, Peacock S, Lehman CD. Characterization of ductal carcinoma in situ on diffusion weighted breast MRI. Eur Radiol. 2011;21(9):2011–9.

Rodríguez MC, Secades AL, Angulo JM. Best cases from the AFIP: intracystic papillary carcinoma of the breast. Radiographics. 2010;30:2021–7.

Sabate JM, Clotet M, Torrubia S, Gomez A, Guerrero R, de las Heras P, Lerma E. Radiologic evaluation of breast disorders related to pregnancy and lactation. Radiographics. 2007;27:S101–24.

Sakamoto N, Tozaki M, Hoshi K, Fukuma E. Is MRI useful for the prediction of nipple involvement? Breast Cancer. 2013;20:316–22.

Santamaría G, Velasco M, Bargalló X, Caparrós X, Farrús B, Luis Fernández P. Radiologic and pathologic findings in breast tumors with high signal intensity on T2-weighted MR images. Radiographics. 2010;30:533–48.

Schnall MD, Blume J, Bluemke DA, Deangelis GA, Debruhl N, Harms S, et al. MRI detection of distinct incidental cancer in women with primary breast cancer studied in IBMC 6883. J Surg Oncol. 2005;92:32–8.

Schneider E, Rohling K, Schnall M, Giaquinto RO, Morris EA, Ballon D. An apparatus for MR-guided breast lesion localization and core biopsy: design and preliminary results. J Magn Reson Imaging. 2001;14(3):243–53.

Scripcaru G, Zardawi IM. Mammary ductal carcinoma in situ: a fresh look at architectural patterns. Int J Surg Oncol. 2012;2012:979521.

Soo MS, Williford ME, Walsh R, Bentley RC, Kornguth PJ. Papillary carcinoma of the breast: imaging findings. AJR Am J Roentgenol. 1995;164:321–6.

Steen ST, Chung AP, Han SH, Vinstein AL, Yoon JL, Giuliano AE. Predicting nipple-areolar involvement using preoperative breast MRI and primary tumor characteristics. Ann Surg Oncol. 2013;20:633–9.

Turnbull L, Brown S, Harvey I, Olivier C, Drew P, Napp V, et al. Comparative effectiveness of MRI in breast cancer (COMICE) trial: a randomized controlled trial. Lancet. 2010;375:563–71.

Van Goethem M, Schelfout K, Dijckmans L, Van Der Auwera JC, Weyler J, Verslegers I, et al. MR mammography in the pre-operative staging of breast cancer in patients with dense breast tissue: comparison with mammography and ultrasound. Eur Radiol. 2004;14:809–16.

Vashi R, Hooley R, Butler R, Geisel J, Philpotts L. Breast imaging of the pregnant and lactating patient: physiologic changes and common benign entities. AJR Am J Roentgenol. 2013;200:329–36.

Wagner AE, Middleton LP, Whitman GJ. Intracystic papillary carcinoma of the breast with invasion. AJR Am J Roentgenol. 2004;183:1516.

Wells CJ, O'Donoghue C, Ojeda-Fournier H, Retallack HEG, Esserman LJ. Evolving paradigm for imaging, diagnosis, and management of DCIS. J Am Coll Radiol. 2013;10(12):918–23.

Woodhams R, Matsunaga K, Kan S, et al. ADC mapping of benign and malignant breast tumors. Magn Reson Med Sci. 2005;4(1):35–42.

Yang WT, Tse GMK. Sonographic, mammographic, and histopathologic correlation of symptomatic ductal carcinoma in situ. Am J Roentgenol. 2004;182(1):101–10.

Yoo JL, Woo OH, Kim YK, Cho KR, Yong HS, Seo BK, et al. Can MR imaging contribute in characterizing well-circumscribed breast carcinomas? Radiographics. 2010;30:1689–702.

High Risk

4

Lauren Friedlander, Victoria Mango,
Karen Weinshelbaum, and Richard Ha

L. Friedlander, MD
Director of Breast and Body Imaging Fellowship,
Division of Breast Imaging, Assistant Professor of Radiology,
Columbia University Medical Center, New York, NY, USA
e-mail: lf2386@columbia.edu

V. Mango, MD
Director of Breast and Body Imaging Fellowship,
Breast Imaging Service, Memorial Sloan-Kettering Cancer Center,
Assistant Professor of Radiology, Weill Cornell Medical College,
New York, NY, USA
e-mail: vlm2125@columbia.edu

K. Weinshelbaum, MD
Department of Radiology, Newark Beth Israel Medical Center,
Newark, NJ, USA
e-mail: kbw747@gmail.com

R. Ha, MD (✉)
Director of Education and Research,
Division of Breast Imaging, Assistant Professor of Radiology,
Columbia University Medical Center, New York, NY, USA
e-mail: rh2616@cumc.columbia.edu

R. Ha et al. (eds.), Breast MRI Teaching Atlas, DOI 10.1007/978-1-4939-6409-3_4

4.1 History

25-year-old patient with Cowden syndrome undergoing screening breast MRI (Figs. 4.1, 4.2, 4.3, and 4.4).

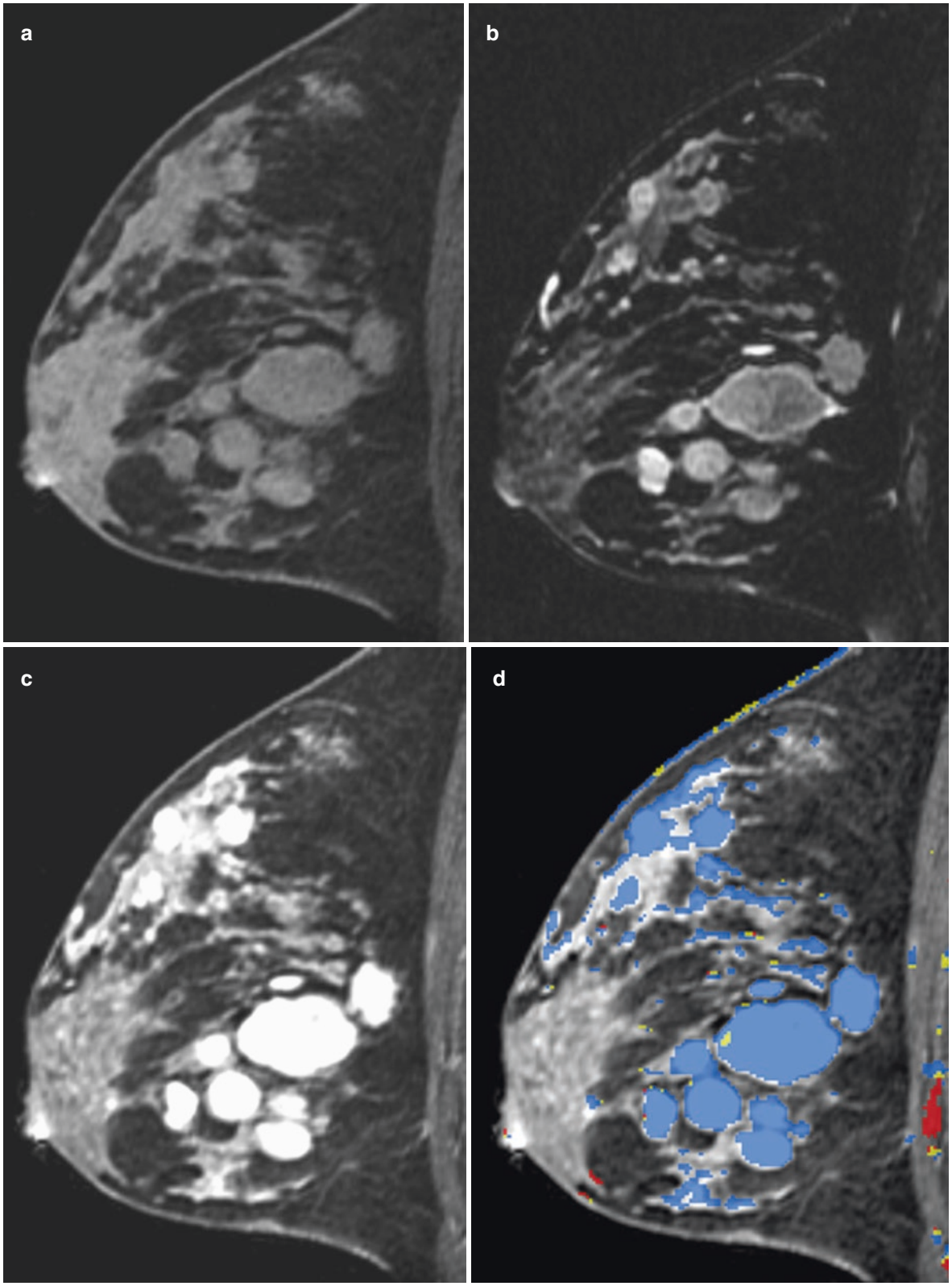

Fig. 4.1 Sagittal MRI images of the left breast. (**a**) T1-weighted fat-saturated image. (**b**) T2-weighted fat-saturated image. (**c**) T1-weighted fat-saturated post-contrast image, with corresponding computer-aided detection (CAD) kinetics analysis color overlay (**d**)

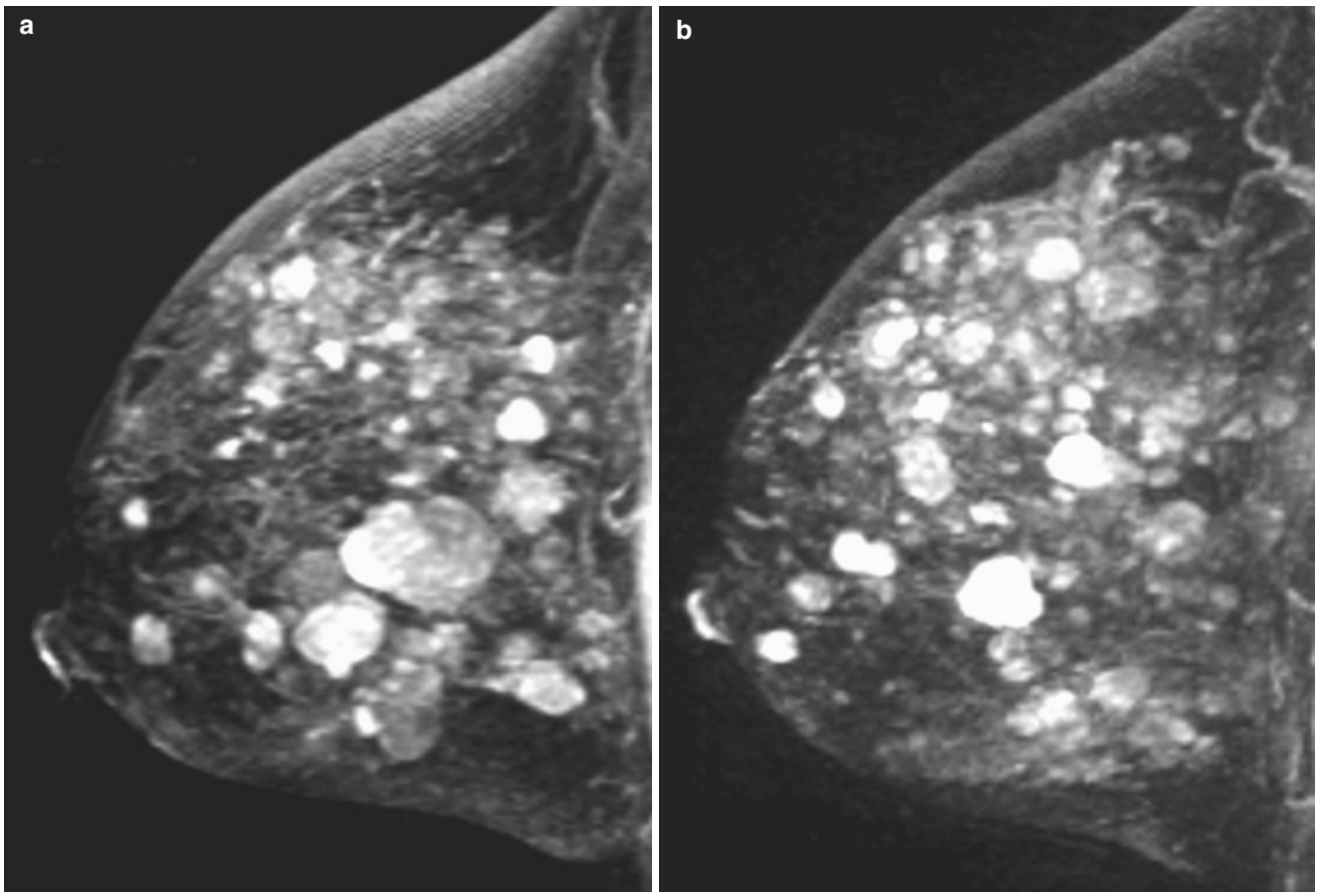

Fig. 4.2 Sagittal post-contrast subtraction maximum intensity projection (MIP) images of the left breast (**a**) and right breast (**b**)

4.1 Cowden Syndrome

Teaching Points Cowden syndrome is an uncommon, autosomal dominant disease in patients with the *PTEN* gene mutation. It is characterized by multiple hamartomas of the skin, mucous membranes, brain, breast, thyroid, and gastrointestinal tract and increased susceptibility to breast cancer. The lifetime risk for breast carcinoma in patients with Cowden syndrome is estimated to be 25–50 %, compared with 12 % in the general female population.

Patients with Cowden syndrome can have bilateral multiple fibroadenomas, as illustrated in this case, which makes breast cancer detection challenging. Fibroadenomas usually enhance homogeneously, have associated T2 hyperintensity and can demonstrate nonenhancing septations. The degree of enhancement and T2 signal intensity can vary. The National Comprehensive Cancer Network (NCCN) recommends breast self-examination beginning at the age of 18 years and annual screening with breast MRI and mammography starting between 30 and 35 years of age and not earlier than 25 years. After establishing a baseline, any change should prompt a workup to exclude malignancy.

Image Findings

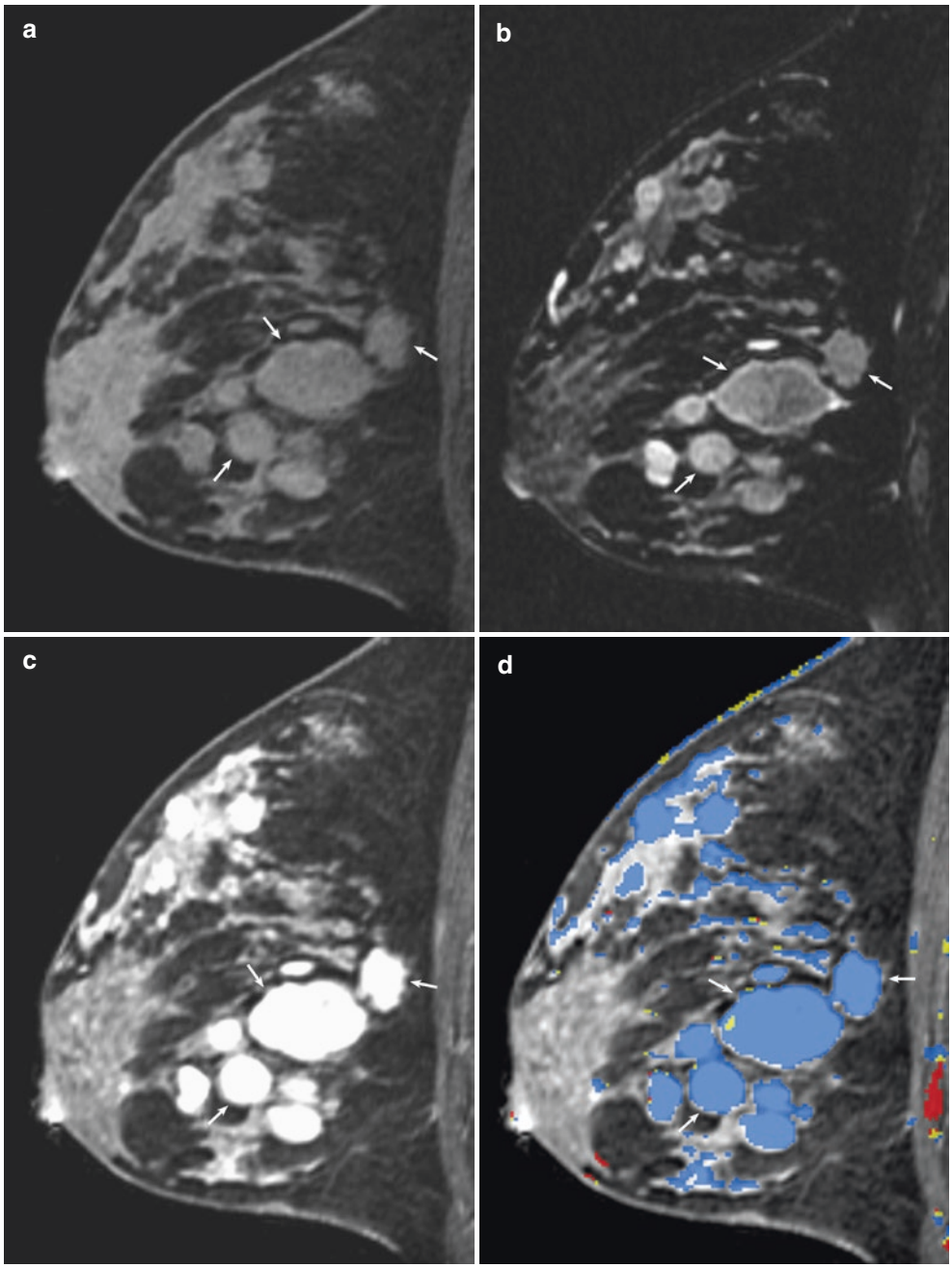

Fig. 4.3 MRI performed for multiple breast masses. A sagittal T1-weighted fat-saturated image (**a**) and a T2-weighted fat-saturated image (**b**) of the left breast demonstrate multiple masses with T1 hypointensity and T2 hyperintensity (*arrowhead*) and T1 hypointensity and T2 minimal to mild hyperintensity (*arrows*). A T1-weighted fat-saturated post-contrast image (**c**) shows homogeneous enhancement in these masses (*arrows*), with persistent delayed enhancement color-coded as blue on the CAD overlay (**d**)

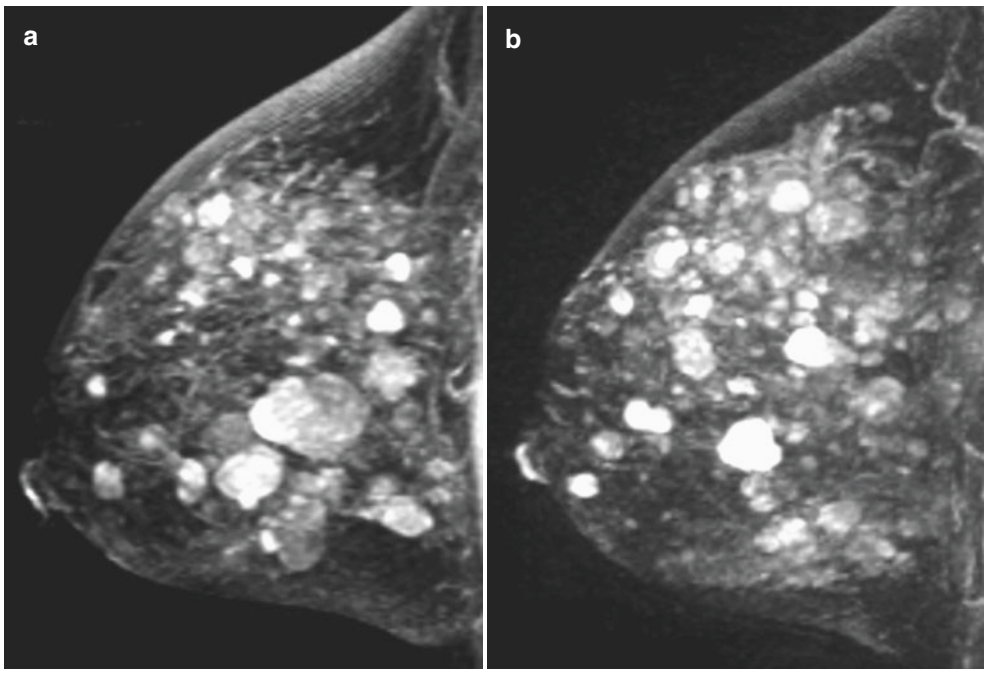

Fig. 4.4 Sagittal post-contrast subtraction MIP images of the left breast (**a**) and right breast (**b**) show multiple masses in both breasts

4.2 History

36-year-old woman with history of right breast cancer who underwent lumpectomy 3 years ago. Screening breast MRI (Figs. 4.5 and 4.6).

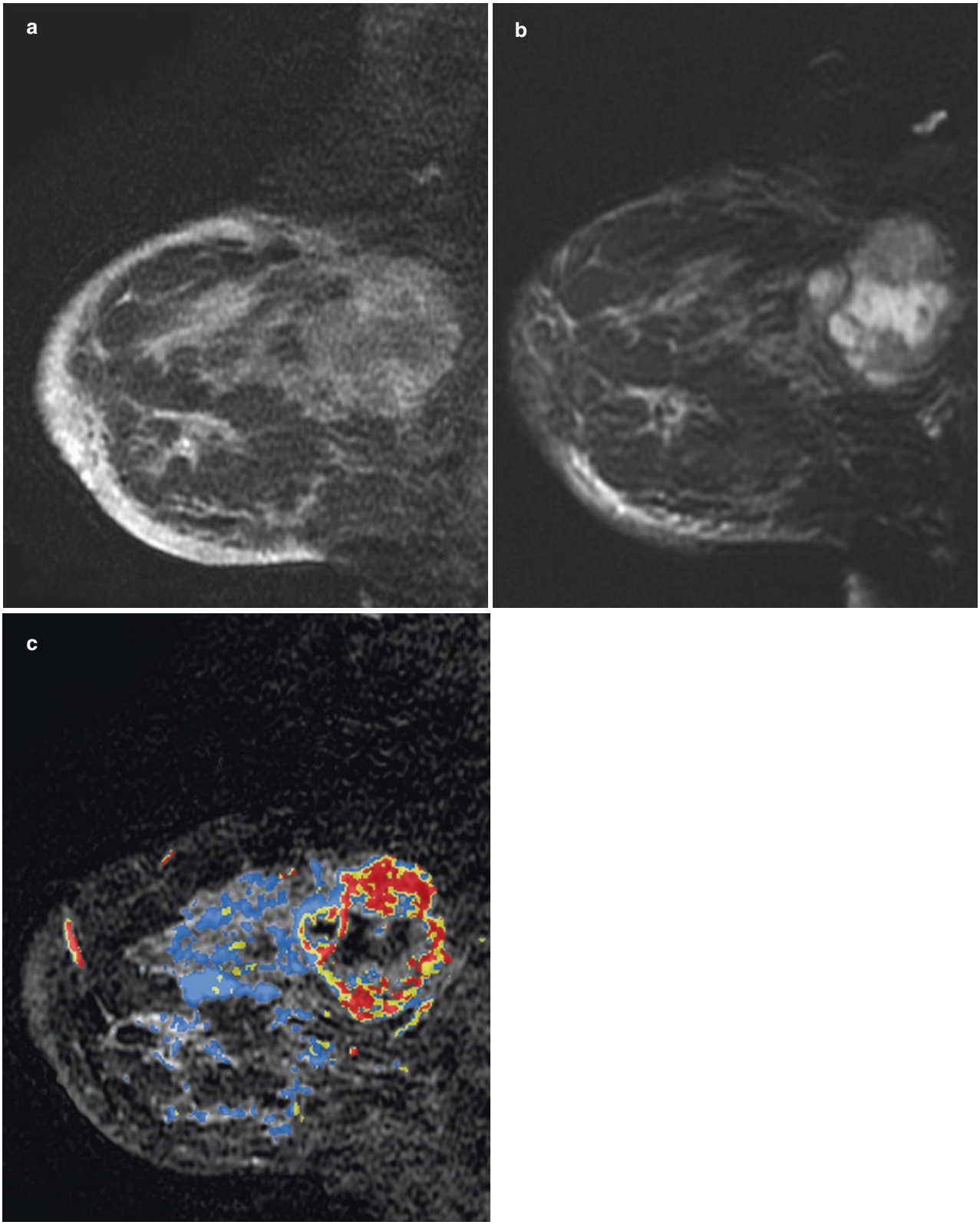

Fig. 4.5 Sagittal MRI images of the right breast. (**a**) T1-weighted fat-saturated. (**b**) T2-weighted fat-sturated. (**c**) Post-contrast subtraction with CAD color overlay

4.2 Personal History of Breast Cancer

Teaching Points Post-lumpectomy tumor recurrence rates are about 1–2 % per year, usually discovered later than 18–24 months after treatment. Detection of treatment failure in these women while still asymptomatic improves relative survival by 27–47 %.

The lumpectomy site is a common site of recurrence, as illustrated in this case. Patients with recurrence following initial treatment with lumpectomy and radiation are usually treated with salvage mastectomy. Breast MRI has a high sensitivity (94–100 %) in the detection of breast cancer. MRI screening of women with only a personal history of breast cancer was clinically valuable in finding malignancies in 12 % of the patients in a study published by Brennan et al. (2010), but personal history is generally not an accepted indication for screening breast MRI.

Image Findings

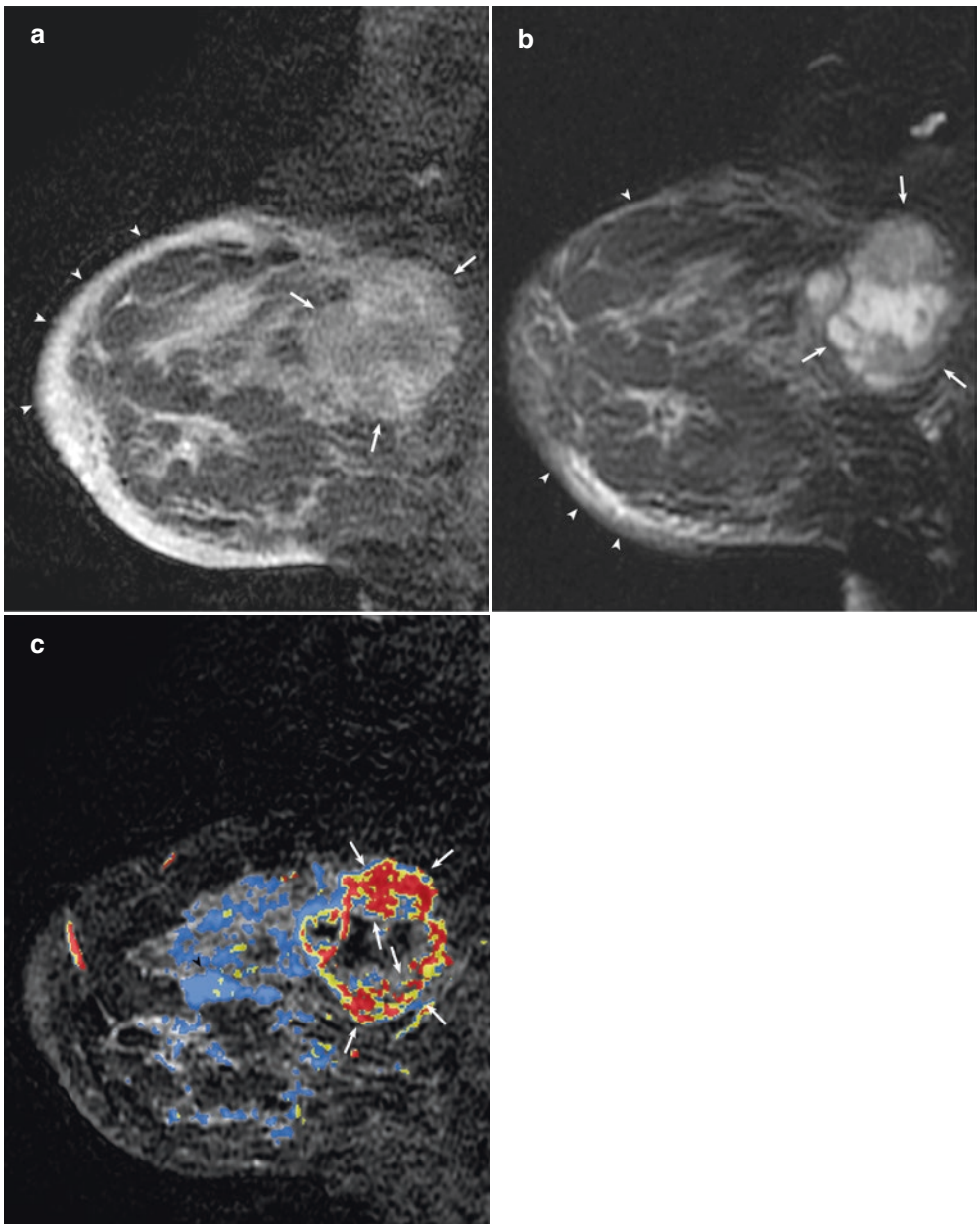

Fig. 4.6 Breast cancer recurrence. Sagittal T1-weighted pre-contrast (**a**) and T2-weighted (**b**) images of the right breast demonstrate post-radiation skin thickening (*arrowheads*) and the lumpectomy site (*arrows*), which is heterogeneously T2 hyperintense. (**c**) Sagittal T1-weighted FS post-contrast image with CAD color overlay demonstrates irregular thick rim enhancement with washout kinetics (*red, arrows*) and adjacent background parenchymal enhancement with persistent kinetics (*blue*)

4.3 History

33-year-old woman with *BRCA1* mutation undergoing high-risk screening mammogram and breast MRI (Figs. 4.7, 4.8, 4.9, and 4.10).

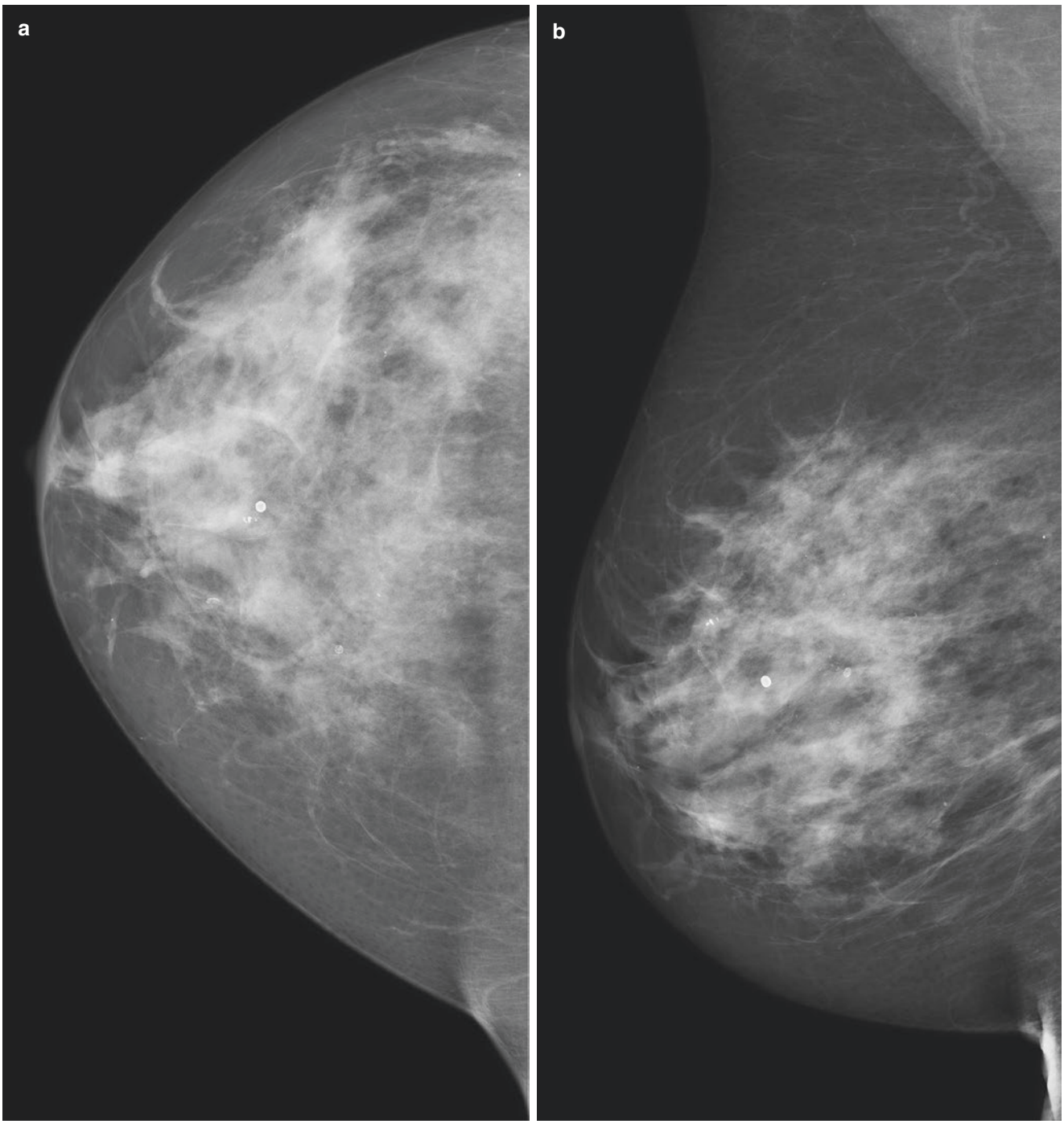

Fig. 4.7 Craniocaudal (CC) mammographic view (**a**) and mediolateral oblique (MLO) mammographic view (**b**) of the left breast

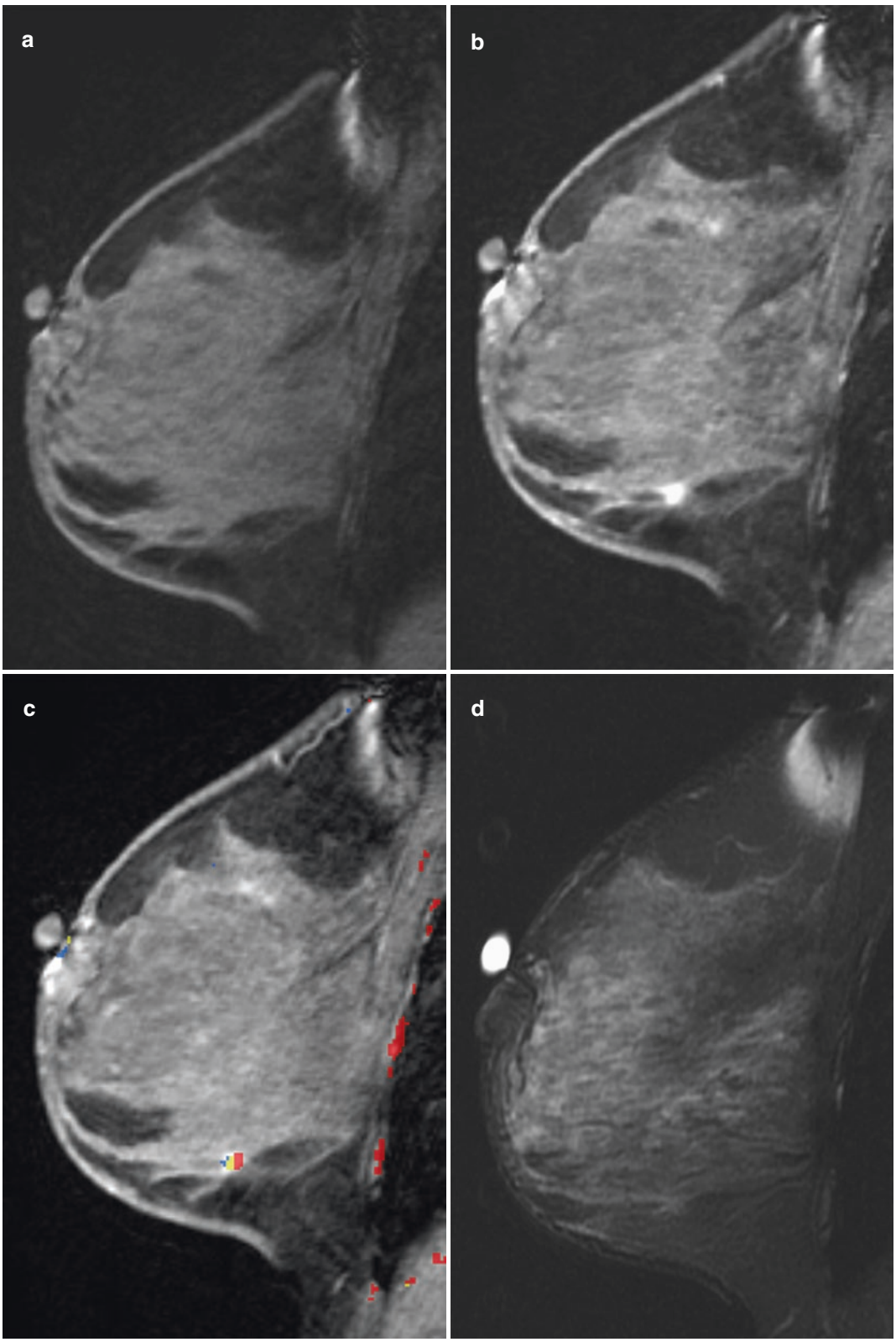

Fig. 4.8 Sagittal MR images of the left breast. T1-weighted fat-saturated pre-contrast image (**a**) and post-contrast image (**b**) with CAD color overlay (**c**). (**d**) T2-weighted fat-saturated image

4.3 *BRCA1* Mutation

Teaching Points Teaching points: see next companion case.

Image Findings

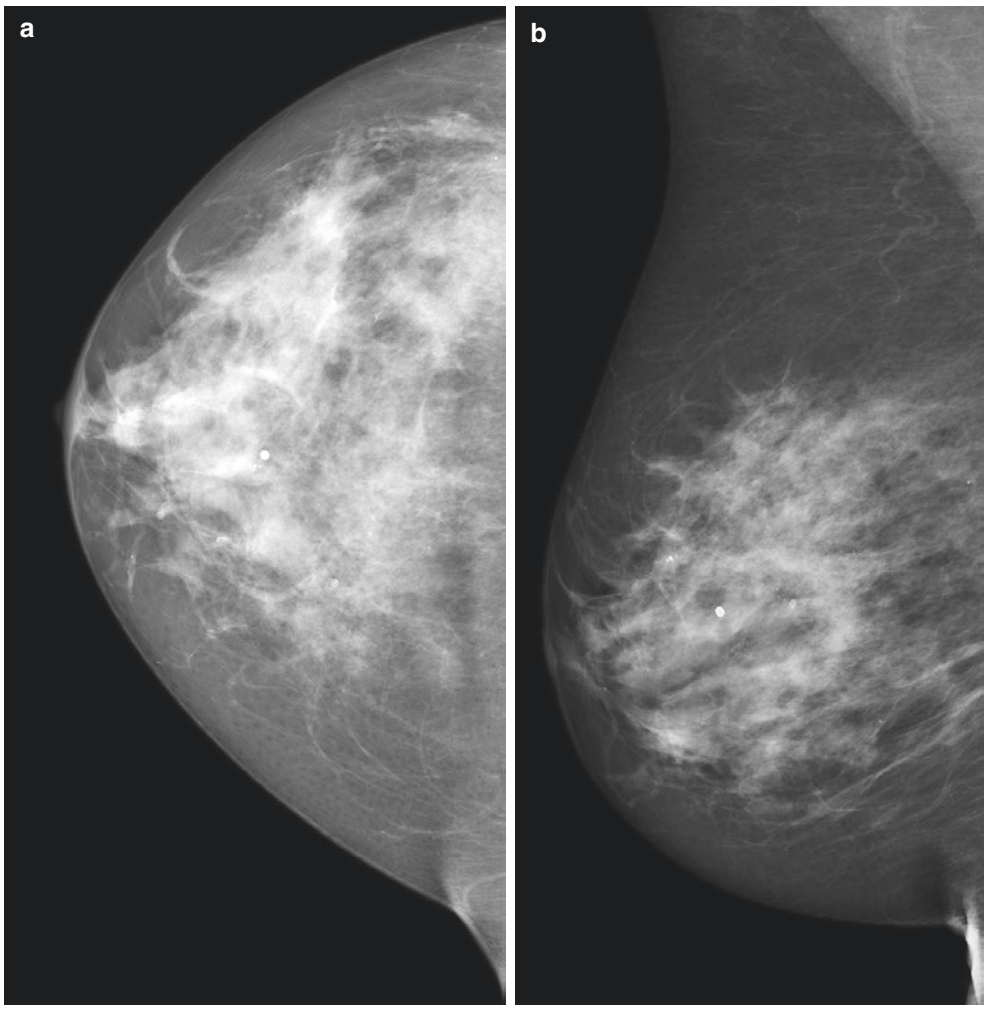

Fig. 4.9 Screening mammograms. CC view (**a**) and MLO view (**b**) of the left breast demonstrate heterogeneously dense tissue. There is no suspicious mass, architectural distortion, or microcalcifications

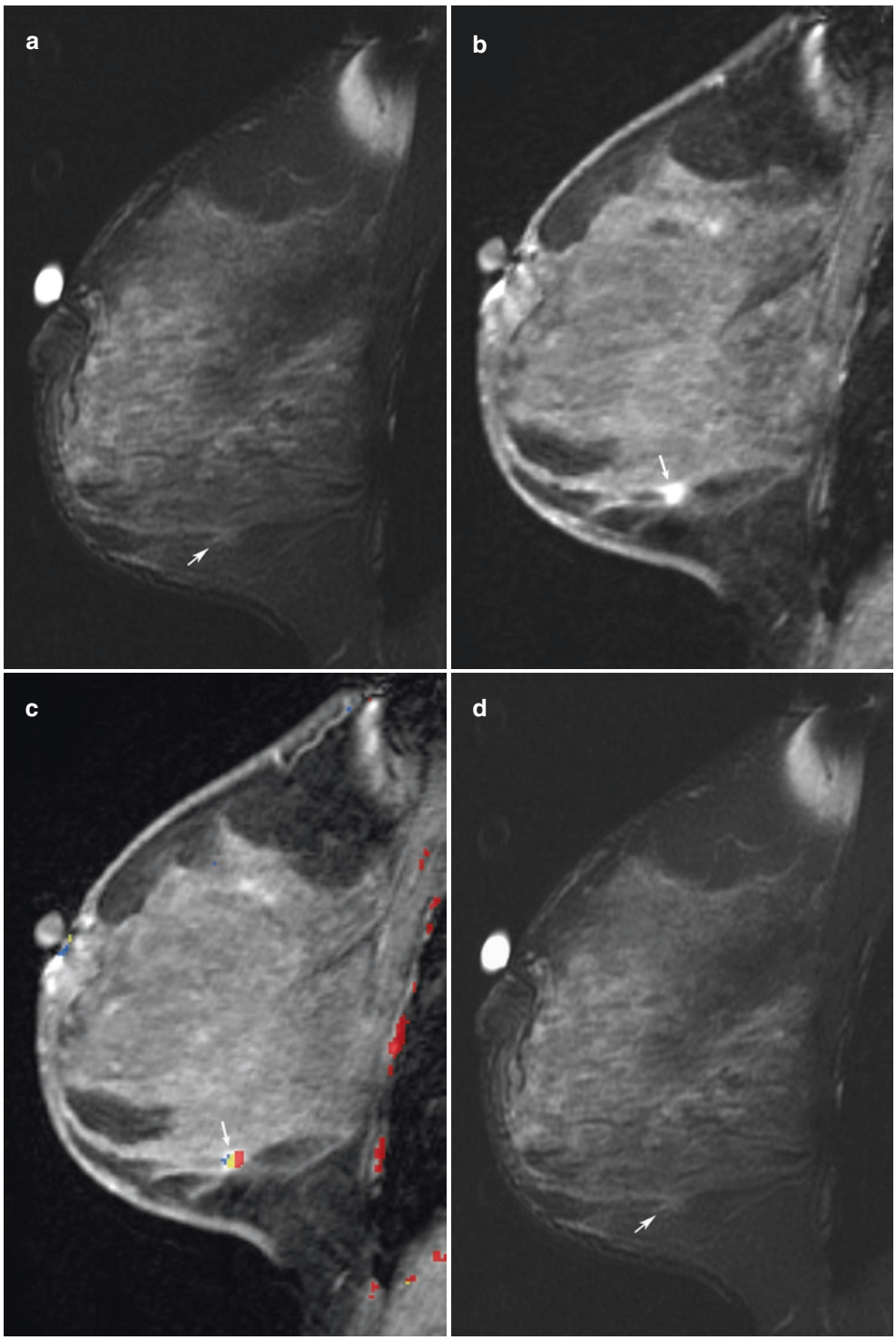

Fig. 4.10 Screening breast MRI. The sagittal T1-weighted fat-saturated pre-contrast image (**a**) and post-contrast image (**b**) demonstrate a suspicious, enhancing irregular mass in the lower breast (*arrow*). CAD analysis (**c**) demonstrates washout enhancement kinetics. No mammographic correlate was noted. The corresponding T2-weighted fat-saturated image (**d**) demonstrates no T2-hyperintense correlate (*arrow*)

4.4 History

33-year-old *BRCA2* mutation carrier undergoing screening breast MRI (Figs. 4.11 and 4.12).

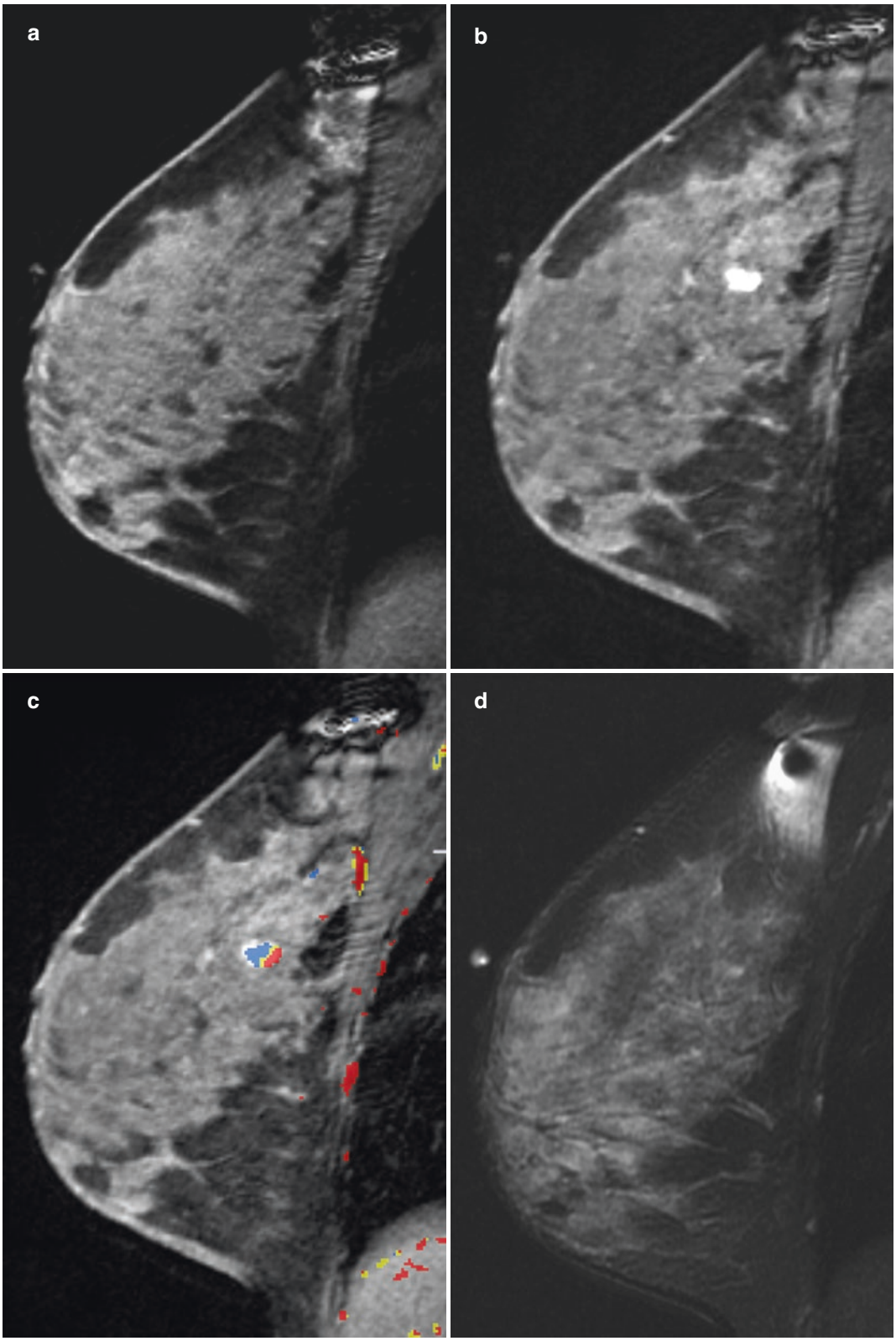

Fig. 4.11 Sagittal MR images of the right breast. T1-weighted fat-saturated pre-contrast image (**a**) and post-contrast image (**b**), with corresponding CAD color overlay image (**c**). (**d**) T2-weighted fat-saturated image

4.4 *BRCA2* Mutation

Teaching Points Although there is no direct evidence that screening with MRI will reduce mortality, it is thought that early detection by using annual MRI surveillance, in addition to mammography, may be useful for high-risk women. The American Cancer Society recommends that screening MRI should be performed for women who are at high risk for breast cancer, based on certain factors:

- Women with 20–25 % or greater lifetime risk of breast cancer, according to risk assessment tools that are based mainly on family history
- Women with known *BRCA1* or *BRCA2* gene mutation
- Women with a first-degree relative with a *BRCA1* or *BRCA2* gene mutation who have not had genetic testing themselves
- Women who had radiation therapy to the chest between the ages of 10–30 years
- Women who have Li-Fraumeni syndrome, Cowden syndrome, or Bannayan-Riley-Ruvalcaba syndrome or have first-degree relatives with one of these syndromes

BRCA1 and *BRCA2* are tumor-suppressor genes that play a role in DNA repair; mutations in either gene are associated with an autosomal dominant inherited form of breast and/or ovarian cancer. The two cases illustrate high sensitivity of breast MRI in detecting clinically favorable early breast cancers in patients with high risk for breast cancer, including patients with *BRCA1* and *BRCA2* gene mutations. Lack of a hyperintense T2 correlate should elevate the level of suspicion, and biopsy should be performed in these high-risk patients even without a corresponding sonographic correlate.

Image Findings

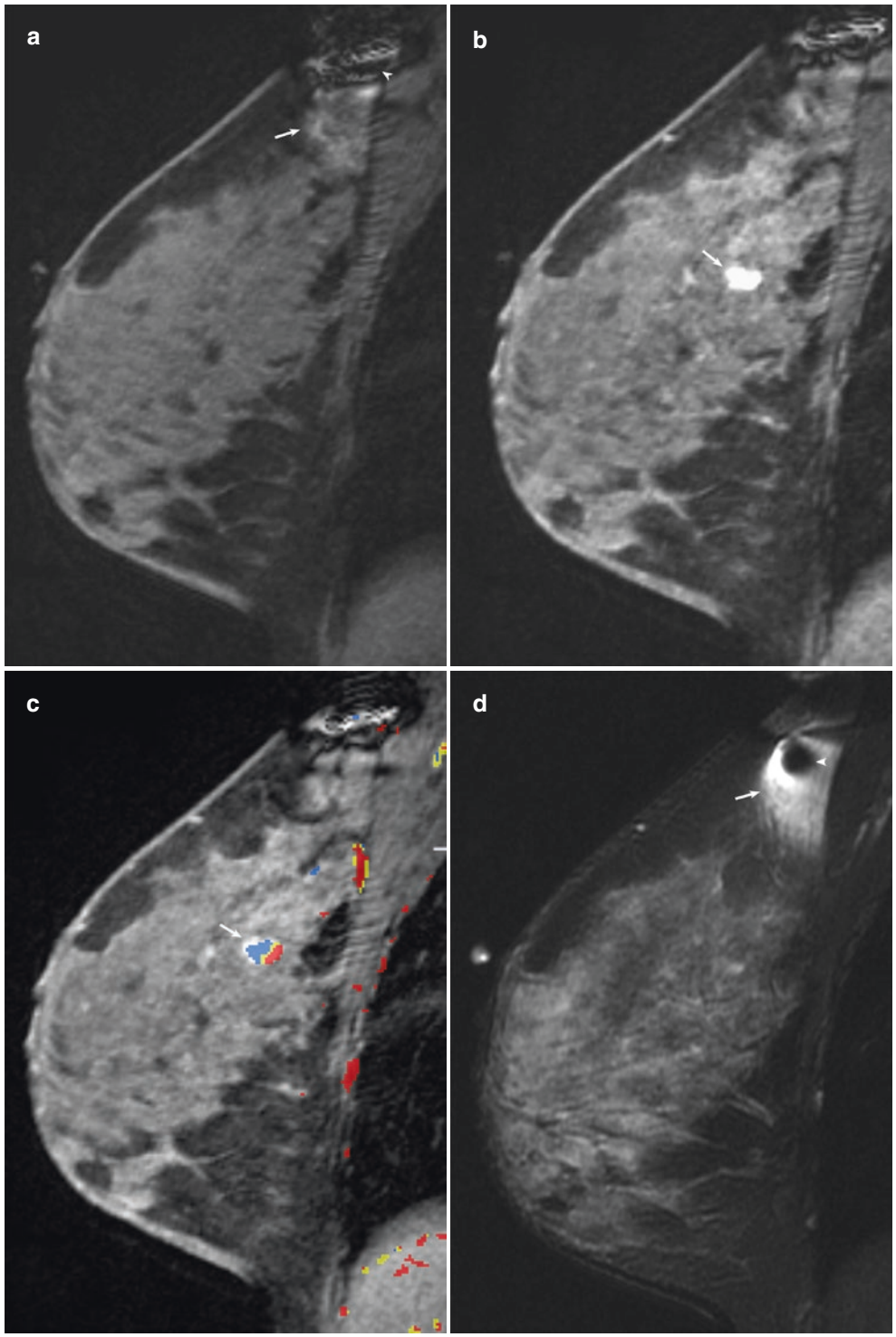

Fig. 4.12 Mammographically and sonographically occult invasive ductal carcinoma (IDC). Sagittal T1-weighted fat-saturated pre-contrast image (**a**) and post-contrast image (**b**) and corresponding CAD color overlay image (**c**) demonstrate a homogeneously enhancing round mass (*arrow*) with washout kinetics. (**d**) No corresponding T2 signal hyperintensity was present. (Incidentally noted are metal artifact (*arrowhead*) and poor fat saturation (*arrow*) in the axilla.) The mass was not identified on second-look ultrasound. MRI-guided biopsy yielded IDC

4.5 History

33-year-old patient undergoing high-risk screening breast MRI (Figs. 4.13 and 4.14).

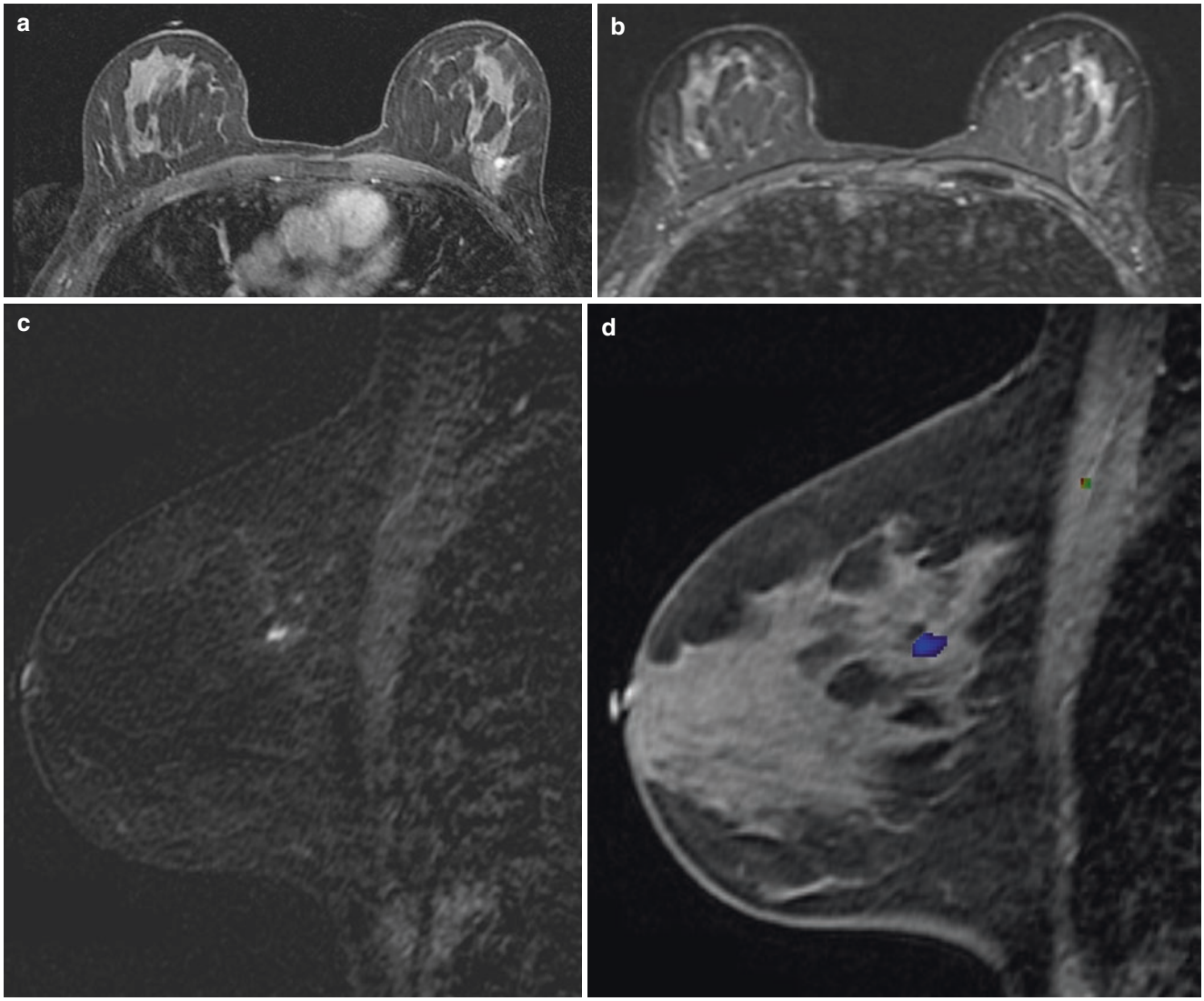

Fig. 4.13 Axial T1-weighted fat-suppressed post-contrast image (**a**) and axial T2-weighted fat-suppressed image (**b**) of both breasts. Sagittal post-contrast subtraction image of the left breast (**c**) with CAD color overlay (**d**)

4.5 Lobular Carcinoma In Situ (LCIS)

Teaching Points Lobular carcinoma in situ (LCIS) is a non-invasive proliferation of lobular cells, a known risk factor for future breast cancer development. Existing data suggest that pleomorphic histology or large volumes of LCIS may be predictive of a more focally aggressive carcinoma. LCIS is usually an incidental finding at core biopsy, as it has no reliable imaging features. The most common imaging features associated with LCIS are grouped, amorphous calcifications on mammography and focus or non–mass-like enhancement with persistent enhancement kinetics on MRI. No specific features have been identified sonographically. The current management recommendation for LCIS diagnosed at core biopsy usually is surgical excision of biopsy sites, particularly those of pleomorphic type.

Image Findings

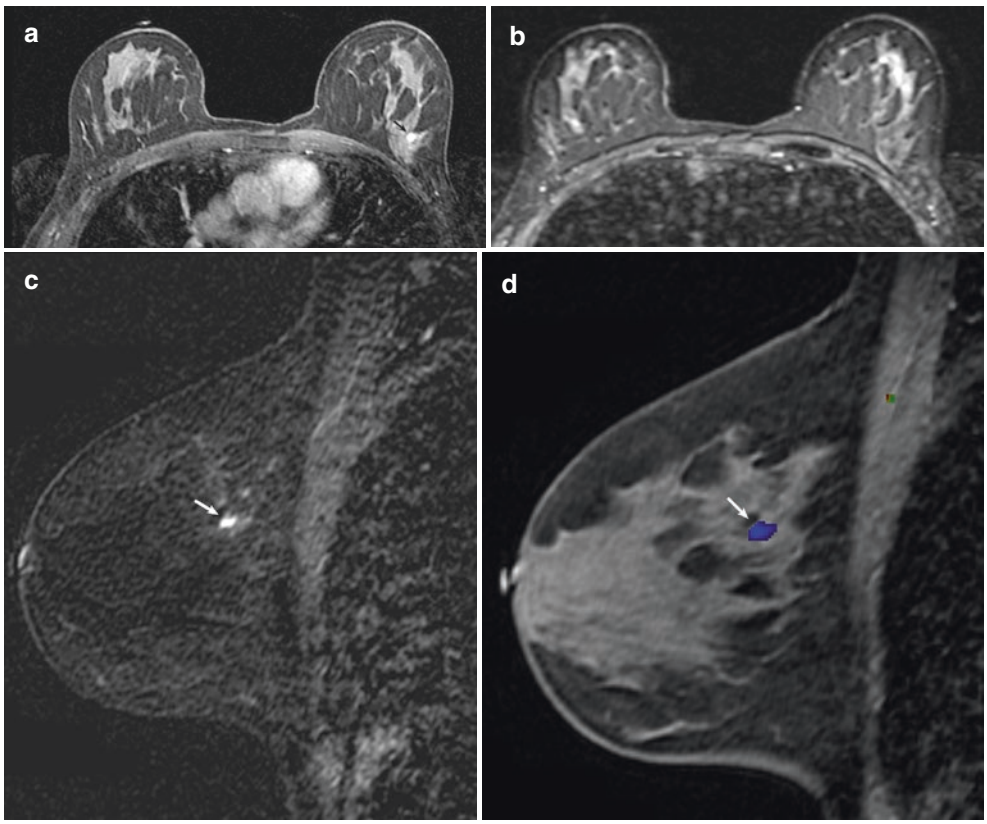

Fig. 4.14 Axial T1-weighted fat-suppressed post-contrast image (**a**) demonstrates a 4-mm focus of enhancement in the posterior upper outer left breast (*arrow*), which does not have a correlate on the T2-weighted fat-suppressed image (**b**). The sagittal post-contrast subtraction image (**c**) of the left breast redemonstrates the 4-mm focus of enhancement (*arrow*), which shows a persistent delayed enhancement pattern on CAD analysis (**d**, *blue color*)

4.6 History

41-year-old woman undergoing high-risk screening breast MRI (Figs. 4.15, 4.16, 4.17, and 4.18).

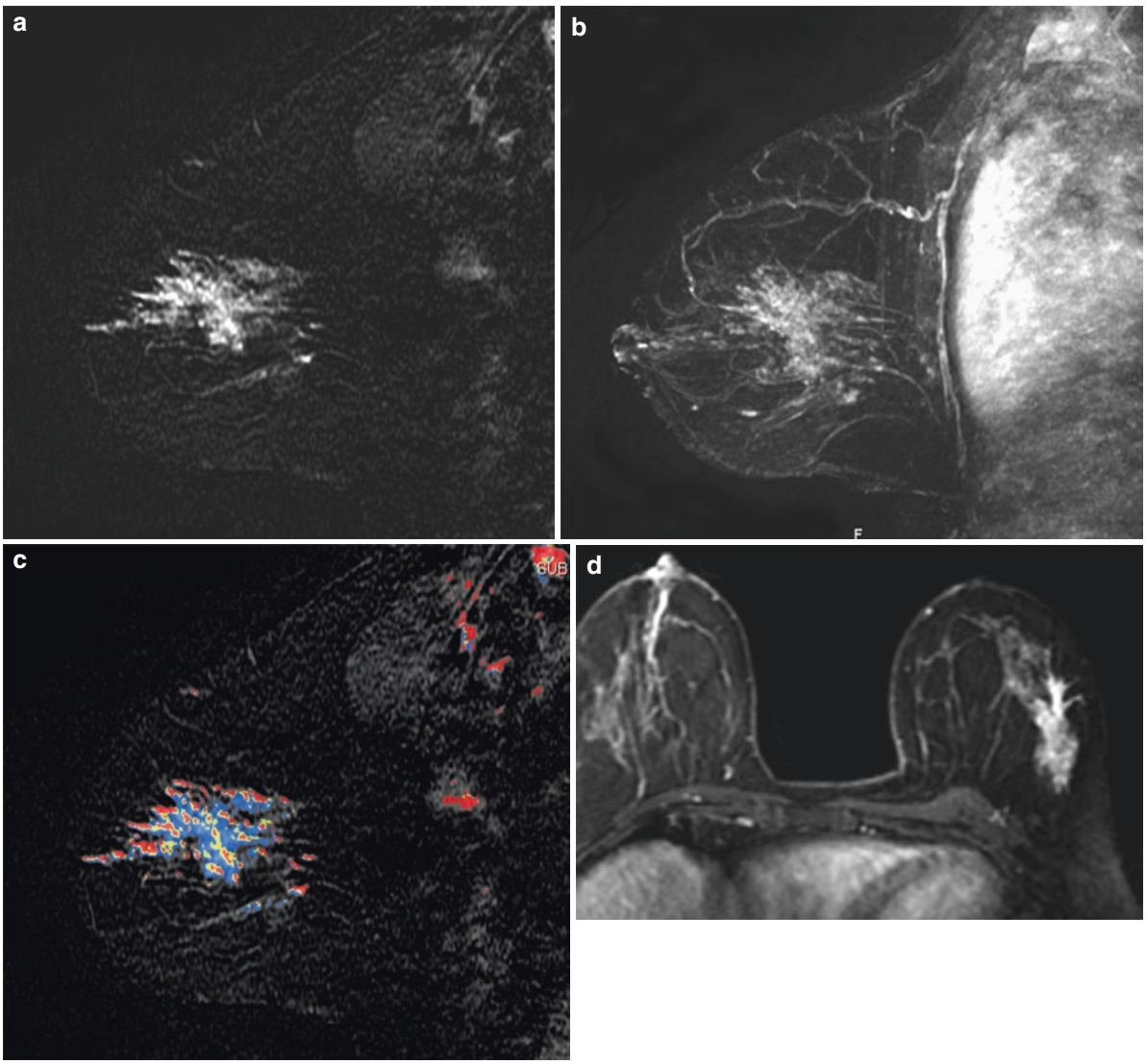

Fig. 4.15 Sagittal post-contrast subtraction image (**a**), sagittal post-contrast 3D MIP image (**b**), and sagittal post-contrast subtraction image with CAD color overlay (**c**) of the left breast. (**d**) Axial T1-weighted fat-suppressed post-contrast image of both breasts

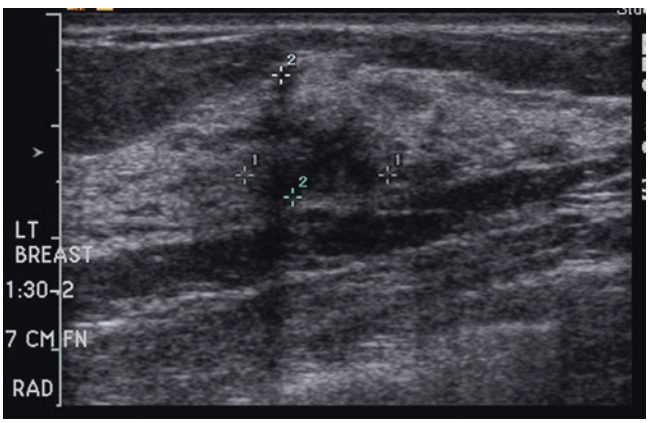

Fig. 4.16 Targeted ultrasound image of the left breast

4.6 Radial Scar

Teaching Points Radial scar is a benign breast lesion characterized by a central fibroelastic core with entrapped ducts surrounded by cystic ducts and lobules showing a spectrum of proliferative changes. They typically measure less than 1 cm and are usually called *complex sclerosing lesions* if 1 cm or greater. Radial scars are typically seen in women younger than 50 years of age. The most common MR imaging feature is nonmass enhancement, including linear or clumped distribution, with associated distortion and type 2 or 3 enhancement kinetics.

Radial scars are associated with an elevated risk for subsequent development of breast cancer; many studies have reported association with malignancy in up to 40 % of cases. The current management recommendation is surgical excision, but some published reviews suggest that excision of radial scars should only be performed if associated with atypia.

Image Findings

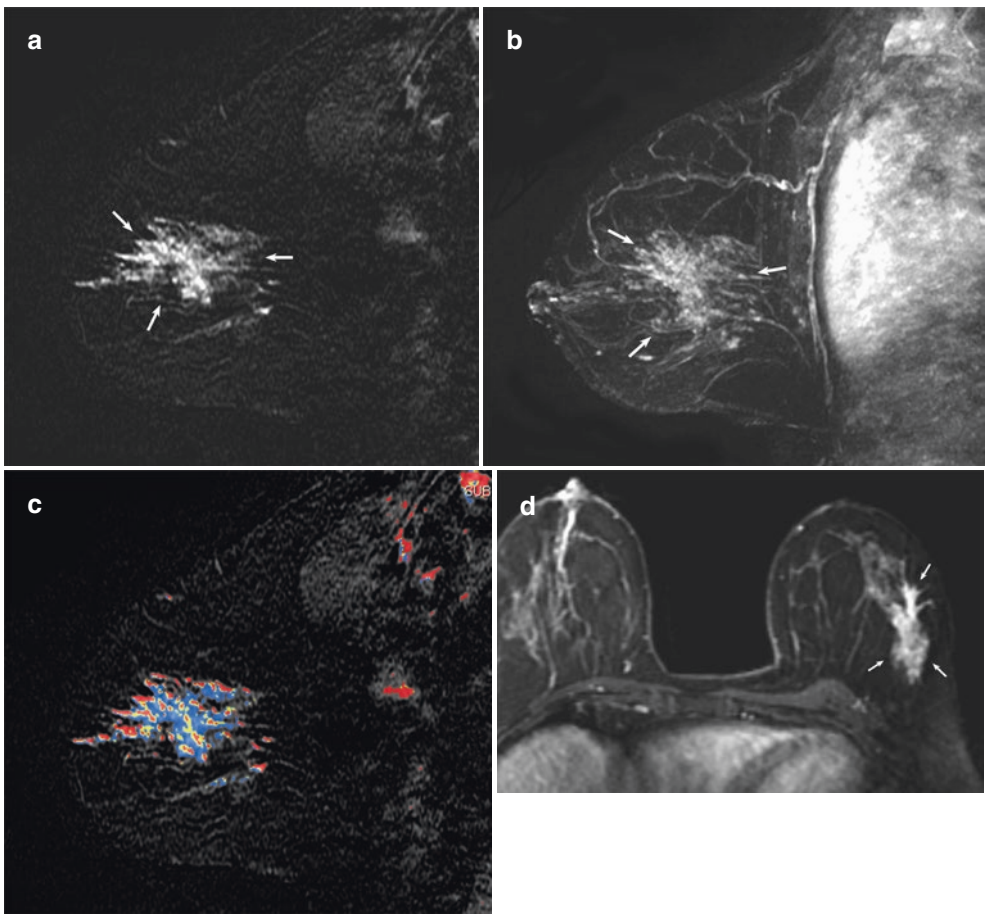

Fig. 4.17 Radial scar. A sagittal post-contrast subtraction image (**a**) and sagittal post-contrast 3D MIP image (**b**) of the left breast demonstrate an irregular enhancing mass in the central breast (*arrows*), with washout enhancement kinetics on CAD analysis (**c**). (**d**) The axial T1-weighted fat-suppressed post-contrast image redemonstrates the irregular enhancing mass (*arrows*) along the lateral aspect of the left breast, with associated architectural distortion

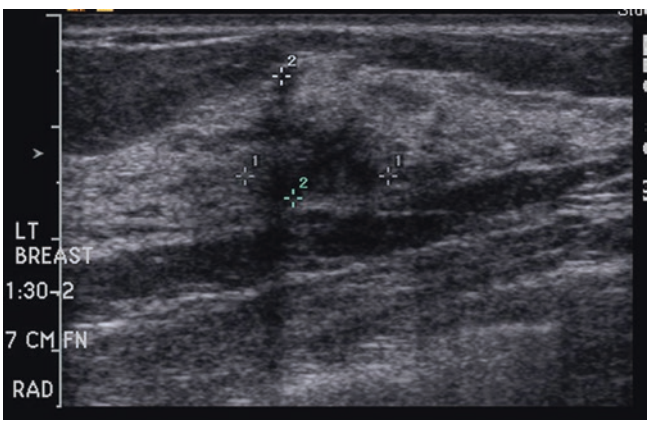

Fig. 4.18 Targeted ultrasound image of the left breast demonstrates a corresponding ill-defined hypoechoic mass with posterior acoustic shadowing. Both the core biopsy and subsequent surgical excision yielded radial scar without atypia or malignancy

4.7 History

48-year-old patient undergoing high-risk screening MRI because of a personal history of breast cancer (Figs. 4.19 and 4.20).

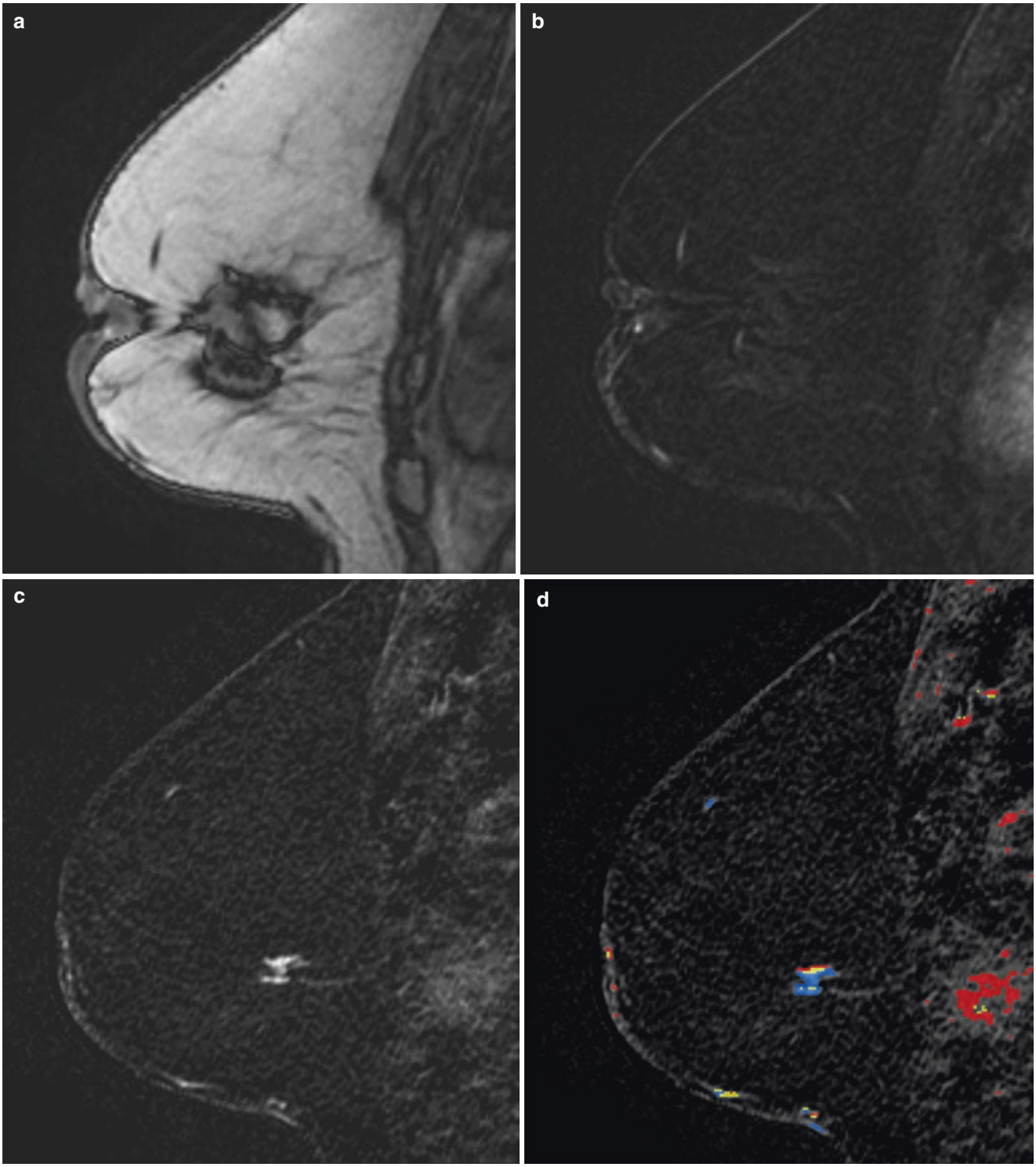

Fig. 4.19 Sagittal T1-weighted image (**a**) and sagittal post-contrast subtraction image (**b**) through the lumpectomy bed. Sagittal post-contrast subtraction image of the more lateral left breast (**c**) with CAD analysis color overlay (**d**)

4.7 Atypical Ductal Hyperplasia (ADH)

Teaching Points Atypical ductal hyperplasia (ADH) is the most common high-risk lesion of the breast. It consists of ductal proliferation that increases a woman's lifetime risk of developing ductal carcinoma. In 20–50 % of cases, depending on the needle gauge used for biopsy, ADH is upgraded histologically to ductal carcinoma in situ (DCIS) or invasive cancer at the time of surgical excision.

According to a review published in 2012 by Heller and Moy, no studies showed specific predictive morphologic or kinetic MRI characteristics for high-risk lesions. Moreover, there were no imaging features that could reliably predict subsequent upgrade to malignancy. The MRI appearance of ADH is variable, ranging from a mass to linear nonmass enhancement mimicking ductal carcinoma in situ (DCIS).

In our case example, ADH was diagnosed on breast MRI in a patient with personal history of cancer. The American Cancer Society recommendations, however, remain controversial regarding performing yearly MRI screening for patients with personal history of breast cancer, DCIS, or high-risk lesions such as ADH, atypical lobular hyperplasia (ALH), and lobular carcinoma in situ (LCIS).

Image Findings

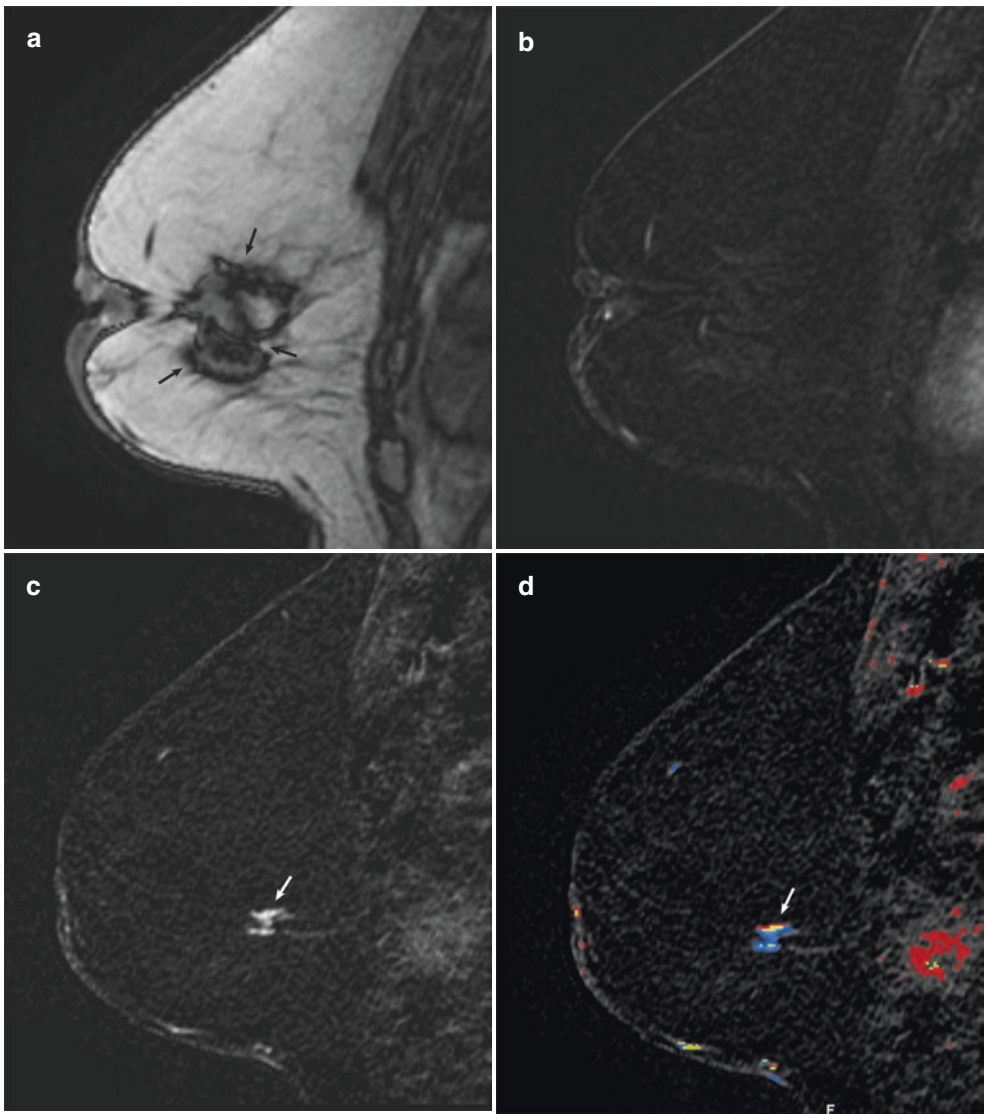

Fig. 4.20 (**a**) Sagittal T1-weighted image of the left breast demonstrates surgical alteration (*arrows*) in the central left breast from prior lumpectomy. (**b**) Sagittal post-contrast subtraction image demonstrate no suspicious enhancement within the lumpectomy bed. Sagittal post-contrast subtraction image without (**c**) and with (**d**) CAD color overlay demonstrates a 1.2-cm area of suspicious linear nonmass enhancement (*arrow*) lateral to the lumpectomy site, with mixed enhancement kinetics. No sonographic or mammographic correlate was identified. The area underwent MRI-guided biopsy, which yielded atypical ductal hyperplasia (ADH)

4.8 History

47-year-old woman undergoing high-risk screening breast MRI (Figs. 4.21 and 4.22).

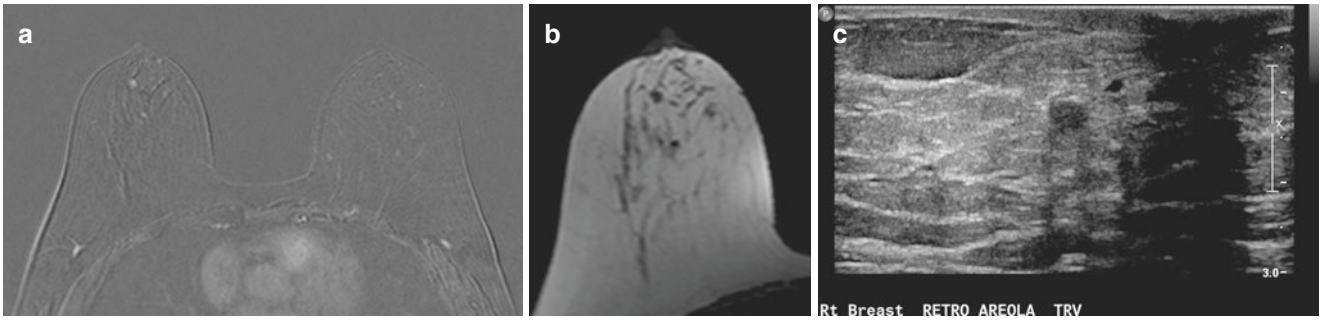

Fig. 4.21 (**a**) Selected axial T1-post-contrast fat-saturated image. (**b**) Corresponding T1 pre-contrast non-fat saturated image. (**c**) Targeted ultrasound image shows a 5-mm, round, hypoechoic mass with mildly irregular margin corresponding to the MRI mass

4.8 Papilloma

Teaching Points Papillary lesions are characterized pathologically by a fibrovascular core, lined by myoepithelial and epithelial layers, extending from a duct wall into the lumen. When symptomatic, patients present commonly with bloody or clear nipple discharge with or without a palpable lump. The benign papillary lesions include solitary intraductal papilloma, multiple intraductal papillomas, and papilloma with atypical hyperplasia. Solitary papillomas are usually retroareolar as in this case whereas multiple papillomas are usually peripheral. Papillomas with and without atypia are associated with an increased risk of developing breast cancer, a risk considered to be higher with multiple papillomas and atypia.

Mammographically, papillomas may be obscured in the retroareolar breast tissue. If visualized in the retroareolar breast, or if seen peripherally, the mass often appears round or oval with circumscribed margins. A papilloma extending throughout a duct may appear as a tubular shaped or even a branching mass mammographically. Benign papillomas are not infrequently associated with calcifications on mammography. Galactography may demonstrate a filling defect in the duct lumen. Sonographically, papillomas may be seen as a mural-based mass surrounded by fluid within a dilated duct. This mass can extend along a duct and branch as the ducts divide. Its margins may be smooth or irregular within the duct as surrounding fluid can highlight its frond-like growth. Vascularity may be detectable within the stalk of the papilloma. A papilloma that does not appear as an intraductal mass may appear round or oval with circumscribed margins. Multiple papillomas can be smaller and less well-defined masses.

As on mammography and sonography, the appearance of papillomas on MRI is variable and unreliably distinguished from malignancy. Small papillomas may be occult on MRI. When solitary, the masses are frequently oval, circumscribed, and homogeneously enhancing, located anteriorly within the breast. It may be associated with a dilated duct or have peri-lesional bright fluid on T2- and sometimes T1-weighted sequences. However, some of its common features are similar to malignancy including being hypointense or isointense on T1- and T2-weighted images. Furthermore, it can have irregular margins mimicking invasive cancer. Diffusion-weighted imaging has not shown a statistically significant difference between papillomas and malignancy. The inability to reliably distinguish papillomas from malignancy on MRI generally leads to a recommendation of biopsy through MRI or ultrasound if visible sonographically.

Papillomas with atypia on biopsy are routinely surgically excised. Management of papillomas without atypia diagnosed on core needle biopsy is the subject of ongoing debate but commonly undergo excision at most academic centers. Some studies lend support to observation for incidental or benign and concordant asymptomatic solitary intraductal papillomas.

Image Findings

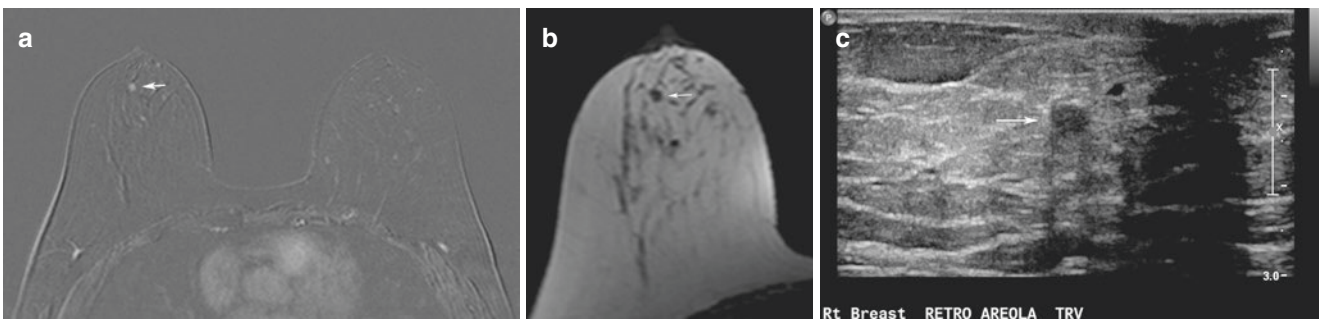

Fig. 4.22 Papilloma. (**a**) There is a 5-mm, round, enhancing mass present in the retroareolar right breast (*arrow*) with hypointensity on T1-weighted pre-contrast image (**b**, *arrow*) and on T2 image (*not shown*). This underwent ultrasound-guided biopsy yielding papilloma. (**c**) Targeted ultrasound image shows a 5-mm round hypoechoic mass with mildly irregular margin corresponding to the MRI mass. This underwent ultrasound-guided biopsy yielding papilloma

4.9 History

36-year-old woman with spontaneous right nipple discharge (Figs. 4.23 and 4.24).

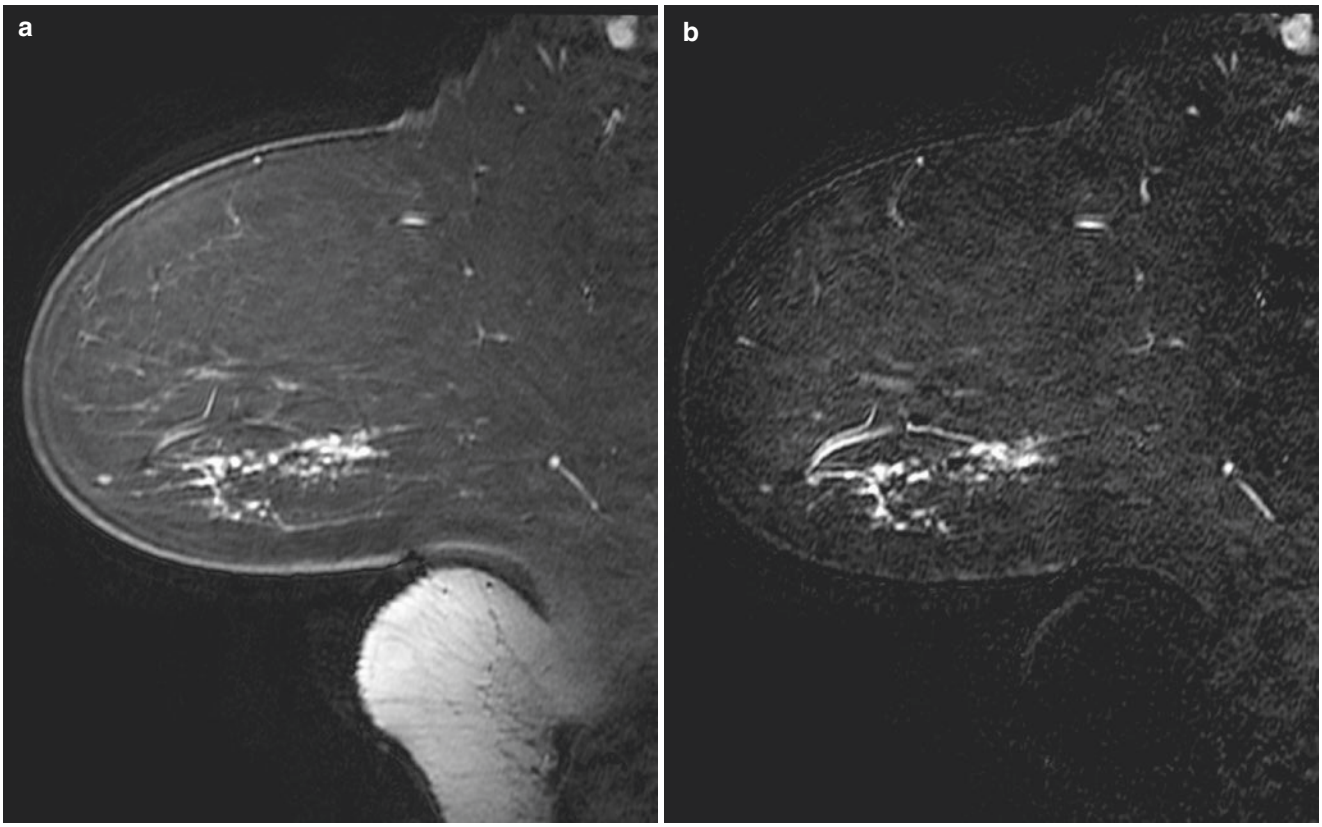

Fig. 4.23 (**a**) Selected sagittal T1-weighted post-contrast fat-saturated image of the right breast. (**b**) Corresponding sagittal T1-weighted post-contrast subtracted image of the right breast

4.9 Papillomatosis and ALH

Teaching Points Multiple papillomatosis occurs in approximately 10% of cases of intraductal papillomas. It occurs more commonly in younger patients and is usually peripheral in location as illustrated in our cases. Multiple papillomatosis are more frequently associated with radial scar, hyperplasia, atypia, sclerosing adenosis, and DCIS. Our case was associated with atypical lobular hyperplasia (ALH). The appearance of papillomas on MRI is variable and unreliably distinguished from malignancy. Non-mass enhancement pattern can be associated with multiple papillomas/papillomatosis as illustrated in this case. It may be associated with a dilated duct or have peri-lesional bright fluid on T2- and sometimes T1-weighted sequences. The inability to reliably distinguish papillomas from malignancy on MRI generally leads to a recommendation of biopsy through MRI or ultrasound if visible sonographically. Papillomas with atypia on biopsy are routinely surgically excised. The patients in this case underwent excision without evidence of malignancy on the surgical specimen. Management of papillomas without atypia diagnosed on core needle biopsy is the subject of ongoing debate.

Atypical lobular hyperplasia (ALH) is a pre-malignant lesion of the breast and is considered a part of borderline breast disease. ALH represents a proliferation of monomorphic cells, which is morphologically identical to lobular carcinoma in situ (LCIS). ALH can be distinguished from LCIS by a non-distended lobule or small lobular duct. LCIS is characterized by distention. It is usually asymptomatic and often found incidentally in a biopsy specimen obtained for another lesion as illustrated in this case. When identified, MRI features of ALH are often round or lobular with irregular margins and heterogeneous enhancement. ALH is typically small in size, measuring 1 cm or less. The treatment for ALH alone is controversial. Some centers surgical excise while others do not.

Image Findings

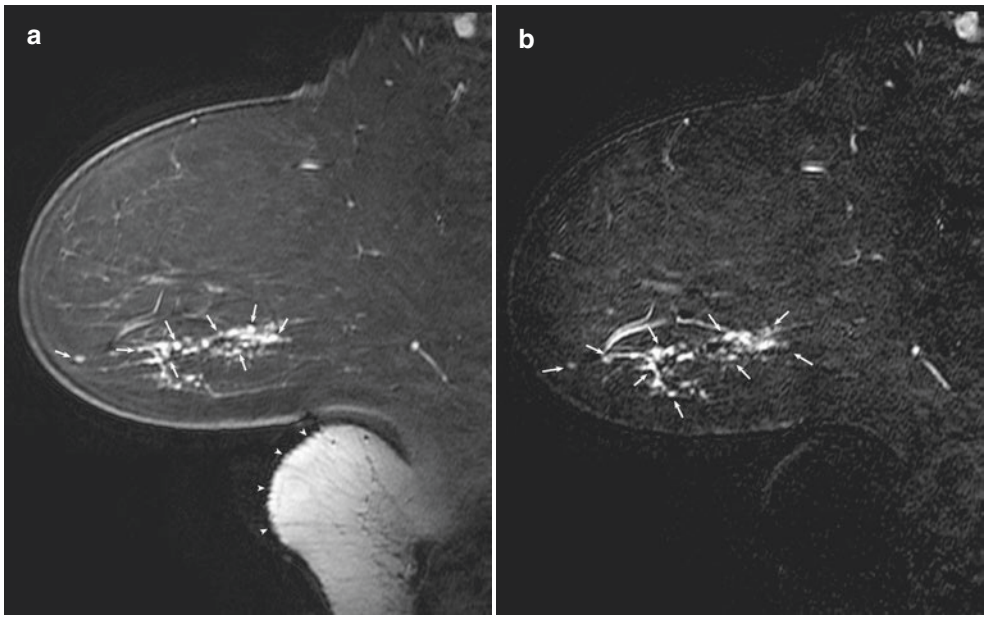

Fig. 4.24 Papillomatosis. (**a**, **b**) There are multiple foci and small linear non-mass enhancements in the lower outer mid right breast in segmental distribution spanning 6 cm. This area underwent MRI-guided biopsy, yielding multiple papillomas and an incidental focus of ALH

Suggested Reading

American College of Radiology Practice Parameter for the Performance of Contrast-Enhanced Magnetic Resonance Imaging (MRI) of the Breast. Amended 2014. http://www.acr.org/~/media/2a0eb28eb59041e2825179afb72ef624.pdf. Accessed 25 Oct 2015.

Atkins KA, Cohen MA, Nicholson B, Rao S. Atypical lobular hyperplasia and lobular carcinoma in situ at core breast biopsy: use of careful radiologic-pathologic correlation to recommend excision or observation. Radiology. 2013;269:340–7.

Becker L, Trop I, David J, Latour M, Ouimet-Oliva D, Gaboury L, Lalonde L. Management of radial scars found at percutaneous breast biopsy. Can Assoc Radiol J. 2006;57:72–8.

Berg WA, Mrose HE, Ioffe OB. Atypical lobular hyperplasia or lobular carcinoma in situ at core-needle breast biopsy. Radiology. 2001;218(2):503–9.

Brennan S, Liberman L, Dershaw DD, Morris E. Breast MRI screening of women with a personal history of breast cancer. AJR Am J Roentgenol. 2010;195:510–6.

Chadashvili T, Ghosh E, Fein-Zachary V, Mehta TS, Venkataraman S, Dialani V, Slanetz PJ. Nonmass enhancement on breast MRI: review of patterns with radiologic-pathologic correlation and discussion of management. AJR Am J Roentgenol. 2015;204:219–27.

Chansakul T, Lai KC, Slanetz PJ. The postconservation breast: part 2, Imaging findings of tumor recurrence and other long-term sequelae. AJR Am J Roentgenol. 2012;198:331–43.

Daniel BL, Gardner RW, Birdwell RL, Nowels KW, Johnson D. Magnetic resonance imaging of intraductal papilloma of the breast. Magn Reson Imaging. 2003;21(8):887–92.

Eiada R, Chong J, Kulkarni S, Goldberg F, Muradali D. Papillary lesions of the breast: MRI, ultrasound, and mammographic appearances. Am J Roentgenol. 2012;198(2):264–71.

Heller SL, Moy L. Imaging features and management of high-risk lesions on contrast-enhanced dynamic breast MRI. AJR Am J Roentgenol. 2012;198:249–55.

Kohr JR, Eby PR, Allison KH, DeMartini WB, Gutierrez RL, Peacock S, Lehman CD. Risk of upgrade of atypical ductal hyperplasia after stereotactic breast biopsy: effects of number of foci and complete removal of calcifications. Radiology. 2010;255:723–30.

Lourenco AP, Khalil H, Sanford M, Donegan L. High-risk lesions at MRI-guided breast biopsy: frequency and rate of underestimation. AJR Am J Roentgenol. 2014;203:682–6.

MacGrogan G, Moinfar F, Raju U. Intraductal papillary neoplasms. In: Tavassoli FA, Devilee P, editors. World Health Organization Classification of tumours: pathology and genetics of tumours of the breast and female genital organs. Lyon, France: IARC; 2003. p. 76–88.

Mulligan AM, O'Malley FP. Papillary lesions of the breast: a review. Adv Anat Pathol. 2007;14(2):108–19.

Nakhlis F, Ahmadiyeh N, Lester S, Raza S, Lotfi P, Golshan M. Papilloma on core biopsy: excision vs. observation. Ann Surg Oncol. 2015;22(5):1479–82.

Neal L, Sandhu NP, Hieken TJ, Glazebrook KN, Mac Bride MB, Dilaveri CA, et al. Diagnosis and management of benign, atypical, and indeterminate breast lesions detected on core needle biopsy. Mayo Clin Proc. 2014;89(4):536–47.

Pal T, Permuth-Wey J, Betts JA, Krischer JP, Fiorica J, Arango H, et al. *BRCA1* and *BRCA2* mutations account for a large proportion of ovarian carcinoma cases. Cancer. 005;104:2807–16.

Peiró G, Adrover E, Guijarro J, Ballester I, Jimenez MJ, Planelles M, Catasús L. Synchronous bilateral breast carcinoma in a patient with cowden syndrome: a case report with morphologic, immunohistochemical and genetic analysis. Breast J. 2010;16:77–81.

Sarica O, Uluc F, Tasmali D. Magnetic resonance imaging features of papillary breast lesions. Eur J Radiol. 2014;83(3):524–30.

Scoggins M, Krishnamurthy S, Santiago L, Yang W. Lobular carcinoma in situ of the breast: clinical, radiological, and pathological correlation. Acad Radiol. 2013;20:463–70.

Seo M, Cho N, Ahn HS, Moon HG. Cowden syndrome presenting as breast cancer: imaging and clinical features. Korean J Radiol. 2014;15:586–90.

Sohn VY, Causey MW, Steele SR, Keylock JB, Brown TA. The treatment of radial scars in the modern era—surgical excision is not required. Am Surg. 2010;76:522–5.

Subhawong A, Subhawong T, Khouri N, Tsangaris T, Nassar H. Incidental minimal atypical lobular hyperplasia on core needle biopsy: correlation with findings on follow-up excision. Am J Surg Pathol. 2010;34(6):822–8.

Wang W, Ding J, Yang W, Li Y, Zhou L, Zhang S, et al. MRI characteristics of intraductal papilloma. Acta Radiol. 2015;56(3):276–83.

Zhu Y, Zhang S, Liu P, Lu H, Xu Y, Yang WT. Solitary intraductal papillomas of the breast: MRI features and differentiation from small invasive ductal carcinomas. Am J Roentgenol. 2012;199(4):936–42.

Interesting Cases

5

Victoria Mango, Lauren Friedlander,
Elizabeth A. Morris, and Richard Ha

V. Mango, MD
Director of Breast and Body Imaging Fellowship,
Breast Imaging Service, Memorial Sloan-Kettering Cancer Center,
Assistant Professor of Radiology, Weill Cornell Medical College,
New York, NY, USA
e-mail: vlm2125@columbia.edu

L. Friedlander, MD
Director of Breast and Body Imaging Fellowship,
Division of Breast Imaging, Assistant Professor of Radiology,
Columbia University Medical Center, New York, NY, USA
e-mail: lf2386@columbia.edu

E.A. Morris, MD
Chief, Breast Imaging Service
Memorial Sloan-Kettering Cancer Center
New York, NY, USA

Professor of Radiology
Weill Cornell Medical College
New York, NY, USA
e-mail: morrise@mskcc.org

R. Ha, MD (✉)
Director of Education and Research,
Division of Breast Imaging, Assistant Professor of Radiology,
Columbia University Medical Center, New York, NY, USA
e-mail: rh2616@cumc.columbia.edu

R. Ha et al. (eds.), Breast MRI Teaching Atlas, DOI 10.1007/978-1-4939-6409-3_5

5.1 History

49-year-old with history of desmoid tumor resection (Figs. 5.1 and 5.2).

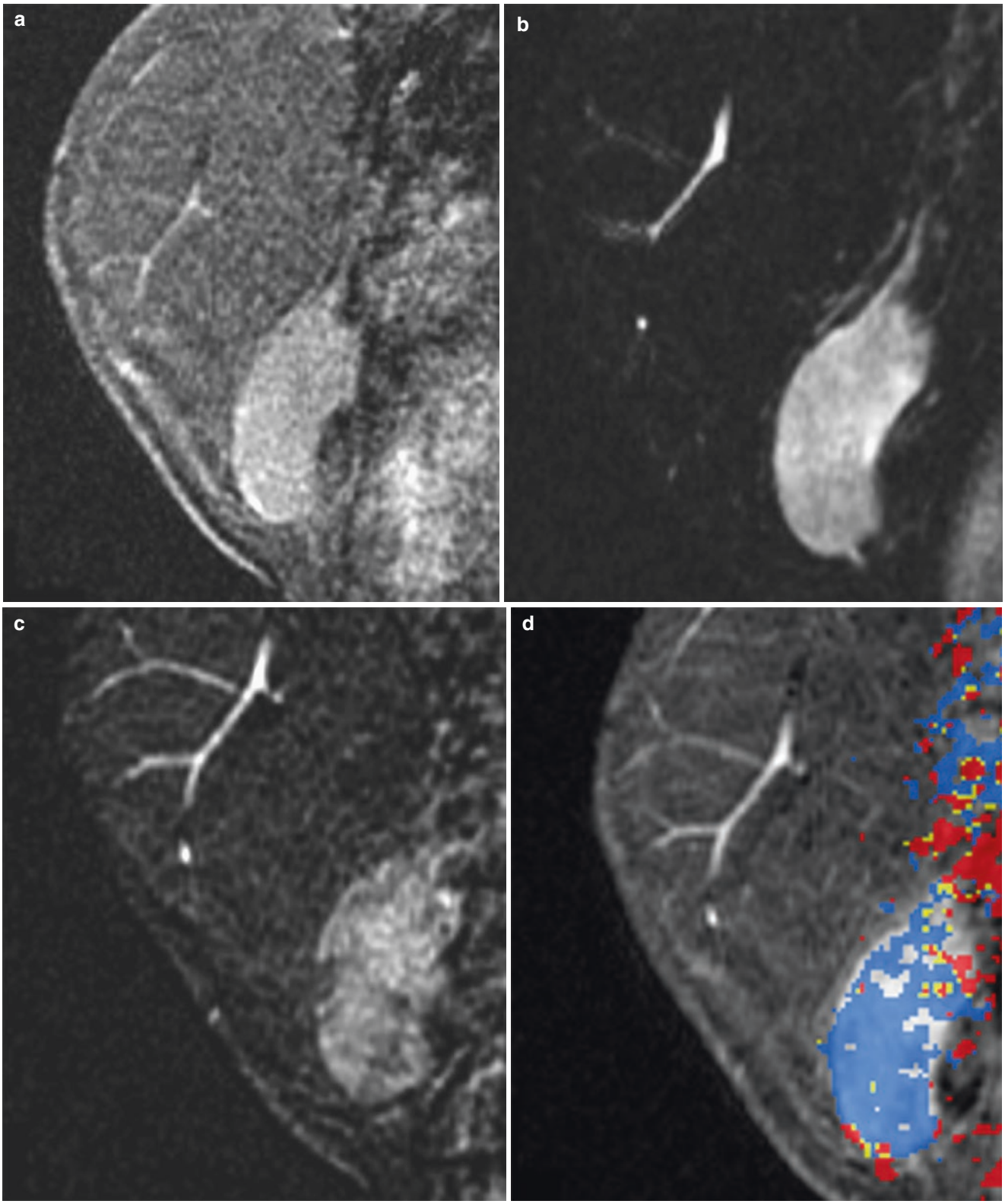

Fig. 5.1 Sagittal MR images of the left breast. (**a**) T1-weighted fat-saturated image. (**b**) T2-weighted fat-saturated image. (**c**) Post-contrast subtraction image. (**d**) T1-weighted fat-saturated post-contrast image with computer-aided detection (CAD) color overlay

5.1 Desmoid Tumor

Teaching Points Desmoid tumor, also known as fibromatosis of the breast, is a rare benign entity, accounting for only 0.2 % of all breast tumors. It is characterized by low-grade, uniform spindle-cell proliferation carrying no malignant potential, but it has shown a significant risk for local recurrence. Therefore, the current management of desmoid tumors is wide excision with clear margins. The mammographic and sonographic features mimic those of malignancy. On MR imaging, a desmoid tumor can appear as an ill-defined or circumscribed mass with low to intermediate signal intensity on the T1-weighted images and increased signal on the T2-weighted images. Progressive enhancement kinetics is usually seen on dynamic contrast imaging. Although these imaging features are nonspecific, MRI can be useful to show chest wall involvement important for surgical planning.

Image Findings

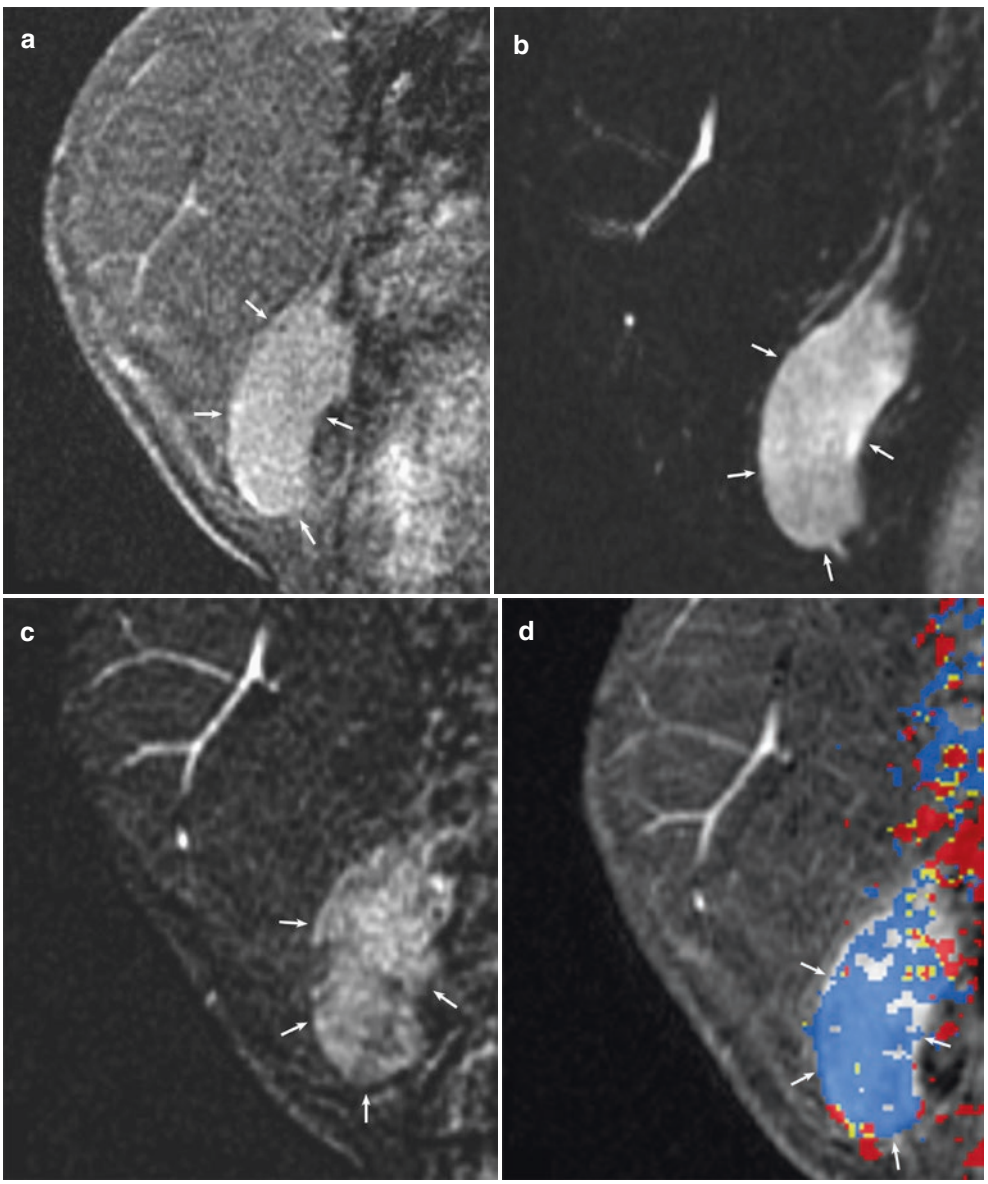

Fig. 5.2 Desmoid tumor local recurrence. (**a**, **b**) Sagittal T1-weighted fat-saturated non-contrast image and corresponding T2-weighted fat-saturated image demonstrate an oval, circumscribed T1- and T2-hyperintense mass (*arrows*) in the lower breast. (**c**, **d**) Sagittal post-contrast subtraction image and corresponding CAD enhancement kinetic analysis demonstrate a circumscribed, homogeneously enhancing mass (*arrows*) with progressive enhancement kinetics

5.2 History

44-year-old with history of pheochromocytoma status post resection 4 years ago, with recent surveillance nuclear medicine scan showing uptake in the left breast. Breast MRI was performed for further evaluation (Figs. 5.3 and 5.4).

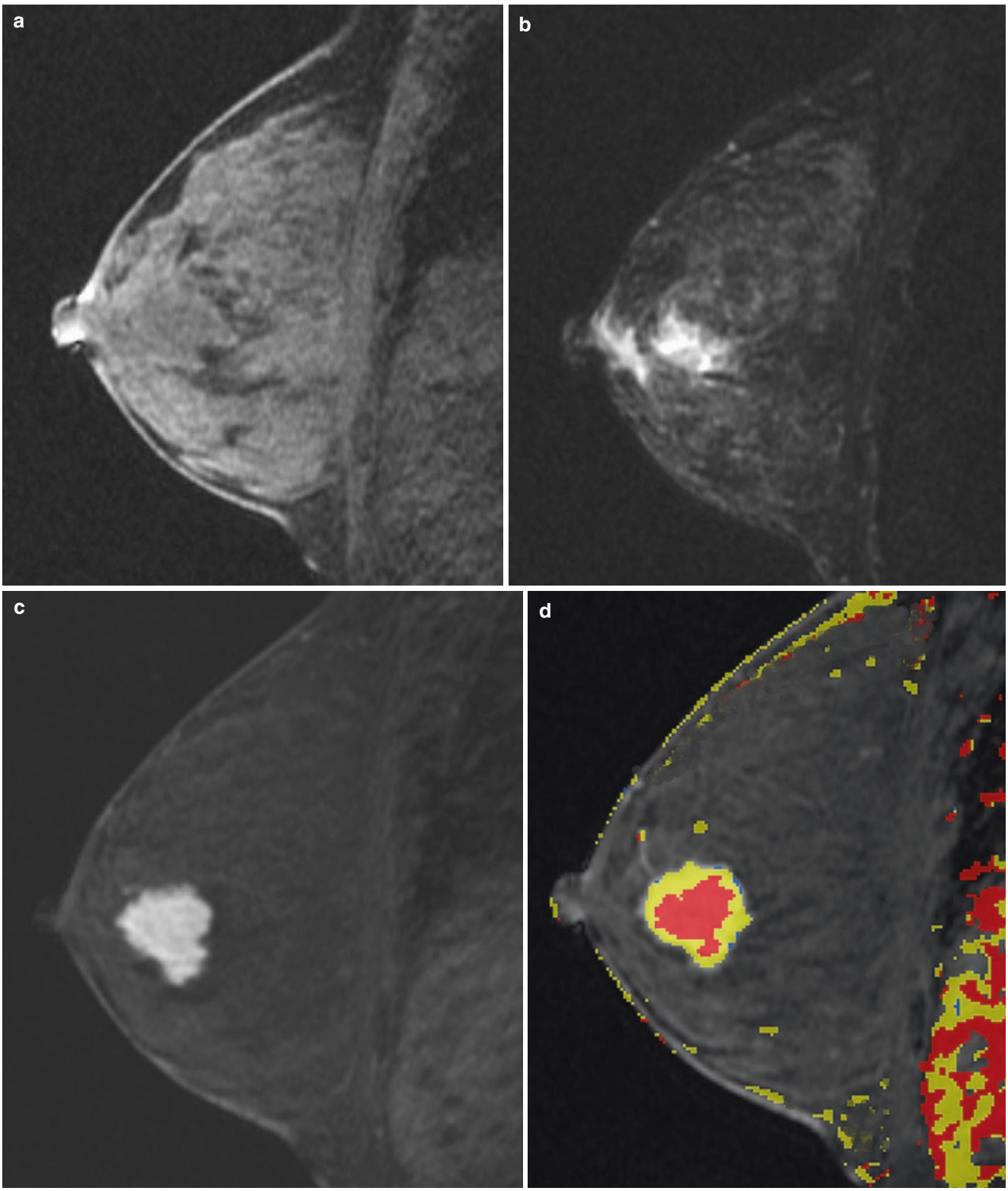

Fig. 5.3 Sagittal MR images of the left breast. (**a**) T1-weighted fat-saturated image. (**b**) T2-weighted fat-saturated image. (**c**) T1-weighted fat-saturated post-contrast image. (**d**) Corresponding CAD color overlay

5.2 Pheochromocytoma

Teaching Points Pheochromocytomas are an uncommon tumor of the adrenal gland. The tumors generally follow a 10 % rule:

- ~10 % are extra-adrenal, as illustrated in this case
- ~10 % are bilateral
- ~10 % are malignant
- ~10 % are found in children
- ~10 % are familial
- ~10 % are not associated with hypertension
- ~10 % contain calcification

On MRI, pheochromocytoma has been described as an intensely enhancing mass having characteristic high signal intensity on T2-weighted imaging, typically heterogeneous as illustrated in this case. This "light bulb bright" signal on T2-weighted imaging is neither specific nor sensitive for pheochromocytoma. A characteristic salt-and-pepper pattern has also been described.

Image Findings

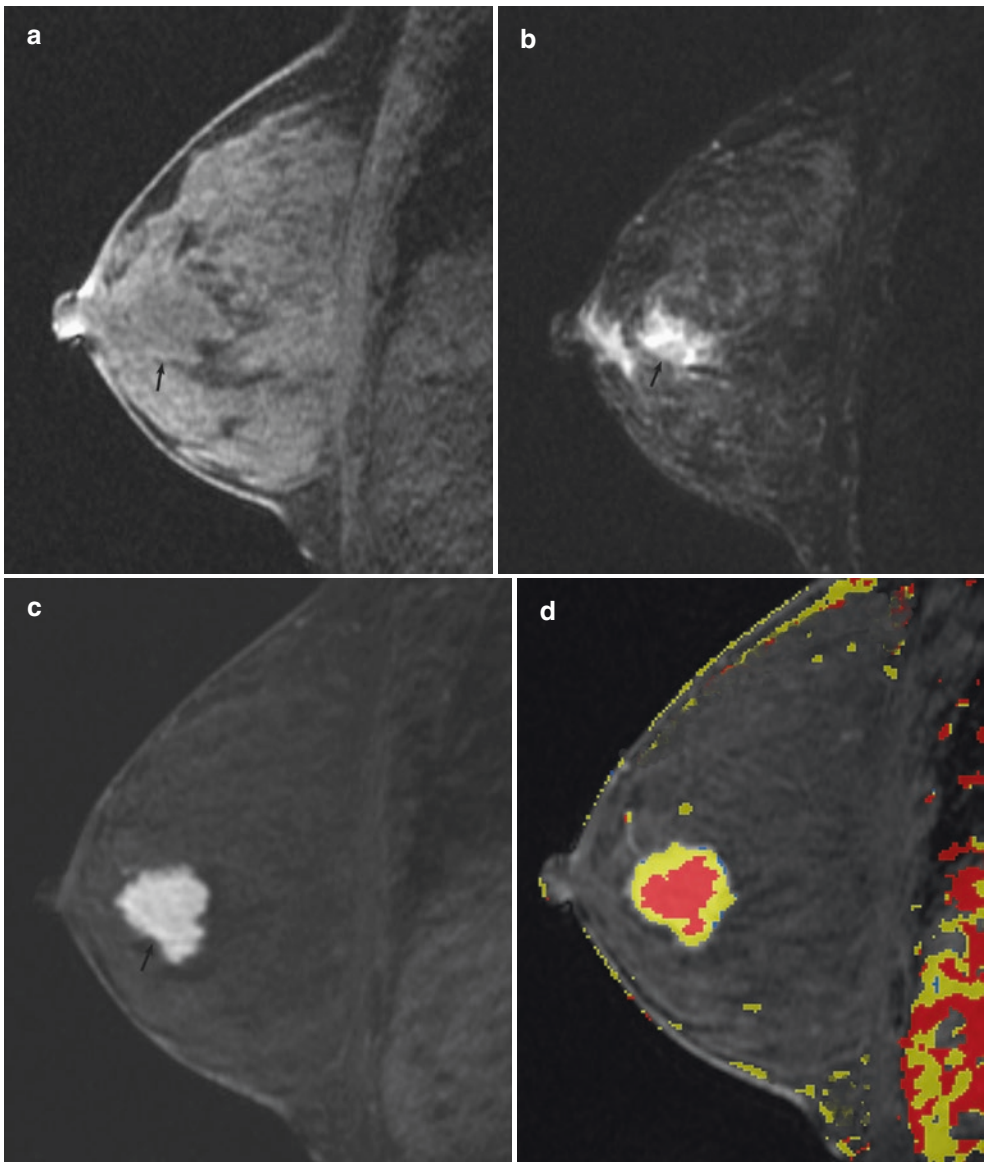

Fig. 5.4 Extra-adrenal pheochromocytoma. Sagittal T1-weighted fat-saturated pre-contrast image (**a**) and corresponding T2-weighted fat-saturated image (**b**) of the left breast demonstrate a T1-isointense and heterogeneously T2-hyperintense subareolar mass (*arrows*). A corresponding T1-weighted fat-saturated post-contrast image (**c**) demonstrates an intensely homogeneously enhancing 2.9-cm irregular mass (*arrow*) in the subareolar region, with central washout pattern on CAD kinetics analysis (**d**)

5.3 History

Screening breast MRI (Figs. 5.5, 5.6, 5.7, and 5.8).

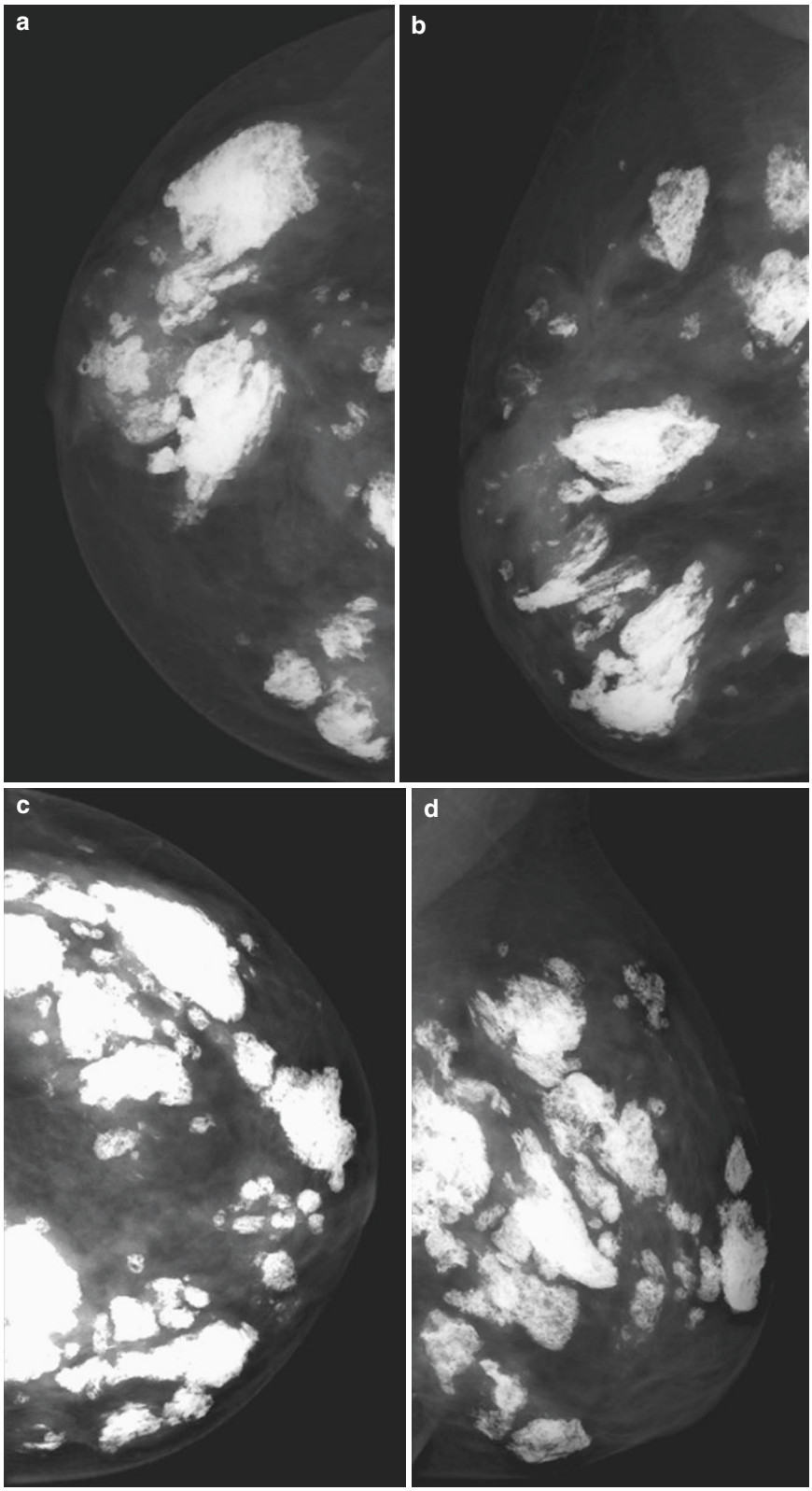

Fig. 5.5 Mammographic views of both breasts. (**a**) Left craniocaudal (CC) view. (**b**) Left mediolateral oblique (MLO) view. (**c**) Right CC view. (**d**) Right MLO view

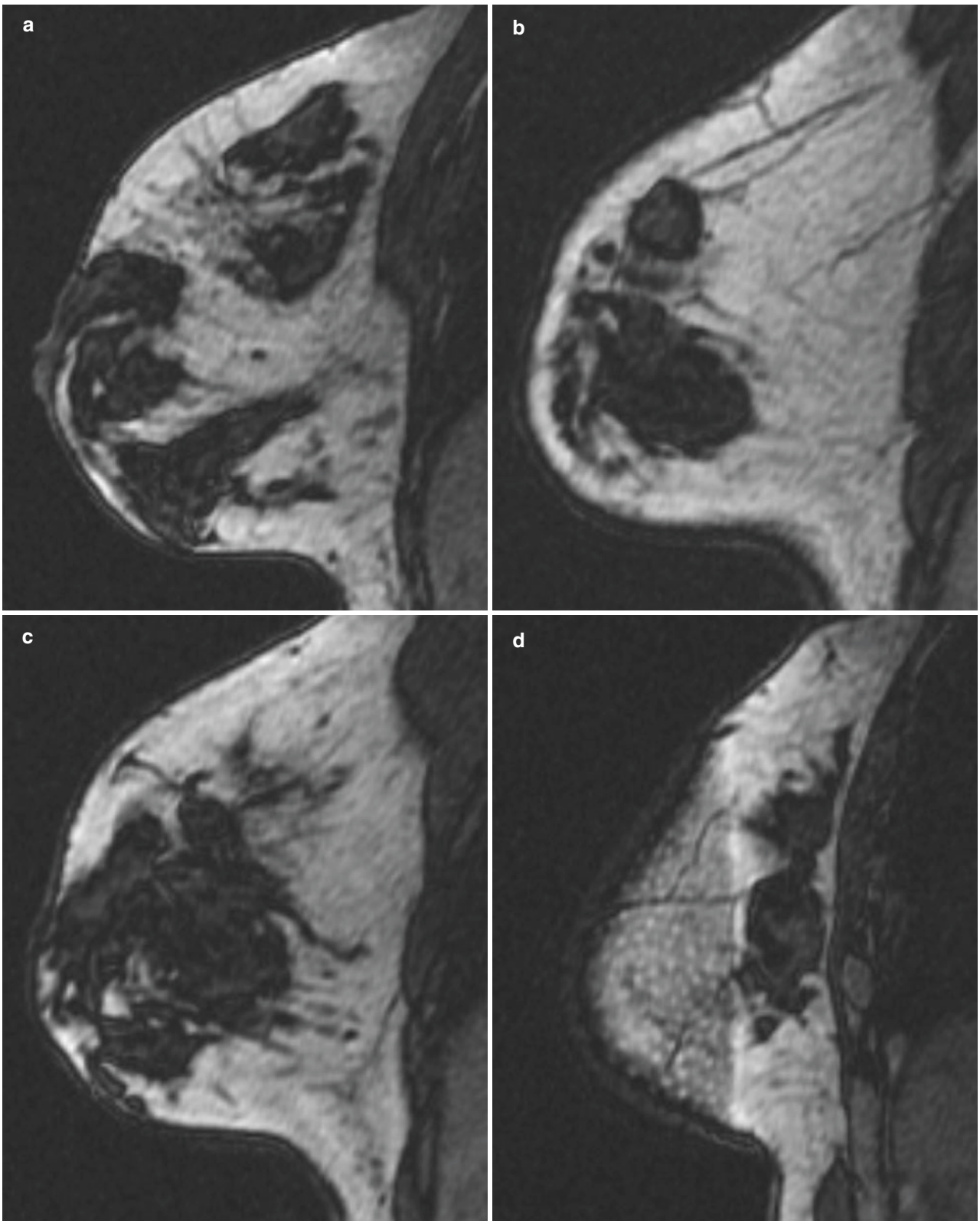

Fig. 5.6 Sagittal MRI images of both breasts. (**a**–**d**) T1-weighted images. (**e**) T2-weighted fat-saturated image. (**f**, **g**) T1-weighted fat-saturated pre-contrast and post-contrast images. (**h**) Image from **g** with CAD color overlay

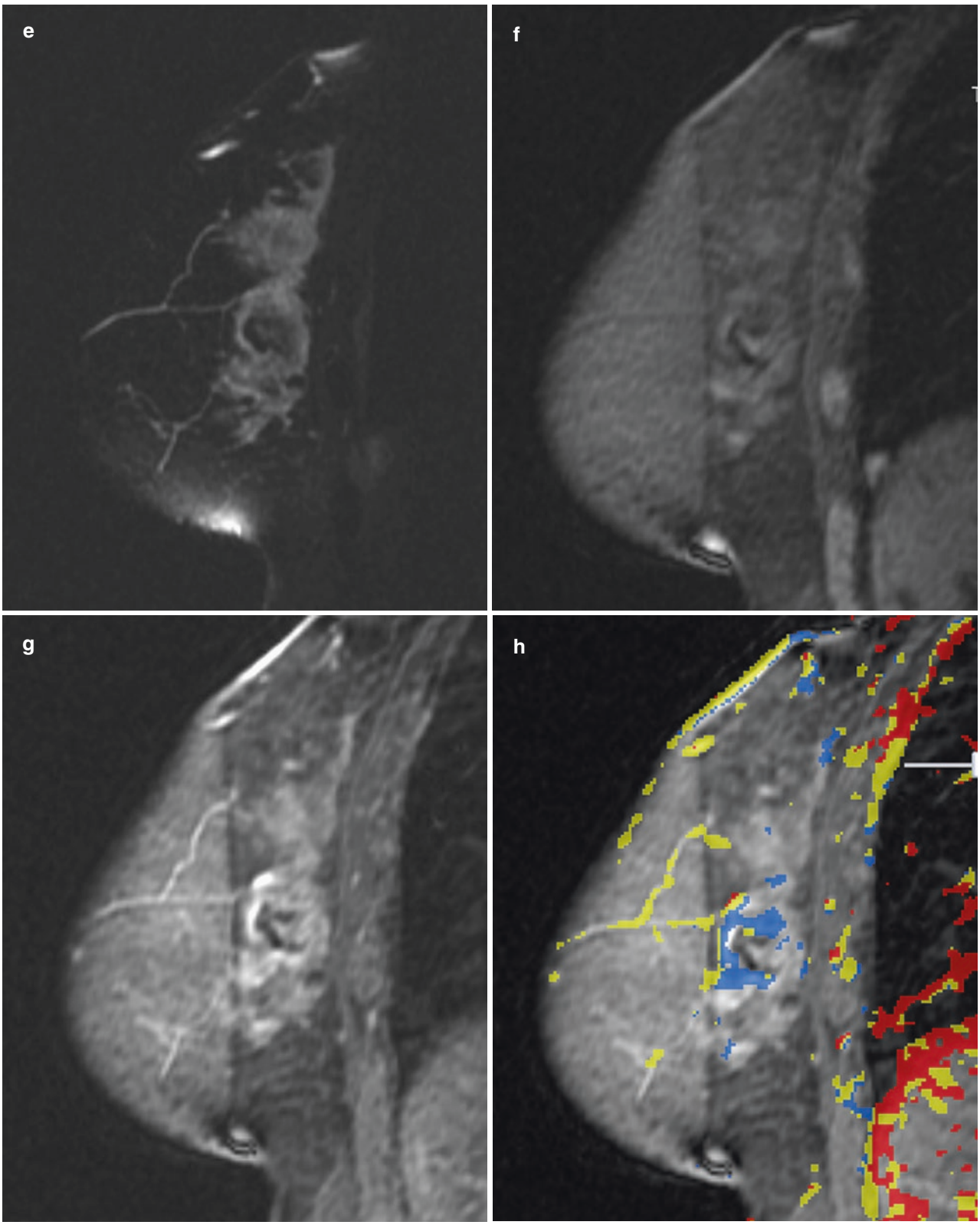

Fig. 5.6 (continued)

5.3 Amyloidosis

Teaching Points Primary breast amyloidosis is rare, and breast involvement is usually part of the systemic disease. Similar to amyloid deposits elsewhere in the body, calcifications can develop in the breast. Mammographic features of breast amyloidosis include irregular or circumscribed masses with coarse, dystrophic calcifications (Fig. 5.5). On MRI examination, lesions generally demonstrate decreased T1 signal intensity with associated increased T2 signal corresponding with edema and inflammation. Delayed progressive enhancement pattern is usually noted on the post-contrast images. Core biopsy is recommended in most cases of indeterminate findings to confidently exclude co-existent malignancy.

Image Findings

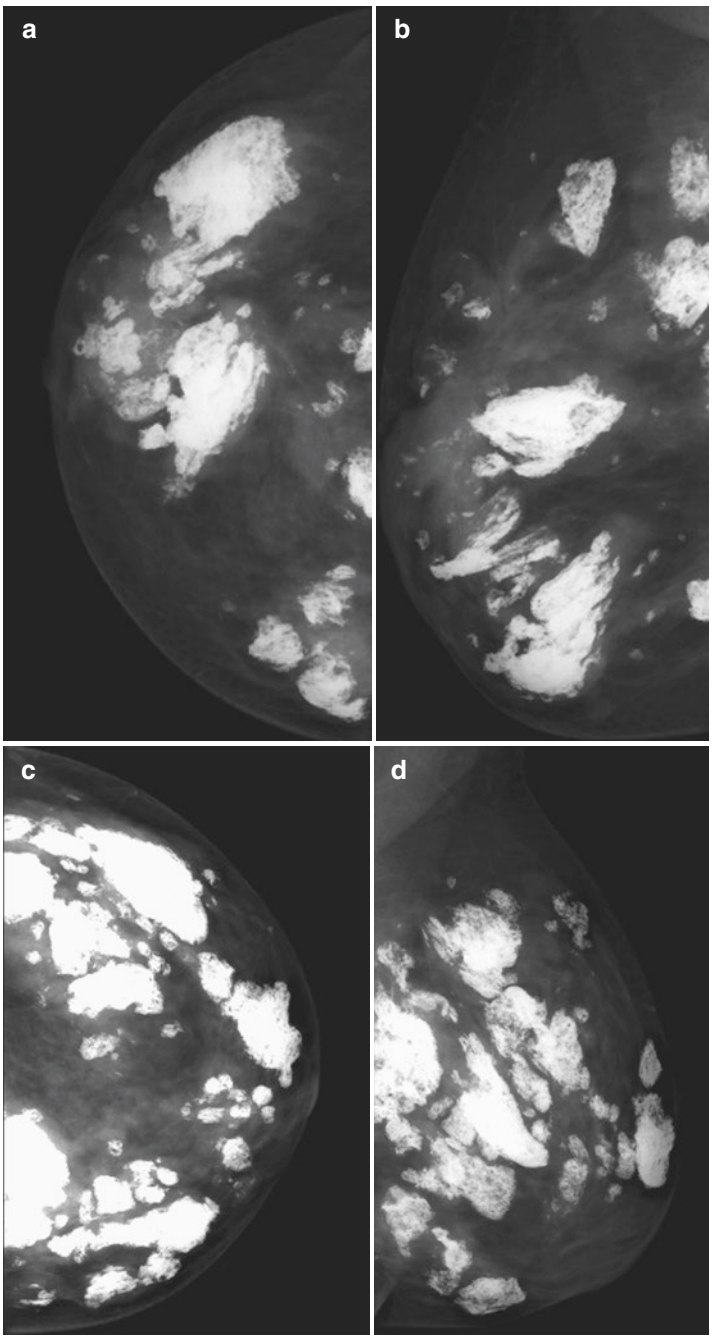

Fig. 5.7 Amyloidosis with associated dense calcifications on mammography, limiting assessment. Left CC (**a**) and MLO (**b**) images and right CC (**c**) and MLO (**d**) images demonstrate bilateral dense calcifications

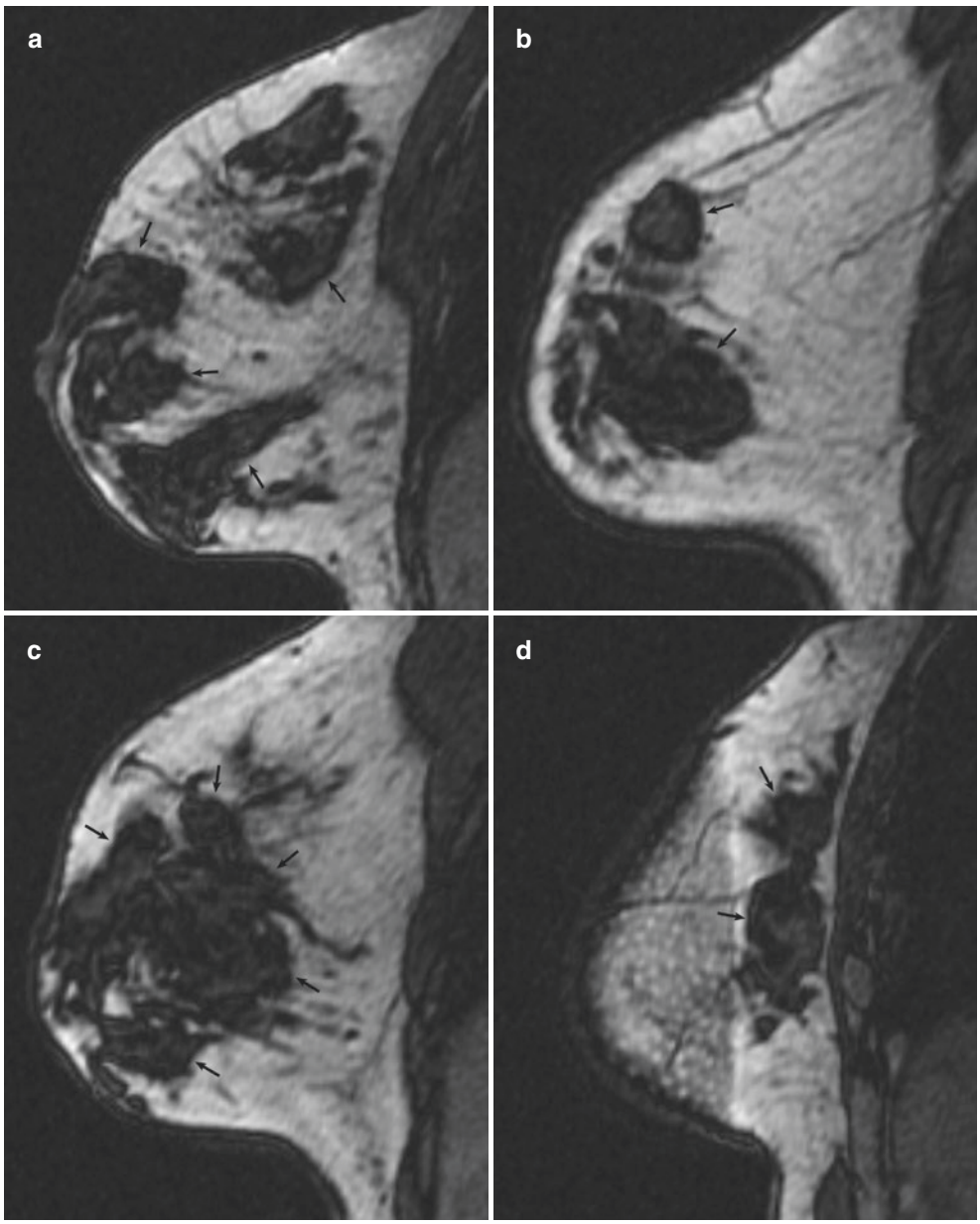

Fig. 5.8 Amyloidosis on breast MRI. (**a**–**d**) Selected sagittal T1-weighted sequences demonstrate large, conglomerate hypointense areas (*arrows*) corresponding to areas of dense calcification on mammography. (**e**) A sagittal T2-weighted fat-saturated image demonstrates corresponding hypointense areas (*arrows*) with associated peripheral T2 hyperintensity. (**f**, **g**) Sagittal T1-weighted fat-saturated pre-contrast and post-contrast images demonstrate mild T1 hyperintensity (*arrows*) and heterogeneous rim enhancement (*arrows*) corresponding to the T2-hyperintense regions. No focal suspicious enhancement was identified. (**h**) CAD enhancement kinetics analysis (*arrows*) demonstrates a predominantly progressive pattern

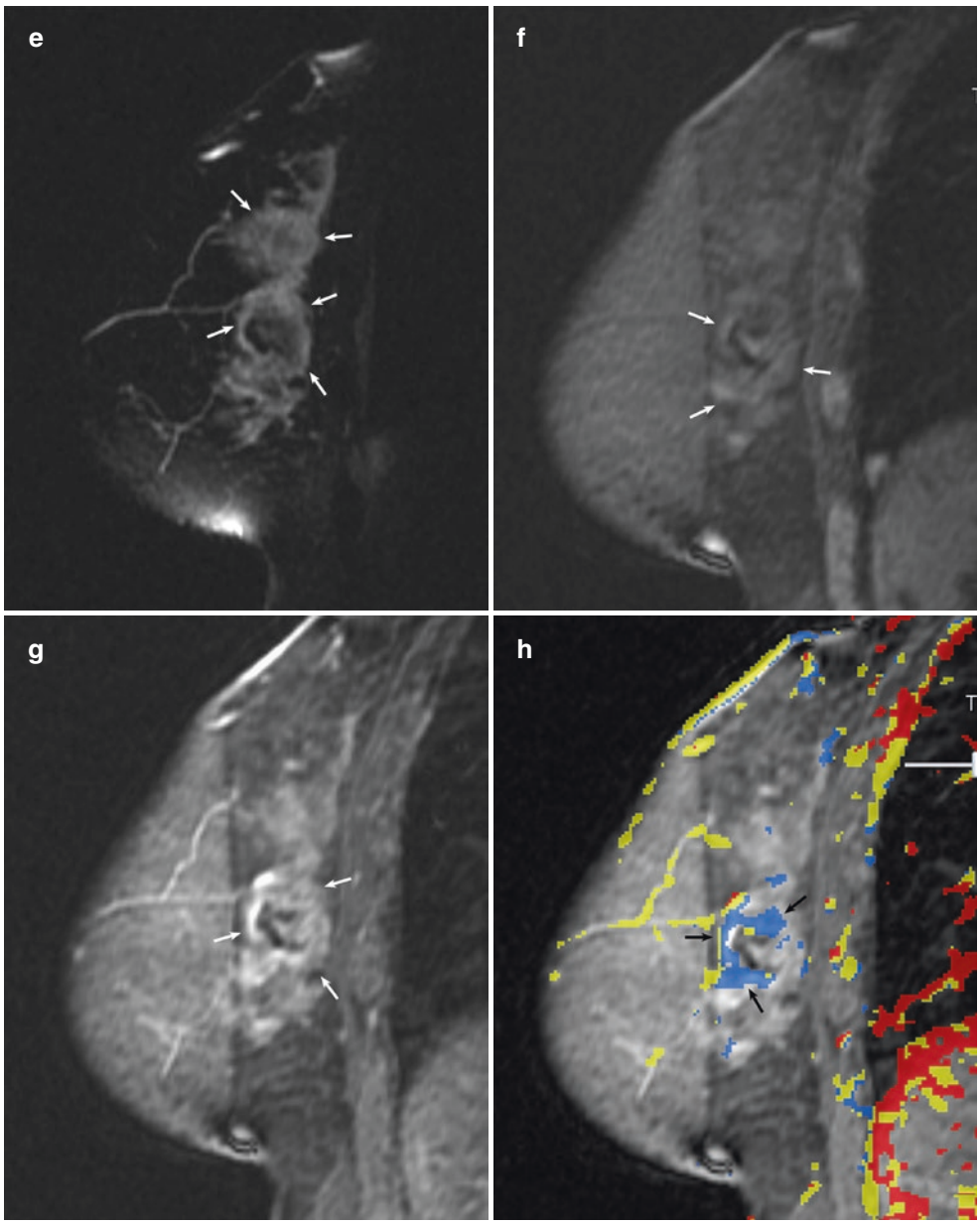

Fig. 5.8 (continued)

5.4 History

Extent of disease evaluation (Figs. 5.9 and 5.10).

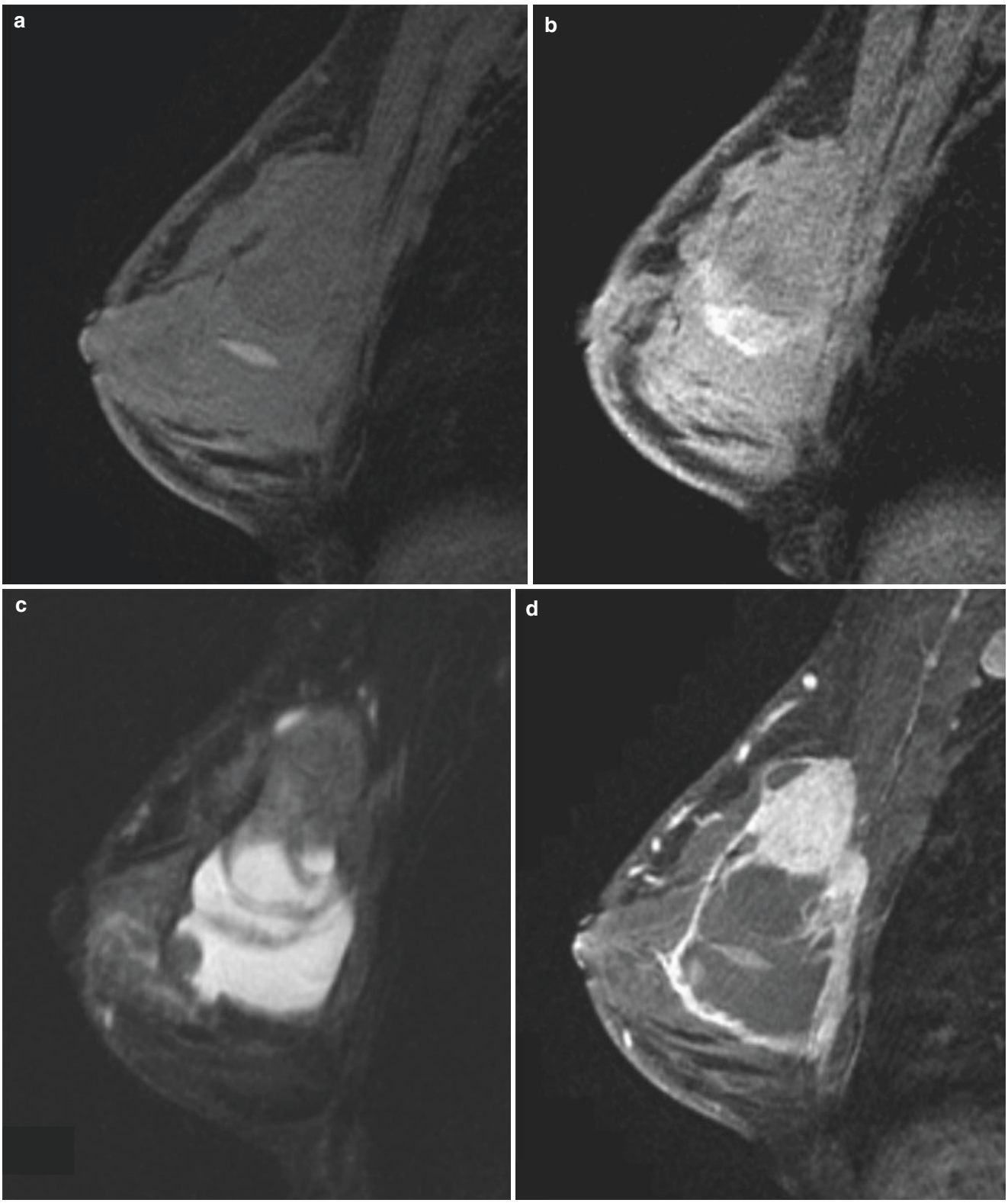

Fig. 5.9 Sagittal MR images of the right breast. (**a**, **b**) T1-weighted fat-saturated images. (**c**) T2-weighted fat-saturated image. (**d**) T1-weighted fat-saturated post-contrast image. (**e**) Corresponding CAD color overlay image

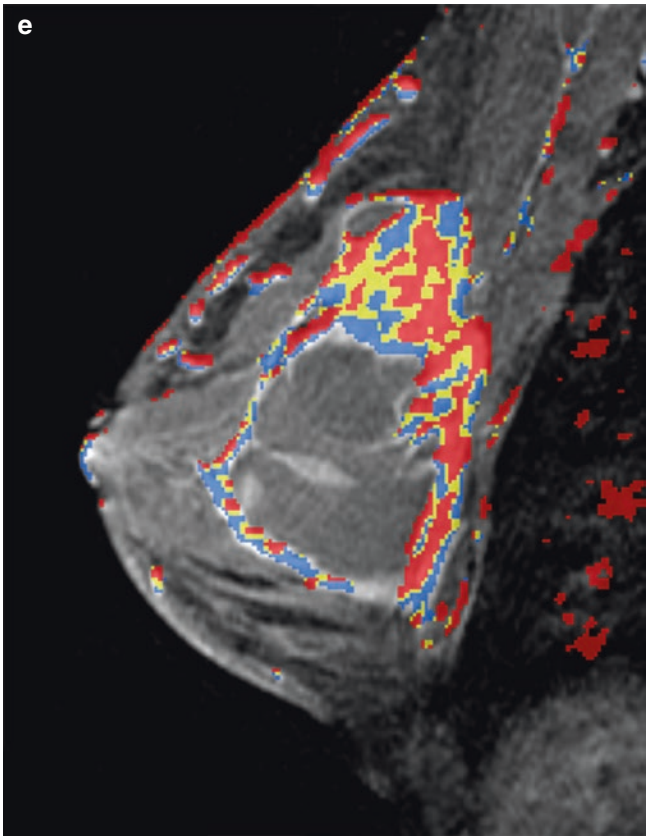

Fig. 5.9 (continued)

5.4 Sarcoma

Teaching Points Angiosarcoma of the breast is a rare malignancy of endovascular origin. It accounts for about 0.04 % of all malignant breast tumors and 8 % of breast sarcomas. It usually affects younger women in their third and fourth decade. Angiosarcoma of the breast tends to metastasize hematogenously rather than lymphogenously, so metastasis to axillary lymph nodes is very rare. The prognosis of angiosarcoma is thought to depend on the histologic grade, with higher-grade lesions more prone to developing recurrence and demonstrating a lower survival rate.

Misdiagnosis of angiosarcoma is not uncommon. It is sometimes due to the variety of possible clinical presentations, including mammographic and sonographic findings. Identifying a mass on mammography is difficult because angiosarcoma affects young women who have denser breast tissue. Associated skin thickening and calcifications may be seen. Ultrasound tends to be nonspecific and only seems to have equivocal additional value if a mass is visible at mammography.

On MRI, angiosarcomas are usually lobular-shaped masses with indistinct borders. On T2-weighted images, the periphery of the mass demonstrates a very bright signal that likely represents the presence of vascular channels containing slow-flowing blood. Angiosarcomas enhance intensely with washout kinetic features at dynamic imaging. Cystic cavities representing venous lakes are characteristic features, as seen in the example.

Image Findings

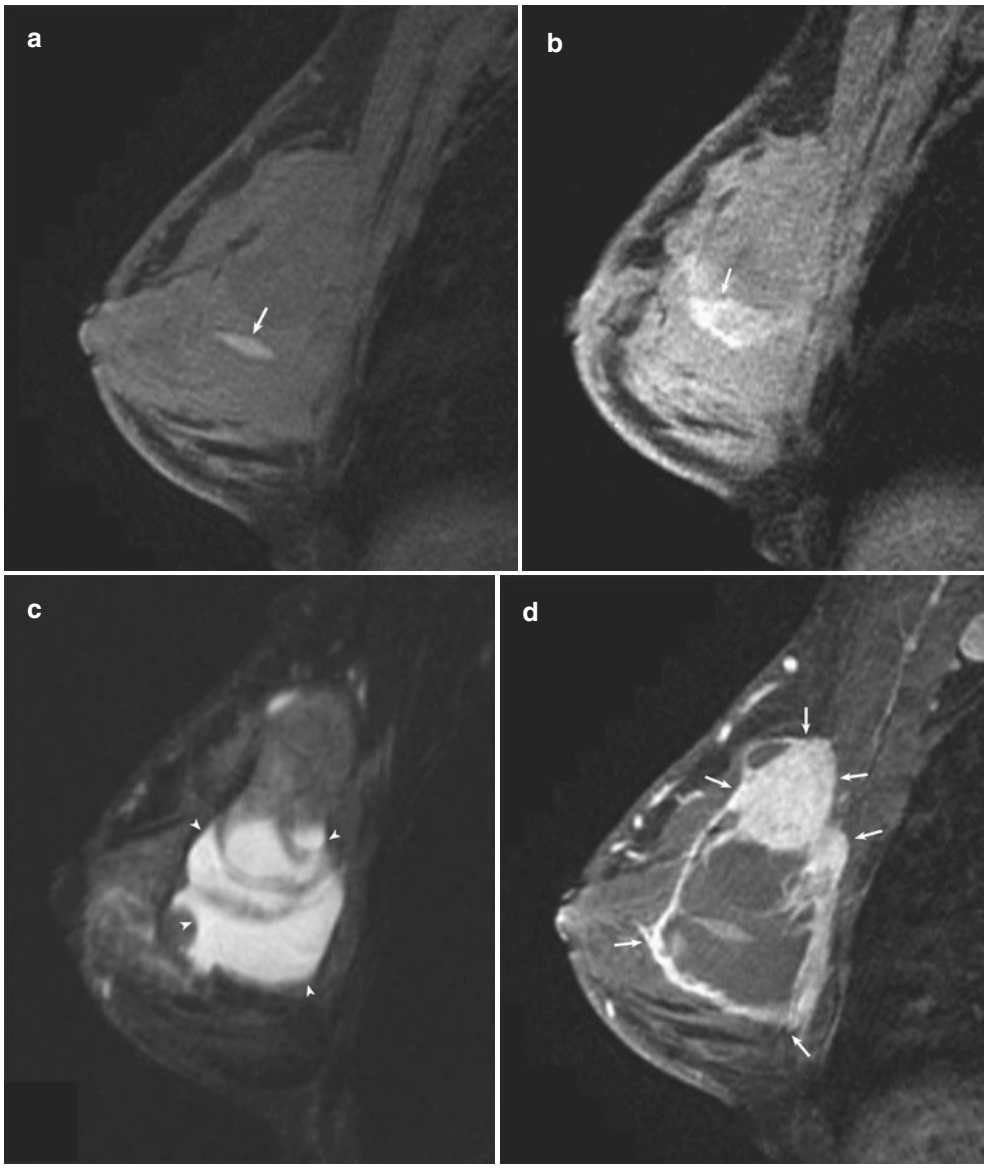

Fig. 5.10 Sagittal T1-weighted fat-saturated pre-contrast images (**a**, **b**) and a sagittal T2-weighted fat-saturated image (**c**) demonstrate irregular masses that are heterogeneously T1-hypointense to isointense and heterogeneously T2-hyperintense. These masses also contain irregular areas of T1 hyperintensity (*arrows*) reflecting the hemorrhagic nature of the tumors and their markedly heterogeneous architecture. Cystic cavities (*arrowheads*) representing venous lakes are present on T2 images. Marked enhancement of the masses (*arrows*) is noted on the sagittal T1-weighted fat-saturated post-contrast image (**d**), and CAD analysis (**e**) demonstrates washout enhancement kinetics

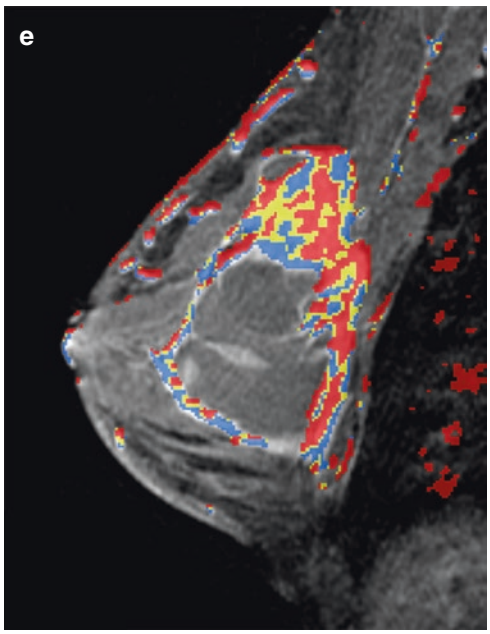

Fig. 5.10 (continued)

5.5 History

49-year-old woman with family history of breast cancer for high-risk screening breast MRI. History of melanoma 2 years ago status post resection (Figs. 5.11, 5.12, 5.13, and 5.14).

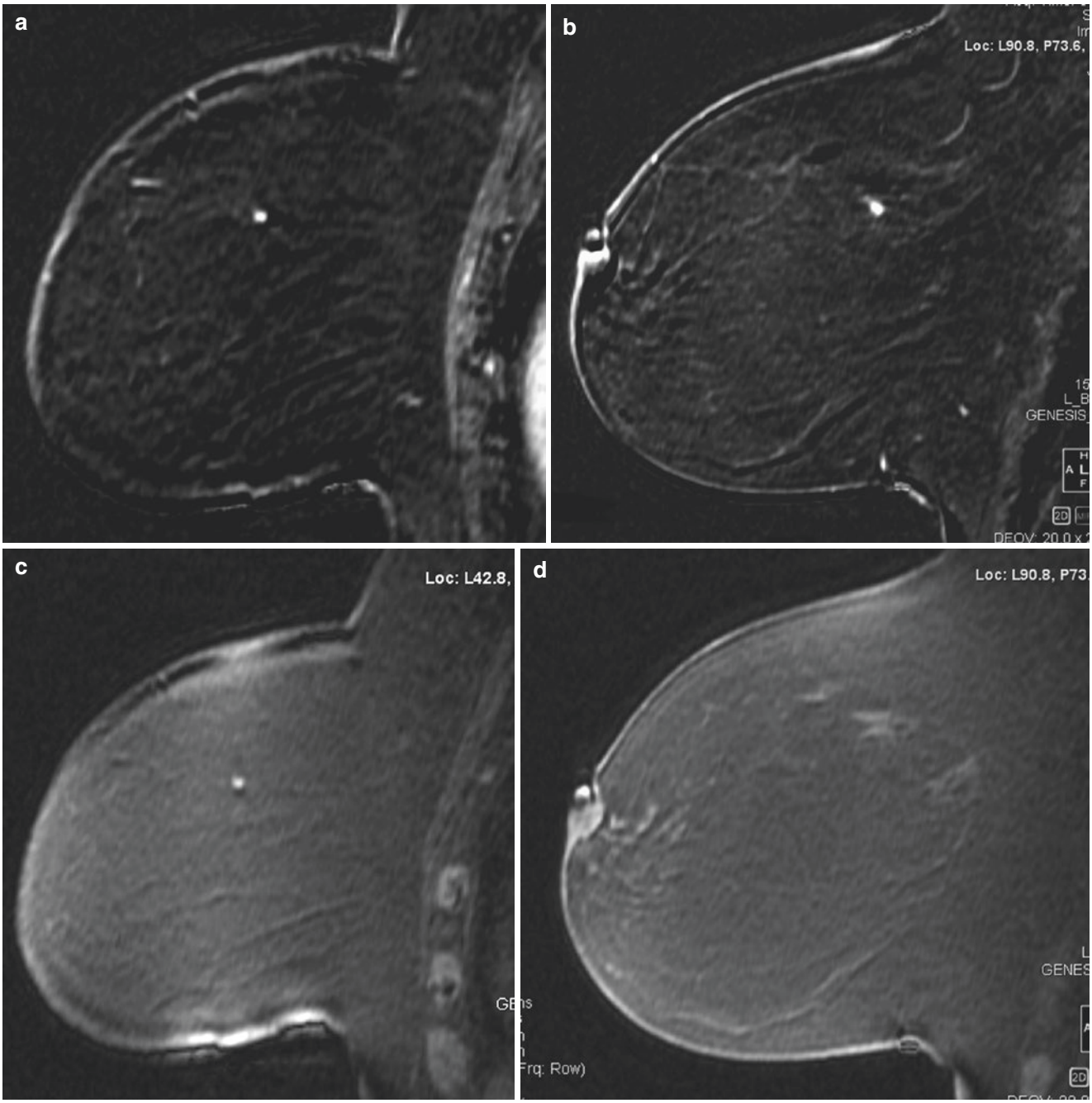

Fig. 5.11 Sagittal MR images of the left breast. (**a**, **b**) Post-contrast subtraction images. (**c**, **d**) T1-weighted fat-saturated images

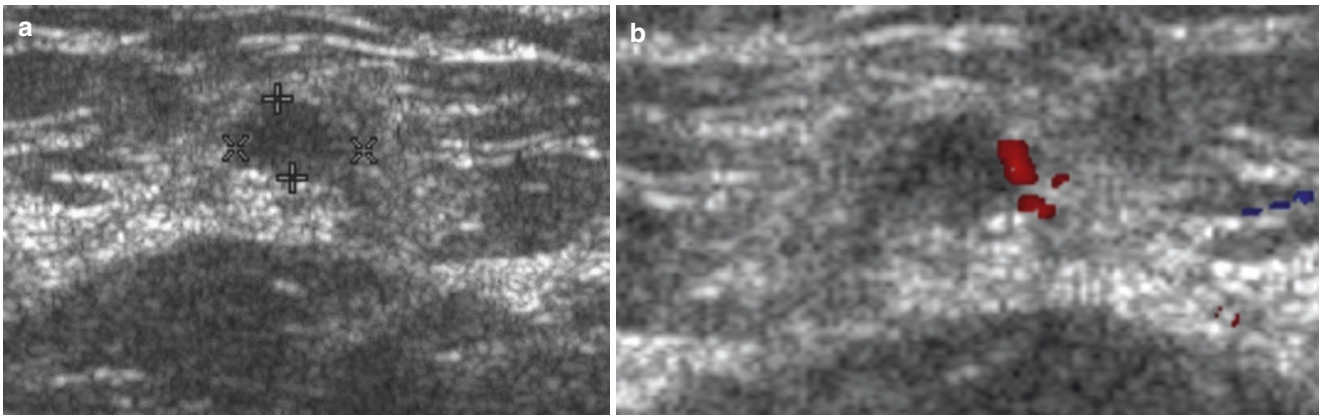

Fig. 5.12 Grayscale (**a**) and color Doppler (**b**) targeted ultrasound images of the left breast

5.5 Melanoma

Teaching Points Although metastasis to the breast is rare, melanoma is among the primary tumors most commonly reported to metastasize to the breast; metastasis should be suspected in patients with a prior history of melanoma even years after the primary tumor has been removed. Melanoma is typically T1-hyperintense secondary to hemorrhage or melanin, but it can be variable, as illustrated in this case. These lesions are typically hypointense on T2-weighted images. Post-contrast enhancement is typically heterogeneous or peripheral rim enhancement.

Image Findings

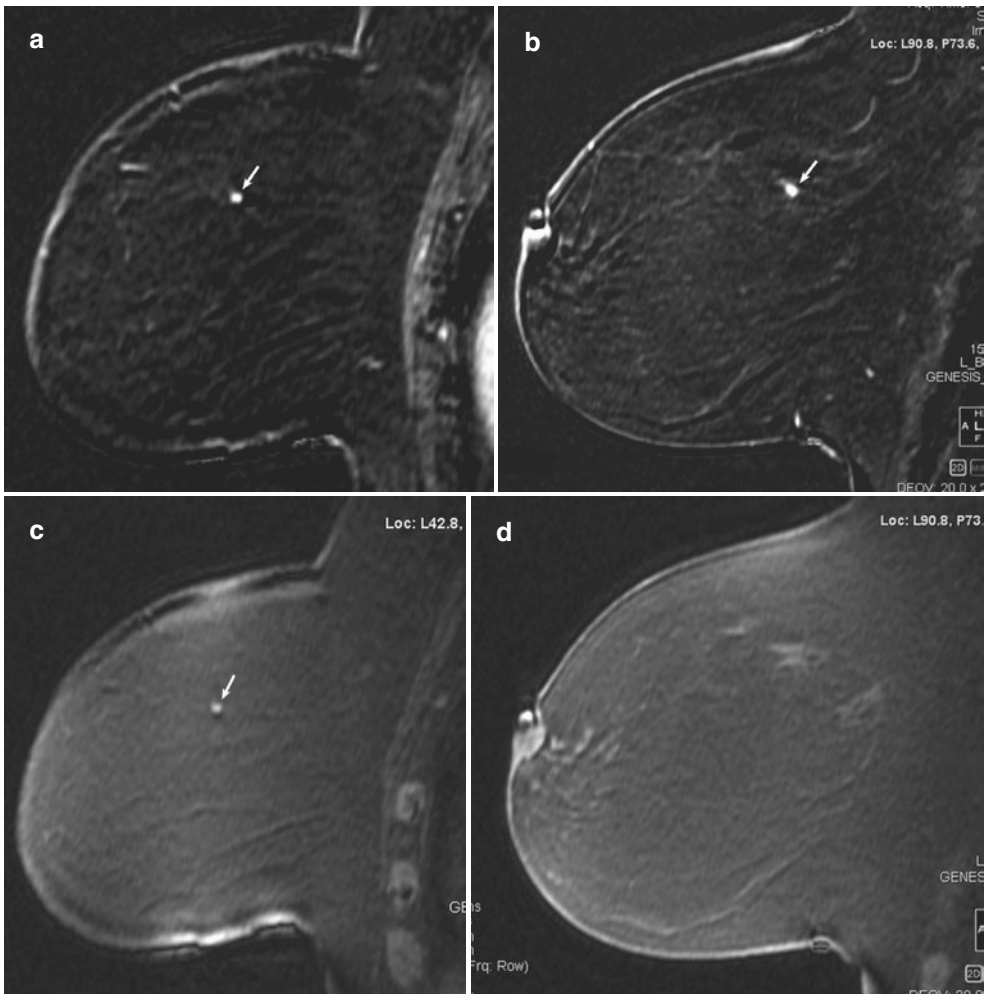

Fig. 5.13 Metastatic melanoma to the left breast on breast MRI. The patient was status post–surgical resection of a melanoma, with findings in the left breast seen incidentally on an abdominal MRI and further evaluated on a dedicated breast MRI. (**a**, **b**) Selected sagittal post-contrast subtraction images of the left breast demonstrate 3-mm and 4-mm enhancing foci (*arrows*) in the upper inner mid left breast. (**c**) The 3-mm enhancing focus has a T1-hyperintense correlate on the T1-weighted fat-saturated non-contrast image. (**d**) The 4-mm enhancing focus has no corresponding signal abnormality on the T1-weighted fat-saturated non-contrast image

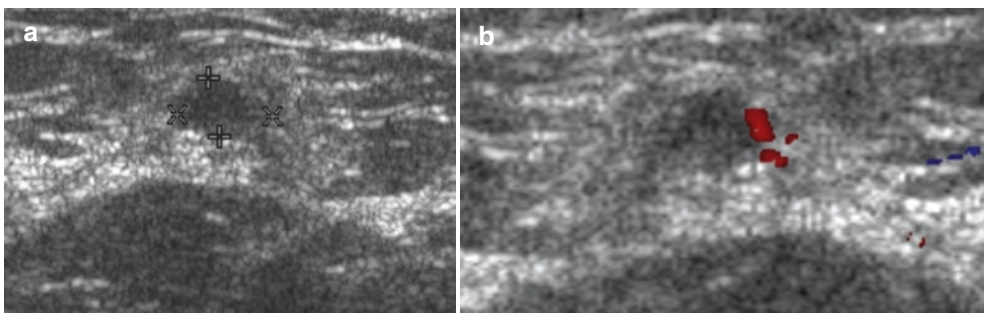

Fig. 5.14 Metastatic melanoma on targeted left breast ultrasound. Correlative grayscale (**a**) and color Doppler (**b**) ultrasound images of the left breast demonstrate two irregular, hypoechoic masses with internal vascularity, corresponding to the breast MRI findings. Ultrasound-guided core needle biopsy yielded metastatic melanoma at both sites

5.6 History

Extent of disease evaluation (Figs. 5.15 and 5.16).

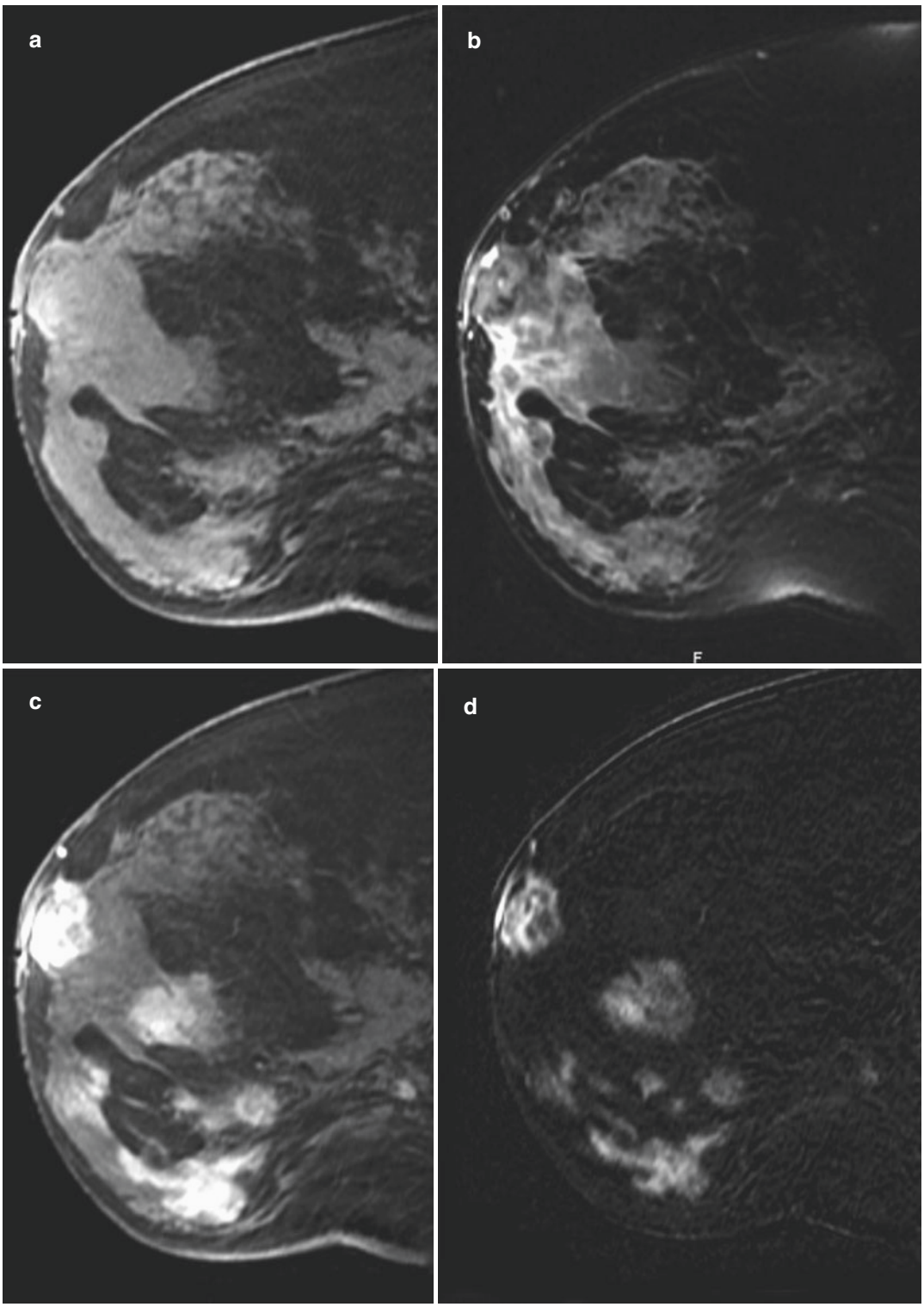

Fig. 5.15 Sagittal MR images of the left breast. (**a**) T1-weighted fat-saturated image. (**b**) T2-weighted fat-saturated image. (**c**) T1-weighted fat-saturated post-contrast image. (**d**) Post-contrast subtraction image. (**e**) Image from **d** with CAD color overlay. (**f**) Post-contrast maximum intensity projection (MIP) image

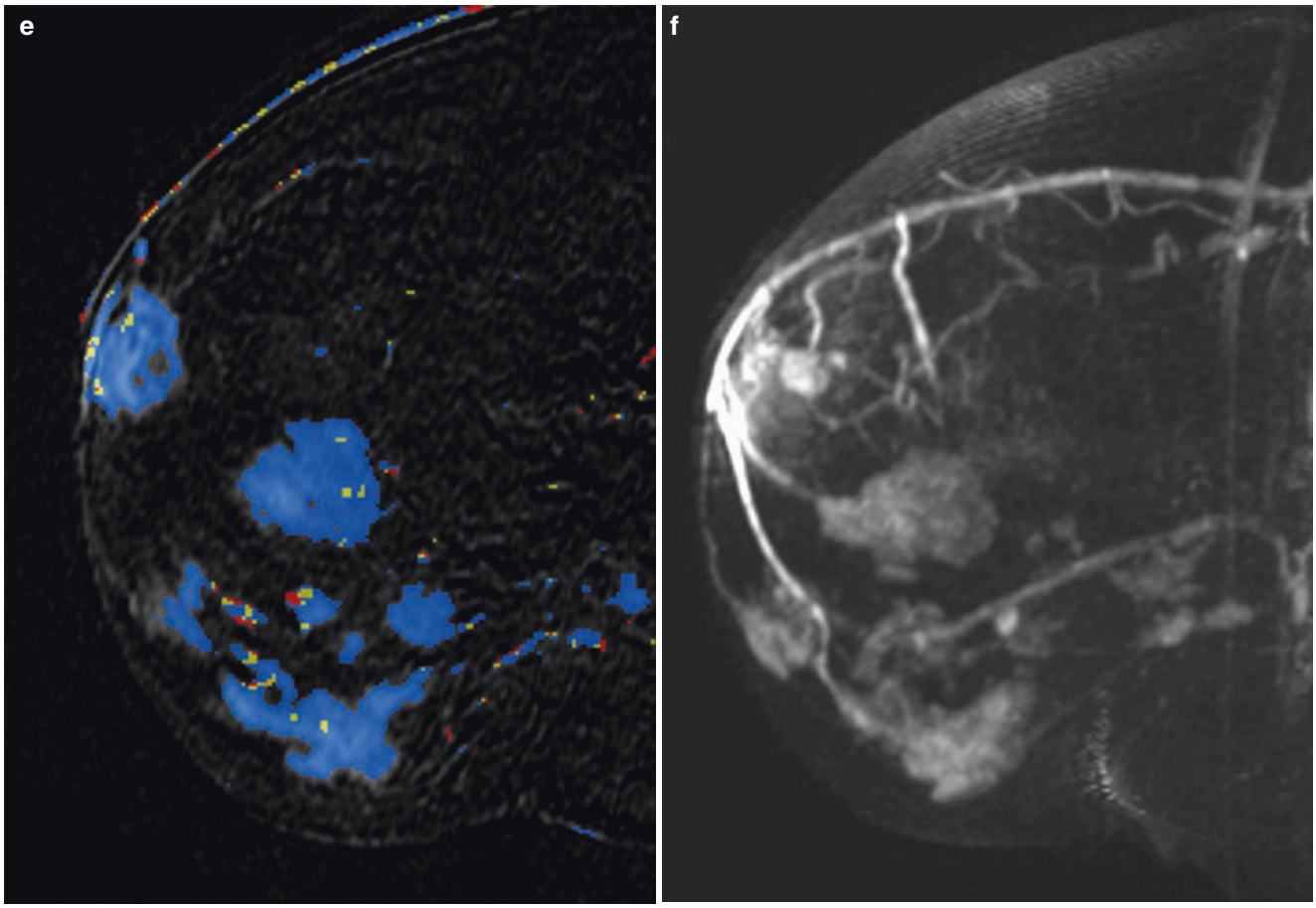

Fig. 5.15 (continued)

5.6 Lymphoma

Teaching Points Lymphoma of the breast is uncommon and constitutes 0.04–0.5 % of malignant breast neoplasms. The small amount of lymphoid tissue in the breast accounts for the rarity of primary breast lymphoma when compared with other organs. Differentiating primary from secondary lymphoma remains challenging. The presence of breast tissue in or adjacent to the lymphomatous infiltrate, the absence of concurrent nodal disease (except for the ipsilateral axillary lymph nodes), and the absence of a history of lymphoma involving other organs are suggestive of primary disease.

Mammographically, lymphoma typically presents as a large, circumscribed or indistinctly marginated mass without associated calcifications or architectural distortion. On ultrasound, it can be hypoechoic to nearly anechoic, mimicking a cyst. On MR imaging, the mass is usually isointense to hypointense on T1-weighted imaging and isointense to hyperintense on T2-weighted imaging, with progressive enhancing kinetics on dynamic contrast imaging as seen in Figs. 5.15e and 5.16e.

Image Findings

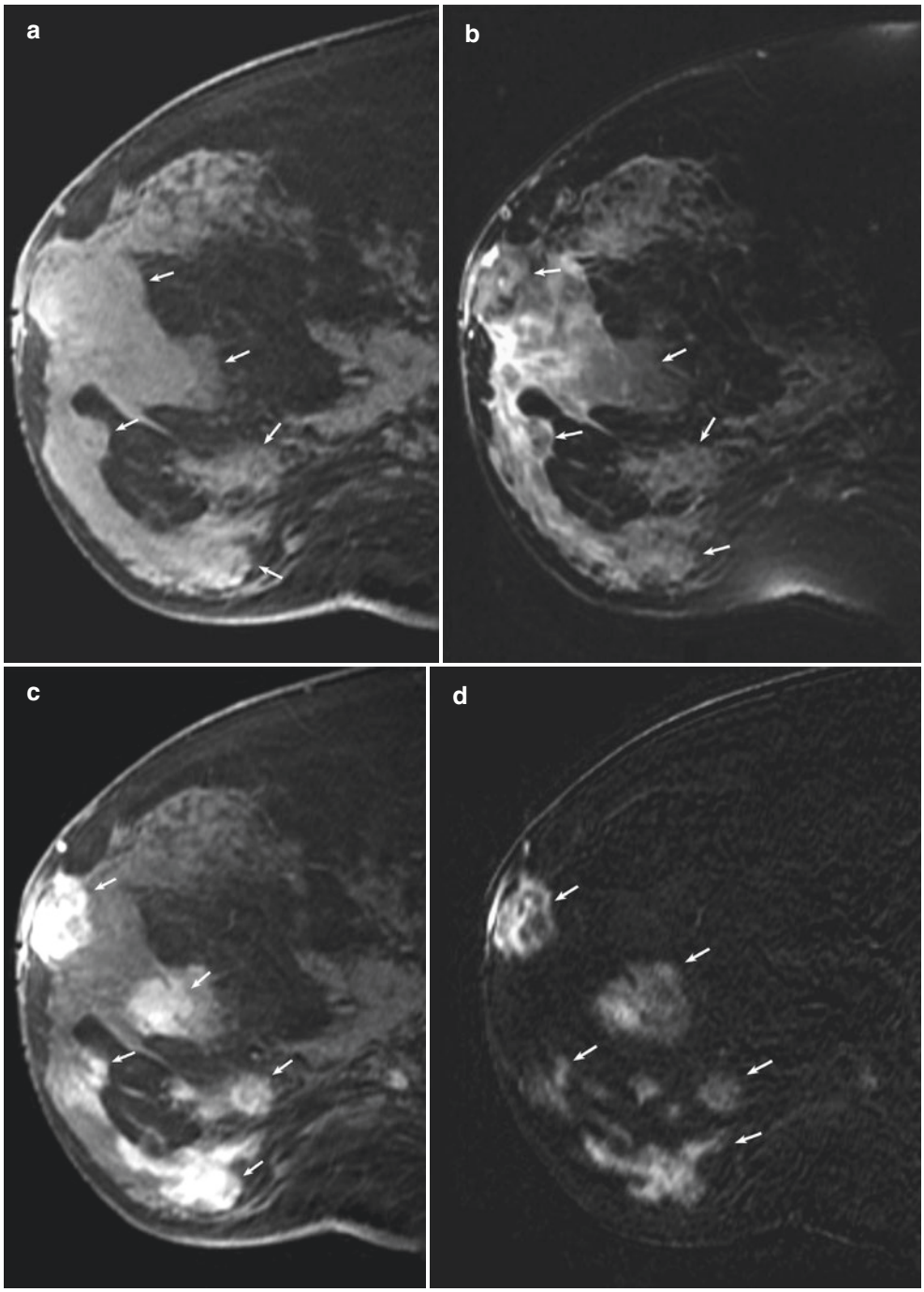

Fig. 5.16 Left breast lymphoma. The sagittal T1-weighted fat-saturated image (**a**) and T2-weighted fat-saturated image (**b**) demonstrate T1-isointense to mildly hypointense and T2-isointense to hyperintense masses throughout the breast (*arrows*). A T1-weighted fat-saturated post-contrast image (**c**), post-contrast subtraction image (**d**), and CAD kinetic analysis image (**e**) demonstrate heterogeneously enhancing irregular masses (*arrows*) with progressive enhancement kinetics. (**f**) A post-contrast MIP demonstrates the multiple enhancing, irregular masses (*arrows*)

Fig. 5.16 (continued)

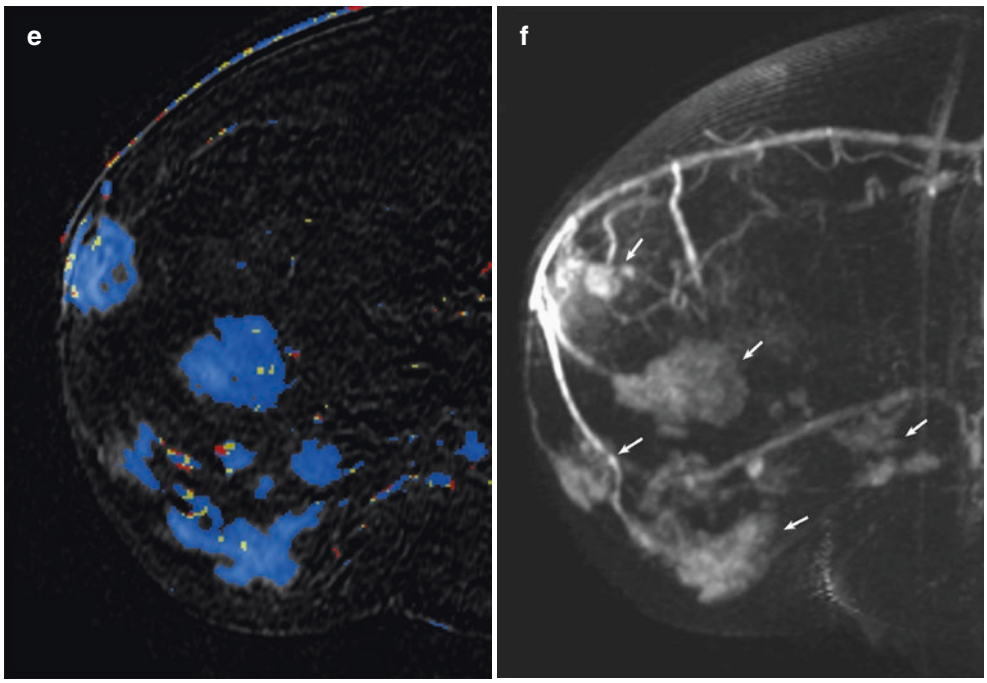

5.7 History

51-year-old with bilateral axillary enlarged lymph nodes (Figs. 5.17, 5.18, 5.19, and 5.20).

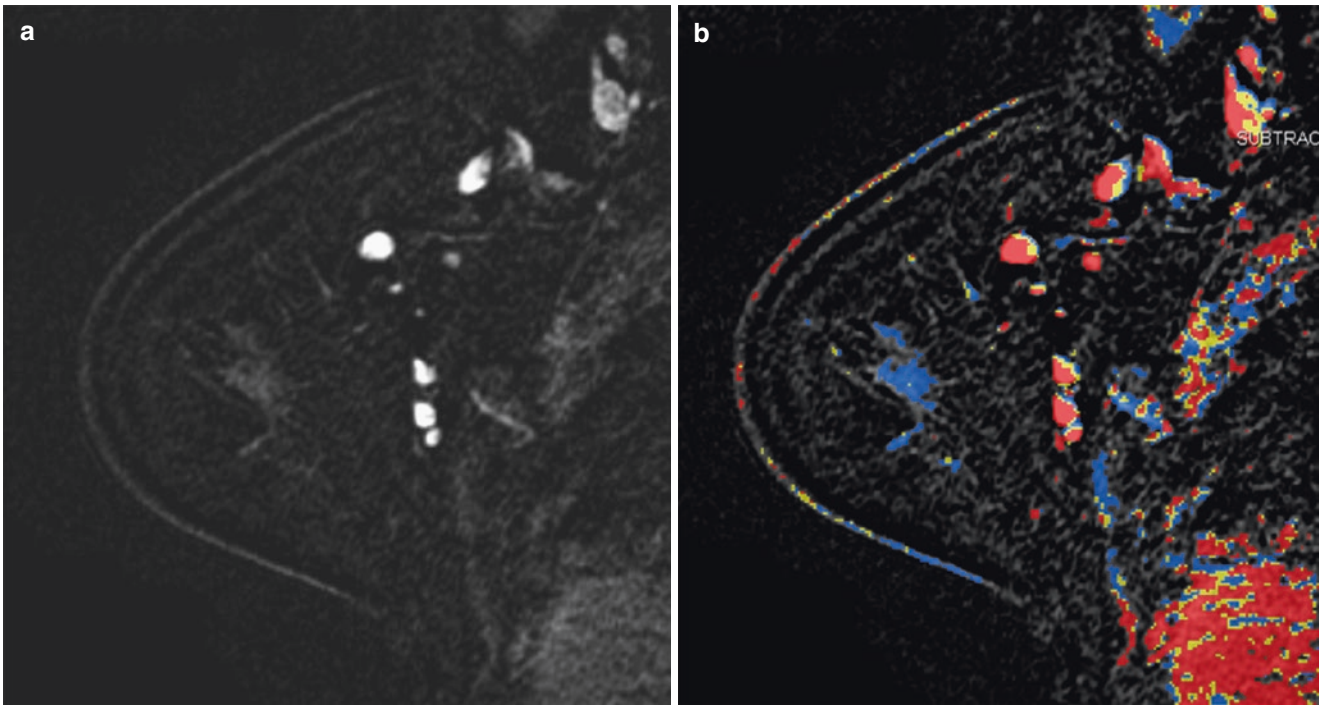

Fig. 5.17 (**a**) Sagittal post-contrast subtraction image of the right breast. (**b**) Corresponding CAD color overlay image

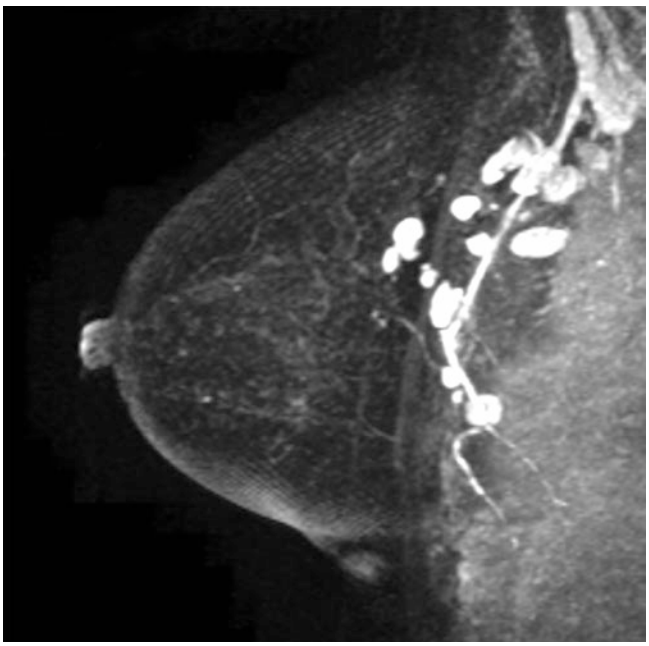

Fig. 5.18 Left breast post-contrast MIP from a breast MRI

5.7 HIV Infection

Teaching Points Multiple bilateral, enlarged axillary lymph nodes may be seen incidentally on screening mammogram, ultrasound, or MRI in female patients infected with HIV. Other common causes of bilateral axillary lymphadenopathy include sarcoidosis, rheumatoid arthritis, lymphoma (CLL), and leukemia. Obtaining a thorough clinical history from patients provides critical information to guide their management. In the absence of a systemic disease, biopsy or fine-needle aspiration (FNA) could be indicated to evaluate for occult breast malignancy.

Image Findings

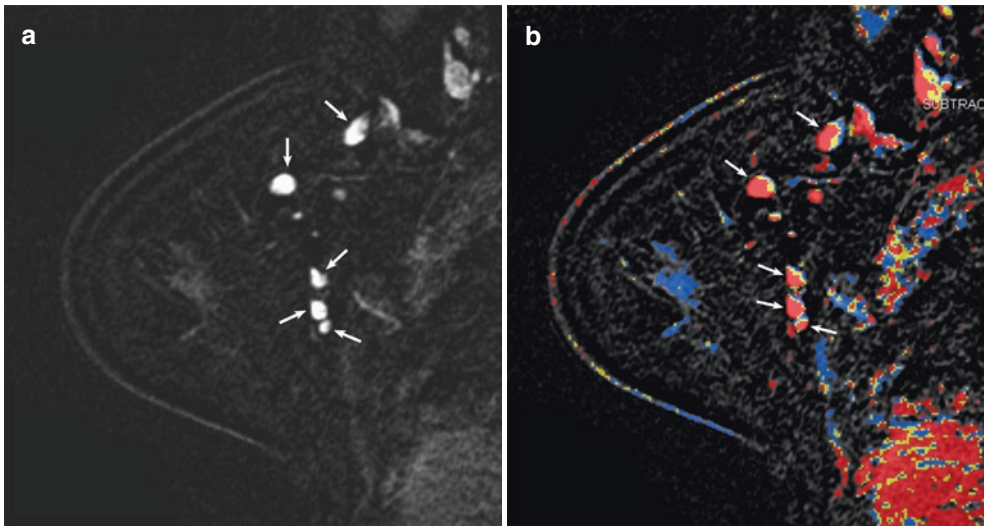

Fig. 5.19 Bilateral lymphadenopathy secondary to HIV infection. (**a**) Sagittal post-contrast subtraction image of the right breast demonstrates multiple, enlarged right axillary lymph nodes (*arrows*). (**b**) CAD kinetics analysis shows the expected washout pattern (*arrows*)

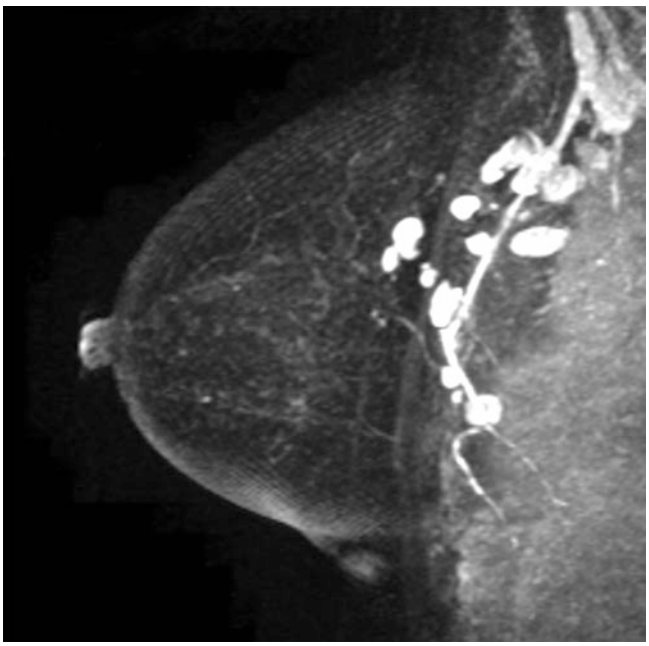

Fig. 5.20 Left breast post-contrast MIP, also showing enlarged left axillary lymph nodes

Suggested Reading

Díaz-Bustamante T, Iríbar M, Vilarrasa A, Benito A, López-Ríos F. Primary amyloidosis of the breast presenting solely as microcalcifications. AJR Am J Roentgenol. 2001;177:903–4.

Ebrahim L, Parry J, Taylor DB. Fibromatosis of the breast: a pictorial review of the imaging and histopathology findings. Clin Radiol. 2014;69:1077–83.

Eghtedari M, Dogan BE, Gilcrease M, Roberts J, Cook ED, Yang WT. Imaging and pathologic characteristics of breast amyloidosis. Breast J. 2015;21:197–9.

Elsayes KM, Narra VR, Leyendecker JR, Francis IR, Lewis Jr JS, Brown JJ. MRI of adrenal and extraadrenal pheochromocytoma. AJR Am J Roentgenol. 2005;184:860–7.

Erguvan-Dogan B, Dempsey PJ, Ayyar G, Gilcrease MZ. Primary desmoid tumor (extraabdominal fibromatosis) of the breast. AJR Am J Roentgenol. 2005;185:488–9.

Görkem SB, O'Connell AM. Abnormal axillary lymph nodes on negative mammograms: causes other than breast cancer. Diagn Interv Radiol. 2012;18:473–9.

Ha KY, Deleon P, Hamilton R. Breast fibromatosis mimicking breast carcinoma. Proc (Bayl Univ Med Cent). 2013;26:22–4.

Irshad A, Ackerman SJ, Pope TL, Moses CK, Rumboldt T, Panzegrau B. Rare breast lesions: correlation of imaging and histologic features with WHO classification. Radiographics. 2008;28:1399–414.

Kikawa Y, Konishi Y, Nakamoto Y, Harada T, Takeo M, Ogata M, et al. Angiosarcoma of the breast – specific findings of MRI. Breast Cancer. 2006;13:369–73.

Leung K, Stamm M, Raja A, Low G. Pheochromocytoma: the range of appearances on ultrasound, CT, MRI, and functional imaging. AJR Am J Roentgenol. 2013;200:370–8.

Lim RF, Goei R. Best cases from the AFIP: angiosarcoma of the breast. Radiographics. 2007;27 Suppl 1:S125–30.

Loffeld A, Marsden JR. Management of melanoma metastasis to the breast: case series and review of the literature. Br J Dermatol. 2005;152:1206–10.

Meerkotter D, Rubin G, Joske F, Angunawela P, Khalafallah A. Primary breast lymphoma: a rare entity. J Radiol Case Rep. 2011;5:1–9.

O'Brien J, Aherne S, McCormack O, Jeffers M, McInerney D. MRI features of bilateral amyloidosis of breast. Breast J. 2013;19:338–9.

Orgüç S, Başara I, Pekindil G, Coşkun T. Contribution of kinetic characteristics of axillary lymph nodes to the diagnosis in breast magnetic resonance imaging. Balkan Med J. 2012;29:285–9.

Ravdel L, Robinson WA, Lewis K, Gonzalez R. Metastatic melanoma in the breast: a report of 27 cases. J Surg Oncol. 2006;94:101–4.

Rizzo S, Preda L, Villa G, Brambilla S, Pruneri G, Alietti A, et al. Magnetic resonance imaging of primary breast lymphoma. Radiol Med. 2009;114:915–24.

Yang WT, Hennessy BT, Dryden MJ, Valero V, Hunt KK, Krishnamurthy S. Mammary angiosarcomas: imaging findings in 24 patients. Radiology. 2007;242:725–34.

Breast Implants

6

Christopher E. Comstock, Lauren Friedlander,
Victoria Mango, and Richard Ha

Christopher E. Comstock
Breast Imaging Service, Memorial Sloan-Kettering Cancer Center,
New York, NY, USA

Associate Professor of Radiology, Weill Cornell Medical College,
New York, NY, USA

L. Friedlander, MD
Director of Breast and Body Imaging Fellowship,
Division of Breast Imaging, Assistant Professor of Radiology,
Columbia University Medical Center, New York, NY, USA
e-mail: lf2386@columbia.edu

V. Mango, MD
Director of Breast and Body Imaging Fellowship,
Breast Imaging Service, Memorial Sloan-Kettering Cancer Center,
Assistant Professor of Radiology, Weill Cornell Medical College,
New York, NY, USA
e-mail: vlm2125@columbia.edu

R. Ha, MD (✉)
Director of Education and Research,
Division of Breast Imaging, Assistant Professor of Radiology,
Columbia University Medical Center, New York, NY, USA
e-mail: rh2616@cumc.columbia.edu

R. Ha et al. (eds.), Breast MRI Teaching Atlas, DOI 10.1007/978-1-4939-6409-3_6

6.1 History

39-year-old woman undergoing high-risk screening MRI.

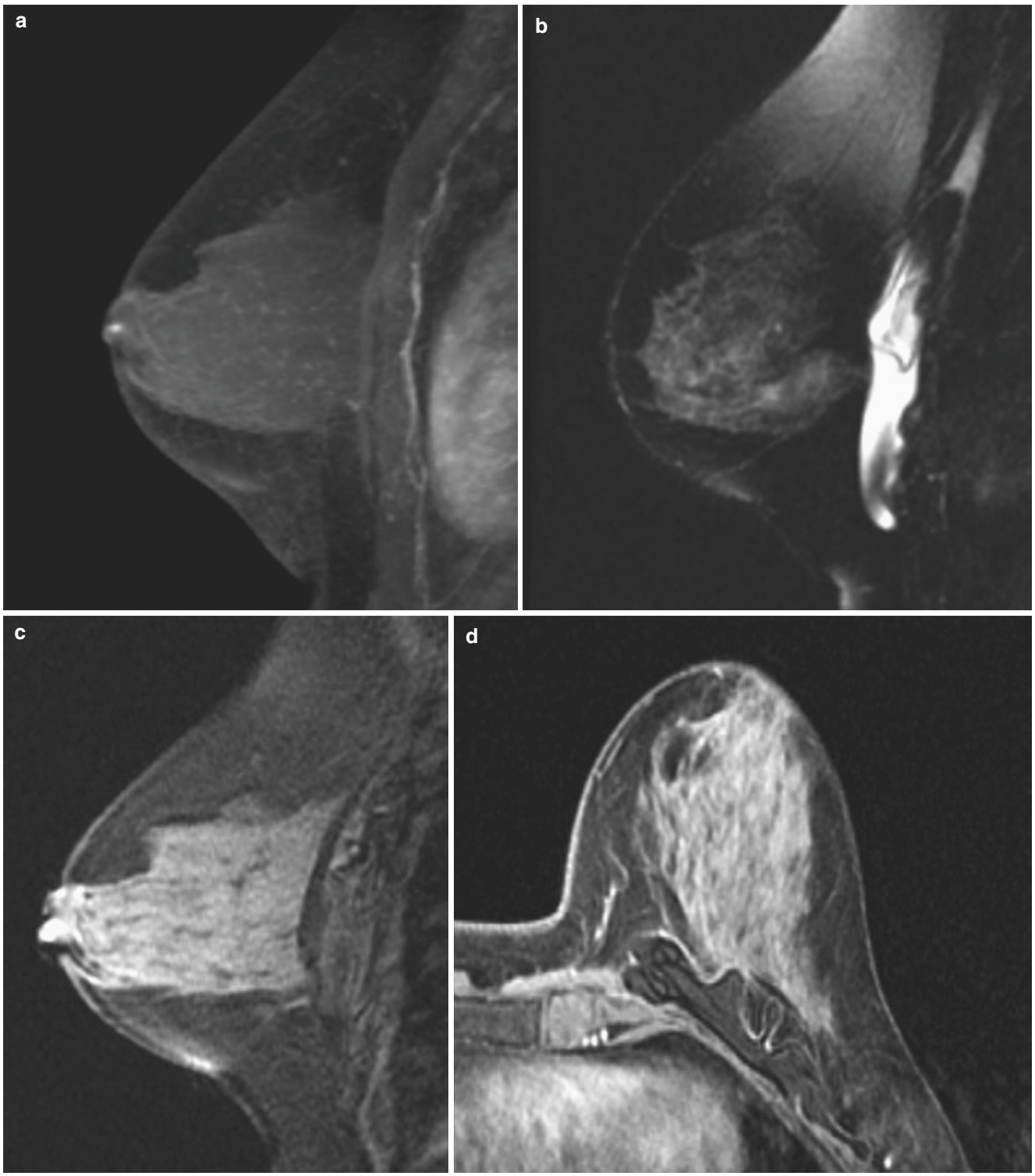

Fig. 6.1 Sagittal T1-weighted fat-saturated post-contrast maximum intensity projection (MIP) image (**a**), sagittal T2-weighted fat-saturated image (**b**), sagittal T1-weighted fat-saturated image (**c**), and axial T1-weighted fat-saturated image (**d**)

6.1 Saline Rupture

Teaching Points Implant rupture is a well-known complication and is the main cause of implant removal. Most ruptures have no obvious traumatic origin, and rupture is sometimes present in asymptomatic patients. MRI is generally accepted as the technique of choice for evaluating the integrity of silicone implants, with a sensitivity of 70–94 % and a specificity of 85–100 %. Patients with saline implant rupture usually report an obvious change in size with fluid extrusion, for which breast MRI is not necessary for diagnosis. Saline implants follow fluid signal on all sequences and have a valve to allow volume adjustment, which helps to identify them on MRI. In our case example (Figs. 6.1 and 6.2), saline implant rupture with complete collapse was incidentally found on a high-risk screening breast MRI.

Image Findings

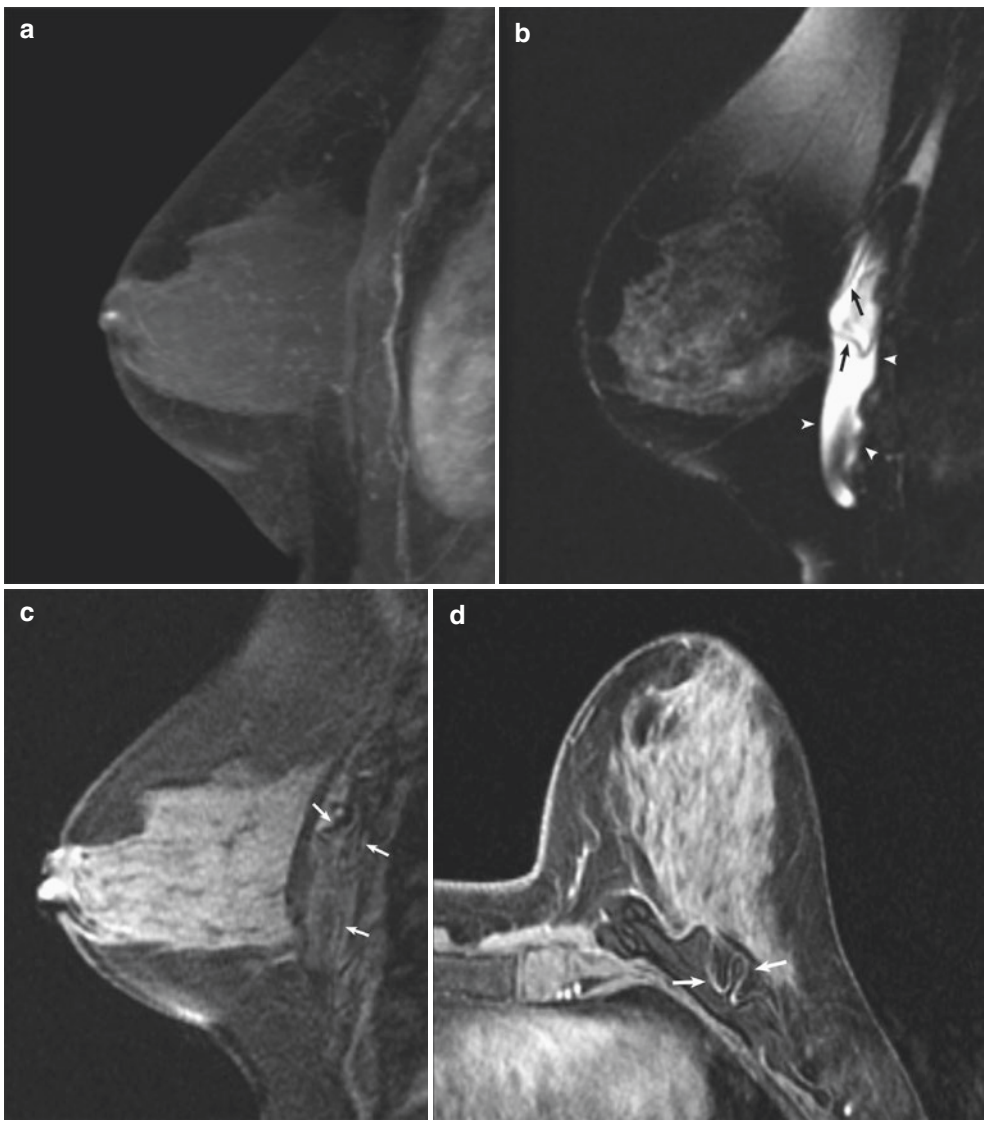

Fig. 6.2 Saline implant rupture. (**a**) Sagittal T1-weighted post-contrast MIP demonstrates no suspicious enhancement. (**b**) Sagittal T2-weighted fat-saturated image demonstrates a collapsed saline implant (*arrows*) with surrounding T2 hyperintensity (*arrowheads*). Sagittal (**c**) and axial (**d**) T1-weighted fat-saturated images demonstrate corresponding T1 hypointensity surrounding the collapsed implant (*arrows*)

6.2 History

32-year-old woman status post motor vehicle accident. History of implant (Fig. 6.3).

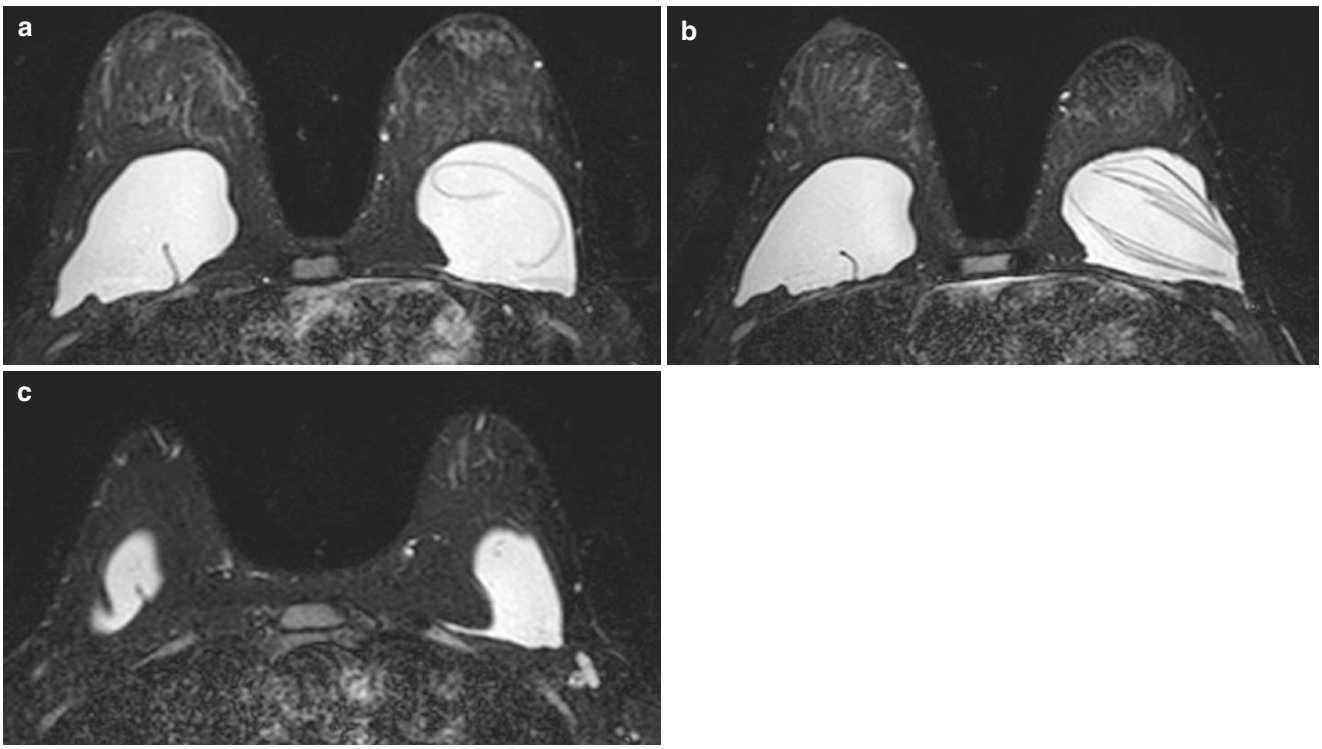

Fig. 6.3 (**a**–**c**) Axial T2-weighted fat-saturated MR images through both breasts

6.2 Silicone Implant Rupture 1

Teaching Points MR imaging can diagnose silicone breast implant rupture with a high sensitivity and specificity, with a positive predictive value of about 99 %. Silicone implant rupture is usually unnoticed by the patient because free silicone is kept in place by the surrounding fibrous capsule, which begins forming immediately after surgery as a natural foreign body reaction.

Extracapsular silicone implant rupture is defined as rupture of both the implant shell and the fibrous capsule, with macroscopic silicone leakage extending beyond the fibrous capsule into surrounding tissues and rarely to distant body regions (Fig. 6.4). *Intracapsular* rupture is defined as rupture of the implant shell with an intact fibrous capsule. The "linguine sign" (the presence of multiple curvilinear, low–signal-intensity lines within the silicone implant) is considered the most reliable MRI characteristic for intracapsular rupture and is often seen with extracapsular implant ruptures.

Radial folds, which are considered to be normal variants, are infoldings of the implant membrane into the silicone implant. On MRI, they appear as blind-ending lines extending from the surface of the implant (Fig. 6.4c).

Image Findings

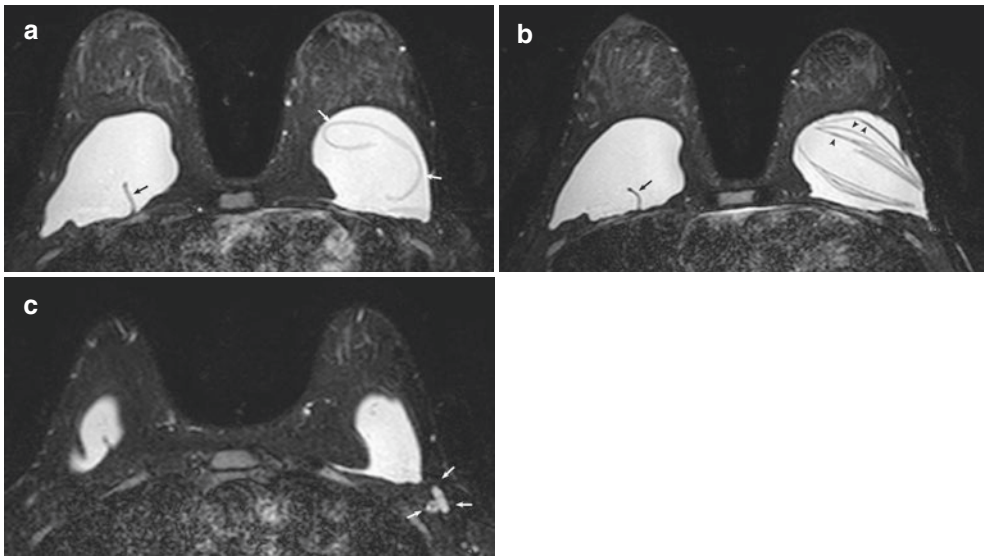

Fig. 6.4 Left extracapsular silicone implant rupture and right silicone implant radial fold. (**a**, **b**) Selected axial T2-weighted fat-saturated images demonstrate collapse of the left silicone implant shell (*white arrows*) with extravasation of silicone into the fibrous capsule. The "linguini sign" (*black arrowheads* in **b**) of intracapsular rupture is evident. Complex radial folds (*black arrow* in **b**) are present involving the right silicone implant shell without evidence of right implant rupture. (**c**) On a more inferior T2-weighted fat-saturated axial image, there is extracapsular leak of silicone (*white arrows*) laterally into the soft tissue along the left chest wall

6.3 History

41-year-old woman with recent chest trauma. History of implants (Figs. 6.5, 6.6, 6.7, and 6.8).

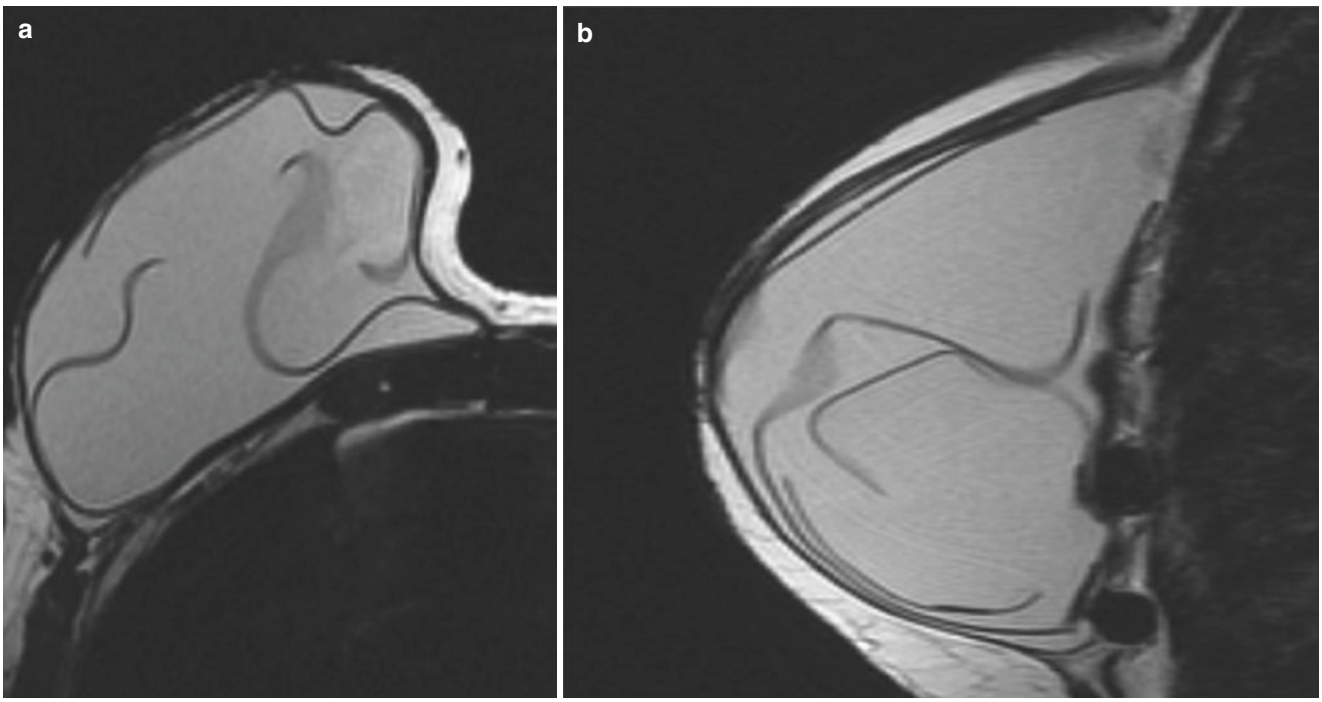

Fig. 6.5 Axial T2-weighted water-saturated image (**a**) and sagittal T2-weighted image (**b**) of the right breast from an implant protocol breast MRI

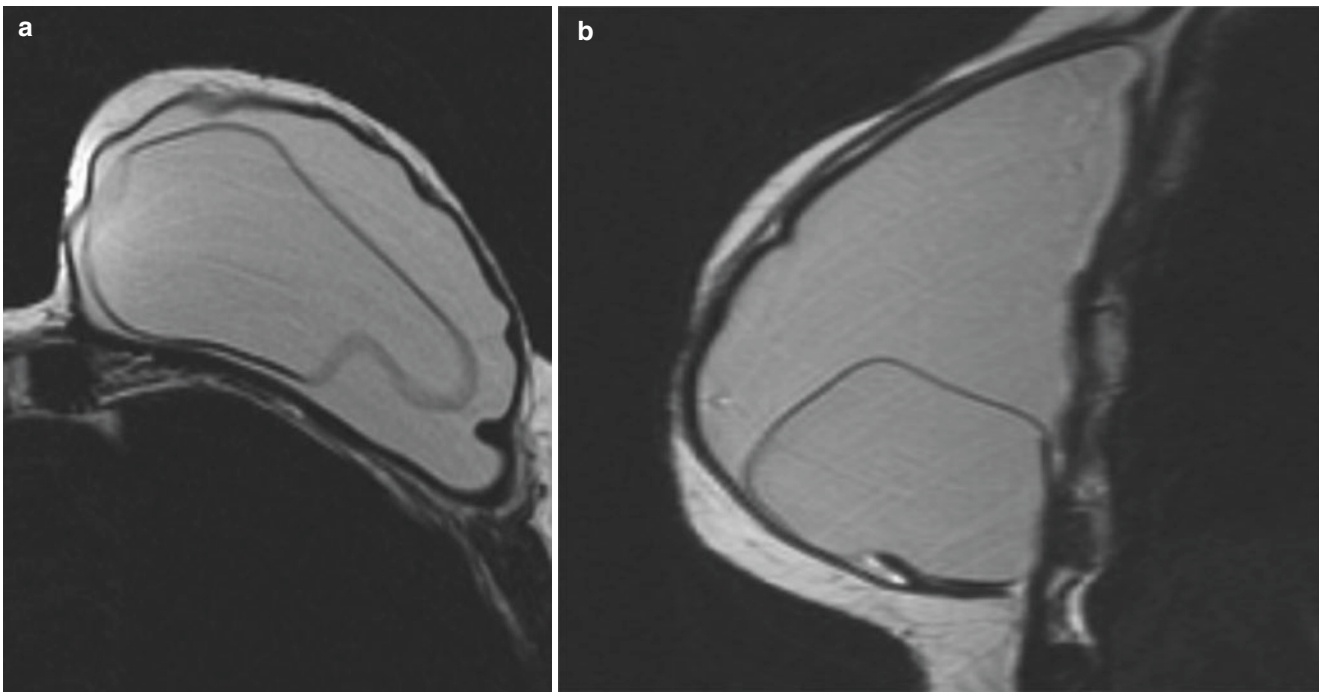

Fig. 6.6 Axial T2-weighted water-saturated image (**a**) and sagittal T2-weighted image (**b**) of the left breast from an implant protocol breast MRI

6.3 Double-Lumen Implant

Teaching Points Double-lumen implants are less commonly used. They typically have a fixed, smaller outer lumen filled with saline surrounding a larger inner lumen of high–signal-intensity silicone. A rupture diagnosis for a double-lumen implant requires both membranes to be ruptured.

Image Findings

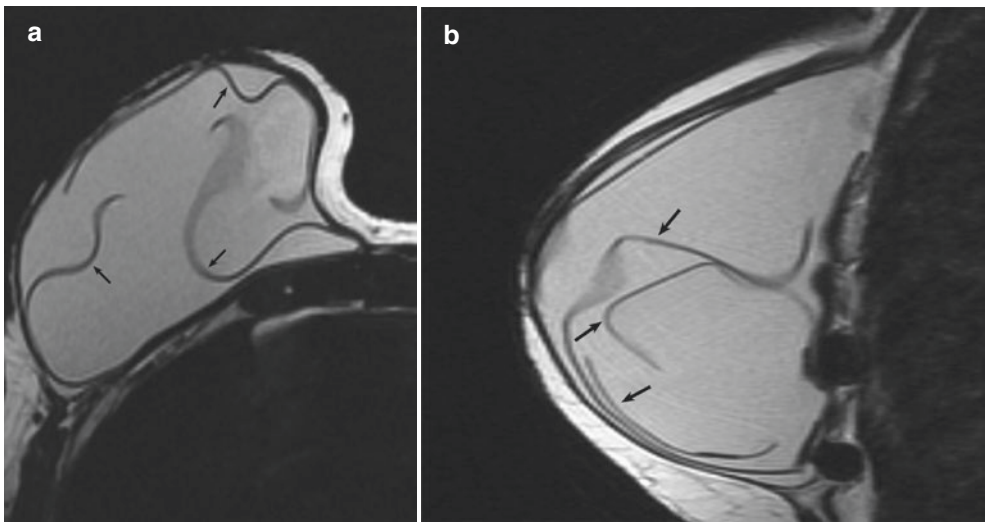

Fig. 6.7 Intracapsular rupture of right double-lumen implant. The axial T2-weighted water-saturated image (**a**) and the sagittal T2-weighted image (**b**) of the right breast demonstrate multiple low-intensity curvilinear lines (*arrows*) contained within the fibrous capsule, representing the collapsed implant shell ("linguine sign"). There is no extrusion of silicone beyond the fibrous capsule, compatible with an intra-capsular rupture

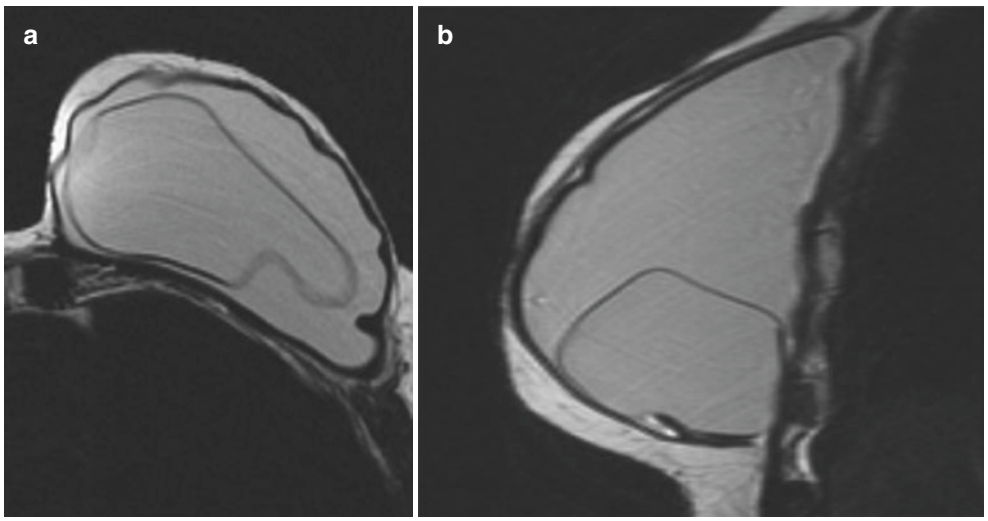

Fig. 6.8 For comparison, the corresponding axial T2-weighted water-saturated image (**a**) and sagittal T2-weighted image (**b**) of the left breast demonstrate an intact double-lumen implant

6.4 History

51-year-old woman with possible silicone implant rupture (Figs. 6.9 and 6.10).

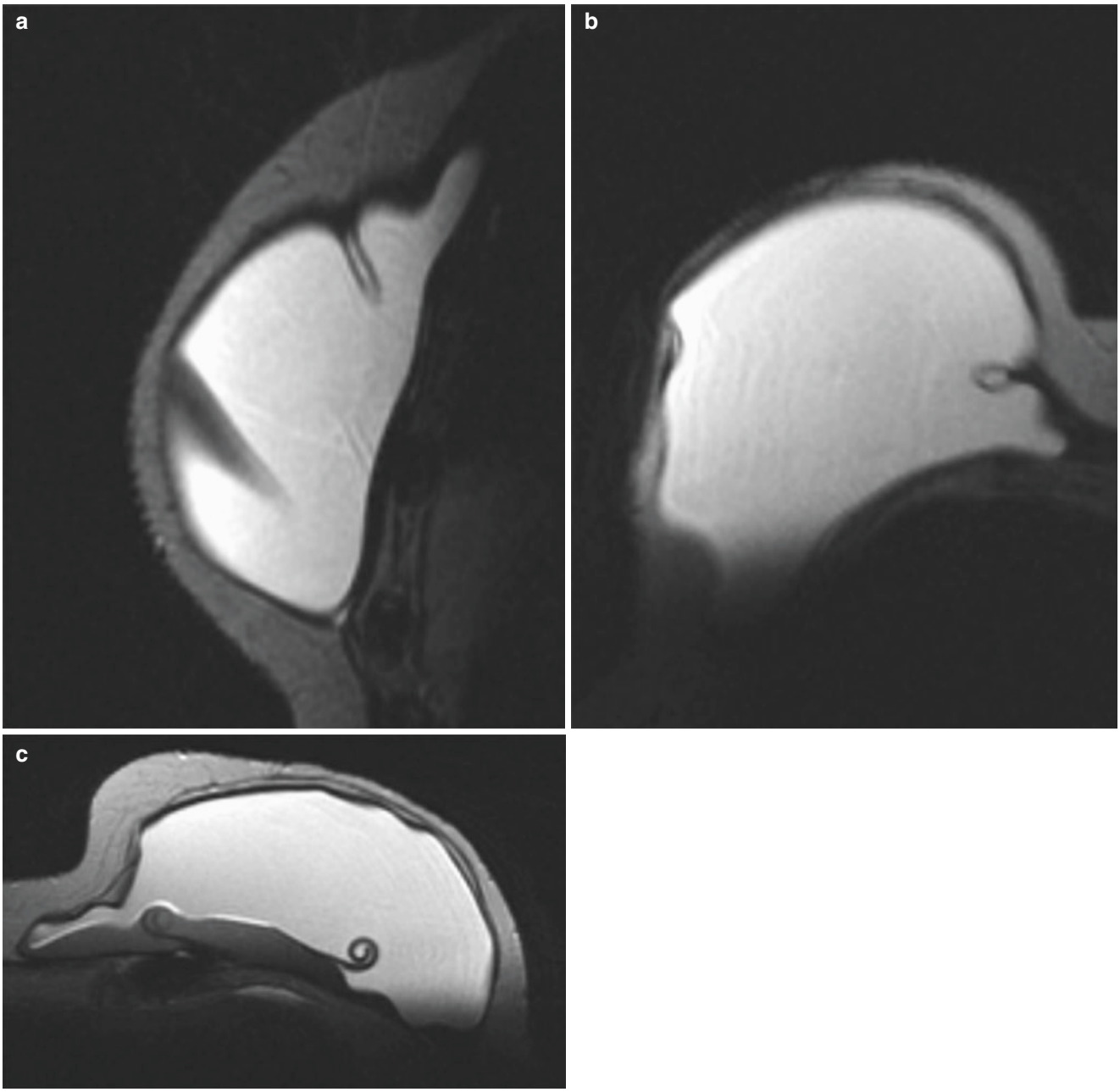

Fig. 6.9 Sagittal T2-weighted water-suppressed image (**a**) and axial T2-weighted image (**b**) of the right breast. (**c**) Axial T2-weighted image of the left breast

6.4 Silicone Implant Rupture 2

Teaching Points Occasionally, focal silicone gel leakage may occur through a small defect in the implant shell. On MRI, this appears as a focal silicone invagination between the implant shell and the fibrous capsule, referred to as a "noose sign," "inverted teardrop sign," or "keyhole sign." Please note that the two membranes do not touch, allowing differentiation between this finding and the teardrop sign (*not shown*).

Image Findings

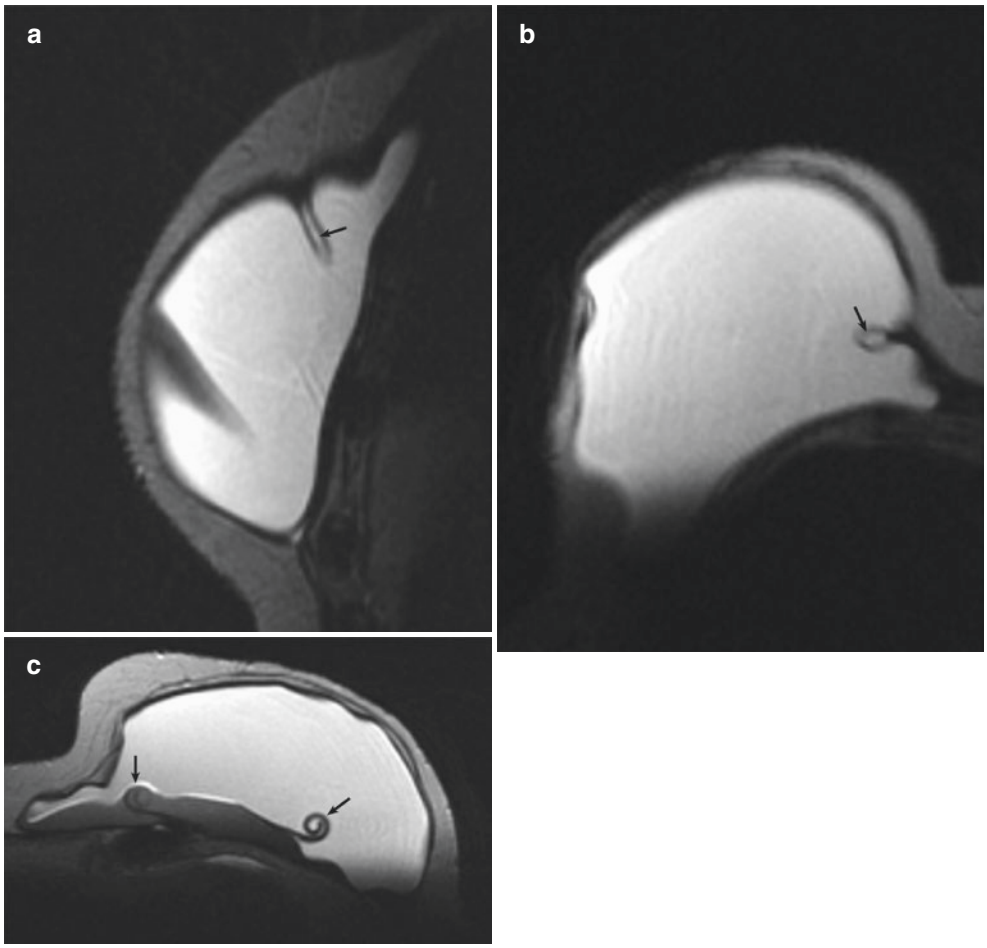

Fig. 6.10 Bilateral intracapsular silicone implant rupture. The sagittal T2-weighted water-suppressed image (**a**) and axial T2-weighted image (**b**) of the right breast show a focus of silicone gel trapped within a fold of the implant shell, known as a "noose sign," "inverted teardrop sign," or "keyhole sign" (*arrows*). (**c**) An axial T2-weighted image of the left breast shows low–signal-intensity, curvilinear lines (*arrows*) contained within the fibrous capsule, representing the collapsed implant shell. These are signs of bilateral intracapsular rupture

6.5 History

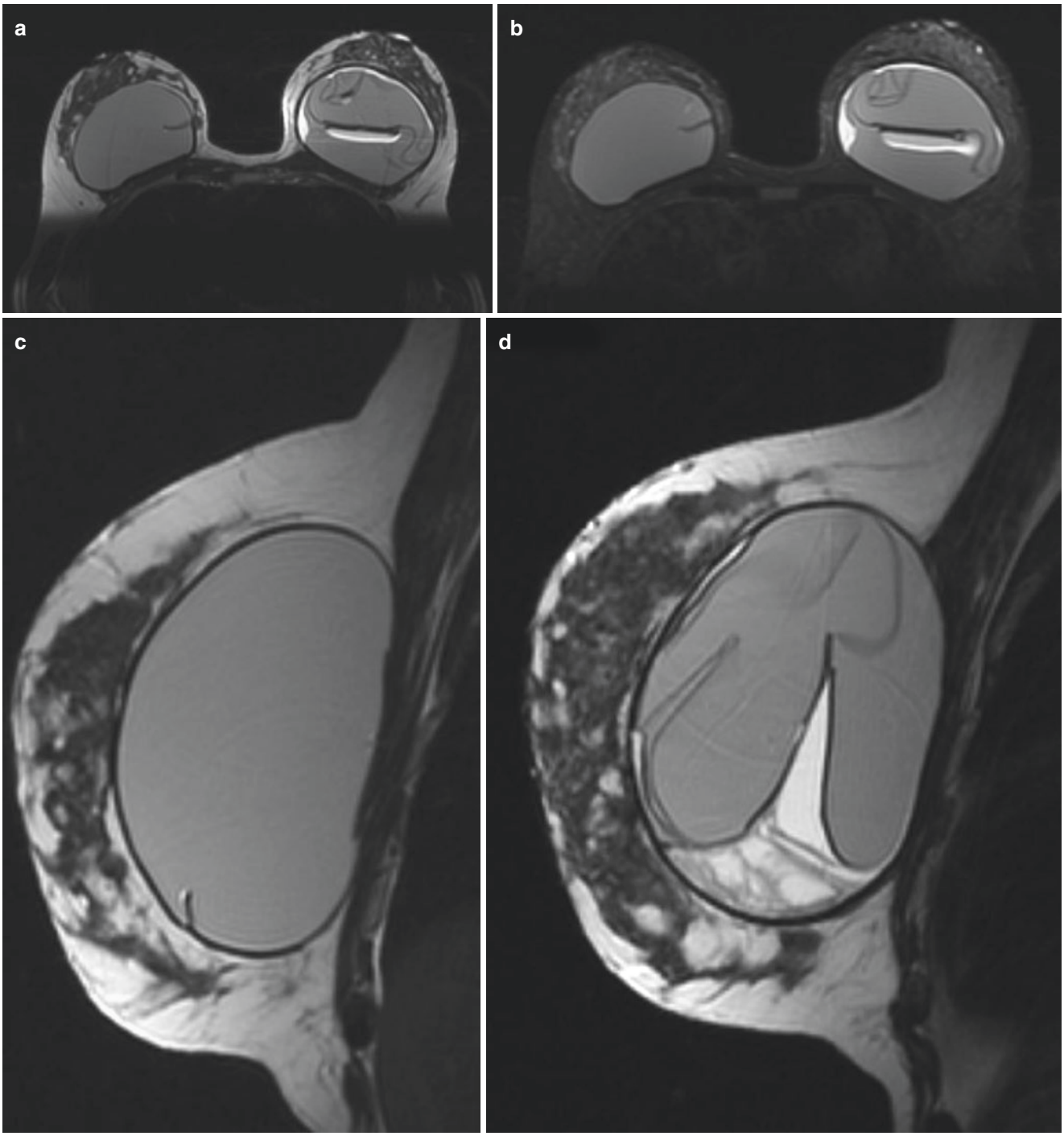

Fig. 6.11 Axial T2-weighted image (**a**) and axial T2-weighted fat-suppressed image (**b**) of both breasts. Sagittal T2-weighted image of the right breast (**c**) and left breast (**d**). Sagittal water-suppressed short T1 inversion recovery (STIR) image (**e**) of the left breast

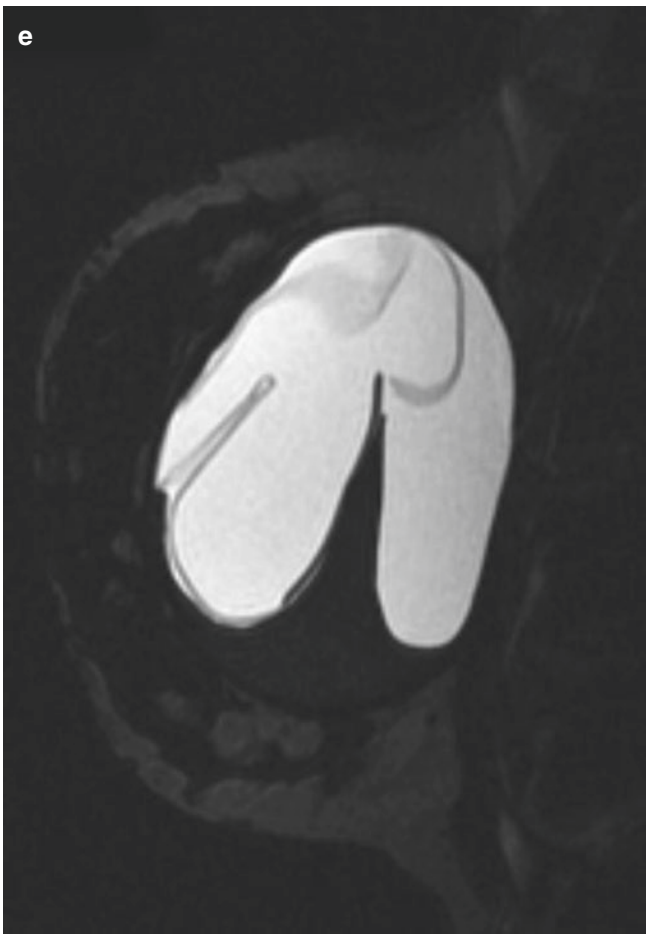

Fig. 6.11 (continued)

6.5 Silicone Implant Rupture 3

Teaching Points 46-year-old woman undergoing breast MRI for evaluation of possible implant rupture (Figs. 6.11 and 6.12).

Image Findings

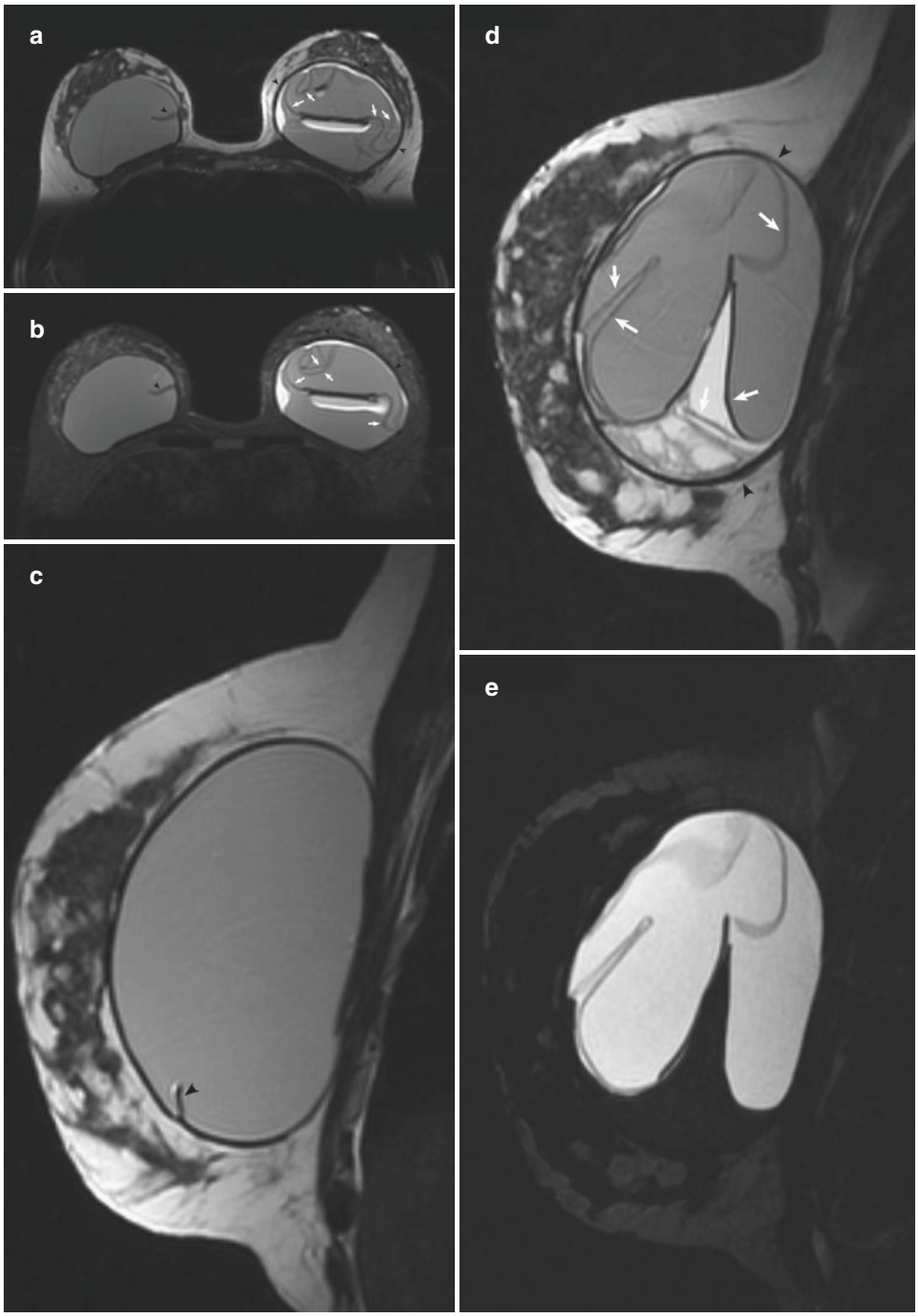

Fig. 6.12 Intracapsular rupture of left retroglandular silicone implant. Axial T2-weighted image of both breasts (**a**), axial T2-weighted fat-suppressed image of both breasts (**b**), and sagittal T2-weighted images of the right breast (**c**) and left breast (**d**) demonstrate an intact right retroglandular silicone implant with radial fold (*black arrowhead*). The left breast implant has a collapsed implant capsule with fluid and silicone external to the collapsed implant capsule, but contained within the fibrous capsule (*black arrowheads*). The multiple low–signal-intensity lines (*white arrows*) are from the collapsed implant capsule, creating the "linguine sign." (**e**) Sagittal water-suppressed STIR image of the left breast (in which only silicone is bright) demonstrates no extracapsular silicone

Suggested Reading

Di Benedetto G, Cecchini S, Grassetti L, Baldassarre S, Valeri G, Leva L, et al. Comparative study of breast implant rupture using mammography, sonography, and magnetic resonance imaging: correlation with surgical findings. Breast J. 2008;14:532–7.

Hölmich LR, Vejborg I, Conrad C, Sletting S, McLaughlin JK. The diagnosis of breast implant rupture: MRI findings compared with findings at explantation. Eur J Radiol. 2005;53:213–25.

Juanpere S, Perez E, Huc O, Motos N, Pont J, Pedraza S. Imaging of breast implants-a pictorial review. Insights Imaging. 2011;2:653–70.

Kreymerman P, Patrick RJ, Rim A, Djohan R, Crowe JP. Guidelines for using breast magnetic resonance imaging to evaluate implant integrity. Ann Plast Surg. 2009;62:355–7.

Middleton MS. MR evaluation of breast implants. Radiol Clin North Am. 2014;52:591–608.

Index

R. Ha et al. (eds.), Breast MRI Teaching Atlas, DOI 10.1007/978-1-4939-6409-3